HZDR-075

EXPERIMENTS ON VERTICAL GAS-LIQUID PIPE FLOWS USING ULTRAFAST X-RAY TOMOGRAPHY

M. Banowski, M. Beyer, D. Lucas,
D. Hoppe, F. Barthel

Wissenschaftlich-Technische Berichte
HZDR-075 · ISSN 2191-8708

WISSENSCHAFTLICH-
TECHNISCHE BERICHTE

HZDR
HELMHOLTZ
ZENTRUM DRESDEN
ROSSENDORF

Wissenschaftlich-Technische Berichte
HZDR-075

M. Banowski, M. Beyer, D. Lucas,
D. Hoppe, F. Barthel

EXPERIMENTS ON VERTICAL GAS-LIQUID PIPE FLOWS USING ULTRAFAST X-RAY TOMOGRAPHY

HZDR

HELMHOLTZ
ZENTRUM DRESDEN
ROSSENDORF

Druckausgabe: ISSN 2191-8708

Elektronische Ausgabe: ISSN 2191-8716

https://www.hzdr.de/publications/Publ-24563

urn:nbn:de:bsz:d120-qucosa-216088

2016

Herausgegeben vom

Helmholtz-Zentrum Dresden - Rossendorf

Bautzner Landstraße 400

01328 Dresden

Germany

Technischer Fachbericht
Experimente zu vertikalen Gas-Flüssigkeits-Rohrströmungen unter Verwendung der ultraschnellen Röntgentomographie

Technical Report
Experiments on vertical gas-liquid pipe flows using ultrafast X-ray tomography

Reaktorsicherheitsforschung-Vorhaben-Nr./
Reactor Safety Research-project No.: 150 1411

Vorhabenstitel: **TOPFLOW-Experimente, Modellentwicklung und Validierung zur Qualifizierung von CFD-Codes für Zweiphasenströmungen**

Project Title: **TOPFLOW experiments, development and validation of models qualifying of CFD codes for two-phase flows**

Autoren / Author(s): **M. Banowski, M. Beyer, D. Lucas, D. Hoppe, F. Barthel**

Dienststelle der Autoren /
Performing Organisation: **Helmholtz-Zentrum Dresden-Rossendorf**
Institut für Sicherheitsforschung

Berichtsdatum / Publication Date: **Dezember 2016**

Berichts-Nr. / Report-No.: **HZDR-075**

Gefördert durch:

Bundesministerium für Wirtschaft und Energie

aufgrund eines Beschlusses des Deutschen Bundestages

Das diesem Bericht zugrundeliegende Vorhaben wurde mit Mitteln des Bundesministeriums für Wirtschaft und Energie unter dem Förderkennzeichen 150 1411 gefördert. Die Verantwortung für den Inhalt dieser Veröffentlichung liegt bei den Autoren.

Berichtsblatt

1. ISBN oder ISSN Druckausgabe: 2191-8708 Elektronische Ausgabe: 2191-8716	2. Berichtsart Technischer Fachbericht
3. Titel Experimente zu vertikalen Gas-Flüssigkeits-Rohrströmungen unter Verwendung der ultraschnellen Röntgentomographie	
4 Autor(en) [Name(n), Vorname(n)] M. Banowski, M. Beyer, D. Lucas, D. Hoppe, F. Barthel	5. Abschlussdatum des Vorhabens 31.12.2015 6. Veröffentlichungsdatum Dezember 2016 7. Form der Publikation Broschüre
8. Durchführende Institution(en) (Name, Adresse) Helmholtz-Zentrum Dresden-Rossendorf Institut für Fluiddynamik Bautzner Landstr. 400 01328 Dresden	9. Ber.Nr. Durchführende Institution HZDR-075 10. Förderkennzeichen 150 1411 11. Seitenzahl 305
13. Fördernde Institution (Name, Adresse) Bundesministerium für Wirtschaft und Energie (BMWi) 11019 Berlin	12. Literaturangaben 14. Tabellen 15. Abbildungen
16. Zusätzliche Angaben	
17. Vorgelegt bei (Titel, Ort, Datum)	

18. Kurzfassung

Die Qualifizierung und Validierung von CFD-Modellen für Zweiphasenströmungen erfordert zielgerichtete Experimente, die Daten in einer hohen Orts- und Zeitauflösung liefern. Charakteristische Parameter der Strömung wie der Volumengasgehalt, die Blasengrößenverteilung, Geschwindigkeiten der Phasen sowie Turbulenzparameter müssen lokal gemessen werden. Um eine Beeinflussung der Strömung durch die Messinstrumente zu vermeiden sind strahlungsbasierte tomographische Methoden für solche Messungen besonders geeignet. In den vorliegenden Experimenten wurde die kürzlich am Helmholtz-Zentrum Dresden – Rossendorf entwickelte ultraschnelle Röntgentomographie zur Bestimmung der lokalen und instantanen Volumengasgehaltsverteilung in einem vertikalen Rohr genutzt. Um eine genügend hohe Bildfrequenz der tomographischen Querschnittsbilder zu erreichen, wird eine rotierende Röntgenquelle durch einen sehr schnell ablenkbaren Elektronenstrahl erzeugt. Die Durchstrahlung des Objekts wird durch einen statischen Detektorring gemessen.

Experimente an vertikalen Rohren sind für die Entwicklung und Validierung von CFD-Modellen für Zweiphasenströmungen besonders geeignet. Die Strömung ist axialsymmetrisch und die Randbedingungen sind gut definiert. Außerdem kann die Entwicklung der Strömung entlang des Rohrs gut vermessen werden.

Dieser Bericht dokumentiert Experimente, die für aufwärts und abwärts gerichtete Gleichströmungen mit Luft-Wasser und Wasserdampf-Wasser durchgeführt wurden, sowie für gegen gerichtete Dampf-Wasser Strömungen. Versuchsaufbau, Versuchsdurchführung, Messtechnik und Datenauswertung werden im Detail dargestellt. Der Bericht beinhaltet außerdem eine Diskussion ausgewählter Ergebnisse sowie Angaben zur Genauigkeit der Daten.

19. Schlagwörter

Experiment, CFD, Zweiphasenströmung, Rohrströmung, Tomographie

20. Verlag	21. Preis

Document Control Sheet

1. ISBN or ISSN Printed: 2191-8708 Electronic: 2191-8716	2. type of document Technical Report
3. title Experiments on vertical gas-liquid pipe flows using ultrafast X-ray tomography	
4. author(s) (family name, first name(s)) M. Banowski, M. Beyer, D. Lucas, D. Hoppe, F. Barthel	5. end of project 31.12.2015
	6. publication date December 2016
	7. form of publication Booklet
8. performing organization(s) (name, address) Helmholtz-Zentrum Dresden-Rossendorf Institut für Fluiddynamik Bautzner Landstr. 400 01328 Dresden	9. originator's report no. HZDR-075
	10. reference no. 150 1411
	11. no. of pages 305
13. sponsoring agency (name, address) Federal Ministry for Economic Affairs and Energy (BMWi) 11019 Berlin	12. no. of references
	14. no. of tables
	no. of figures
16. supplementary notes	
17. presented at (title, place, date)	
18. abstract For the qualification and validation of two-phase CFD-models for medium and large-scale industrial applications dedicated experiments providing data with high temporal and spatial resolution are required. Fluid dynamic parameter like gas volume fraction, bubble size distribution, velocity or turbulent kinetic energy should be measured locally. Considering the fact, that the used measurement techniques should not affect the flow characteristics, radiation based tomographic methods are the favourite candidate for such measurements. Here the recently developed ultrafast X-ray tomography, is applied to measure the local and temporal gas volume fraction distribution in a vertical pipe. To obtain the required frame rate a rotating X-ray source by a massless electron beam and a static detector ring are used. Experiments on a vertical pipe are well suited for development and validation of closure models for two-phase flows. While vertical pipe flows are axially symmetrically, the boundary conditions are well defined. The evolution of the flow along the pipe can be investigated as well. This report documents the experiments done for co-current upwards and downwards air-water and steam-water flows as well as for counter-current air-water flows. The details of the setup, measuring technique and data evaluation are given. The report also includes a discussion on selected results obtained and on uncertainties.	
19. keywords experiment, CFD, two-phase flow, pipe flow, tomography	
20. publisher	21. price

Content

1. Introduction

The qualification and validation of two-phase CFD-models for medium and large-scale industrial applications is an important task of research. For the development and validation of such models dedicated experiments providing data with high temporal and spatial resolution are required. Fluid dynamic parameter like temperature, pressure, gas volume fraction, velocity or turbulent kinetic energy should be measured locally. Considering the fact, that the used measurement techniques should not affect the flow characteristics, radiation based tomographic methods are the favorite candidate for such measurements.

Tomographic measurement systems are used for many technical and medical applications. The physical basis is radiographing an object and measuring the intensity of the attenuated ray. To get cross-sectional images of the investigated object such projections have to include a sufficient angular range to enable a full reconstruction. In most conventional tomographic applications steady state investigations of the object are done. Thus, it is not possible to scan transient processes with usual tomography systems where the ray source and detectors rotate around the object. The image frequency is limited by centrifugal forces to about 3 images per second. If the number of constructed sources and detectors is increased around the object, the image frequency will be increased to about 300 images per second. However, for two-phase flows with bubble velocities in the order of 1 m/s this frame rate is still too low. The idea of increasing source numbers around the object results in a rotating X-ray source by a massless electron beam and a static detector ring. Using such a technique very high frame rates can be achieved.

Experiments on a vertical pipe are well suited for development and validation of closure models for poly-disperse two-phase flows. While vertical pipe flows are axially symmetrically, the boundary conditions are well defined. The evolution of the flow along the pipe can be investigated as well. Experiments on vertical pipe flows were already conducted at the TOPFLOW facility of the Institute of Fluid Dynamics in Helmholtz-Zentrum Dresden-Rossendorf. Wire mesh sensors were used for investigating two-phase flows in pipes with ID 50 and ID 200 with air-water and steam-water flow regimes up to 6.5 MPa, see e.g. Beyer et al. (2008), Lucas et al. (2011), Prasser et al. (2001), (2003) and (2007).

Disadvantages of these existing experiments are the intrusive measurement technique and the necessity of a variable gas injection system due the fact, that the wire mesh sensors disturb the downstream flow. Therefore, the gas injection has to be re-adjusted whenever the measurement position is changed. This procedure provokes discontinuous experimental conditions and needs a relatively long time to reach steady state.

In this technical report, the test facility and the applied measurement techniques are presented (chapters 2, 3 and 4). Additional in chapter 3 processing steps of the measurement data to obtain quantitative data is presented. After appraising measurement uncertainties in chapter 5, selected experimental results are discussed for upward, counter-current as well as downward flows in chapter 6.

2. Objectives and test facility

2.1. Objectives of the experimental series

The objective of the experimental series is to provide detailed experimental data on gas-liquid flows for a wide range of flow conditions. As part of nuclear safety research, CFD-codes have to be qualified for analyzing safety relevant flows in nuclear light water power plants. Especially processes in the primary loop are in focus of these R&D activities, because the three dimensional two-phase flow phenomena have an important effect on cooling of the reactor pressure vessel.

With previous experiments on vertical pipes a large database of vertical two-phase flows basing on the wire mesh sensor technique is available. In these experimental series co-current counter-gravity air-water as well as steam-water flows were investigated at different pressures up to 6.5 MPa. They provided valuable quantitative data, but also gave deep insights into two-phase flow structures. A disadvantage of the used wire mesh sensors is their intrusive measurement principle. To minimize the intrusive effects most of the investigated flows had liquid superficial velocities larger than 0.4 m/s. At lower liquid superficial velocities, the gas holdup is overestimated due to the bubble interaction with the wire mesh.

Using the non-invasive tomography technique, this disadvantage is resolved. Therefore, the aim of these new experiments on vertical two-phase pipe flows is to enlarge the existing upward two-phase flow database especially in low liquid flow regimes. But also in the range of already investigated flow regimes using WMS, new data were obtained. Furthermore, downward two-phase flow regimes are investigated. The experiments are conducted with air-water as well as steam-water flows. Finally, results of WMS and tomography are compared for assessing the measurement accuracy.

2.2. Setup of the facility „Vertical titanium pipe“

The vertical test section “Titanium Pipe” is a 4.95 m long pipe with an inner diameter of 54.8 mm and a wall thickness of 1.6 mm. It was manufactured from 6 pipe sections with lengths between 998 mm and 347 mm which were connected by high-quality WIG orbital welding. For the current test series the “Titanium Pipe” was installed in the test section circuit of the TOPFLOW facility which supplied the pipe with water, dry air or saturated steam flows respectively. The isometric drawings of the vertical test section and the inlet and outlet pipes are attached to this report as digital appendix.

Figure 2.1 shows 3 different configurations of the test section circuit that involves of the vertical test sections “Titanium Pipe” and “Variable Gas Injection”, the steam drum and the test section pump as well as an air and steam supply system. During all measurements the steam drum was used as separation and water storage tank. Additionally its gas blow-off valves were used to control the pressure in the circuit. The test section pump circulated the water from the steam drum through the vertical pipes. Downstream the pressure side of the pump, the water flow control and measurement devices were arranged in 3 parallel lines to allow a good measurement quality in a parameter range up to 50 kg/s. The air flow was provided by the compressed air system which feeds the test sections with a gas norm volume flow up to 850 m³/h by using one of 6 parallel devices. For non-adiabatic tests the TOPFLOW

facility can supply a maximum saturated steam mass flow of 1.4 kg/s. Thereby the steam flow can be controlled and measured by 2 parallel lines.

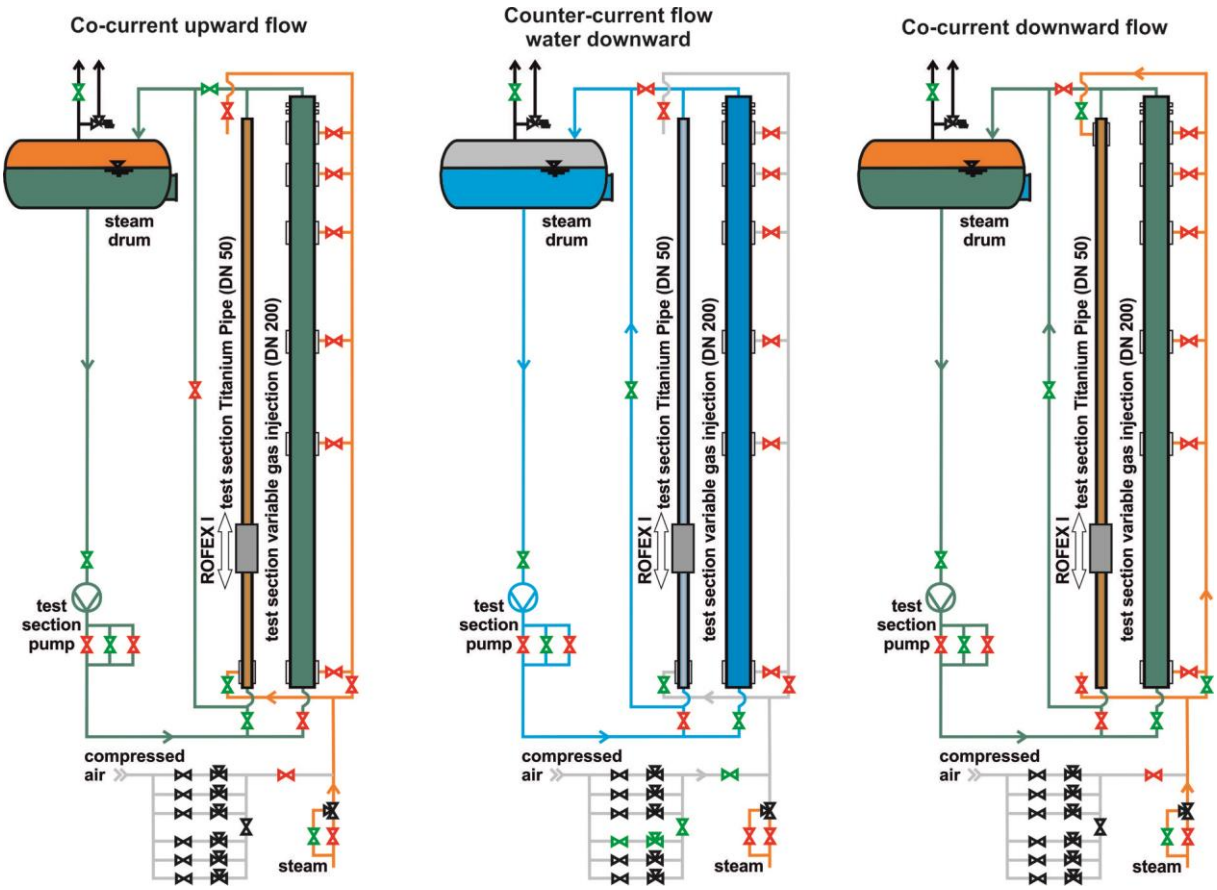

Figure 2.1: Schematic view of the TOPFLOW test section circuit with the Titanium Pipe: left hand side – configuration for co-current upward flow; middle part – for counter-current flow and right hand side – for co-current downward flow, red marked valves are closed during operation, while the green marked are open.

This report presents all the different tests conducted in the vertical Titanium Pipe. The non-invasive ultra-fast X-ray tomography was used to measure important flow characteristics. For co-current upward and downward two-phase flows adiabatic tests with air-water flows as well as almost adiabatic experiments with saturated steam and slightly sub-cooled water were executed. Furthermore, some measurements were carried out with counter-current flows, however in this case only an air-water mixture was analyzed. To analyze different flow regimes the combination of gas and liquid superficial velocities in the pipe was varied over a wide range. For this reason 2 types of gas injection modules were applied, which ensures an almost symmetrical gas distribution in the pipe cross section. A detailed description of both gas injectors is given in section 2.2.2.Table 2.1 assigns the different types of tests to the measurement series numbers, their boundary conditions and used gas injection modules.

Table 2.1: List of the Titanium Pipe measurement series and their range of boundary conditions

Series	Flow condition	Pressure [MPa]	Temperature [°C]	Gas injection module
L16	Co-current upward (air)	0.4	29 - 31	M3
L18	Co-current upward (air)	0.4	29 - 31	M4
D19	Co-current upward (steam)	4 and 6.5	Saturation	M4
L17	Counter-current (air)	0.4	29 - 31	M3
L20	Co-current downward (air)	0.4	29 - 31	M3
L21	Co-current downward (air)	0.4	29 – 31	M4
D20	Co-current downward (steam)	4 and 6.5	Saturation	M4

2.2.1 Test procedure

As aforementioned, in the test section Titanium Pipe air-water as well as steam-water tests were executed. Hence, the TOPFLOW test section circuit works under different conditions. First the preparation for air-water experiments will be described.

After assembling of the piping and a final measurement technique check, the water in the circuit was heated-up to 29 °C using the test section pump. Parallel the pressure in the system was increased to the nominal value (0.4 MPa) by gas injection into the test section. Then the operational data acquisition system was activated. The next step was the adjustment of the matrix parameter for the water mass flow and the norm gas volume flow corresponding to both superficial velocities. Additional the gas blow-off valves of the steam drum were used to control the pressure in the Vertical Titanium Pipe. When all parameters were constant, the operators waited about 15 minutes to have constant pressure condition also in the gas feeding pipes upstream the injection module. Then the X-ray tomography was moved to the first measurement position and the measurement was conducted. After copying and checking the measurement data for accuracy, the next tomography position was adjusted and the pipe flow was measured. After finishing the measurements for all levels, the next matrix parameters were set and the measurement procedure was started again. Beside these measurements the necessary reference data for the calibration of the X-ray tomography were recorded. For the pure water references the air injection was closed by two ball valves, while the water circulation kept working. The void references were measured after draining the Titanium Pipe.

During the operation of the test section pump, the water temperature increases while the water is circulated. To keep the temperature of the fluid in the test section constant, warm water inside the steam drum was substituted partly with cold water from the blow-off tank of the TOPFLOW facility.

As shown in *Table 2.1* different flow conditions were applied. For co-current upward flow (Figure 2.1; left hand side; steam operation) the liquid and gas were injected directly at the bottom of the test section. Then the mixture rose up inside the Titanium Pipe and flowed to the steam drum.

For co-current downward flow the gas injection module was shifted to the top of the Titanium Pipe. To supply the gas to the top injection module the gas-feeder of the test section Variable Gas Injection (VGI; thick vertical pipe in Figure 2.1; right hand side; steam operation) was used. The liquid was directed from the pressure side of the test section pump through the VGI to the top of the Titanium Pipe. This flow regime will work under steady-state condition only if the water superficial velocity is higher than the gas drift velocity. The matrix of the series L20, L21 and D20 (see section 6.3 for further details) satisfied this requirement. From the bottom of the Titanium Pipe the two phase mixture returned into the steam drum.

For counter-current flow the liquid path was the same as for downward flow, while the gas phase was injected at the bottom of the Titanium Pipe (Figure 2.1; middle part; air operation). In this case the liquid superficial velocity was set lower than the relative velocity of the gas phase, in order to get a two-phase flow with rising bubbles in the vertical test section. This led the gas to accumulate and displace the water in the pipes above the vertical test sections. This effect has to be considered in the data evaluation and analysis. To minimize the gas accumulation effect, the time between two tomographic measurements was used to flush the Titanium Pipe and the top pipes. For this an upward water flow through both vertical test sections was arranged.

Beside air-water flows almost adiabatic steam-water mixtures were investigated. These tests required a more complex facility preparation. In addition to the test section circuit the steam generator of the TOPFLOW facility and the auxiliary systems had to be set into operation. Since the most operational procedures are less interesting for the reported tests, in this chapter only the relevant activities are considered. At first the test section circuit was heated-up. For this the water circulation through the Titanium pipe was started and heating steam was injected into the steam drum. Due to steam condensation the water temperature in the circuit increased. During this procedure, the blow-off valves were closed. Hence, the pressure in the steam drum increased too.

The half-filled steam drum and the upper pipes are the highest points of the test section circuit, so air accumulates there. High quality steam-water tests require the removal of non-condensable gases. For this fact, the steam drum is equipped with a degasification pipe which allows the release of the air steam mixture directly above the water level. This is the best place for degasification, because the heavier air (related to the steam density) concentrates there. During the heating-up of the test section circuit the degasification was activated periodically after the liquid temperature exceeded 150 °C. The degasification process was controlled by the comparison of the saturation temperature as function of the pressure in the steam drum and the temperature of the gas volume inside the tank. If the last is practically equal to the saturation temperature, the circuit will be free of non-condensable gases. Furthermore the feed water of the TOPFLOW steam generator was degassed by membrane contactors to avoid additional entry of non-condensable gases into the test section by steam injection.

The water and steam mass flows into the vertical Titanium Pipe were adjusted after heat-up and pressure increase up to the nominal values. As soon as all parameters were constant, the tomographic measurements along the vertical test section were done similar to the air-water flow measurements. Also for steam-water tests the pure water and the void references for tomographic reconstruction were recorded.

The analysis of steam-water test data of previous experiments revealed, that condensation in the steam pipes between the mass flow measurements and the gas injection modules cannot be neglected. It occurs due to heat losses in the steam pipes and is relevant for low pressure tests, because the low steam density leads to very small nominal steam mass flows for the interesting volume flow range. For this reason the current steam tests were carried out only at high pressures, e.g. 4 and 6.5 MPa to reduce this effect.

Furthermore, it is important to mention, that the injected water was slightly sub-cooled. In the storage tank (steam drum) the liquid has saturation temperature. Due to the hydrostatic pressure, the pressure increase by the test section pump and heat losses, the liquid temperature on the test section inlet is a few degrees below saturation state. The steam at the injection point can be accounted as saturated, because in steam feeding pipes non-separated condensate is carried as droplets away. Both inlet temperatures were stored in the operational data file for data evaluation.

2.2.2 Gas injection modules

All tests were done in a wide range of parameters. Two different gas injection modules were applied for a continuous gas injection as well as homogeneous cross-sectional gas distribution.

For small gas flows (up to 0.09 m/s) a two-stage injector with one or three injection needles was used (M3). A parallel operation with 4 needles is also possible. Figure 2.2 shows this device. It consists of a pressure-proofed bottom part with 2 gas distribution chambers and the connecting gas tubes. Based on this a double pipe rise up to the gas injection level, where 3 injection needles are connected to the outer pipe and 1 to the inner one. The inner diameter of all 4 needles amounts 0.8 mm. 6 metal sheets are welded around the circumference of the outer pipe which work as water flow straightener. The long distance between the bottom part and the gas injection level results on the one hand from the CFD requirement of knowledge about the flow structure directly downstream the gas injector. On the other hand the design of the X-ray tomograph specifies the distance between the detector (measurement) level and the end of the radiation protection shield.

For high gas volume flows the 2nd gas injection module M4 was constructed (Figure 2.3). It is also a two-stage injector which provides 6 injection pipes each with one orifice as well as 12 pipes each with 4 holes. All orifices have an inner diameter of 1.2 mm. A parallel operation of all 54 holes is also possible. To reduce the pressure drop of the gas injection pipes, they were designed with a minimal length. Hence the gas injection takes place near the gas distribution chambers which were included in the pressure proofed basis. So the two-phase flow was generated far from the tomographic detection level. To get nevertheless flow data near the gas injection an

additional mesh (step 4 x 4 mm; 1 mm wire diameter) was fixed 345 mm above the gas injection level that serves as flow straightener and distributor. Additional downstream of the gas injection a honeycomb shaped liquid flow straightener was installed. Both modules allow a parallel injection of the gas phase into the liquid.

Appendix 9.3 contains tables with important operational data. They also include information about the applied gas injection module (M3 or M4 – as aforementioned) and the number of worked injection needles (e.g. M3 / 3) for each test.

Figure 2.2: Gas injector M3 for small volume flows

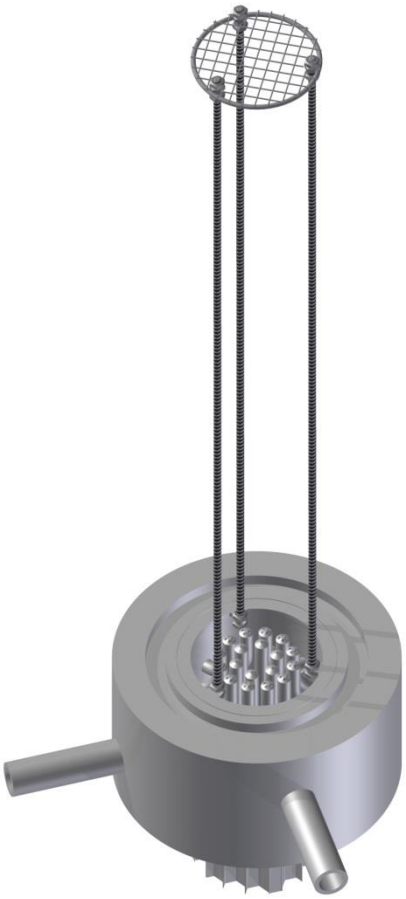

Figure 2.3: Injection module M4 for high volume flows

The technical drawings of both gas injection modules are attached in the digital appendix.

2.2.3 Measurement positions

For investigation of the flow evolution along the vertical pipe it is necessary to observe the flow behavior in different levels, starting near the gas injection and finishing at developed flow state. To meet this requirement, the X-ray tomograph was mounted on an elevation unit (Figure 2.1), which allows a continuous positioning along the Titanium Pipe. Furthermore for all upward co-current tests beside the X-ray scanner a pair of wire-mesh sensors was used, which was installed on the top of the

Titanium Pipe (level S in Table 2.2). All other levels (A - P) correspond to tomographic measurements.

Table 2.2 lists the test series and their associated levels. In this table the numbers are the distance between the gas injection and the measurement level. For clearness the levels corresponding to the downward flows (series L20, L21 and D20) were indicated as negative numbers. For the series L16, L17, L20 and L22 the injection module M3 was applied. Here the gas injection level was the upper end of the capillary tubes. The other tests (L18, L21, L23, D19 and D20) were conducted with the module M4, whereat the injection level was set to the wire-mesh. In both cases the most upstream level is few millimeters away from the steel parts of the injection modules, to ensure a clean tomographic observation. Due to the construction of the X-ray scanner and the flange positions near the vertical Titanium Pipe, the measurement levels near the gas injection and at the widest position from the gas injection differ among the series.

Table 2.2: Test series with associated measurement levels

Series	A	C	D	E	G	J	M	N	NN	P	S
	mm	mm	mm	mm	mm	mm	mm	mm	mm	mm	mm
L16	5		62		171	435	1271			3270	4685
L18	18		62		171	435	1271			3205	4685
D19		18		94	171	435	1271			3202	4685
L17	1		62		171	435	1271			3270	4685
L20	-5		-62		-171	-435	-1271	-3113			
L21	-18		-62		-171	-435	-1271		-3054		
D20	-18		-62		-171	-435	-1271		-3054		

2.2.4 Operational data acquisition

The synchronous recording of relevant operational data is an important task beside all measurements. This information is necessary for assessing the boundary condition of these tests at CFD simulations. The operational data acquisition on TOPFLOW is realized by the commercial software DIAdem, provided by the company National Instruments. This software is connected to an OPC server which works as central data storage of the facility and provide refreshed information each second.

During the preparation of new test series a list of operational parameters is specified. Based on this list, DIAdem application software is developed. This list is mostly very voluminous by technical reasons. During the data evaluation process a summary is generated by DIAdem scripts. While the operational data acquisition software runs continuously and recorded the requested data over the entire time, the X-ray scanner generates a trigger signal during its measurement time for synchronizing with these operational data.

The signal is stored in the operational data file and also serves as trigger for the wire-mesh sensor measurement if necessary. Additionally the trigger is used by the DIAdem script to create the summary for each test that contains values of the most important parameters, averaged over the measurement time. The DIAdem software is a commercial product and is not generally available. Therefore, the information of the summaries has to be transferred to the common Microsoft Excel format, where it is stored in sheets, sorted by test numbers. After completion of the data evaluation the Excel files are available for further test analysis.

Figure 2.4 shows the position of relevant operational measurements at the vertical pipe. The pressure and differential pressure are illustrated with red color. On top of the test section 2 sensors are installed: PI4-200 and PI4-201. While the first one is used for air-water tests with a maximal pressure of 0.6 MPa, the second one covers the entire range up to 10.0 MPa for steam experiments. This solution ensures a high accuracy in a wide pressure range.

Furthermore the devices for air volume flow (FIC4-10 – FIC4-15) as well as steam (FIC4-04, FIC4-05) and water mass flow (FIC4-01 – FIC4-03) are shown blue colored.

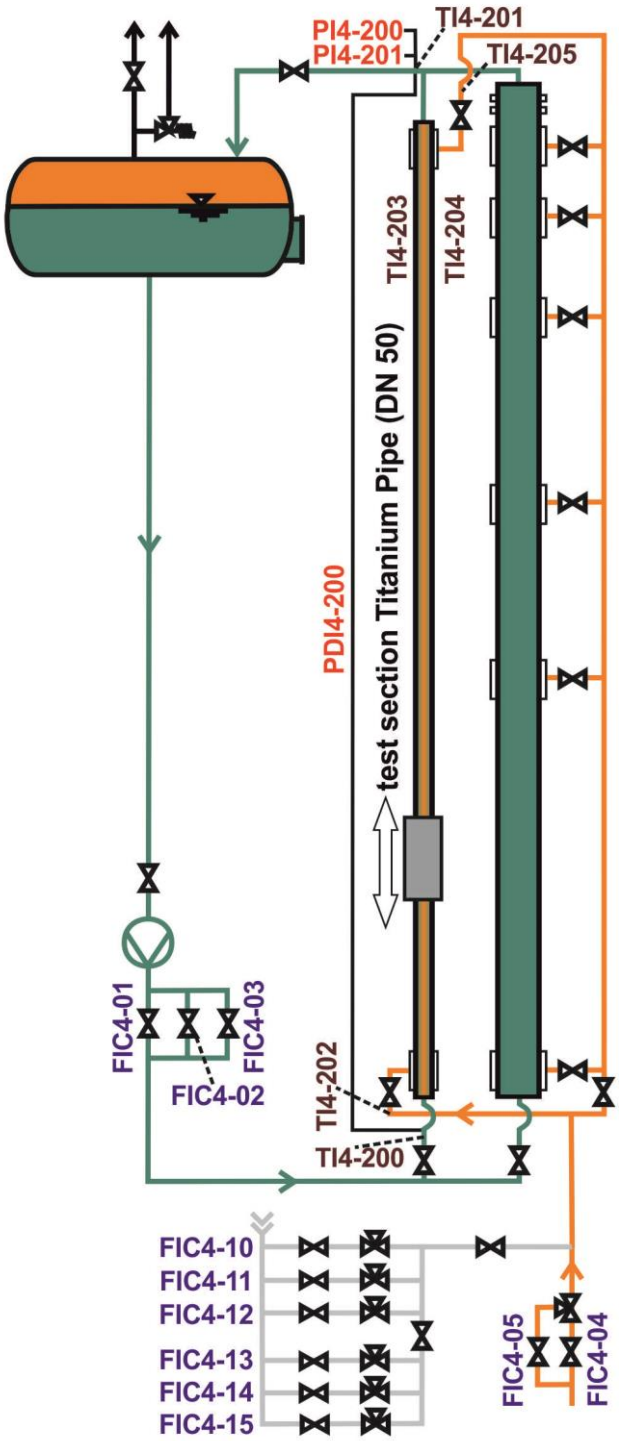

Figure 2.4: Vertical test section Titanium Pipe with pressure, temperature and flow sensors

At the top and bottom of the Titanium Pipe thermocouples are mounted to measure the water (TI4-201, TI4-200) and gas temperature (TI4-205, TI4-202). The other 2 thermocouples (TI4-203 and TI4-204) are fixed at the outer surface of the thermal insulation. Their indication was used to check the thermal load of the X-ray tomography.

Regarding to the vertical Titanium Pipe the relevant operational parameters depend on the flow regime (Figure 2.1) and on the media. Table 2.3 summarizes all parameters and shows their correlation to the test series. Additional it contains the calibration range, the measurement uncertainty and the calibration data. The parameter listed in Table 2.3 includes the differential pressure PDI4-200. This value is presented in the operational data files of all test series. It is important to consider, that the pure measurement values of PDI4-200 are included in the files. It indicates the pressure difference between the fulfilled impulse pipe and the test section. For further data analysis it have to be considered, that the real pressure drop over the test section can be determined using the distance between both measurement connections (5.73 m) and the water density in the impulse pipe. Furthermore Table 2.3 contains the pressure values PI4-202 and PI4-203 for downward flows. Both parameters are calculation results. While PI4-202 bases on PI4-200 (low pressure) and on PDI4-200, PI4-203 was calculated with PI4-201 (high pressure) and PDI4-200.

The nominal pressure of 0.4 MPa for air-water and 4 or 6.5 MPa for steam-water tests was set:

- upward and counter-current flows (series L16, L18, D19, L17) at PI4-200 / PI4-201 above the WMS position; the impulse pipe is connected to the pipe after the first elbow above the Ti test section (150 mm above the upper WMS mounting flange) and
- downward flows (series L20, L21 and D20) at PI4-202 / PI4-203 downstream the Ti test section mounting flange; the impulse pipe is connected to the fluid outlet pipe 100 mm below the bottom mounting flange.

The real pressure values together with the corresponding operational parameters for each test contain the tables in appendix 9.3.

A further boundary condition is the temperature of the liquid and gas phase. In consideration with Fig. 2.4 the liquid inlet temperature was measured with the sensors TI4-200 (upward) or TI4-201 (downward). Their nominal value was set to 30 °C ± 1K for all air-water tests. For steam-water tests it was slightly sub-cooled due to technical reasons. The real water temperatures for each test are listed in the operational data tables in the appendix 9.3.

The air was injected with uncontrollable temperatures. The measured values are also included in the operational data tables in app. 9.3. Here 2 sensors are important: For co-current upward and counter-current flow the gas was injected at the bottom part of the Ti-pipe – so the TI4-202 is valid. Regarding the downward flow the gas was injected at the top side of the test section and was measured with TI4-205. The steam temperature was at saturation level depending of the pressure at gas injection.

The water inlet flow is specified as water mass flow and was converted to the liquid superficial velocity (appendix 9.3). The nominal gas volume flow was calculated from the nominal gas superficial velocity from HZDR matrix under consideration of the nominal pressure of 0,4 MPa for air-water tests (4 or 6,5 MPa respectively for steam tests). For technical reasons the nominal pressure could not be adjusted at gas injection level. Hence, the injected gas superficial velocity at injection level was

slightly different from the matrix value. This fact has to be considered during data analysis.

Table 2.3: Operational parameters and measurement uncertainties

Parameter	L16 L18	D19	L20 L21	D20	L17	L22 L23	Calibration range	Meas. uncertainty	Calibration data
FIC4-14	X		X		X	X	0,05 – 0,5 nm³/h	-1.8 – 0.1 %	06.2010
FIC4-13	X		X			X	0,5 – 5 nm³/h	-3.0 – 0.9 %	
FIC4-12	X		X			X	5 – 50 nm³/h	-2.5 – 1.1 %	
FIC4-11						X	50 – 500 nm³/h	-0.5 – 6.0 %	
FIC4-01	X					X	5 – 50 kg/s	± 0.2 %	12.2008
FIC4-02	X	X	X	X		X	0,5 – 5 kg/s	± 0.1 %	
FIC4-03	X				X	X	0,05 – 0,5 kg/s	± 0.2 %	
FIC4-04		X					0,16 – 1,6 kg/s	± 2.1 %	12.2008
FIC4-05		X		X			0,016 – 0,16 kg/s	± 2.1 %	
PI4-200	X				X	X	0 – 0,6 MPa	± 0,15 %	06.2012 03.2013
PI4-201		X		X			0,1 – 10 MPa	± 0,1 %	06.2011
PI4-202			X					± 1 %	calculation
PI4-203				X				± 1 %	calculation
PDI4-200	X	X	X	X	X	X	-100 – 100 kPa	± 0.8 %	09.2011 04.2013
TI4-200	X	X	X	X	X	X	20 – 300 °C	± 0.5 K	06.2012 03.2013
TI4-201	X	X	X	X	X	X	20 – 300 °C	± 0.5 K	
TI4-202	X	X			X	X	20 – 300 °C	± 0.5 K	
TI4-203		X		X				± 1 K	factory
TI4-204		X		X				± 1 K	factory
TI4-205			X	X			20 – 300 °C	± 0.5 K	06.2012 03.2013

The table above also presents the calibration data of the measurement devices. Thereby the water mass flow on TOPFLOW is measured by Coriolis devices. They were obtained at the end of 2008 with factory calibration. Due to the fact, that the uncertainty of Coriolis flow meters is very small and their drift is very low, the operators decided that a calibration all 10 years is sufficient. The measuring orifices

FIC4-04 and FIC4-05 were also calibrated at the manufacturer. Due to the low steam operation time of the TOPFLOW facility the erosion of the orifices is insignificant. So for these devices the calibration time is alright. The thermocouples TI4-203 and TI4-204 were used only for internal monitoring. Thus, an extra calibration was not necessary.

All relative values in the column “measurement uncertainty” are related to the measurement values.

3. Ultrafast X-ray tomography

Ultrafast X-ray computed tomography is a non-intrusive imaging technique, which provides cross-sectional slice images of the propagating flow with very high temporal and spatial resolution. The ROFEX device (ROssendorf Fast Electron beam X-ray tomograph) was developed at HZDR for such measurements.

3.1. Setup and working principle of ROFEX

X-ray tomography systems acquire radiography data of an investigated object from many angles of view. From these data cross-sectional slice images are reconstructed. Conventional X-ray tomography systems are limited in measuring speed by centrifugal forces, caused by inertia of mechanically rotated X-ray source and detector. But, for investigation of two-phase flows with high internal dynamics a frame rate of at least 1000 images per second is needed.

Therefore, the ultrafast electron beam X-ray tomography was developed at the HZDR. The principle is as follows: An electron gun produces a free electron beam of sufficient energy. The beam is formed and focused on a circular ring target, which surrounds the object with an angle of 240°. This limitation of the target angle was introduced to enable the implementation of a pipe. The electron beam focus spot (i.e. X-ray source spot) is swept rapidly along this target, by deflection coils. Thus, a fast rotating X-ray source is produced. The radiation passes the object in the centre of setup and the X-ray intensity behind the object is measured by fast static detectors which are arranged as a full 360° ring. By rotating the X-ray spot and recording attenuation data continuously, a set of projections per revolution of the beam is acquired. From these data a superposition free slice image is reconstructed using conventional convolution back projection algorithm (see section 3.2). The systems provides dual-layer CT mode, which means acquisition of projection data from two different imaging layers with an axial distance of 10.2 mm (time multiplexed). This allows to obtain the bubble velocity information from the two-phase flow. The ROFEX-scanner can be moved vertically in arbitrary positions by an elevation unit. In Figure 3.1 a) a schematic drawing of the working principle of ROFEX is presented. Photography of the ROFEX application on the vertical test section is shown in Figure 3.1 b).

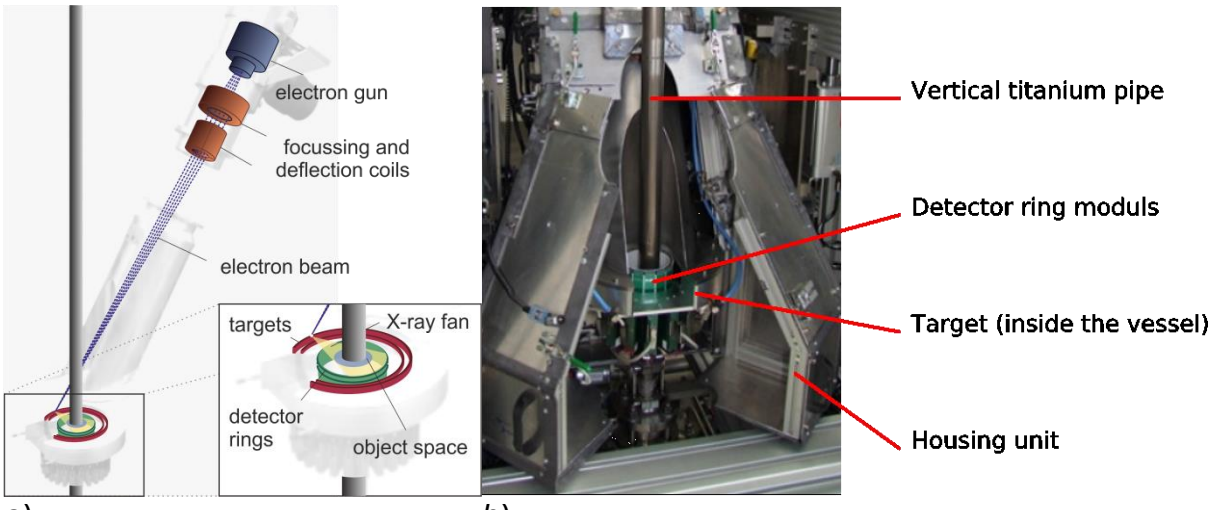

a) *b)*

Figure 3.1: a) Schematic design and working principle of ROFEX. b) Detailed photographic image of ROFEX

The X-ray energy is 150 keV with a maximum beam power of 10 kW. The detector consists of 576 room-temperature semiconductor cadmium-tellurite pixels with an active area of 1.33 mm x 1.33 mm, arranged on a full circle in two layers. The X-ray photons create electron-hole pairs in the detector crystal which are collected by a bias field and eventually converted into a voltage signal. The detector readings are sampled by a 12 bit ADC with a frequency of 1 MHz. The measured raw data is stored intermediately in a 24 GB detector memory and downloaded using Gigabit Ethernet to the controlling PC after each measurement. Further information on ROFEX tomography system is presented by Fischer and Hampel (2010), Fischer et al. (2008), Hampel et al. (2013).

The spatial resolution in the reconstructed images significantly depends on attenuation behavior of investigated object and temporal resolution in the scan as well. Phantom measurements for the application on vertical test section at TOPFLOW facility resulted in 2 mm gas bubble size at measuring speed of 5000 frames per second.

For the setup of vertical titanium test section at the TOPFLOW facility the system achieves a spatial resolution of 2 mm at a temporal resolution of 5000 frames per second at best conditions.

3.2. Reconstruction

3.2.1 Filtered back projection

The tomographic image reconstruction bases on the assumption of a linear path of radiation from a dot-shaped X-ray source spot to the detectors at which a location-dependent attenuation inside the investigated object occurs. With other words: the corresponding “shadow” of the object is projected on the static ring of detectors. (see section 3.1). The detectors and the X-ray source spot are approximately in the same plane forming a measurement plane. As mentioned before ROFEX has two such measuring planes which are parallel to each other. Between object and tomography system (containing X-ray source spot and detectors) there is a relative rotation inside this plane, whereat the fulcrum is inside the object preferably. The entity of measured attenuation values from a 360° tomography rotation are called sinogram. They are stored in matrices where the rows represent the detector numbers and the columns the different angular steps. In Figure 3.2 a scaled sinogram is presented. Sinogram scaling means dividing each element of the sinogram obtained for the object of interest (titanium pipe and two-phase flow) by the corresponding elements of a sinogram without object (free radiation path). This scaling is the first step of tomographic reconstruction.

The electron beam continuously rotates over the full circle, but a signal is existent only for an angle of 240° caused by the horseshoe shaped target (compare to Figure 3.2). This limitation is unproblematic since many radiation paths are measured twice and can be reassembled for this reason. Using this redundancy all attenuation values are existent for the remaining angle range of 120°. Therefore, the full tomographic image reconstruction is possible.

It should be noted here, that in principle the radiation paths of the existing X-ray fan projections could be regrouped in a way to get parallel projections. This would allow a

large reduction of computing time. However, it would be connected with a loss of information (no use of redundancies) and lead to additional numerical errors. In the result, it would lead to a lower quality of the reconstructed image (lower sharpness and larger noise). For this reason, the fan projection is used for the tomographic image reconstruction although it requires much more computational resources.

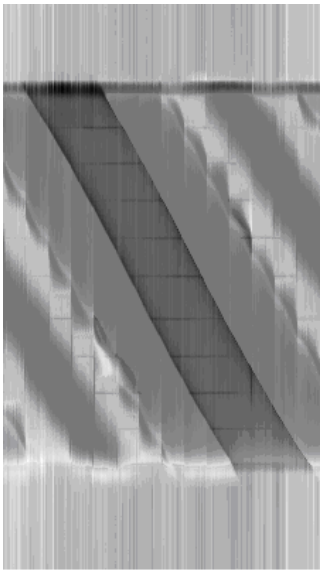

Figure 3.2: Example for a matrix of scaled measured attenuation values (sinogram). The rows present the different angles for the full circle, the columns of the single detectors.

The dark diagonal strip in Figure 3.2 is the shadow of the scanned titanium pipe. The reconstruction of this stripe and a small surrounding region is shown in Figure 3.3. The formation of the projections can be described by a mathematical operation called radon transformation (see Kak and Slaney, 2001), whereat mainly line integrals are calculated along the paths of rays. Accordingly, the image reconstruction basing on the inverse radon transformation is a differential operation, which is inversely to the integration. A disadvantage of this differentiation is the non-determined absolute value at the reconstructed image. However, using a-priori knowledge the correct absolute term can be restored.

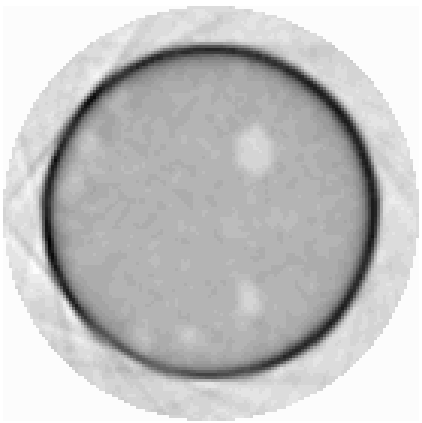

Figure 3.3: Tomographic cross-sectional image of vertical titanium pipe including water and bubbles

The estimation of the absolute term and hence the gas volume fraction is explained firstly in an abstract presentation and illustrated by an example afterwards. A linear relationship is defined between reconstructed grey value image g and real distribution of attenuation coefficients μ according to

$$\mu = a(g + b + c) \tag{3.1}$$

where a, b and c are constants. The constant c considers model uncertainties like scattered radiation or beam hardening. These image artefacts are caused mainly by the titanium pipe and are not subject to variations between different measurements. So, c is assumed to be invariant. In contrast, the constant b represents the absolute term of the reconstructed images and has to be estimated individually for each image. Assuming an invariant amplification of the tomography system the constant a is invariant as well.

To estimate the constant b three different measurements are used: the unknown gas-liquid flow measurement U, the empty tube one E (only gas filled) and a full liquid filled tube one F. Attention should be paid to guarantee identical conditions for temperature, pressure, frequency etc. during the reference measurements and the unknown gas-liquid measurement. Using E and F, a scale can be defined to determine U. Clearly it must be assumed that the titanium pipe has the same position in the images of U, E and F. Possible local offsets have to be be corrected before this scaling (cf. section 3.4). According equation (3.1) it applies

$$\begin{aligned} \mu_U &= a(g_U + b_U + c) \\ \mu_E &= a(g_E + b_E + c) \\ \mu_F &= a(g_F + b_F + c) \end{aligned} \tag{3.2}$$

The constant c is cancelled out by calculating the differences from the equations (3.11):

$$\begin{aligned} \mu_U - \mu_F &= a(g_U - g_F + b_U - b_F) \quad resp. \\ \mu_{U-F} &= a(g_{U-F} + b_{U-F}) \end{aligned} \tag{3.3}$$

as well as

$$\begin{aligned} \mu_E - \mu_F &= a(g_E - g_F + b_E - b_F) \quad resp. \\ \mu_{E-F} &= a(g_{E-F} + b_{E-F}) \end{aligned} \tag{3.4}$$

The constant b can be determined from regions in the scanned object which are not a subject of change. Independent from the material present for such non-changing regions the differences above have to be identical to zero. A ring shaped region outside of the pipe is chosen as such a non-changing region as presented in Figure 3.4. In this region $\mu_{U-F} and\ \mu_{E-F}$. are set to zero. In the result

$$b_{U-F} = -g_{U-F,ref}$$
$$b_{L-F} = -g_{L-F,ref} \tag{3.5}$$

are obtained. Combining (3.12), (3.13) and (3.14), the gas volume fraction can be calculated according to

$$\varepsilon = \frac{\mu_{U-F}}{\mu_{E-F}} = \frac{g_{U-F} - g_{U-F,ref}}{g_{E-F} - g_{E-F,ref}} \in [0;1]. \tag{3.6}$$

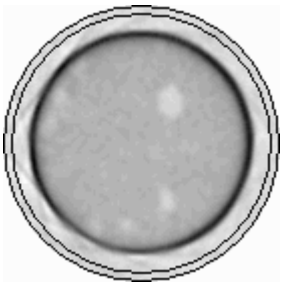

Figure 3.4: Ring shaped constant region, which is used as reference region

In Figure 3.5, examples for measurements of empty tube *E* (the presented case is an air reference measurement), liquid filled tube *F* and unknown gas-liquid flow *U* are shown.

Figure 3.5: Exemplary images of empty tube measurement E (left), liquid filled tube measurement F (center) and unknown gas-liquid measurement U (right)

According to equations (3.12) and (3.13), the differences E-F and U-F are calculated. In Figure 3.6 these differences are presented.

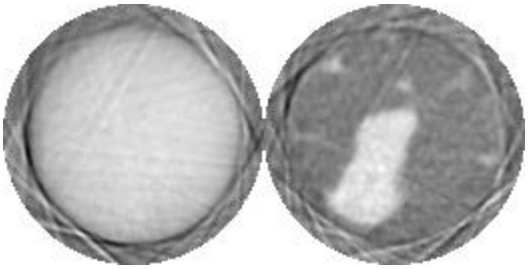

Figure 3.6: The differences E-F and U-F of presented examples in Figure 3.5

Althrough the region of the pipe wall is invariant, it is not fully canceled out in all cases. To avoid that these remaining pipe fragments affect the gas volume fraction values near the wall, a ring shaped mask is used which is slightly broader than the pipe wall. The ring position and width is adjusted individually for each measurement.

The local and temporal gas volume fraction can be determined by a pixel wise calculation of the quotient according to equation (3.15). These gas volume fraction values are scaled to the relative gas fraction values (0% for liquid and 100% for gas), independent from pressure and temperature conditions.

This procedure is done for all sinograms of each measurement. The cross-sectional size of the reconstructed image is chosen to 108x108 pixels (0.5 mm per pixel). The stack of all reconstructed frames per measurement is saved in a binary file with extension '*.rtv' (X-ray tomography void file) as signed 16 bit integer values.

3.2.2 Image centering

As aforementioned, the reconstructed images of the unknown gas-liquid flow as well as the reference images must have the same centered position. To do this, an image K is defined which contains a centered ring reflecting accurately the titanium pipe size. This ring is cross-correlated with the reconstructed, non-centered image R (such may be the images U, E or F from the section before) which usually are not centered:

$$\psi_{xy}(x', y') = R * K = \int R(x, y) \cdot K(x + x', y + y')dxdy \tag{3.7}$$

Here x and y are spatial coordinates. The maximum value at $(\hat{x}, \hat{y})$ of the two-dimensional function ψ_{xy} is usually not in the image center (x_0, y_0) as shown in Figure 3.7.

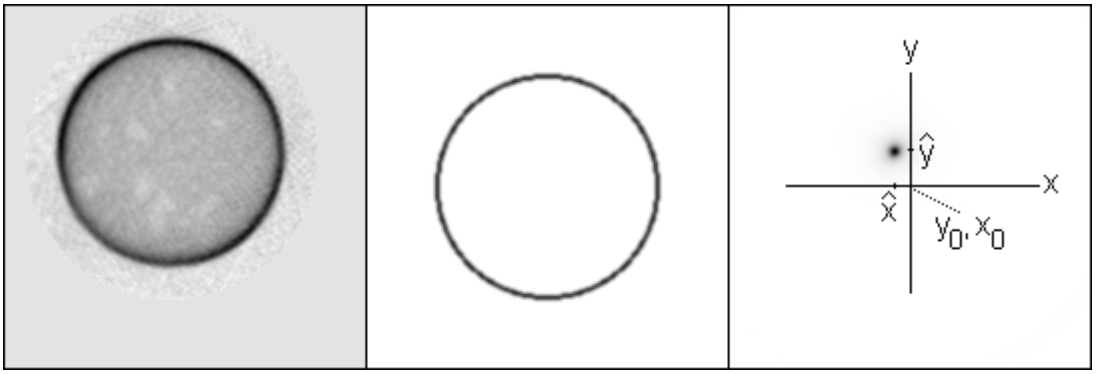

Figure 3.7: Reconstructed, non-centered image R (left), ring image K (center), cross-correlation function ψ_{xy} (right)

The deviation $(\hat{x} - x_0, \hat{y} - y_0)$ specifies the displacement of the titanium pipe in R from the image center. This makes possible to shift the pipe in image R into the center:

$$R' = R(x - \hat{x}, y - \hat{y}) \tag{3.8}$$

Since a pixel wise displacement would be too rough, the shifting is done using a linear interpolation.

3.2.3 Noise reduction filter

The separation of single bubbles can be hindered seriously by the noise of the reconstructed tomography data. Therefore, very small bubbles are difficult to be distinguished from noisy artefacts. A filtering within single images would not meaningful for noise suppression because the noise is rather coarsely and bubbles would hardly to be separable from noise. The random parts between succeeding frames can be considered as statistical independent. Therefore, the high-frequency spectra parts can be suppressed without the risk to loose bubble signals.

For the definition of a filter it is assumed that bubbles spread over 2 frames in minimum. So it is possible to limit the spectra to the range lower than half of the Nyquist frequency (which is equal to a quarter from the sampling frequency). This corresponds to a weak low-pass filter. To avoid overshoots (Gibbs phenomenon) a filtering function with smoothed edges is advantageously. So the edges are defined as sigmoid function

$$sig(t) = \frac{1}{1+e^{-t}} \tag{3.9}$$

Combining two sigmoid functions a filter characteristic is created according to Figure 3.8. The smoothing result using this filter is shown in Figure 3.9.

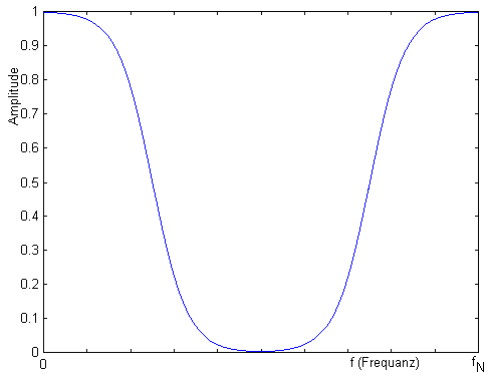

Figure 3.8: Frequency characteristics of the noise reduction filter. (f_N: sampling frequency, N: number of sampling steps)

Comparing the unfiltered image and the filtered one in Figure 3.9 it is obvious that a much more reliable segmentation of bubbles is possible after the filtering. This data processing step requires huge computationally resources but is appraised as necessary and helpful. For this reason it is applied to all data. All reconstructed data are filtered before the *.rtv-files are stored.

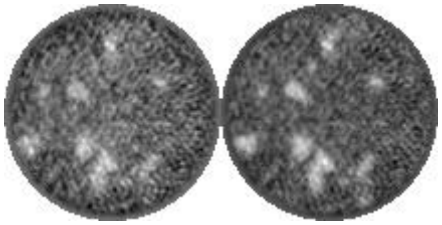

Figure 3.9: Comparison of reconstructed images, left: unfiltered, right: after filtering

3.3. Segmentation and bubble identifying

3.3.1 Working principle

For further processing, the 3D grey value arrays have to be binarized. The basic idea is to agglomerate pixels to a bubble by beginning at grey values which are local maxima. So, no bubble cores have to be defined as marker before. The flow chart of this algorithm is shown in Figure 3.10.

First the noisy data set is smoothed using an average box filter with a size of [5, 5, 5]. A new 3D matrix with the same dimensions as the matrix containing the grey values (108 * 108 * 25.000) is initialized. It is used to store the bubble numbers assigned to each pixel which belongs to an identified bubble. The assignment of the pixels to bubbles is done stepwise considering a defined range of grey values only. The maximum grey value gmax,i of all not yet assigned pixels is determined and all pixels of the data set array H with grey values g in the range 0.95 * gmax,i < g are selected for the present assignment step. The indices of these pixels are stored in a field of “pixels to assign”. Priority has the agglomeration of these selected pixels to an existing bubble by checking the neighborhood of each selected pixel. For this check, a 3D connectivity considering 6 neighbors is chosen, since the consideration of 26 neighbors did not improve the algorithm. If a pixel from the selection range g is bordered to a bubble (i.e. to a pixel to which a bubble number has already been assigned), this pixel will be assigned to this bubble. To do that the bubble number of this neighboring pixel will be written into the array of bubble numbers B. Pixels with more than one bordered bubbles are assigned to the bubble with the most connections. This is done for all pixels selected for this step. The pixels which could be assigned to an existing bubble during this step are removed from the field of “pixels to assign”. Since possibly the new assigned pixels may allow the assignment of neighboring pixels in the selection range, this agglomeration step is repeated until selected pixels are no longer allocable.

The second step is the creation of new bubbles. Starting from one of the remaining pixels in the above mentioned field of “pixels to assign” a connected region of pixels with grey values between the maximum value of this step gmax,i and 90% of the previously defined lower limit for this step (which is 95% of the maximum as described above, i.e. gmin,new bubble,i = gmax,i * 0.95 * 0.9) is determined. A new bubble is only created if there is no overlap of such a region with already existing bubbles, i.e. with pixels which are already assigned to a bubble. If there is no overlap of the connected region with an existing bubble, all these pixels will be marked as a new bubble. To do this all pixels of this connected region will be assigned to a new number. If there is an overlap with already assigned pixels no new bubble is generated. The pixels remain marked as unassigned. This step is repeated until no new bubbles can be generated from the remaining pixels. The remaining pixels are considered in the next assignment step. However for the determination of gmax,i+1 their grey values remain disregarded.
The assignment steps go down to an abort criterion. This abort criterion depends on the signal-noise-ratio of each single measurement array. Assigning of pixels with values below the abort criterion isn’t meaningful, because in this range the influence of noise effects exceeds the signal obtained from bubbles. The bubble regions determined by this procedure are in general larger than the real bubble size since the gas-liquid interface is located at least for large bubbles at higher grey values than the abort criterion for the data set. Hence, an individual threshold k(gmax, f) per bubble

depending on the bubble maximum value is applied. The determination of the individual threshold k is described in section 3.3.2. Pixels less than this threshold are removed from this bubble region and are set to zero (i.e. assigned to liquid phase). In the result the algorithm provides a segmentation of the 3D array into liquid regions and individual bubbles marked by a number. This segmentation is used by further algorithms to extract quantitative data like radial gas profiles, velocity profiles and bubble size distributions.

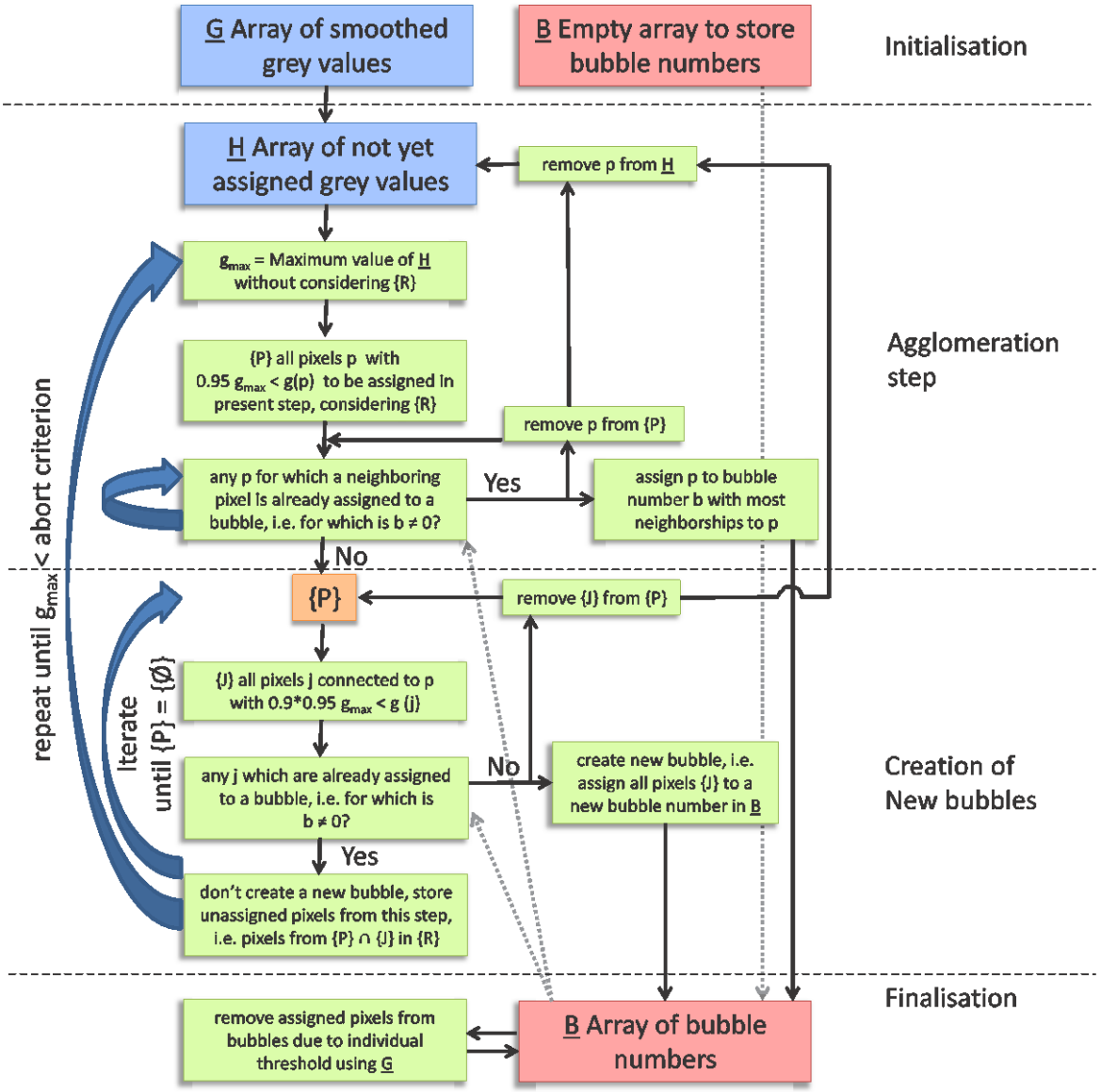

Figure 3.10: Flow chart of the new segmentation algorithm

General, the abort criterion should be the grey value, at which the ratio of gas signal to noisy water signal amounts one. This value depends on different conditions: The global gas volume fraction of the flow regime, the chosen frequency depending on the gas velocity as well as all noise effects mentioned above. The asymmetrical shape of the water peak in the histograms can be used to estimate an abort criterion. Asymmetrical shape means that the left peak side conforms to Gaussian distribution (noise distribution) and the right peak side is a superposition of the Gaussian distribution and gas signal values. As visible in Figure 3.11 there is in general also a shift of the peak, i.e. it is not centered exactly at zero. This is also true for a second

example given in Figure 3.11, where the dotted line shows the right side of the water peak taken from the histogram. Therefore, first the peak position is estimated after smoothing. For the example case the maximum of the smoothed water peak p is located at -2.5. Second, the left side is subtracted from the right side resulting in the solid line in Figure 3.11. Finally, this curve is scaled to the right side of the peak (dotted line in Figure 3.11). This leads to the S-shaped dashed line. This curve is fitted as a sigmoid function according to

$$y = \frac{1}{b^{i-x} + 1} \tag{3.10}$$

While the parameter b determines the incline of the curve, i corresponds the inflection point of the sigmoid function which is equal to the function value amounting 0.5. At the grey value equal i, the number of gas signal pixels and noise pixels of the water peak is identical. Therefore the sigmoid function parameter i provide a suitable abort criterion as described above. This procedure is used for all measurement arrays to estimate their individual abort criterion.

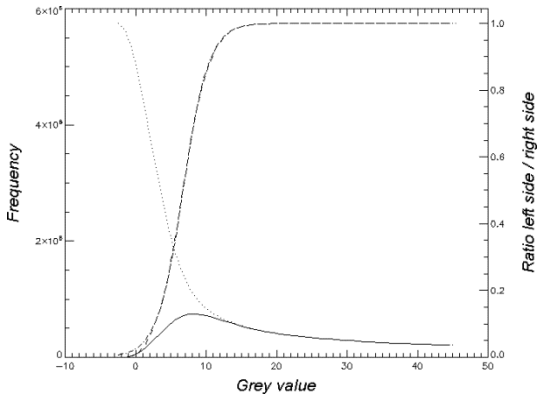

Figure 3.11: Exemplary result for estimating the sigmoid function. Dotted line – right side of water peak, solid line – difference between right and left side of water peak, dashed line – ratio of difference to right side, dash dot line – fitted sigmoid function

Sometimes it is impossible to fit a sigmoid function with plausible inflection point i. For such cases it is necessary to use all the experimental data with different flow regimes and different gas volume fractions for estimating the sigmoid function parameters. These parameters should be applied as functions or constant values in case of non-plausible sigmoid function parameters. The example in Figure 3.11 is for a two-phase flow regime with an expected gas volume fraction of about 12%. The basis b has the value 1.7319 and the inflection point i is located at 6.72. For this example, the abort criterion amounts 7 (there are only integer values in G).

Now, all pertinent pixels are assigned to bubble regions. Due the fact, that there are few bubble regions which have a maximum grey value less a sigmoid value 1, there are doubts, that these regions are real bubbles and no agglomerated noisy pixels. Therefore, all bubble regions are set to water phase again, which have a maximum grey value less than position where the sigmoid function is equal 0.95. Further information are presented by Banowski et al. (2015).

3.3.2 Qualification and validation

Since the agglomeration process in general leads to too large bubble regions, some pixel in the region of a bubble interface have to be reset to water region. An individual bubble threshold is estimated accordingly. To determine such an individual bubble threshold function, two bubble structured phantoms are used. These phantoms each consist of a stack of 301 milled plastic slides with a diameter of 54 mm and a height of 0.5 mm. The titanium pipe wall is simulated by a 0.5 mm steel wall. One phantom simulates a two-phase flow with a low gas volume fraction, the other one simulates a two-phase flow with a medium gas volume fraction. These phantoms were scanned with ROFEX at different frequencies as well as with a volumetric µCT to get a reference data set. In Figure 3.12, photos, a milling template for an exemplary plastic slide as well as the µCT result of the same plastic slide of the phantom 1 are shown. The µCT measurement is done with a spatial resolution of 68 µm and a measurement time of about 20 min. So, the interfacial contrast of this µCT measurement is high enough, that the transition from the milled whole (“gas phase”) to the plastic (“liquid phase”) has a width of only one pixel.

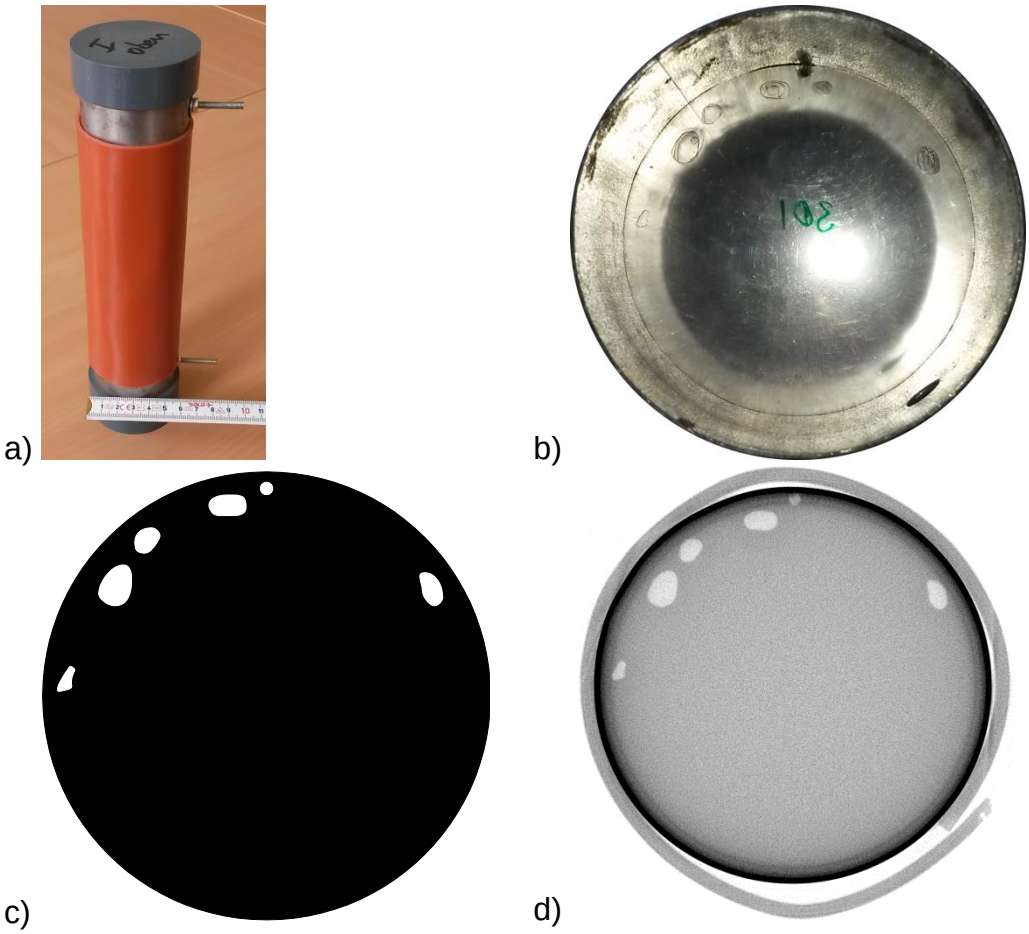

Figure 3.12: Phantom 1. a) photo of the whole phantom including the steel wall, b) inside photo with a view on the last plastic slide of the stack, c) milling template of this plastic slide, d) cross-sectional µCT image of this plastic slide

Therefore, the segmentation of this data set is done using a threshold value; spaced wholes are separated completely due the high contrast and resolution. The

discretisation error of the bubble volume V using the sphere equivalent bubble diameter

$$d_{eq} = \sqrt[3]{\frac{6}{\pi} \cdot V} \tag{3.11}$$

accords to the propagation of uncertainty:

$$\frac{\Delta V}{V} = \left|\frac{dV}{dd_{eq}}\right| \cdot \frac{\Delta d_{eq}}{V} = \frac{3 \cdot \Delta d_{eq}}{d_{eq}} \tag{3.12}$$

As maximum deviation the double resolution is chosen as uncertainty of the sphere equivalent bubble diameters d_{eq}. The maximum discretization error of the bubble volume V is shown in Figure 3.13. Therefore the maximum uncertainty for bubble diameters greater than d_{eq} = 2 mm is less than 20%; for $d_{eq} \geq$ 4 mm less than 10% as well as for $d_{eq} \geq$ 8 mm less than 5%.

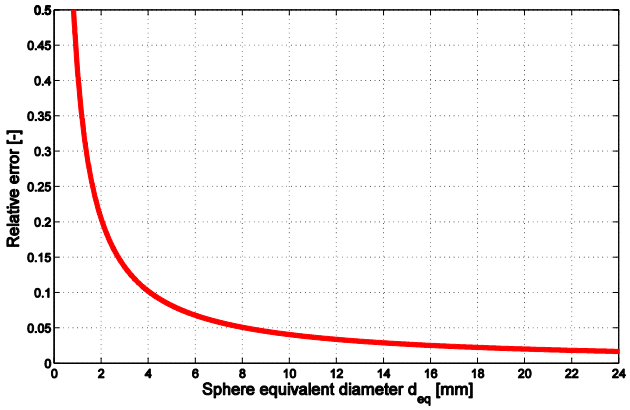

Figure 3.13: Maximum uncertainty of the µCT sphere equivalent bubble diameter

Parameter studies were done for both ROFEX phantom data sets (both planes and 3 different frequencies for each plane: 1000Hz / 2000Hz / 2500Hz) to compare bubble size distributions and global gas volume fractions. In the result functions for the individual threshold depending on the maximum bubble grey value within the bubble were determined separately for each measuring frequency. The individual bubble threshold is obtained by multiplying the maximal grey value gmax of the bubble by the value from this function. All functions have a decreasing linear part and a constant part. The constant part has a value about 0.36 – 0.40 for all measurement frequencies. Only the decreasing linear parts have different parameters. This is caused by the increasing noise effects at increasing measurement frequencies. The general function accords to

$$k_i(g_{max,i}, f) = \max\left(-m(f) \cdot g_{max,i} + n(f), c(f)\right) \tag{3.13}$$

The corresponding values for m, n and c are given in Table 3.1. In Figure 3.14 the individual threshold functions for 3 chosen frequencies are plotted.

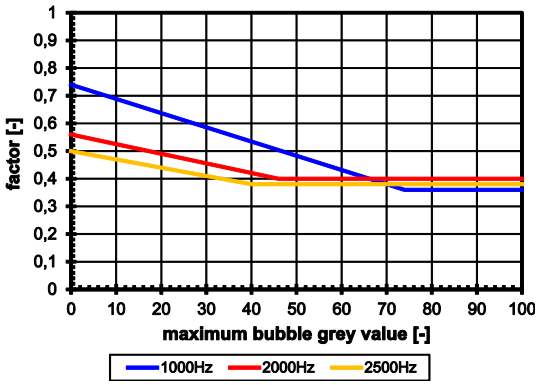

Figure 3.14: Individual bubble threshold function k(g_{max}, f)

Table 3.1: Corresponding values for m, n and c used in equation (3.13) and plotted in Figure 3.14

Frequency *f*	*m*	*n*	*c*
2x1000Hz	0.005135	0.74	0.36
2x2000Hz	0.003478	0.56	0.4
2x2500Hz	0.003	0.5	0.38

In Figure 3.15 the resulting bubble size distributions of the ROFEX phantom measurements are plotted for frequencies f = 1000Hz, 2000Hz and 2500Hz for the upper plane together with the µCT reference distribution. In all cases, a reasonable agreement is obtained. At the bubble size distribution of phantom 2, there are two bubbles with a sphere equivalent diameter of about 20 mm in the µCT. The larger bubble contains many spaced bubbles, which are joined together by the milling process of the phantom slides. For this reason they are evaluated as one bubble in the µCT measurement, while they are separated to some extent again in the ROFEX measurement. This results from the capability of the algorithm to disconnect also bubbles separated by a thin liquid film.

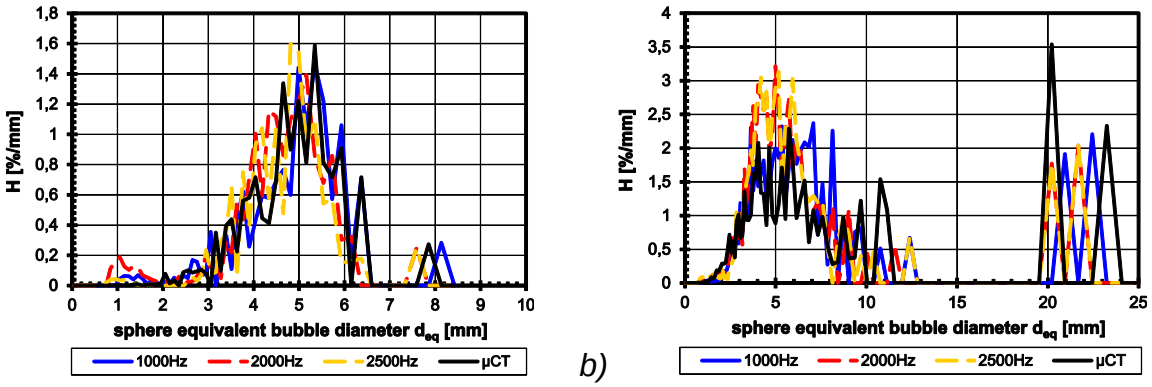

Figure 3.15: Bubble size distributions of both ROFEX phantom data sets at different frequencies compared with µCT. a) Phantom 1, b) Phantom 2

In Figure 3.16 different cross sectional views of both phantoms with different frequencies are shown. On the left side, the ROFEX raw data is plotted, in the middle the segmentation result of the algorithm is shown and on the right side the downscaled µCT is presented for comparison. In general, all cross sectional images of the binary results agree very well to the ROFEX data and the µCT results. The

different colors of the bubbles show separate detected bubbles. The colors are chosen randomly for each result and aren't comparable among themselves. The shapes and the size of the cut bubbles are in agreement with µCT cross sectional views and ROFEX raw data. In part (d) there are two examples of subsequent separation of joined bubbles by milling process (The green one in the µCT and the blue and green one in the binary result).

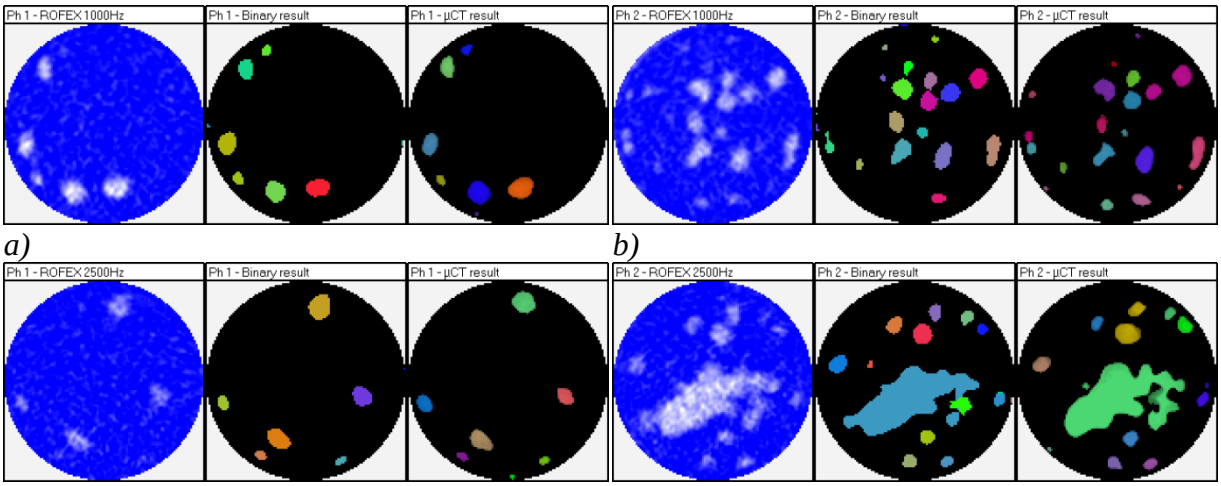

Figure 3.16: Cross sectional views to phantom data: (left) ROFEX raw data, (middle) binary result, (right) µCT result; a) Phantom 1 – 1000Hz, b) Phantom 2 – 1000Hz, c) Phantom 1 – 2500Hz, d) Phantom 2 – 2500Hz

3.4. Revising the reconstructed data

Results of the gas volume fraction (section 3.5) make it possible to check the results of reconstruction and segmentation. With the assumption, that the gas distribution in the pipe is symmetrical, the time averaged local gas fractions of the pipe cross-section (*.epsxy) have to display such a symmetrical distribution. In some cases, there are spots with an increased local gas volume fraction. The reason is mostly a local increased liquid peak level of the grey values. These distortions take grey values higher the abort criterion of segmentation but less than bubble grey values. Therefore, these spots are identified as bubbles by the segmentation algorithm. To reduce these errors, the grey value distribution has to be rescaled locally.

First, the pipe cross section is classified into 10 ring shaped domains. For each domain, their average gas fraction value is estimated from the *.epsxy-file. To reduce boundary effects on crossing between two annuli, the averaged values of neighboring domains is considered too. Each cross sectional point is masked, where the conditions

$$\varepsilon_{epsxy}(x,y) > 1.1 \cdot \bar{\varepsilon}_{epsxy,ring} \quad \cup \quad \varepsilon_{epsxy}(x,y) > \bar{\varepsilon}_{epsxy,ring} + 5\% \tag{3.14}$$

are complied. The second condition guarantees that small fluctuations in the epsxy-file of small gas volume fraction flow regimes aren't masked. An example for the steps of the revision process is shown in Figure 3.17. The spots of increased local

gas volume fractions after segmentation are also discernible as spot in the reconstruction raw data. These regions are masked.

For all unmasked cross sectional pixels the global grey value histogram is estimated. Additionally the position of the water peak p_w, global is ascertained using a Gaussian distribution approximation.

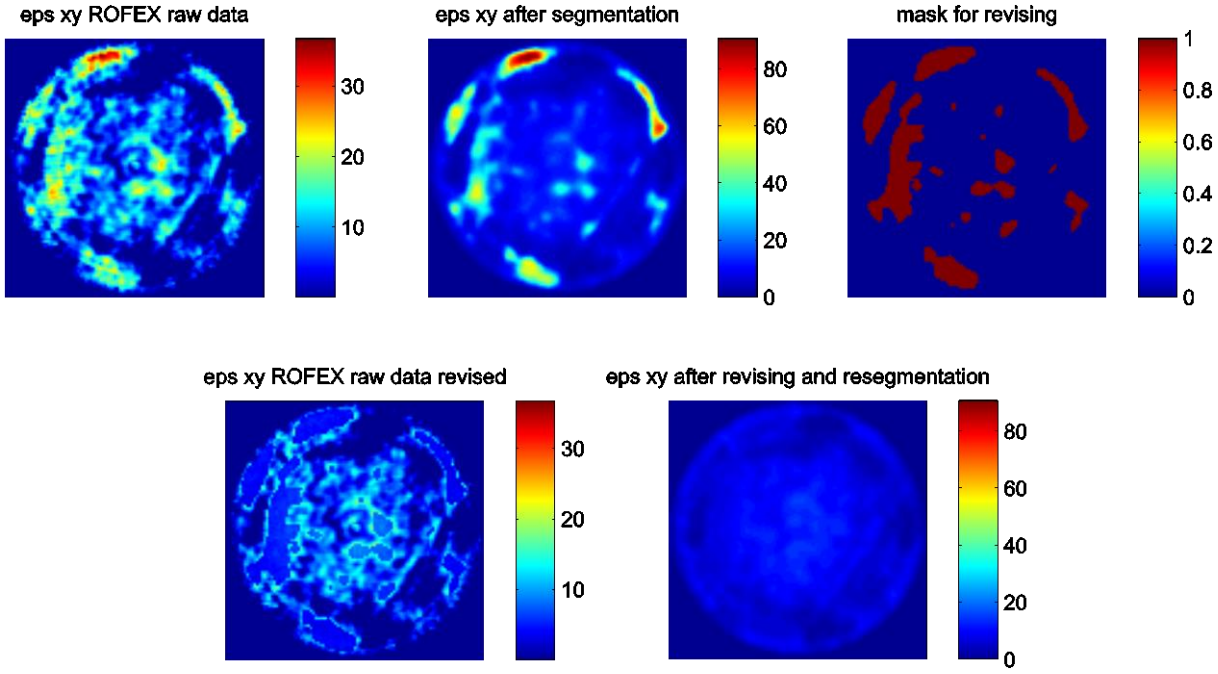

Figure 3.17: Intermediate steps of revising raw data. Upper line, left to right: time averaged reconstruction result, epsxy-file after segmentation, masked pixels. Lower line, left to right: time averaged revised reconstruction result, epsxy-file after revising and re-segmentation

For every cross sectional point, its grey value distribution is created. The cross sectional water peak position $p_w(x,y)$ is ascertained using a Gaussian distribution approximation. With the knowledge of both water peak positions, the vector of each cross sectional point (x,y) against the time is rescaled with

$$\varepsilon_{x,y,rescaled}(t) = m \cdot \varepsilon_{x,y}(t) + n, \quad with \quad m = \frac{100 - p_{w,global}}{100 - p_w(x,y)}, \qquad n = 100 - 100 \cdot m \tag{3.15}$$

to its conditions of each reconstruction array. Using equation (3.15), only the position of the local water peak is rescaled. The assumed gas peak position is remained at 100%, because the gas peak position can't be estimated satisfying every time due less gas fraction values. The result is shown in the lower line Figure 3.17. At the positions of the spots from the upper line, the time-averaged values are less. The results of the re-segmentation show a better symmetrical gas fraction distribution. In the presented example, the global gas fraction is reduced due rescaling from 12.2%

to 7.3%. The expected gas fraction value amounts 7.5%, estimated by drift flux model considering the hydrostatic pressure.

This method gives the possibility to reverse the completely reconstructed measurement array. After revising the reconstruction data, the evaluation processing can be restarted with segmentation and following estimation of quantitative data.

3.5. Gas volume fraction

After segmentation, the data present the local instantaneous volumetric void fraction $\varepsilon_{i,j,k}$ (i, j are the indices of the grid points in the measurement plane and k is the number of the frame). In order to obtain quantitative information on the flow, a time averaging of the void fraction data can be used (Prasser et al., 2002). In contrast to the wire mesh sensor, no weight coefficients are used for cross-sectional averaging because as result from the reconstruction, only pixels with their full area in the cross-sectional frame are available. In total 9216 Pixels $N_{cross\text{-}section}$ lie inside the open pipe cross section.

$$\bar{\varepsilon}_k = \varepsilon(t) = \frac{1}{N_{cross-section}} \sum_i \sum_j \varepsilon_{i,j,k} \tag{3.16}$$

The result of the data evaluation with equation (3.) is a sequence of instantaneous average volumetric gas fractions, which is available with the full measurement frequency. These values are stored in a separate file.

Another option is the averaging in time. Two-dimensional void fraction distributions are provided by the following equation:

$$\bar{\varepsilon}_{i,j} = \frac{1}{k_{\max}} \sum_{k=1}^{k_{\max}} \varepsilon_{i,j,k} \tag{3.17}$$

With equations (3.) and (3.) an average void fraction for the total measurement cross-section can be obtained as follows:

$$\bar{\varepsilon} = \frac{1}{N_{cross-section}} \sum_i \sum_j \bar{\varepsilon}_{i,j} = \frac{1}{k_{\max}} \sum_{k=1}^{k_{\max}} \bar{\varepsilon}_k \tag{3.18}$$

Moreover, a radial gas fraction profile can be calculated by averaging the local instantaneous gas fractions over the measurement period of 10 s and over a number of ring-shaped domains. The latter is done by the following equation:

$$\bar{\varepsilon}_m = \frac{1}{k_{\max}} \sum_k \sum_i \sum_j a_{i,j,m} \cdot \varepsilon_{i,j,k} \tag{3.19}$$

where $a_{i,j,m}$ are weight coefficients denoting the contribution of each pixel with the indexes i,j to a ring with the number m (Figure 3.18).

$$(m-1)\cdot\frac{R_{sensor}}{m_{\max}} \le r \le m\cdot\frac{R_{sensor}}{m_{\max}} \qquad (3.20)$$

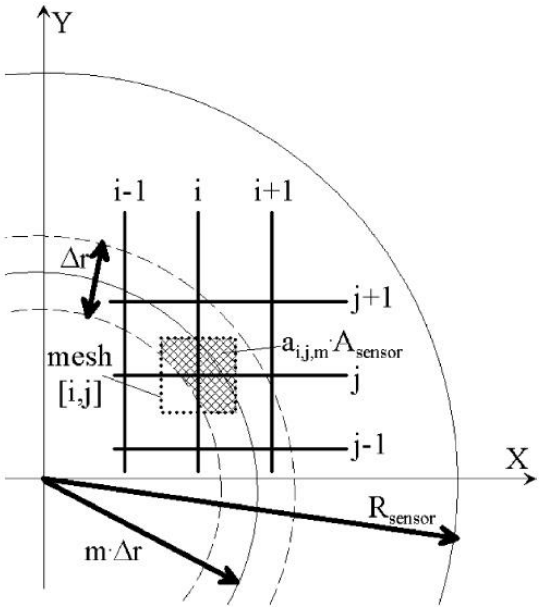

Figure 3.18: Weight coefficients for the cross-section averaging of local gas fractions over a number of ring-shape domains

This ring-shaped averaging domain covers a given radial distance from the centre of the pipe, where mmax is the total number of radial steps, in the case of the present experiments mmax was set to 20.

Additionally, gas fraction profiles can be obtained considering a limited range of the bubble sizes (volume fraction profiles, decomposed according to the bubble size, see Prasser et al. 2002 and section 3.8). This requires a bubble identification and bubble size determination, which will be described in the following chapter.

Thus, azimuthally and time averaged gas volume fraction profiles (*.epsrad_20), as well as the time averaged local gas fractions for each measurement point of the pipe cross-section (*.epsxy) are available. Furthermore, the time and space averaged gas volume fractions (eps_all.asc) according to equation (3.18) can be used to check dependencies on flow rates, the evolution of the flow along the pipe and others.

3.6. Bubble identification and properties

As a result from the bubble segmentation, all connected pixel regions detected as bubbles, are labelled. To each element which belongs to one bubble, the same identification number is assigned. Different bubbles receive different identification numbers. These numbers are stored in the elements $b_{i,j,k}$ of a second array. This array has the same dimension as the void fraction array (compare to section 3.3). Together with the information about the gas fraction, now important parameters can be determined for each bubble. It has to be noted that in the code the index k refers to the serial number of the frames, while i and j, in this case, serve as indices in the

measurement plane. This assignment of the indices is also used in the equations given in this section.

The volume of a bubble with the number n is obtained by multiplying the number of pixel belonging to the bubble N_n with the pixel size in the horizontal plane and the vertical dimension of a pixel which can be obtained from the bubble velocity:

$$V_n = \Delta x \Delta y \Delta t \cdot w_n \cdot N_n \quad , \qquad \forall [i,j,k] : b_{i,j,k} = n \tag{3.21}$$

with the pixel size and the time between two measured cross-section images:

$$\Delta x = \Delta y = 0.5\ mm \text{ and } \Delta t = \frac{1}{f_{meas}} \tag{3.22}$$

The velocity can be taken from both velocity estimation methods: Cross-correlation as well as bubble pair finding. In the case of using the cross-correlation method, the individual bubble velocity is taken as an approximation at the location of the center of mass $x_{CM,n}$ and $y_{CM,n}$ of the given bubble:

$$w_n = w_G(r_n) \text{ with } r_n = \sqrt{\left(x_{CM,n} - x_0\right)^2 + \left(y_{CM,n} - y_0\right)^2} \tag{3.23}$$

By using the individual velocity obtained by the bubble pair finding algorithm, the individual volume can be estimated without approximation.

The coordinates of the center of mass can be obtained by averaging the measurement coordinates of all elements belonging to the selected bubble:

$$x_{CM,n} = \frac{\sum_i i \cdot \Delta x}{N_n}; \quad y_{CM,n} = \frac{\sum_j j \cdot \Delta y}{N_n}; \quad z_{CM,n} = \frac{\sum_k k \cdot \Delta t}{N_n}; \qquad \forall [i,j,k] : b_{i,j,k} = n \tag{3.24}$$

After that, the equivalent diameter of the bubble can be determined, which is defined as the diameter of a sphere that has the volume according to equation (3.21):

$$D_{b,n} = \sqrt[3]{\frac{6V_n}{\pi}} \tag{3.25}$$

For the evaluation of asymmetries of the bubble, moments for each bubble are determined. Likewise, the void fraction served as weight function:

$$rm_{x,n} = \sqrt{\frac{5 \cdot \sum_i \left(i \cdot \Delta x - x_{CM,n}\right)^2}{N_n}}; \quad rm_{y,n} = \sqrt{\frac{5 \cdot \sum_j \left(j \cdot \Delta y - y_{CM,n}\right)^2}{N_n}}$$
$$rm_{z,n} = \sqrt{\frac{5 \cdot \sum_k \left(k \cdot \Delta' t - z_{CM,n}\right)^2}{N_n}}; \quad \forall [i,j,k] : b_{i,j,k} = n \tag{3.26}$$

From the moments for the coordinates x and y in the measurement plane of the tomography, the radial moment results:

$$rm_{xy,n} = \sqrt{rm_{x,n}^2 + rm_{y,n}^2} \tag{3.27}$$

Further information on the distortion of the bubble can be obtained by calculating the maximum equivalent diameter in the x-y plane. For this matter, the area being occupied by the bubble in the x-y plane is added. Similar to equation (3.21), the sum of the number of pixels of the measurement volumes belonging to the bubble is multiplied by cross-sectional resolution. This procedure is done for each single sampling time characterized by index k:

$$A_{xy,n,k} = \Delta x \Delta y \sum_{i,j} N_{n,i,j,k} \quad \forall [i,j,k] : b_{i,j,k} = n \tag{3.28}$$

The maximum area is found and converted into the diameter of an area equivalent circle:

$$D_{xy,n,\max} = \sqrt{\frac{4A_{xy,n,\max}}{\pi}} \quad mit \quad A_{xy,n,\max} = \max\left(A_{xy,n,k}\right) \tag{3.29}$$

In addition to these bubble characteristics, the minimum and maximum coordinates $x_{front,n}$, $y_{front,n}$, $z_{front,n}$ as well as $x_{back,n}$, $y_{back,n}$, $z_{back,n}$ of the bubbles are determined. Another important parameter for the characterization of gas bubbles is the volume fraction of the bubble related to the total volume of the flow:

$$\varepsilon_n = \frac{N_n}{N_{ges}}; \quad N_{ges} = t_{meas} \cdot f_{meas} \cdot \sum_j \sum_k a_{j,k} \tag{3.30}$$

The parameter $a_{j,k}$ will be set to 1, if the cross-sectional pixel position is inside the measurement range.

Apart from the already mentioned parameters, the maximum gas fraction and the number of measurement volumes per bubble are determined. All values are stored in an ASCII file (*.a) as table for each identified bubble n.

3.7. Velocity estimation

The use of a dual-layer tomography allows the determination of the bubble velocities. In analogy to the wire-mesh sensor technique the cross-correlation method is used. In addition a method for bubble pair finding between both tomography layers was deveopled. In the case of counter-current flows, morphological bubble properties are used as third velocity estimation method.

3.7.1 Cross-correlation method

To determine time averaged gas velocities, the signals from both measurement planes are cross-correlated separately for each pair of cross-sectional pixels, which have the same indices. For time-discrete series of this fluctuation components of the

local instantaneous void fraction from the first measurement plane ($\varepsilon'_{1,i,j,k}$) and the second plane ($\varepsilon'_{2,i,j,k}$), the cross-correlation can be defined as follows:

$$F_{i,j,\Delta k} = \frac{\sum_k \varepsilon'_{1,i,j,k} \cdot \varepsilon'_{2,i,j,k+\Delta k}}{\sqrt{\sum_k \varepsilon'^2_{1,i,j,k}} \cdot \sqrt{\sum_k \varepsilon'^2_{2,i,j,k}}} \tag{3.31}$$

The index Δk corresponds to the time-shift of $\Delta t = \Delta k / f_{meas}$. Fluctuation components were calculated by subtracting the time-average from the instantaneous value: $\varepsilon'_{i,j,k} = \varepsilon_{i,j,k} - \bar{\varepsilon}_{i,j}$. The cross-correlation was carried out by means of Fast Fourier Transformation (FFT). The obtained cross-correlation functions were averaged in circumferential direction for different radii (m) using the same weight coefficients as for the calculation of radial gas fraction profiles:

$$F_{m,\Delta k} = \frac{1}{k_{\max}} \sum_i \sum_j a_{i,j,m} \cdot F_{i,j,\Delta k} \tag{3.32}$$

In the next step, the location of the maximum in the cross-correlation functions averaged by equation (3.32) was found. The average gas-phase velocity for the given radius is calculated from the corresponding time-shift:

$$w_G(r) = w_G(m) = \frac{\Delta L}{\Delta k_{\max}} \cdot f_{meas}, \tag{3.33}$$

with Δk_{max} corresponding to $F_{m,\Delta k max} = \max(F_{m,\Delta k})$.

In equation (3.33) ΔL = 10.2 mm is the axial distance between the two planes of tomography. The technique of averaging the cross-correlation functions before searching for the maximum has proven to supply more stable velocity values, than the velocities directly deduced from the result of a point-to-point cross-correlation according to equation (3.31), which suffers from a high scattering of the results.

For the documentation of the evaluation process, the results of the point-to-point cross-correlation are stored as time averaged cross-sectional velocity matrix in a ASCII file (*.velxy). The azimuthally averaged gas velocities and the centre radii of the 20 rings are stored in the ASCII files *.vel. Graphs showing the radial profiles of the gas velocities can be found in Appendix 9.1.

3.7.2 Bubble pair finding

In order to calculate individual bubble velocities a new method was developed. It is based on the assumption that a bubble detected at the upstream measurement plane, should be also be detected at the downstream measurement plane. Even though bubble coalescences or breakup may occur between both measurement planes, the probability to have the same bubble detected in both planes is quite high since the distance between both measurement planes is short (10.2 mm). By finding the identical bubble on both measurement planes, the bubble traveling time and bubble lateral movement which are needed for velocity calculation are obtained. According to its working principle this method is called „bubble pair method“. Even

though the idea sounds quite simple, it will be tricky to estimate correct bubble pairs from both measurement planes, in cases with dense flows where a large number of gas bubbles is present. Bubble parameters like bubble size, lateral position and a range for the expected bubble velocity are used for pairing. The algorithm is processing a size sorted bubble lists b_1 (upstream plane) and b_2 (downstream plane) starting at the largest bubble. The number of large bubbles is less than small bubbles and thus it is easier to find bubble pairs for large bubbles. Also, large Taylor-like bubbles cause a strong distortion of the local liquid flow field, which has to be considered for the expected velocity range for smaller bubbles.

For all possible bubble combinations a probability is calculated for being the same bubble, as presented in equation (3.34). It bases on the bubble volume $\varphi_{\mathrm{volume}}$, the cross sectional position $\varphi_{\mathrm{position}}$ and resulting velocity $\varphi_{\mathrm{velocity}}$. The bubble pair with the highest total probability value Φ is chosen as correct bubble pair.

$$\boldsymbol{\Phi(b_1, b_2) = \varphi_{volume}(b_1, b_2) \circ \varphi_{position}(b_1, b_2) \circ \varphi_{velocity}(b_1, b_2)} \tag{3.34}$$

Bubble volume Probability

The bubble pair with the most similar volume has to get the highest probability value. Since the real bubble volume depends on the still to determine bubble velocity, the used bubble volume is calculated using the individual axial velocity for each possible bubble pair. To estimate a probability value, the Gaussian distribution is used:

$$\boldsymbol{\varphi_{volume}^{1\to2}(b_1, b_2) = e^{-0.5\left(\frac{V(b_2)-V(b_1)}{\sigma_{volume}(b_1)}\right)^2}}$$
$$\boldsymbol{\sigma_{volume}(b_1) = \begin{cases} V(d(b_1) + 0.5mm) - V(b_1), & d(b_1) < 5mm \\ V\left(1.1 \cdot d(b_1)\right) - V(b_1), & d(b_1) \geq 5mm \end{cases}} \tag{3.35}$$

For the standard deviation sigma in general a tolerance range of 10% for the sphere equivalent diameter is chosen. In addition it is assumed that the uncertainty of bubble diameter is at least one pixel, i.e. 0.5 mm. Sigma in equation (3.35) depends only on the size of the bubble b1. In order to obtain symmetry, the volume probability value $\varphi_{\mathrm{volume}}^{2\to1}(\mathrm{b}_1, \mathrm{b}_2)$ has to be estimated using $\sigma_{\mathrm{volume}}(\mathrm{b}_2)$. As volume probability value for equation (3.34) the product of both partial probability values is used.

Bubble lateral position probability

The bubble lateral position probability is estimated also by using the Gaussian distribution as shown in equation (3.35)). Larger differences of bubble positions in lower and upper measuring plane make it less probably that it is the same bubble. Random lateral bubble migration caused by turbulence, bubble oscillations as well as directed migration caused by bubble forces are possible in general. However, as larger the bubble velocity is, as lower gets the possible distance for horizontal bubble moving because of the short passing time across measurement planes and vice versa. Therefore, sigma for the position probability is indirect proportional to the vertical velocity of the bubble pair $(\mathrm{b}_1, \mathrm{b}_2)$.

$$\varphi_{\text{position}}(b_1, b_2) = e^{-0.5\left(\frac{\Delta_{position}(b_1,b_2)}{\sigma_{position}(b_1,b_2)}\right)^2}$$

$$\Delta_{\text{position}}(b_1, b_2) = \sqrt{\left(X(b_2) - X(b_1)\right)^2 + \left(Y(b_2) - Y(b_1)\right)^2} \tag{3.36}$$

$$\sigma_{\text{position}}(b_1, b_2) = \frac{2.5\frac{mm^2}{ms}}{\text{u}_{\text{axial}}(b_1, b_2)}$$

The value of the sigma parameter in equation (3.36) is chosen with 2.5 mm2/ms for bubbly flow.

Bubble Velocity Probability

The bubble pair finding process uses searching a window for the shift of the bubble in the stack of time slices which corresponds to a range of velocities. On the one hand it helps to exclude the consideration of unphysical bubble velocities by the use of a priory knowledge. On the other hand a manipulation of the velocity result due the searching window has to be avoided. According to this fact, the Gaussian distribution is not useful to calculate a velocity probability value and a flat roof shaped function is applied instead. This function is plotted in Figure 3.19.

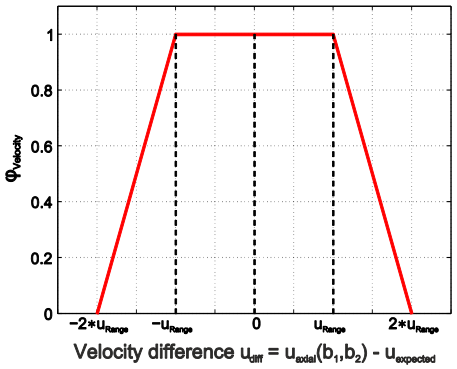

Figure 3.19: Velocity probability function

To estimate the velocity probability value $\varphi_{velocity}(b_1, b_2)$ the difference of the axial bubble pair velocity $\text{u}_{\text{axial}}(b_1, b_2)$ and an expected velocity value for this bubble pair is used.

$$\boldsymbol{u_{diff}(b_1, b_2) = u_{axial}(b_1, b_2) - u_{expected}(b_1)} \tag{3.37}$$

The calculation of the expected velocities depends on flow regions and is described in detail below. If the velocity difference u_{diff} is in the range of $\pm\,\text{u}_{\text{Range}}$, the velocity probability value $\varphi_{\text{velocity}}(\text{b}_1, \text{b}_2)$ is set equal to 1. If the velocity difference is greater than the range as well as less than the doubled range, the velocity probability value is linear decreasing from 1 to 0. The range velocity is estimated by:

$$\boldsymbol{u_{Range}(b_1, b_2) = min\,(0.375 \cdot u_{expected}(b_1),\, u_{Drift})} \tag{3.38}$$

The bubble drift velocity $\mathrm{u_{Drift}}$ is calculated using Harmathy (1960). For air-water pipe flows at a temperature of 30°C and a pressure at 0.4 MPa, the drift velocity amounts about 0.25 m/s.

Because individual bubble velocities strongly depend on the local flow conditions the expected velocities are calculated in dependency on the flow pattern. It is distinguished between bubbly flow region, Taylor bubble, falling film region beside the Taylor bubble and the wake region after a Taylor bubble. Since the defining of such regions depends on the presence of Taylor bubbles, the algorithm sorts the bubbles to decreasing bubble size before processing and the Taylor bubbles can be detected.

According to the fact, that the expected bubble velocity depends only on one of both bubbles, the velocity probability value for a possible bubble pair $\varphi_{\mathrm{velocity}}(\mathrm{b_1}, \mathrm{b_2})$ is estimated for both bubbles analogue to the volume probability value.

Bubbly flow region

The bubble region is assumed in case there is no Taylor bubble detected. For the calculation of expected velocity, the liquid velocity is estimated using the power equation of turbulent flow from Beyerlein et al. (1985), Ishii et al. (2004). The bubble drift velocity is approached with theoretical prediction given by Harmathy (1960). Both equations are presented as sum in equation (3.39). The condition of turbulent flow as well as the condition of ellipsoidal bubbles is satisfied quite well for the most pipe flow cases.

$$\begin{aligned} u_{expected}(b_1) &= u_{liquid}\left(b_{1_{position}}\right) + u_{Drift} \\ &= u_{liquid,max} \cdot \left(1 - \frac{r(b_1)}{R}\right)^{\frac{1}{n}} + u_{Drift} \\ &= \frac{(n+1)(2n+1)}{2n^2} \cdot \frac{u_{liquid}}{1-\varepsilon} \cdot \left(1 - \frac{r(b_1)}{R}\right)^{\frac{1}{n}} + 1.53\left(\frac{g \cdot \Delta\rho \cdot \sigma}{\rho_{liquid}}\right)^{\frac{1}{4}} \end{aligned} \tag{3.39}$$

$$n = 2.95 \cdot Re_{liquid}^{0.0805}$$

The liquid Reynolds number is known through the injection condition of each obtained two-phase flow. The range of possible values of n is 5.6 …8.1 resulting in a total factor in front of $\mathrm{u_{avg}}$ from 1.28 down to 1.19. According the velocity range in Figure 3.19, the error by using this power law approximation is rather small.

Taylor and large Cap Bubble regions

If one or more Taylor bubbles are detected, three additional regions beside the bubbly flow region are considered: The Taylor bubble itself, the falling film as well as

the bubble wake. In this procedure, the meaning of “Taylor bubble” includes large cap bubbles, since the effects on the surrounding liquid flow like the existence of a liquid film beside the bubbly or wake vortices are similar generally. Therefore, all bubbles with a maximum detected cross-sectional circle equivalent diameter larger than 35 mm are defined as “Taylor bubble”. This parameter is chosen because the average liquid velocity of the liquid film between Taylor bubble and pipe wall is modified significantly with increasing Taylor bubble cross sectional area beginning at about this value. In the following sections, only the differences to the bubble flow cases are described.

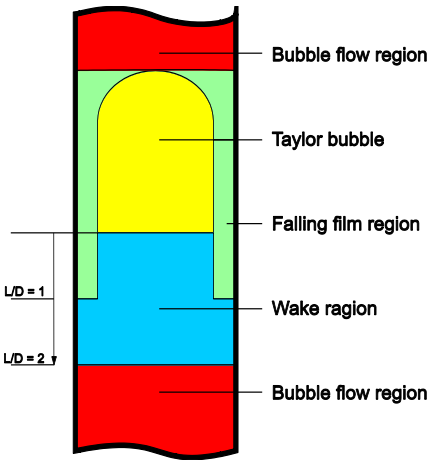

Figure 3.20: Different regions at slug flows

The expected velocity of the Taylor bubble is taken from Nicklin et al. (1962), see equation (3.40).

$$\boldsymbol{u_{expected,TB} = 1.2 \cdot j_{avg} + 0.35 \cdot \sqrt{gD}} \qquad (3.40)$$

$$\boldsymbol{j_{avg} = j_{liquid} + j_{gas}}$$

Falling Film Region

This region is the ring region between Taylor bubble and pipe wall. It reaches from the bubble nose until 1D after Taylor bubble ending. The specification of 1D after the Taylor bubble ending was taken from Kawaji et al. (1997), who found out that the falling film region decays rapidly around 1D to 1.25D after the Taylor bubble ending. For the calculation of the length of time in the stacked data, the expected Taylor bubble velocity is used. The expected liquid velocity of the falling film region results from the continuity equation, similar to Ahmad et al. (1998) and using the assumption $\mathrm{A} = \mathrm{A_{TB}} + \mathrm{A_{FF}}$:

$$u_{avg} \cdot A = u_{TB} \cdot A_{TB} + u_{FF} \cdot A_{FF}$$

$$u_{FF} = u_{avg} - (u_{TB} - u_{avg}) \frac{A_{TB}}{A_{FF}} \tag{3.41}$$

To calculate the bubble velocity in the falling film it is assumed that it is given by the liquid falling film velocity plus the drift velocity by Harmathy (1960).

$$u_{FF_{Bubble}} = u_{FF} + u_{Drift}$$
$$= u_{avg} - (u_{TB} - u_{avg}) \frac{A_{TB}}{A_{FF}} + 1.53 \left(\frac{g \cdot \Delta\rho \cdot \sigma}{\rho_{liquid}} \right)^{\frac{1}{4}} \tag{3.42}$$

Wake Region

The wake region is defined here as a region which is not assigned to the falling film region and located from Taylor bubble ending until 2D behind Taylor bubble. This value is taken from van Hout et al. (2002) and is confirmed in Liu et al. (2013). General, the wake region is approached similar to the bubble region. The equation (3.39) is also used for calculation of the expected velocity. However in order to resolve the problem of high dynamics in bubble coalescence and break up, sigma volume parameter shown in equation (3.35) is multiplied by two. All possible regions of slug flow are illustrated in Figure 3.20.

Bubble Pair Finding and Velocity Calculation

After calculating the total probability Φ using equation (3.34), the bubbles are assigned to pairs starting from the maximum value in the matrix Φ. For each assigned pair, the probability values are set equal to zero and the procedure is continued with the next maximum probability value. In this pair assigning step, all probability values greater equal 1% are considered. Probability values smaller than 1% are effects from noisy bubbles. If the bubble pairs are assigned, the individual bubble velocities is calculated, whereby the parameter k means the temporal detection of the bubble:

$$u_{axial}(b_1, b_2) = \frac{10.2\ mm}{k(b_2) - k(b_1)} \tag{3.43}$$

According to the axial velocity in equation (3.43), the radial velocities are calculated also:

$$u_{radial}(b_1, b_2) = \frac{r_2 - r_1}{k(b_2) - k(b_1)} \tag{3.44}$$

For a better understanding of calculation azimuthal velocities, the geometrical basics are presented in Figure 3.21. Firstly, a fictive bubble position b_2'(i,j) is estimated, where the vector direction from the pipe center is the same as the original bubbles position b_2(i,j) and the radial position is the same as the radial position at b_1(i,j). Now, the distance s between b_1 and b_2 is calculated.

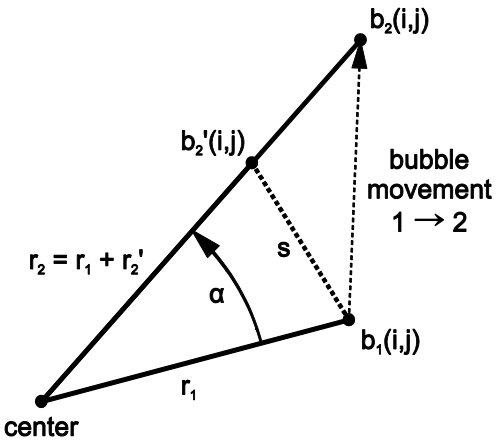

Figure 3.21: Geometrical basics of calculating azimuthal velocities

According to this figure, the movement angle α can be calculated:

$$\alpha = \arccos\left(1 - \frac{s^2}{2 \cdot {r_1}^2}\right) = 2 \cdot \arcsin\left(\frac{s}{2 \cdot r_1}\right) \tag{3.45}$$

Due the fact, that equation (3.47) gives back no direction sign, the orientation is estimated additionally by vector product of the positions b1(i,j) and b2(i,j):

$$orientation = \begin{cases} -1, & b_1 \times b_2 < 0 \\ 1, & b_1 \times b_2 \geq 0 \end{cases} \tag{3.46}$$

Further, the azimuthal velocity can be calculated:

$$\boldsymbol{u_{azimuthal}(b_1, b_2) = orientation \cdot \frac{\alpha \cdot r_1}{k(b_2) - k(b_1)}} \tag{3.47}$$

For large bubbles the shape can change caused by oscillations, which may modify the position of the center of mass. In addition, coalescence and breakup processes may cause such a modification. For this reason, the reference point to calculate the bubble time i is adapted depending on their size. For small bubbles with a maximum cross-sectional circle equivalent diameter less than 6 mm, the detected center of mass is used as reference point i. If the maximum cross-sectional circle equivalent diameter is greater than 20 mm, the detected bubble nose will be used as reference point i. For all bubbles with a size between $6\,\mathrm{mm} < \mathrm{d_{xy,max}} \leq 20\,\mathrm{mm}$, a virtual reference point i is calculated by linear interpolation between center of mass and bubble nose. With the knowledge of the individual bubble velocity, their real bubble

volume $\mathrm{V}(\mathrm{b}_1)$ as well as the real sphere equivalent bubble diameter $\mathrm{d}_{\mathrm{eq}}(\mathrm{b}_1)$ can be calculated using the equations (3.48):

$$\boldsymbol{V(b_1) = v(b_1) \cdot u_{axial}(b_1)}$$

$$d_{eq}(b_1) = \sqrt[3]{\frac{6}{\pi} \cdot V(b_1)} \tag{3.48}$$

The results are saved in files with extensions from the cross-correlation method, but added with "_pair".

3.7.3 Morphological algorithm

In the case of small bubble velocities, the dwell time of bubbles between the two tomography layers gets high. If this large dwell time is superposed with a high fluctuating velocity field, the bubble velocity is very difficult to estimate with both presented methods – the cross-correlation as well as pair finding method. Especially at counter-current flows such situations are observed. To illustrate this, in Figure 3.22, two exemplary side cut views are presented.

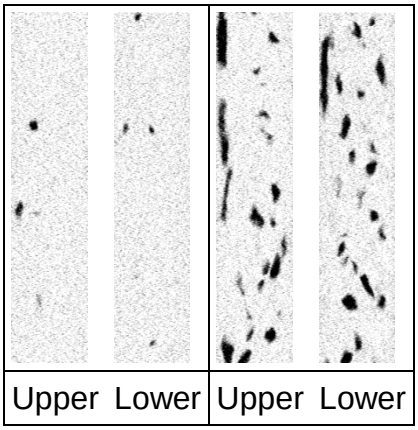

Figure 3.22: Two examples for different results between upper and lower tomography layer at counter-current two-phase flows

For such flows a third algorithm is developed which uses a prior knowledge on the morphological properties of the bubbles. With equation (3.29) the maximum detected equivalent diameter of the bubble in cross-sectional cut is known. Using the EÖTVÖS- and MORTEN-number for air-water flows

$$Eo(b) = \frac{\Delta\varrho \cdot g \cdot D_{xy,n,max}^2(b)}{\sigma}, \qquad Mo = 2.56 \cdot 10^{-11} \tag{3.49}$$

the aspect ratio $\overline{\mathrm{E}}$ of each bubble can be estimated with

$$\overline{E(b)} = \frac{1}{(1 + 0.163 \cdot Eo(b)^{0.757})} \tag{3.50}$$

as given by Clift (1978). The individual bubble velocity can be calculated using maximum cross-sectional diameter $D_{xy,n,max}$, aspect ratio $\overline{E}$ and time detection length dt from the bubble properties:

$$u_{axial}(b) = \frac{D_{xy,n,max}(b) \cdot \overline{E(b)}}{dt(b)} \tag{3.51}$$

$u_{axial}(b)$ is the absolute average axial velocity of the bubble b. The flow direction of bubbles can be estimated by approximating the center of mass at each time step k of each bubble to a line: The radial and azimuthal displacement of this line at beginning and ending of the bubble can be used as input into the equations (3.44) and (3.47). Instead of two tomography layers, the beginning and ending of the bubble is meant in this case, of course.

The results are saved in files with extensions from the cross-correlation method, but added with "_morph" for a better distinction.

3.8. Bubble sizes

After evaluation of the data described in the previous sections, three-dimensional information for gas volume fraction distribution and for bubble sizes is available. Additionally, a list with characteristics of each bubble is generated.

The combination of these data makes it possible to obtain bubble size distributions. To do this, histograms are calculated in which the void fraction per bubble class is summed up. This is done related to the volume equivalent diameter according to equation (3.25) as well as related to the area equivalent diameter of the gas bubbles according to equation (3.29). This information is available in a representation with a linear bubble class width of 0.25 mm and also for a logarithmically increasing width of the bubble classes. The smallest bubble size class for the logarithmic representation has a lower boundary of 0.1 mm. The bubble size distributions are stored in ASCII files with the extensions *.his_lin and *.his_log, respectively. The linear distributions are preferably used for the numerical investigations and the logarithmic information for visualisation (bubble size distributions in appendix 9.1).

In both types of bubble size distributions, the void fraction that is related to the bubble class width is represented by ($\Delta\varepsilon/\Delta D_b$), which gives:

$$\varepsilon_{ges} = \sum_{0}^{D_{b,max}} \frac{\Delta\varepsilon}{\Delta D_b} \cdot \Delta D_b \tag{3.52}$$

In addition these distributions related to the total gas content ($\Delta\varepsilon/\Delta D_b/\varepsilon_{ges}$) are listed in both files. Furthermore, the files contain the bubble number distributions in which the absolute number of bubbles per bubble class is referred to the bubble class width and the total measurement time.

The data also enable to present the azimuthally and time averaged gas fraction distributions (as defined by equation (3.19) decomposed according to bubble size). Such data are stored in the files *.epsrad_20_bub in dependence on the radius and a division into four bubble classes (0 - 4 mm, 4 mm - 5.8 mm, 5.8 mm - 7 mm and 7 mm - 200 mm). For the air-water flow, at the boundary conditions presented above the Tomiyama lift force changes its direction at an equivalent bubble diameter of about 5.8 mm. For this reason, two bubble classes with a smaller width were chosen above and below this value, as well as two classes containing the void fraction for the remaining bubbles. Additionally, these files contain the total void fraction per radial ring.

In addition, the previously described linear bubble size distributions (*.his_lin) were split up for the single radial rings. To do that, position (i,j) and diameter (Db) of each reconstructed bubble is checked and the related void fraction is assigned to a two-dimensional array according to the associated bubble class and the respective radial ring m(r). Again the weight coefficient ai,j,m (see also Figure 3.18 is used for this procedure. These void fraction distributions are related to the bubble class width, as in the *.his_lin files. The cross section averaged bubble size distributions discussed above $\Delta\varepsilon(r)/\Delta D_b$ can be obtained from these data according to:

$$\frac{\Delta\varepsilon}{\Delta D_b} = \frac{1}{2 \cdot R_{Sensor}^2} \sum_{r=1}^{R_{Sensor}} \frac{\Delta\varepsilon(r)}{\Delta D_b} \cdot r \cdot \Delta r \tag{3.53}$$

Furthermore, these results were related to the total void fraction per radial ring: $\Delta\varepsilon(r)/\Delta D_b/\varepsilon_{ges}(r)$. For the determination of the bubble number distribution, the following conditions were considered: Each bubble is only once registered per radial ring. If a bubble penetrates several radius rings, then it is detected separately in each ring.

These data are available in the files *.his_lin_r as 20 individual bubble size distributions, each per radius ring described in equation (3.20). To enable some checks, these files contain at the end the bubble size distribution, an integration over the radius according to equation (3.53)), which corresponds to the data in the *.his_lin file.

4. Wire mesh sensor

As mentioned before a pair of wire-mesh sensors was installed at the upper end of the pipe in case of upwards liquid flows for comparison of the measuring methods. Electrode-mesh sensors are based on a measurement of the local instantaneous conductivity of the two-phase mixture. In case of a gas/liquid two-phase flow, the liquid phase is slightly conducting, while the gas phase is practically an ideal insulator. A direct conductivity measurement between pairs of crossing wires is applied to avoid tomographic reconstruction algorithms (Prasser et al., 1998)) and to increase time resolution.

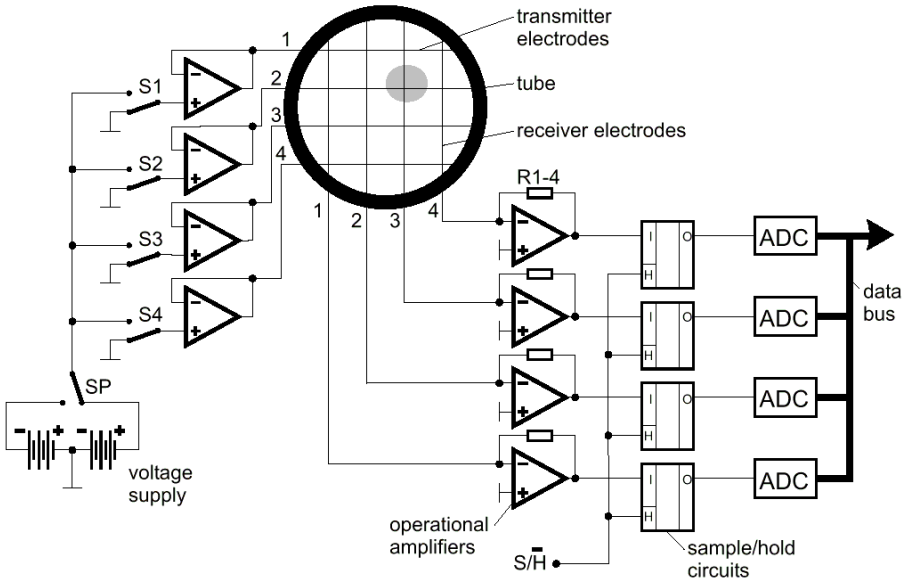

Figure 4.1: Measuring principal of wire-mesh sensors, simplified scheme of a wire-mesh sensor with 2x4 electrode wires

From the point of view of the general arrangement of electrode wires, the used sensors are quite similar to the ones developed firstly by Johnson (1987). The sensor consists of two grids of parallel wires which span over the measuring cross section. The wires of both planes cross under an angle of 90 deg. During the signal acquisition, one grid of electrode wires is used as transmitter, the other one as receiver plane (Figure 4.1). The transmitter electrodes are activated by supplying them with voltage pulses in a successive order. The current at a receiver wire resulting from the activation of a given transmitter wire is a measure of the conductivity of the fluid in the corresponding control volume close to the crossing point of the two wires. The currents from all receiver wires are sampled simultaneously. This procedure is repeated for all transmitter electrodes. After activating the last transmitter wire, a complete matrix of measured values is stored in the computer, which represents the complete two-dimensional conductivity distribution in the sensor cross section at the time of measurement. The used sensor can be operated up to 7 MPa and 286 °C (Pietruske and Prasser, 2007). The spatial and temporal resolutions amount 3 mm and up to 10 kHz respectively. The chosen measurement frequency for all measurements amounts 5 kHz. The sensor is equipped with a matrix of 16x16 wires and has an inner diameter of 52.3 mm.

A CAD view is shown in Figure 4.2. Two identical sensors of this kind were manufactured and placed into the test pipe in a distance of 63 mm behind each other. This

allowed to additionally measure steam velocities by cross-correlating the signals of both sensors (see 3.7.1).

Further information are available e.g. in Prasser et al., (1998), (2001), (2007).

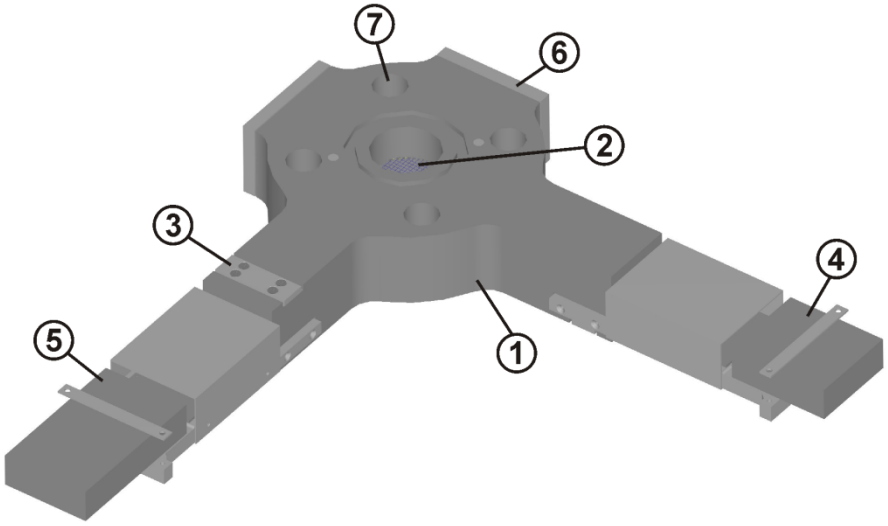

Figure 4.2: CAD view of the complete sensor for a 52.3 mm inner diameter pipe, 16x16 electrodes: (1) sensor body, (2) measuring plane with wires, (3) location of sealed bushings (without cooling bodies), (4) driver unit, (5) receiver pre-amplifier, (6) cap, (7) bolt hole of flange connection

As aforementioned in section 2.2, the inner diameter of the titanium pipe is 54.8 mm. So, there is a diameter difference of 2.5 mm to the wire-mesh sensor. To minimize the influence of decreasing the cross-sectional area, the lower and upper edges of the wire-mesh sensors are chamfered with 1.25x15°. Nevertheless there are different cross-sectional areas, which have to be considered at comparison of evaluated data.

5. Measurement uncertainties

Uncertainties in the measurements are influenced by flow regime conditions (pressure, temperature, mass and volume flow), the measurement technique and the data processing algorithms. The uncertainties of the process control measurements are considered more detailed in section 2.2.4. The measurement uncertainties of the used wire mesh sensor are reported by Beyer et al. (2008). The accuracy of the X-ray tomography system is discussed by Fischer et al. (2008), Fischer and Hampel (2013). Estimating the uncertainties of the data obtained by X-ray tomography is more difficult because noise and systematic uncertainties may have an important influence on the segmentation process. Therefore, the discussion on the estimation of uncertainties is split into two parts: frequency and segmentation.

5.1. Frequency and discretization error

The measurement frequency was chosen basing on the expected bubble velocities. On one hand the frequencies have to be high enough to resolve small bubbles with a minimum of voxel and on the other hand the data quality decreases at high frequencies. So, the optimal frequency has to be defined. The following conditions and assumptions are applied for choosing the measurement frequency:

- The resulting discretization error for estimating the velocity may not extend 10%.
- Bubbles with the minimum detectable size of 2mm should have a detection length of 2 frames at least.
- The bubble velocity was estimated here as the sum of the total superficial velocity and the drift velocity.

Considering these conditions, the minimum necessary frequencies can be calculated for the different combinations of gas and liquid superficial velocities according to the general HZDR test matrix. They are given in Table 5.1.

Table 5.1: Test matrix with minimum necessary frequencies for upward flows

[m/s]		*Superficial gas velocity*																	
		0,0025	*0,0040*	*0,0062*	*0,0096*	*0,0151*	*0,0235*	*0,0368*	*0,0574*	*0,0898*	*0,1400*	*0,219*	*0,342*	*0,534*	*0,835*	*1,305*	*2,038*	*3,185*
Superficial liquid velocity	*4,047*	4300	4301	4303	4307	4312	4321	4334	4354	4387	4437	4516	4639	4831	5132	5602	6335	7482
	2,554	2807	2808	2810	2814	2819	2828	2841	2861	2894	2944	3023	3146	3338	3639	4109	4842	5989
	1,611	1864	1865	1867	1871	1876	1885	1898	1918	1951	2001	2080	2203	2395	2696	3166	3899	5046
	1,017	1270	1271	1273	1277	1282	1291	1304	1324	1357	1407	1486	1609	1801	2102	2572	3305	4452
	0,641	894	895	897	901	906	915	928	948	981	1031	1110	1233	1425	1726	2196	2929	4076
	0,406	659	660	662	666	671	680	693	713	746	796	875	998	1190	1491	1961	2694	3841
	0,255	508	509	511	515	520	529	542	562	595	645	724	847	1039	1340	1810	2543	3690
	0,161	414	415	417	421	426	435	448	468	501	551	630	753	945	1246	1716	2449	3596
	0,102	355	356	358	362	367	376	389	409	442	492	571	694	886	1187	1657	2390	3537
	0,064	317	318	320	324	329	338	351	372	404	454	533	656	848	1149	1619	2352	3499
	0,041	293	295	297	300	306	314	327	348	380	431	510	633	825	1126	1596	2329	3476

Considering the afore mentioned maximum scanning frequency of 5000 frames per second for a single layer, the black typed matrix points can be scanned with dual-layer and the red typed ones with single layer. The points marked with orange background were not investigated, because the reconstruction quality condition of minimum 200 projections is considered. Basing on Table 5.1, the frequencies were set. To avoid many different values and different measurement settings, two main frequencies are set: 1000 and 2500Hz. In some cases of the downward flows,

2000Hz are used. It results in point specific discretization errors for the bubble velocity as shown in Table 5.2.

Table 5.2: Test matrix with resulting discretization errors for upward flows

[%]	Superficial gas velocity																
Superficial liquid velocity	0,0025	0,0040	0,0062	0,0096	0,0151	0,0235	0,0368	0,0574	0,0898	0,1400	0,219	0,342	0,534	0,835	1,305	2,038	3,185
4,047	16,9	16,9	16,9	16,9	16,9	16,9	17,0	17,1	17,2	17,4	17,7	18,2	18,9	20,1	22,0	24,8	29,3
2,554	11,0	11,0	11,0	11,0	11,1	11,1	11,1	11,2	11,3	11,5	11,9	12,3	13,1	14,3	16,1	19,0	23,5
1,611	7,3	7,3	7,3	7,3	7,4	7,4	7,4	7,5	7,7	7,8	8,2	8,6	9,4	10,6	12,4	15,3	19,8
1,017	5,0	5,0	5,0	5,0	5,0	5,1	5,1	5,2	5,3	5,5	5,8	6,3	7,1	8,2	10,1	13,0	17,5
0,641	8,8	8,8	8,8	8,8	8,9	9,0	9,1	9,3	3,8	4,0	4,4	4,8	5,6	6,8	8,6	11,5	16,0
0,406	6,5	6,5	6,5	6,5	6,6	6,7	6,8	7,0	7,3	7,8	8,6	3,9	4,7	5,8	7,7	10,6	15,1
0,255	5,0	5,0	5,0	5,0	5,1	5,2	5,3	5,5	5,8	6,3	7,1	8,3	4,1	5,3	7,1	10,0	14,5
0,161	4,1	4,1	4,1	4,1	4,2	4,3	4,4	4,6	4,9	5,4	6,2	7,4	9,3	4,9	6,7	9,6	14,1
0,102	3,5	3,5	3,5	3,5	3,6	3,7	3,8	4,0	4,3	4,8	5,6	6,8	8,7	4,7	6,5	9,4	13,9
0,064	3,1	3,1	3,1	3,2	3,2	3,3	3,4	3,6	4,0	4,5	5,2	6,4	8,3	4,5	6,3	9,2	13,7
0,041	2,9	2,9	2,9	2,9	3,0	3,1	3,2	3,4	3,7	4,2	5,0	6,2	8,1	4,4	6,3	9,1	13,6

The blue marked values are calculated for a frequency of 2500Hz, the black ones are for a frequency of 1000Hz. The color stratified distribution is caused by the reducing of the frequency from 2500 to 1000 Hz. The same procedure is done for counter-current flows as well as downward flows. The results are shown in Tables 5.3 and 5.4. At the downward flows, the red colored values are calculated with a frequency of 2000Hz.

Table 5.3: Test matrix with resulting discretisation error for counter-current flows

[%]	Superficial gas velocity																
Superficial liquid velocity	0,0025	0,0040	0,0062	0,0096	0,0151	0,0235	0,0368	0,0574	0,0898	0,1400	0,219	0,342	0,534	0,835	1,305	2,038	3,185
-4,047																	
-2,554																	
-1,611																	
-1,017																	
-0,641																	
-0,406																	
-0,255																	
-0,161	0,9	0,9	0,9	1,0	1,0	1,1	1,2	1,4	1,8	2,2	3,0	4,2	6,1	9,1	5,5	8,3	12,8
-0,102	1,5	1,5	1,5	1,5	1,6	1,7	1,8	2,0	2,3	2,8	3,6	4,8	6,7	9,6	5,7	8,6	13,1
-0,064	1,8	1,9	1,9	1,9	2,0	2,1	2,2	2,4	2,7	3,2	4,0	5,2	7,1	4,0	5,8	8,7	13,2
-0,041	2,1	2,1	2,1	2,1	2,2	2,3	2,4	2,6	2,9	3,4	4,2	5,4	7,3	4,1	5,9	8,8	13,3

Table 5.4: Test matrix with resulting discretisation error for co-current downward flows

[%]	Superficial gas velocity																
Superficial liquid velocity	-0,0025	-0,0040	-0,0062	-0,0096	-0,0151	-0,0235	-0,0368	-0,0574	-0,0898	-0,1400	-0,219	-0,342	-0,534	-0,835	-1,305	-2,038	-3,185
-4,047	14,9	14,9	14,9	14,9	14,9	15,0	15,0	15,1	15,2	15,4	15,7	16,2	17,0	18,2	20,0	22,9	27,4
-2,554	9,0	9,1	9,1	9,1	9,1	9,1	9,2	9,3	9,4	9,6	9,9	10,4	11,1	12,3	14,2	17,0	21,5
-1,611	6,7	6,7	6,7	6,7	6,7	6,8	6,9	7,0	7,1	7,4	6,2	6,7	7,4	8,6	10,5	13,3	17,8
-1,017	7,5	7,6	7,6	7,6	7,7	7,8	7,9	8,1	8,4	8,9	9,7	5,4	5,1	6,3	8,1	11,0	15,5
-0,641	3,9	3,9	3,9	3,9	4,0	4,1	4,2	4,4	4,7	5,2	6,0	3,6	4,5	6,0	6,7	9,5	14,0
-0,406	1,6	1,6	1,6	1,6	1,7	1,8	1,9	2,1	2,4	2,9	3,7	4,9	6,8	4,9	5,7	8,6	13,1
-0,255																	
-0,161																	
-0,102																	
-0,064																	
-0,041																	

5.2. Segmentation

The uncertainty of the segmentation depends on the processing algorithm as well as the reconstruction quality determined by the number of projections in the sinogram (depending on frequency). In section 3.3.2 some considerations about the quality of the segmentation were done using bubble size distributions of phantom measurements. These phantoms were made using real two-phase flow data from former measurements.

To get some quantitative impression on uncertainties at different bubble sizes, additional phantom measurements were conducted with the frequencies 1000 and 2500Hz. These 3D phantoms have empty spheres milled into plastic, the first one - with 4 mm diameter (180 bubbles), the other - with 2 mm diameter (560 bubbles). Therefore, the segmentation and also measurement uncertainty for small bubbles near to the resolution limit was evaluated. The phantom was moved through the ROFEX with a constant speed of 0.5 m/s.

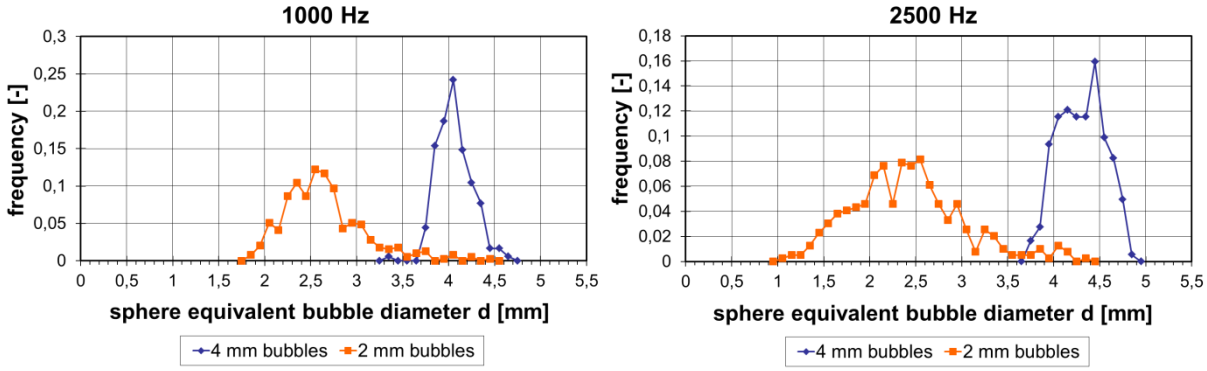

a) *b)*

Figure 5.1: Bubble size distributions of the phantom a) 1000 Hz and b) 2500 Hz measurements

In Figure 5.1 bubble size distributions of both phantom measurements are presented. It is obvious, that the width of the distributions increases with increasing frequency. The 2 mm bubbles have a very width distribution, which in addition is shifted to larger diameters. This is caused mainly by following facts:

- The discretization error has a very large influence to the volume of the small bubbles,
- Due the known resolution limit of ROFEX, there is defined a minimum detectable bubble size,
- Artificial coalescence effects of spaced bubbles (orange distribution at diameters greater than 3.5 mm) as well as
- Noisy pixels joined to detected bubble regions.

The last point is mostly the reason for increasing distribution width with increasing frequency: The number of available projections for each frame is decreasing and the number of information for reconstructing reduces. Therefore, noise effects become stronger in the reconstructed frame.

Table 5.5: Statistic results from phantom measurements for 2 and 4 mm bubbles

	1000 Hz				2500 Hz			
	2 mm		4 mm		2 mm		4 mm	
Mean value	2.64 mm		4.06 mm		2.41 mm		4.30 mm	
Standard deviation (P=68.3%)	0.43 mm	16.4%	0.19 mm	4,64%	0.60 mm	25,1%	0.25 mm	5,82%
Deviation with P=95% / uncertainty	0.85 mm	32,1%	0.37 mm	9,10%	1.18 mm	49,1%	0.49 mm	11,4%

In Table 5.5 the statistical results from Figure 5.1 are presented. In all four cases the mean values are overestimated, but a view to the uncertainties (deviation with a confidence interval of P=95%) reveals, that the mean value is not outside of this region. In both frequency cases of the 2 mm bubbles the relative uncertainties are very large. Considering the lower uncertainty values for the 4 mm bubbles and the items above, the uncertainties for bubbles greater 4 mm can be assumed as less than 10%.

6. Experiments and results

Experimental series were done as co-current upward, counter-current and co-current downward flows. Air-water experiments were conducted for all these flows, while steam-water experiments were done only for co-current upward and downward flows. The test conditions and measurement positions are given in *Table 2.1* and Table 2.2. All measurements were done with a measuring time of 10 s. The data was reconstructed, segmented and evaluated using the presented algorithms in sections 3.2-3.8. For the upward and counter-current flows, in addition to the X-ray tomography measurements, a wire-mesh sensor was used at measurement position S.

6.1. Upward flows

6.1.1 Air-water flows

The investigated co-current upward air-water flow regimes are shown in Figure 6.1. The measurement series include 19 (L16) and 13 (L18) measurement points. The measuring frequencies used are 2x1000 and 2x2500 Hz for dual layer measurements and additionally 1x5000 Hz for single layer measurements at flows for which very high bubble velocities were expected. For the tomography measurements, the L/D ratio increases along the measurement positions A, D, G, J, M and P. The pressure was adjusted in a way that it is always 0.4 MPa at the upper end of the pipe (see 2.2.4). The temperature is kept constant at 30°C ± 1K for the water.

		Superficial velocity gaseous phase																
	[m/s]	0,0025	0,0040	0,0062	0,0096	0,0151	0,0235	0,0368	0,0574	0,0898	0,1400	0,2190	0,3420	0,5340	0,8350	1,3050	2,0380	3,1850
Superficial velocity liquid phase	4,0470	011	022	033	044	055	066	077	088	099	110	121	132	143	154	165	176	187
	2,5540	010	021	032	043	054	065	076	087	098	109	120	131	142	153	164	175	186
	1,6110	009	020	031	042	053	064	075	086	097	108	119	130	141	152	163	174	185
	1,0170	008	019	030	041	052	063	074	085	096	107	118	129	140	151	162	173	184
	0,6410	007	018	029	040	051	062	073	084	095	106	117	128	139	150	161	172	183
	0,4050	006	017	028	039	050	061	072	083	094	105	116	127	138	149	160	171	182
	0,2550	005	016	027	038	049	060	071	082	093	104	115	126	137	148	159	170	181
	0,1610	004	015	026	037	048	059	070	081	092	103	114	125	136	147	158	169	180
	0,1020	003	014	025	036	047	058	069	080	091	102	113	124	135	146	157	168	179
	0,0641	002	013	024	035	046	057	068	079	090	101	112	123	134	145	156	167	178
	0,0405	001	012	023	034	045	056	067	078	089	100	111	122	133	144	155	166	177

Figure 6.1: Test matrix for co-current upward air-water flow regimes. Blue marked: L16 series with gas injector M3, orange marked: L18 series with gas injector M4

In Figure 6.2 the investigated matrix points from Figure 6.1 are shown in a flow map which bases on Taitel et al. (1980) for L/D=60 (measurement position P). The given transition lines could be confirmed by the present measurements. A small deviation is obtained only at the transition between bubbly flow and slug flow: A small band for “cap bubble flow” as transition region is missed left from the plotted transition line. The Point 118 (jl = 1.017 m/s; jg = 0.219 m/s, marked with a green circle) would be categorized as cap bubble flow regime, while the points 089, 116 and 140 (the three points very closed to the transition line, marked with a purple circle) are categorized clearly as slug flows.

In Figure 6.3 central cut views of six chosen air-water upward flow examples are presented. These flow patterns confirm the observations described above: The flow regime at 118 represents a cap bubble flow as transition from bubble to slug flow. The 140 pattern show clearly a slug flow regime, while the 162 represents a churn turbulent flow.

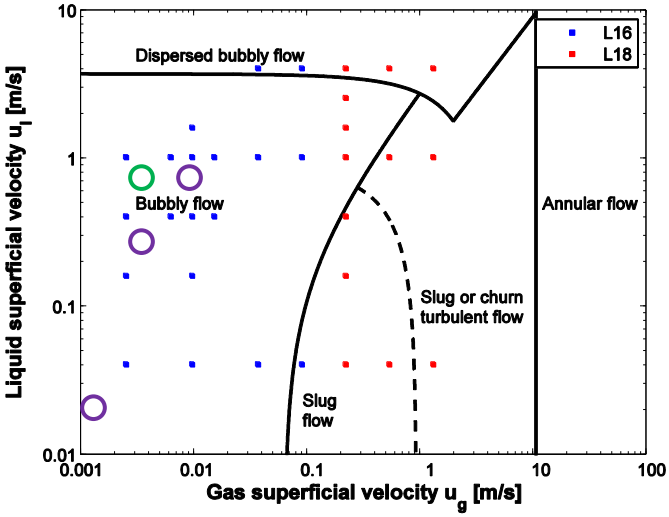

Figure 6.2: Flow map for L16 and L18 series, transition lines basing on Taitel, Bornea, and Dukler (1980)

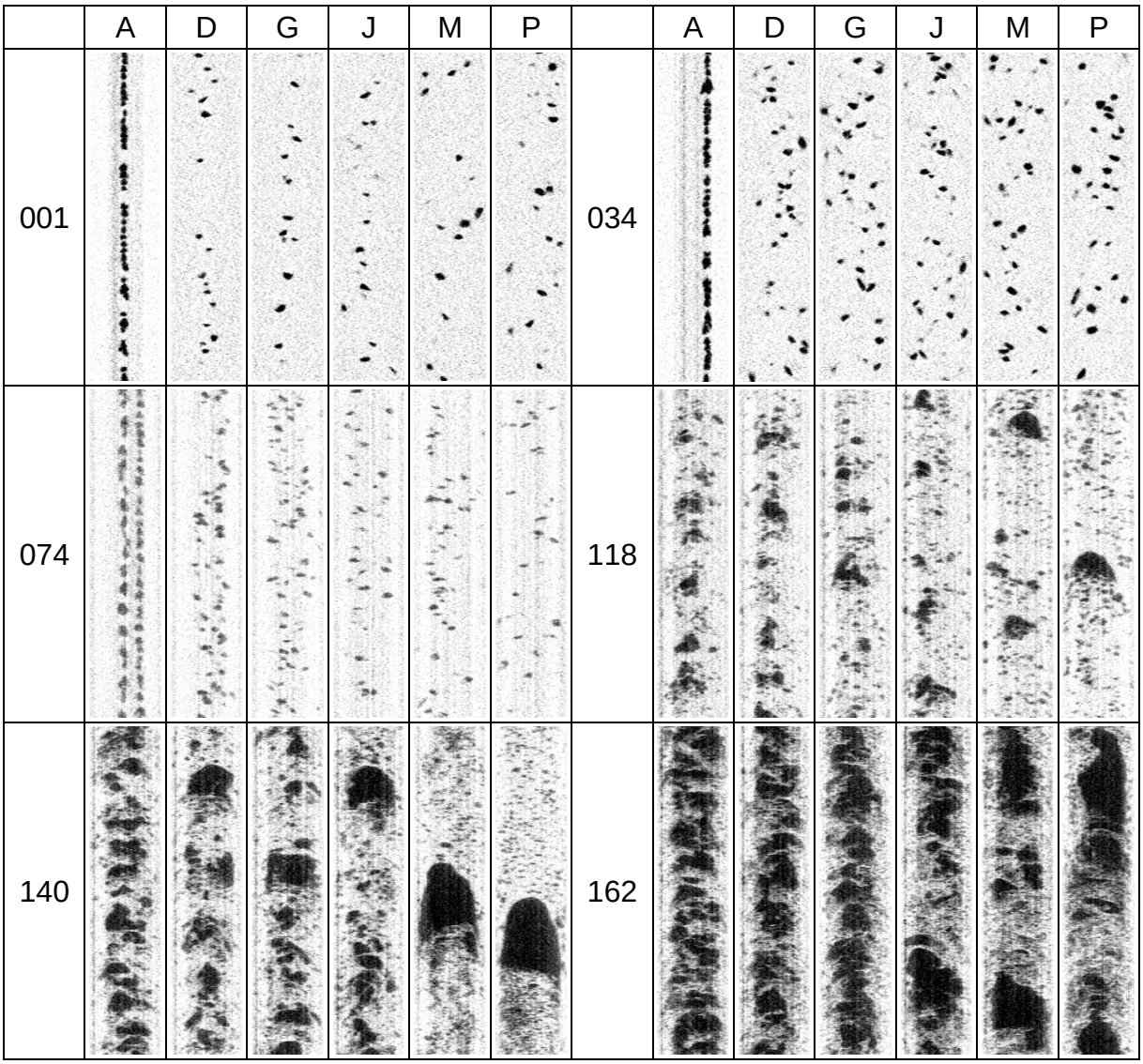

Figure 6.3: Exemplary central cuts illustrating the flow pattern for 6 measured matrix points

The evolution of the flow caused by horizontal bubble migration and by coalescence and breakup is also illustrated by these side cut views. Especially for the low flow rates with bubbly flow (points 001, 034 and 074) the bubble migration from the gas injection in the center region over the whole cross-section can be observed along the pipe. With increasing gas volume fraction, gas bubbles agglomerate and coalescence to large bubbles with increasing flow length. Before the bubble size is large enough to fill the cross-sectional pipe area, the cap bubbles are observable in the pipe center (118, 140 A-J, 162 A-G).

Examples for gas volume fraction values obtained after the segmentation process are listed in Table 6.1. Additional, the expected gas volume fraction values at the position P (L/D = 60) as well as the wire mesh sensor results at position S (L/D=85) are included. The results of the tomography at level P show generally a slight underestimation of the expected gas volume fraction. This is caused by the spatial resolution of the tomography system. General, the underestimation is inside the in the segmentation uncertainty limit of ±0.5% absolutely for small gas volume fractions and ±8% relatively for medium and high gas volume fractions (Banowski et al., 2015). The deviations are in a similar range for the wire mesh sensor results.

Table 6.1: Gas volume fraction values for selected measurements at all measured positions, compared with theoretical value and wire mesh sensor measurements (position S)

Matrix point	A [%]	D [%]	G [%]	J [%]	M [%]	P [%]	Expected value at P [%]	WMSS [%]	Expected value at S [%]
001	0.378	0.614	0.640	0.730	0.730	0.777	1.028	1.146	1.096
034	1.159	2.824	3.303	3.132	3.364	3.440	3.821	5.082	4.056
074	0.461	2.562	2.667	2.656	2.800	2.931	3.245	3.298	3.447
118	14.32	12.65	14.35	15.77	16.74	16.24	16.38	16.70	17.10
140	24.73	24.90	26.32	29.53	31.68	31.77	31.85	31.35	32.73
162	38.10	38.31	40.99	44.75	47.61	50.26	52.60	48.70	53.28

The gas volume fraction values from Table 6.1 are plotted against the length to diameter (L/D) ratio in Figure 6.4 for illustrating their evolution along the pipe. The charts for the L16 measurements accord mainly to the expectations, there are only some deviations inside the uncertainty limits. All three plots show a slight increasing trend with increasing height position. This is caused by the decreasing absolute pressure due the hydrostatic condition. The smaller values close to the injection probably result from the rather high gas velocities because of the injection from the small injection cannulas. The plots shown for the L18 measurements have a more inclined trend than the L16 ones. Possible reasons are discussed in the following.

The bubble size distribution of L18 – 118 shown on the bottom right side in Figure 6.5 shows an increase of the peak of small bubbles, along the pipe. It may be connected with the resolution limit of the tomography system. Above the injection, an additional mesh was installed which serves as flow straightener and distributor (see section 2.2.2). The two-phase flow is accelerated at this position because of the smaller cross-sectional area and the wires create shear forces. This may lead to bubble breakup generating a considerable amount of bubbles with sizes less than the special resolution. Along the pipe, these bubbles coalesce and are added to the measured small bubbles peak. This explanation is supported by the facts that this

peak begins at the limit for the spatial resolution, i.e. at an equivalent sphere diameter of 2 mm and looks asymmetrically with a steep flange at the left side for lower measuring positions.

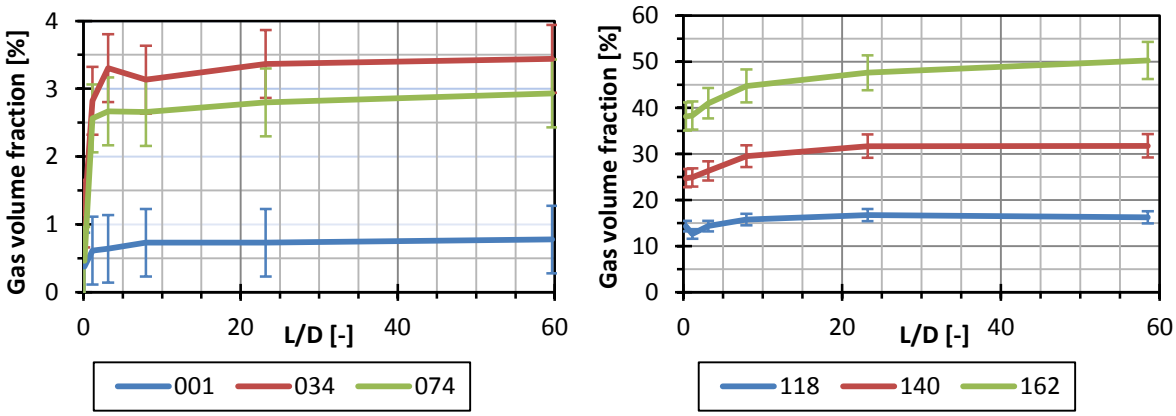

Figure 6.4: Development of gas volume fraction along the pipe. left: examples from the L16 measurements, right: examples from the L18 measurements

In the top row of Figure 6.5, the radial gas volume fraction profiles are presented. In both cases, the development from center peaked gas distribution near the injection to a more flattened gas distribution can be observed. The radial WMS gas fraction profile of L16 – 001 reveals the disadvantage of the WMS technique: At slow velocities, the momentum of the bubbles is too low to push them through the mesh. So, the mesh decelerates bubbles and catches them. The measured gas volume fraction is too high. This effect is not relevant at L18 – 118, because the bubbles are pushed well through the mesh by the higher liquid velocity. However, an ongoing flattening trend from P position to WMS position S is explainable with the slight straightening effect of the wires. Comparing the measured and theoretical values from Table 6.1, the values are according quite well.

Due the slight bubble jam at both wire-mesh sensors in the 001 case, the velocity result is ignored in the L16 – 001 velocity chart, which bases on bubble pair finding results. The profile trends correspond with the radial gas profiles, indicated especially between D and P profiles. In the L18 – 118 flow case, a slight flattening process can be observed with increasing position height. This is induced by the mainly central injection of the gas phase, whereby a faster gas path is created in the pipe core. The WMS velocity plot seems to have too high values. Caused by different cross sectional areas of Titanium pipe and wire-mesh sensor, the correcting factor $k = A_{WMS} / A_{TiP}$ is multiplied with the WMS velocity values and the radial position steps are also adjusted. In the pipe centre, the deviation amounts only 6.25% between S and P position. This deviation is near to the discretization error of the tomography measurement with 5.8%, calculated using mean velocities. Near the pipe wall, local narrowing effects can be an explanation. Nevertheless, the bubble size distribution shows similar results for both measurement systems in the L18 – 118 flow regime. The light shifting to the right side can be explained with the larger velocity values and the less small bubble peak can be explained with the slight greater special resolution of 3 mm at the wire-mesh sensor instead 2 mm of the tomography system. The big differences at the L16 – 001 flow regime are caused by the wrong velocity estimation by the wire-mesh sensor. All investigated bubbles have mostly a sphere equivalent diameter less than 8 mm.

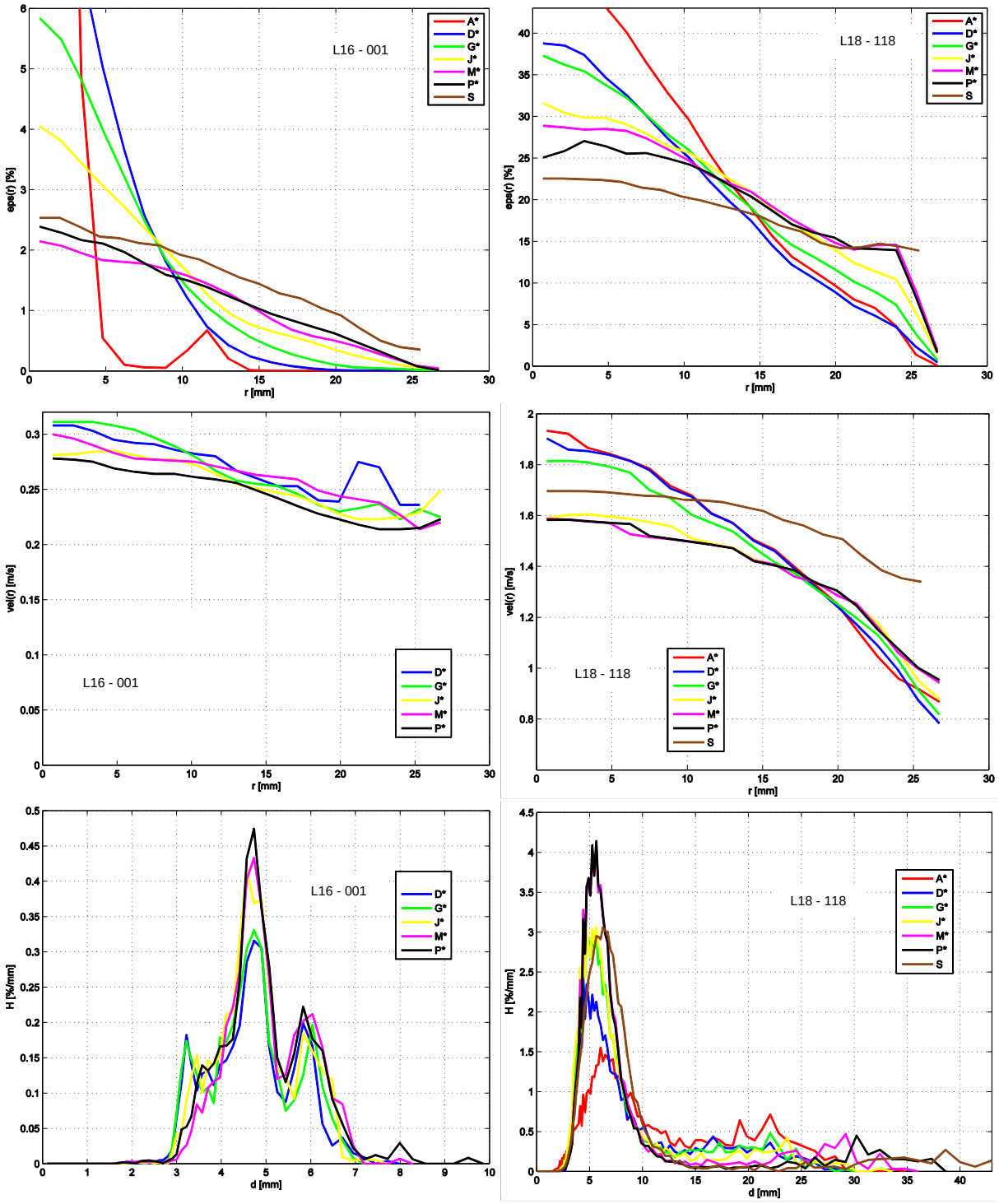

Figure 6.5: Radial gas volume fraction profiles (top), radial bubble velocity profile (middle) and bubble size distribution (bottom) for point 001 (left hand side) and point 118 (right hand side) measurements. The measurement position A is not included for gas velocity and bubble size distribution for L16 – 001 due their extremal values. The gas velocity results are taken from bubble pair algorithm for L16 – 001 and from cross-correlation for L18 – 118.

In Figure 6.6 radial velocity profiles from L16 - 034 and 074 measurements are plotted comparing results from cross-correlation method and bubble pair method. While for higher liquid velocity cases the result is quite similar, there is a deviation of about 40% relative and 0.1 m/s absolute at the 034 flow regime. This disagreement can be explained with the working principles of both methods: While the cross-

correlation estimates only time-averaged velocities for each cross-sectional pixel, the bubble pair method considers different bubble velocities. This fact combined with some noise effects segmented artificially, the cross-correlation method uses a slight different data bases for velocity estimation. Additional, the cross-correlation needs a lot of phase changes for reliable results, so few small artificially noise structures have an influence to the cross-correlation result. Due this fact, the cross-correlation results have to be positive; the velocity values are shifted slightly to greater values. Nevertheless, in the right chart of Figure 6.6, the range of sigma is added to the bubble pair results. It is obvious, that the differences between bubble pair and cross-correlation results have the same magnitude as the sigma value from the bubble pair distribution.

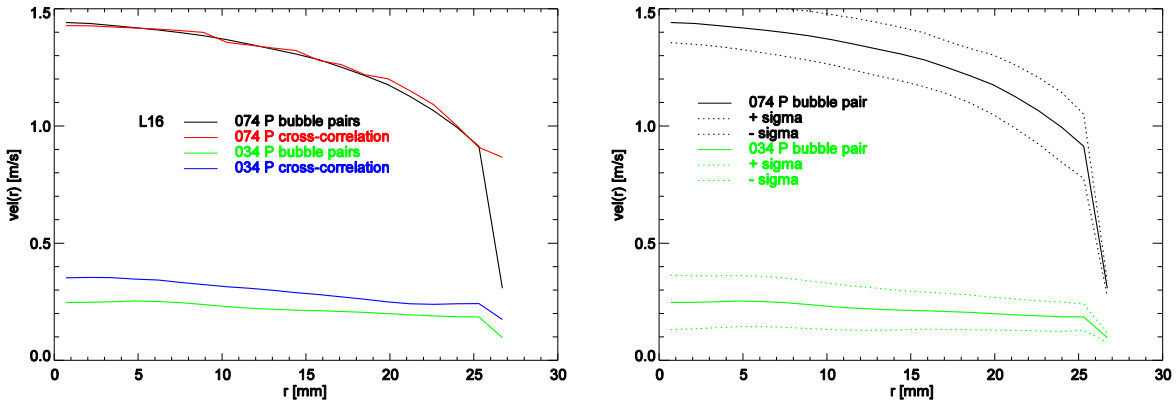

Figure 6.6: Left: Comparison of velocity results between bubble pair method and cross-correlation method. Right: Bubble pair results and their ranges of sigma. The measurements are taken at position P (L/D = 60).

Using bubble pair results, it is possible to decompose gas volume fraction values to different bubble size classes. In Figure 6.7, such bubble size depending radial gas fraction profiles are presented for the L16 – 034 (left hand side) and 074 (right hand side) flow regimes at measurement position P. So, the probability of presence for a bubble with known size can be estimated. Comparing both presented results, it seems that liquid velocity has a strong influence to the radial position: While all profiles of 034 have a decreasing trend from pipe centre to wall, bubbles with diameter less than 4.5 mm will be only near to the wall in the 074 flow regime. Bubbles with a size greater than 5.5 mm are mostly in the pipe centre. The diameter range 4.5 to 5.5 mm seems to be a transition range. Therefore, using this data, conclusions can be draw to the influence of the lift force in turbulent vertical pipe flows.

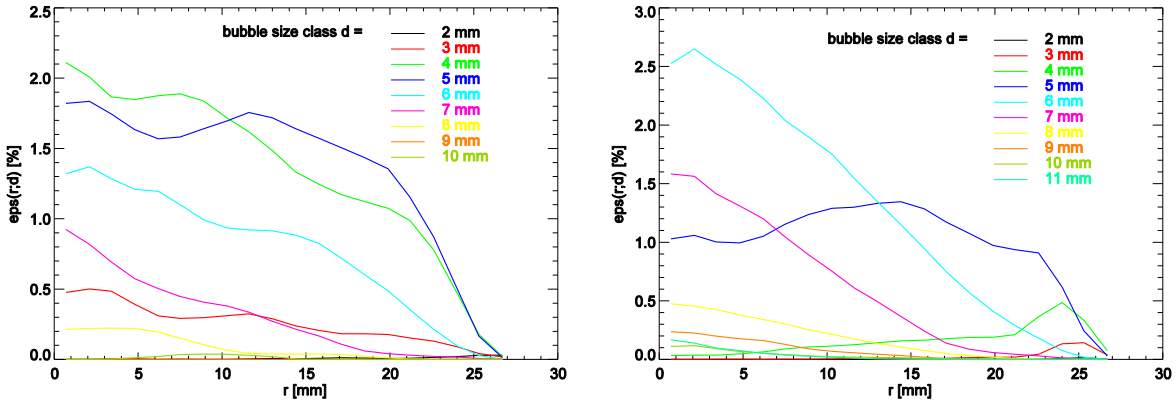

Figure 6.7: Radial gas volume fraction profiles separated to bubble size classes for L16 – 034 (left hand side) and L16 – 074 (right hand side) at position P.

An important method for quality check of the measured values (especially gas volume fraction and bubble velocities) is to estimate the superficial gas velocity according to Beyer et al. (2008). In Table 6.2 the estimated superficial gas velocities from tomography and wire mesh measurements are listed. These values are computed considering the pressure differences between measurement position and injection with Boyle's law:

$$j_{g,meas} = \frac{\dot{V}_G}{A} = \frac{2}{R^2}\int_0^R u_G(r)\cdot\varepsilon(r)\cdot r\cdot dr = <\varepsilon\cdot u_G>. \qquad (6.1)$$

$$j_{g,inj} = j_{g,meas}.\frac{p_{meas}}{p_{inj}}$$

The L16 results are calculated using cross-correlation results. These results show an underestimating for most cases. The L16 WMS results show clearly overestimated values, especially in the 001 and 034 cases with low water velocity. With greater liquid velocity, like in the 074 case, this overestimation is reduced. The reason is the low momentum of the rising bubbles which are caught in the sensor mesh. This overestimation goes on slightly in the L18 examples, where the liquid velocity is high enough. However, general, the WMS results at the L18 examples agree well with the injection condition. The tomography results are computed using cross-correlation results. The underestimation can be explained also with the spatial resolution limit. In the 140 and 162 cases, an additional effect must be considered: The used measurement frequency amounts nearly the minimum frequency taken from Table 5.1. Therefore, small bubbles near to the resolution limit could be lost in the segmentation process. The general underestimation trend is strengthened.

However, also the different methods for the determination of the gas velocity lead to very different results regarding the reconstructed superficies. The values are listed in annex 10.2. For the examples shown in Table 6.2 for the L16 test series the values are much closer to the injected values for the morphology method. For this reason further investigations on this topic seem to be necessary. In any case the results

presented in annex 9.1 should be considered to evaluate the reliability of the single measurements.

Table 6.2: Estimated superficial gas velocity from tomography and wire mesh measurements

j_g [m/s]	injected	A	D	G	J	M	P	S
L16 - 001	0.0025	0.0043	0.0021	0.0022	0.0022	0.0021	0.0020	0.0277
L16 - 034	0.0096	0.0361	0.0090	0.0093	0.0090	0.0097	0.0091	0.1187
L16 - 074	0.0368	0.0047	0.0314	0.0343	0.0349	0.0351	0.0342	0.0456
L18 - 118	0.219	0.222	0.195	0.211	0.217	0.221	0.207	0.2605
L18 - 140	0.534	0.457	0.450	0.455	0.477	0.502	0.502	0.6440
L18 - 162	1.305	0.947	0.918	0.987	0.945	0.997	1.067	1.3863

In Figure 6.8 the pressure corrected superficial gas velocity results are presented for done measurements at jl = 0.0405 and 1.017 m/s and the measurement position P. The sizes of the error bars are calculated by error propagation. The trend shows a slight underestimation, which is expected.

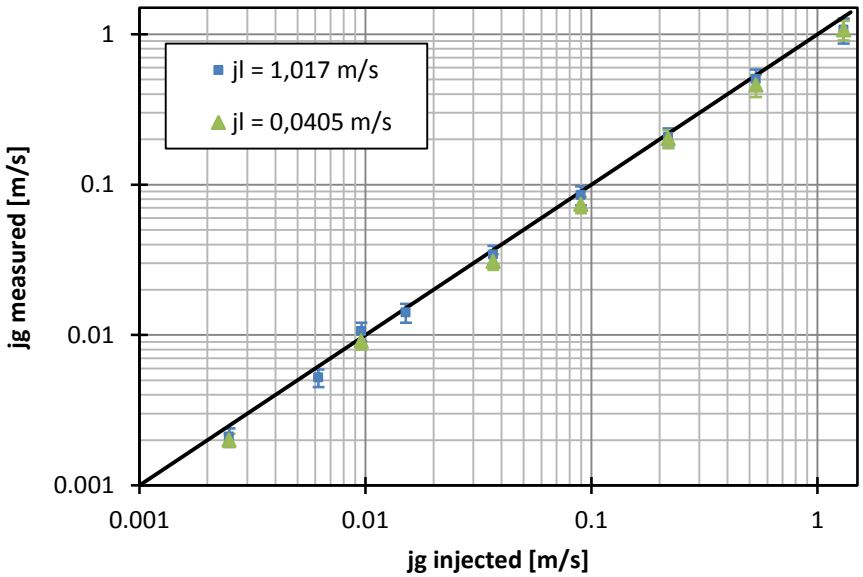

Figure 6.8: Comparison of estimated and injected superficial gas velocities of L16 / L18 measurements with j_l = 0.0405 and 1.017 m/s at position P

6.1.2 Steam-water flows

In Figure 6.9 the investigated combinations superficial velocities for steam and water upward flow are presented. These measurements were conducted at 4.0 and 6.5 MPa and the corresponding saturation temperatures of 250 and 281°C. All points were measured with 2x2500Hz at the positions C, E, G, J, M, and P. The points 163 and 173 were investigated additionally by 1x5000Hz measurements. The range of matrix points which can be used for these experiments is rather small. The reason is the minimum steam flux for which the flow rate can be measured accurately. The measured data were not revised as described in section 3.4.

		Superficial velocity gaseous phase																
	[m/s]	0,0025	0,0040	0,0062	0,0096	0,0151	0,0235	0,0368	0,0574	0,0898	0,1400	0,2190	0,3420	0,5340	0,8350	1,3050	2,0380	3,1850
Superficial velocity liquid phase	4,0470	011	022	033	044	055	066	077	088	099	110	121	132	143	154	165	176	187
	2,5540	010	021	032	043	054	065	076	087	098	109	120	131	142	153	164	175	186
	1,6110	009	020	031	042	053	064	075	086	097	108	119	130	141	152	163	174	185
	1,0170	008	019	030	041	052	063	074	085	096	107	118	129	140	151	162	173	184
	0,6410	007	018	029	040	051	062	073	084	095	106	117	128	139	150	161	172	183
	0,4050	006	017	028	039	050	061	072	083	094	105	116	127	138	149	160	171	182
	0,2550	005	016	027	038	049	060	071	082	093	104	115	126	137	148	159	170	181
	0,1610	004	015	026	037	048	059	070	081	092	103	114	125	136	147	158	169	180
	0,1020	003	014	025	036	047	058	069	080	091	102	113	124	135	146	157	168	179
	0,0641	002	013	024	035	046	057	068	079	090	101	112	123	134	145	156	167	178
	0,0405	001	012	023	034	045	056	067	078	089	100	111	122	133	144	155	166	177

Figure 6.9. Test matrix for co-current upward steam-water flows (D19)

The flow regime can be expected as churn-turbulent flow for the chosen matrix points. This is supported by side cut views shown in Figure 6.10. Three observations can be made:

- The steam-water flows have a churned pattern since steam injection and with increasing measurement height, the bubble sizes increases due bubble coalescence.
- Especially small bubbles are vanishing due condensation effects mostly since position J.
- This condensation effects at 6.5 MPa are less important than at the 4.0 MPa measurements.

The first aspect is similar to the observations from upward air-water flow. The second aspect is more interesting: As aforementioned in section 2.2.1, the temperature of injected water is slightly subcooled. This fact is caused mainly by heat loss and depends sensitively on the liquid mass flow. Nevertheless, at the injection position the temperature difference is still the largest between liquid and gas phase; the temperature difference is between 2.5 K and 6 K, roughly (listed in Table 6.3). According to this, the main part of condensation occurs near the injection. If the saturation temperature is achieved, the ongoing condensation is caused by the heat loss at the Titanium pipe.

	4.0 MPa						6.5 MPa					
	C	E	G	J	M	P	C	E	G	J	M	P
151	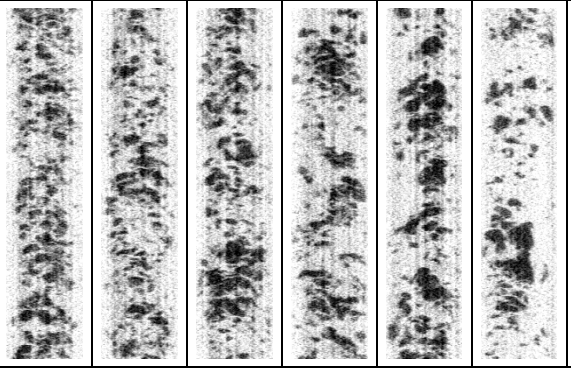						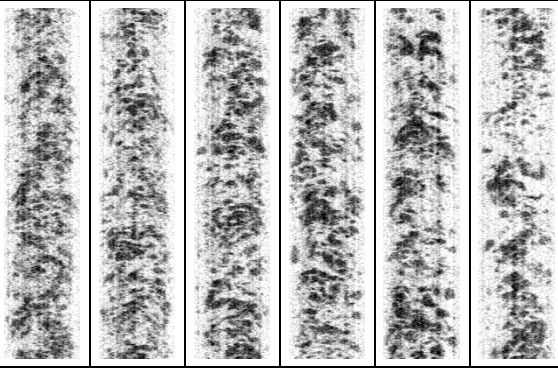					
163	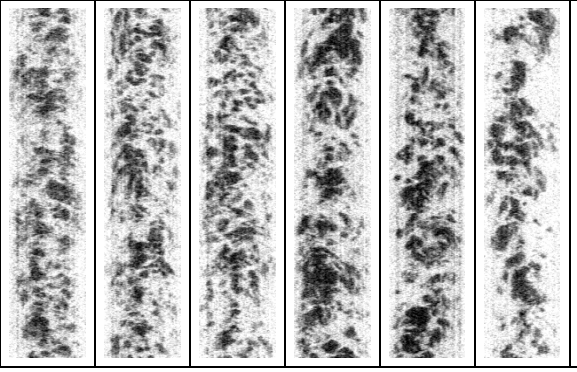						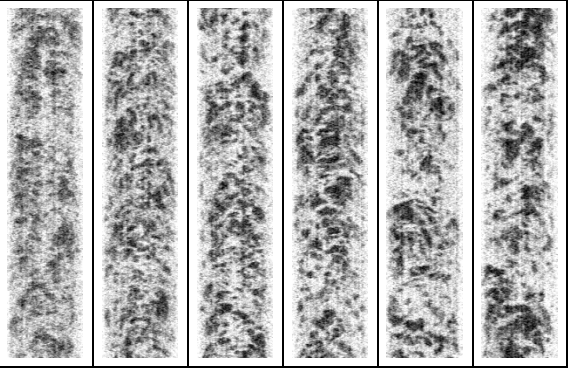					

Figure 6.10: Side cut views for exemplary D19 measurements 151 (2x2500Hz) and 163 (1x5000Hz) for all measurement positions

For the third aspect, decreasing condensation with increasing pressure, assessed values obtained from operational system are listed in Table 6.3. To assess the condensation rate, a flow and heat balances were used basing on measured operational variables. Knowing the liquid sub-cooling at water inlet, heat loss in steam titanium pipe as well as pressure and temperature, the change of internal energy can be estimated. Considering the evaporation enthalpy, the condensing steam mass flow can be assessed. This absolute condensing mass flow is for both pressure stages mostly similar. The reason for the lower condensation rate at 6.5 MPa lays in the larger injection gas mass flow. Because of the different pressure, the density values of steam are different: 20.090 kg/m³ at 4.0 MPa and 33.639 kg/m³ at 6.5 MPa. Therefore, the injected steam mass flow must be still higher and the condensation rate is less, which can be observed in the side cut views in Figure 6.10.

Table 6.3: Assessed condensation at D19 measurements using operational data

	4.0 MPa			6.5 MPa		
	Sub-cooling @ water inlet [K]	Condensed gas mass flow [kg/s]	Condensation rate [%]	Sub-cooling @ water inlet [K]	Condensed gas mass flow [kg/s]	Condensation rate [%]
151	2.70	0.0159	39.64	2.39	0.0162	24.54
160	4.46	0.0108	17.51	5.97	0.0160	15.43
163	2.29	0.0209	33.73	2.29	0.0239	22.98
173	3.26	0.0189	19.46	2.98	0.0198	12.26

Quantitative data are presented in Figure 6.11, Figure 6.13 and Figure 6.14 for the examples shown in Figure 6.10. All radial gas volume fraction profiles show a core peak and a decrease towards the pipe wall. This is caused by the near centre position of large bubbles, similar to the upward air-water flows, and the condensation of smaller bubbles due the temperature gradient near to the pipe wall. As described above, the gas volume fraction at 6.5 MPa experiments is larger than at 4.0 MPa ones caused by the lower relative condensation.

The profiles reflect the observed condensation effects described above: The gas distribution profiles with the highest values are at position C in all cases. Steam condensates up to position J due the subcooled injected water.

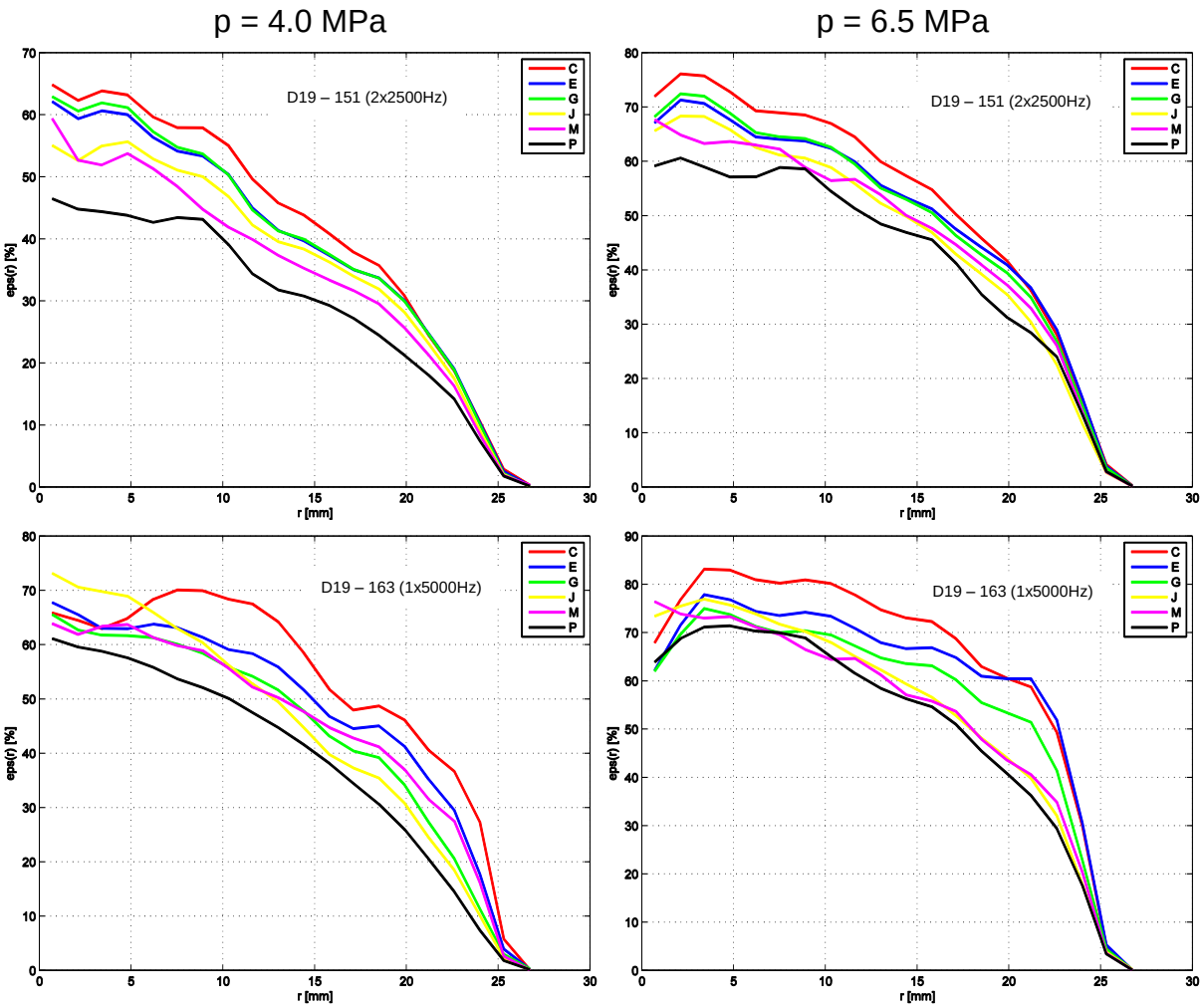

Figure 6.11: Radial gas fraction profiles for exemplary D19 measurements 151 (2x2500Hz) and 163 (1x5000Hz)

A deeper view into the condensation effect is given in Figure 6.12, where the integral gas volume fraction values are plotted against the diameter length of the measurement positions. The general trend of these sequences shows a rapidly decreasing near to the injection, followed by a slightly gas volume fraction decreasing. In some cases, at position M (L/D = 23) the gas volume fraction value is little bit greater than at the surrounding values. Combined with the error bars of 8% of measured value, these increased values are inside of measurement uncertainties. Only the measurement 160 at 4.0 MPa shows a slight continuous increasing of gas

volume fraction. Despite careful checkups, there was found no reason for this single result.

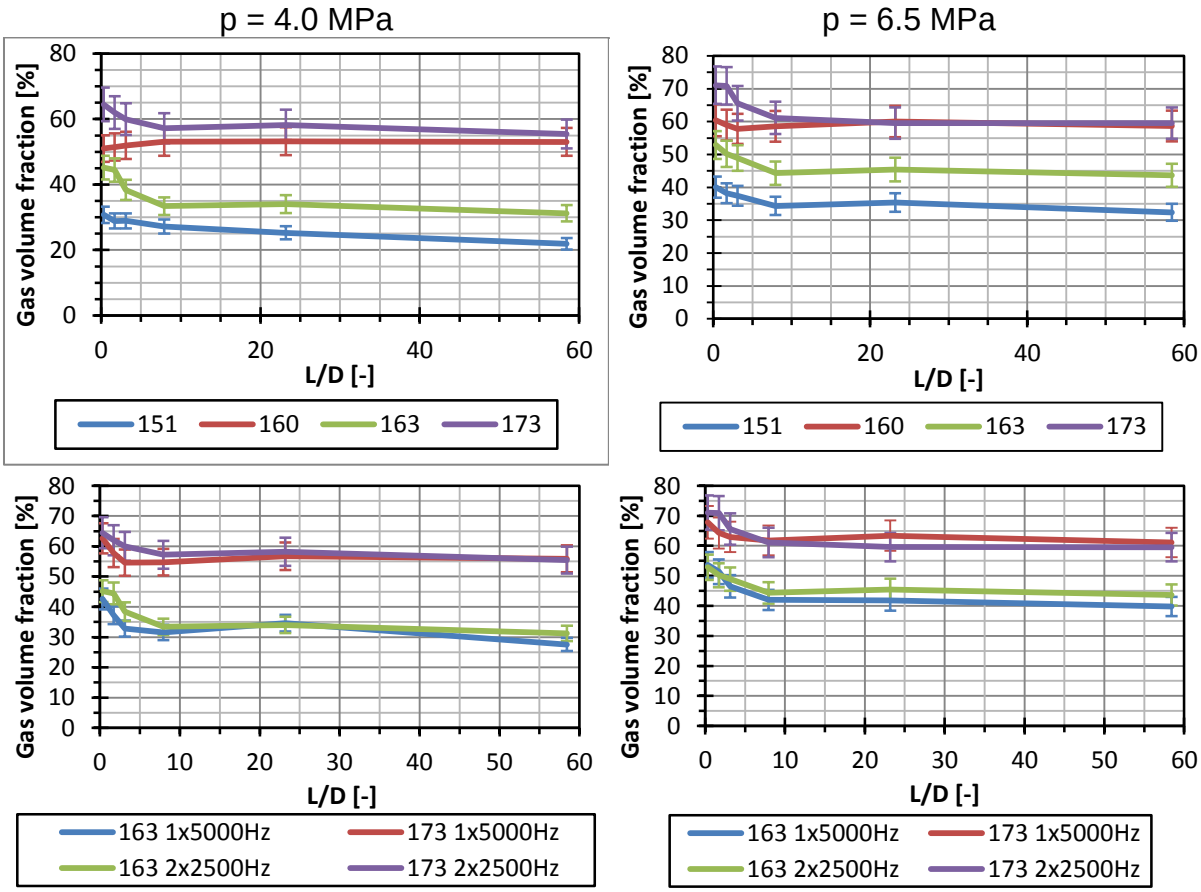

Figure 6.12: Development of gas volume fraction against measurement position in diameter length. Upper row: 2x2500Hz measurements, Lower row: Comparison of 1x5000Hz measurements with 2x2500Hz ones

In Figure 6.13 examples for radial velocity profiles are presented. A general trend is obviously: With increasing flow length, the steam center velocity is decreasing as well as the steam velocity near the wall is increasing slightly. This effect can be explained mainly with one reason: Obstacle effects due the gas injection module M4. Remembering to the mesh above the injection bends shown in Figure 2.3, the resulting narrowing provokes an acceleration of gas which flows particularly in the center (due the 2 mm ring of the mesh near to the wall). So a calmed range near to the wall is created. These reasons are confirmed due the still similar profiles of positions J, M P, where the main part of flow development after an obstacle is occurred up to the position J, where L/D=8. The mostly constant averaged velocity values are presented in Table 6.4. So the profile shape changing is caused mainly by the gas injection module.

An effect, which was expected but not observed is the decrease of specific volume due condensation. If steam condenses the volume flow will decrease. According to the continuity relationship, the velocity will decrease slightly too.

Table 6.4: Averaged velocity for exemplary D19 measurements 151 (2x2500Hz) and 163 (2x2500Hz)

	Averaged gas velocity $\bar{u}_{axial}$ [m/s]			
	4.0 MPa		6.5 MPa	
	151	163	151	163
C	1.479	2.292	1.512	2.378
E	1.482	2.268	1.521	2.348
G	1.483	2.262	1.526	2.390
J	1.482	2.267	1.536	2.414
M	1.470	2.264	1.534	2.376
P	1.449	2.266	1.543	2.369

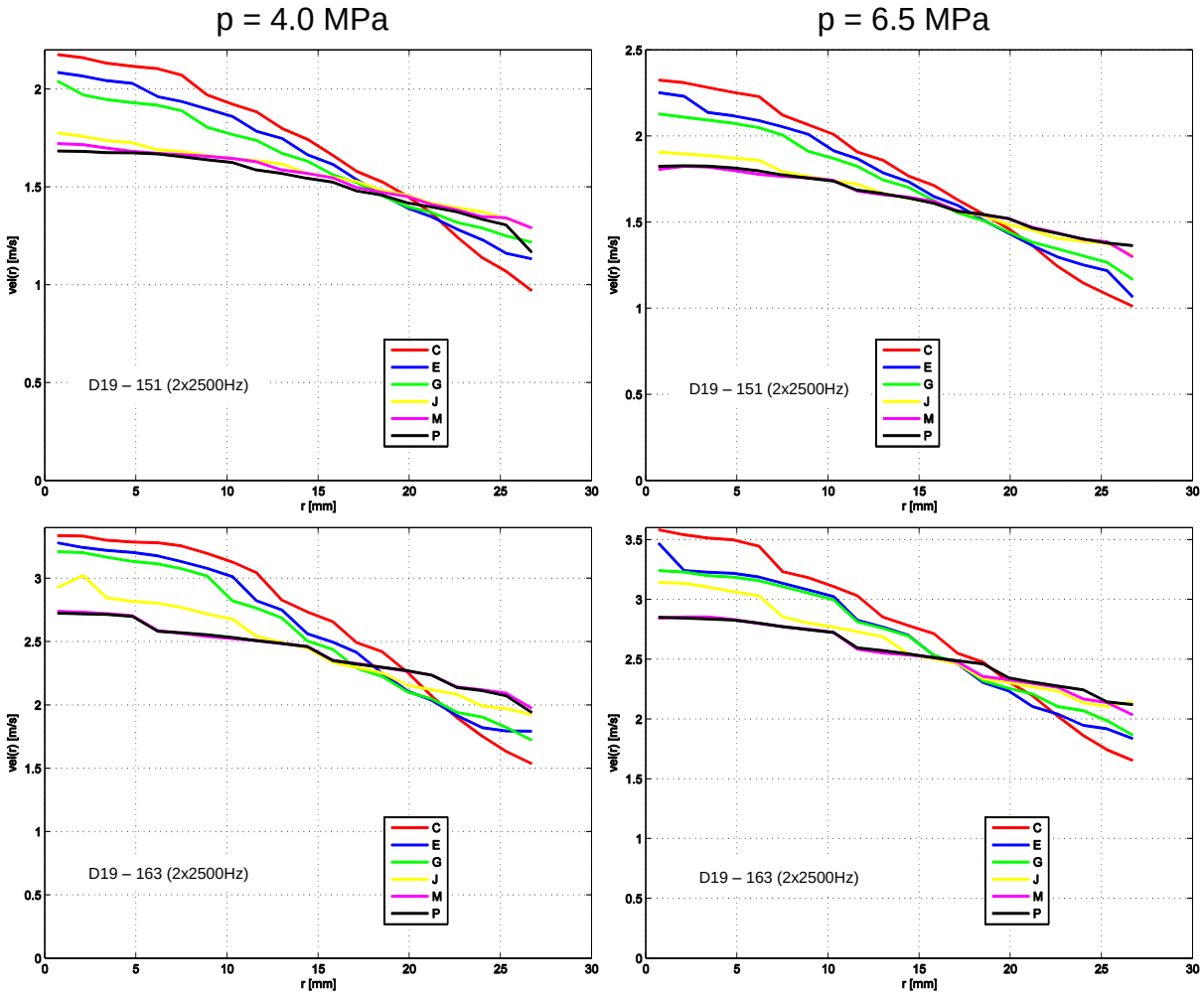

Figure 6.13: Radial velocity profiles using cross-correlation for exemplary D19 measurements 151 (2x2500Hz) and 163 (2x2500Hz)

Bubble size distributions are shown in Figure 6.14. The condensation effects described above and flow distribution effects are visibly. Near to the injection there are mostly small bubbles with a sphere equivalent diameter up to 15 mm. Larger bubbles are created by bubble coalescences. So, at the M and P positions the part of large bubble structures is the highest, the number of small bubbles is reduced mostly by condensation at the pipe wall due heat loss. For the positions J, M and P, the distributions are similar. This fact endorses the observation described above, that the main part of condensation is done in the lower pipe section by the warming of injected subcooled water.

In all shown bubble size distributions the result at position G shows a little bit larger bubbles than at position C. While the integral gas holds up values show good results, the bubble sizes at position C are a little bit overestimated due spaced small bubbles. Therefore, a lot of them are coalesced artificially.

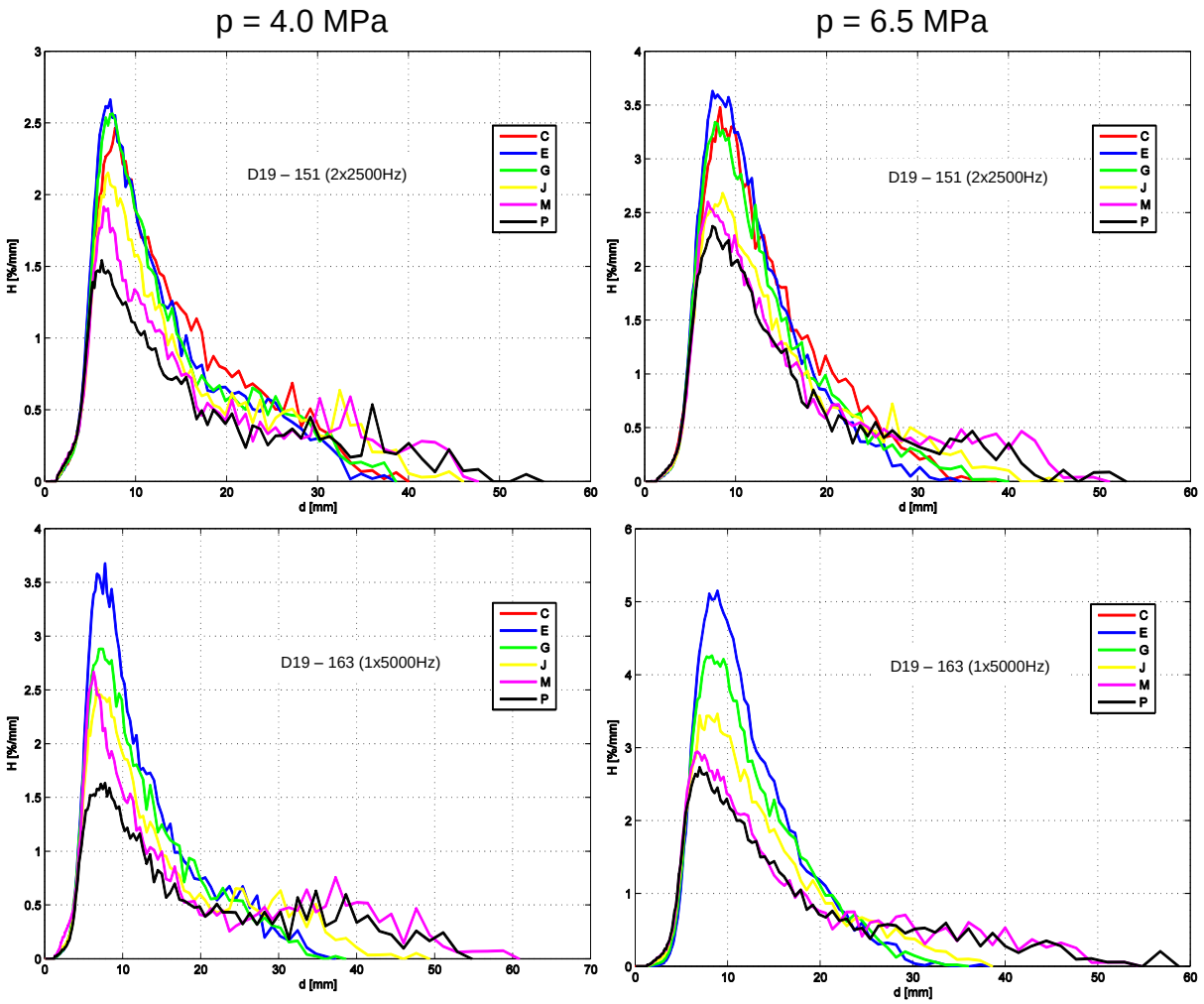

Figure 6.14: Bubble size distributions for exemplary D19 measurements 151 (2x2500Hz) and 163 (1x5000Hz, with velocities from 2x2500Hz measurements)

In Table 6.5 the resulting superficial gas velocity is estimated using the measurements of ROFEX and WMS. The assessed values are calculated with operational data: The condensed steam mass flow is calculated from the heat balance considering heat losses at titanium and steam pipe. The thermodynamic properties of water and steam are estimated using Wagner and Kretzschmar (2008). The difference between injected steam mass flow and condensed mass flow is assumed as steam mass flow at the top of the pipe. So it is assumed also, that the condensation of steam between P position of ROFEX, WMS position and pipe outlet can be neglected. This assumption is endorsed by the results presented above. Knowing the steam mass flow, steam density and cross sectional pipe area, the gas superficial velocity can be calculated.

The uncertainties in Table 6.5 are estimated by error propagation, where the maximum uncertainties are taken. For the ROFEX uncertainties the void error is assumed with 8% (Banowski et al., 2015) and the velocity one is taken from Table 5.2. The error of the WMS is calculated with void underestimation up to -4% (Prasser,

et al., 2005) and a velocity discretization error estimated similar to Table 5.2. The assessment error is estimated using the uncertainties from Table 2.3. In Figure 6.15 the values from Table 6.5 are presented as chart diagram.

Table 6.5: Comparison of injected, assessed and measured gas superficial velocities for the D19 2x2500Hz measurements at ROFEX and WMS as well as their uncertainties

		j_g injected [m/s]	j_g Measurement [m/s]			Uncertainties [%]			
			Assess-ment	ROFEX	WMS	Assess-ment	ROFEX	Upper error WMS	Lower error WMS
4.0 MPa	151	0.835	0.5094	0.3485	0.4586	14.90	16.27	4.62	0.65
	160	1.305	1.0748	0.7076	0.8333	5.56	15.74	4.64	0.62
	163	1.305	0.8668	0.7661	0.7236	12.77	20.49	4.84	0.97
	173	2.038	1.6484	1.2662	1.4505	6.19	21.16	4.98	1.03
6.5 MPa	151	0.835	0.6283	0.4691	0.5789	9.42	18.03	4.61	0.66
	160	1.305	1.1083	0.7117	0.8403	4.57	16.35	4.62	0.62
	163	1.305	1.0092	0.8456	0.9033	8.57	23.00	4.89	0.99
	173	2.038	1.7896	1.3032	1.6159	4.76	22.44	4.98	1.03

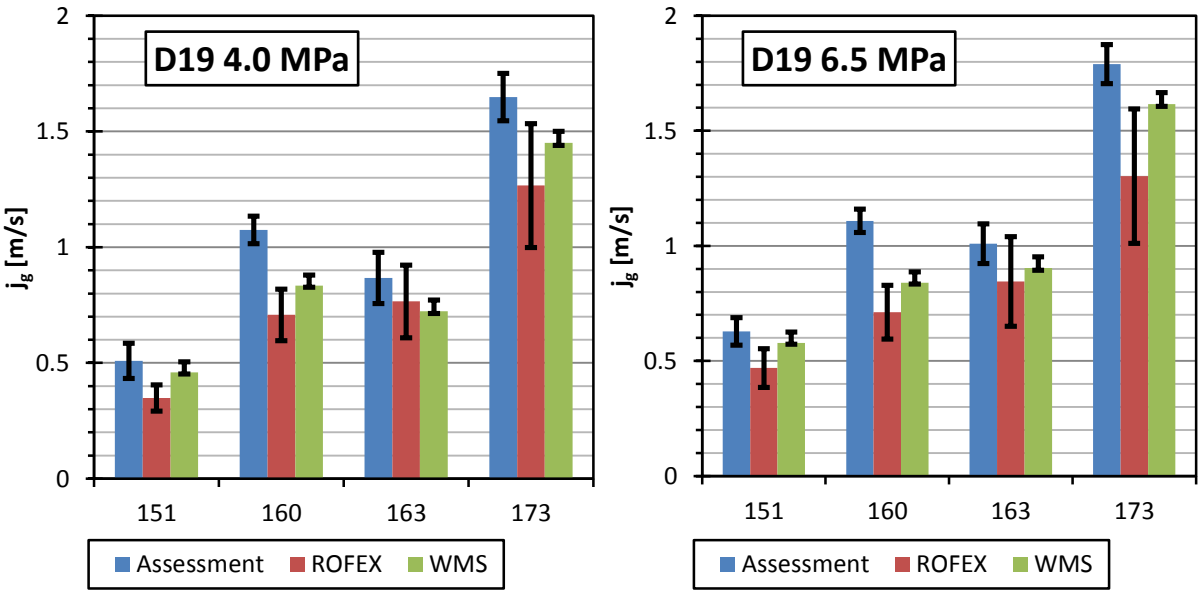

Figure 6.15: Chart of assessed and measured gas superficial velocities of D19 measurements at ROFEX and WMS, given in Table 6.5

6.2. Counter current flows

Counter-current flow is obtained for cases with low downward liquid flow rates, which allow the bubbles to rise upwards.

Figure 6.16 presents the test matrix. The flooding line published by Taitel and Barnea (1983) is added. Beside the condition of low liquid downward velocity there is also a limitation in gas flow rate since the gas accumulates in the pipes above the vertical test section during the experiment (see section 2.2.1). To limit this effect only gas superficial velocities below 0.01 m/s were investigated. Under these conditions, the developing gas cushion on the highest point of the test facility is small enough to neglect the increasing pressure condition during the experiments. All six points were

measured with 2x1000 Hz at the measurement positions A, D, G, J, M and P. The module M3 was used as gas injection module. The overall measurement time amounts 10 s per position. At the top of the pipe, a fixed pressure of 0.4 MPa was adjusted (see 2.2.4). For detailed information about the liquid and gas temperatures see 2.2.4 and appendix 9.3.

		Superficial velocity gaseous phase																
	[m/s]	0,0025	0,004	0,0062	0,0096	0,0151	0,0235	0,0368	0,0574	0,0898	0,14	0,219	0,342	0,534	0,835	1,305	2,038	3,185
Superficial velocity liquid phase	-4,0470	011	022	033	044	055	066	077	088	099	110	121	132	143	154	165	176	187
	-2,5540	010	021	032	043	054	065	076	087	098	109	120	131	142	153	164	175	186
	-1,6110	009	020	031	042	053	064	075	086	097	108	119	130	141	152	163	174	185
	-1,0170	008	019	030	041	052	063	074	085	096	107	118	129	140	151	162	173	184
	-0,6410	007	018	029	040	051	062	073	084	095	106	117	128	139	150	161	172	183
	-0,4050	006	017	028	039	050	061	072	083	094	105	116	127	138	149	160	171	182
	-0,2550	005	016	027	038	049	060	071	082	093	104	115	126	137	148	159	170	181
	-0,1610	004	015	026	037	048	059	070	081	092	103	114	125	136	147	158	169	180
	-0,1020	003	014	025	036	047	058	069	080	091	102	113	124	135	146	157	168	179
	-0,0641	002	013	024	035	046	057	068	079	090	101	112	123	134	145	156	167	178
	-0,0405	001	012	023	034	045	056	067	078	089	100	111	122	133	144	155	166	177

Figure 6.16: Test matrix for the counter-current air-water flow regimes (L17). The red line represents the flooding line and the part below the blue line the only region for bubble flows given by Taitel and Barnea (1983). The liquid superficial velocities deviate from the matrix values! The corrected values are given in Table 6.6.

Two effects concerning the data acquisition were noticed after conducting the measurements: First, a water mass flow device had a wrong zero-point-calibration function. Using the recalibration function, the measured liquid mass flow and therefore the superficial liquid velocity was corrected. Second, due the fact of gas accumulation in the pipe system above the vertical titanium pipe, the gas displace the water as discussed above. This increasing gas volume provokes an increasing downward liquid superficial velocity. The increase amounts exactly the value of the injected superficial gas velocity. In Table 6.6 the corrected superficial liquid velocities considering the described effects above are presented.

Table 6.6: Corrected values for superficial liquid velocities at L17 measurements

Matrix point	001mod	002mod	003mod	034mod	035mod	036mod
Corrected j_{liquid} [m/s]	-0.0352	-0.0601	-0.0997	-0.0422	-0.0672	-0.1067

All the investigated matrix points are in the bubbly flows regime. Figure 6.17 presents side cut views of the matrix point 36 with the highest gas volume fraction in the bubble flow region of Figure 6.16. The large sausage-shaped bubbles at the measurement positions M and P are very slow bubbles. In the position A the differences between the two layers are caused by the small distance between the injection and the first tomography layer. It is only 1 mm above the injection needles, while the upper layer position amounts 11 mm above the needles. Maybe, there is much calescence of bubble very close to the injection. The bubble line is not in the center because the gas injection was done using 3 needles.

	A		D		G		J		M		P	
	Upper	Lower	Upper	Lower	Upper	Lower	Upper	Lower	Upper	Lower	Upper	Lower
036	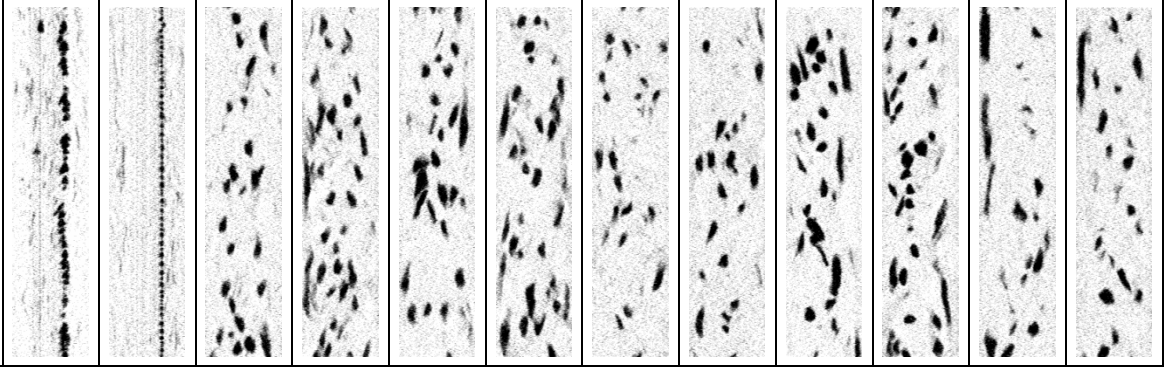											

Figure 6.17: Side cut views of reconstructed raw data of the measurement L17 – 036

Table 6.7 presents the gas volume fraction averaged over time, cross section and both measuring layers. The position A values are taken only from the upper plane, caused by the bubble effect described above. In addition the values are plotted against their measurement positions in diameter/length-ratio (L/D) in Figure 6.18. For the three measurements with higher gas flow rate (34 - 36), the values at D and G tend to form a maximum. Eventually these increased gas volume fractions could results from a recirculation zone above the injection module. Caused by the central gas injection, the bubbles displace the liquid towards the pipe periphery, where it is accelerated. The local liquid velocity is larger than the bubble drift velocity and some bubbles move downward. Considering the upward bubble injection, a recirculation zone can possibly be created. Such an effect was also observed in pre-tests for counter-current slug flows in a transparent pipe. Due to the larger injected gas volume fraction in these pre-tests, the resulting downward liquid velocity was more increased as for the L17 tests, so that the recirculation zone may caught the injection module. Hence the recirculation zone for the L17 tests stays near the positions D and G caused by the lower gas volume fraction. General, the increasing gas volume fraction with increasing measurement level agrees with the decreasing hydrostatic pressure.

Table 6.7: Gas volume fraction results from the L17 measurements

Matrix point	A [%]	D [%]	G [%]	J [%]	M [%]	P [%]	S [%]	Expected value [%]
001	0.634	0.776	0.945	0.980	1.013	1.221	2.069	1.236
002	1.022	0.990	0.966	1.060	1.086	1.152	2.151	1.409
003	0.861	1.045	1.176	1.330	1.439	1.602	2.798	1.814
034	2.994	4.865	4.783	4.692	4.878	5.127	8.170	4.743
035	2.861	6.348	5.679	5.474	6.206	6.356	8.875	5.411
036	5.465	10.748	11.269	7.909	9.222	8.120	10.690	6.962

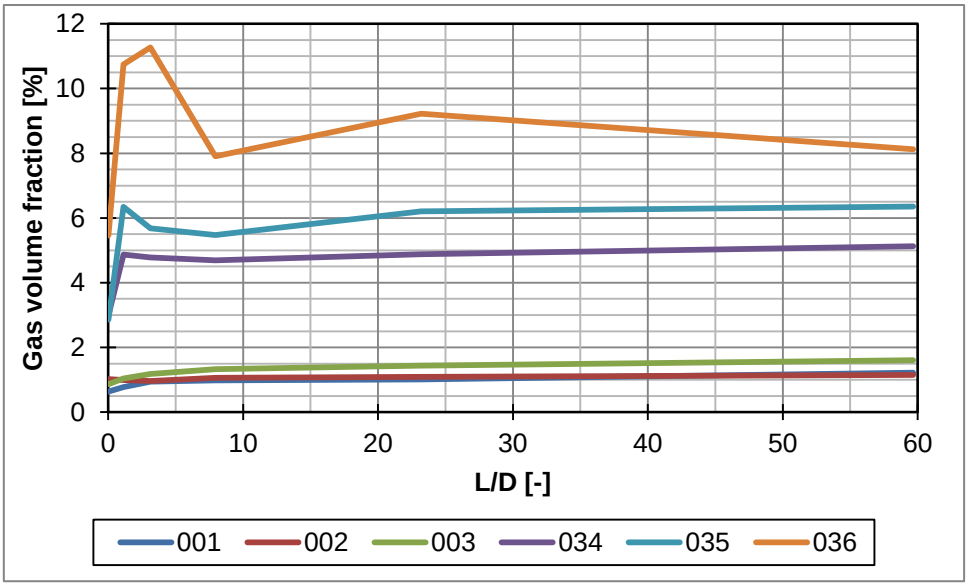

Figure 6.18: Gas volume fraction values from Table 6.7 plotted against L/D of measurement position

In Figure 6.19 exemplary radial gas profiles of the points 003 and 035 are shown; the resulting profile for the position A shows very large and rapidly decreasing gas peaks above the injection needles (in the center for 003 and above the 3 outer needles in case 035). In the 003 case, the evolution of the profiles is dominated by a flattening with increasing level. The 035 case shows approximately a homogeneous gas distribution starting from position D. This is the effect of the recirculation zone. The profile development from D to J tend to a slight core peaking, before the profiles in M and P become flatter.

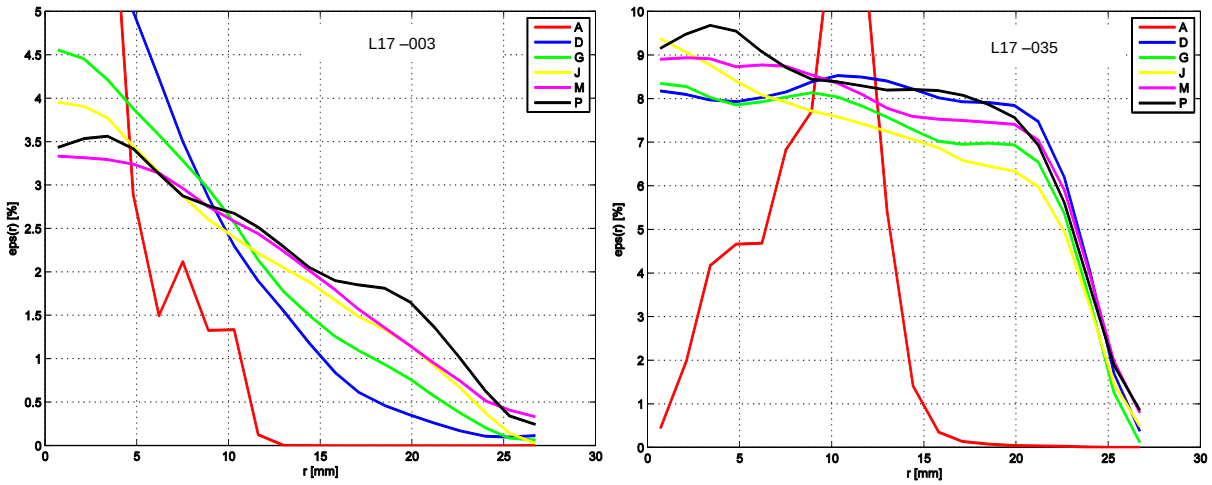

Figure 6.19: Radial gas volume fraction profiles. Left side: 003, right side: 035. All profiles show the results from the upper layer

In Figure 6.20 velocity profiles and bubble size distributions are presented for 035 measurements using two different methods for the evaluation of the gas velocity, the morphological one as well as the cross-correlation one. General, the profiles in the region between the pipe center and the radial position r = 20 mm are rather similar. The flatting profiles start from about bubble drift velocity (0.235 m/s) in the center and decrease down to about 0.1 m/s. Near pipe wall the morphological velocity profiles show a rapid increase to center velocities. This is in clear contrast to the cross-correlation results. With a view to both bubble size distributions, all bubbles have a

sphere equivalent diameter less 10 mm. Therefore, the bubble drift velocity can be assumed to about 0.23 – 0.25 m/s. Subtracting this value from the profiles, the liquid velocity profile can be estimated. While the liquid profile from the morphological method fulfil the wall adhesion condition $u_{liquid,\ wall} \approx 0$ m/s, the near wall downward velocity of liquid phase would be high according to the velocity profiles obtained by the cross-correlation method. Therefore, the velocity profiles estimated by the morphological method seem to be more reliable. Because of the individual bubble velocity, the bubble size distribution is also probably more accurate. Comparing both distributions, the one obtained by the morphological method is clearly sharper. The peak position for all measurement positions is still the same between 5 mm and 6 mm.

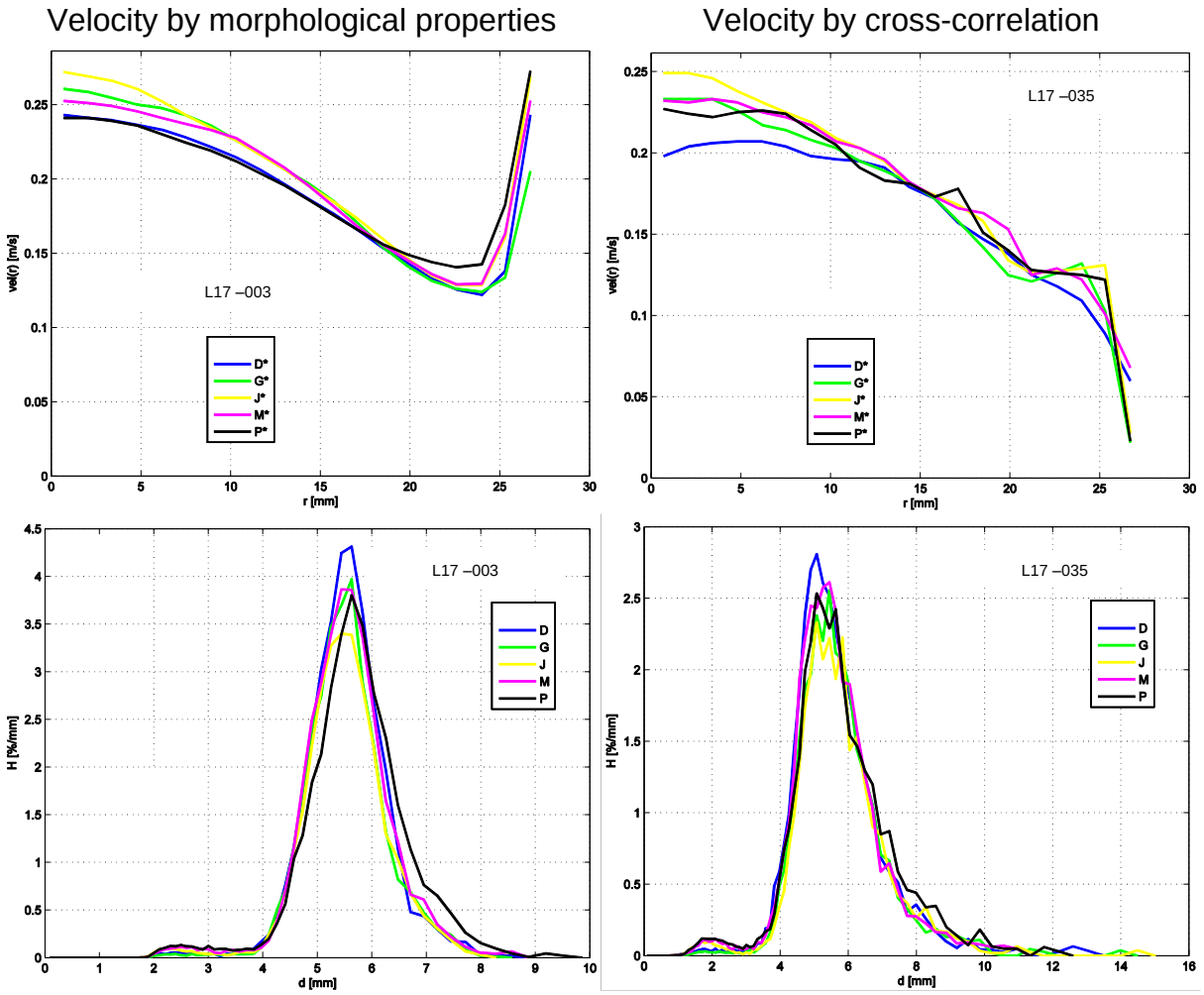

Figure 6.20: Velocity profiles (upper ones) and bubble size distributions (lower ones) of L17 035, upper layer. Left side: Velocity estimated by morphological bubble properties, right side: velocity estimated by cross-correlation method

An important tool for checking the accuracy of measurement and evaluation is the calculation of gas superficial velocity using gas volume fraction and velocity results according to Beyer et al. (2008). In Table 6.8 these results are presented for all L17 measurements at all levels using the morphology method. Similar to Table 6.7, the results are averaged from lower and upper tomography layer. Only at position A, the superficial velocities are too small, caused by the injection effect. The overestimation in the values for 036 D and G is probably caused by the aforementioned recirculation zone and the limitation of the morphological method to consider only positive

velocities. Comparing all other values, the latter effect of only positive bubble velocities comes not strongly into the picture.

Table 6.8: Estimated superficial gas velocity from morphological velocity method, pressure corrected to injection condition

Matrix point	A [m/s]	D [m/s]	G [m/s]	J [m/s]	M [m/s]	P [m/s]	j_g [m/s]
001	0.0014	0.0023	0.0025	0.0024	0.0024	0.0026	0.0025
002	0.0021	0.0023	0.0024	0.0023	0.0023	0.0020	0.0025
003	0.0017	0.0022	0.0022	0.0023	0.0024	0.0024	0.0025
034	0.0052	0.0092	0.0096	0.0095	0.0092	0.0094	0.0096
035	0.0052	0.0101	0.0094	0.0093	0.0101	0.0098	0.0096
036	0.0081	0.0112	0.0108	0.0096	0.0096	0.0092	0.0096

6.3. Downward flows

6.3.1 Air-water flows

The test matrix for air-water downward flows is presented in Figure 6.21. The two experimental series correspond to the different gas injector modules M3 (L20) and M4 (L21), similar to the upward flows. The chosen frequencies are 2x1000 Hz, 2x2000 Hz and 2x2500Hz, depending on the expected velocities. The measurement positions are A, D, G, J, M and N for L20 as well as NN for L21. The different measurement positions N and NN are caused by technical limitations at the bottom mounting flange. The different values for level A have to be accepted due to the different gas injection modules. At the highest position, the sifting is limited by the maximum elevation length for the tomography system. Nevertheless, both positions have a flow length of L/D=56, rounded to an integer value.

The overall measurement time is again 10 s for each single measurement. The pressure and temperature boundary conditions were described in 2.2.4.

		Superficial velocity gaseous phase																
	[m/s]	-0,0025	-0,0040	-0,0062	-0,0096	-0,0151	-0,0235	-0,0368	-0,0574	-0,0898	-0,1400	-0,2190	-0,3420	-0,5340	-0,8350	-1,3050	-2,0380	-3,1850
Superficial velocity liquid phase	-4,0470	011	022	033	044	055	066	077	088	099	110	121	132	143	154	165	176	187
	-2,5540	010	021	032	043	054	065	076	087	098	109	120	131	142	153	164	175	186
	-1,6110	009	020	031	042	053	064	075	086	097	108	119	130	141	152	163	174	185
	-1,0170	008	019	030	041	052	063	074	085	096	107	118	129	140	151	162	173	184
	-0,6410	007	018	029	040	051	062	073	084	095	106	117	128	139	150	161	172	183
	-0,4050	006	017	028	039	050	061	072	083	094	105	116	127	138	149	160	171	182
	-0,2550	005	016	027	038	049	060	071	082	093	104	115	126	137	148	159	170	181
	-0,1610	004	015	026	037	048	059	070	081	092	103	114	125	136	147	158	169	180
	-0,1020	003	014	025	036	047	058	069	080	091	102	113	124	135	146	157	168	179
	-0,0641	002	013	024	035	046	057	068	079	090	101	112	123	134	145	156	167	178
	-0,0405	001	012	023	034	045	056	067	078	089	100	111	122	133	144	155	166	177

Figure 6.21: Test matrix for co-current downward air-water flow measurements. Yellow: L20 series with gas injection module M3, ruby: L21 series with M4 gas injection module

In Figure 6.22 side cut views of all investigated matrix points are shown for the measurement position L/D=56. The flow pattern in general agrees with the flow pattern map presented by Barnea et al. (1982).

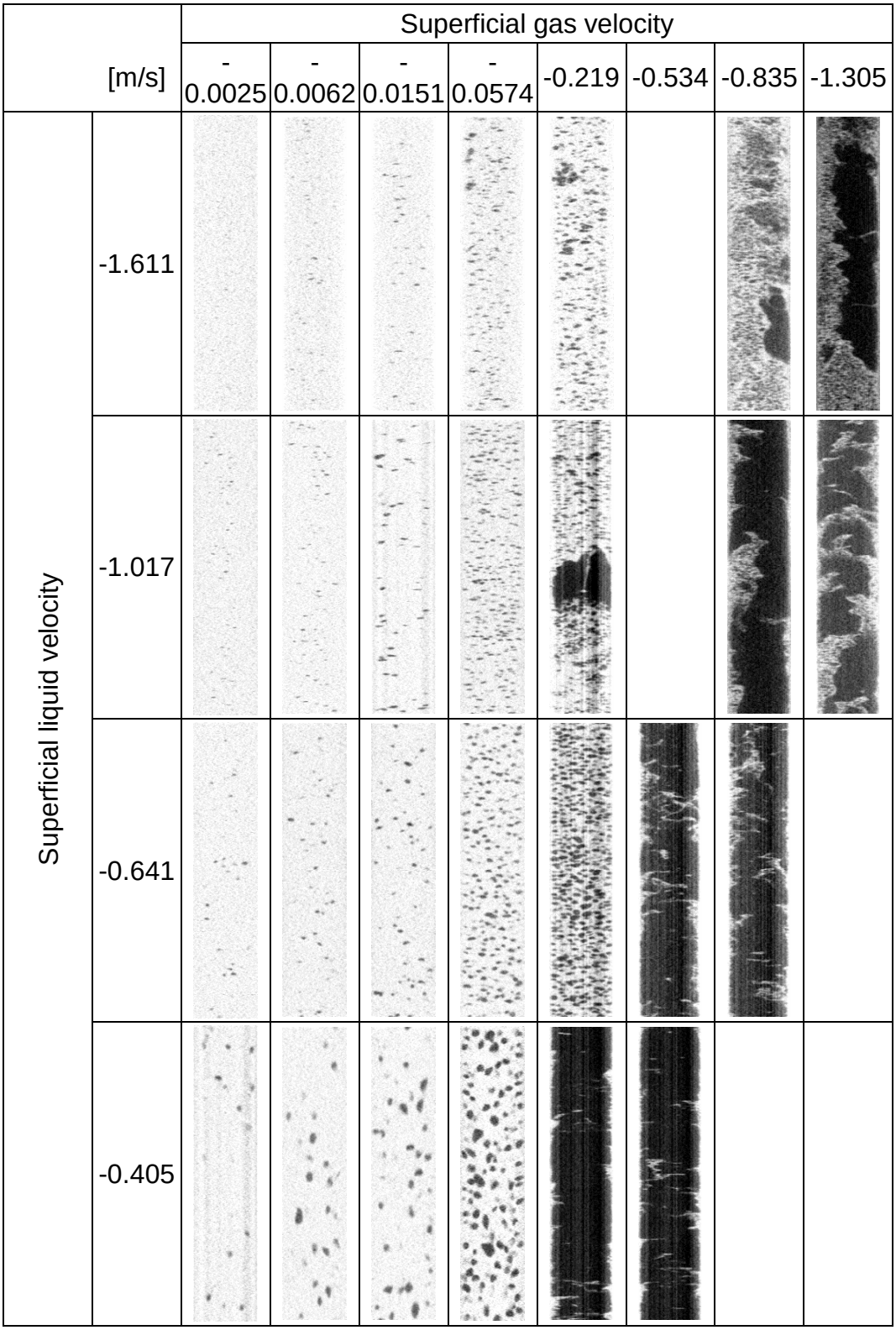

Figure 6.22: Side cut views of downward air-water flow raw data at L/D = 56

The side cut views can also be well discussed basing on the downward two-phase flow map presented by Ishii et al. (2004). In Figure 6.23 this flow map is shown including the conducted L20 and L21 measurements. Basing on the clear regime transitions at upward flows from bubbles via slugs to annular flow the two side cut views at jg = -0.219 m/s and jl = -0.641 and -1.017 m/s seem to be interchanged. However, both regimes are part of the “Kinematic shock existence” region observed

by Ishii et al. (2004). This region represents the abrupt transition from bubbly to annular flow regime within the test section and for this reason it is connected with instabilities.

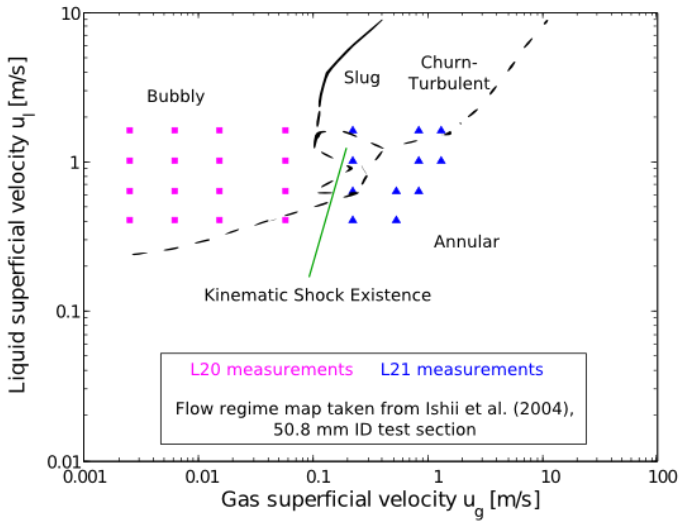

Figure 6.23: The test matrix overlaid by the downward two-phase flow map presented by Ishii et al. (2004)

Additionally in Figure 6.24 side cut views of six selected matrix points are shown for each measured level. For the case 086 of the L20 series (where the injection module M3 was used) a large gas bubble is created at the injection needles. The creation of such a bubble depends on liquid velocity and injected gas volume rate. In the case of the 086 measurements, the “normal” bubbles are developed by shearing from the injection bubble near position G. For the L21 – 116 case annular flow establishes along the pipe. While in positions A and D bubbles are caught in a recirculation zone due the screws of the injection module mesh near the wall (see sections 2.2.2 and 6.1.2), in the other positions, a normal annular flow is developed. Large bubbles as in the 163 case are positioned near to the pipe wall, which can be an indication for the inverted lift force due high liquid downward velocity.

During segmentation process, it was found that there are annular domains near the wall with averaged grey values less than the detected water peak position in many reconstruction data sets of downward flows. This effect is a quasi-inverse problem to the hot spot problem described in section 3.4. It was necessary to revise these regions before the segmentation processes get started. In the upper row of Figure 6.25, an exemplary reconstruction result from the L20 031 N, lower plane, is shown. The low grey value ring near the wall with values less than the water peak at -1 is clearly visible. This ring region provokes a water peak shape containing a rucksack on the left peak side. Due this bulge, the sigmoid function for estimating abort criterion cannot be defined correctly: The minimum search level for pixel agglomeration (rounded inflection point i from equation (3.1), in histogram named “sigmoid coefficient”) and the 95% criterion for the minimum possible bubble core grey value (in histogram named “sigmoid level 2”) have too high values. The result would be a too low gas volume fraction after segmentation.

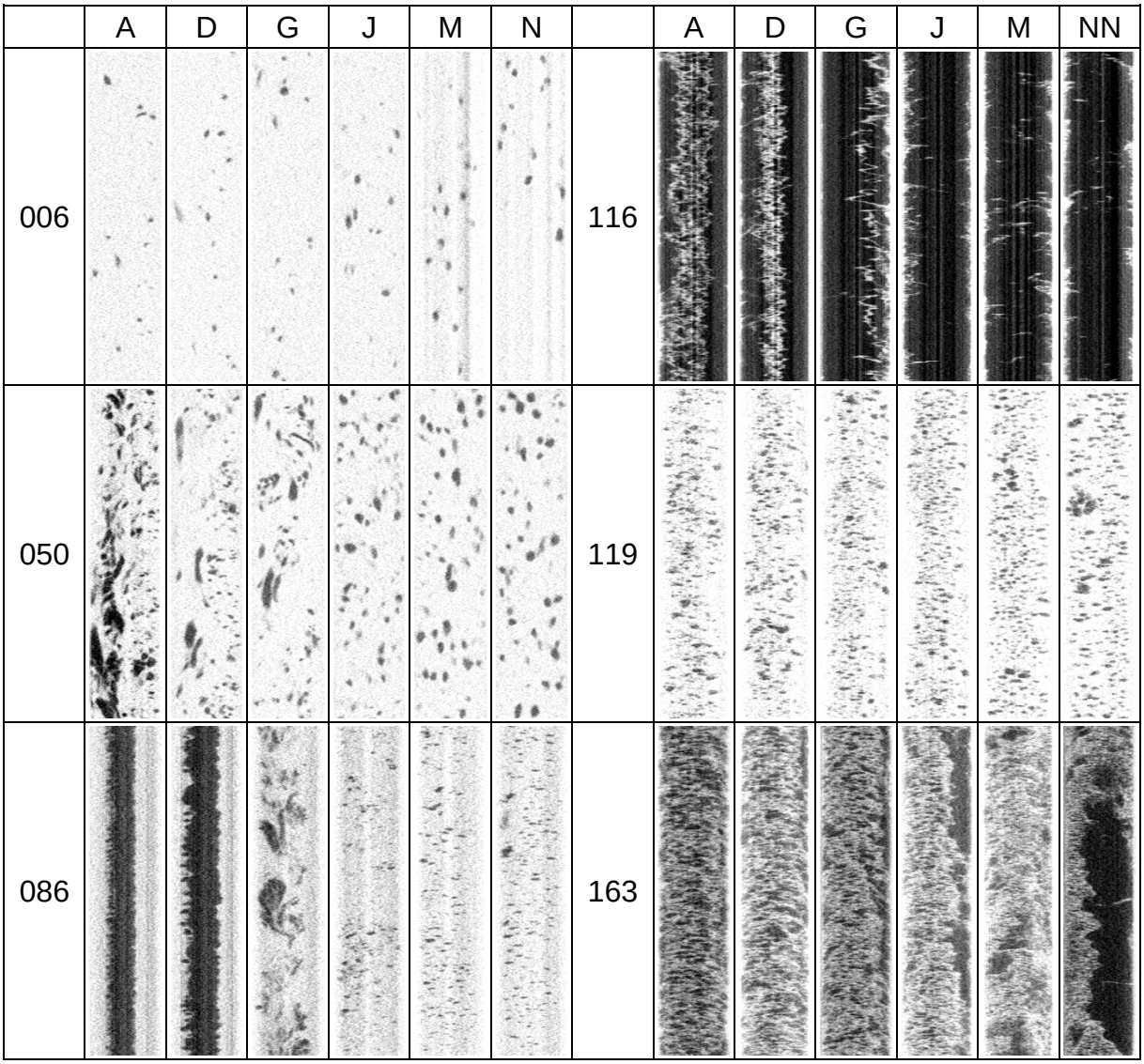

Figure 6.24: Exemplary side cut views for six measured matrix points

To solve this problem, the vectors in time coordinate are recalibrated for all cross-sectional pixels considering the eight-neighbored pixels for a better statistical base. The recalibration was done identically to the one described in section 3.4. The result for the aforementioned example is presented in Figure 6.25, lower row. All pixels inside the ring beside pipe wall have averaged grey values near the detected water peak. As a reason of this histogram recalibration, the sigmoid coefficients can be estimated correctly and therefore, the segmentation of the bubbles can be done satisfyingly.

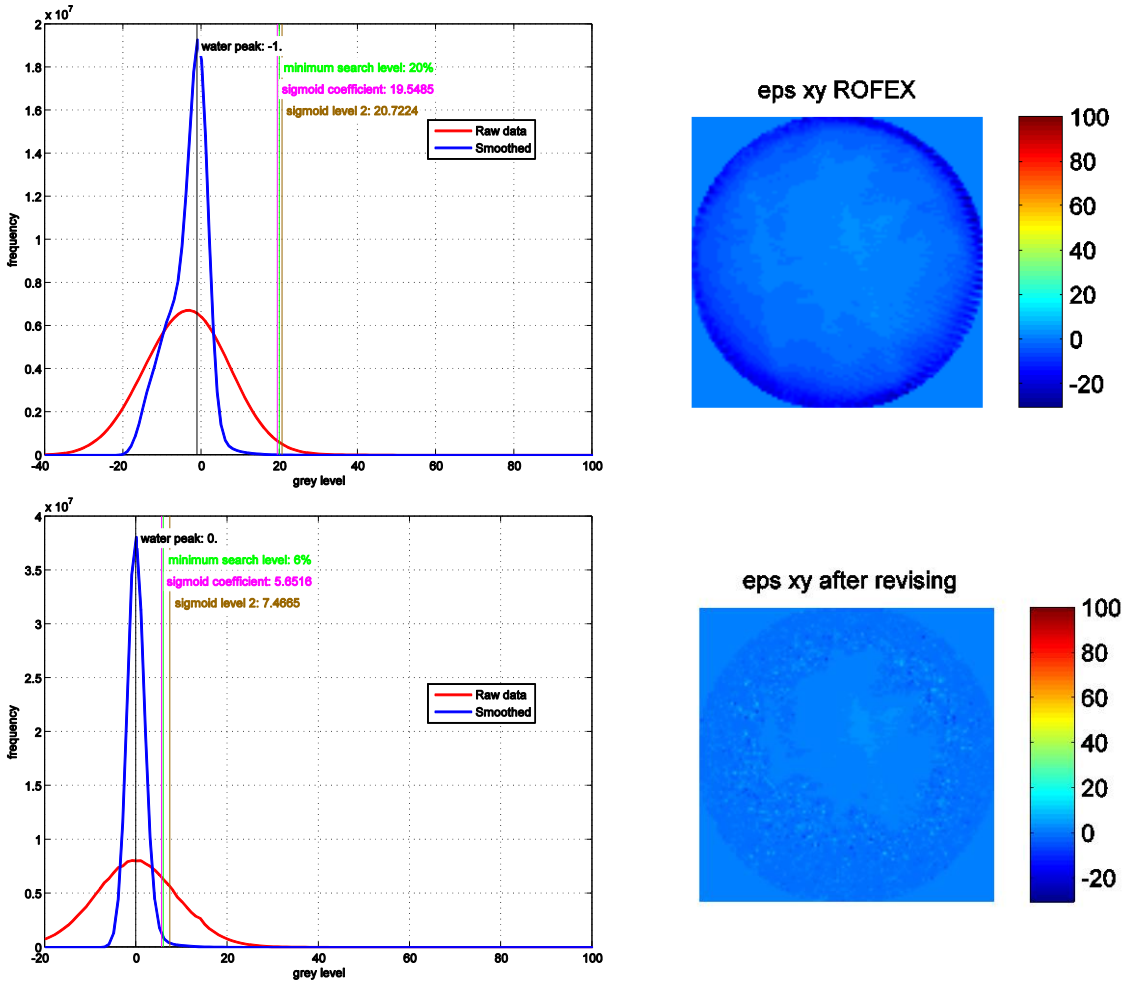

Figure 6.25: Histograms (left side) and time averaged grey value image (right side) of L20 031 N, lower plane measurements. Top: Original reconstruction result, bottom: revised result

In Figure 6.26, radial gas volume fraction profiles for the L20 006 and 050 as well as L21 116 and 119 measurements are presented. While in both L20 examples the injection module affects the profile for position A, all profiles show mostly homogenous cross-sectional gas distribution. Only at the L21 – 119 cases the profile is developing from a decreasing shape to a plateau shape along the flow length. For radius ranges greater than 20 mm, all profiles flatten to zero. This observation confirms the conclusions from Hibiki et al. (2004), Kashinsky and Randin (1999), Oshinowo and Charles (1974), Sun et al. (2004), Usui and Sato (1989), Wang et al. (1987), that gas bubbles in downward flows tend to gas coring effects. The changes of the L21 – 116 profiles from A to G are recirculation effects by the gas injection module as aforementioned.

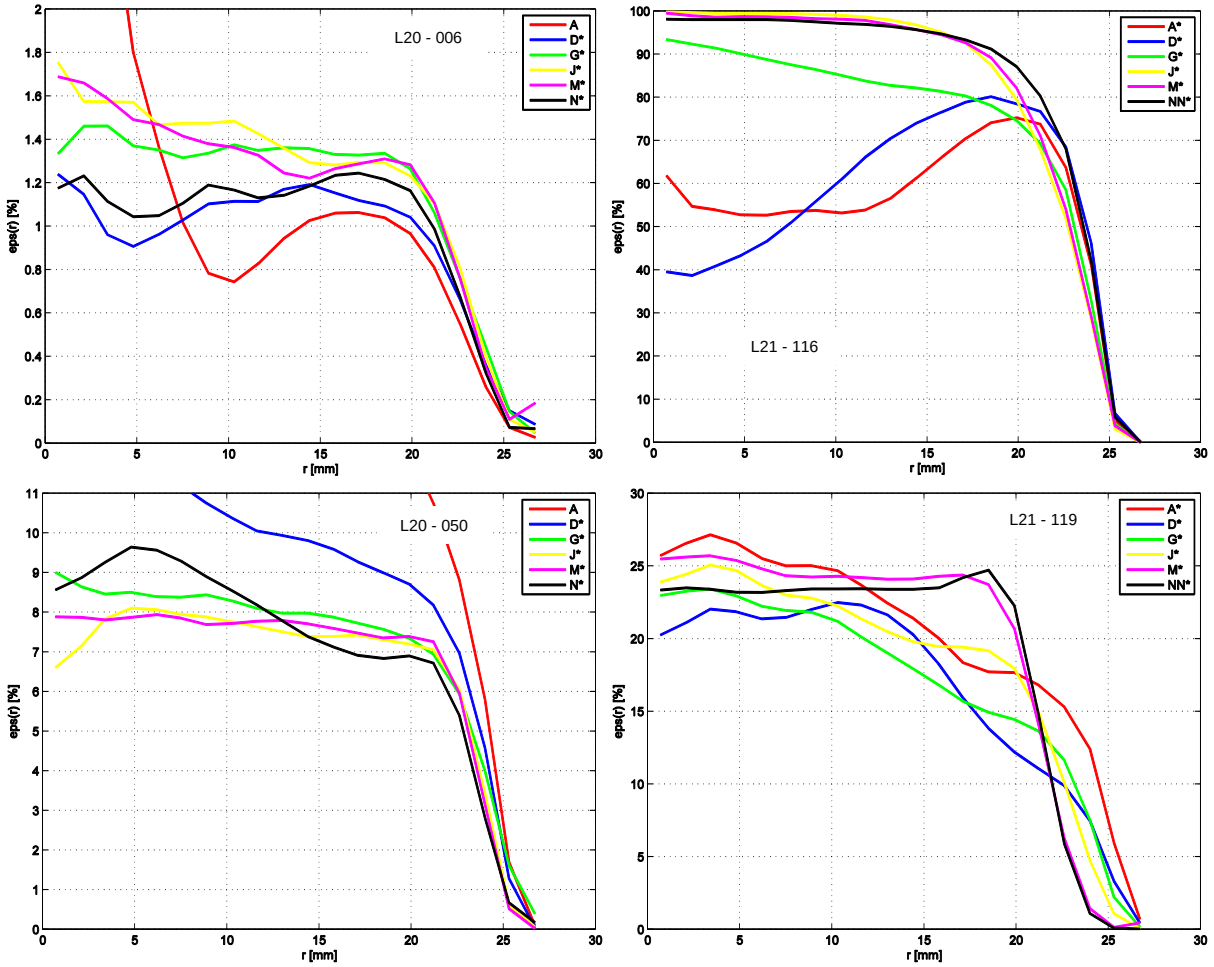

Figure 6.26: Radial gas volume fraction profiles for four exemplary downward two-phase flow cases

The radial gas velocity profiles for the same examples are presented in Figure 6.27. The shown L20 results are determined using the morphological method. In the 006, the profiles near the injection at A and D show the largest velocity values in the radial range where the liquid phase flows between the module and pipe wall. The comparison of the A position profiles of gas distribution and velocity suggest that a recirculation zone exits direct after the injection needle. The bubbles move not directly downwards after center injection, but move a little bit upwards, then to the side into the accelerated downward liquid stream. This explains the high center gas volume fraction and a low downward velocity as well as the low gas volume fraction and high downward velocity at radius range 13 – 22 mm. The velocity profiles for remote positions show a slight flattening profile from center to radius position 23 mm and a fast decreasing toward the pipe wall.

The L20 – 050 profiles show similar trends to the counter-current velocity results. While near the injection the same effect as described above can be observed, the profiles develop to a low velocity range in the center and a larger downward velocity near the wall. Therefore downward bubble flow for this case with relatively low liquid flow rate seems to be very similar to counter current bubble flow with inverse bubble flow direction.

The presented L21 results are determined by using the cross-correlation method. For annular flow as in the L21 – 116 case, the cross-correlation (as also the other

methods) fails to provide the gas velocity. Instead, the velocity of surface waves and notches leads to a maximum in the cross-correlation. Therefore, the velocity values in the 116 profile are too high for the averaged gas velocity. In the bubbly flow case 119, the development of the profiles goes from decreasing shape at position A to a very flat profile shape at position NN. The very high velocity at A is caused by the restriction due the mesh of the gas injector. At D and G, the bubble are decelerated to less velocity values. The rough cross-sectional averaged velocity values of about -1.6 m/s conform to the sum of the superficial gas and liquid as well as the drift velocity.

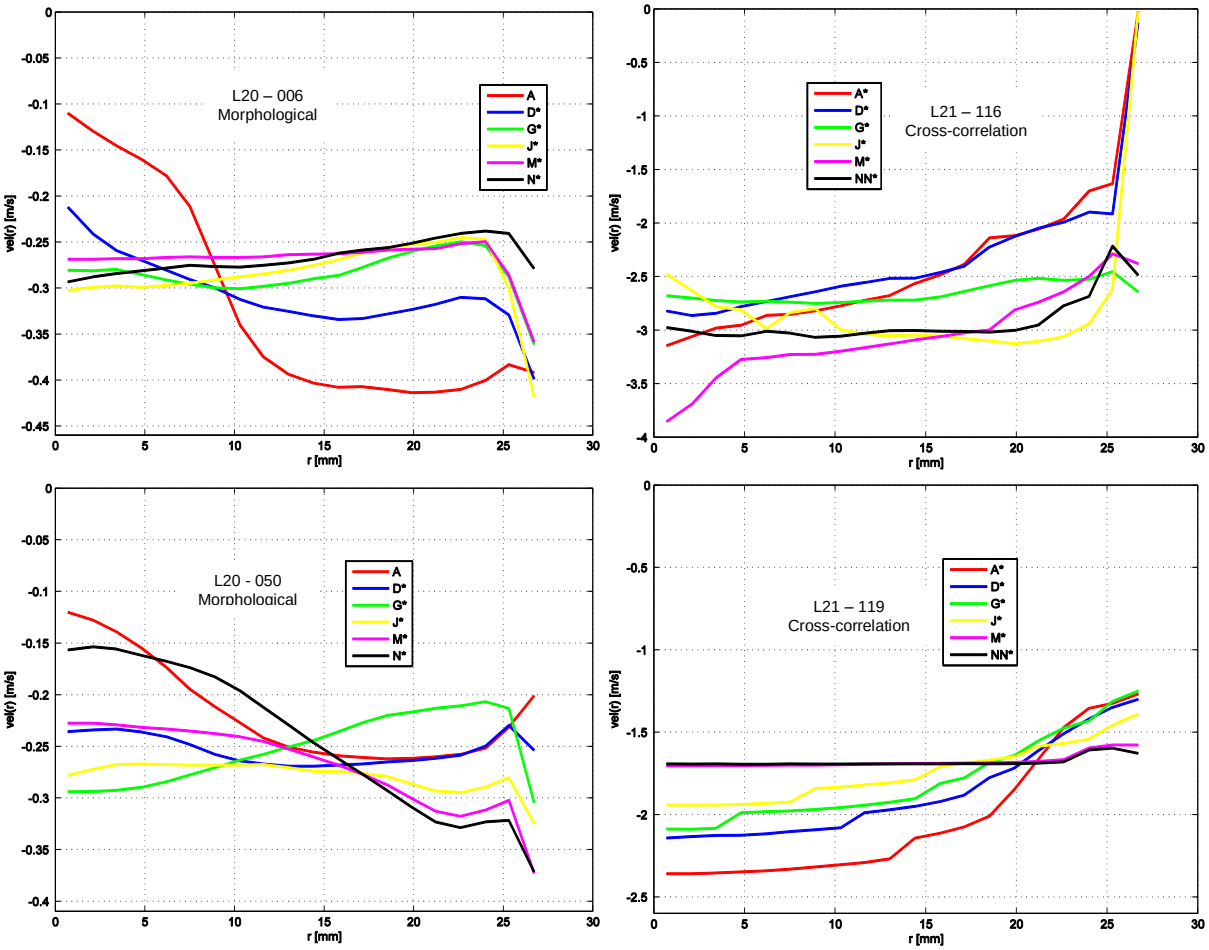

Figure 6.27: Radial gas velocity profiles for four exemplary downward cases

Using the velocity results, the bubble sizes can be calculated. Their distributions are presented in Figure 6.28. For the three cases of bubble flow, the smallest detected bubbles have a sphere equivalent diameter of about 2 mm. The peaks are mostly in the same range of 4 to 6 mm. The peak shifting at L21 – 119 can be explained with very dense bubbles after the injection mesh; therefore, some bubbles are detected coalesced artificially.

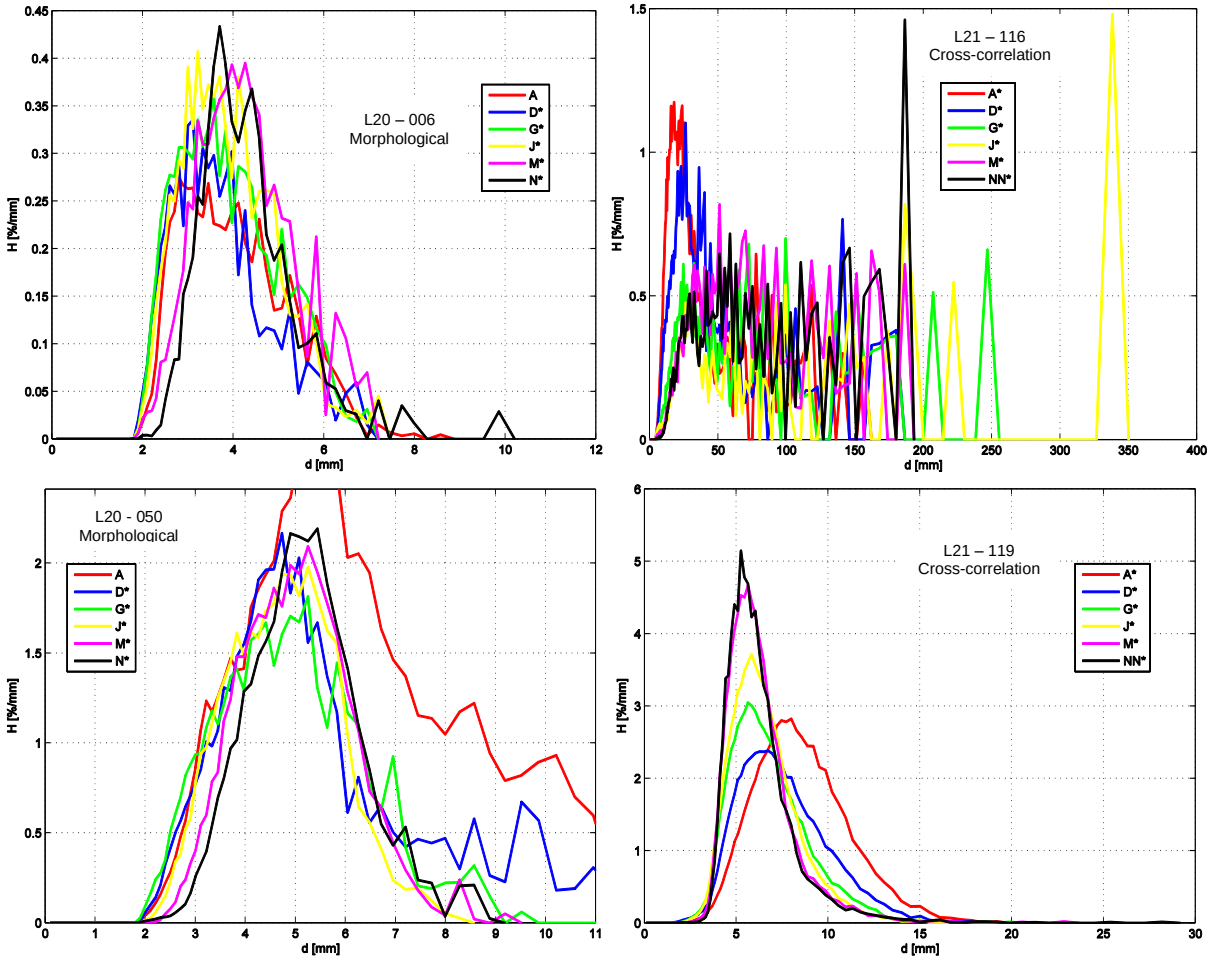

Figure 6.28: Bubble size distributions corresponding to the measurement results presented in Figure 6.26 and Figure 6.27

6.3.2 Steam-water flows

In Figure 6.29 the test matrix for downward steam-water flows is presented. All highlighted matrix points were measured for pressure values of 4 and 6.5 MPa, and the corresponding saturation temperatures of 250 and 281°C, respectively. The measurement positions were A, D, G, J, M and NN (cp. Table 2.2). In difference to the upward steam-water measurements, all matrix points were measured with a frequency amounting 2x2500Hz. Additionally the chosen matrix points are conducted with air-water flow regimes also (L21 series – see Figure 6.20).

As in case of the upward steam-water flows, all investigated flow regimes are in the churn turbulent flow regime as visible in Figure 6.30. There is obviously the same trend that a higher pressure results in a lower condensation of steam volume (see 6.1.2). Some influences of the injection module, which provoke recirculation zones, are visible especially at A and D positions in the 151 measurement at 4.0 MPa: There are long stretched bubbles near the pipe wall on the right side. Comparing this observation with side cut views from the 151 measurement at 6.5 MPa this effect is less pronounced.

		Superficial velocity gaseous phase																
	[m/s]	-0,0025	-0,0040	-0,0062	-0,0096	-0,0151	-0,0235	-0,0368	-0,0574	-0,0898	-0,1400	-0,2190	-0,3420	-0,5340	-0,8350	-1,3050	-2,0380	-3,1850
Superficial velocity liquid phase	-4,0470	011	022	033	044	055	066	077	088	099	110	121	132	143	154	165	176	187
	-2,5540	010	021	032	043	054	065	076	087	098	109	120	131	142	153	164	175	186
	-1,6110	009	020	031	042	053	064	075	086	097	108	119	130	141	152	163	174	185
	-1,0170	008	019	030	041	052	063	074	085	096	107	118	129	140	151	162	173	184
	-0,6410	007	018	029	040	051	062	073	084	095	106	117	128	139	150	161	172	183
	-0,4050	006	017	028	039	050	061	072	083	094	105	116	127	138	149	160	171	182
	-0,2550	005	016	027	038	049	060	071	082	093	104	115	126	137	148	159	170	181
	-0,1610	004	015	026	037	048	059	070	081	092	103	114	125	136	147	158	169	180
	-0,1020	003	014	025	036	047	058	069	080	091	102	113	124	135	146	157	168	179
	-0,0641	002	013	024	035	046	057	068	079	090	101	112	123	134	145	156	167	178
	-0,0405	001	012	023	034	045	056	067	078	089	100	111	122	133	144	155	166	177

Figure 6.29: Test matrix for steam-water downward flows (D20)

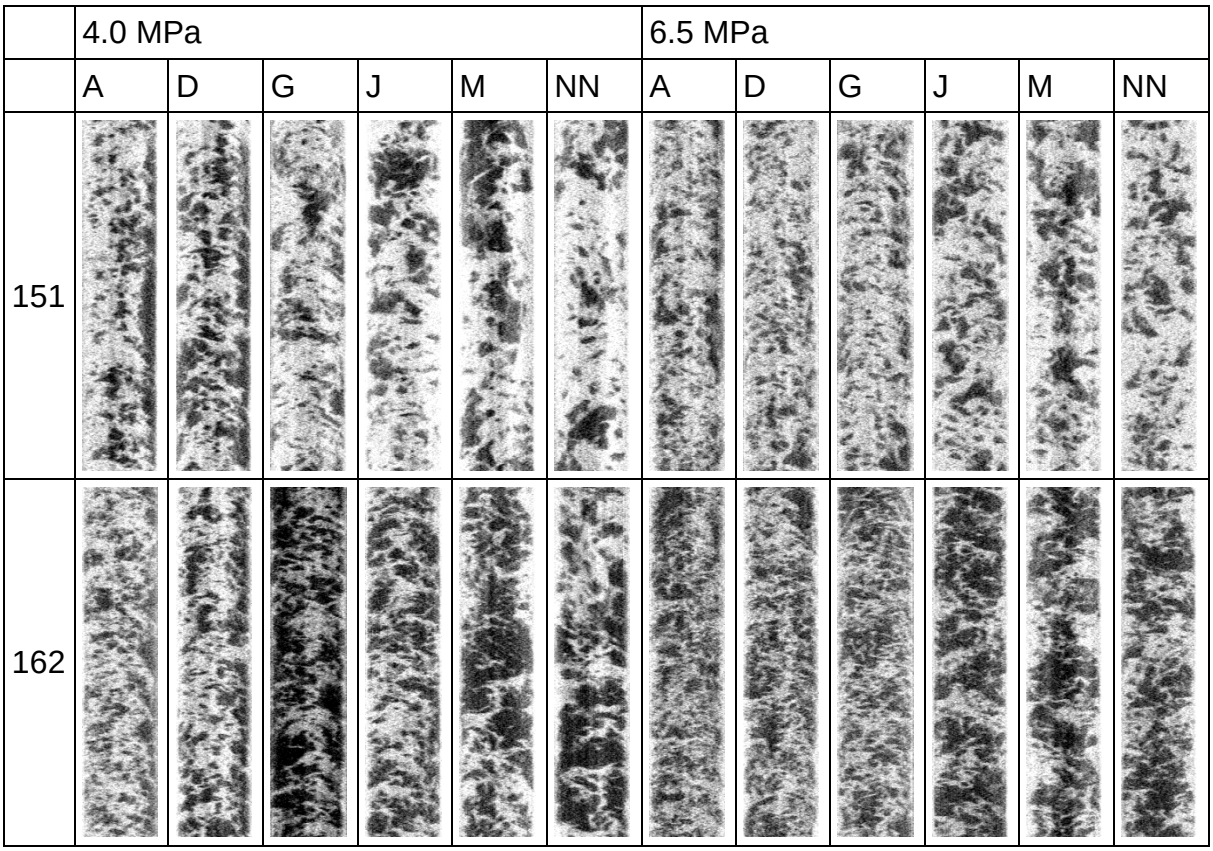

Figure 6.30: Side cut views for examples of D20 measurements at all positions

Comparing the Table 6.3 and Figure 6.11 for the matrix points 151 and 163, the condensation rate is higher at downward experiments than at upward experiments. The main reason is the higher sub-cooling of the liquid phase by the greater pipe length for feeding. The general trend, that the condensation rate is higher at 4 MPa as at 6.5 MPa is the same one like at the upward experiments: The reason for the lower condensation rate at 6.5 MPa lays in the larger injected gas mass flow. Due the different pressure, the density values of steam are still different: 20.090 kg/m³ at 4.0 MPa and 33.639 kg/m³ at 6.5 MPa. Therefore, the injected steam mass flow must be still higher and the condensation rate is less, but the absolute condensing mass flow is for both pressure stages mostly similar.

Table 6.9: Assessed condensation at D20 tests using operational data

	40 bar			65 bar		
	Subcooled temperature [K]	Condensed gas mas flow [kg/s]	Condensation rate [%]	Subcooled temperature [K]	Condensed gas mas flow [kg/s]	Condensation rate [%]
150	4.529	0.0182	45.62%	6.687	0.0294	44.42%
151	3.128	0.0197	49.26%	4.188	0.0293	44.46%
152	2.609	0.0252	62.80%	2.893	0.0318	48.12%
162	3.729	0.0230	37.17%	3.940	0.0278	26.73%
163	2.653	0.0256	41.23%	2.904	0.0319	30.71%

In Figure 6.31 the radial gas fraction profiles of the examples *from Figure 6.30 are* presented. The profile shapes show the same trend as the downward air-water flows: there is a nearly flat profile from pipe center to the radius r ≈ 20 mm and a decreasing trend from this radius position toward the pipe wall. In the measurement positions A, D and G, the local peaks exist caused by the mesh fixture of the injection module.

In Figure 6.32, the void fraction evolution is plotted against the measurement position. The expected decrease of the gas volume fraction caused by condensation effects can be observed especially in the 4.0 MPa experiments. For 6.5 MPa an increase of gas volume fraction with increasing distance from the injection is observed for most of the cases. This is surprising since with increasing L/D, the pressure is increasing slightly and the condensation is ongoing. The inverse observation may be caused by the increase of the bubble sizes along the pipe.

Radial velocity profiles of the same examples as shown in Figure 6.31 are presented in Figure 6.33. These velocity results are determined using the cross-correlation method. So, only time averaged axial velocity components are available. In contrast to the air-water downward flows, the presented velocity profile shapes show a clear decrease towards the pipe wall. The profiles become flatter for the M and NN positions. The result of 151 at 4.0 MPa shows the influence of the condensation effect on the steam-water flow: caused by the steam condensation, the void fraction decreases. Thus, the gas volume flow decreases also, which results in lower axial velocities (considering the different densities of water and steam). The same result can be observed in the 162 measurement at 4.0 MPa.

At the 6.5 MPa experiments the decreasing trend can be ascertained at the pipe center, but the velocity values near the pipe wall increases. So, the mean velocity values remain nearly constant at all positions.

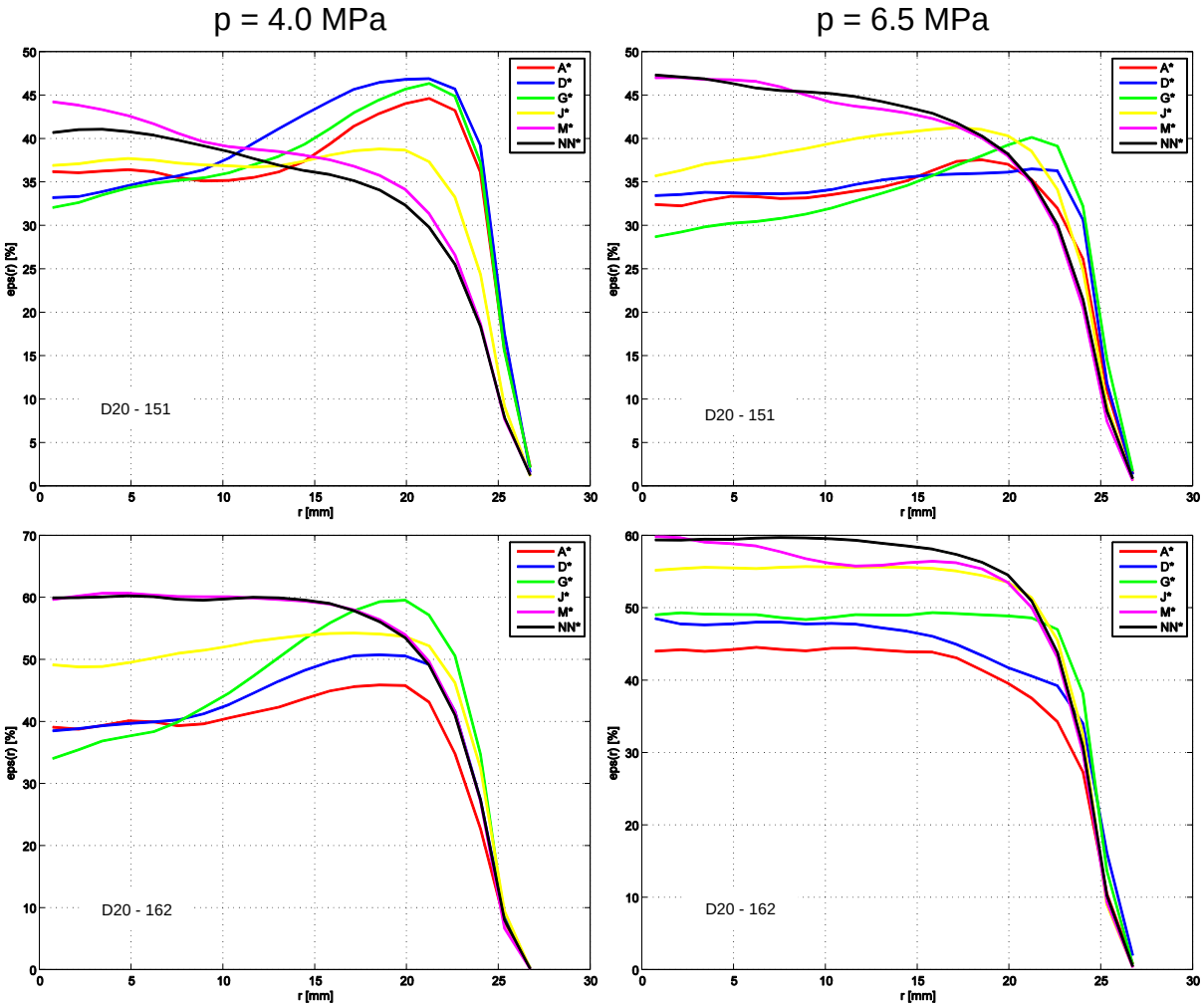

Figure 6.31: Radial gas fraction profiles for exemplary D20 measurements 151 (2x2500Hz) in upper line and 162 (2x2500Hz) in lower line

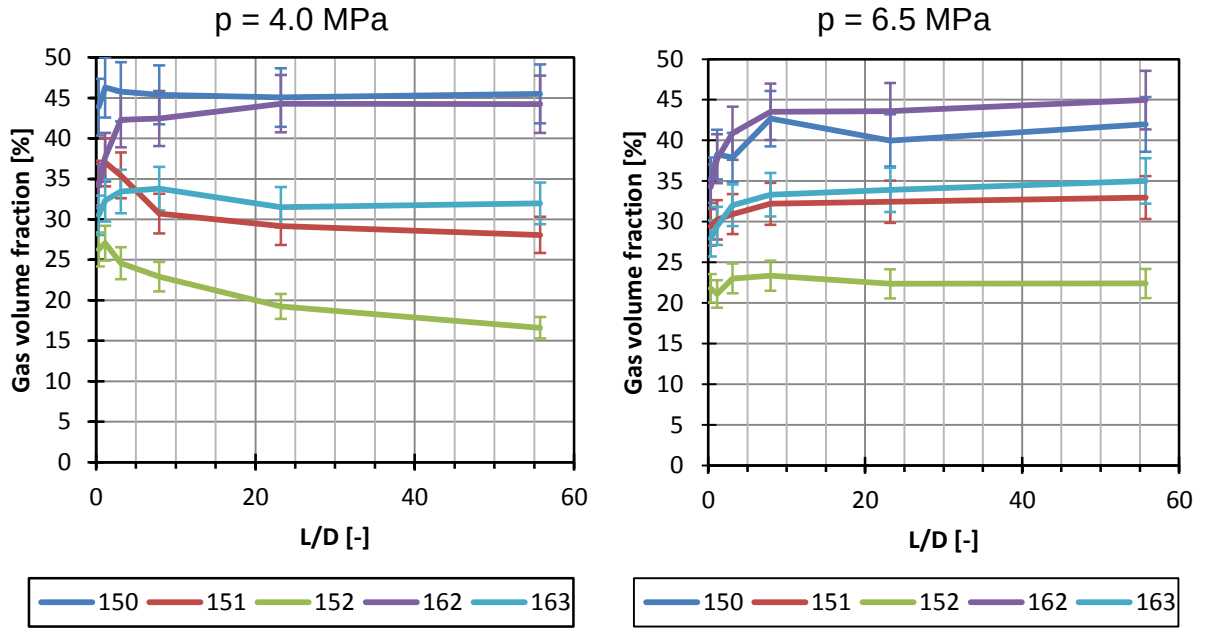

Figure 6.32: Development of gas volume fraction against measurement position in diameter length

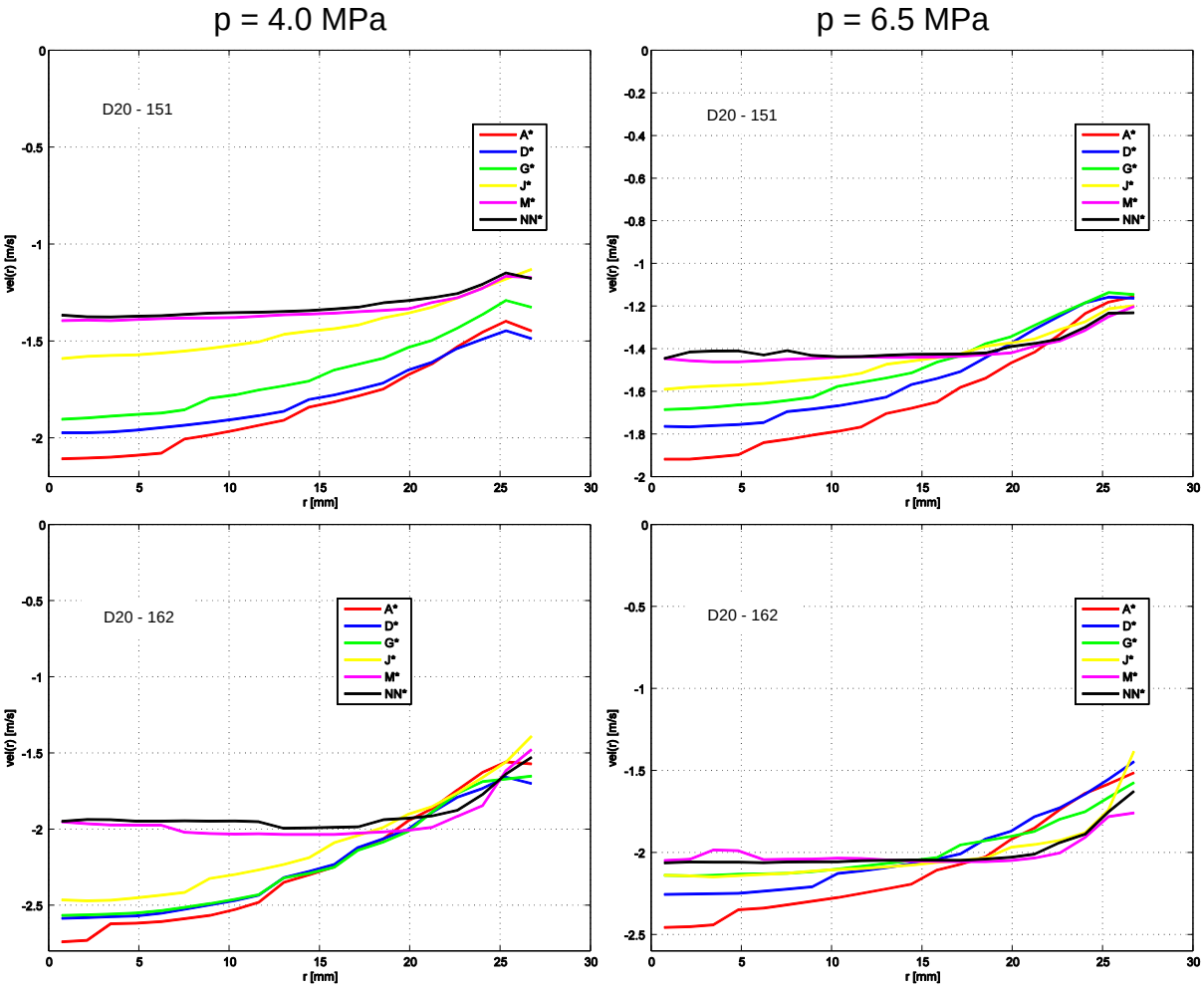

Figure 6.33: Radial velocity profiles using cross-correlation for exemplary D20 measurements 151 (2x2500Hz) and 162 (2x2500Hz)

The bubble size distributions of the downward steam-water measurement examples are presented in Figure 6.34. In all shown cases, a development is visible from bubble sphere equivalent diameter of about 10 mm near the injection to larger bubbles with a diameter about 60-80 mm at the measurement position NN. While at the 4.0 MPa experiments the small bubble peak reduction from injection to the maximal inlet length is an effect of condensation and bubble coalescence, the reduction is probably caused mainly by bubble coalescence for 6.5 MPa.

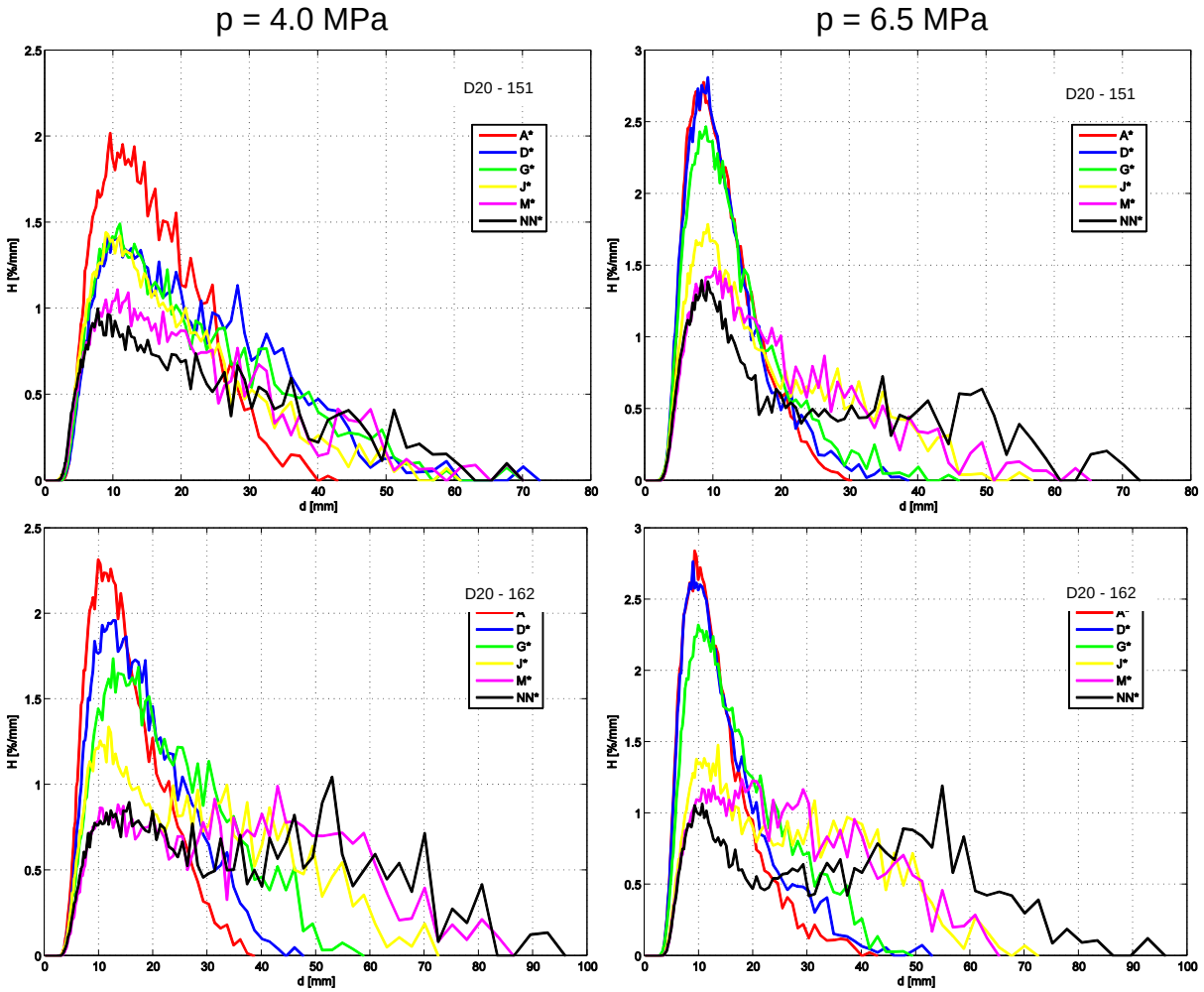

Figure 6.34: Bubble size distributions for exemplary D20 measurements 151 (2x2500Hz) and 162 (2x2500Hz)

To assess the condensation, the same procedure is applied as at the upward steam-water experiments: the condensed steam mass flow is calculated from the heat balance considering heat losses at titanium and steam pipe. The thermodynamic properties of water and steam are estimated using Wagner and Kretzschmar (2008). In difference to the upward experiments, there are no WMS data available. The comparison between assessment and measurement by ROFEX is presented in Table 6.10. Again the presented uncertainties are estimated by error propagation, where the maximum uncertainties are taken. For the ROFEX uncertainties the void error is assumed with 8%, see Banowski, et al. (2015) and the one for the velocity is taken from Table 5.2. The assessment error is estimated using the uncertainties from Table 2.3. In Figure 6.35 the values are presented as chart diagram.

Table 6.10: Comparison of injected, assessed and measured gas superficial velocities for the D20 measurements with ROFEX and their uncertainties at the position NN

		j_g injected [m/s]	j_g Measurement [m/s]		Uncertainties [%]	
			Assessment	ROFEX	Assessment	ROFEX
4.0 MPa	150	-0.835	-0.4590	-0.5799	17.27%	14.00%
	151	-0.835	-0.4290	-0.3671	22.52%	14.27%
	152	-0.835	-0.3147	-0.2772	38.78%	16.61%
	162	-1.305	-0.8200	-0.8547	12.90%	16.13%
	163	-1.305	-0.7693	-0.7322	17.19%	18.45%
6.5 MPa	150	-0.835	-0.4634	-0.4993	13.72%	14.01%
	151	-0.835	-0.4614	-0.4592	16.37%	14.27%
	152	-0.835	-0.4322	-0.4117	21.80%	16.60%
	162	-1.305	-0.9615	-0.9020	8.99%	16.13%
	163	-1.305	-0.9080	-0.8462	11.54%	18.46%

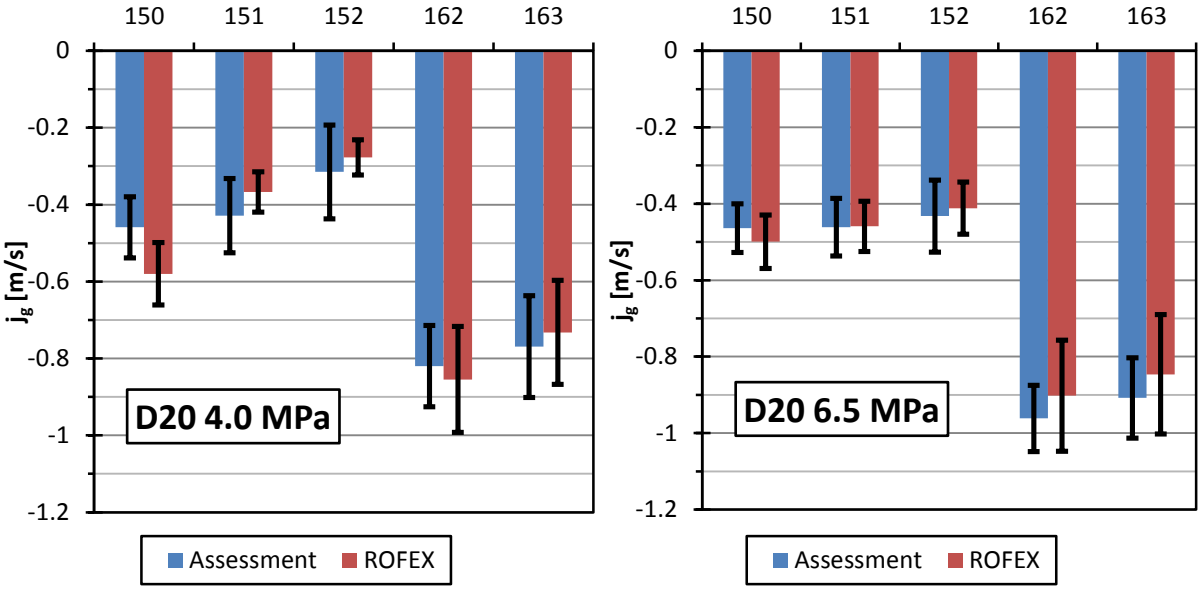

Figure 6.35: Chart of assessed and measured gas superficial velocities of D20 measurements at ROFEX, given in Table 6.10

7. Conclusions

The extensive experimental results presented in this report provide a database for air-water as well as steam-water flows in a vertical pipe with an inner diameter of 54.8 mm. This database can be used for the development and validation of CFD-models for two-phase flows, but also to extract general information on two-phase flow characteristics. Experiments are available for bubbly flows, slug flows and churn-turbulent flows in co-current upward and downward flow direction. Counter-current flow measurements are available only for bubbly flows. In particular, the investigations aim on the evolution of the two-phase flow along the pipe. Therefore, measurements were done at 6 height positions with varying distances from the gas injection for a wide range of combinations of gas and water flow rates. Each of the tests comprises dual layer measurement planes. The pressure at the downstream end of the test section was kept constantly: 0.4 MPa at air-water flow regimes and 4.0 as well as 6.5 MPa at steam-water flow regimes. The water temperature, which significantly influences bubble coalescence and fragmentation, was kept constant at 30 °C for air-water measurements with a maximum deviation amounting 1 K. The water temperatures at steam-water experiments are nearly the saturation temperatures of the different pressure levels with a slight sub-cooling.

All measurements were conducted using the non-invasive ultrafast X-ray tomography technique. Therefore new data evaluation algorithms were developed for identification of the gas structures in the liquid phase and for extracting individual bubble velocity information.

The co-current upward experiments clearly extent the database which is available from previous wire-mesh sensor experiments. The tomography system enables the non-invasive investigation of low velocity flow regimes, where bubble shape information can be extracted as well as bubble pairs can be found to extract individual bubble velocities. New two-phase flow experiments with downward liquid flow were conducted. Depending on the liquid velocity, bubbles rise up or are pushed downward. For both conditions, such comprehensive experiments were conducted first time considering such a depth of extractable bubble information.

The most important quantitative results of these test series are time averaged radial profiles of gas volume fraction and gas axial velocity, as well as time and cross-section averaged bubble size distributions. The velocity profiles as well as the bubble size distributions are determined using different methods. The results are compared and discussed. For steam-water flow experiments the condensation rate is compared between assessed values and calculated values using measurement results.

The uncertainties of algorithms and methods are estimated and discussed. Additional to stated uncertainties, superficial velocities are calculated from measured gas volume fractions and velocities. These results are compared with injection conditions of the experiments providing information on the consistency of the measurements.

8. References

Ahmad, Wayez R., Julio M. DeJesus, and Masahiro Kawaji, 1998, Falling film hydrodynamics in slug flow, Chemical Engineering Science 53, 123–130.

Banowski, Manuel, Dirk Lucas, and Lutz Szalinski, 2015, A new algorithm for segmentation of ultrafast X-ray tomographed gas–liquid flows, International Journal of Thermal Sciences 90, 311–322.

Barnea, Dvora, Ovadia Shoham, and Yehuda Taitel, 1982, Flow pattern transition for vertical downward two phase flow, Chemical Engineering Science 37, 741–744.

Beyer, M., D. Lucas, J. Kusin, and P. Schütz, 2008, Air-water experiments in a vertical DN200-pipe, FZD-505.

Beyerlein, Steven W., Rainer K. Cossmann, and Horst.J. Richter, 1985, Prediction of bubble concentration profiles in vertical turbulent two-phase flow, International Journal of Multiphase Flow 11, 629–641.

Clift, R., 1978, Bubbles, Drops, and Particles (Academic Press, New York).

Fischer, F, D Hoppe, E Schleicher, G Mattausch, H Flaske, R Bartel, and U Hampel, 2008, An ultra fast electron beam x-ray tomography scanner, Measurement Science and Technology 19, 094002.

Fischer, F., and U. Hampel, 2010, Ultra fast electron beam X-ray computed tomography for two-phase flow measurement, Nuclear Engineering and Design 240, 2254–2259.

Hampel, U., E. Krepper, D. Lucas, M. Beyer, L. Szalinski, M. Banowski, F. Barthel, D. Hoppe, A. Bieberle, and T. Barth, 2013, High-resolution two-phase flow measurement techniques for the generation of experimental data for CFD code qualification, Kerntechnik 78, 9–15.

Harmathy, Tibor Z., 1960, Velocity of large drops and bubbles in media of infinite or restricted extent, AIChE Journal 6, 281–288.

Hibiki, T., H. Goda, S. Kim, M. Ishii, and J. Uhle, 2004, Structure of vertical downward bubbly flow, International Journal of Heat and Mass Transfer 47, 1847–1862.

Ishii, M., S.S. Paranjape, S. Kim, and X. Sun, 2004, Interfacial structures and interfacial area transport in downward two-phase bubbly flow, International Journal of Multiphase Flow 30, 779–801.

Johnson, I. D., 1987, Method and apparatus for measuring water in crude oil, .

Kak, Avinash C., and Malcolm Slaney, 2001, Principles of Computerized Tomographic Imaging. Classics in applied mathematics 33 (Society for Industrial and Applied Mathematics, Philadelphia).

Kashinsky, O.N., and V.V. Randin, 1999, Downward bubbly gas–liquid flow in a vertical pipe, International Journal of Multiphase Flow 25, 109–138.

Kawaji, M., J.M. DeJesus, and G. Tudose, 1997, Investigation of flow structures in vertical slug flow, Nuclear Engineering and Design 175, 37–48.

Liu, Yi-Peng, Ping-Yang Wang, Jing Wang, and Zhao-Hui Du, 2013, Investigation of Taylor bubble wake structure in liquid nitrogen by PIV technique, Cryogenics 55-56, 20–29.

Lucas, D., M. Beyer, E. Krepper, C. Vallée, T. Höhne, T. Seidel, L. Szalinski, U. Hampel, M. Schmidtke, E. Schleicher, H. Pietruske, P. Schütz, D. Danciu, Deendarlianto, D. Zhang, F. Barthel, C. Zippe, S. Hänsch, H. Carl, and F.-P. Weiß, 2011, TOPFLOW-Experimente, Modellentwicklung und Validierung von CFD-Codes für Wasser-Dampf-Strömungen mit Phasenübergang, Helmholtz-Zentrum Dresden-Rossendorf, HZDR-11, Nov. 2011.

Nicklin, D. J., J. O. Wilkes, and J. F. Davidson, 1962, Two-phase flow in vertical tubes, Transactions of the Institution of Chemical Engineers 40, 61–68.

Oshinowo, Toks, and M. E. Charles, 1974, Vertical two-phase flow part I. Flow pattern correlations, The Canadian Journal of Chemical Engineering 52, 25–35.

Pietruske, Heiko, and Horst-Michael Prasser, 2007, Wire-mesh sensors for high-resolving two-phase flow studies at high pressures and temperatures, Flow Measurement and Instrumentation 18, 87–94.

Prasser, H.-M, A Böttger, and J Zschau, 1998, A new electrode-mesh tomograph for gas–liquid flows, Flow Measurement and Instrumentation 9, 111–119.

Prasser, H.-M., D. Scholz, and C. Zippe, 2001, Bubble size measurement using wire-mesh sensors, Flow Measurement and Instrumentation 12, 299–312.

Prasser, Horst-Michael, Eckhard Krepper, and Dirk Lucas, 2002, Evolution of the two-phase flow in a vertical tube—decomposition of gas fraction profiles according to bubble size classes using wire-mesh sensors, International Journal of Thermal Sciences 41, 17–28.

Prasser, H.-M., D. Lucas, E. Krepper, D. Baldauf, A. Böttger, U. Rohde, P. Schütz, F.-P. Weiß C. Zippe, W. Zippe, and J. Zschau, 2003, Flow maps and models for transient two-phase flows, Forschungszentrum Dresden, FZR-379.

Prasser, H.-M., M. Misawa, and I. Tiseanu, 2005, Comparison between wire-mesh sensor and ultra-fast X-ray tomograph for an air–water flow in a vertical pipe, Flow Measurement and Instrumentation 16, 73–83.

Prasser, H.-M., H. Carl M. Beyer, A. Manera, H.Pietruske, and P. Schütz, 2007, Experiments on upwards gas/liquid flow in vertical pipes, Forschungszentrum Dresden.

Sun, Xiaodong, Sidharth Paranjape, Seungjin Kim, Basar Ozar, and Mamoru Ishii, 2004, Liquid velocity in upward and downward air–water flows, Annals of Nuclear Energy 31, 357–373.

Taitel, Yehuda, Dvora Bornea, and A. E. Dukler, 1980, Modelling flow pattern transitions for steady upward gas-liquid flow in vertical tubes, AIChE Journal 26, 345–354.

Taitel, Yehuda, and Dvora Barnea, 1983, Counter current gas-liquid vertical flow, model for flow pattern and pressure drop, International Journal of Multiphase Flow 9, 637–647.

Usui, Kensuke, and Kazuo Sato, 1989, Vertically Downward Two-Phase Flow, (I): Void Distribution and Average Void Fraction, Journal of Nuclear Science and Technology 26, 670–680.

Van Hout, R, A Gulitski, D Barnea, and L Shemer, 2002, Experimental investigation of the velocity field induced by a Taylor bubble rising in stagnant water, International Journal of Multiphase Flow 28, 579–596.

Wagner, Wolfgang, and Hans-Joachim Kretzschmar, 2008, International Steam Tables: Properties of Water and Steam Based on the Industrial Formulation IAPWS-IF97: Tables, Algorithms, Diagrams, and CD-ROM Electronic Steam Tables: All of the Equations of IAPWS-IF97 Including a Complete Set of Supplementary Backward Equations for Fast Calculations of Heat Cycles, Boilers, and Steam Turbines. 2nd ed. (Springer, Berlin).

Wang, S. K., S. J. Lee, O. C. Jr Jones, and R. T. Jr Lahey, 1987, 3-D turbulence structure and phase distribution measurements in bubbly two-phase flows, International Journal of Multiphase Flow 13, 327.

9. Appendix

9.1. Characteristic data of the measurement points

On the following pages, the quantitative data of gas volume fraction, velocity and bubble size distributions are presented for each position of each measured flow regimes and series. If the position letter is marked with a star “*”, this measurement data is revised with the procedure described in section 3.4.

L16 – 001 (jl = 0.0405 $^{m}/_{s}$; jg = 0.0025 $^{m}/_{s}$), 2x1000Hz

Void development

Radial gas fraction profiles

Radial velocity profiles
(Cross-correlation)

Bubble size distribution
(Cross-correlation)

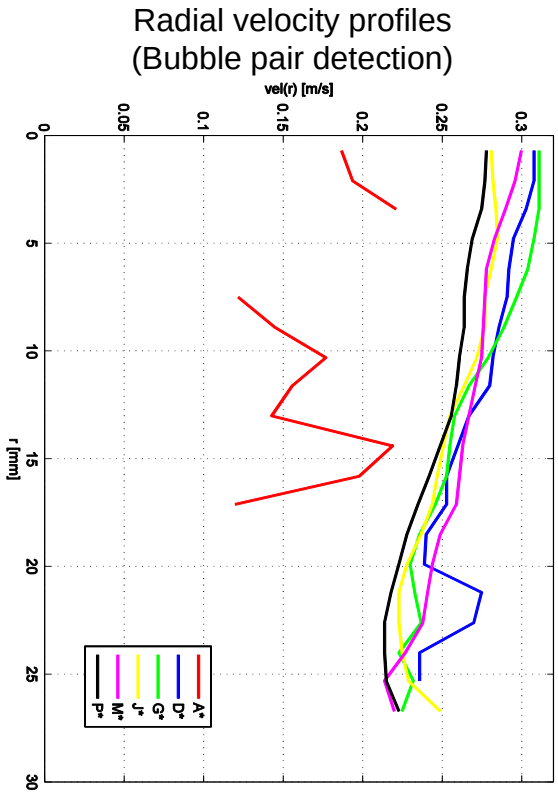
Radial velocity profiles
(Bubble pair detection)
vel(r) [m/s]
r [mm]
P*
M*
J*
G*
D*
A*

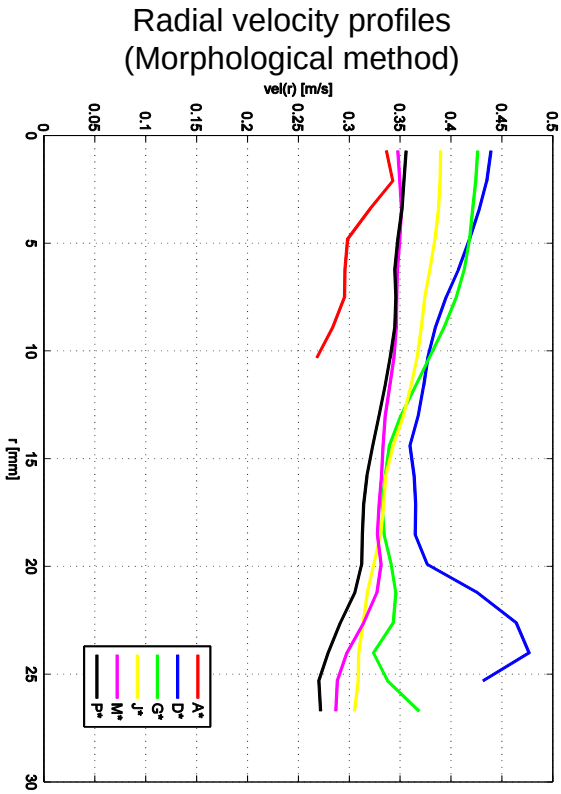
Radial velocity profiles
(Morphological method)
vel(r) [m/s]
r [mm]
P*
M*
J*
G*
D*
A*

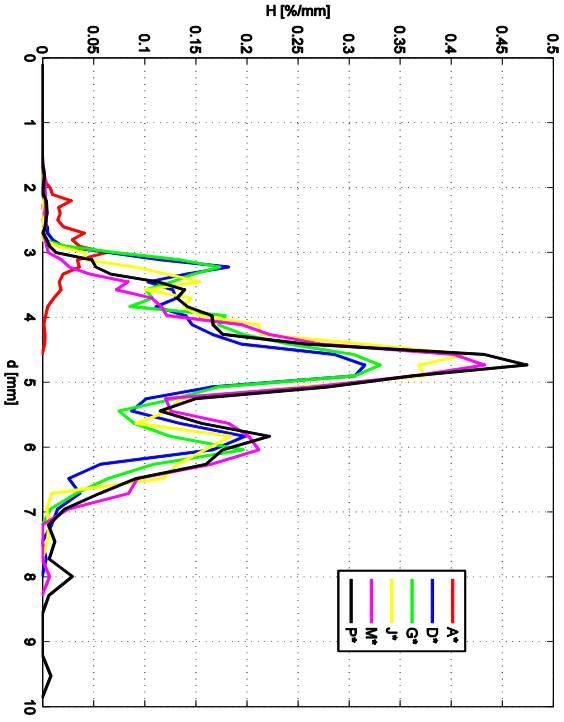
Bubble size distribution
(Bubble pair detection)
H [%/mm]
d [mm]
P*
M*
J*
G*
D*
A*

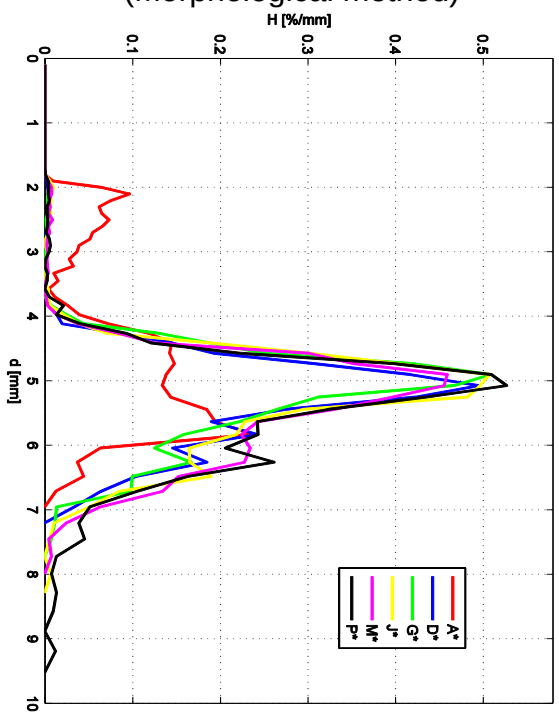
Bubble size distribution
(Morphological method)
H [%/mm]
d [mm]
P*
M*
J*
G*
D*
A*

L16 – 004 (jl = 0.161 m/s; jg = 0.0025 m/s), 2x1000Hz
Void development
eps [%]
L/D [-]
Theory (u_d = 0.235 m/s)
Measurement
Radial gas fraction profiles
eps(r) [%]
r [mm]
A*
D*
G*
J*
M*
P*
Bubble size distribution
(Cross-correlation)
H [%/mm]
d [mm]
Radial velocity profiles
(Cross-correlation)
vel(r) [m/s]
r [mm]

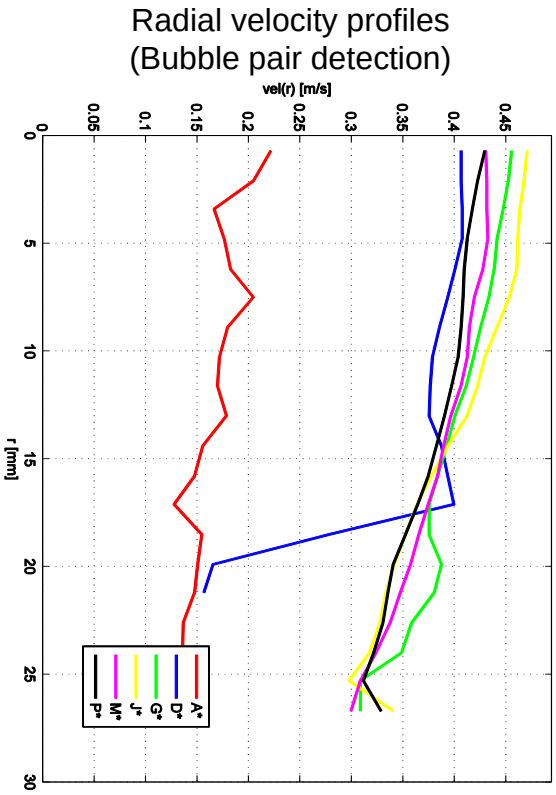
Radial velocity profiles
(Bubble pair detection)
vel(r) [m/s]
r [mm]
P*
M*
J*
G*
D*
A*

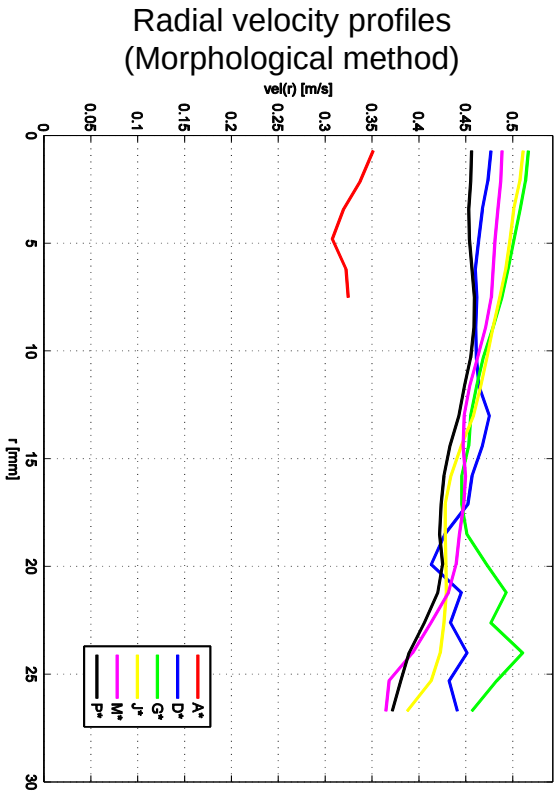
Radial velocity profiles
(Morphological method)
vel(r) [m/s]
r [mm]
P*
M*
J*
G*
D*
A*

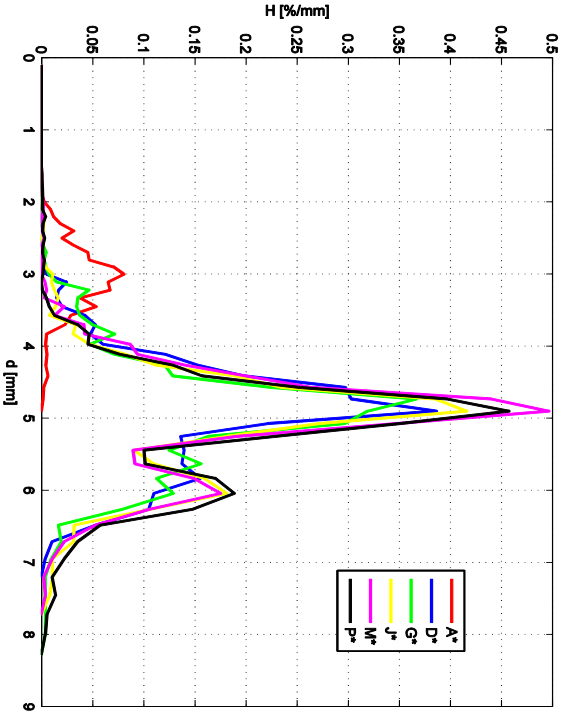
Bubble size distribution
(Bubble pair detection)
H [%/mm]
d [mm]
P*
M*
J*
G*
D*
A*

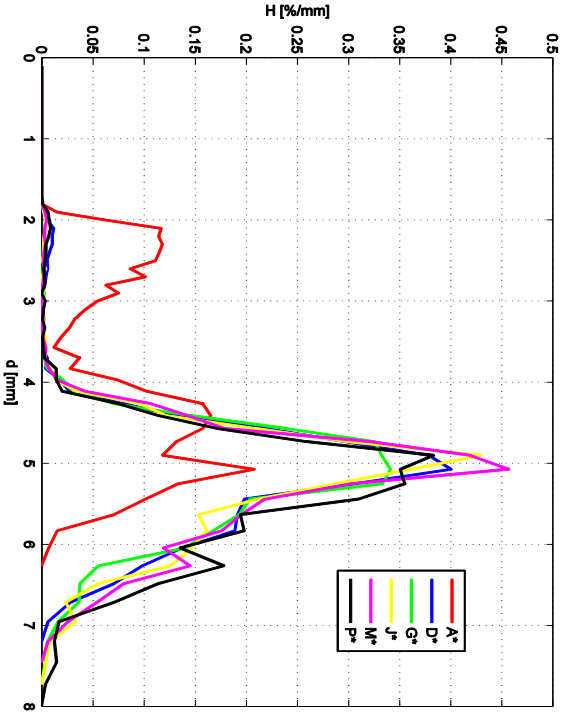
Bubble size distribution
(Morphological method)
H [%/mm]
d [mm]
P*
M*
J*
G*
D*
A*

L16 – 006 (jl = 0.405 $^{m}/_{s}$; jg = 0.0025 $^{m}/_{s}$), 2x1000Hz

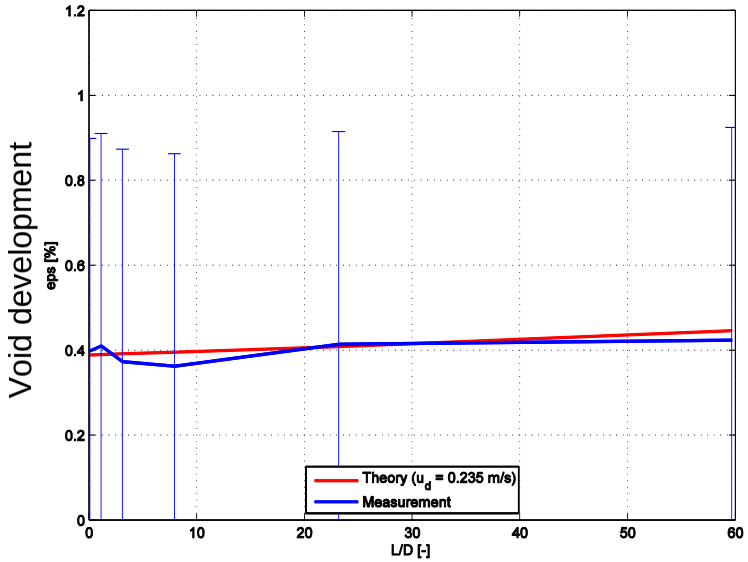

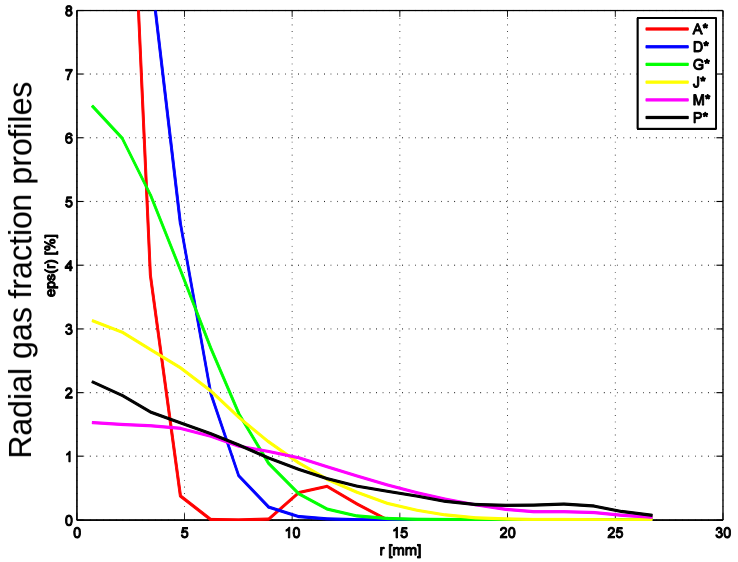

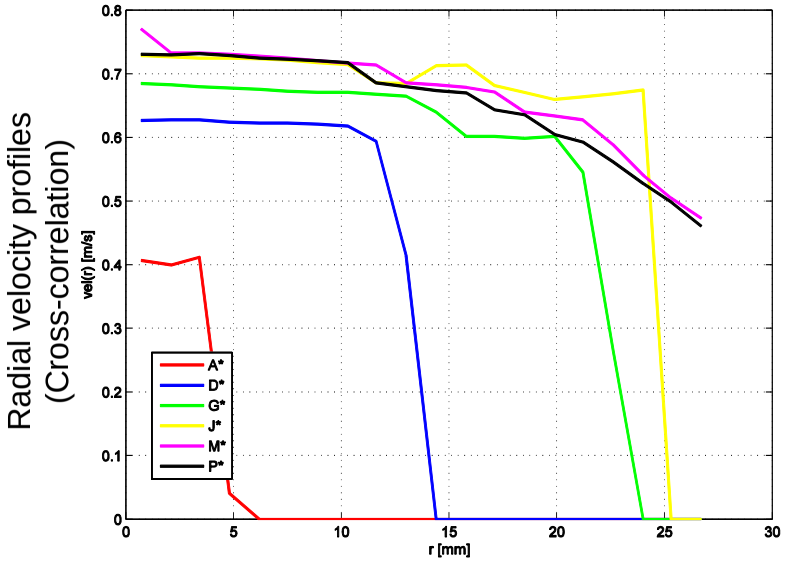

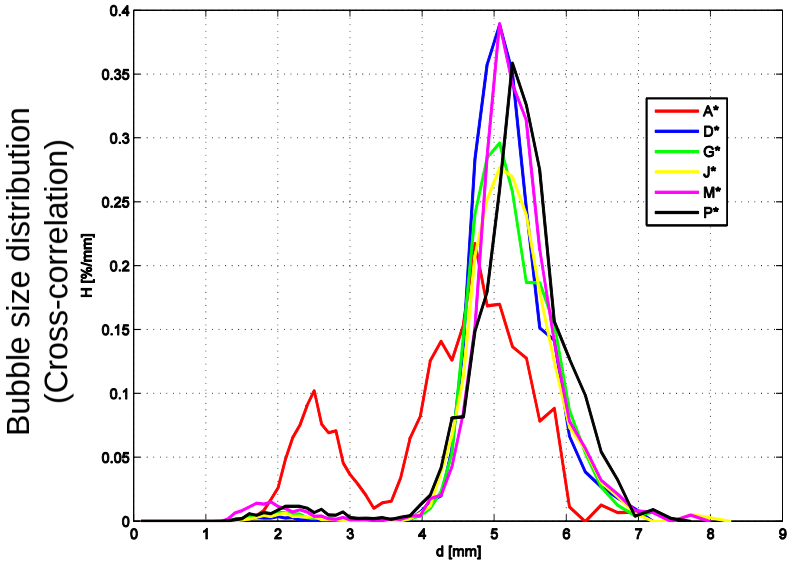

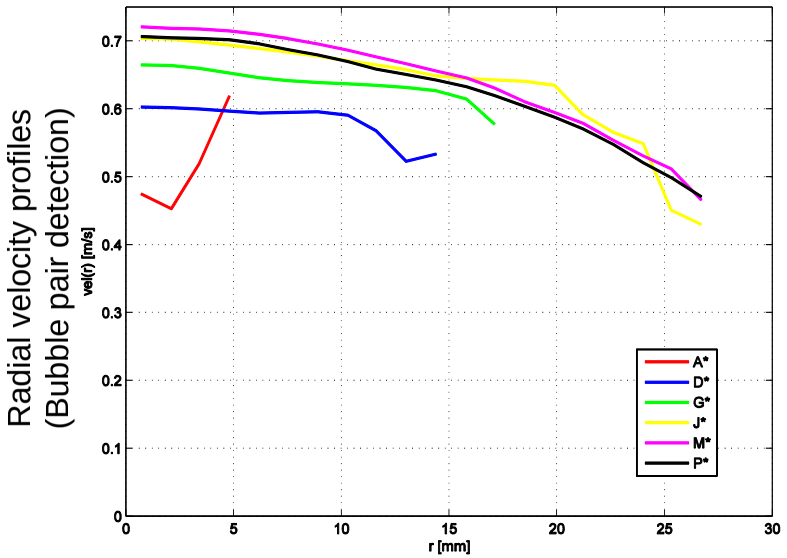
Radial velocity profiles
(Bubble pair detection)
vel(r) [m/s]
r [mm]
A*
D*
G*
J*
M*
P*

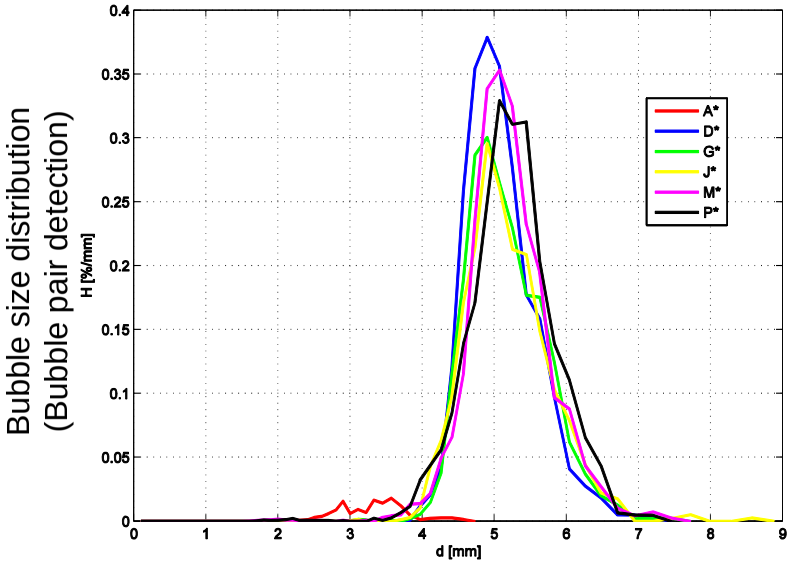
Bubble size distribution
(Bubble pair detection)
H [%/mm]
d [mm]
A*
D*
G*
J*
M*
P*

L16 – 006 (jl = 0.405 $^{m}/_{s}$; jg = 0.0025 $^{m}/_{s}$), 2x2500Hz

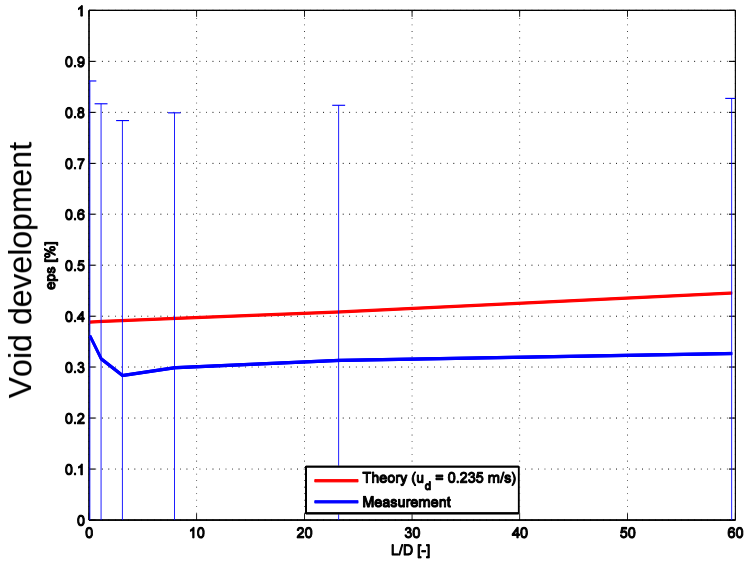

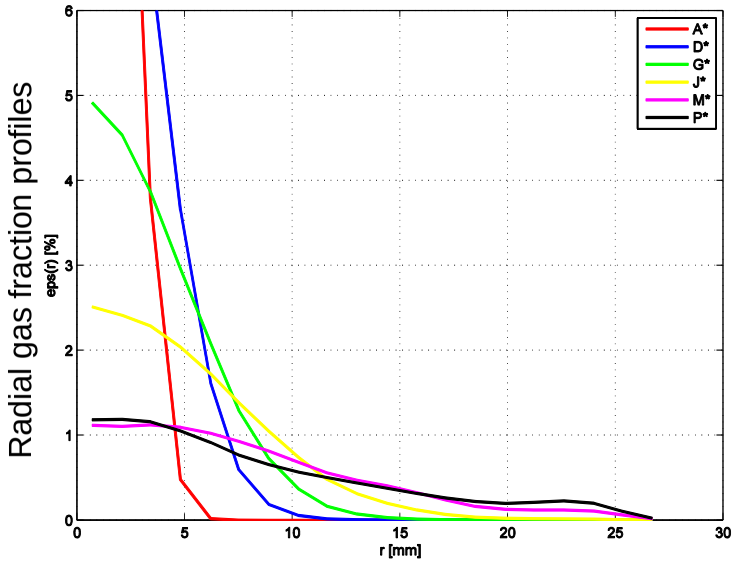

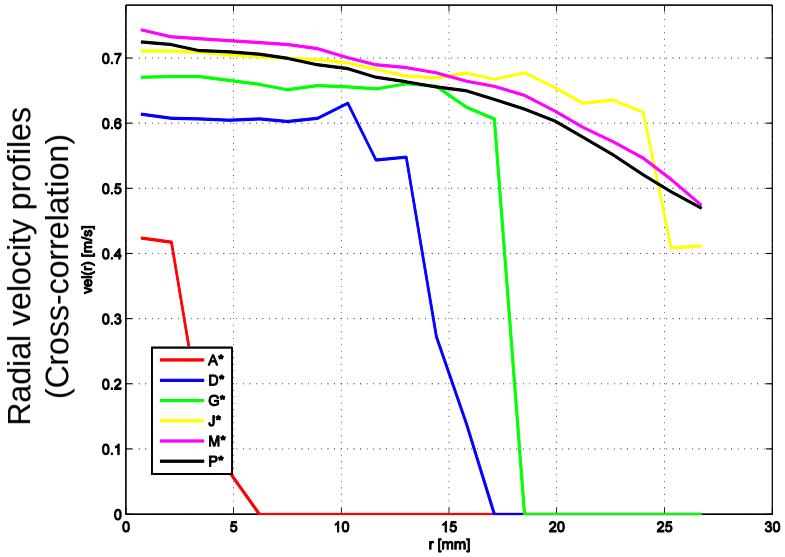

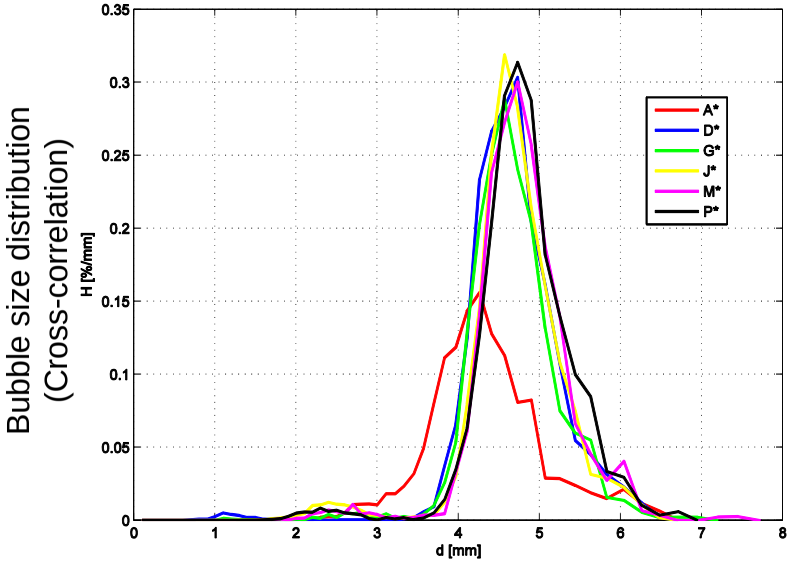

Radial velocity profiles
(Bubble pair detection)

Bubble size distribution
(Bubble pair detection)

L16 – 008 (jl = 1.017 $^{m}/_{s}$; jg = 0.0025 $^{m}/_{s}$), 2x2500Hz

Radial velocity profiles
(Bubble pair detection)

Bubble size distribution
(Bubble pair detection)

L16 – 028 (jl = 0.405 $^{m}/_{s}$; jg = 0.0062 $^{m}/_{s}$), 2x1000Hz

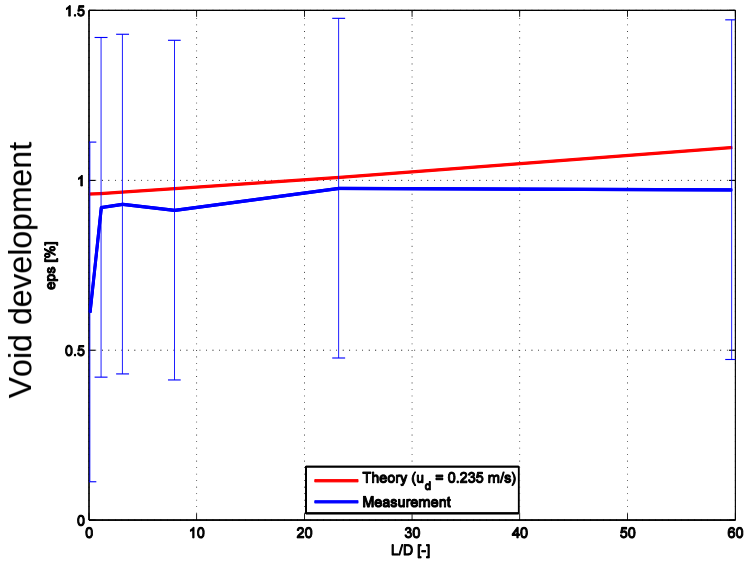

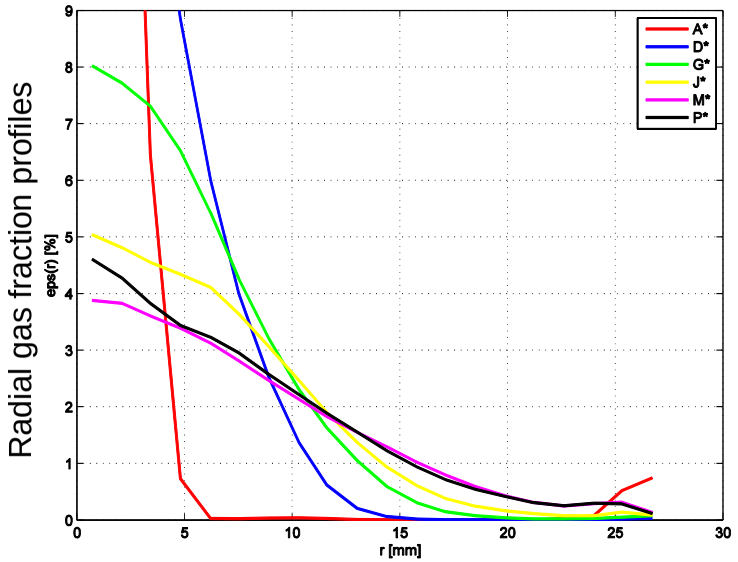

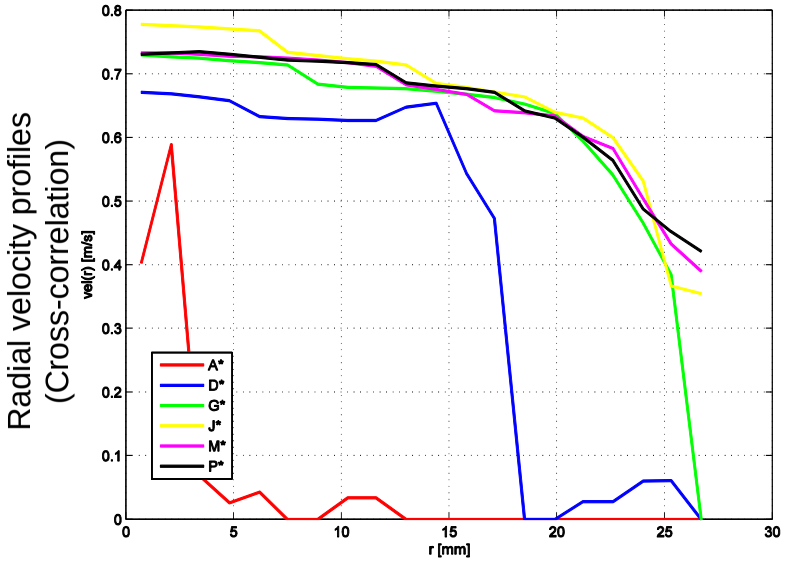

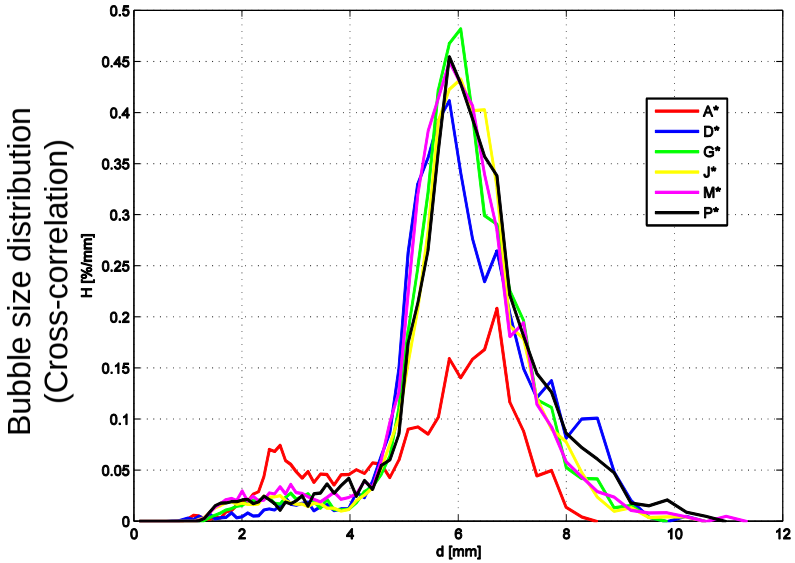

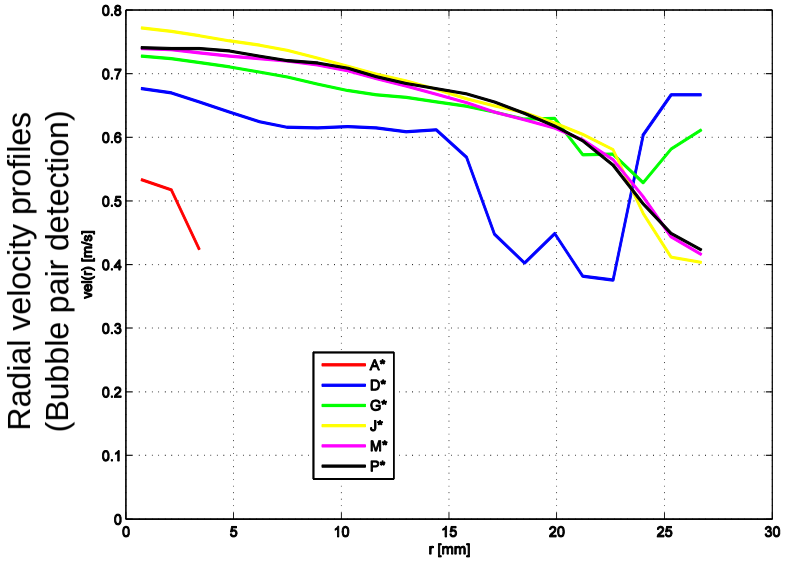
Radial velocity profiles
(Bubble pair detection)
vel(r) [m/s]
r [mm]
A*
D*
G*
J*
M*
P*

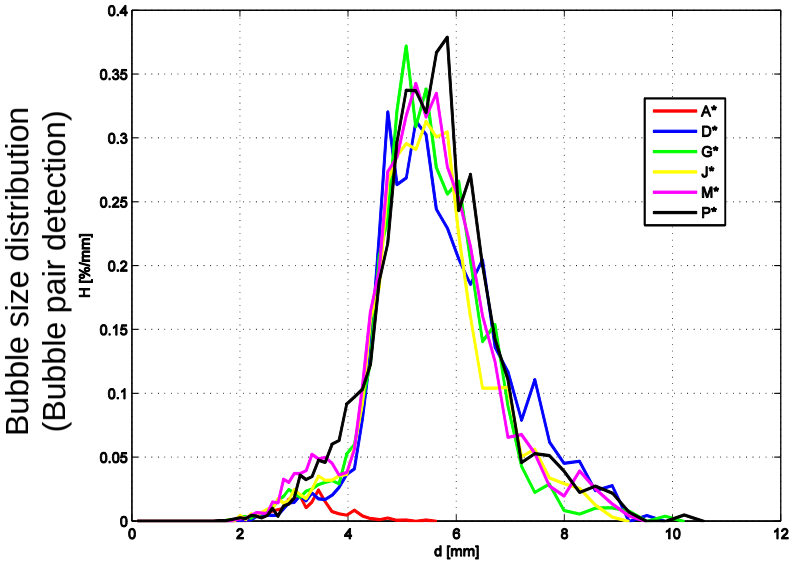
Bubble size distribution
(Bubble pair detection)
H [%/mm]
d [mm]
A*
D*
G*
J*
M*
P*

L16 – 028 (jl = 0.405 m/s; jg = 0.0062 m/s), 2x2500Hz
Void development
eps [%]
L/D [-]
Theory (u_d = 0.235 m/s)
Measurement
Radial gas fraction profiles
eps(r) [%]
r [mm]
A*
D*
G*
J*
M*
P*
Radial velocity profiles
(Cross-correlation)
vel(r) [m/s]
r [mm]
Bubble size distribution
(Cross-correlation)
H [%/mm]
d [mm]

Radial velocity profiles
(Bubble pair detection)

Bubble size distribution
(Bubble pair detection)

L16 – 030 (jl = 1.017 $^{m}/_{s}$; jg = 0.0062 $^{m}/_{s}$), 2x2500Hz

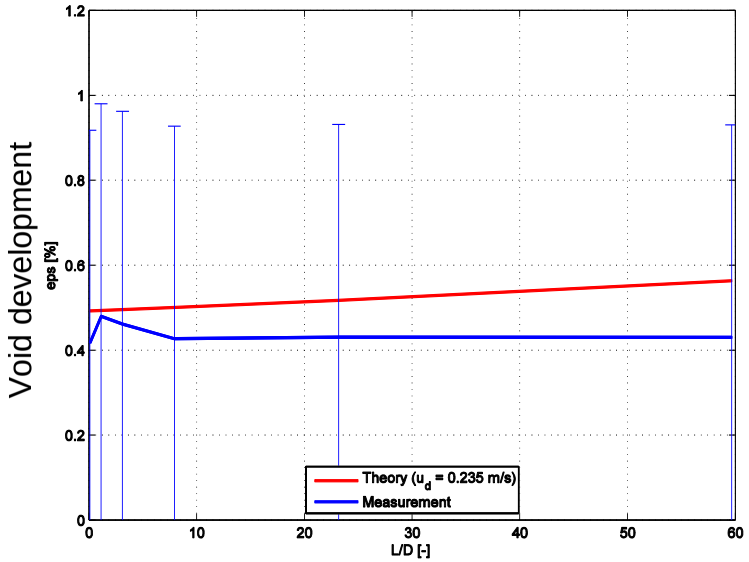

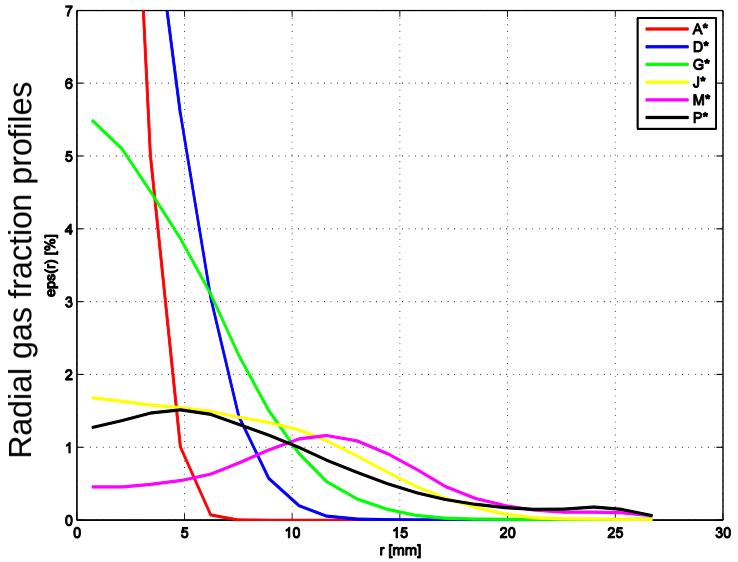

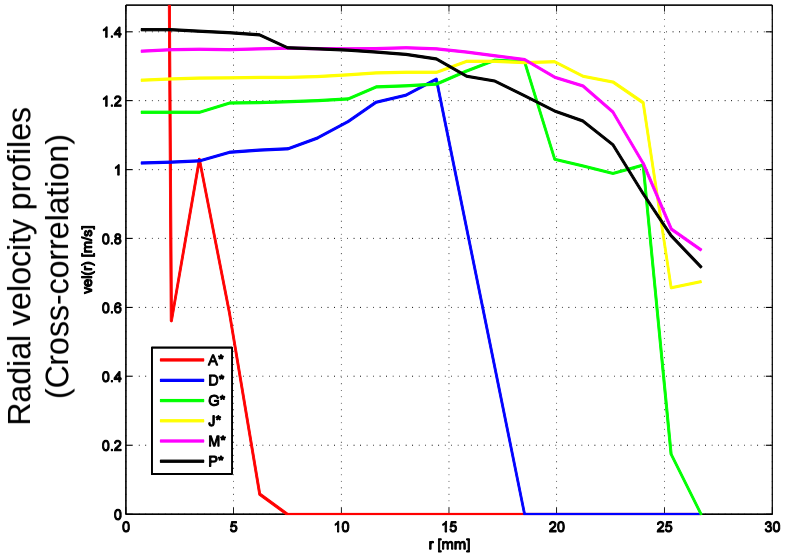

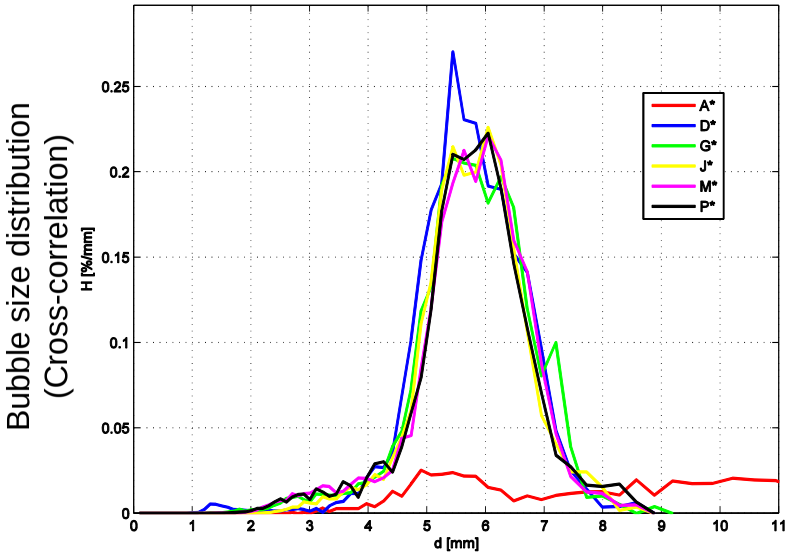

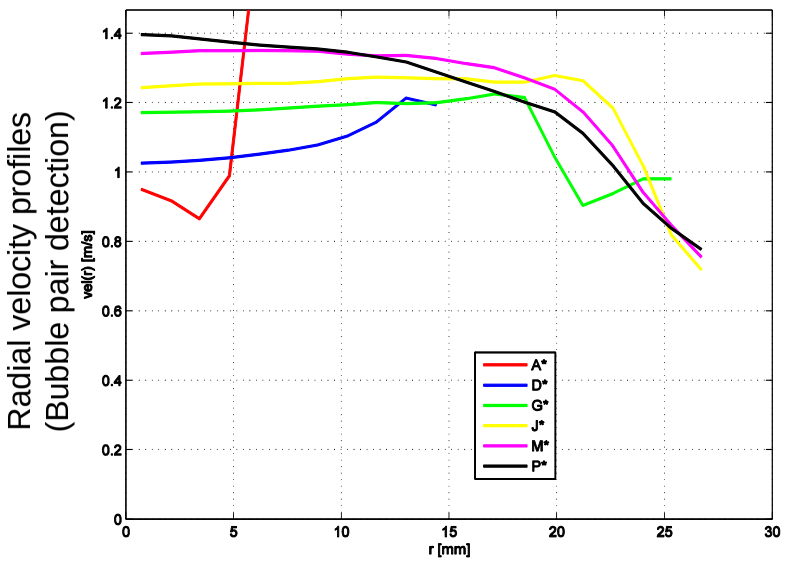
Radial velocity profiles
(Bubble pair detection)
vel(r) [m/s]
r [mm]
A*
D*
G*
J*
M*
P*

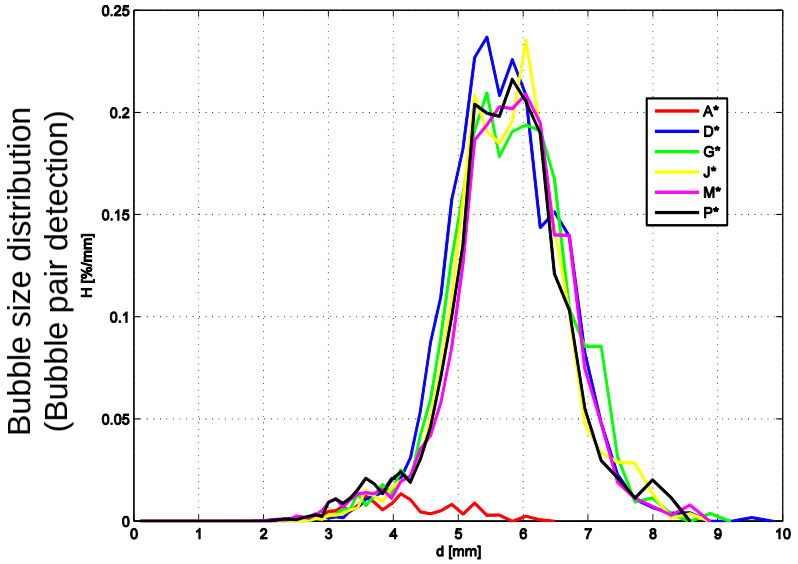
Bubble size distribution
(Bubble pair detection)
H [%/mm]
d [mm]
A*
D*
G*
J*
M*
P*

L16 – 034 (jl = 0.0405 $^{m}/_{s}$; jg = 0.0096 $^{m}/_{s}$), 2x1000Hz

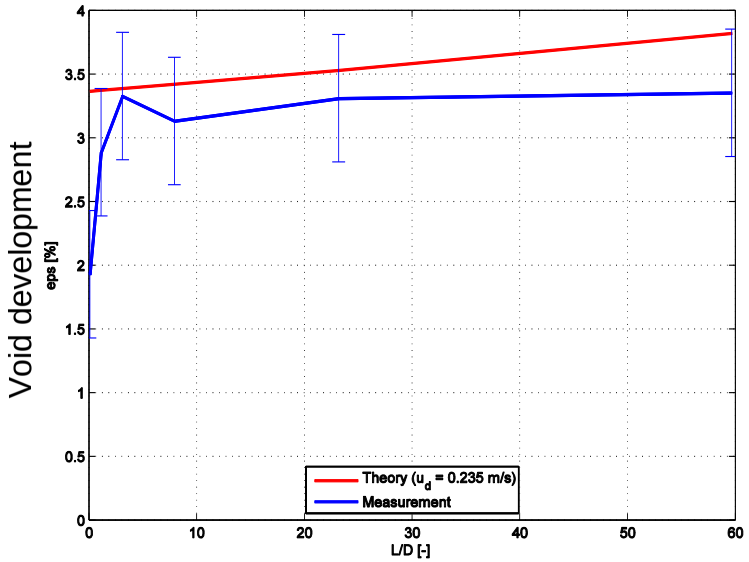

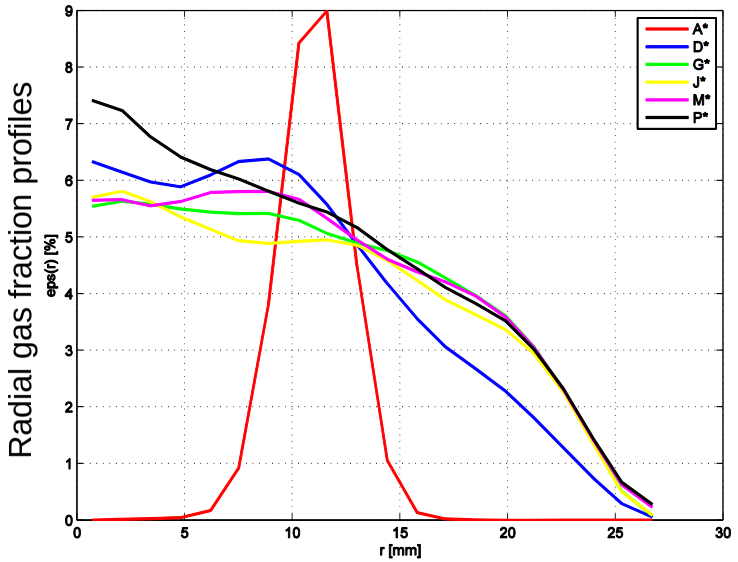

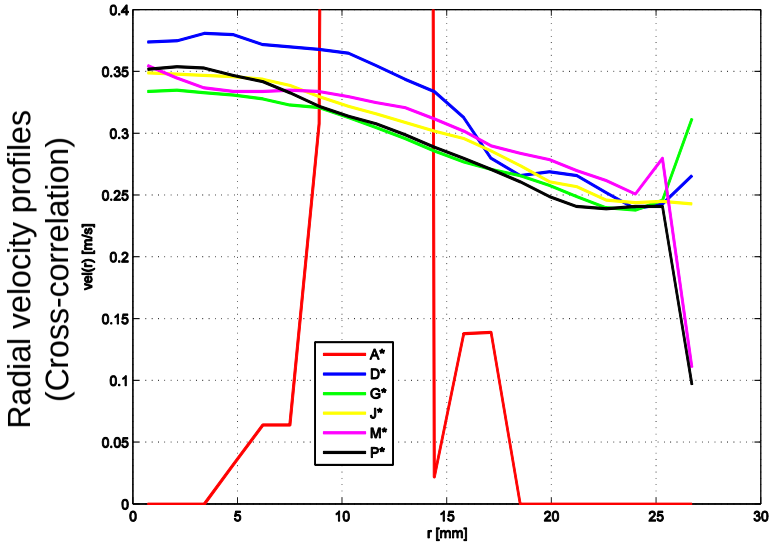

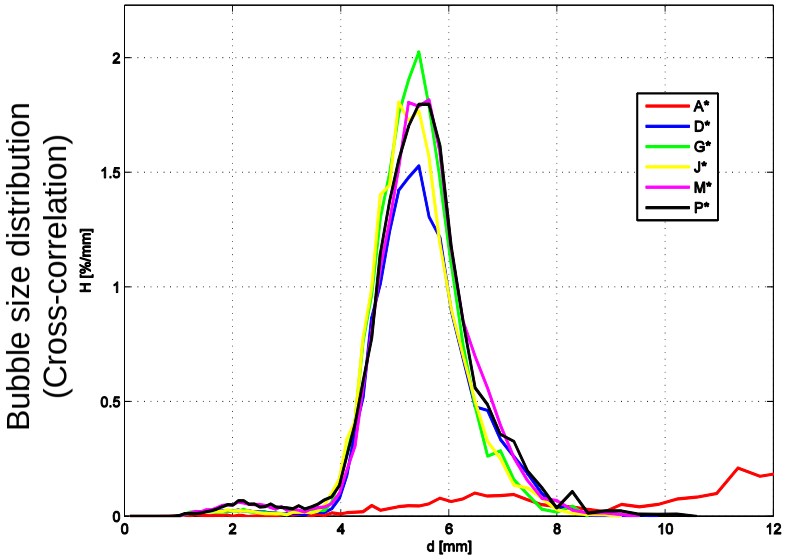

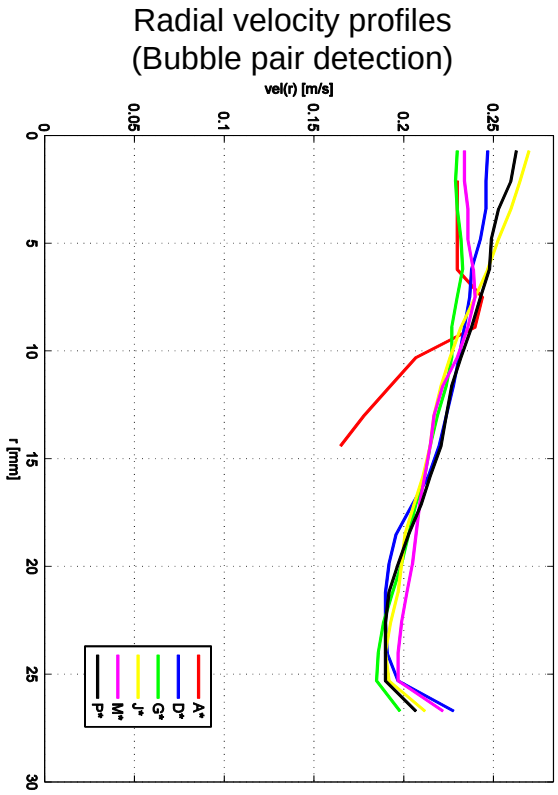
Radial velocity profiles
(Bubble pair detection)
vel(r) [m/s]
r [mm]
P*
M*
J*
G*
D*
A*

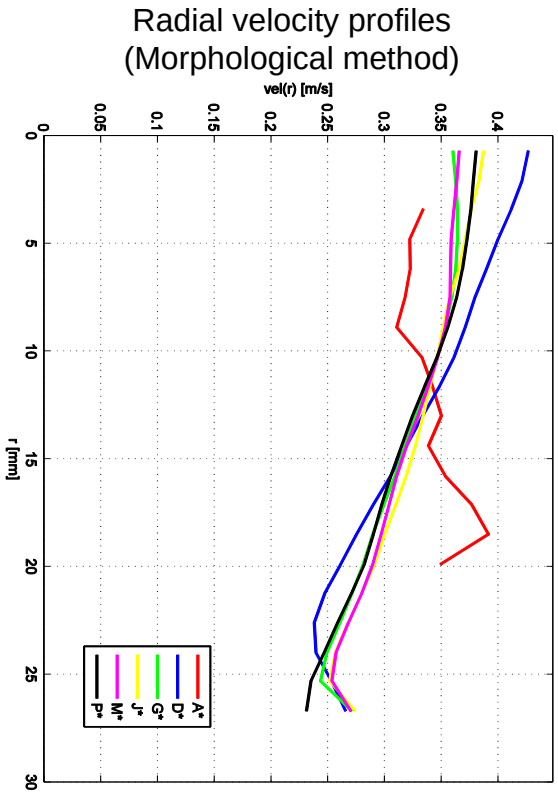
Radial velocity profiles
(Morphological method)
vel(r) [m/s]
r [mm]
P*
M*
J*
G*
D*
A*

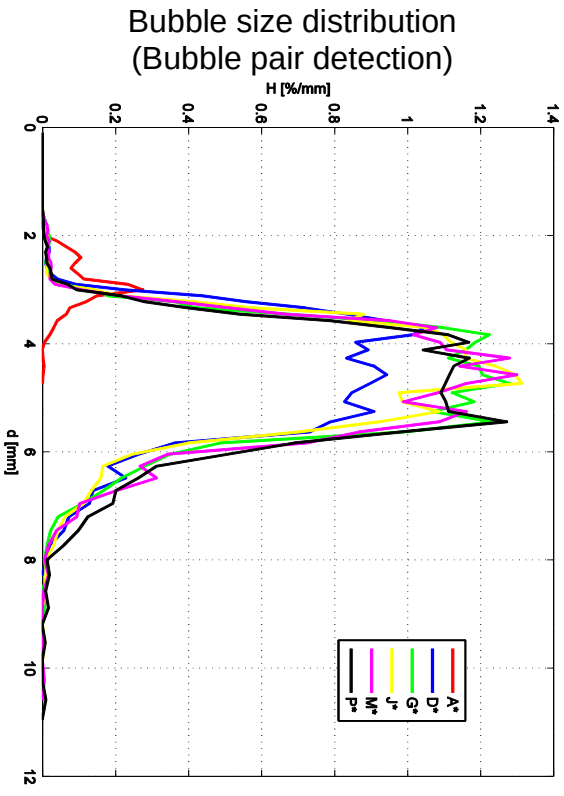
Bubble size distribution
(Bubble pair detection)
H [%/mm]
d [mm]
P*
M*
J*
G*
D*
A*

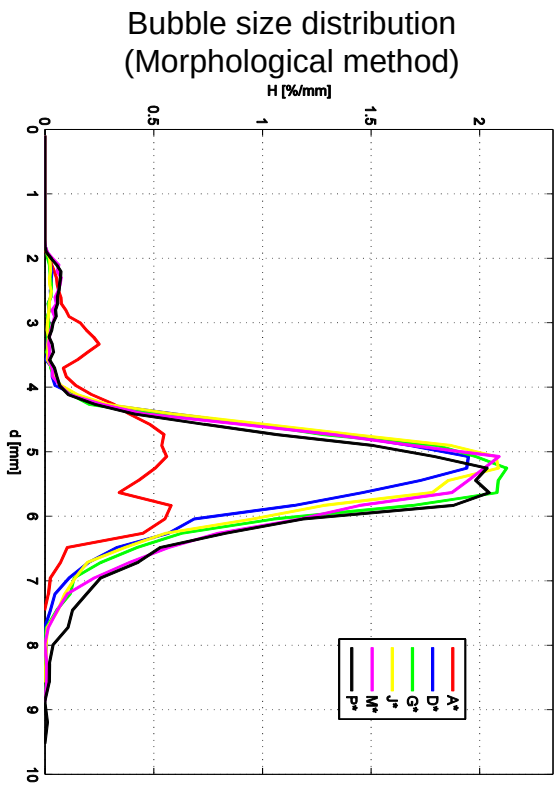
Bubble size distribution
(Morphological method)
H [%/mm]
d [mm]
P*
M*
J*
G*
D*
A*

L16 – 037 (jl = 0.161 m/s; jg = 0.0096 m/s), 2x1000Hz
Void development
eps [%]
L/D [-]
Theory (u_d = 0.235 m/s)
Measurement
Radial gas fraction profiles
eps(r) [%]
r [mm]
A*
D*
G*
J*
M*
P*
Radial velocity profiles
(Cross-correlation)
vel(r) [m/s]
r [mm]
Bubble size distribution
(Cross-correlation)
H [%/mm]
d [mm]

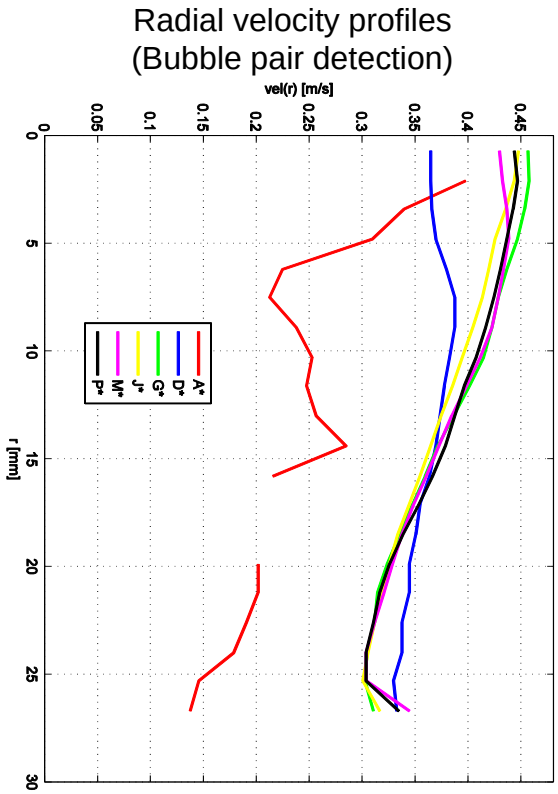
Radial velocity profiles
(Bubble pair detection)
vel(r) [m/s]
r [mm]
P*
M*
J*
G*
D*
A*

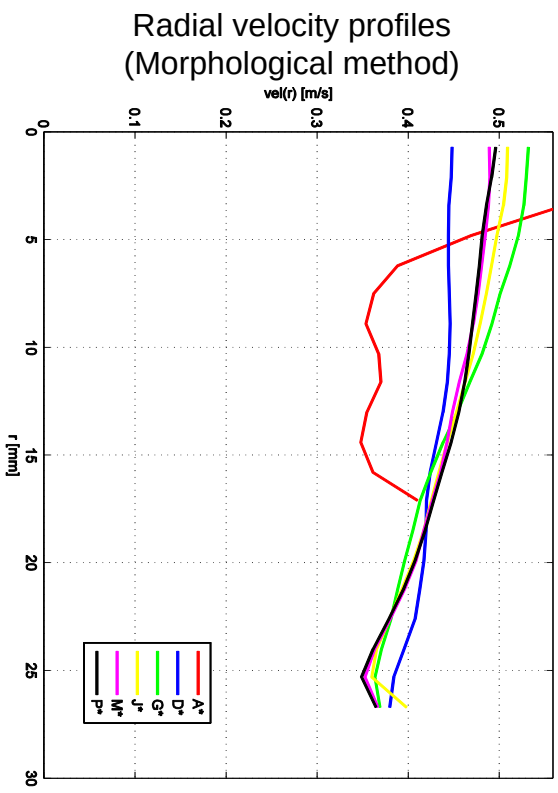
Radial velocity profiles
(Morphological method)
vel(r) [m/s]
r [mm]
P*
M*
J*
G*
D*
A*

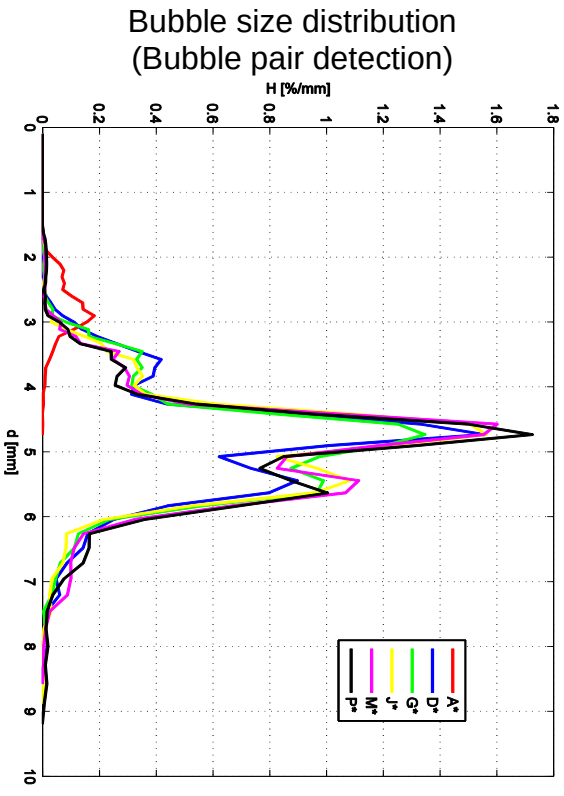
Bubble size distribution
(Bubble pair detection)
H [%/mm]
d [mm]
P*
M*
J*
G*
D*
A*

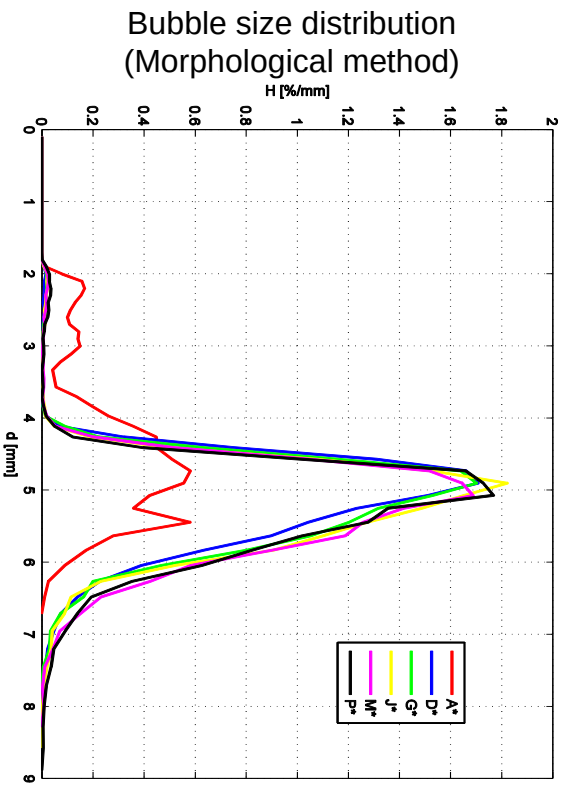
Bubble size distribution
(Morphological method)
H [%/mm]
d [mm]
P*
M*
J*
G*
D*
A*

L16 – 039 (jl = 0.405 m/s; jg = 0.0096 m/s), 2x1000Hz
Void development
eps [%]
L/D [-]
Theory (u_d = 0.235 m/s)
Measurement
Radial gas fraction profiles
eps(r) [%]
r [mm]
A*
D*
G*
J*
M*
P*
Bubble size distribution
(Cross-correlation)
H [%/mm]
d [mm]
Radial velocity profiles
(Cross-correlation)
vel(r) [m/s]
r [mm]

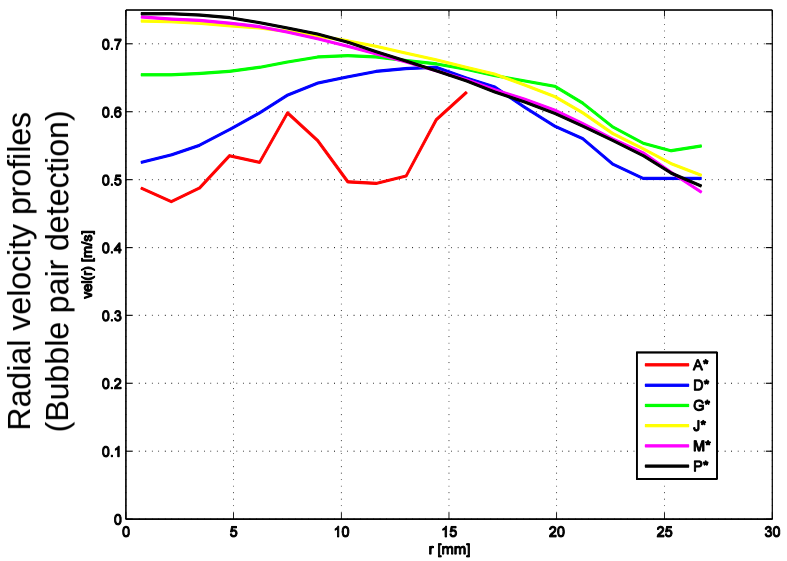
Radial velocity profiles
(Bubble pair detection)
vel(r) [m/s]
r [mm]
A*
D*
G*
J*
M*
P*

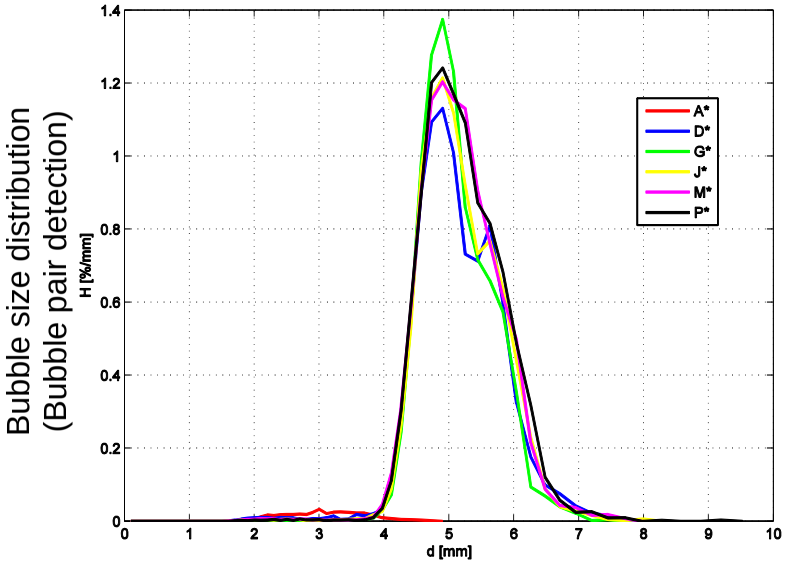
Bubble size distribution
(Bubble pair detection)
H [%/mm]
d [mm]
A*
D*
G*
J*
M*
P*

L16 – 039 (jl = 0.405 $^{m}/_{s}$; jg = 0.0096 $^{m}/_{s}$), 2x2500Hz

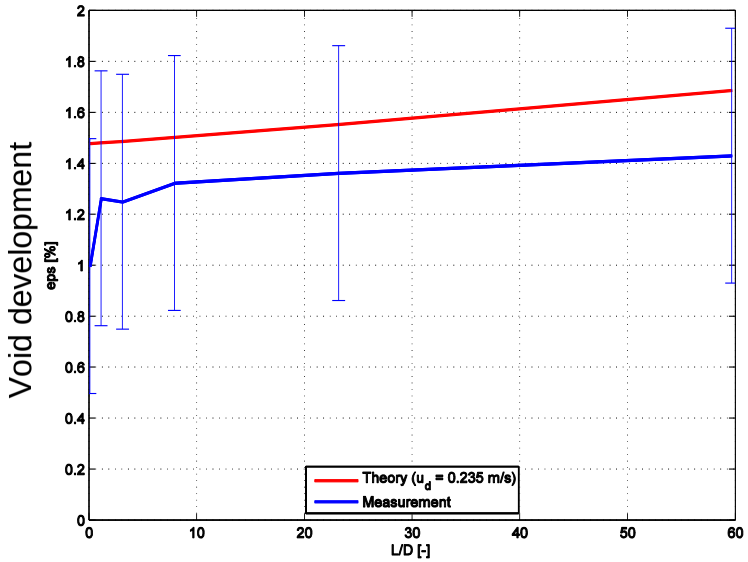

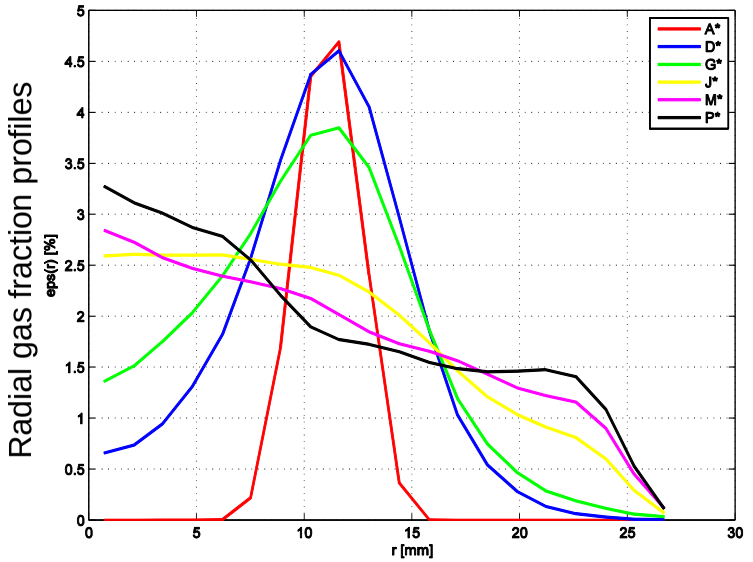

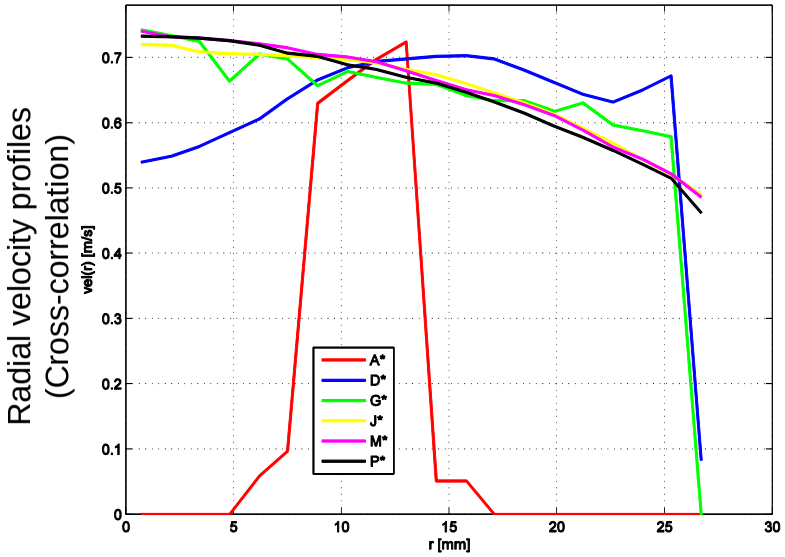

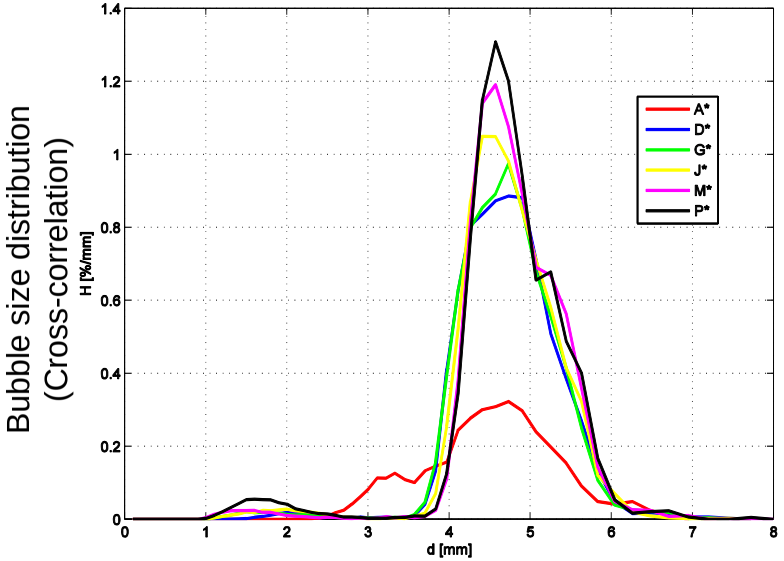

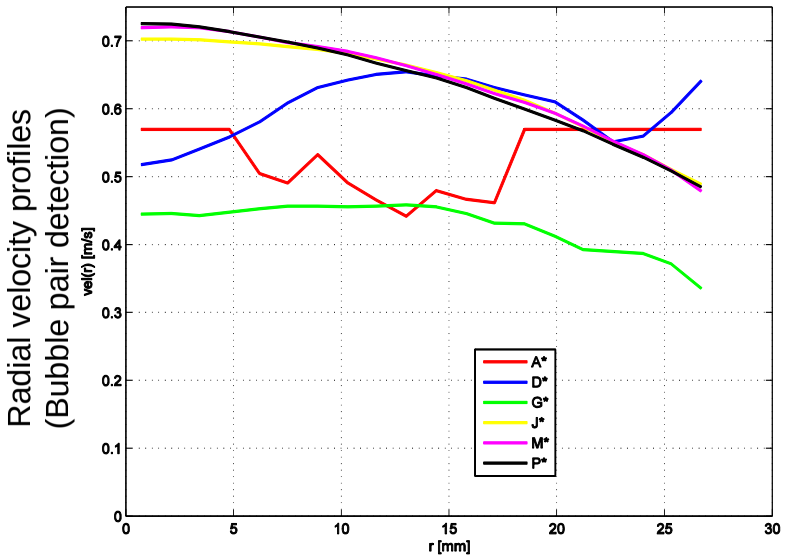
Radial velocity profiles
(Bubble pair detection)
vel(r) [m/s]
r [mm]
A*
D*
G*
J*
M*
P*

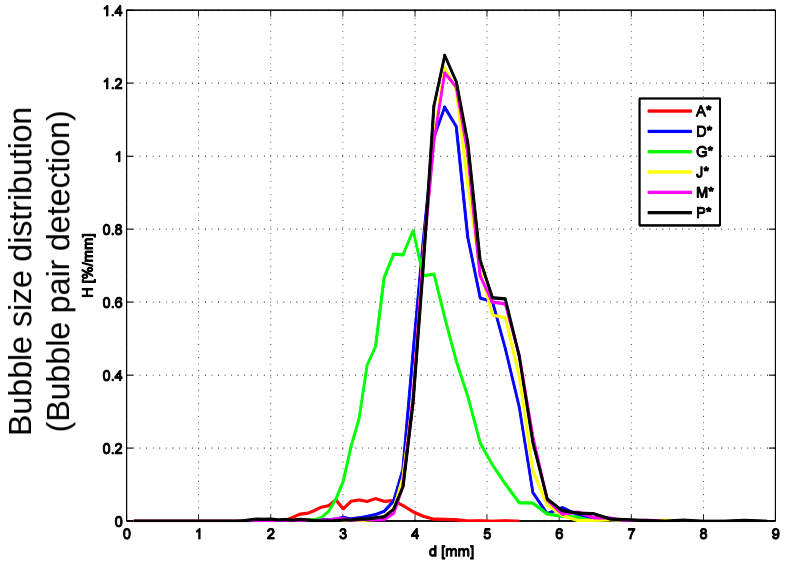
Bubble size distribution
(Bubble pair detection)
H [%/mm]
d [mm]
A*
D*
G*
J*
M*
P*

L16 – 041 (jl = 1.017 $^{m}/_{s}$; jg = 0.0096 $^{m}/_{s}$), 2x2500Hz

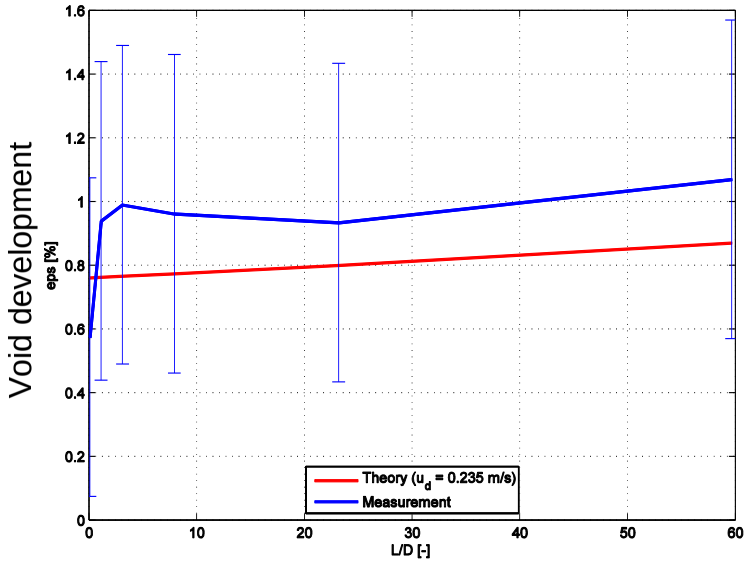

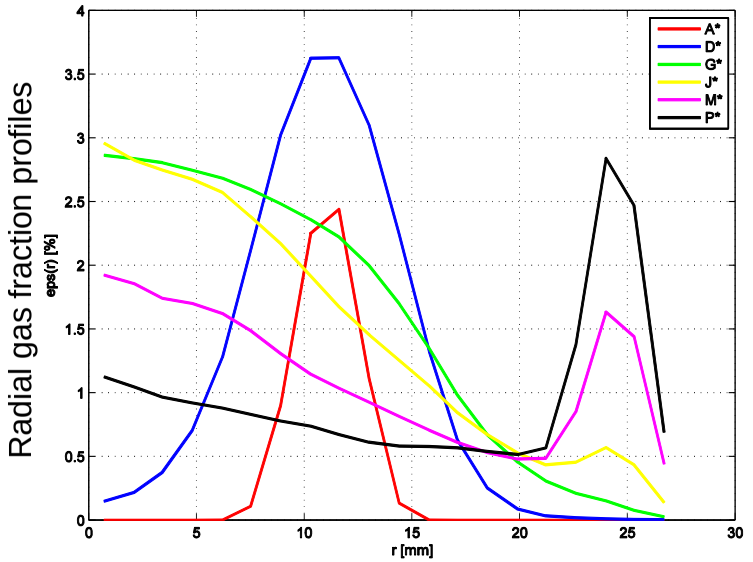

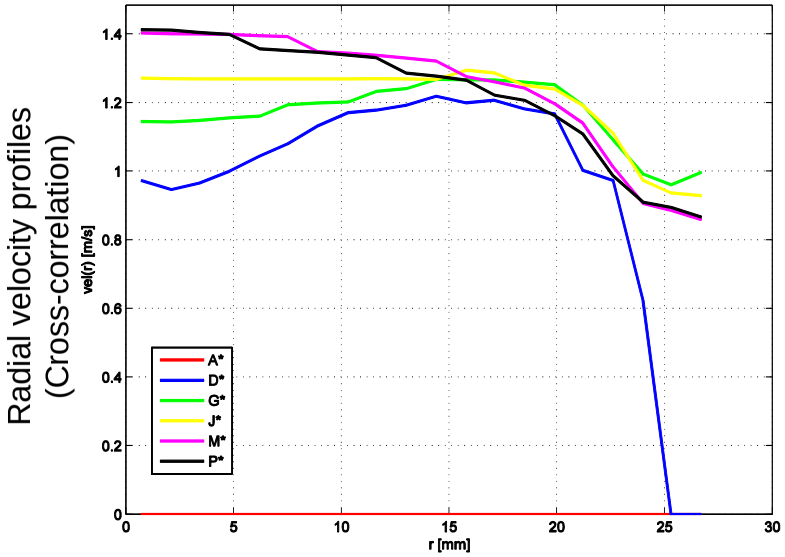

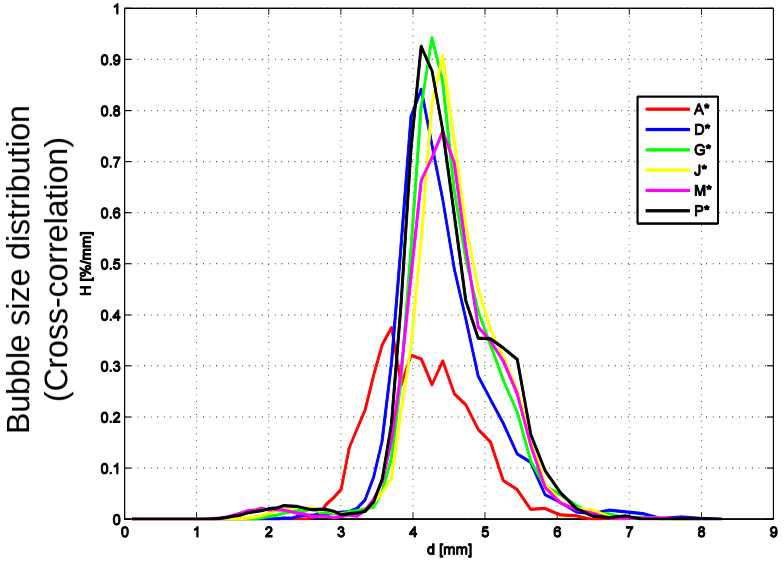

Radial velocity profiles
(Bubble pair detection)

Bubble size distribution
(Bubble pair detection)

L16 – 042 (jl = 1.611 $^{m}/_{s}$; jg = 0.0096$^{m}/_{s}$), 2x2500Hz

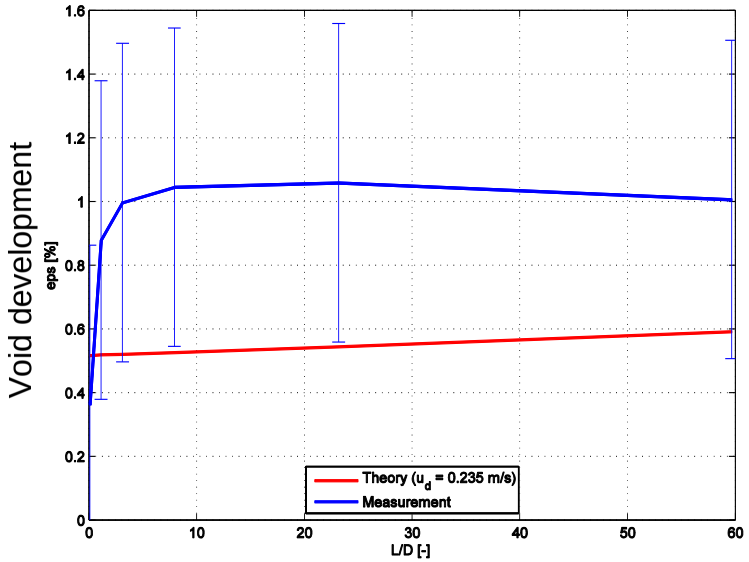

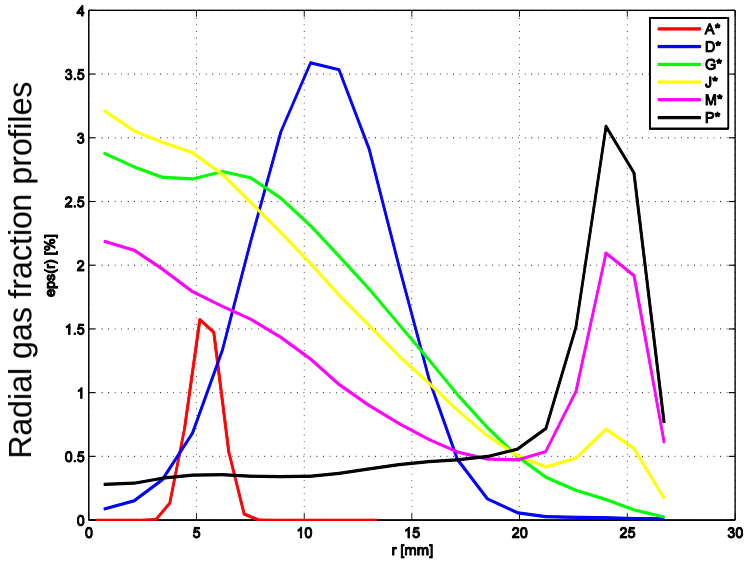

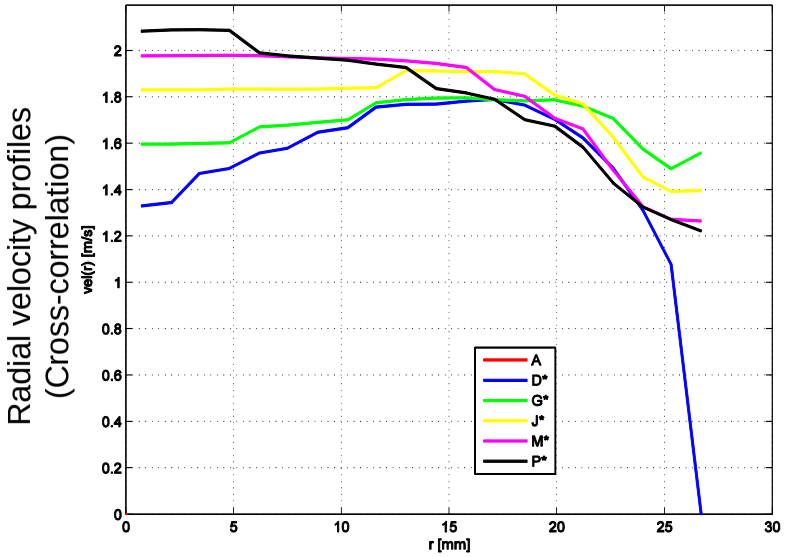

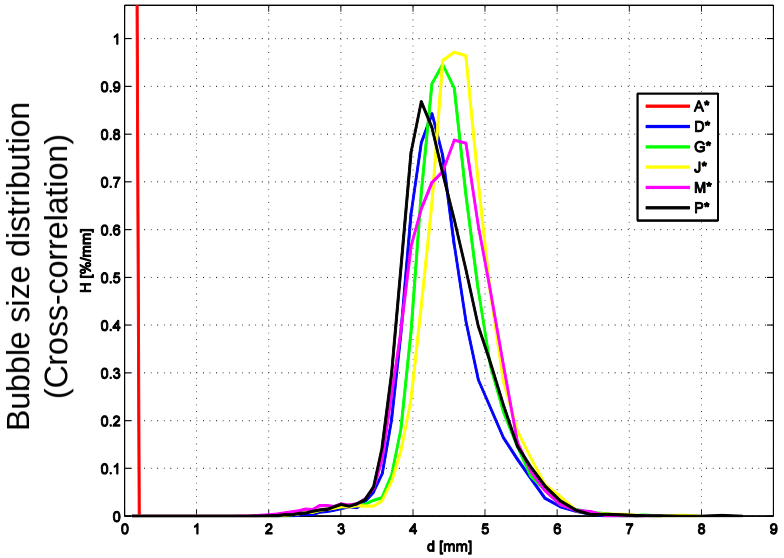

Radial velocity profiles
(Bubble pair detection)

Bubble size distribution
(Bubble pair detection)

L16 – 050 (jl = 0.405 $^{m}/_{s}$; jg = 0.0151 $^{m}/_{s}$), 2x1000Hz

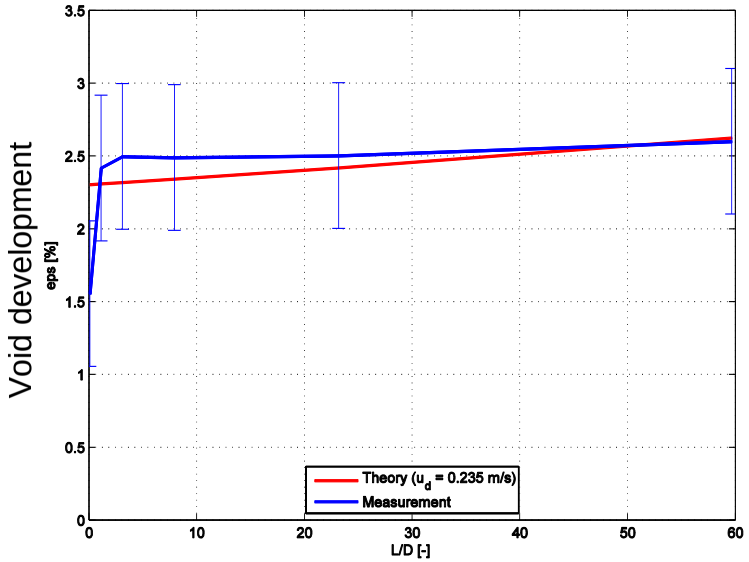

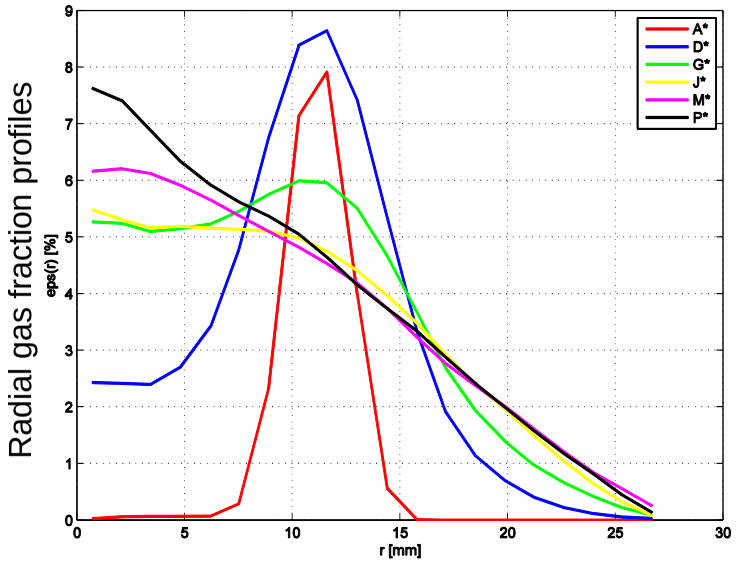

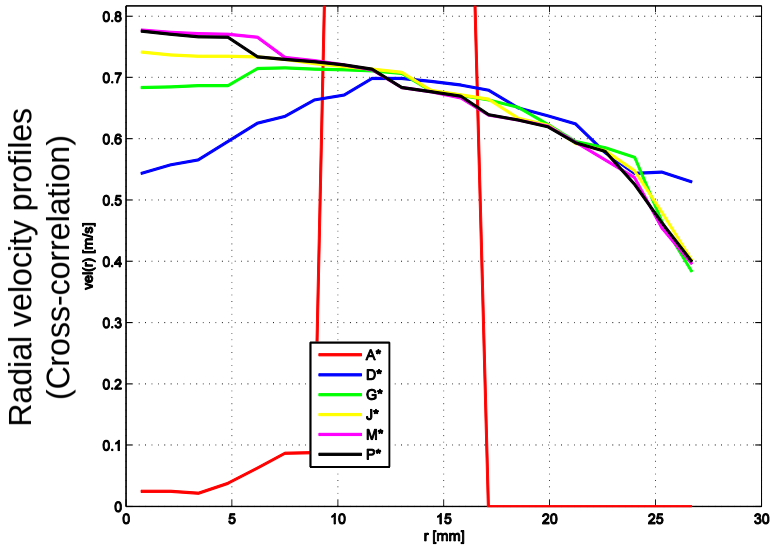

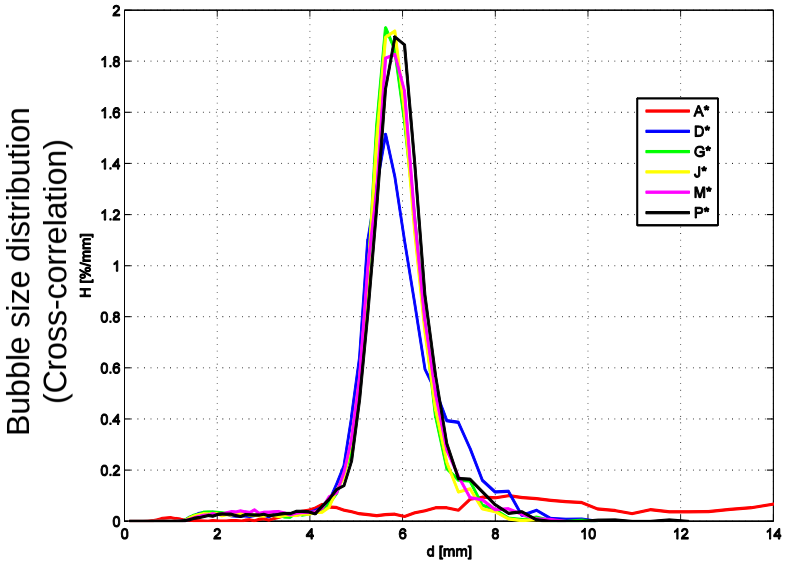

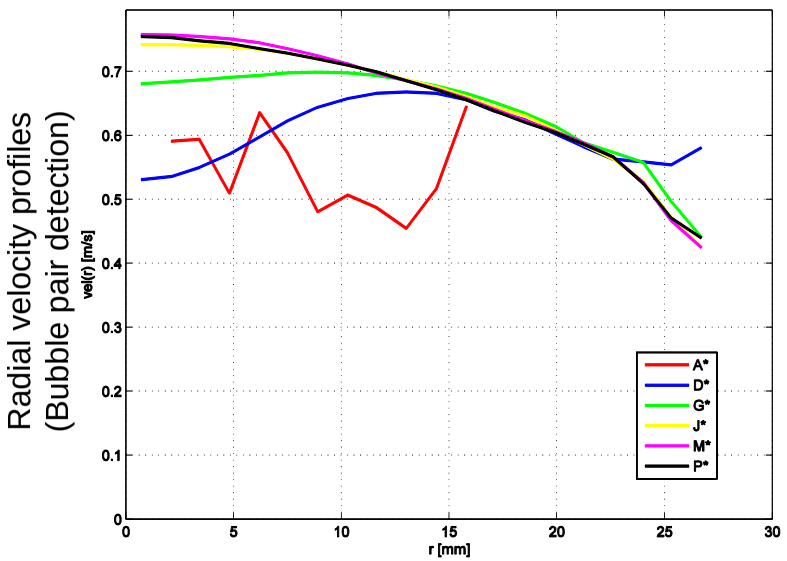
Radial velocity profiles
(Bubble pair detection)
vel(r) [m/s]
r [mm]
A*
D*
G*
J*
M*
P*

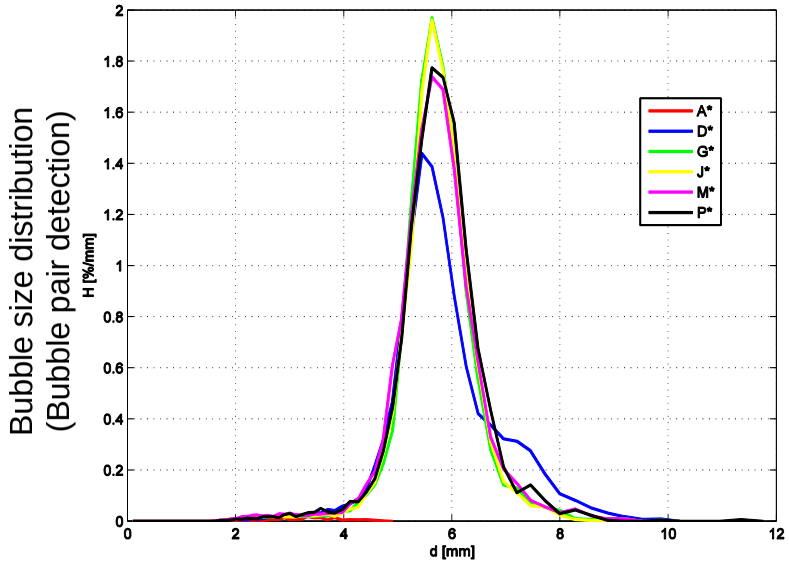
Bubble size distribution
(Bubble pair detection)
H [%/mm]
d [mm]
A*
D*
G*
J*
M*
P*

L16 – 050 (jl = 0.405 $^{m}/_{s}$; jg = 0.0151 $^{m}/_{s}$), 2x2500Hz

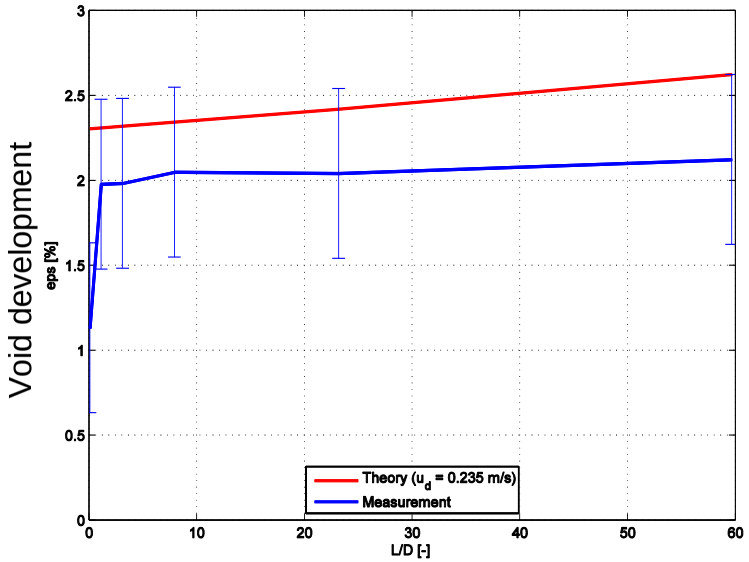

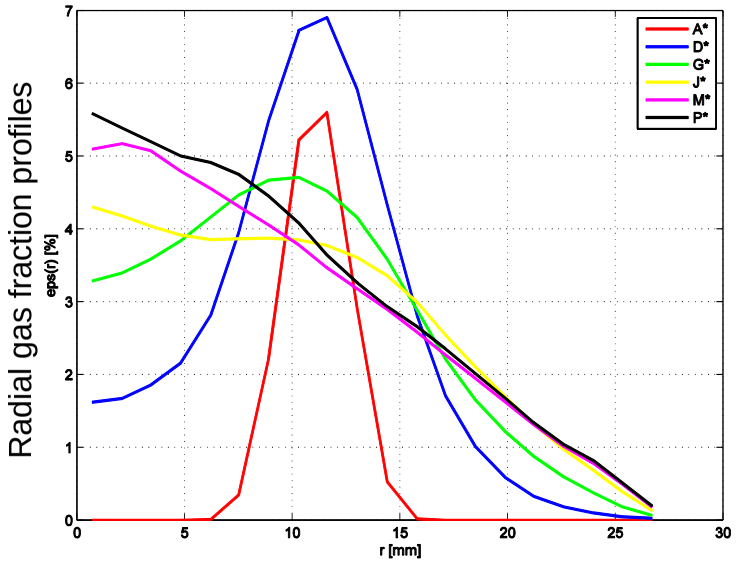

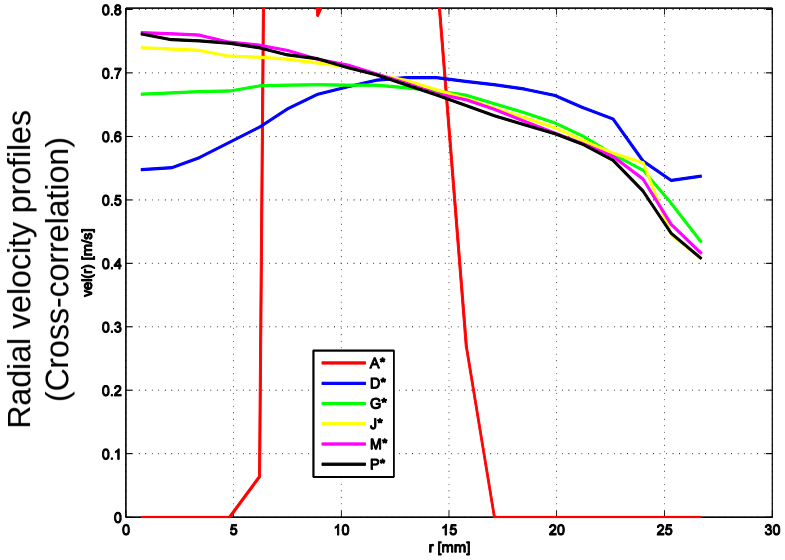

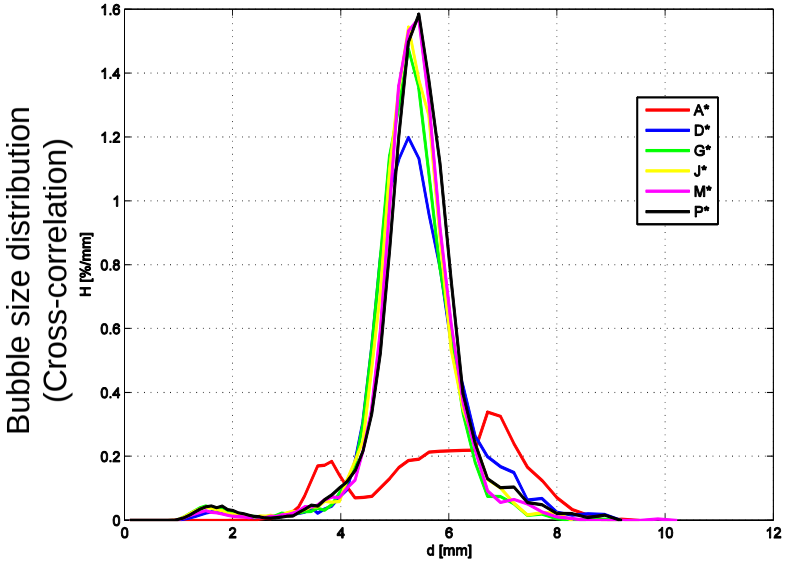

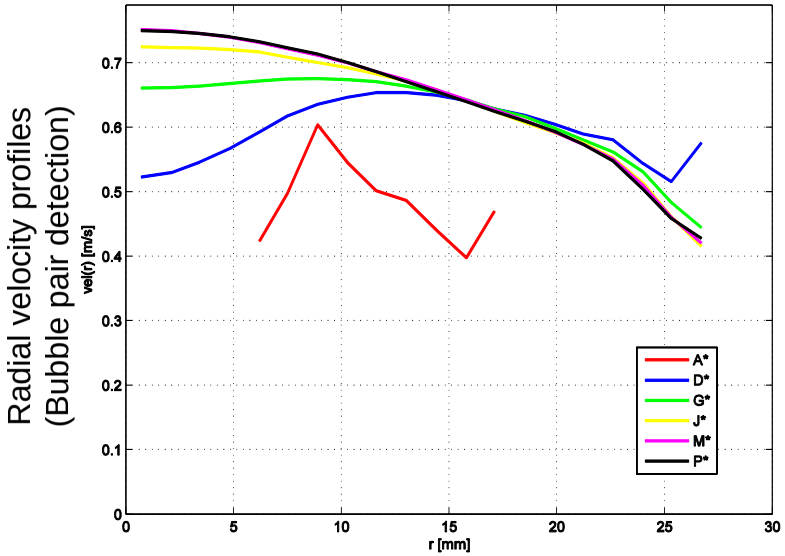
Radial velocity profiles
(Bubble pair detection)
vel(r) [m/s]
r [mm]
A*
D*
G*
J*
M*
P*

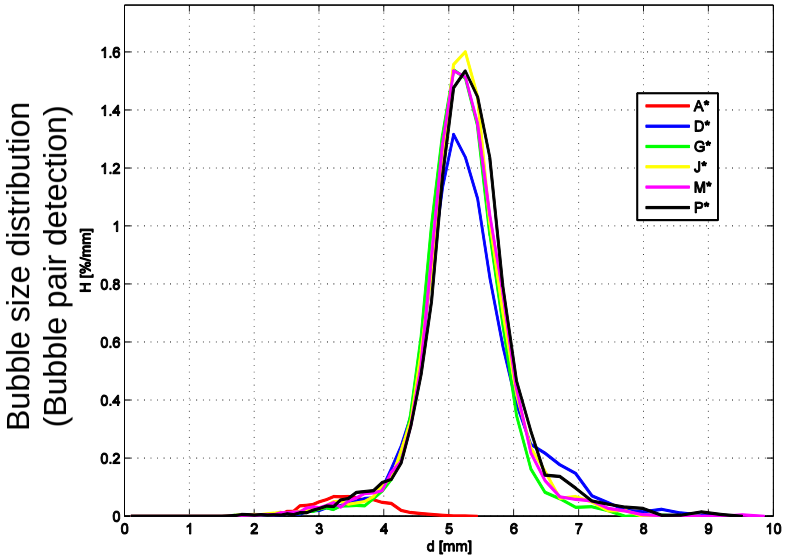
Bubble size distribution
(Bubble pair detection)
H [%/mm]
d [mm]
A*
D*
G*
J*
M*
P*

L16 – 052 (jl = 1.017 $^{m}/_{s}$; jg = 0.0151 $^{m}/_{s}$), 2x2500Hz

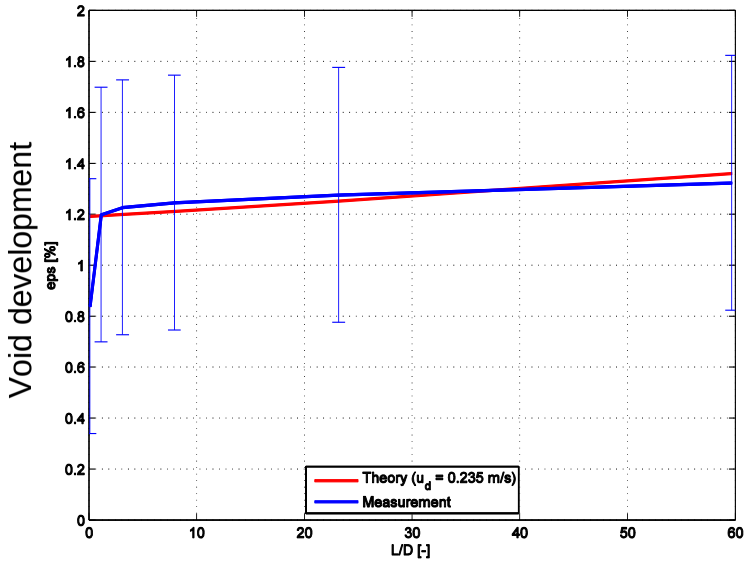

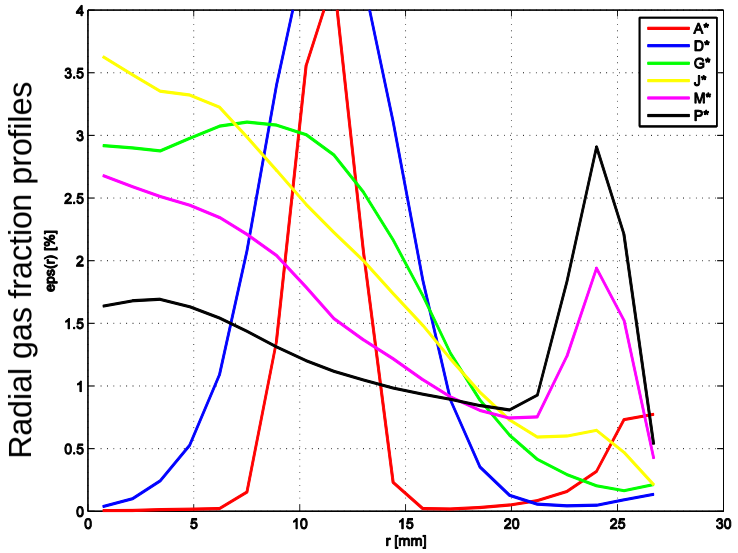

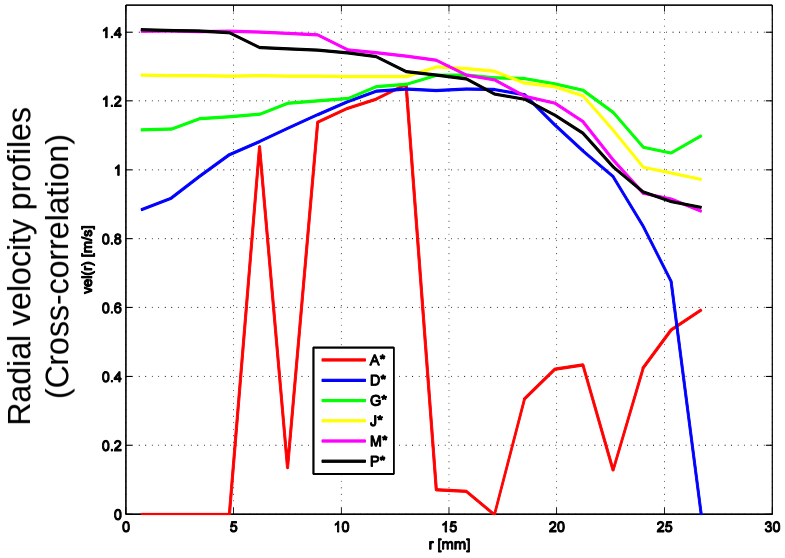

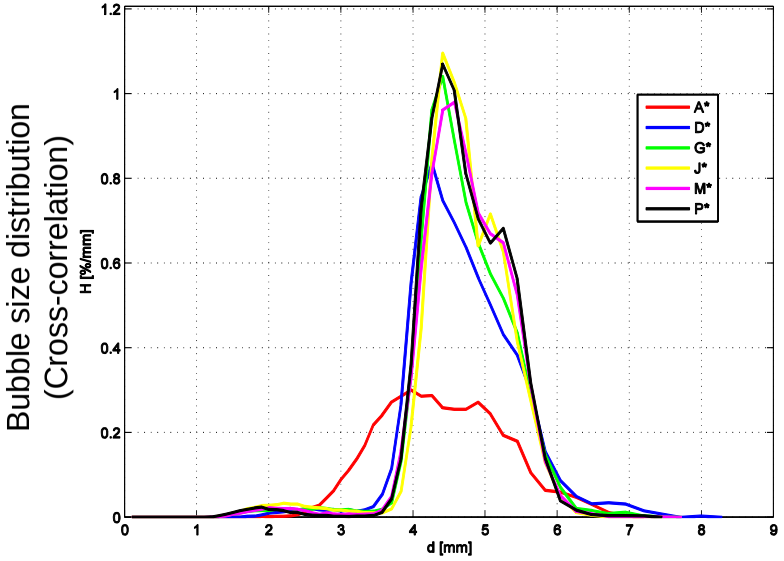

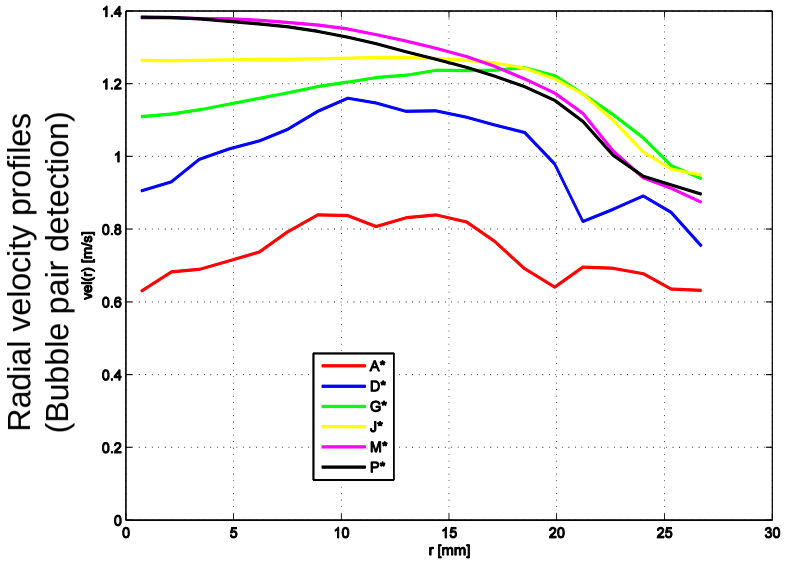
Radial velocity profiles
(Bubble pair detection)
vel(r) [m/s]
r [mm]
A*
D*
G*
J*
M*
P*

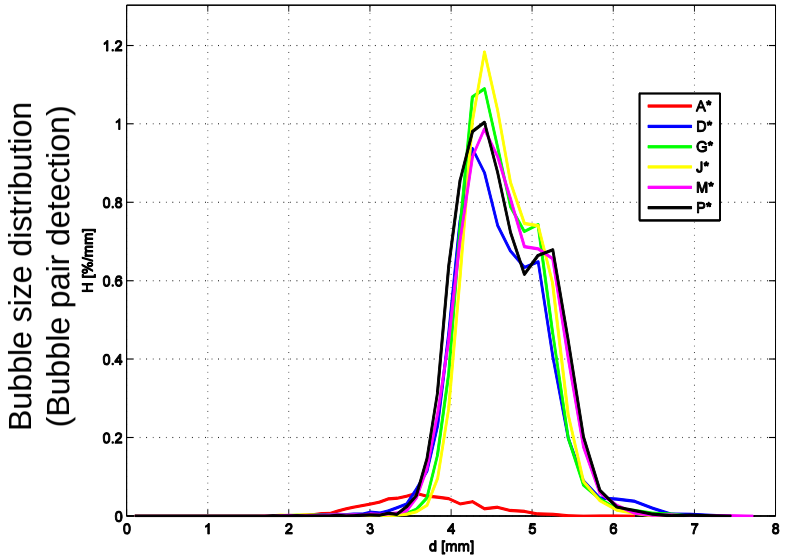
Bubble size distribution
(Bubble pair detection)
H [%/mm]
d [mm]
A*
D*
G*
J*
M*
P*

L16 – 067 (jl = 0.0405 $^{m}/_{s}$; jg = 0.0368 $^{m}/_{s}$), 2x1000Hz

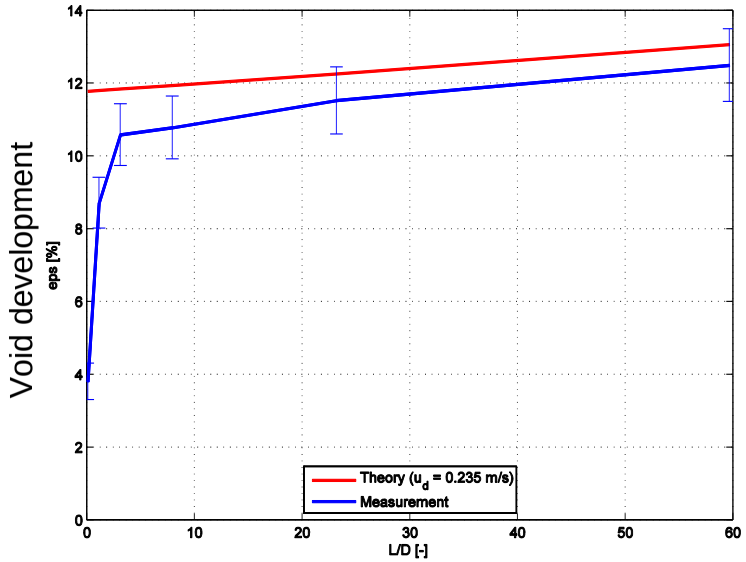

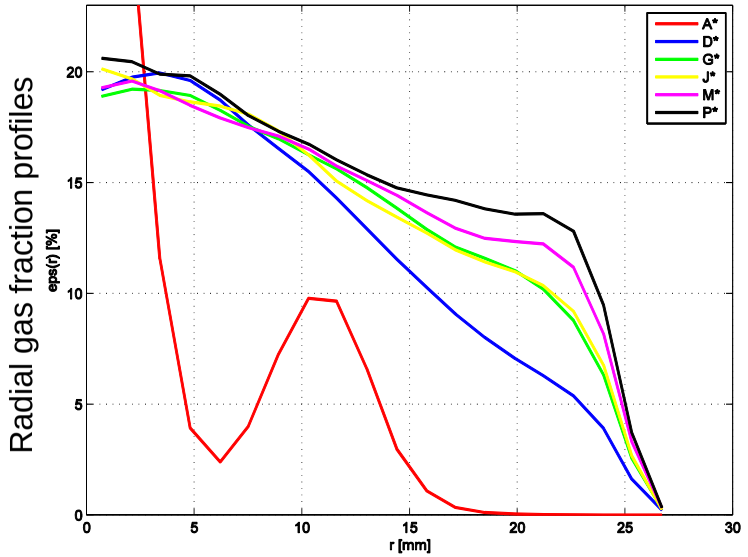

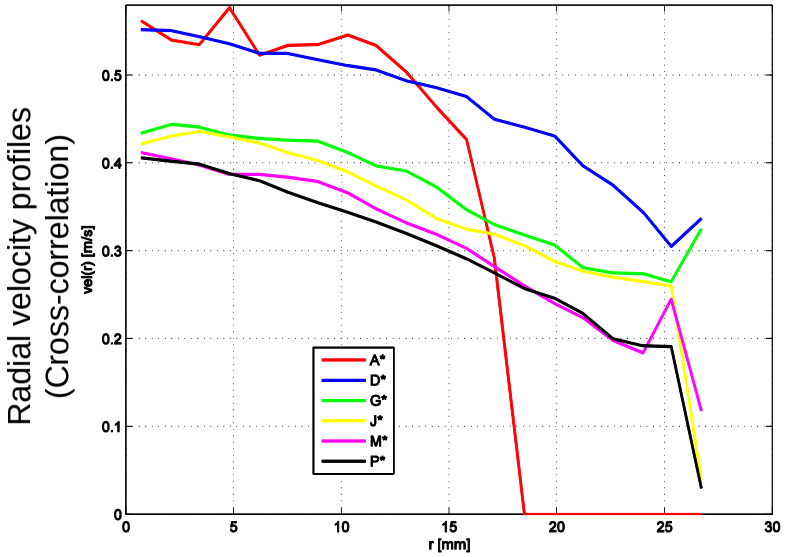

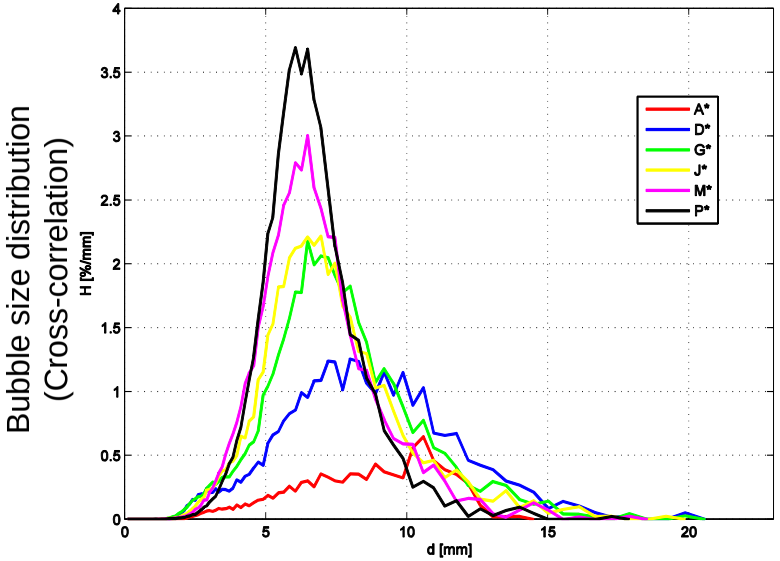

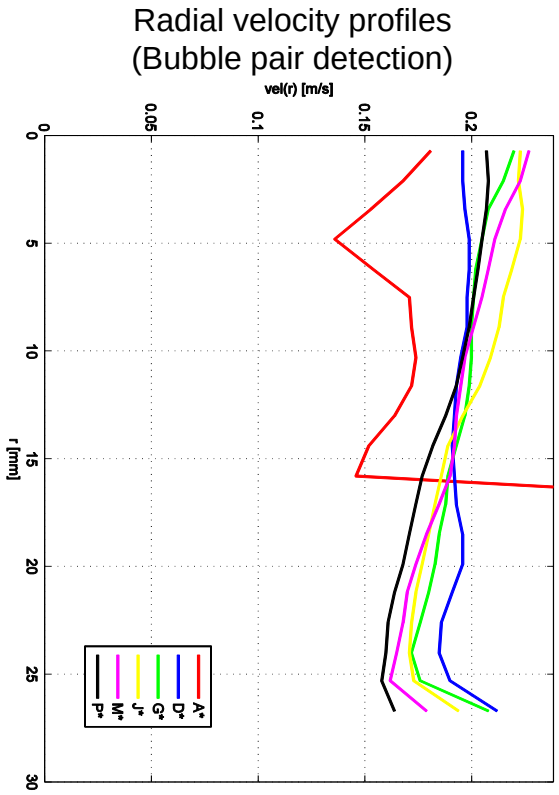
Radial velocity profiles
(Bubble pair detection)
vel(r) [m/s]
r [mm]
P*
M*
J*
G*
D*
A*

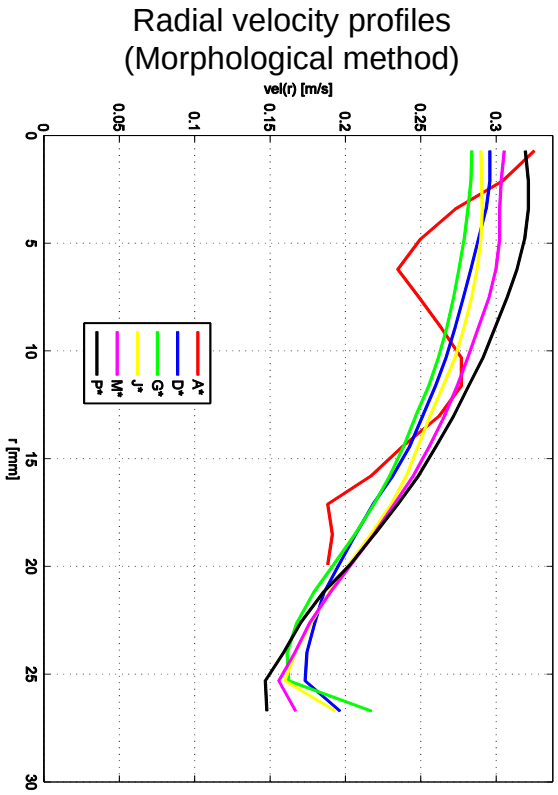
Radial velocity profiles
(Morphological method)
vel(r) [m/s]
r [mm]
P*
M*
J*
G*
D*
A*

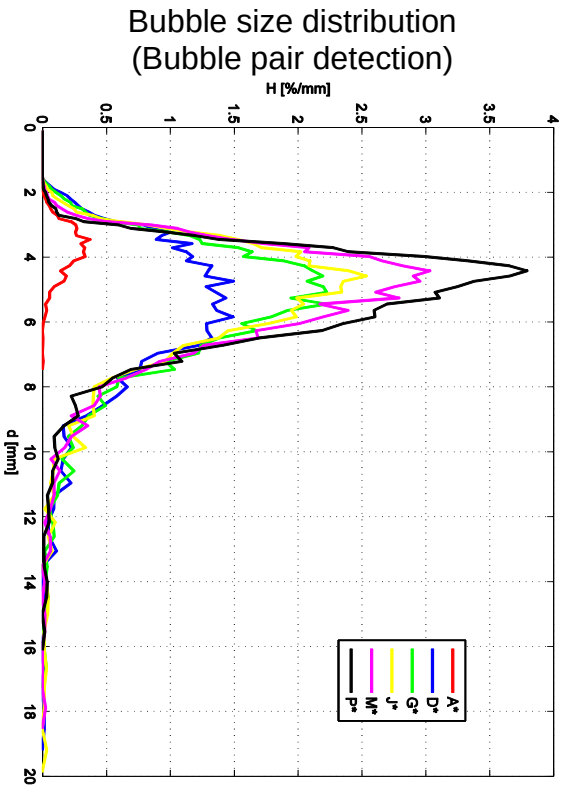
Bubble size distribution
(Bubble pair detection)
H [%/mm]
d [mm]
P*
M*
J*
G*
D*
A*

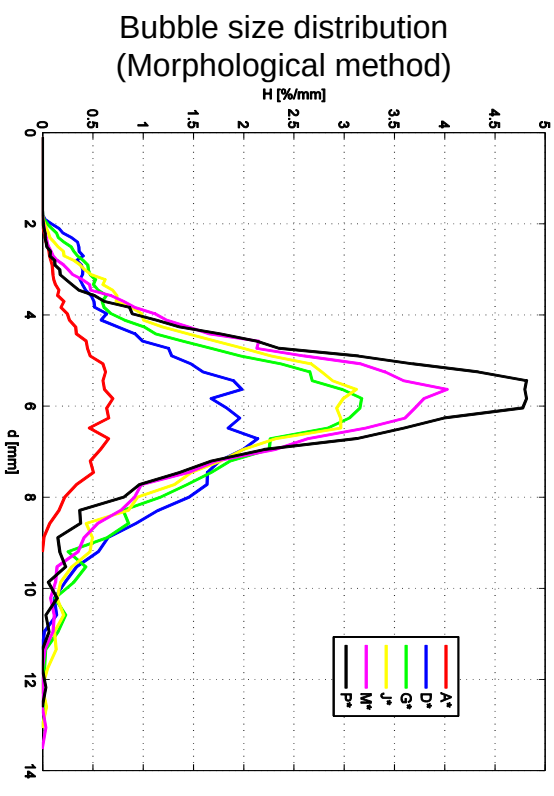
Bubble size distribution
(Morphological method)
H [%/mm]
d [mm]
P*
M*
J*
G*
D*
A*

L16 – 074 (jl = 1.017 m/s; jg = 0.0368 m/s), 2x2500Hz
Void development
eps [%]
L/D [-]
Theory (u_d = 0.235 m/s)
Measurement
Radial gas fraction profiles
eps(r) [%]
r [mm]
A*
D*
G*
J*
M*
P*
Radial velocity profiles
(Cross-correlation)
vel(r) [m/s]
r [mm]
Bubble size distribution
(Cross-correlation)
H [%/mm]
d [mm]

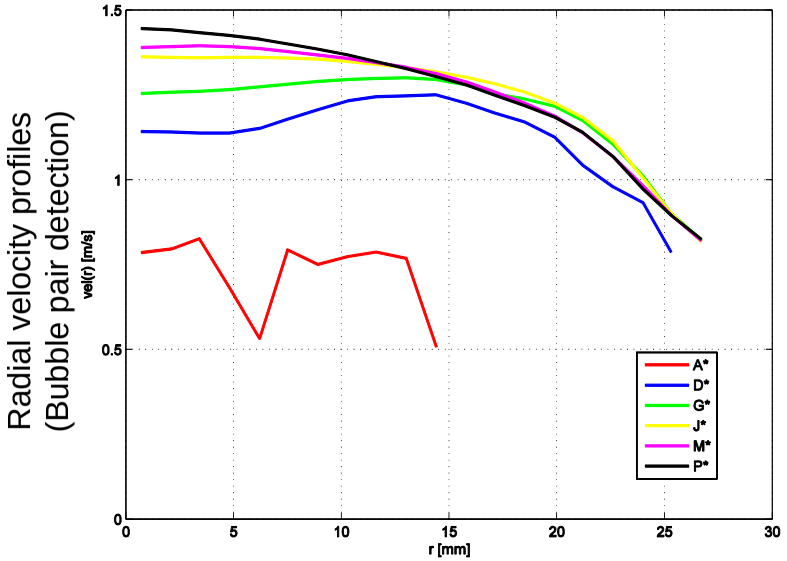
Radial velocity profiles
(Bubble pair detection)
vel(r) [m/s]
r [mm]
A*
D*
G*
J*
M*
P*

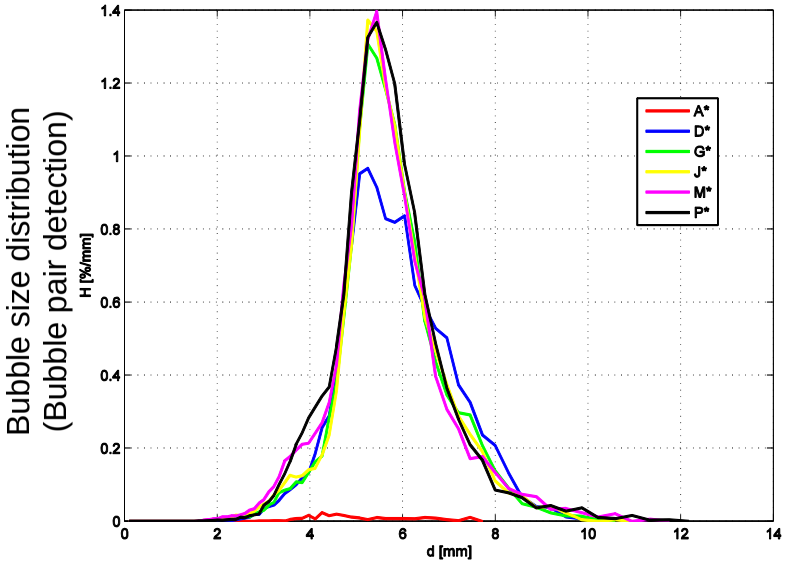
Bubble size distribution
(Bubble pair detection)
H [%/mm]
d [mm]
A*
D*
G*
J*
M*
P*

L16 – 077 (jl = 4.047 $^{m}/_{s}$; jg = 0.0368 $^{m}/_{s}$), 1x5000Hz

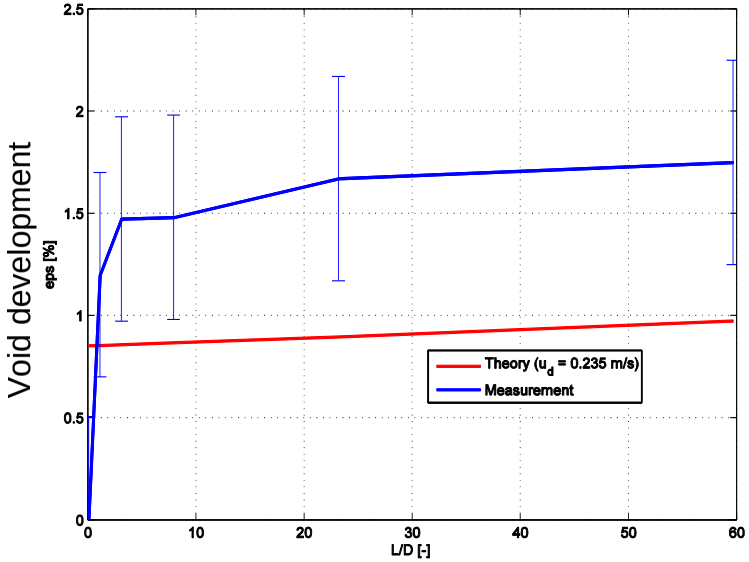

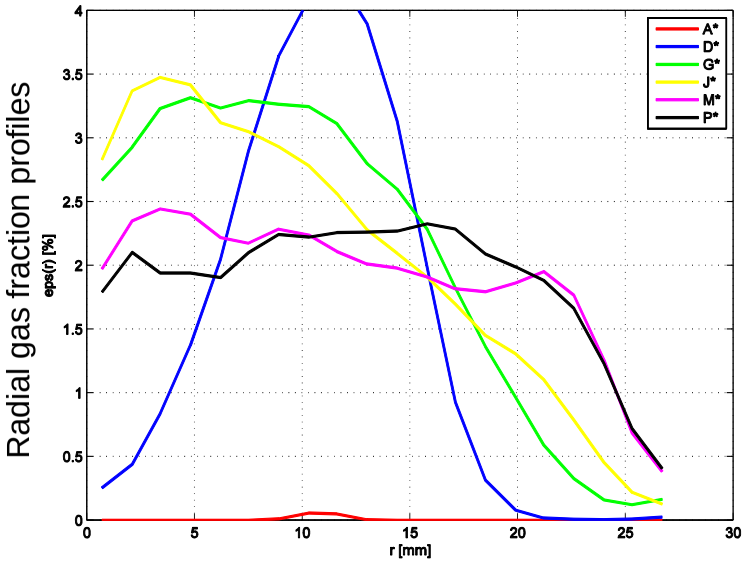

Radial velocity profiles
(Cross-correlation)
2x2500Hz results are used

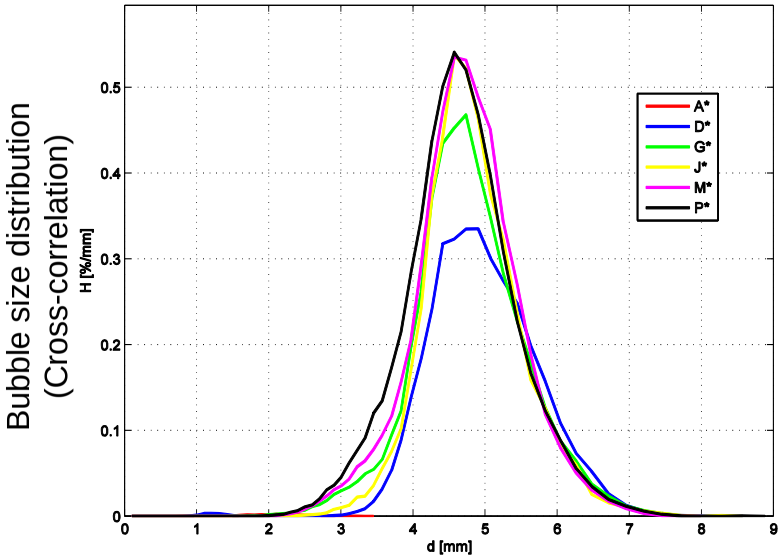

L16 – 077 (jl = 4.047 m/s; jg = 0.0368 m/s), 2x2500Hz
Void development
eps [%]
L/D [-]
Theory (u_d = 0.235 m/s)
Measurement
Radial gas fraction profiles
eps(r) [%]
r [mm]
A*
D*
G*
J*
M*
P*
Bubble size distribution
(Cross-correlation)
H [%/mm]
d [mm]
Radial velocity profiles
(Cross-correlation)
vel(r) [m/s]
r [mm]

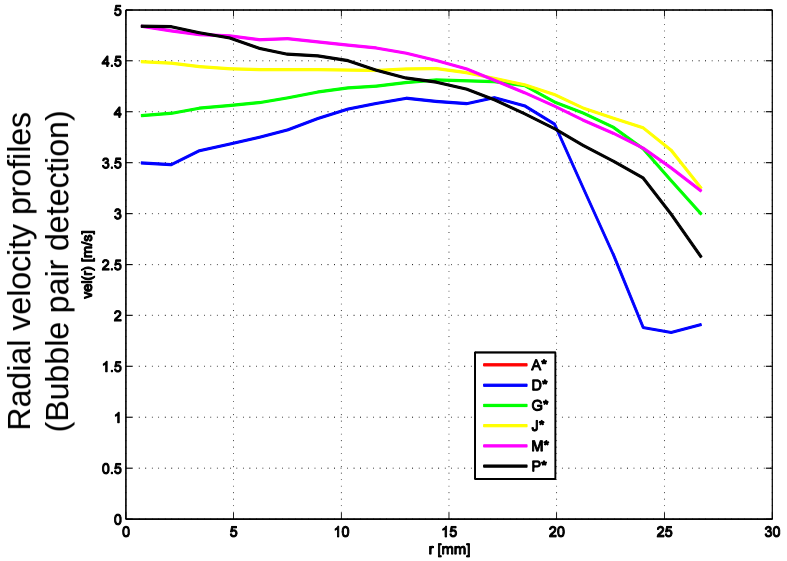
Radial velocity profiles
(Bubble pair detection)
vel(r) [m/s]
r [mm]
A*
D*
G*
J*
M*
P*

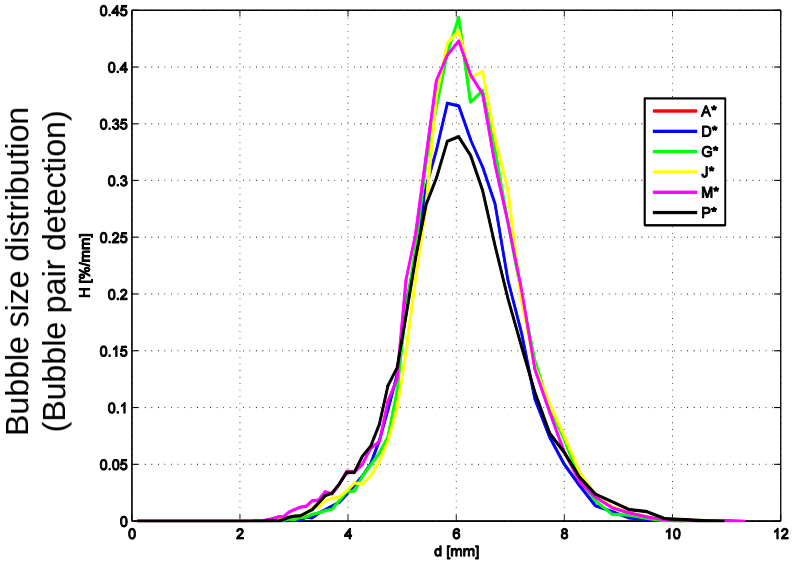
Bubble size distribution
(Bubble pair detection)
H [%/mm]
d [mm]
A*
D*
G*
J*
M*
P*

L16 – 089 (jl = 0.0405 $^{m}/_{s}$; jg = 0.0898 $^{m}/_{s}$), 2x1000Hz

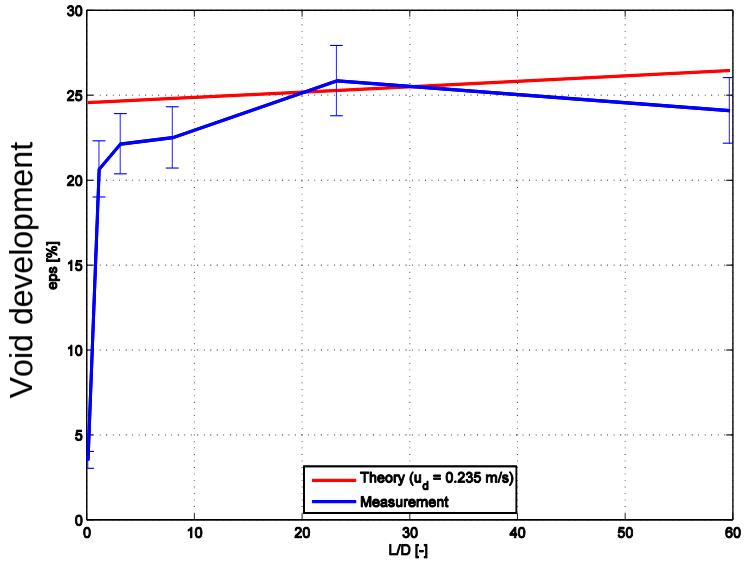

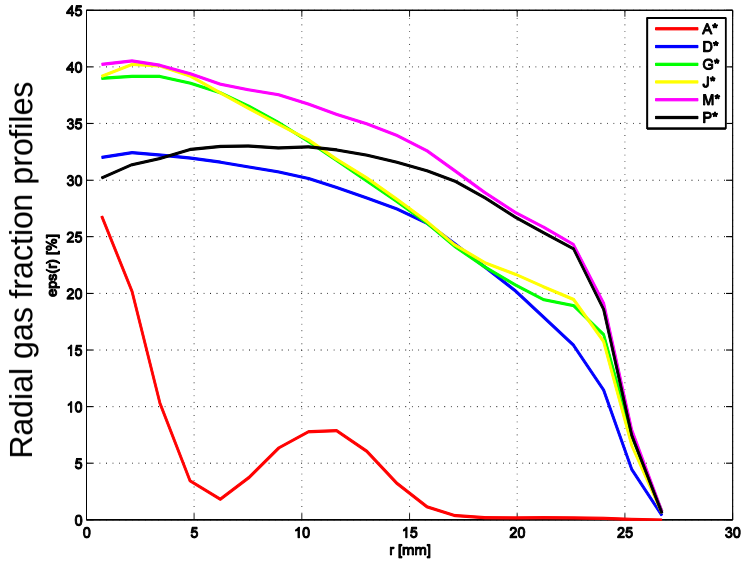

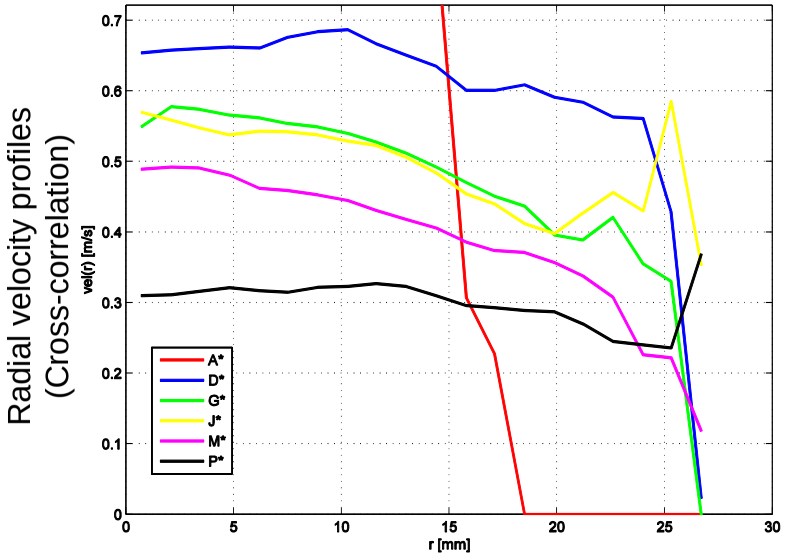

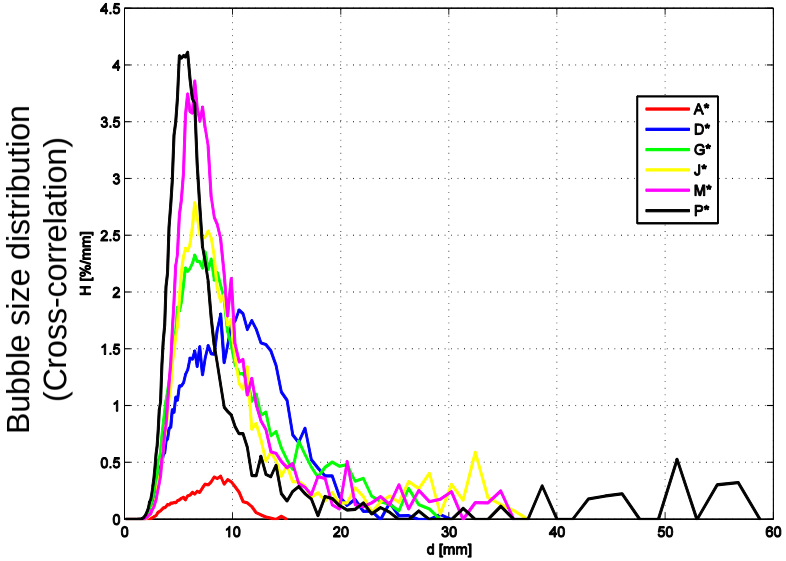

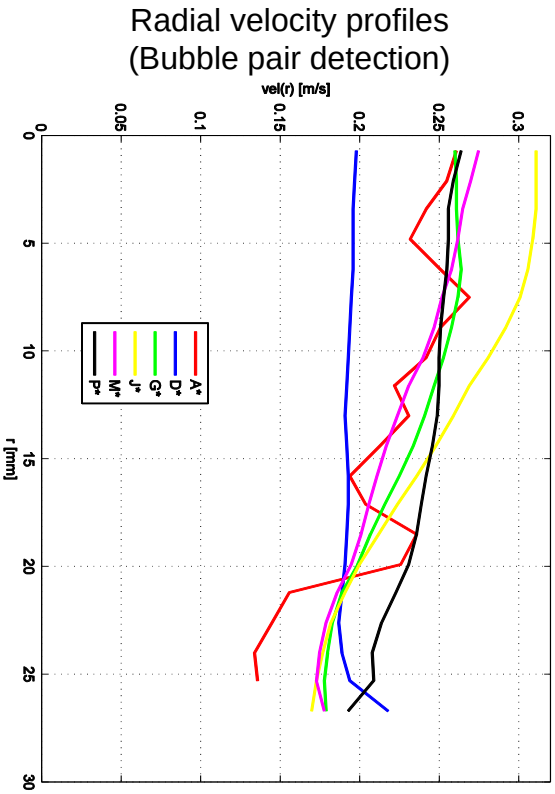
Radial velocity profiles
(Bubble pair detection)
vel(r) [m/s]
r [mm]
P*
M*
J*
G*
D*
A*

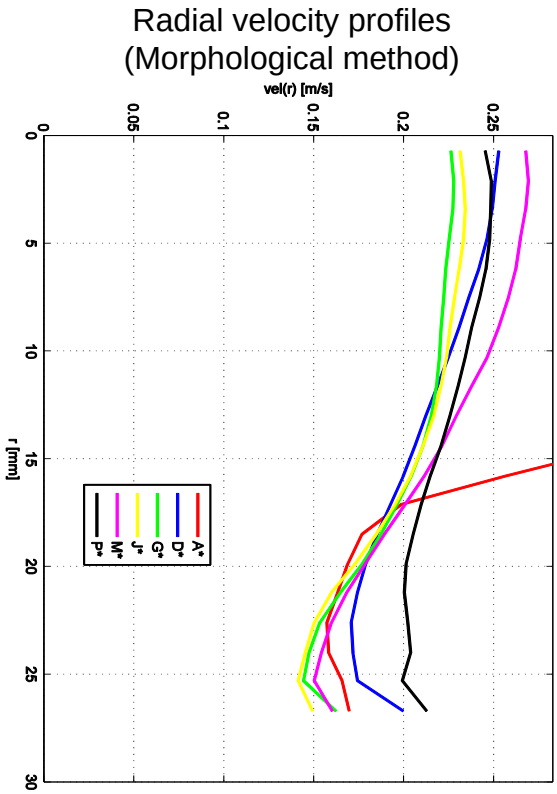
Radial velocity profiles
(Morphological method)
vel(r) [m/s]
r [mm]
P*
M*
J*
G*
D*
A*

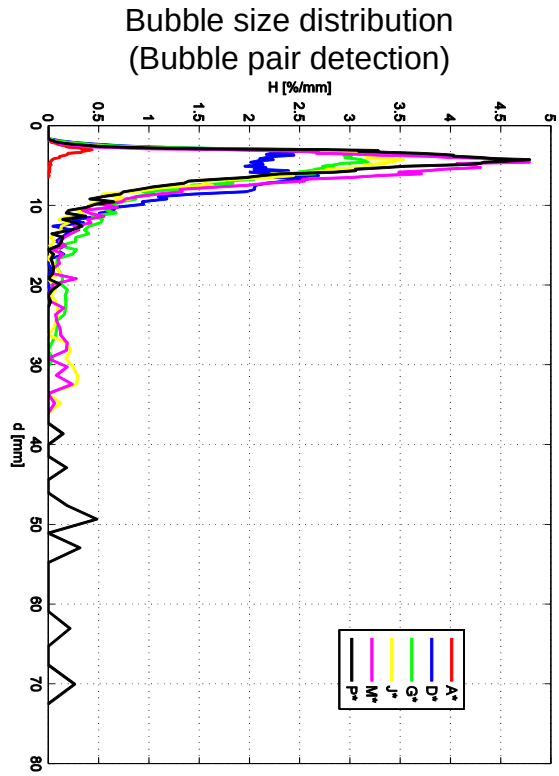
Bubble size distribution
(Bubble pair detection)
H [%/mm]
d [mm]
P*
M*
J*
G*
D*
A*

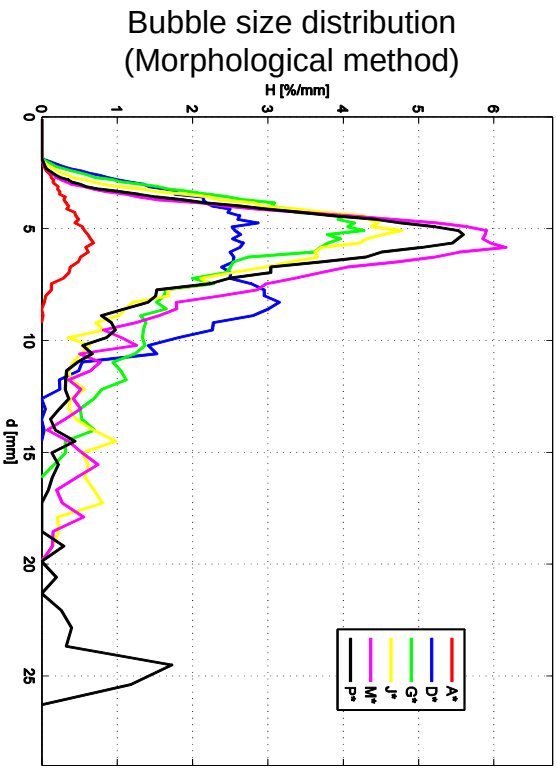
Bubble size distribution
(Morphological method)
H [%/mm]
d [mm]
P*
M*
J*
G*
D*
A*

L16 – 096 (jl = 1.017 $^{m}/_{s}$; jg = 0.0898 $^{m}/_{s}$), 2x2500Hz

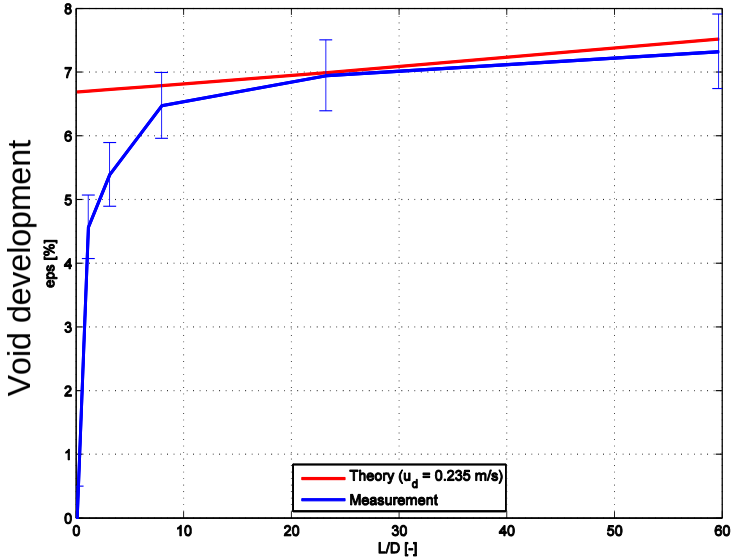

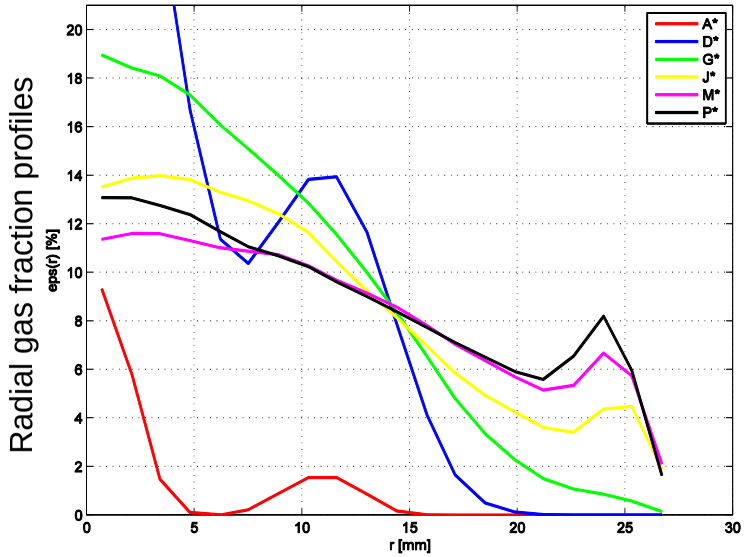

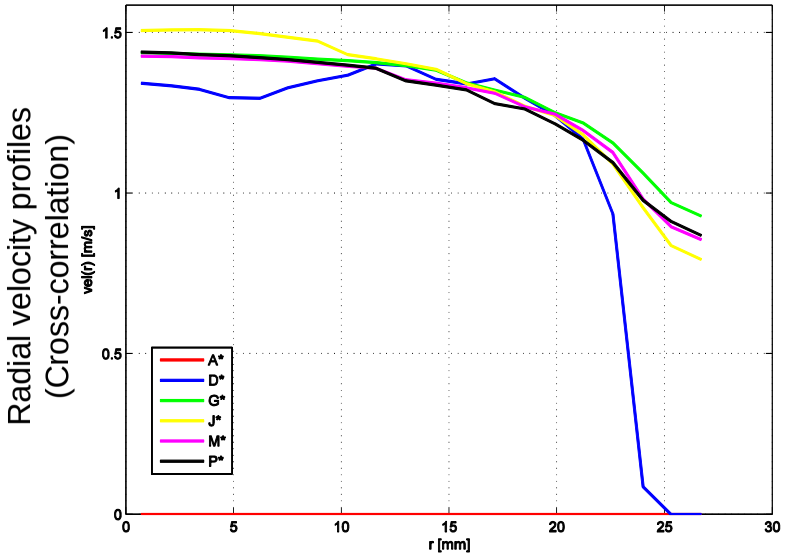

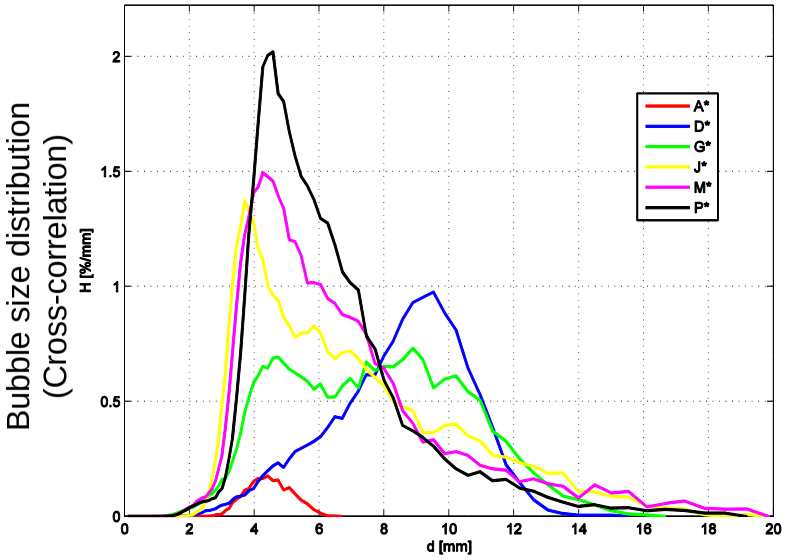

Radial velocity profiles
(Bubble pair detection)

Bubble size distribution
(Bubble pair detection)

L16 – 099 (jl = 4.047 m/s; jg = 0.0898 m/s), 1x5000Hz
Void development
eps [%]
L/D [-]
Theory (u_d = 0.235 m/s)
Measurement
Radial velocity profiles
(Cross-correlation)
2x2500Hz results are used
Radial gas fraction profiles
eps(r) [%]
r [mm]
A*
D*
G*
J*
M*
P*
Bubble size distribution
(Cross-correlation)
H [%/mm]
d [mm]

L16 – 099 (jl = 4.047 $^{m}/_{s}$; jg = 0.0898 $^{m}/_{s}$), 2x2500Hz

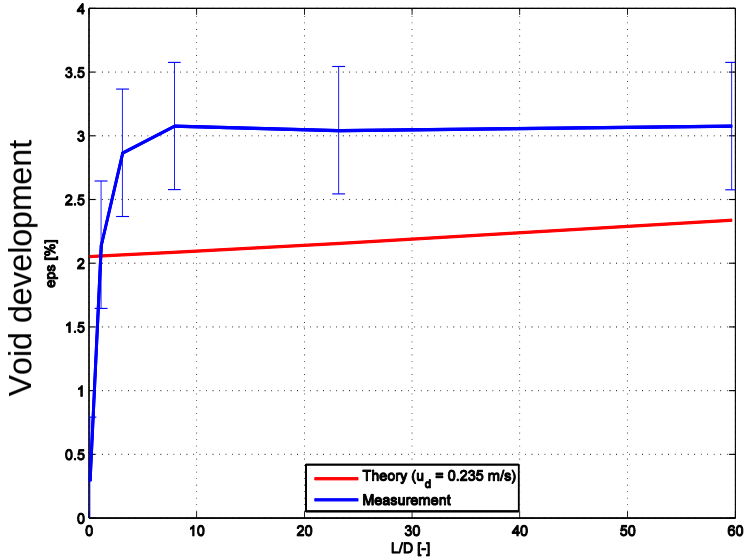

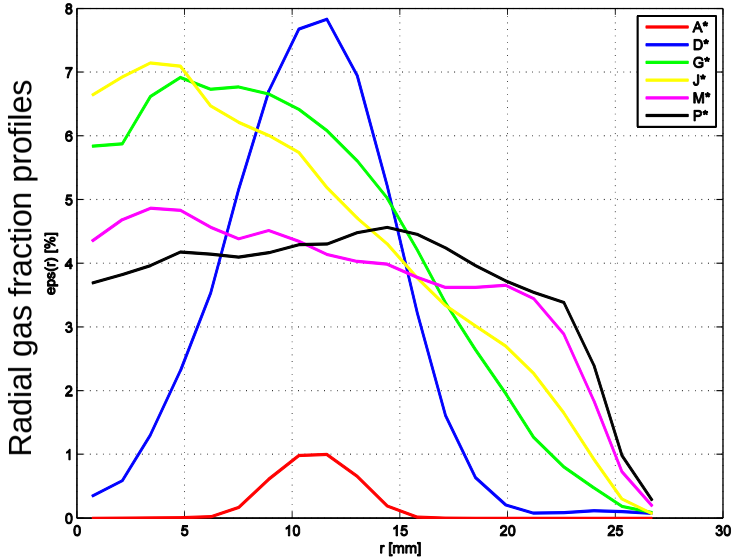

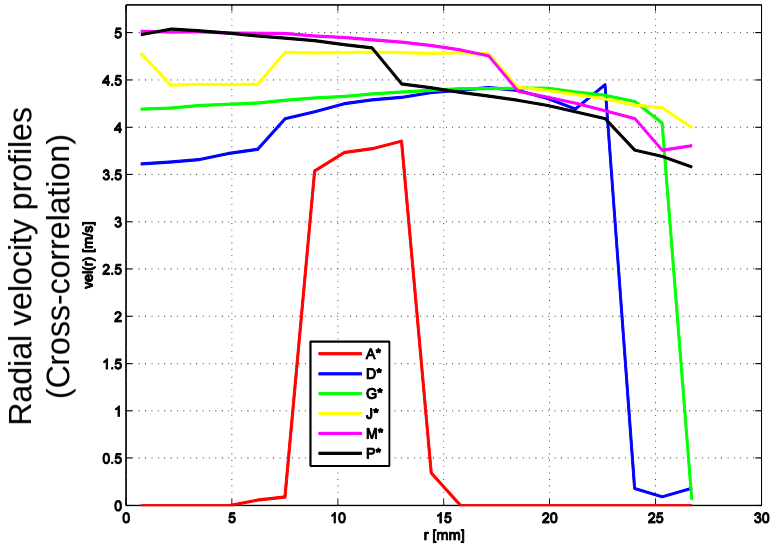

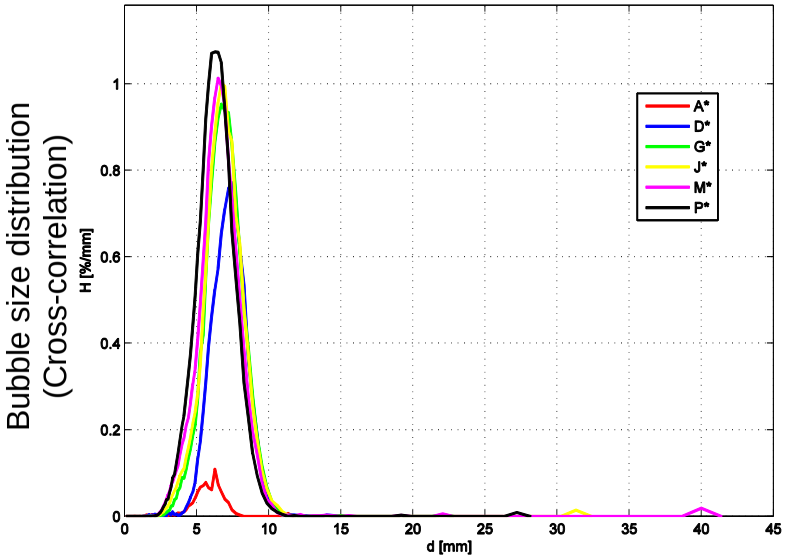

Radial velocity profiles
(Bubble pair detection)

Bubble size distribution
(Bubble pair detection)

L17 – 001mod (jl = -0.0352 $^{m}/_{s}$; jg = 0.0025 $^{m}/_{s}$), 2x1000Hz

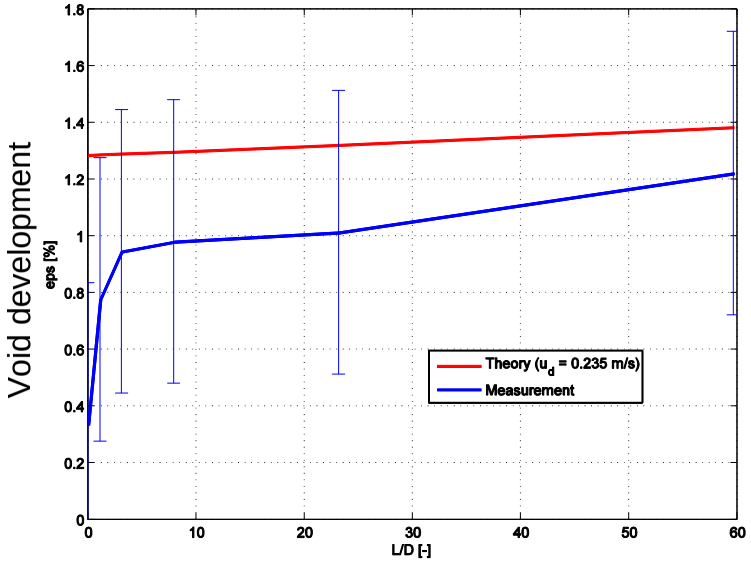

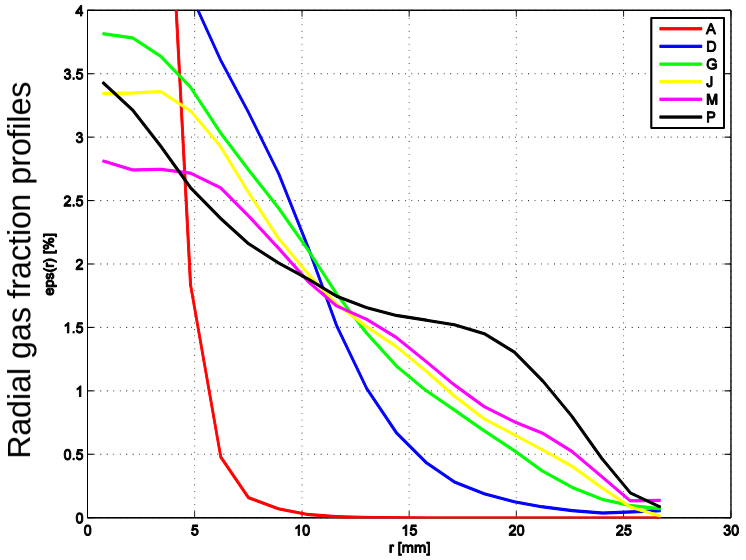

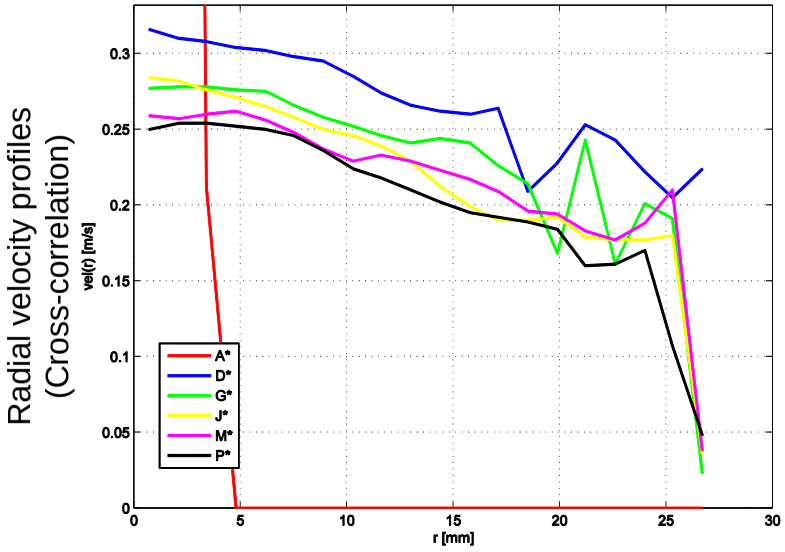

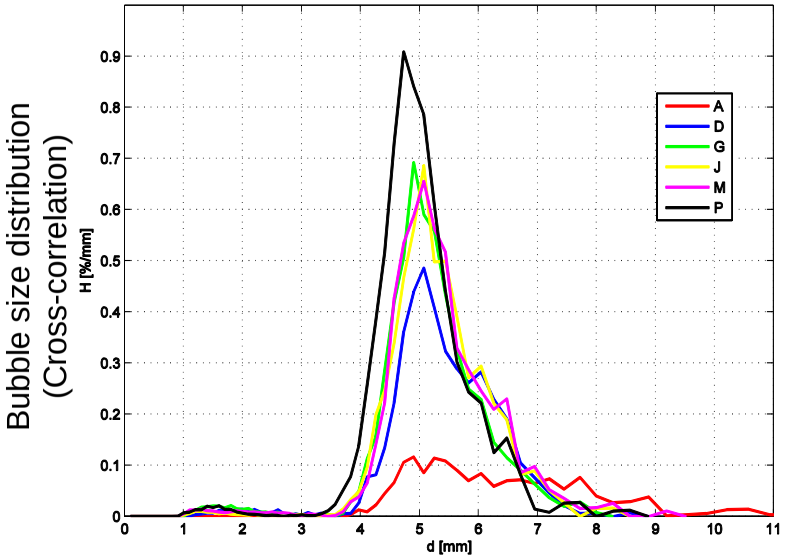

Radial velocity profiles
(Morphological method)

Bubble size distribution
(Morphological method)

L17 – 002mod (jl = -0.0601 m/s; jg = 0.0025 m/s), 2x1000Hz
Void development
eps [%]
L/D [-]
Theory (u_d = 0.235 m/s)
Measurement
Radial gas fraction profiles
eps(r) [%]
r [mm]
A
D
G
J
M
P
Bubble size distribution
(Cross-correlation)
H [%/mm]
d [mm]
Radial velocity profiles
(Cross-correlation)
vel(r) [m/s]
r [mm]
A*
D*
G*
J*
M*
P*

Radial velocity profiles
(Morphological method)

Bubble size distribution
(Morphological method)

L17 – 003mod (jl = -0.0997 $^{m}/_{s}$; jg = 0.0025 $^{m}/_{s}$), 2x1000Hz

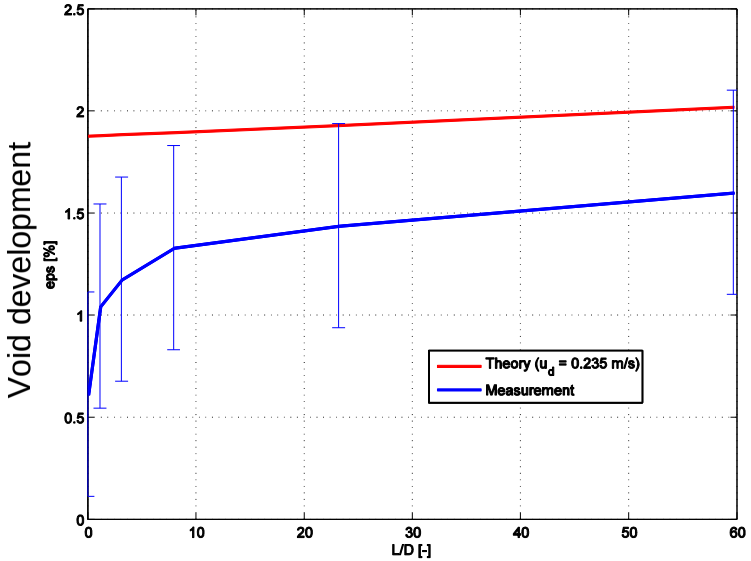

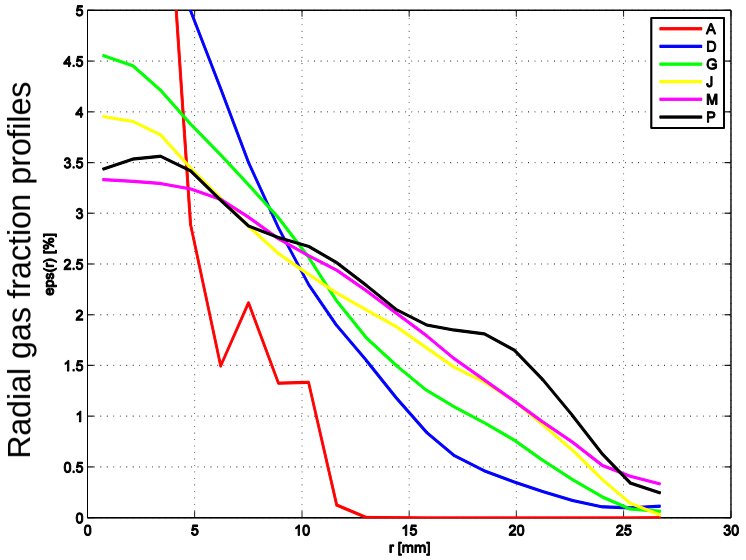

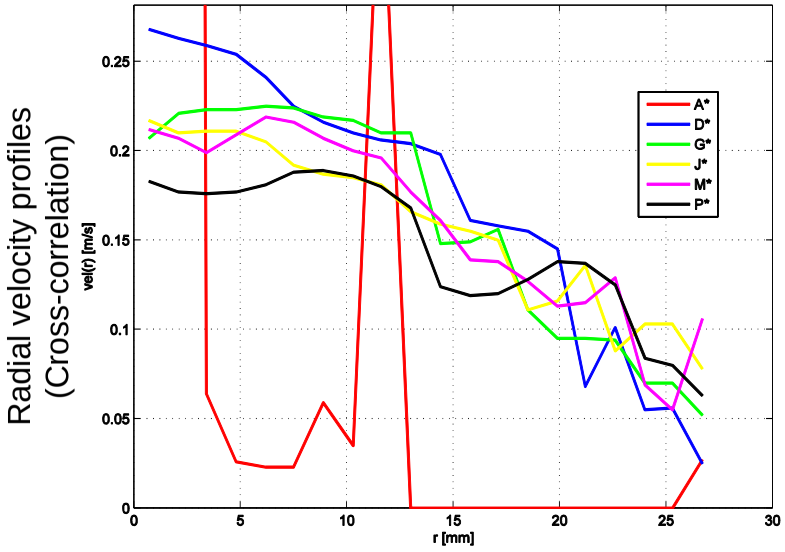

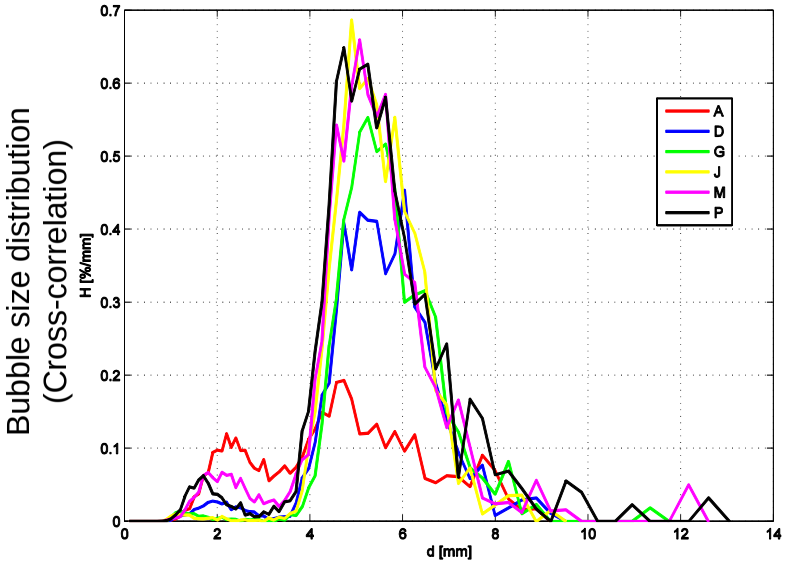

Radial velocity profiles
(Morphological method)

Bubble size distribution
(Morphological method)

L17 – 034mod (jl = -0.0422 m/s; jg = 0.0096 m/s), 2x1000Hz
Void development
eps [%]
L/D [-]
Theory (u_d = 0.235 m/s)
Measurement
Radial gas fraction profiles
eps(r) [%]
r [mm]
A
D
G
J
M
P
Bubble size distribution
(Cross-correlation)
H [%/mm]
d [mm]
Radial velocity profiles
(Cross-correlation)
vel(r) [m/s]
r [mm]
A*
D*
G*
J*
M*
P*

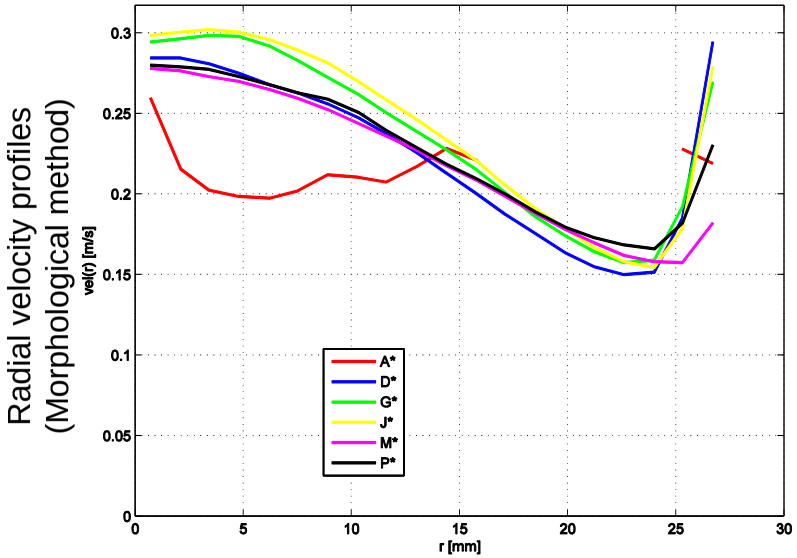
Radial velocity profiles
(Morphological method)
vel(r) [m/s]
r [mm]
A*
D*
G*
J*
M*
P*

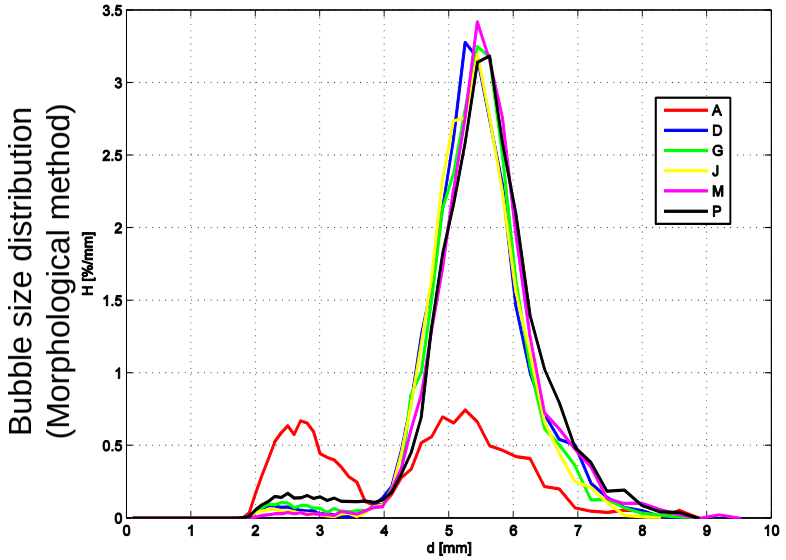
Bubble size distribution
(Morphological method)
H [%/mm]
d [mm]
A
D
G
J
M
P

L17 – 035mod (jl = -0.0672 m/s; jg = 0.0096 m/s), 2x1000Hz
Void development
eps [%]
L/D [-]
Theory (u_d = 0.235 m/s)
Measurement
Radial gas fraction profiles
eps(r) [%]
r [mm]
A
D
G
J
M
P
Bubble size distribution
(Cross-correlation)
H [%/mm]
d [mm]
Radial velocity profiles
(Cross-correlation)
vel(r) [m/s]
r [mm]
A*
D*
G*
J*
M*
P*

Radial velocity profiles
(Morphological method)

Bubble size distribution
(Morphological method)

L17 – 036mod (jl = -0.1067 m/s; jg = 0.0096 m/s), 2x1000Hz
Void development
eps [%]
L/D [-]
Theory (u_d = 0.235 m/s)
Measurement
Radial gas fraction profiles
eps(r) [%]
r [mm]
A
D
G
J
M
P
Radial velocity profiles
(Cross-correlation)
vel(r) [m/s]
r [mm]
A*
D*
G*
J*
M*
P*
Bubble size distribution
(Cross-correlation)
H [%/mm]
d [mm]
A
D
G
J
M
P

Radial velocity profiles
(Morphological method)

Bubble size distribution
(Morphological method)

L18 – 111 (jl = 0.0405 m/s; jg = 0.219 m/s), 2x1000Hz
Void development
eps [%]
L/D [-]
Theory (u_d = 0.235 m/s)
Measurement
Radial gas fraction profiles
eps(r) [%]
r [mm]
A*
D*
G*
J*
M*
P*
Radial velocity profiles
(Cross-correlation)
vel(r) [m/s]
r [mm]
Bubble size distribution
(Cross-correlation)
H [%/mm]
d [mm]

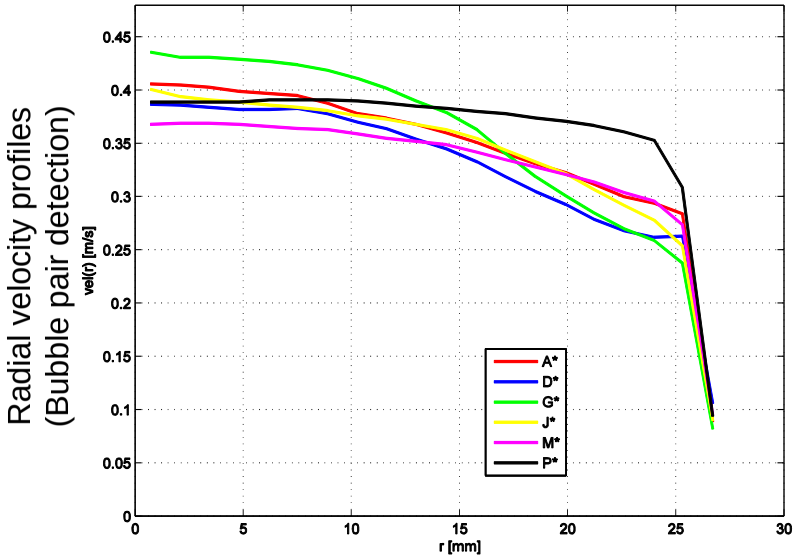
Radial velocity profiles
(Bubble pair detection)
vel(r) [m/s]
r [mm]
A*
D*
G*
J*
M*
P*

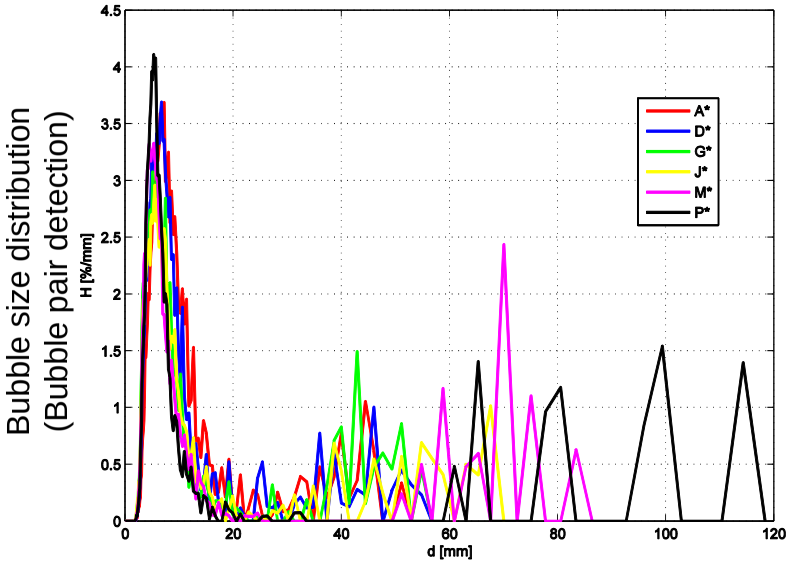
Bubble size distribution
(Bubble pair detection)
H [%/mm]
d [mm]
A*
D*
G*
J*
M*
P*

L18 – 114 (jl = 0.161 $^{m}/_{s}$; jg = 0.219 $^{m}/_{s}$), 2x1000Hz

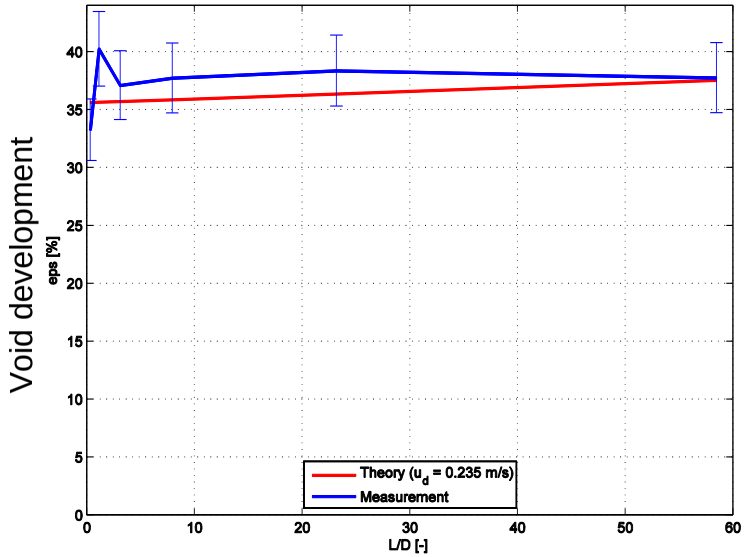

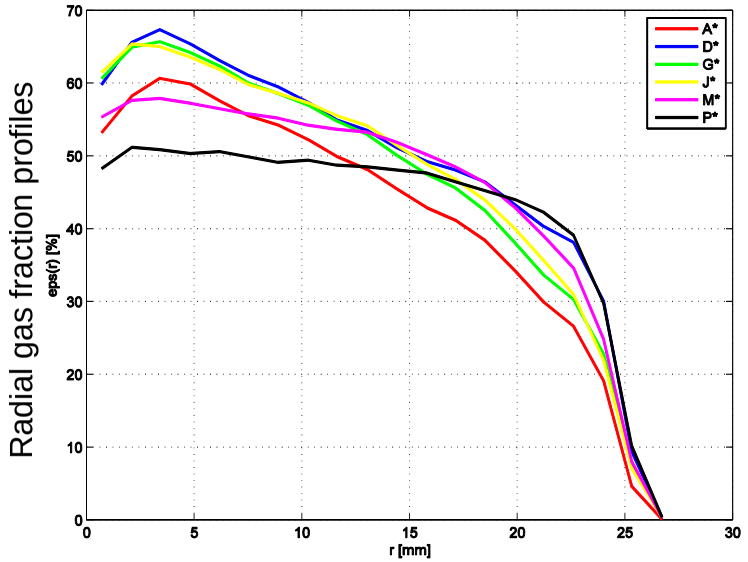

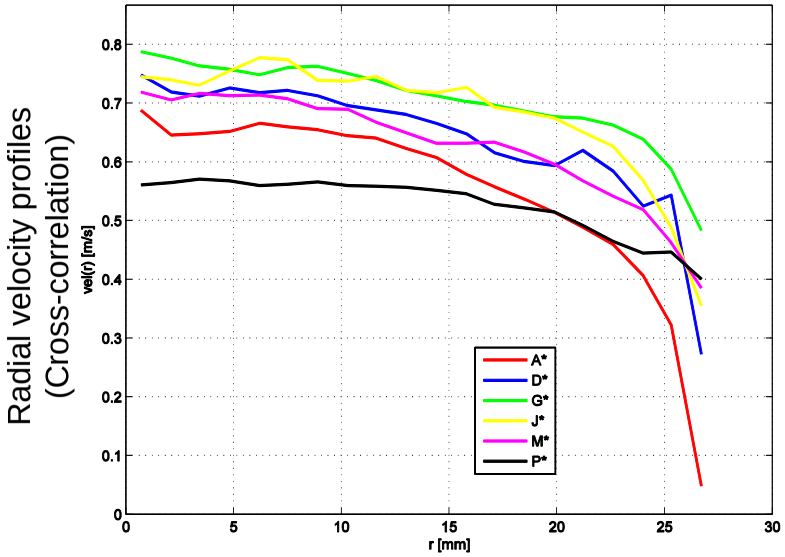

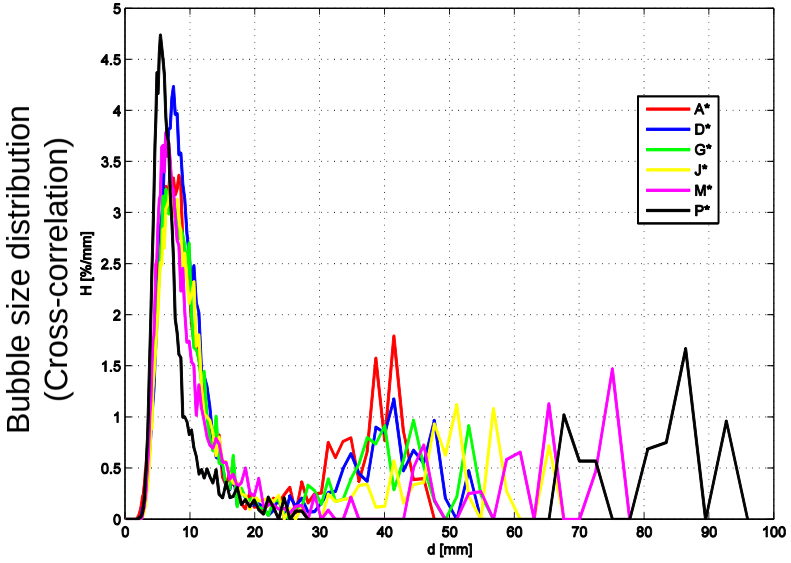

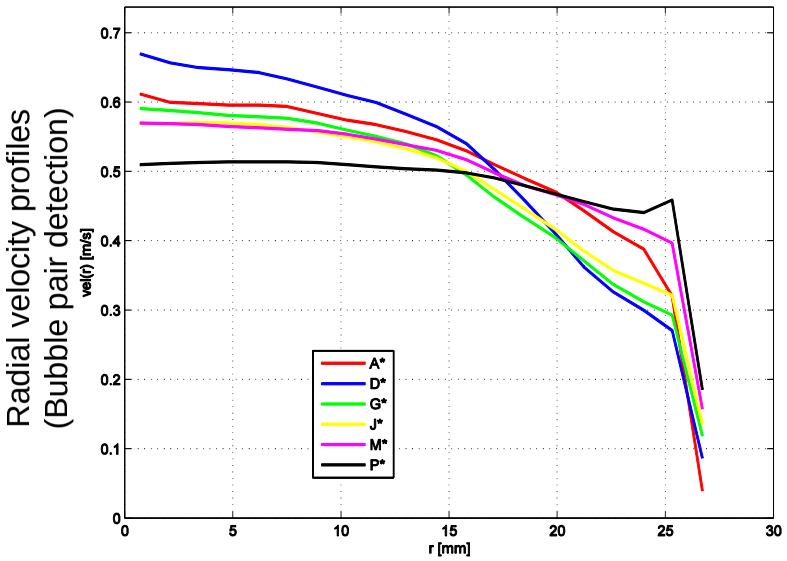
Radial velocity profiles
(Bubble pair detection)
vel(r) [m/s]
r [mm]
A*
D*
G*
J*
M*
P*

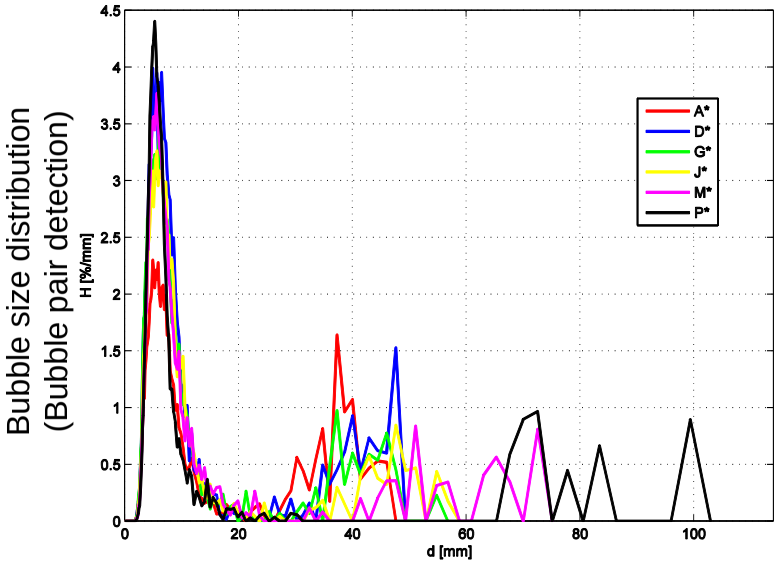
Bubble size distribution
(Bubble pair detection)
H [%/mm]
d [mm]
A*
D*
G*
J*
M*
P*

L18 – 116 (jl = 0.405 m/s; jg = 0.219 m/s), 2x1000Hz
Void development
eps [%]
L/D [-]
Theory (u_d = 0.235 m/s)
Measurement
Radial gas fraction profiles
eps(r) [%]
r [mm]
A*
D*
G*
J*
M*
P*
Bubble size distribution
(Cross-correlation)
H [%/mm]
d [mm]
Radial velocity profiles
(Cross-correlation)
vel(r) [m/s]
r [mm]

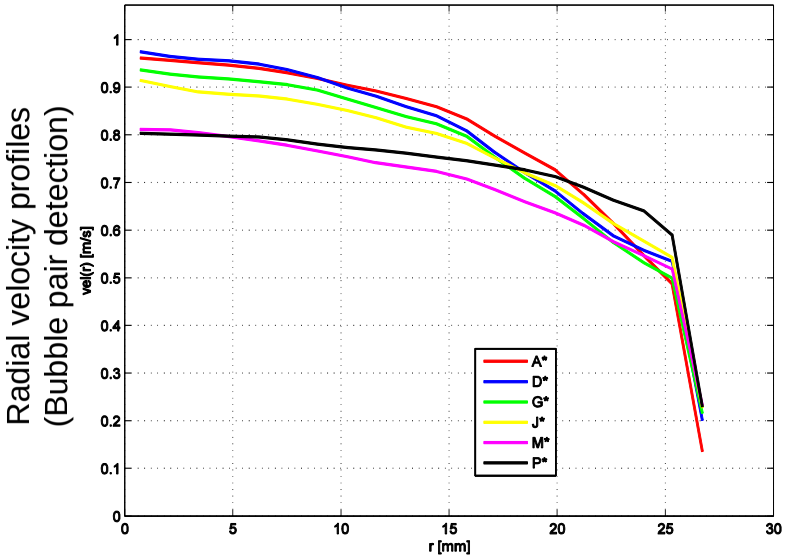
Radial velocity profiles
(Bubble pair detection)
vel(r) [m/s]
r [mm]
A*
D*
G*
J*
M*
P*

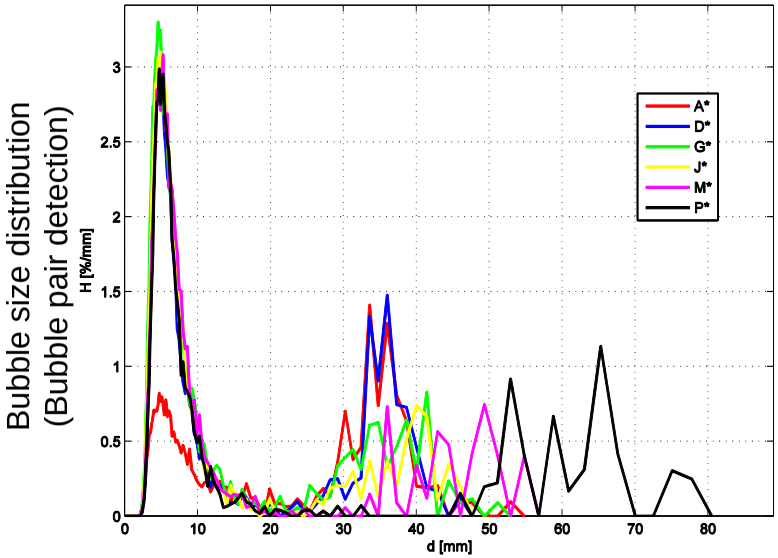
Bubble size distribution
(Bubble pair detection)
H [%/mm]
d [mm]
A*
D*
G*
J*
M*
P*

L18 – 118 (jl = 1.017 $^{m}/_{s}$; jg = 0.219 $^{m}/_{s}$), 2x2500Hz

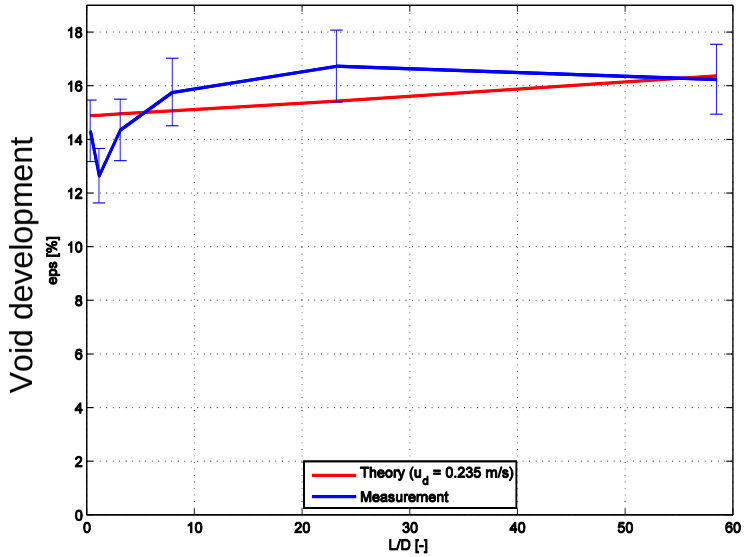

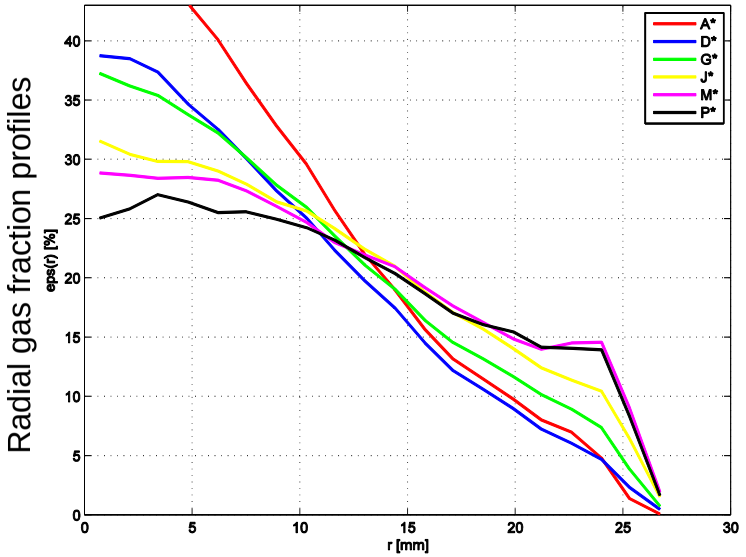

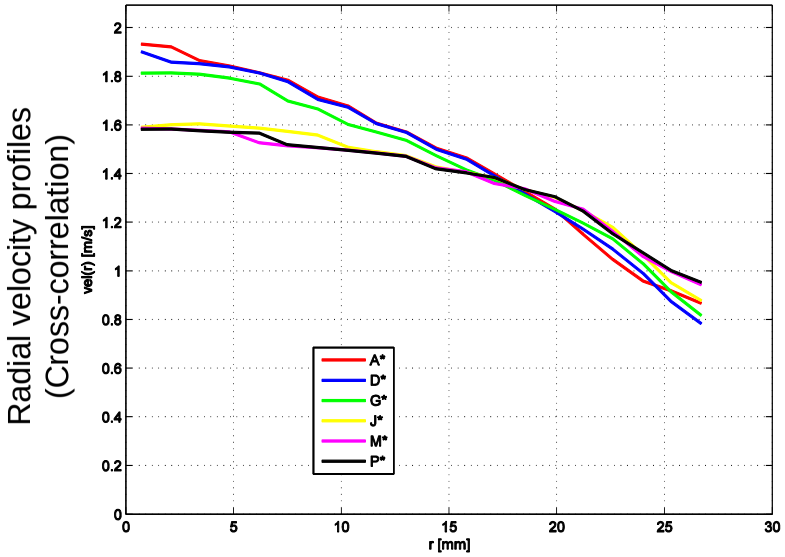

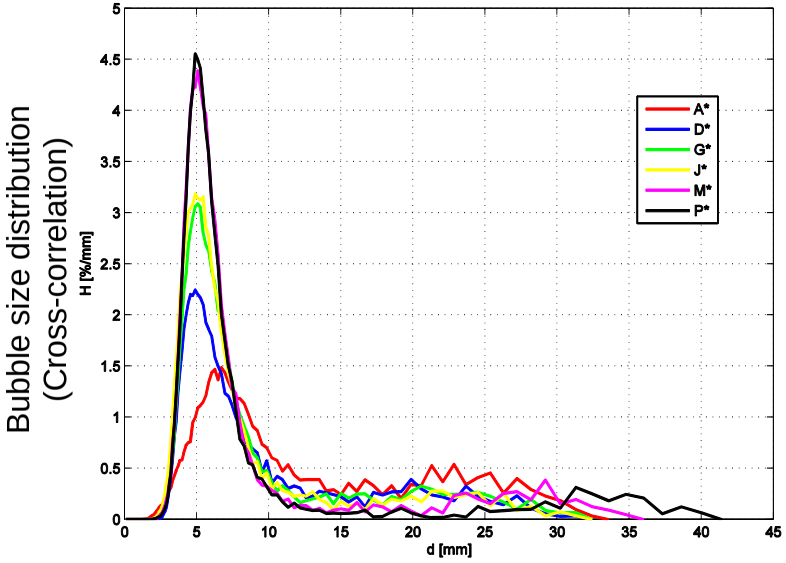

Radial velocity profiles
(Bubble pair detection)

Bubble size distribution
(Bubble pair detection)

L18 – 119 (jl = 1.611 $^{m}/_{s}$; jg = 0.219 $^{m}/_{s}$), 2x2500Hz

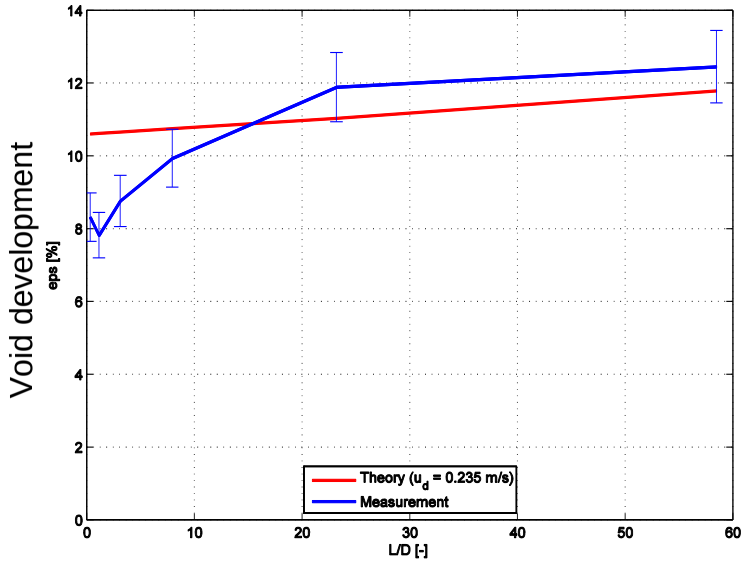

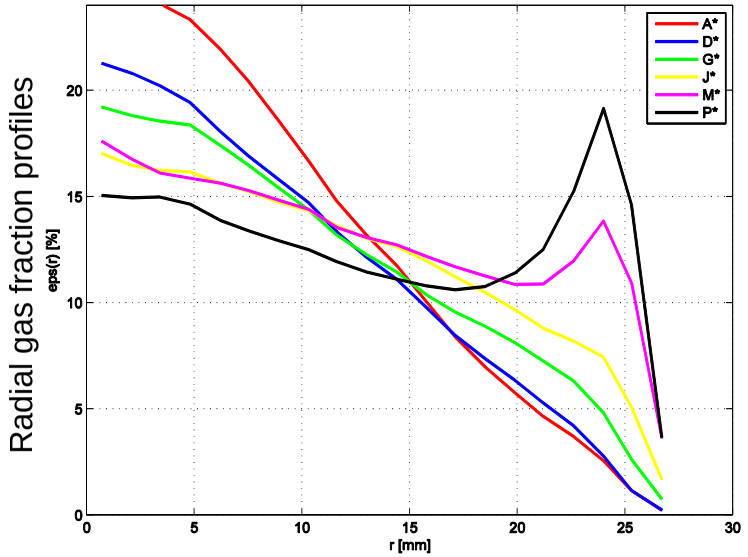

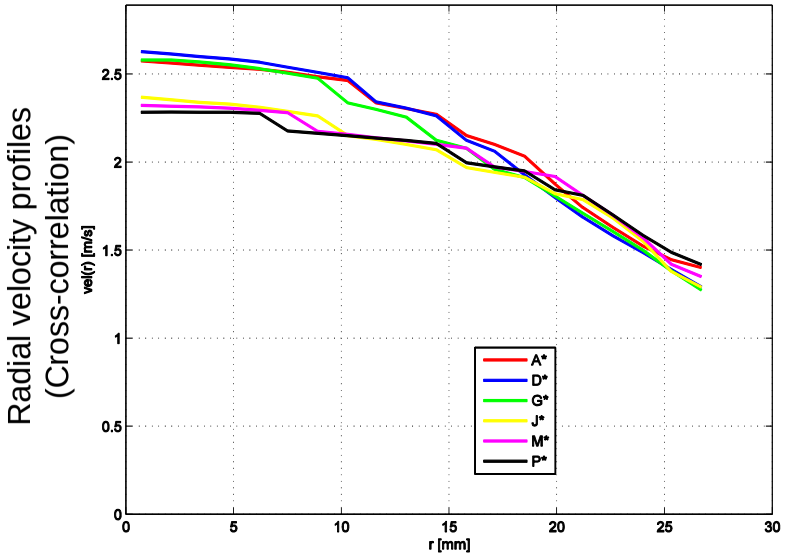

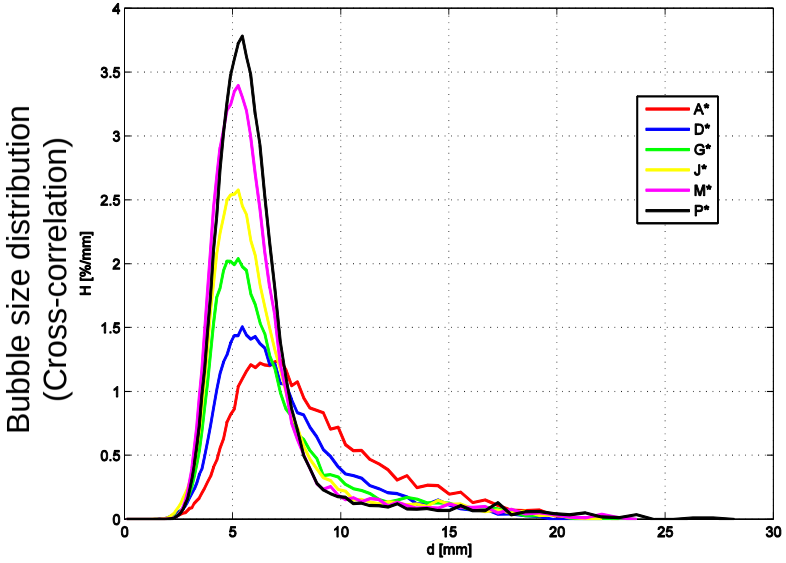

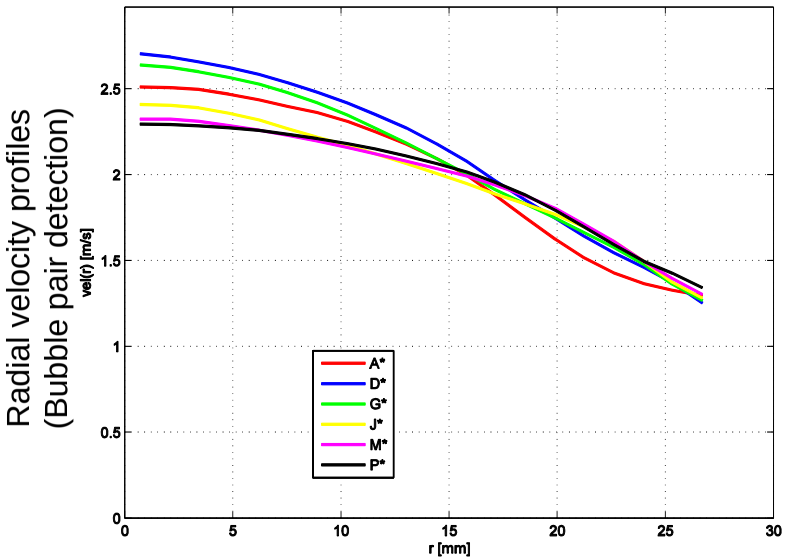
Radial velocity profiles
(Bubble pair detection)
vel(r) [m/s]
r [mm]
A*
D*
G*
J*
M*
P*

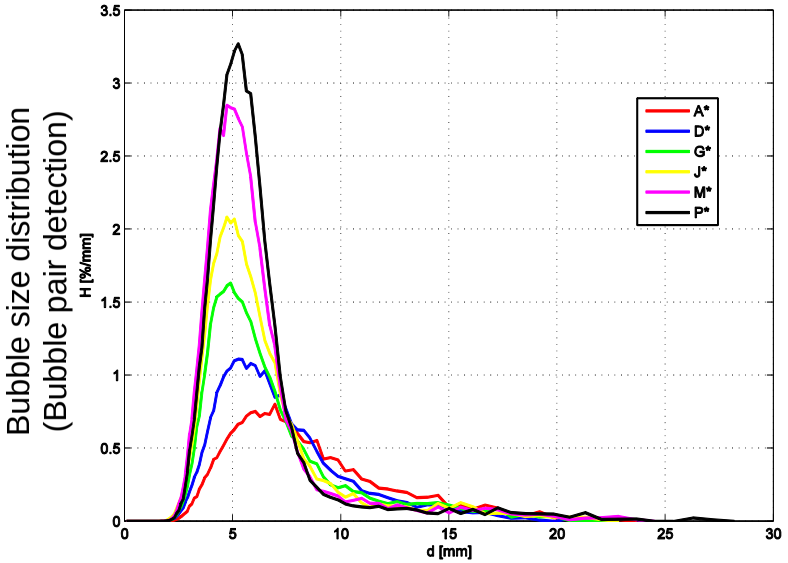
Bubble size distribution
(Bubble pair detection)
H [%/mm]
d [mm]
A*
D*
G*
J*
M*
P*

Radial velocity profiles used from L18 –
120, 2x2500Hz
(Cross-correlation)

L18 – 120 (jl = 2.554 m/s; jg = 0.219 m/s), 2x2500Hz
Void development
eps [%]
L/D [-]
Theory (u_d = 0.235 m/s)
Measurement
Radial gas fraction profiles
eps(r) [%]
r [mm]
A*
D*
G*
J*
M*
P*
Radial velocity profiles
(Cross-correlation)
vel(r) [m/s]
r [mm]
Bubble size distribution
(Cross-correlation)
H [%/mm]
d [mm]

Radial velocity profiles
(Bubble pair detection)

Bubble size distribution
(Bubble pair detection)

L18 – 121 (jl = 4.047 $^{m}/_{s}$; jg = 0.219 $^{m}/_{s}$), 1x5000Hz

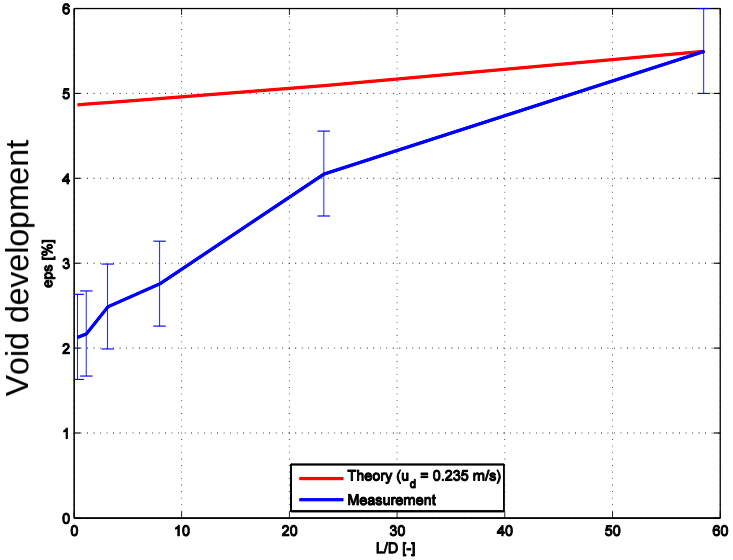

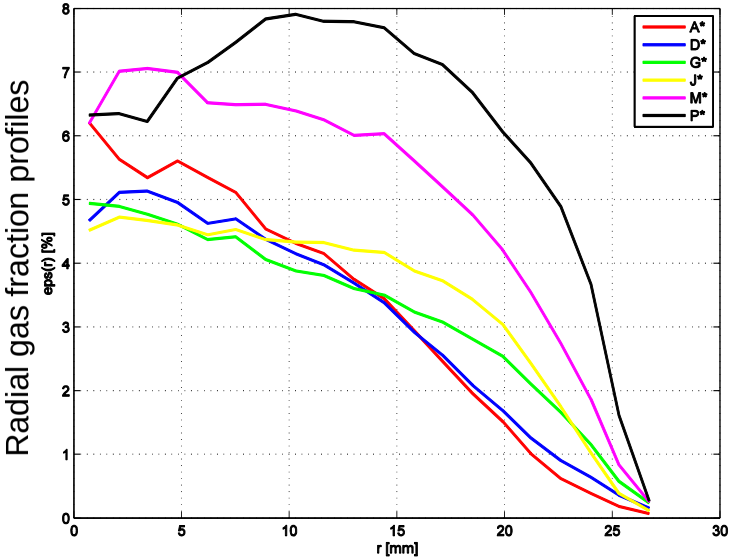

Radial velocity profiles used from L18 – 121, 2x2500Hz (Cross-correlation)

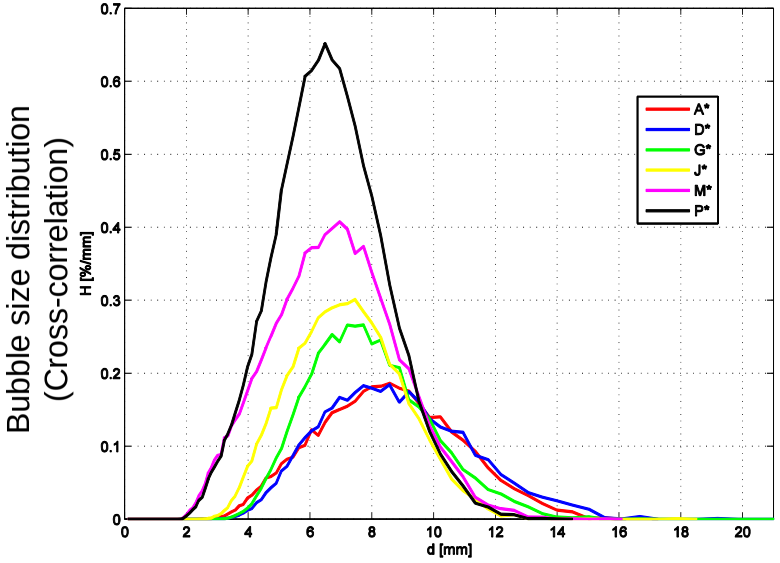

L18 – 121 (jl = 4.047 $^{m}/_{s}$; jg = 0.219 $^{m}/_{s}$), 2x2500Hz

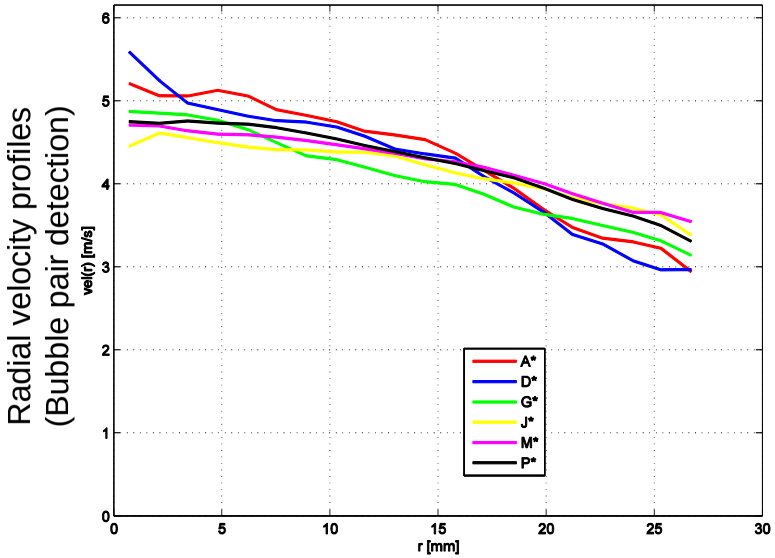
Radial velocity profiles
(Bubble pair detection)
vel(r) [m/s]
r [mm]
A*
D*
G*
J*
M*
P*

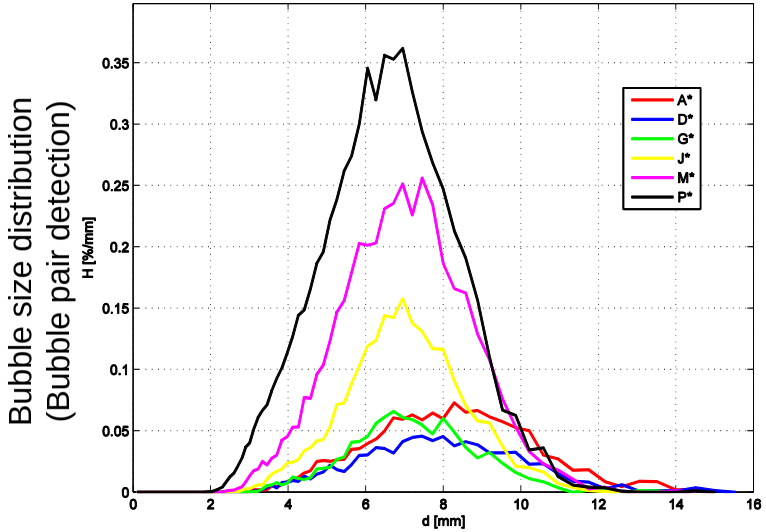
Bubble size distribution
(Bubble pair detection)
H [%/mm]
d [mm]
A*
D*
G*
J*
M*
P*

L18 – 133 (jl = 0.0405 m/s; jg = 0.534 m/s), 2x1000Hz
Void development
eps [%]
L/D [-]
Theory (u_d = 0.235 m/s)
Measurement
Radial gas fraction profiles
eps(r) [%]
r [mm]
A*
D*
G*
J*
M*
P*
Bubble size distribution
(Cross-correlation)
H [%/mm]
d [mm]
Radial velocity profiles
(Cross-correlation)
vel(r) [m/s]
r [mm]

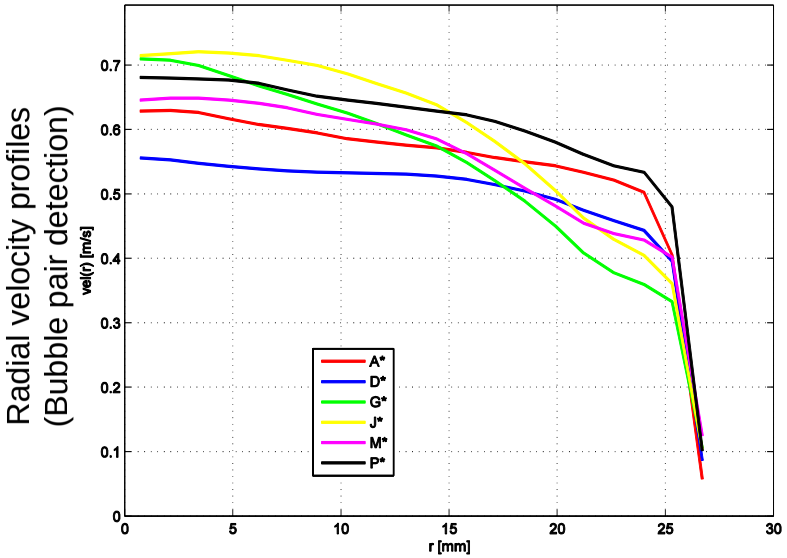
Radial velocity profiles
(Bubble pair detection)
vel(r) [m/s]
r [mm]
A*
D*
G*
J*
M*
P*

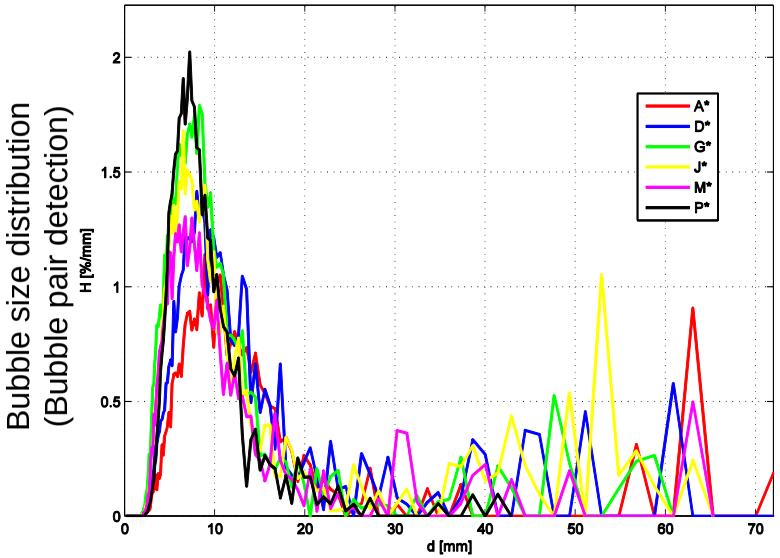
Bubble size distribution
(Bubble pair detection)
H [%/mm]
d [mm]
A*
D*
G*
J*
M*
P*

L18 – 140 (jl = 1.017 $^{m}/_{s}$; jg = 0.534 $^{m}/_{s}$), 2x2500Hz

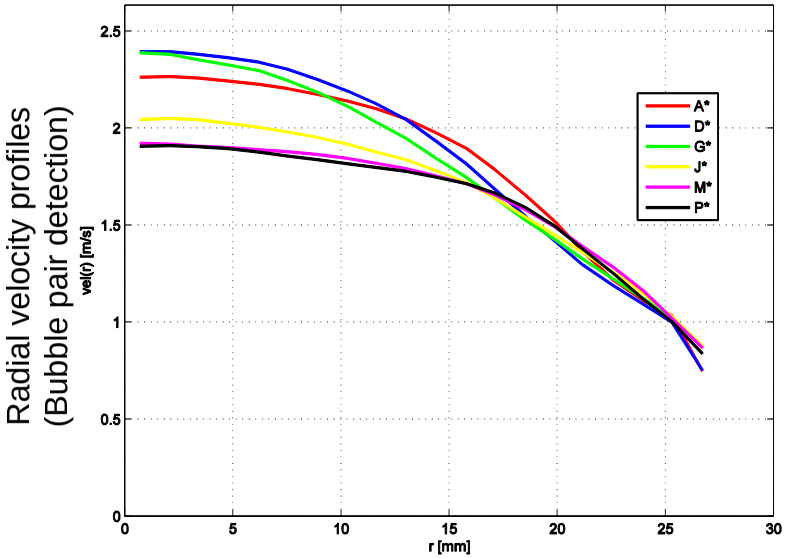
Radial velocity profiles
(Bubble pair detection)
vel(r) [m/s]
r [mm]
A*
D*
G*
J*
M*
P*

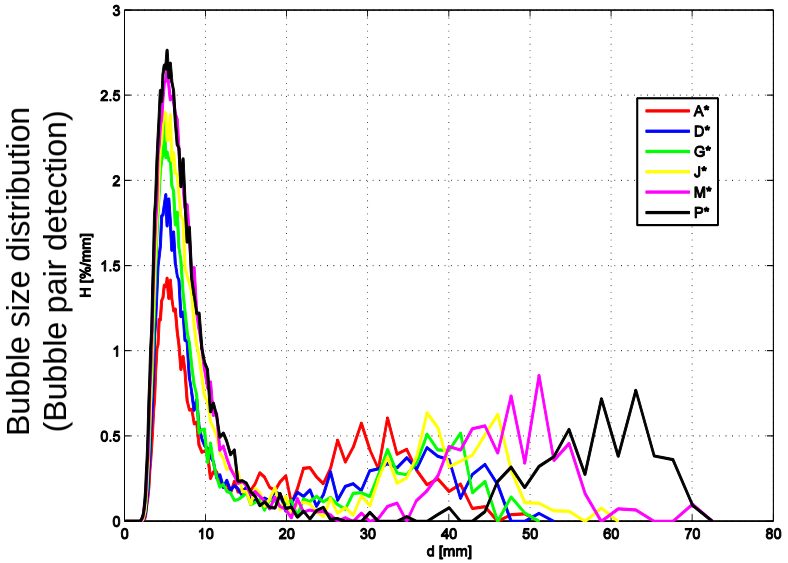
Bubble size distribution
(Bubble pair detection)
H [%/mm]
d [mm]
A*
D*
G*
J*
M*
P*

Radial velocity profiles used from L18 – 143, 2x2500Hz (Cross-correlation)

L18 – 143 (jl = 4.047 $^{m}/_{s}$; jg = 0.534 $^{m}/_{s}$), 2x2500Hz

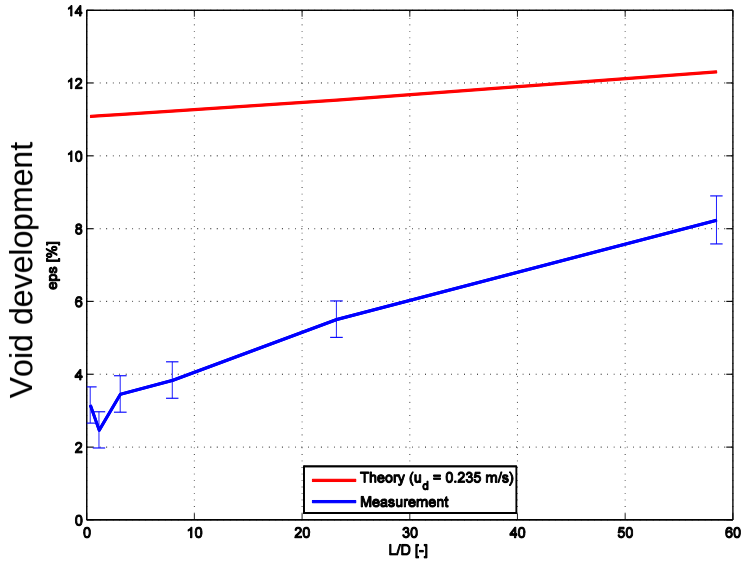

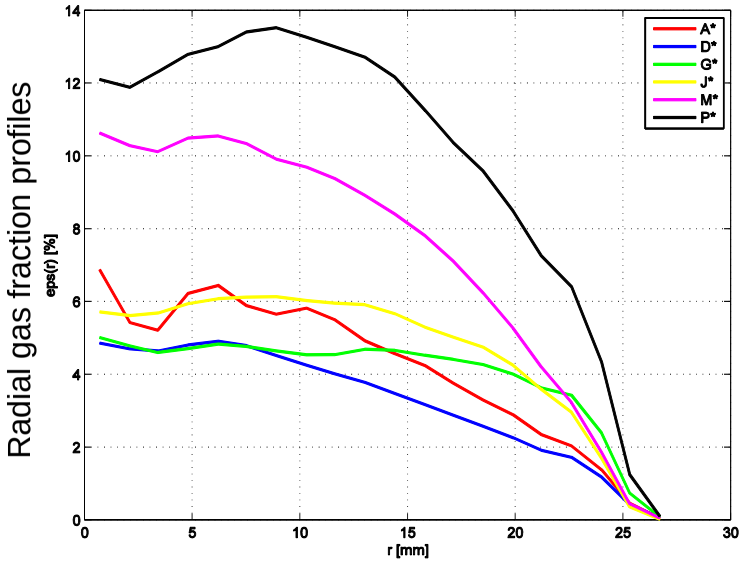

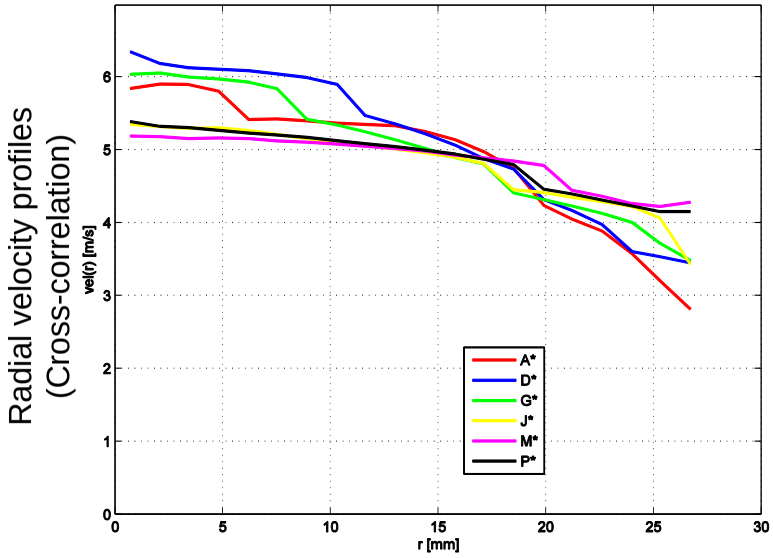

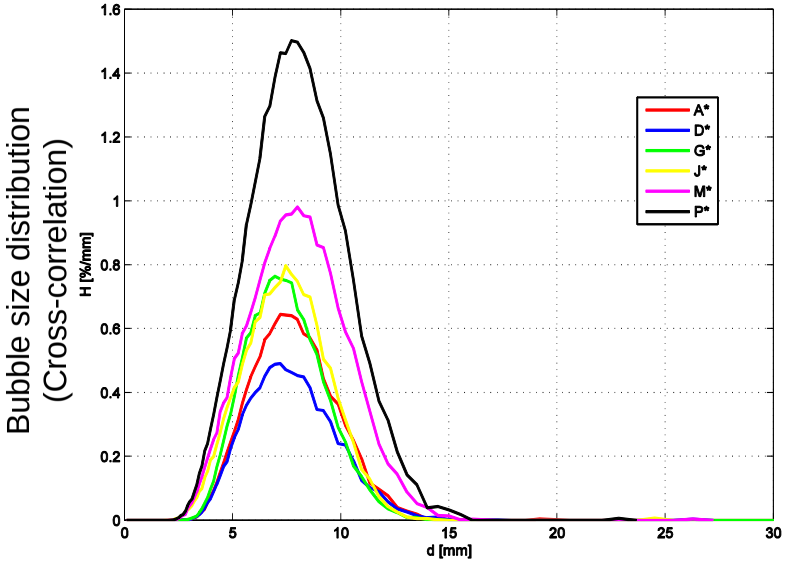

Radial velocity profiles
(Bubble pair detection)

Bubble size distribution
(Bubble pair detection)

L18 – 155 (jl = 0.0405 $^{m}/_{s}$; jg = 1.305 $^{m}/_{s}$), 2x2500Hz

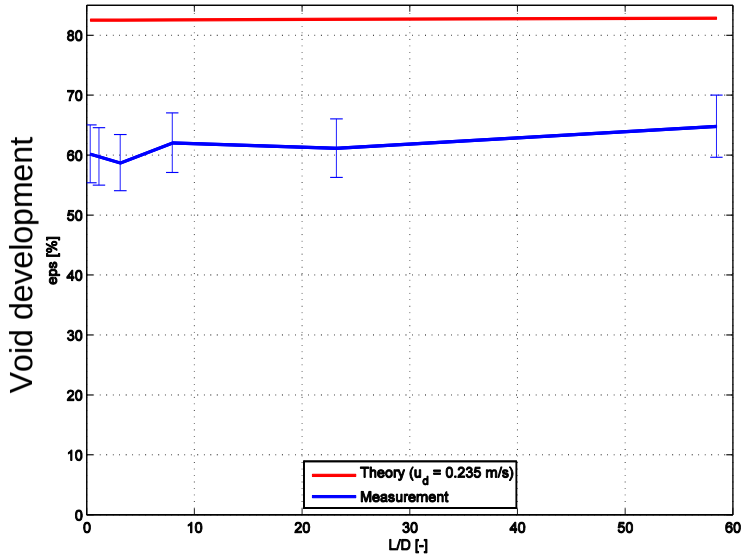

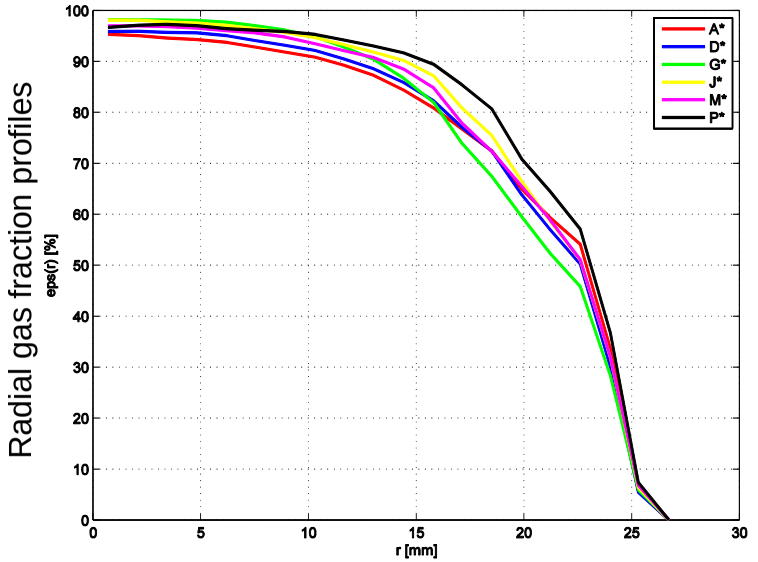

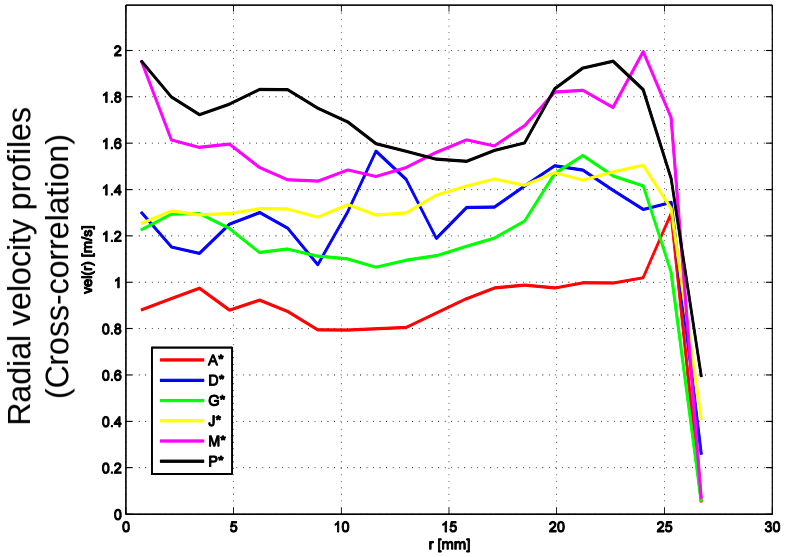

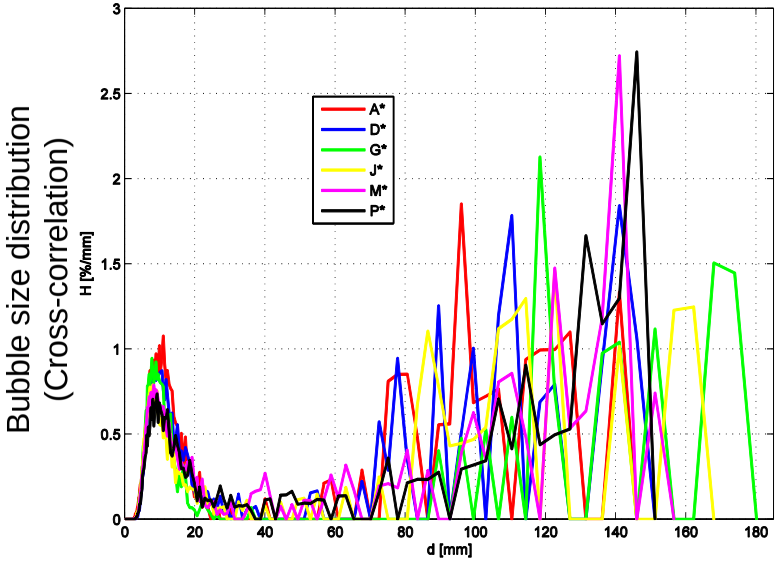

Radial velocity profiles
(Bubble pair detection)

Bubble size distribution
(Bubble pair detection)

Radial velocity profiles used from L18 – 162, 2x2500Hz (Cross-correlation)

Void development

Bubble size distribution (Cross-correlation)

Radial gas fraction profil

es

L18 – 162 (jl = 1.017 $^{m}/_{s}$; jg = 1.305 $^{m}/_{s}$), 1x5000Hz

L18 – 162 (jl = 1.017 $^{m}/_{s}$; jg = 1.305 $^{m}/_{s}$), 2x2500Hz

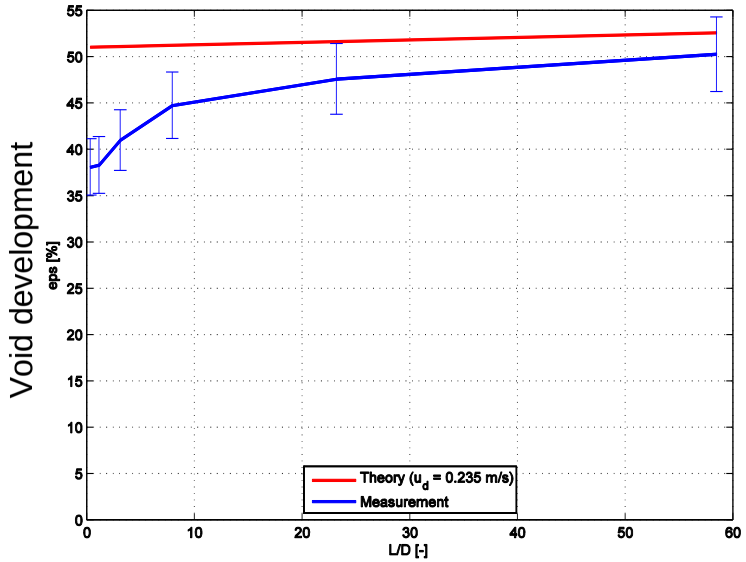

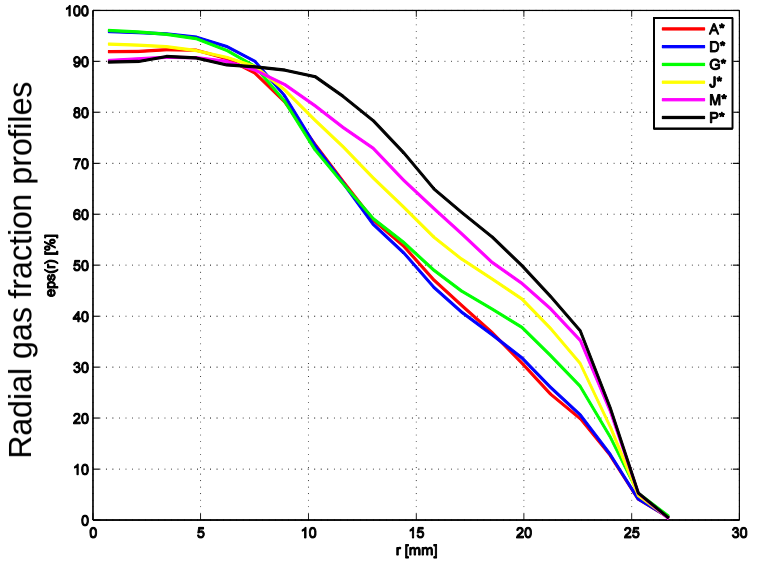

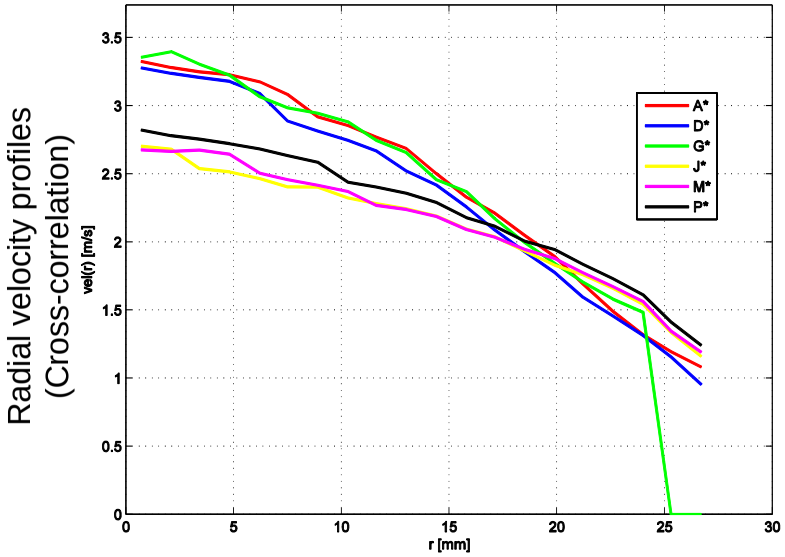

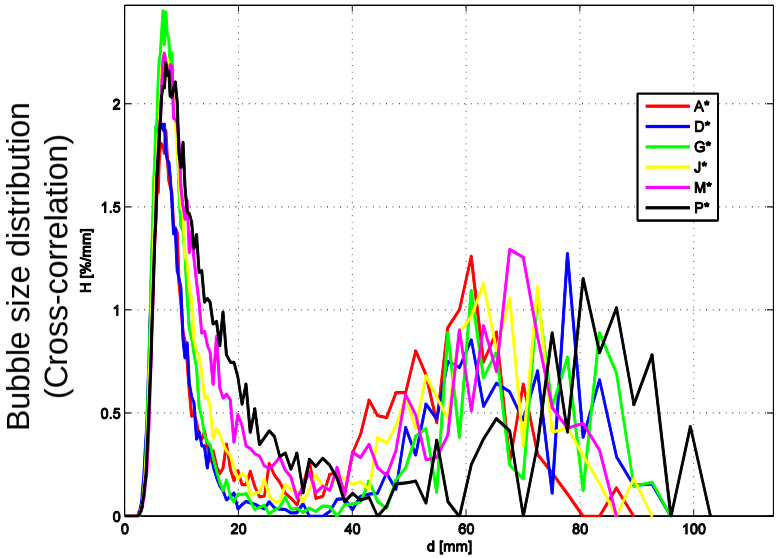

Radial velocity profiles
(Bubble pair detection)

Bubble size distribution
(Bubble pair detection)

Radial velocity profiles used from L18 –
165, 2x2500Hz
(Cross-correlation)

L18 – 165 (jl = 4.047 $^{m}/_{s}$; jg = 1.305 $^{m}/_{s}$), 2x2500Hz

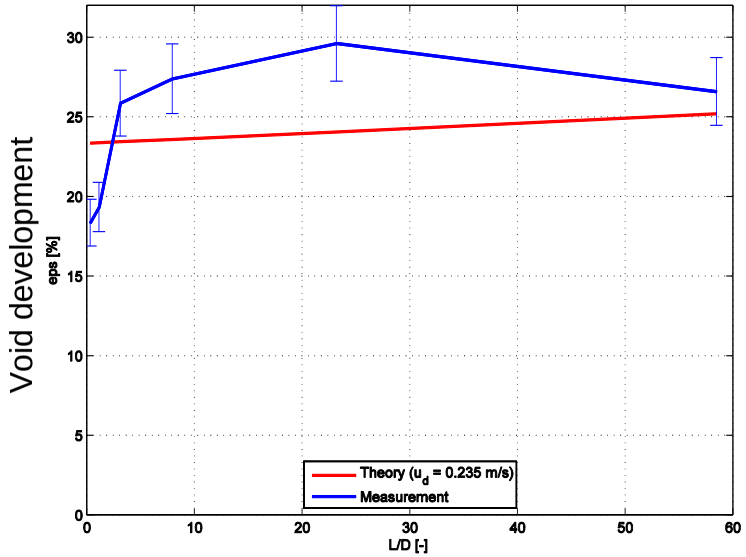

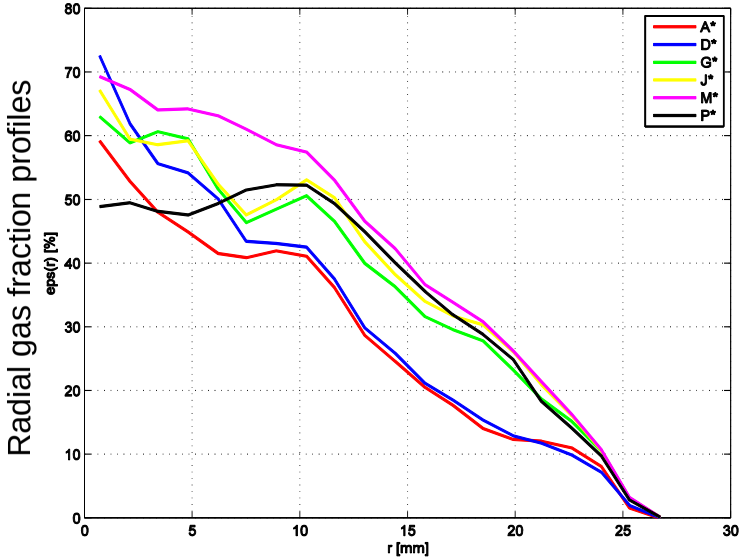

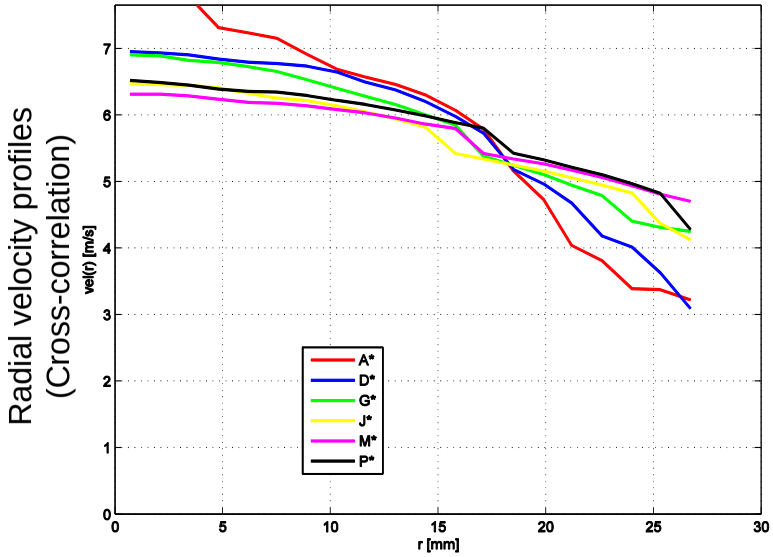

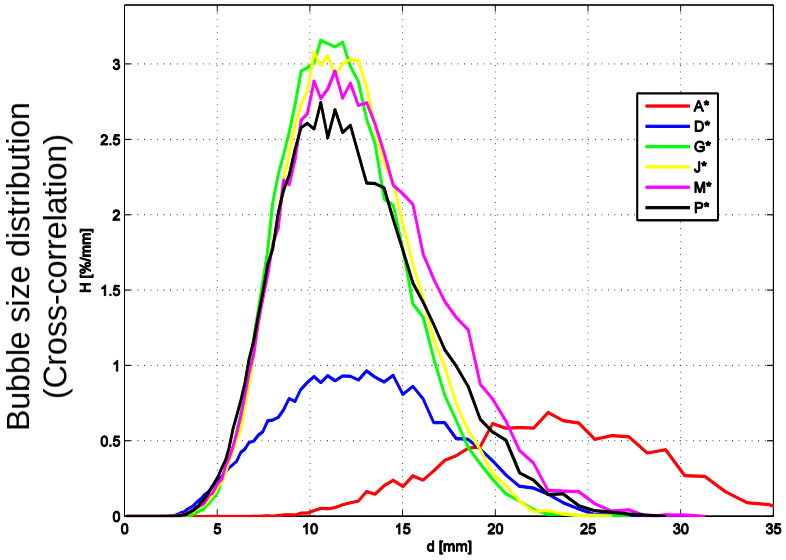

Radial velocity profiles
(Bubble pair detection)

Bubble size distribution
(Bubble pair detection)

L20 – 006 (jl = -0.405 $^{m}/_{s}$; jg = -0.0025 $^{m}/_{s}$), 2x1000Hz

Void development

Radial gas fraction profiles

Radial velocity profiles
(Cross-correlation)

Bubble size distribution
(Cross-correlation)

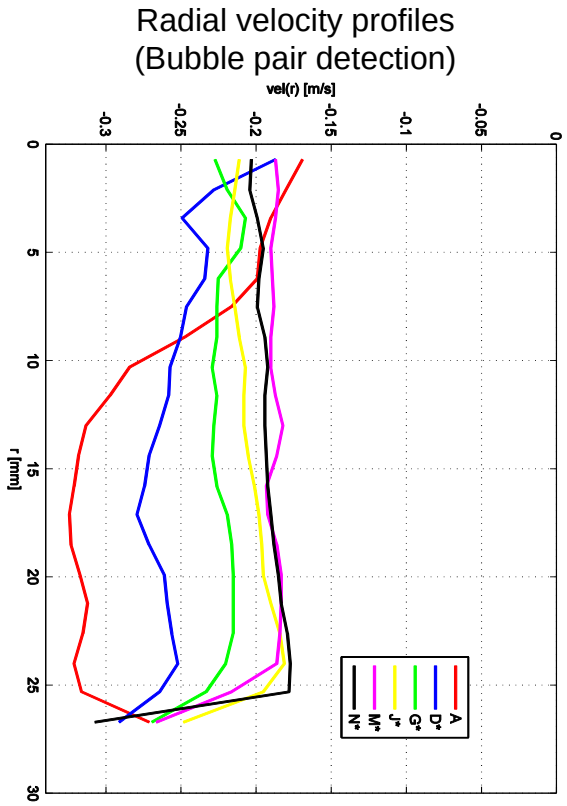
Radial velocity profiles
(Bubble pair detection)
vel(r) [m/s]
r [mm]
A
D*
G*
J*
M*
N*

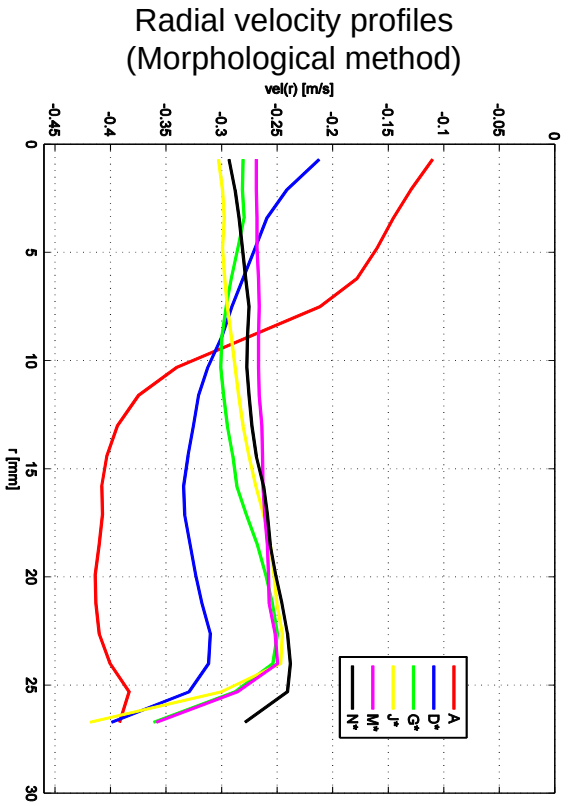
Radial velocity profiles
(Morphological method)
vel(r) [m/s]
r [mm]
A
D*
G*
J*
M*
N*

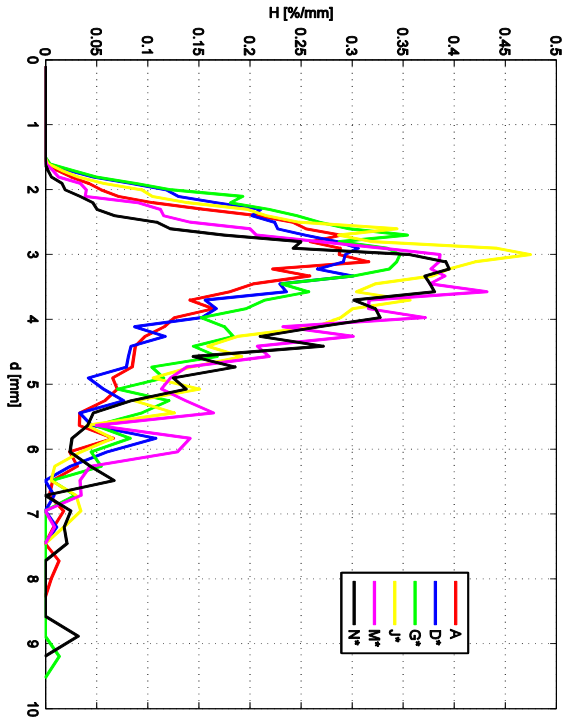
Bubble size distribution
(Bubble pair detection)
H [%/mm]
d [mm]
A
D*
G*
J*
M*
N*

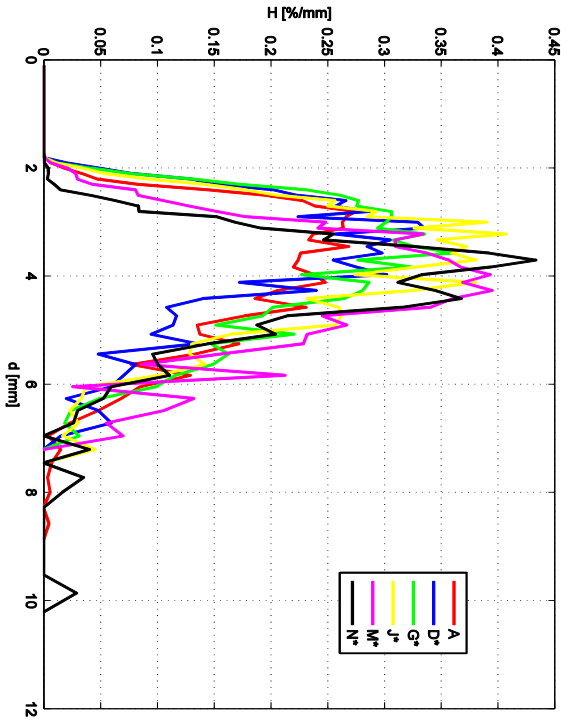
Bubble size distribution
(Morphological method)
H [%/mm]
d [mm]
A
D*
G*
J*
M*
N*

L20 – 007 (jl = -0.641 $^{m}/_{s}$; jg = -0.0025 $^{m}/_{s}$), 2x1000Hz

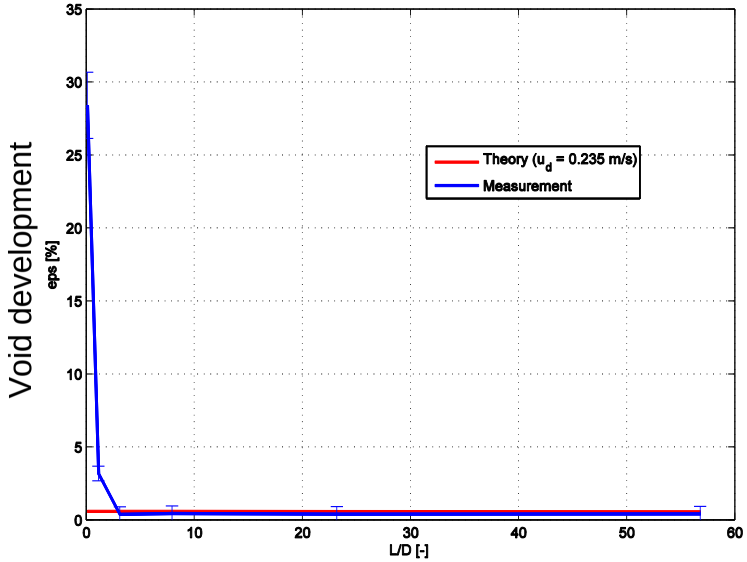

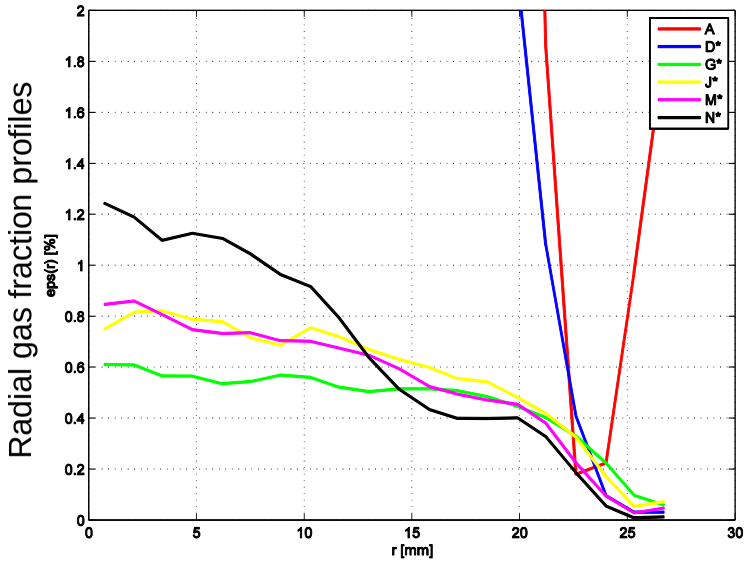

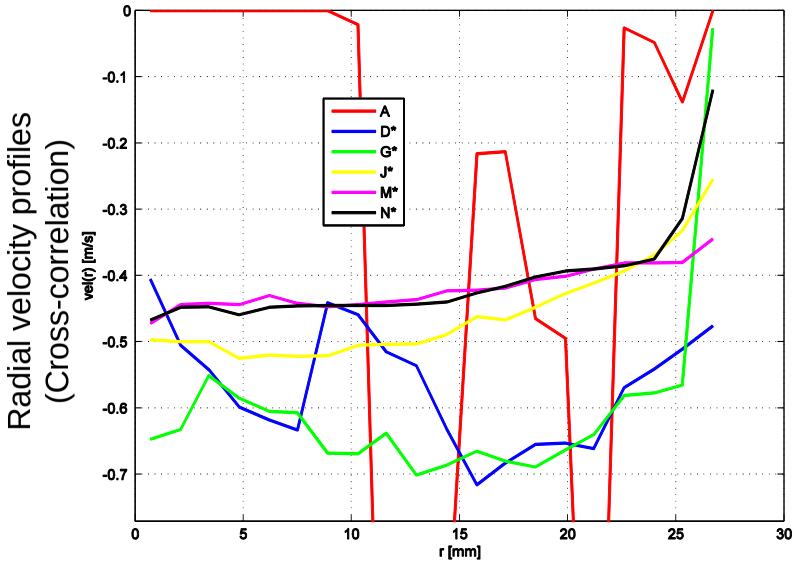

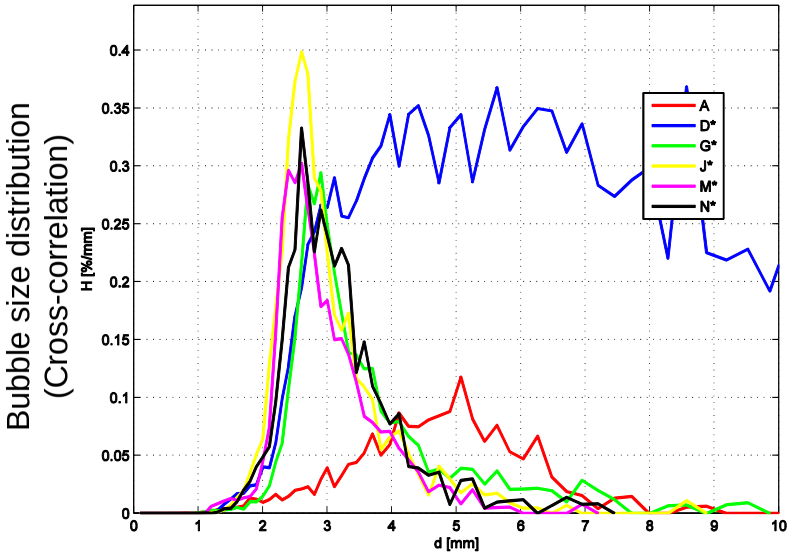

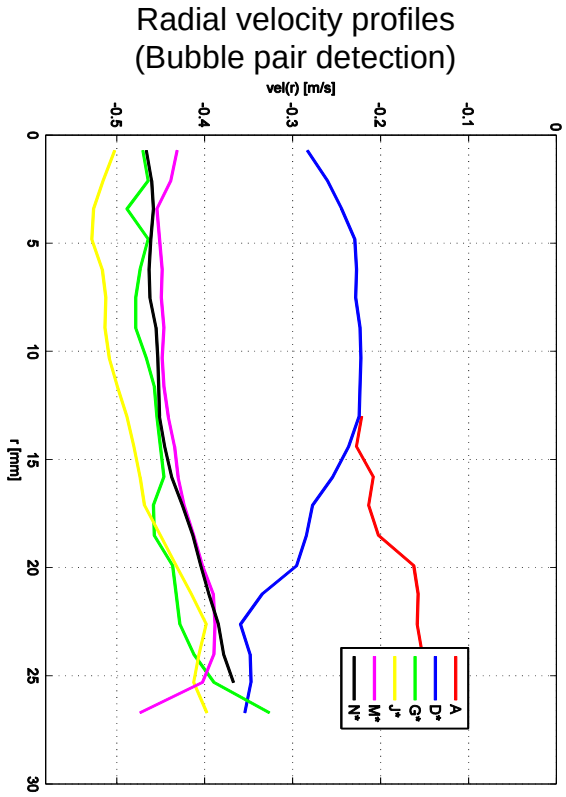
Radial velocity profiles
(Bubble pair detection)
vel(r) [m/s]
r [mm]
N*
M*
J*
G*
D*
A

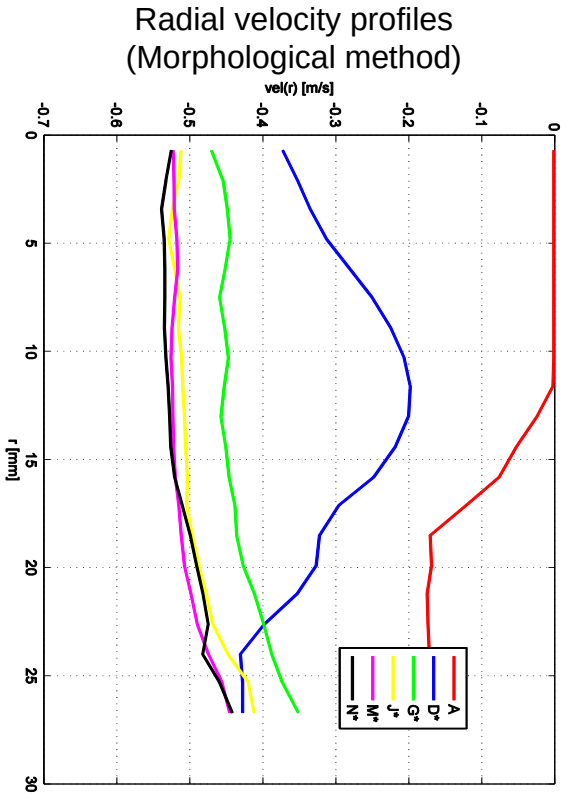
Radial velocity profiles
(Morphological method)
vel(r) [m/s]
r [mm]
N*
M*
J*
G*
D*
A

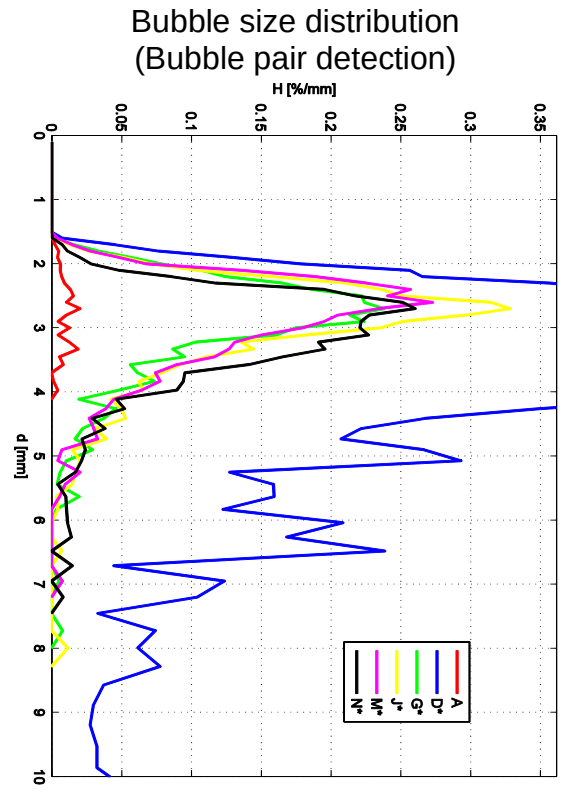
Bubble size distribution
(Bubble pair detection)
H [%/mm]
d [mm]
N*
M*
J*
G*
D*
A

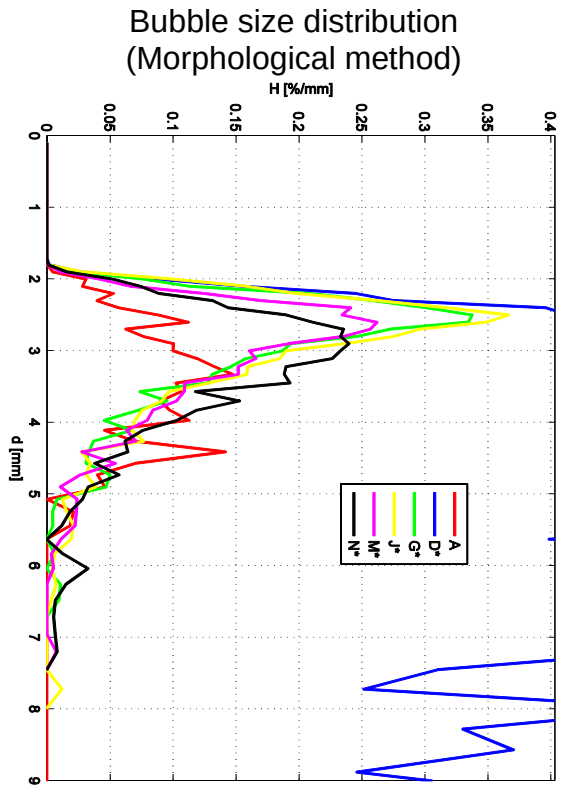
Bubble size distribution
(Morphological method)
H [%/mm]
d [mm]
N*
M*
J*
G*
D*
A

L20 – 008 (jl = -1.017 $^{m}/_{s}$; jg = -0.0025 $^{m}/_{s}$), 2x1000Hz

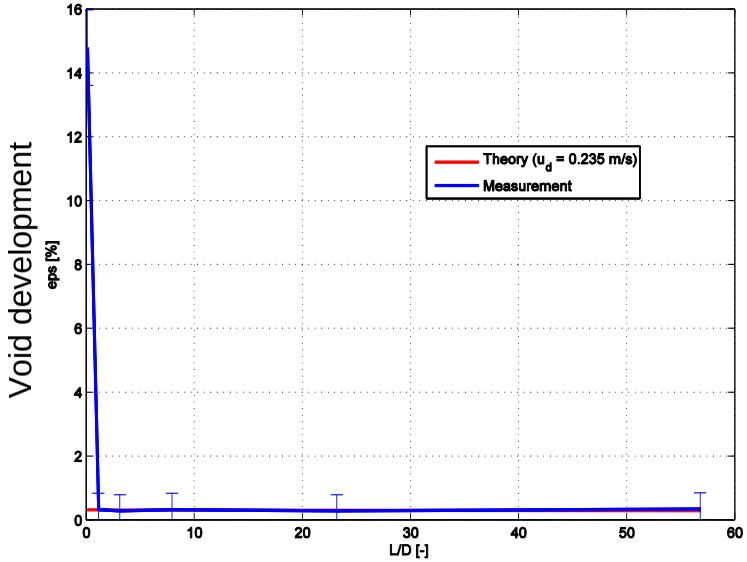

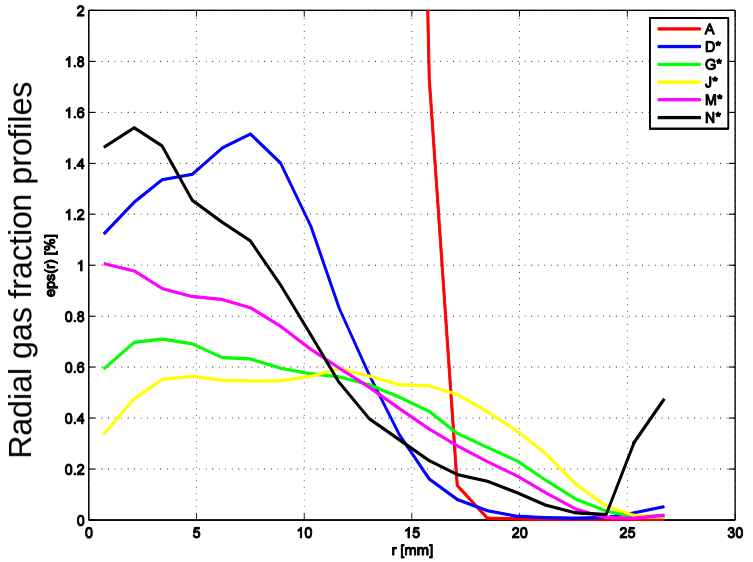

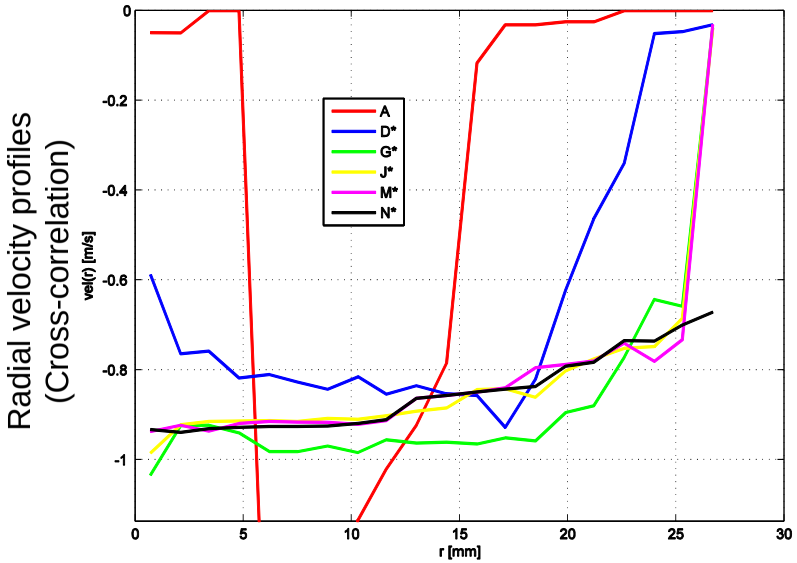

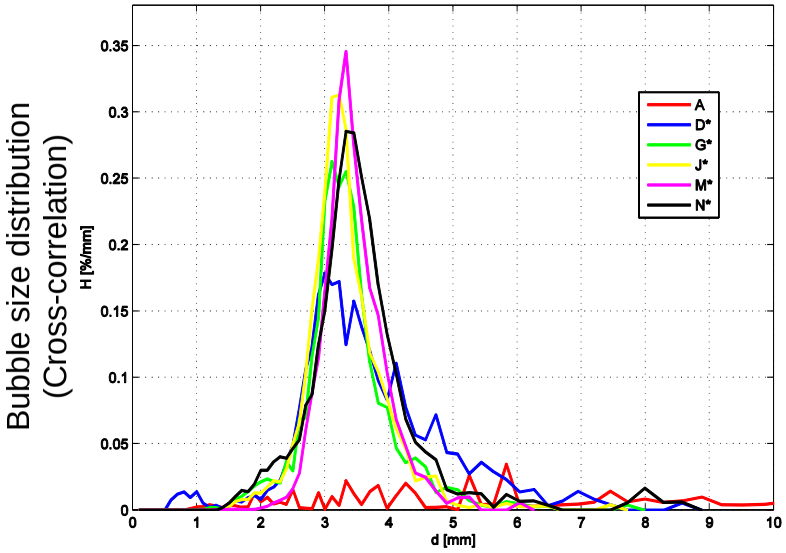

Radial velocity profiles
(Bubble pair detection)

Bubble size distribution
(Bubble pair detection)

L20 – 009 (jl = -1.611 $^{m}/_{s}$; jg = -0.0025 $^{m}/_{s}$), 2x2000Hz

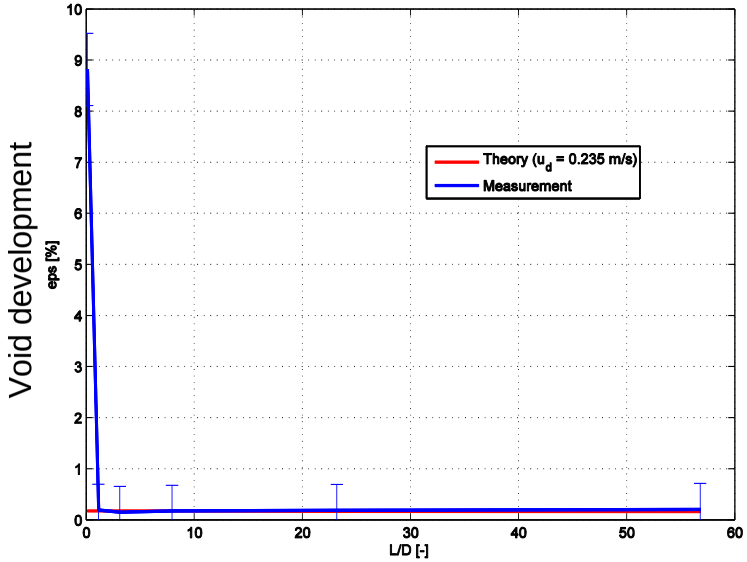

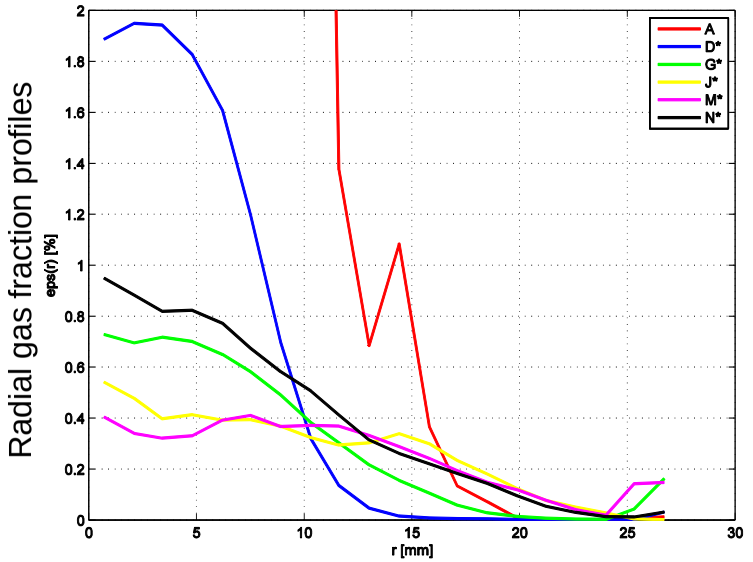

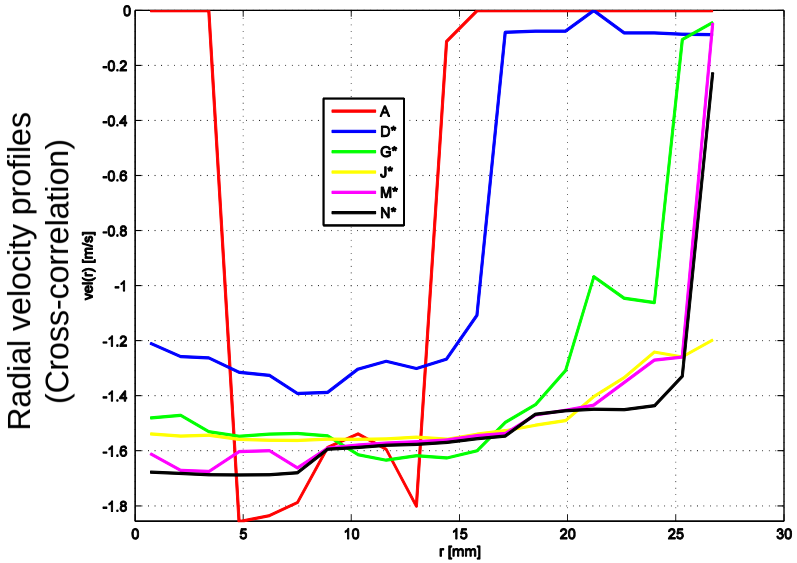

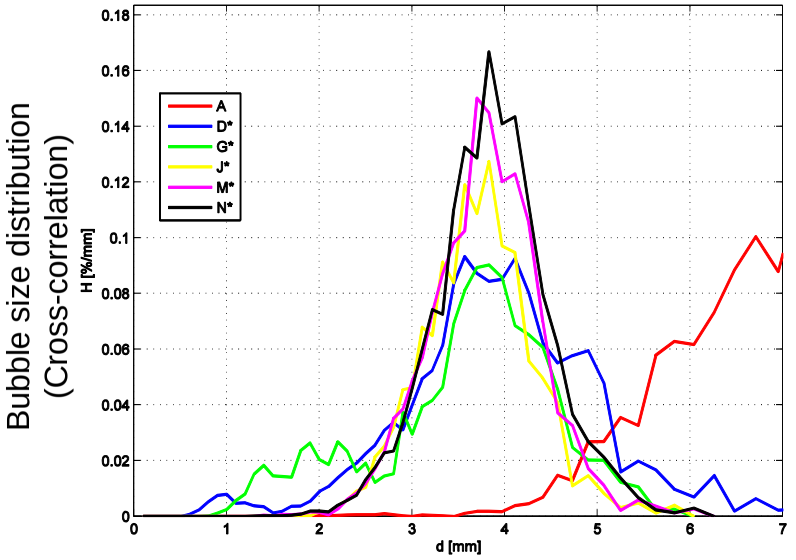

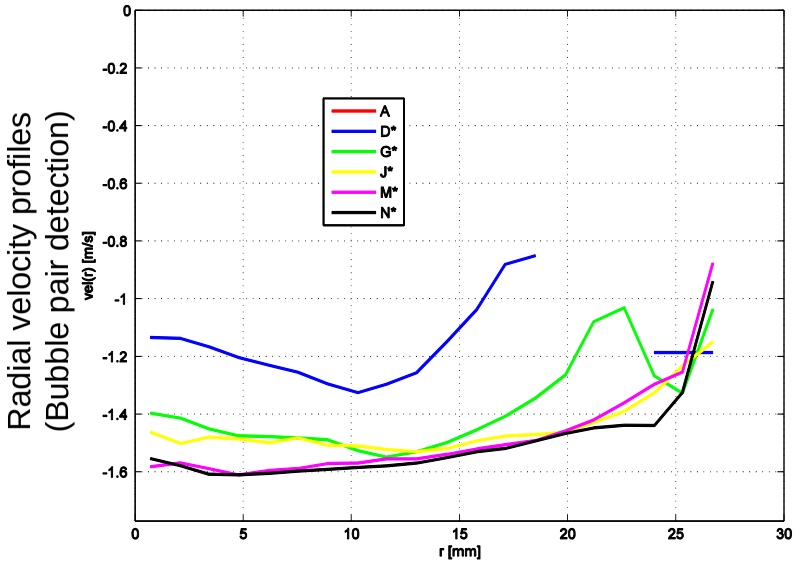
Radial velocity profiles
(Bubble pair detection)
vel(r) [m/s]
r [mm]
A
D*
G*
J*
M*
N*

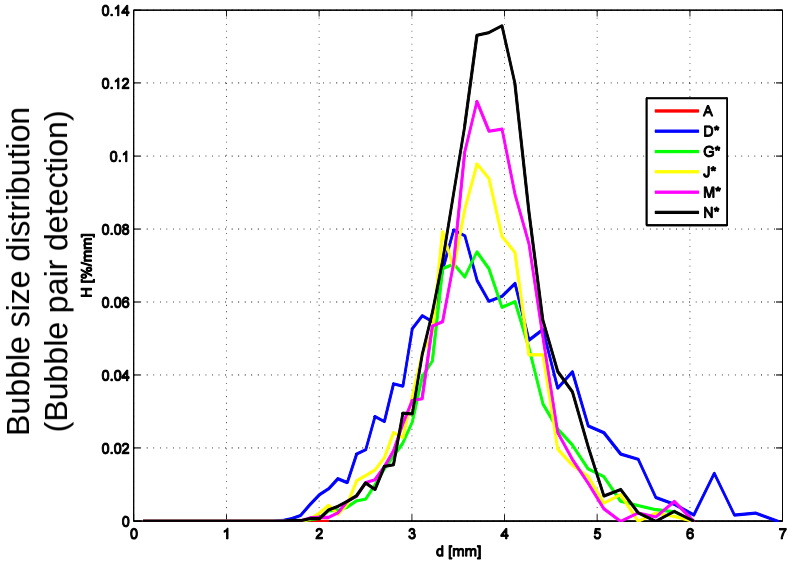
Bubble size distribution
(Bubble pair detection)
H [%/mm]
d [mm]
A
D*
G*
J*
M*
N*

L20 – 028 (jl = -0.405 $^{m}/_{s}$; jg = -0.0062 $^{m}/_{s}$), 2x1000Hz

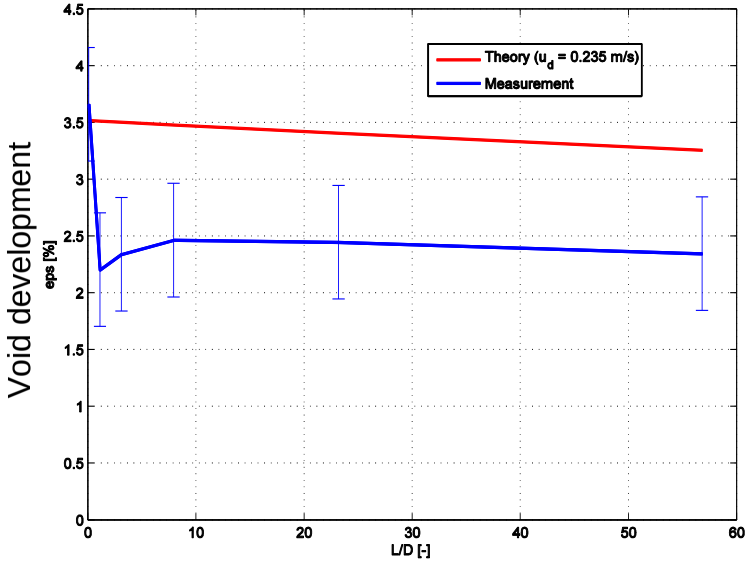

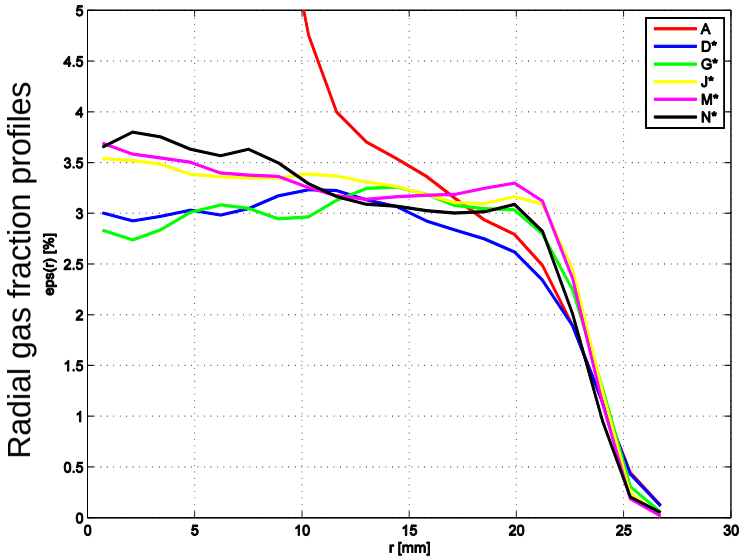

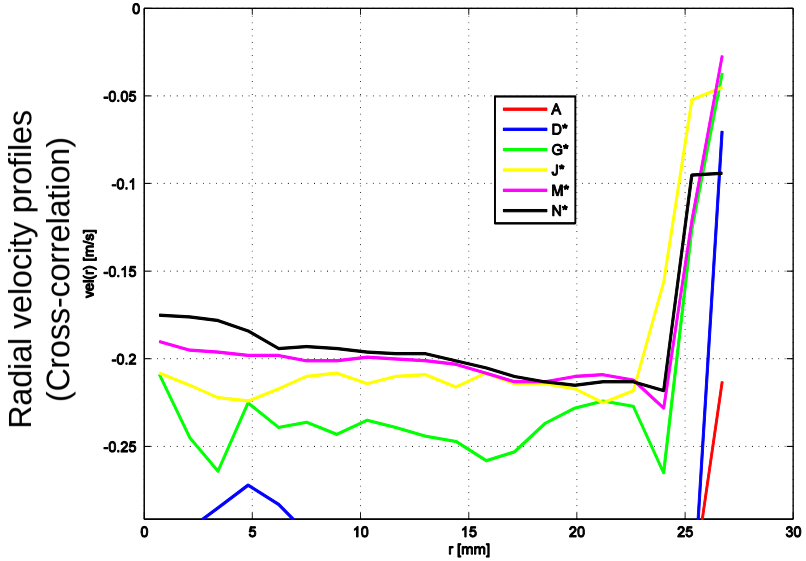

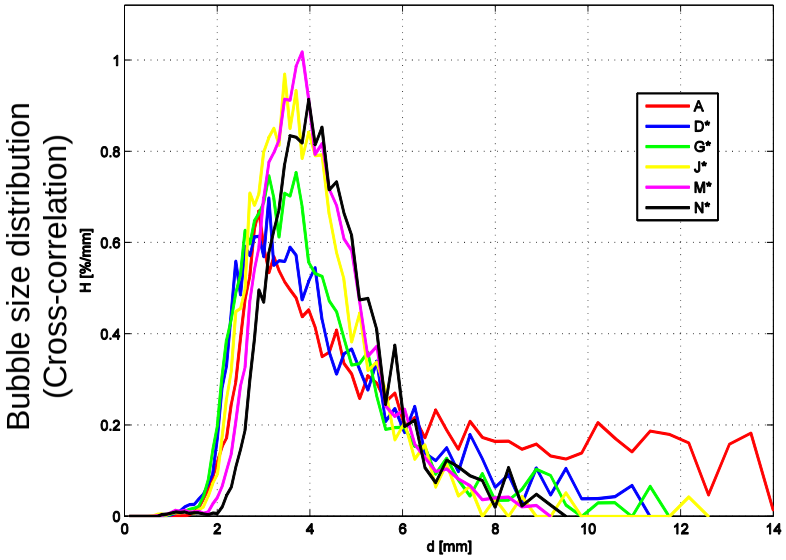

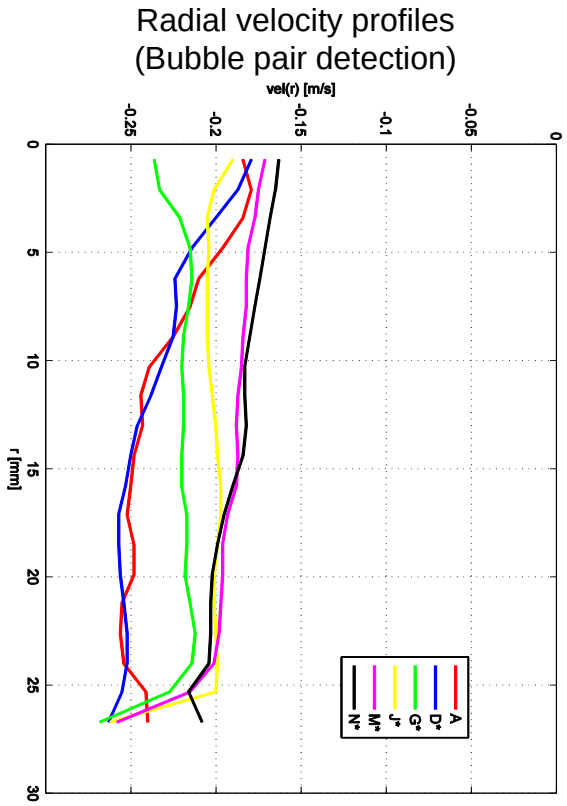
Radial velocity profiles
(Bubble pair detection)
vel(r) [m/s]
r [mm]
A
D*
G*
J*
M*
N*

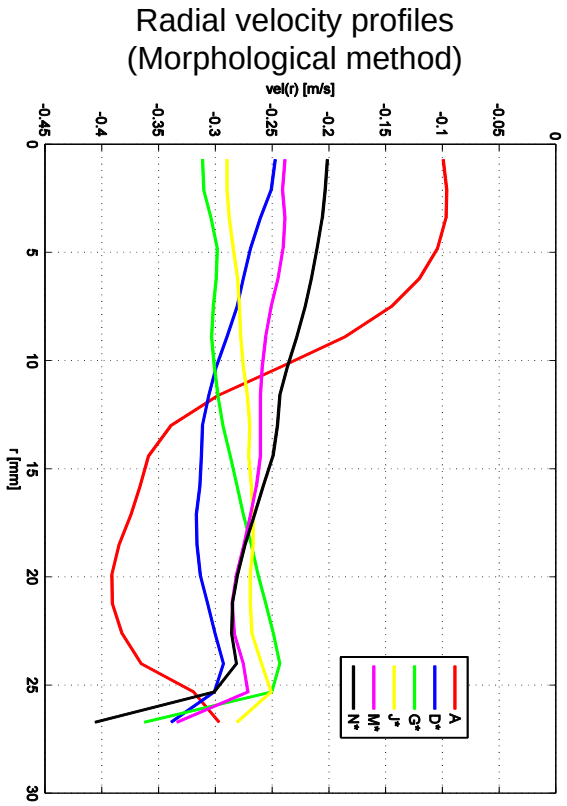
Radial velocity profiles
(Morphological method)
vel(r) [m/s]
r [mm]
A
D*
G*
J*
M*
N*

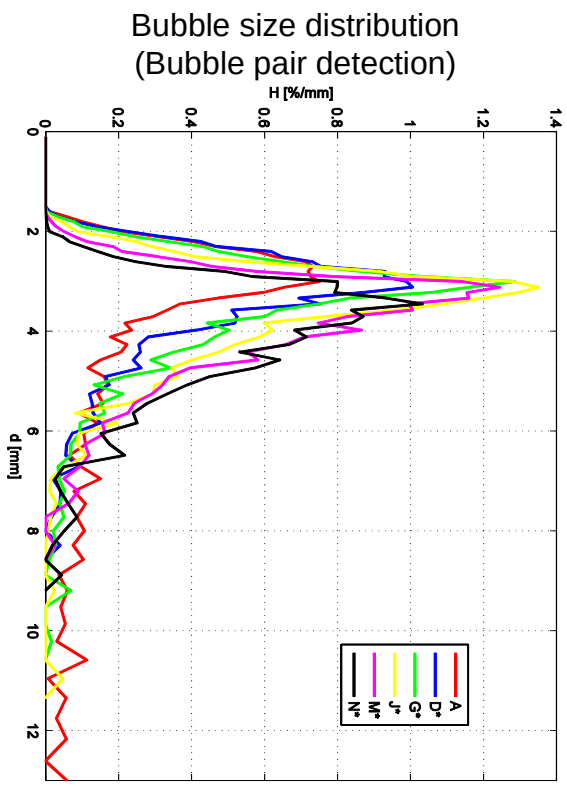
Bubble size distribution
(Bubble pair detection)
H [%/mm]
d [mm]
A
D*
G*
J*
M*
N*

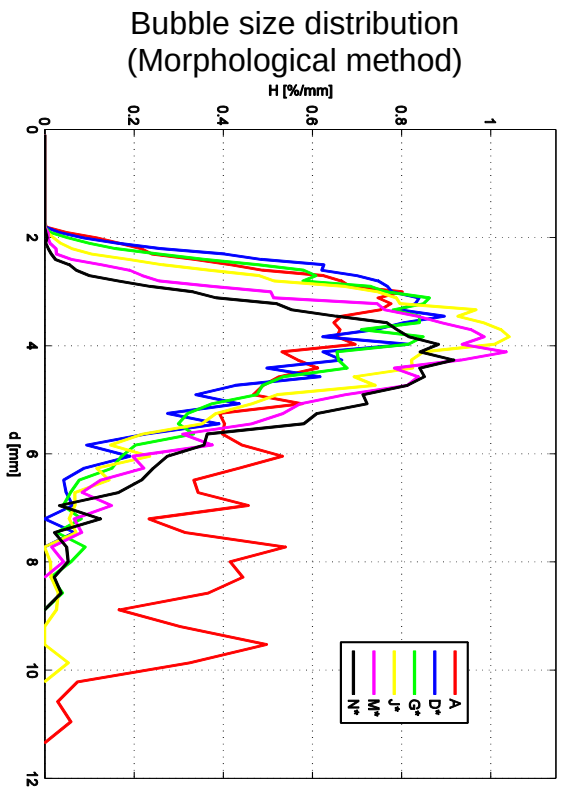
Bubble size distribution
(Morphological method)
H [%/mm]
d [mm]
A
D*
G*
J*
M*
N*

L20 – 029 (jl = -0.641 m/s; jg = -0.0062 m/s), 2x1000Hz
Void development
eps [%]
L/D [-]
Theory (u_d = 0.235 m/s)
Measurement
Radial gas fraction profiles
eps(r) [%]
r [mm]
A
D
G*
J*
M*
N*
Bubble size distribution
(Cross-correlation)
H [%/mm]
d [mm]
Radial velocity profiles
(Cross-correlation)
vel(r) [m/s]
r [mm]

Radial velocity profiles
(Morphological method)

Radial velocity profiles
(Bubble pair detection)

Bubble size distribution
(Morphological method)

Bubble size distribution
(Bubble pair detection)

L20 – 029Wh (jl = -0.641 $^{m}/_{s}$; jg = -0.0062 $^{m}/_{s}$), 2x1000Hz

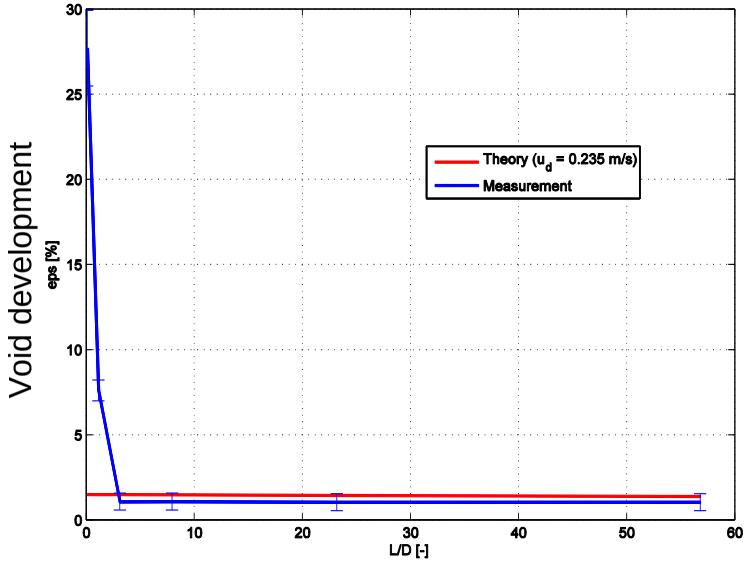

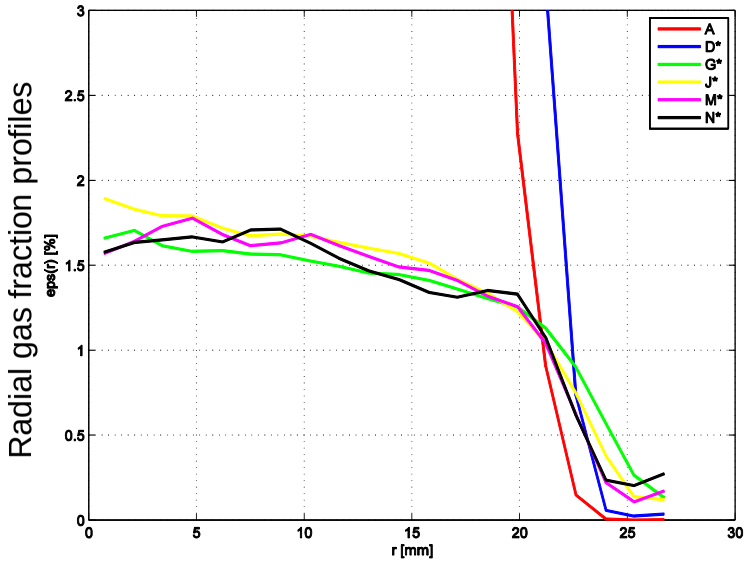

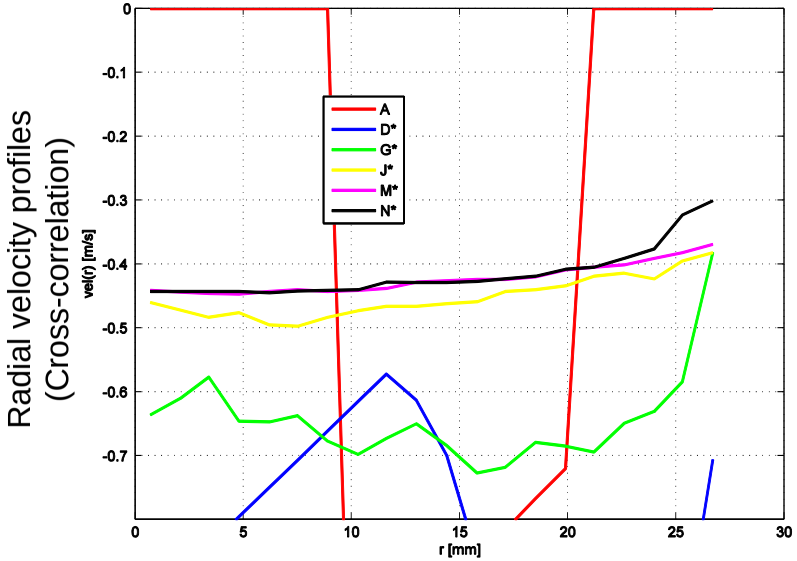

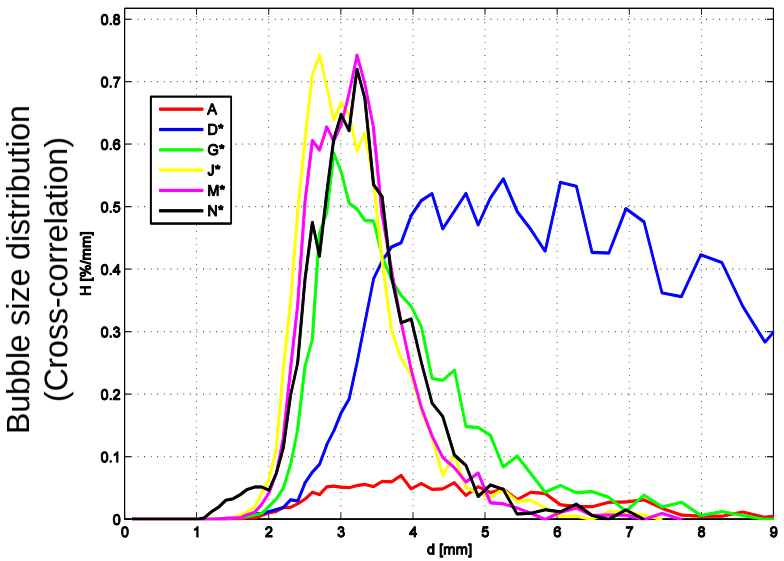

Radial velocity profiles
(Morphological method)

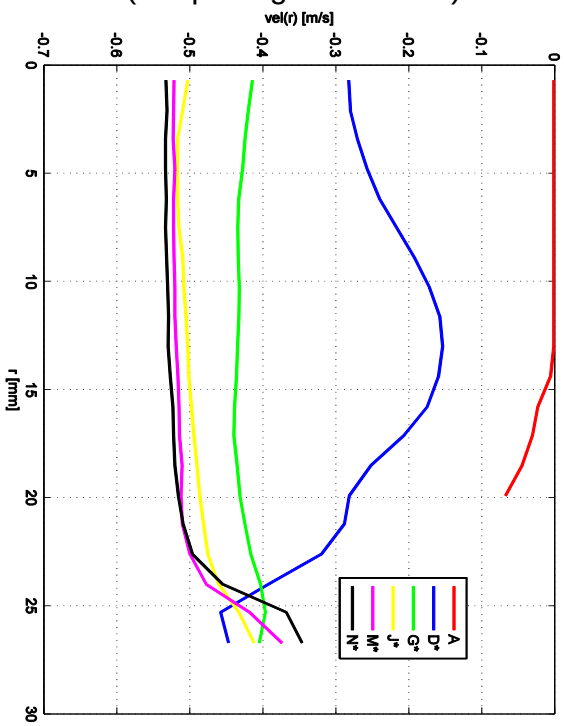

Radial velocity profiles
(Bubble pair detection)

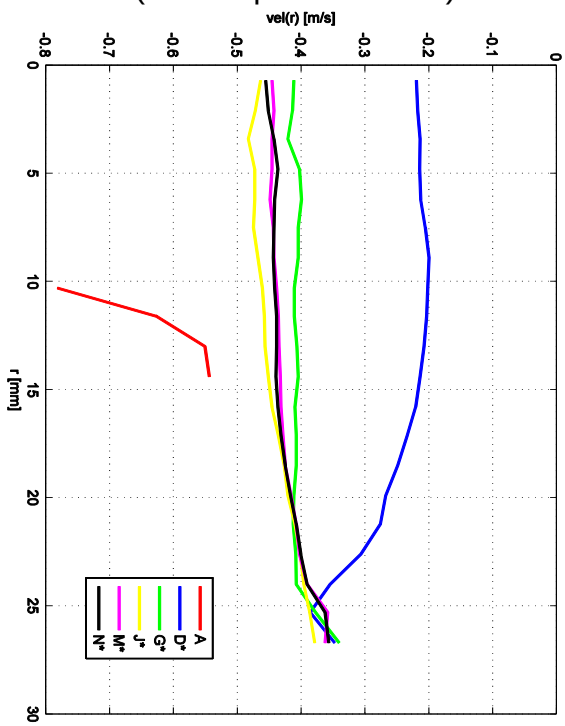

Bubble size distribution
(Morphological method)

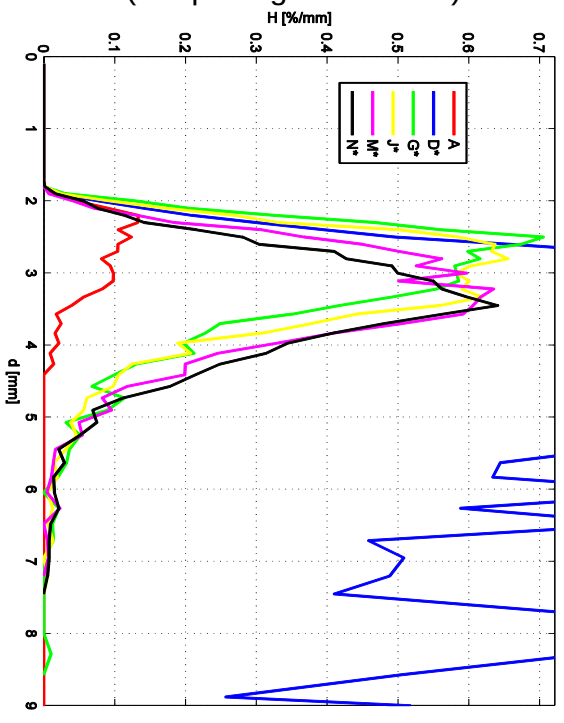

Bubble size distribution
(Bubble pair detection)

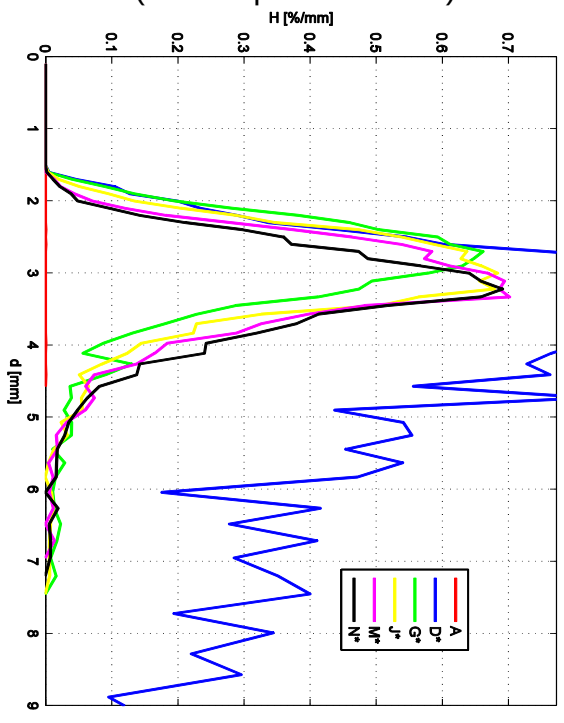

L20 – 030 (jl = -1.017 $^{m}/_{s}$; jg = -0.0062 $^{m}/_{s}$), 2x1000Hz

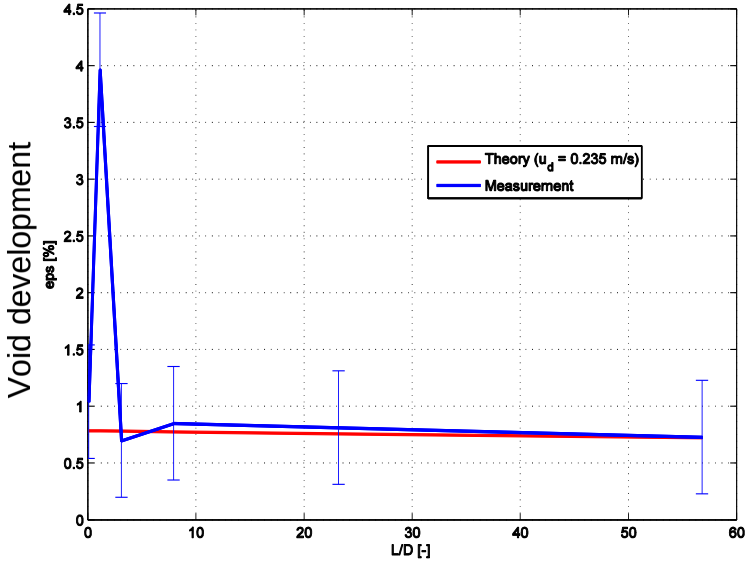

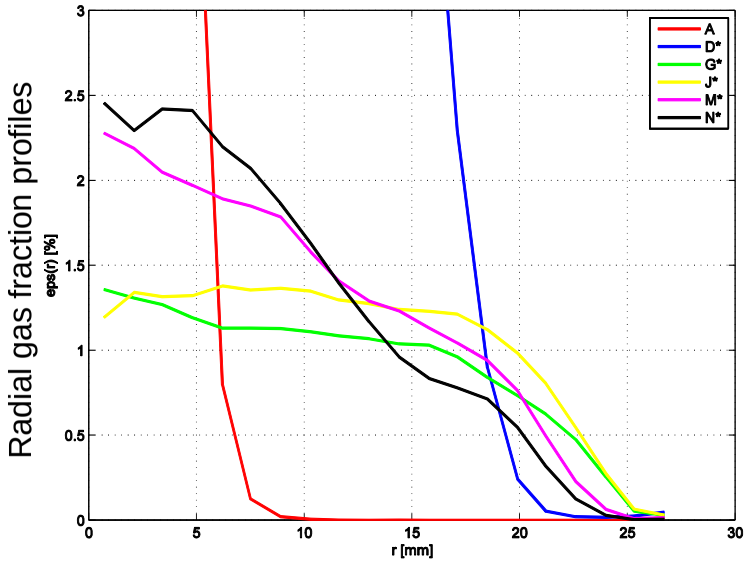

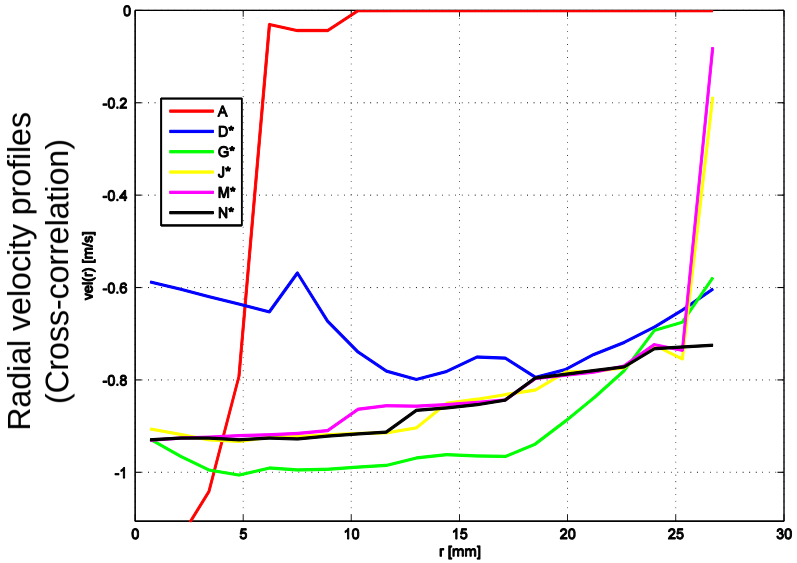

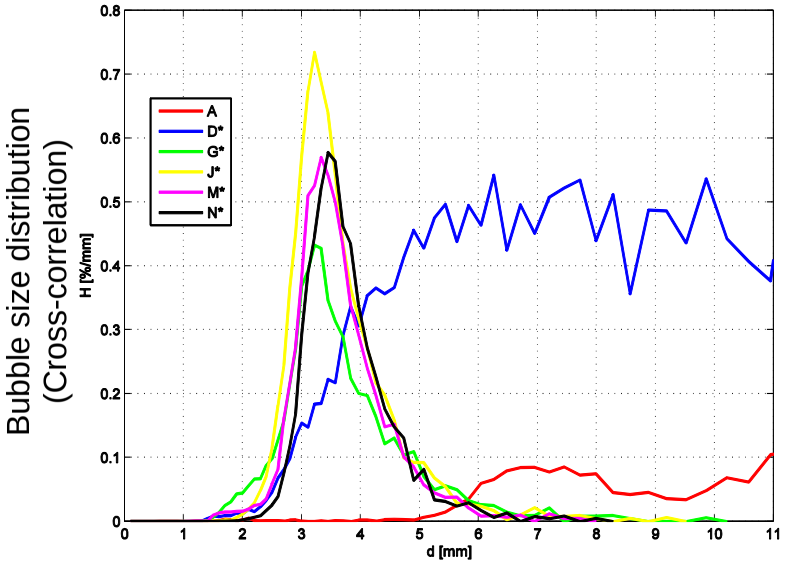

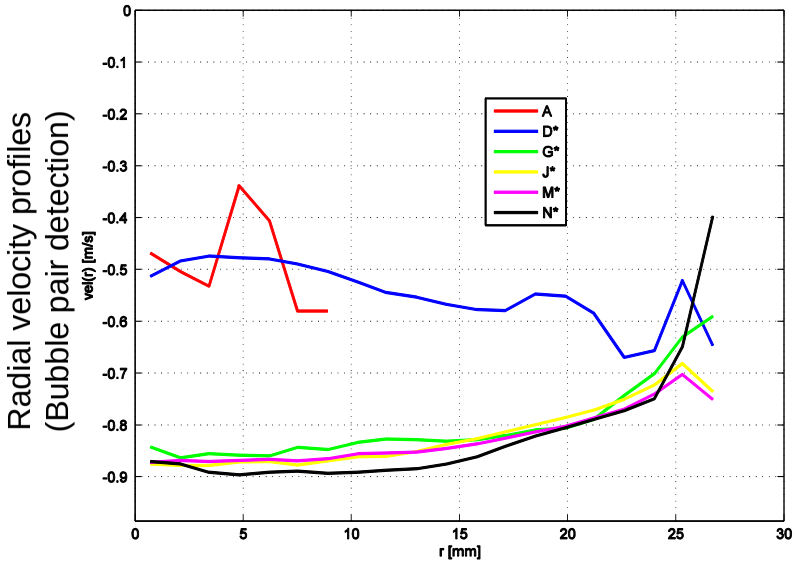
Radial velocity profiles
(Bubble pair detection)
vel(r) [m/s]
r [mm]
A
D*
G*
J*
M*
N*

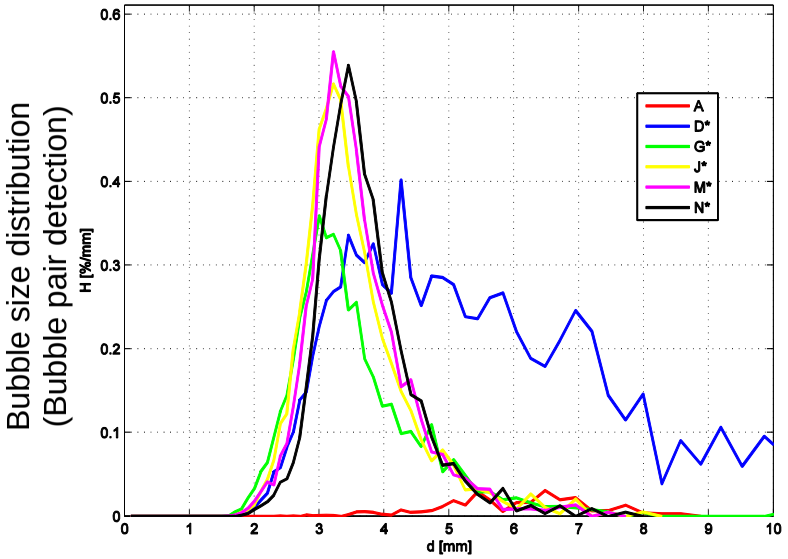
Bubble size distribution
(Bubble pair detection)
H [%/mm]
d [mm]
A
D*
G*
J*
M*
N*

L20 – 031 (jl = -1.611 m/s; jg = -0.0062 m/s), 2x2000Hz
Void development
eps [%]
L/D [-]
Theory (u_d = 0.235 m/s)
Measurement
Radial gas fraction profiles
eps(r) [%]
r [mm]
A
D*
G*
J*
M*
N*
Bubble size distribution
(Cross-correlation)
H [%/mm]
d [mm]
Radial velocity profiles
(Cross-correlation)
vel(r) [m/s]
r [mm]

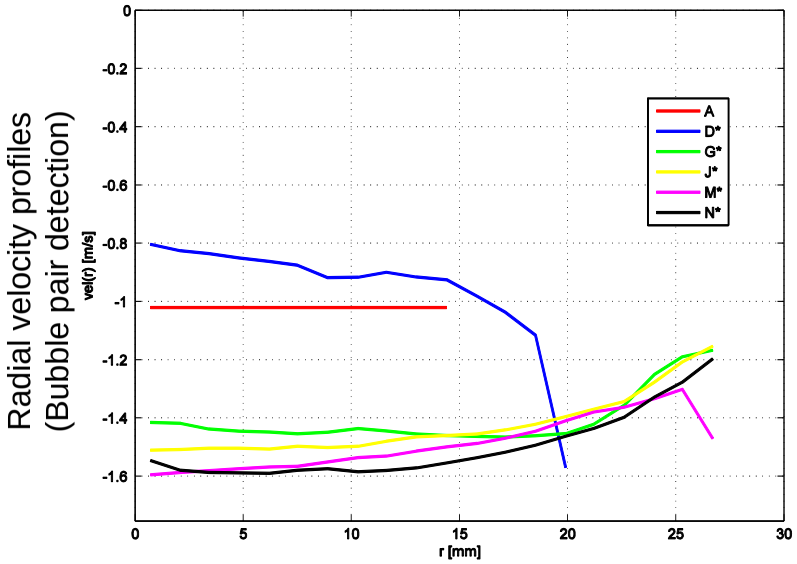
Radial velocity profiles
(Bubble pair detection)
vel(r) [m/s]
r [mm]
A
D*
G*
J*
M*
N*

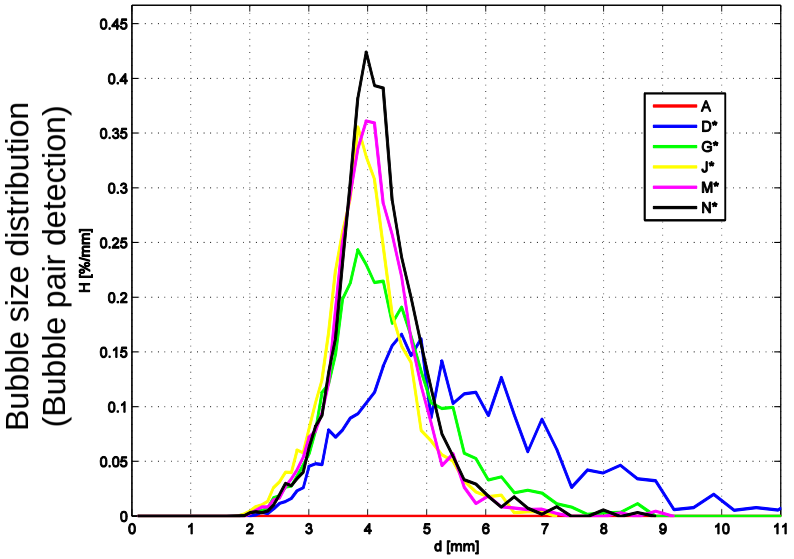
Bubble size distribution
(Bubble pair detection)
H [%/mm]
d [mm]
A
D*
G*
J*
M*
N*

L20 – 050 (jl = -0.405 m/s; jg = -0.0151 m/s), 2x1000Hz
Void development
eps [%]
L/D [-]
Theory (u_d = 0.235 m/s)
Measurement
Radial gas fraction profiles
eps(r) [%]
r [mm]
A
D*
G*
J*
M*
N*
Radial velocity profiles
(Cross-correlation)
vel(r) [m/s]
Bubble size distribution
(Cross-correlation)
H [%/mm]
d [mm]

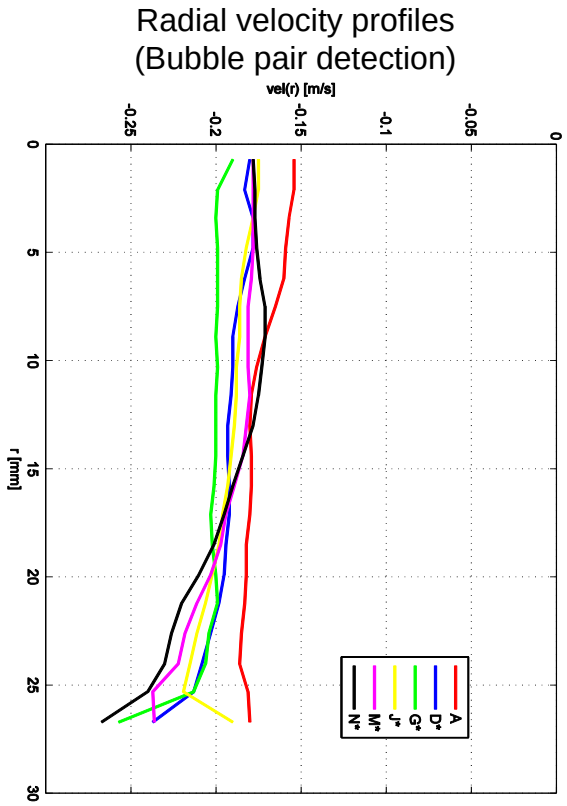
Radial velocity profiles
(Bubble pair detection)
vel(r) [m/s]
r [mm]
N*
M*
J*
G*
D*
A

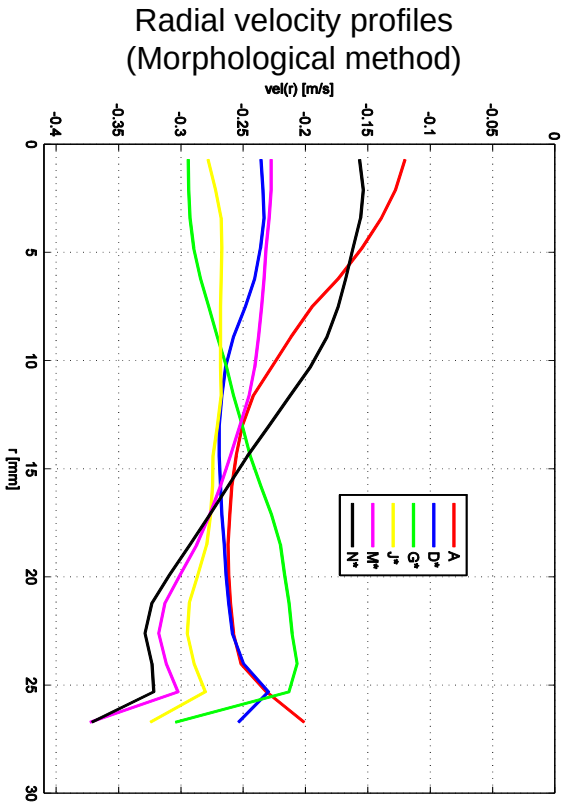
Radial velocity profiles
(Morphological method)
vel(r) [m/s]
r [mm]
N*
M*
J*
G*
D*
A

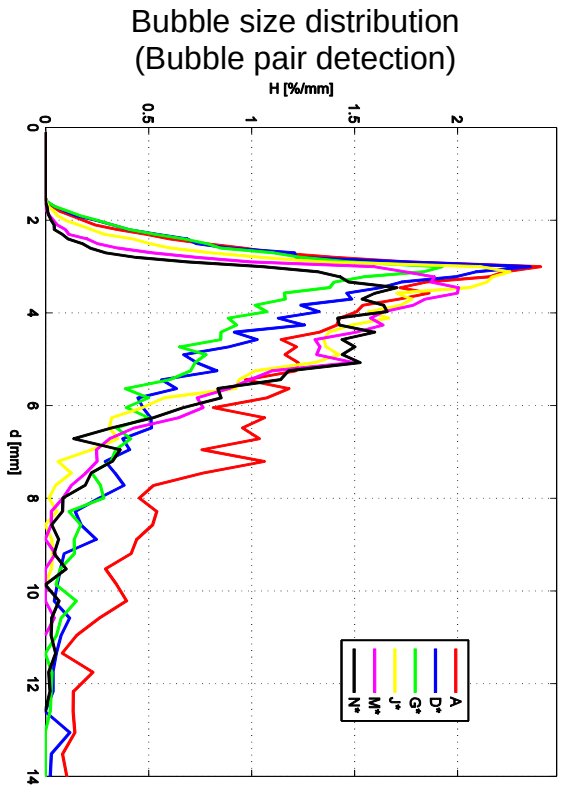
Bubble size distribution
(Bubble pair detection)
H [%/mm]
d [mm]
N*
M*
J*
G*
D*
A

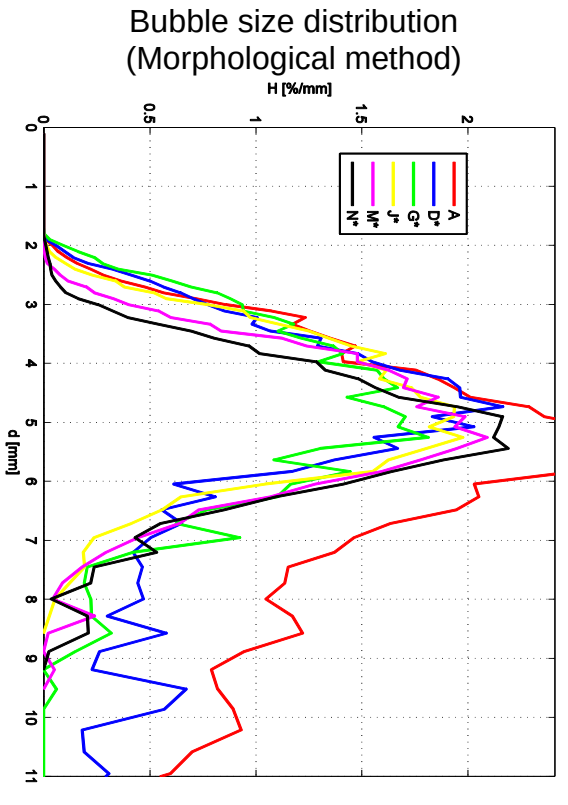
Bubble size distribution
(Morphological method)
H [%/mm]
d [mm]
N*
M*
J*
G*
D*
A

L20 – 051 (jl = -0.641 m/s; jg = -0.0151 m/s), 2x1000Hz
Void development
eps [%]
L/D [-]
Theory (u_d = 0.235 m/s)
Measurement
Radial gas fraction profiles
eps(r) [%]
r [mm]
A
D
G*
J*
M*
N*
Bubble size distribution
(Cross-correlation)
H [%/mm]
d [mm]
Radial velocity profiles
(Cross-correlation)
vel(r) [m/s]
r [mm]

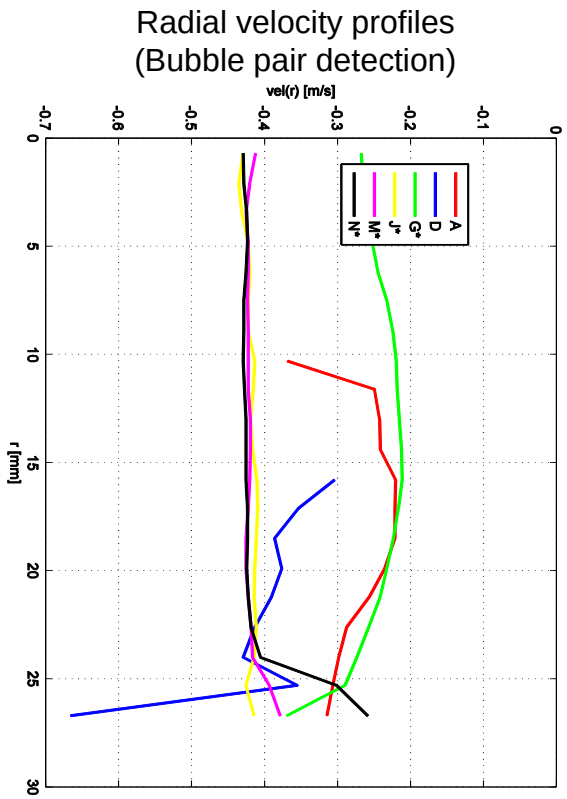
Radial velocity profiles
(Bubble pair detection)
vel(r) [m/s]
r [mm]
A
D
G*
J*
M*
N*

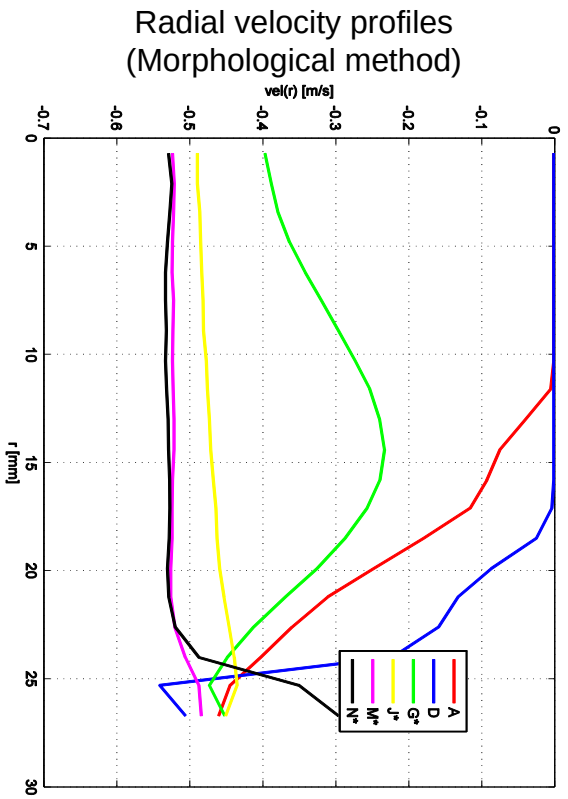
Radial velocity profiles
(Morphological method)
vel(r) [m/s]
r [mm]
A
D
G*
J*
M*
N*

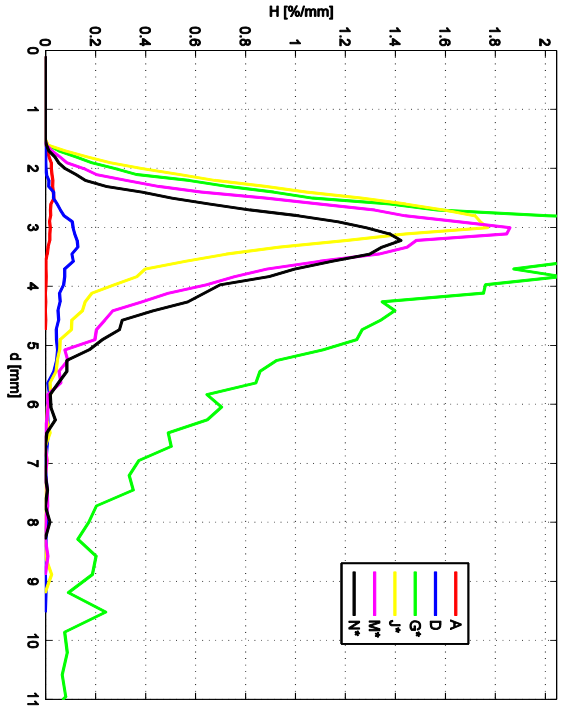
Bubble size distribution
(Bubble pair detection)
H [%/mm]
d [mm]
A
D
G*
J*
M*
N*

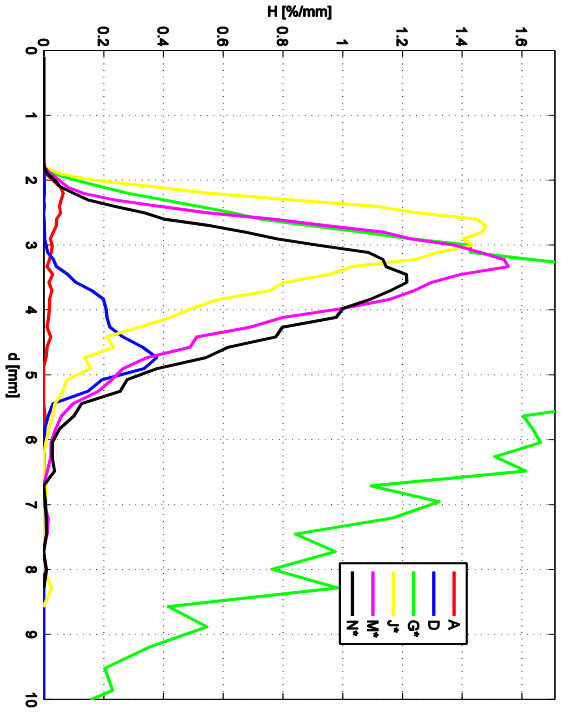
Bubble size distribution
(Morphological method)
H [%/mm]
d [mm]
A
D
G*
J*
M*
N*

L20 – 052 (jl = -1.017 $^{m}/_{s}$; jg = -0.0151 $^{m}/_{s}$), 2x1000Hz

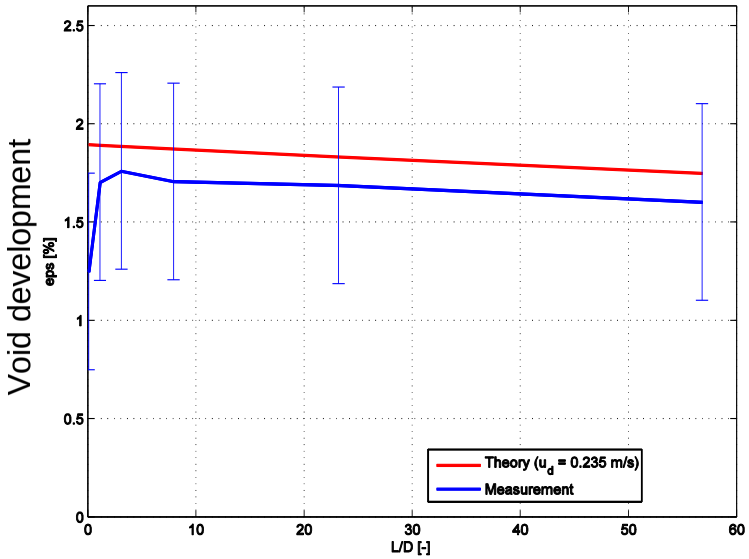

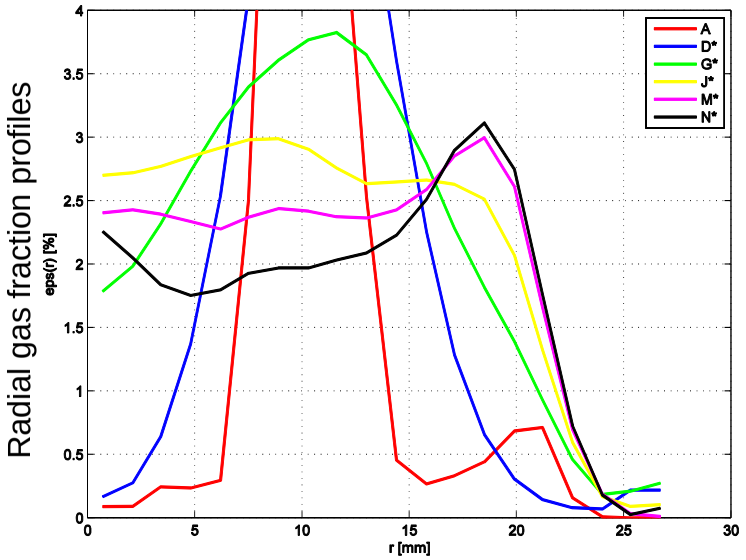

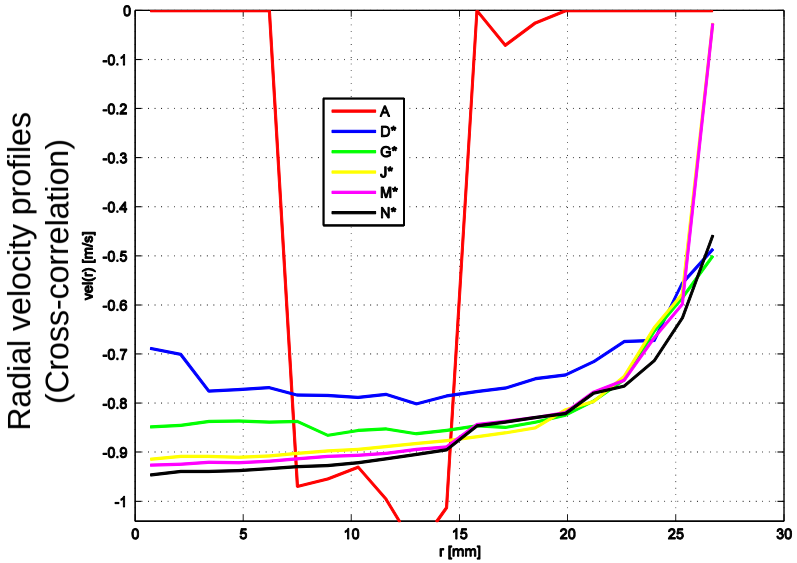

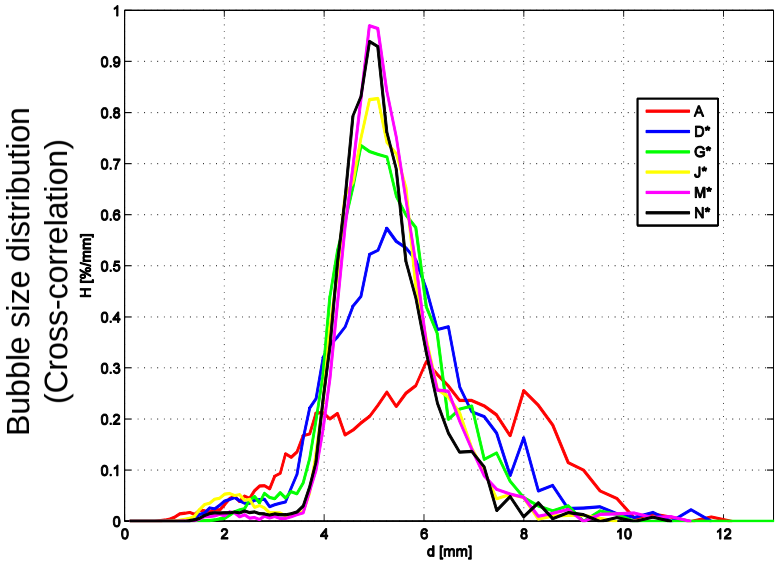

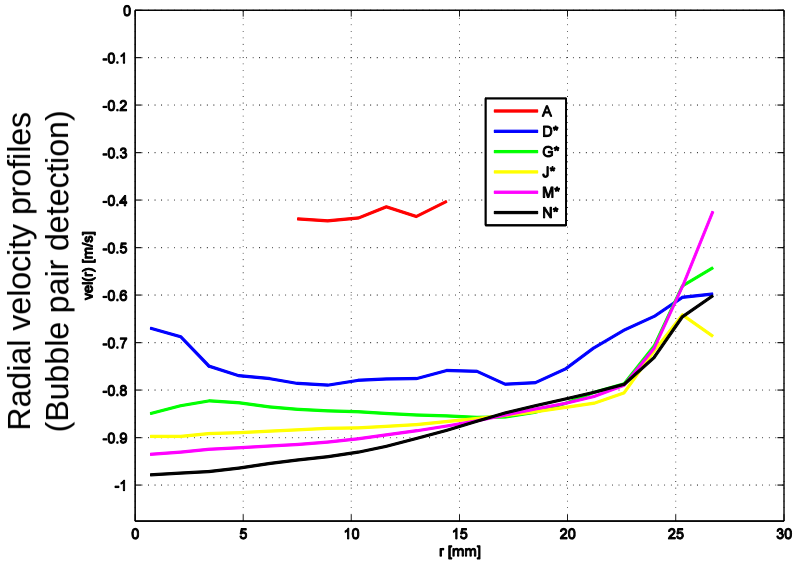
Radial velocity profiles
(Bubble pair detection)
vel(r) [m/s]
r [mm]
A
D*
G*
J*
M*
N*

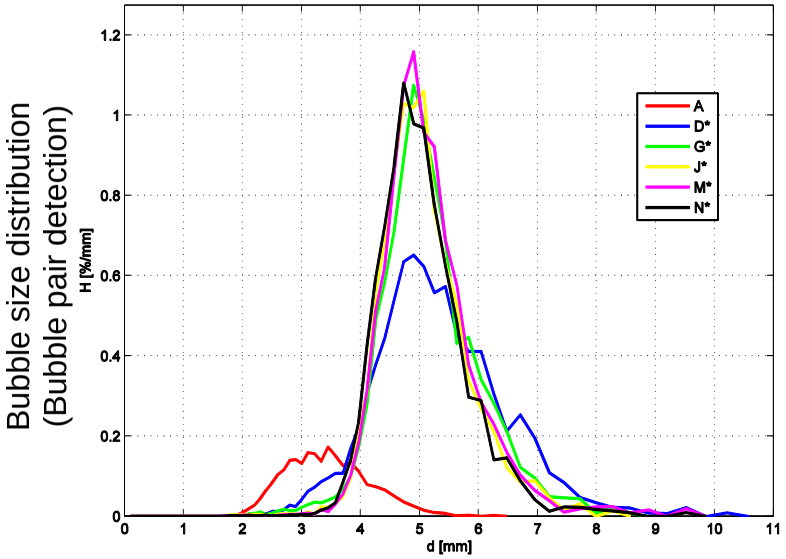
Bubble size distribution
(Bubble pair detection)
H [%/mm]
d [mm]
A
D*
G*
J*
M*
N*

L20 – 053 (jl = -1.611 $^{m}/_{s}$; jg = -0.0151 $^{m}/_{s}$), 2x2000Hz

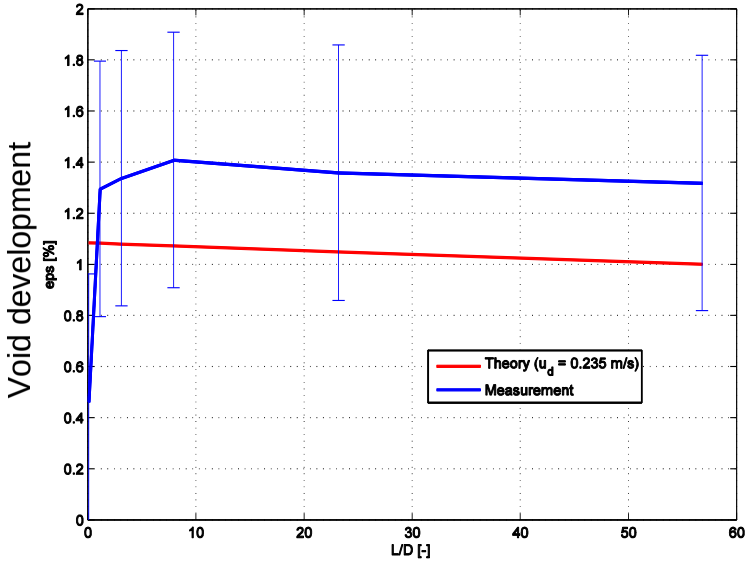

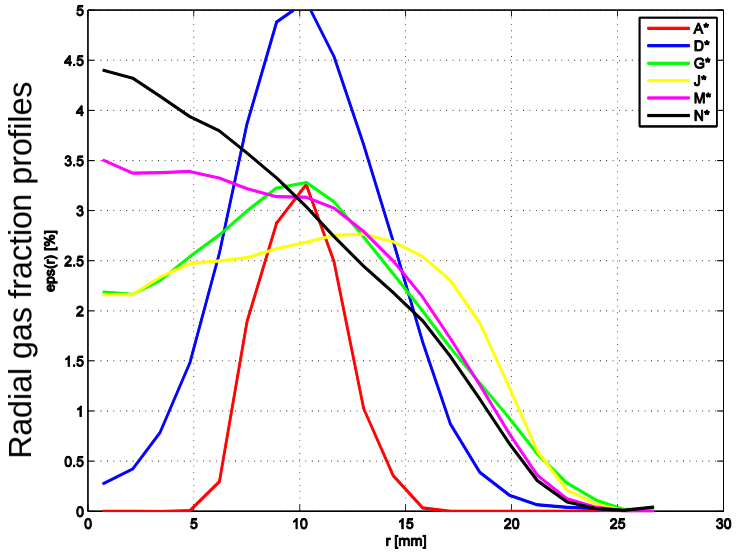

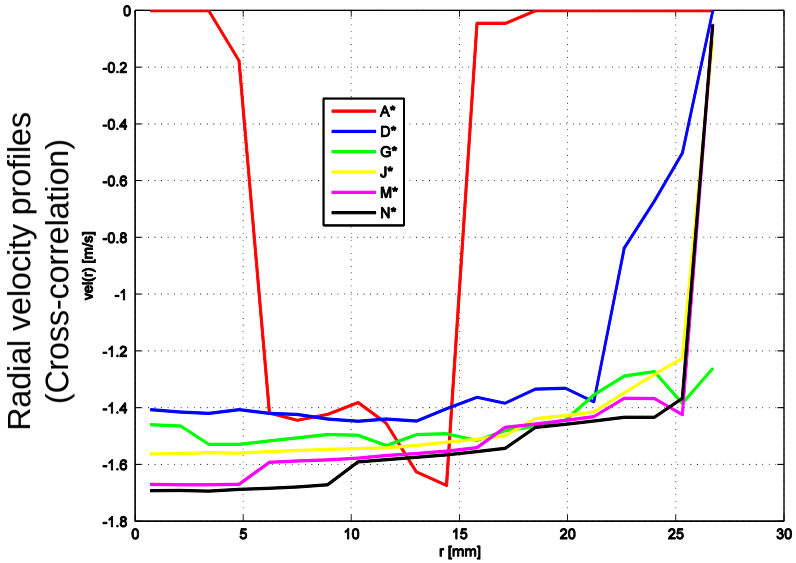

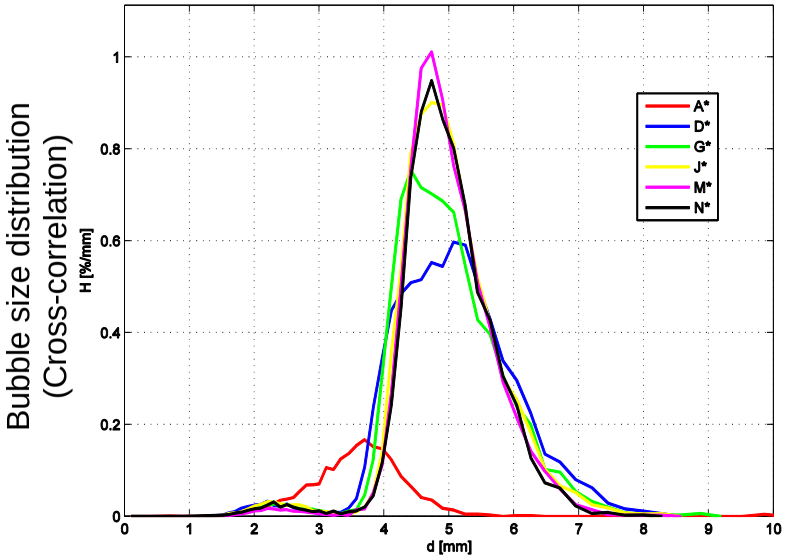

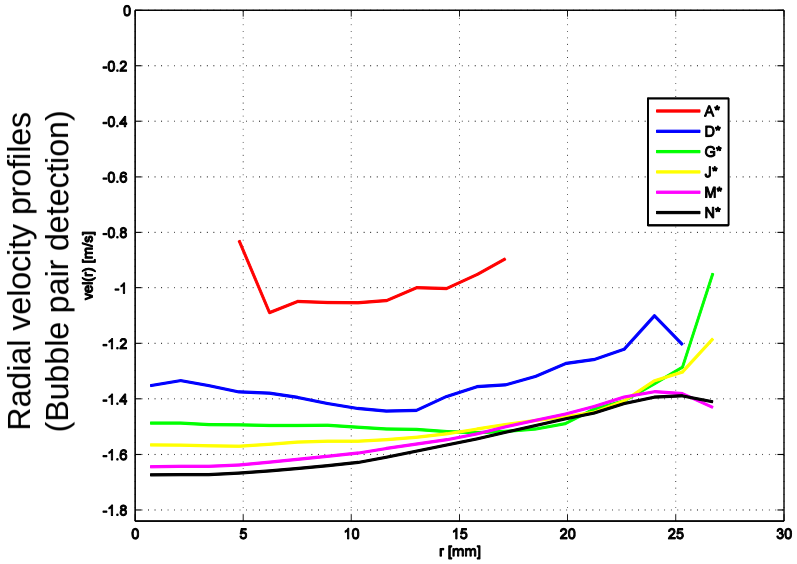
Radial velocity profiles
(Bubble pair detection)
vel(r) [m/s]
r [mm]
A*
D*
G*
J*
M*
N*

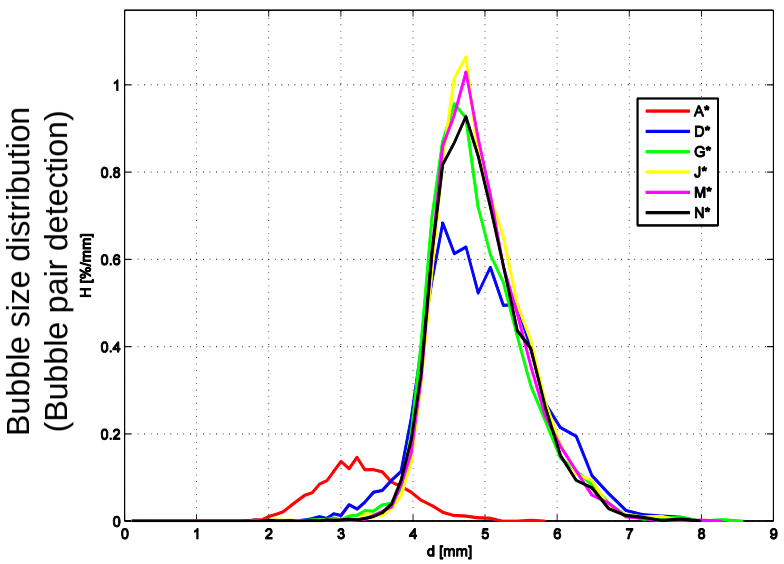
Bubble size distribution
(Bubble pair detection)
H [%/mm]
d [mm]
A*
D*
G*
J*
M*
N*

L20 – 083 (jl = -0.405 m/s; jg = -0.0574 m/s), 2x1000Hz
Void development
eps [%]
L/D [-]
Theory (u_d = 0.235 m/s)
Measurement
Radial gas fraction profiles
eps(r) [%]
r [mm]
A
D*
G*
J*
M*
N*
Bubble size distribution
(Cross-correlation)
H [%/mm]
d [mm]
Radial velocity profiles
(Cross-correlation)
vel(r) [m/s]
r [mm]

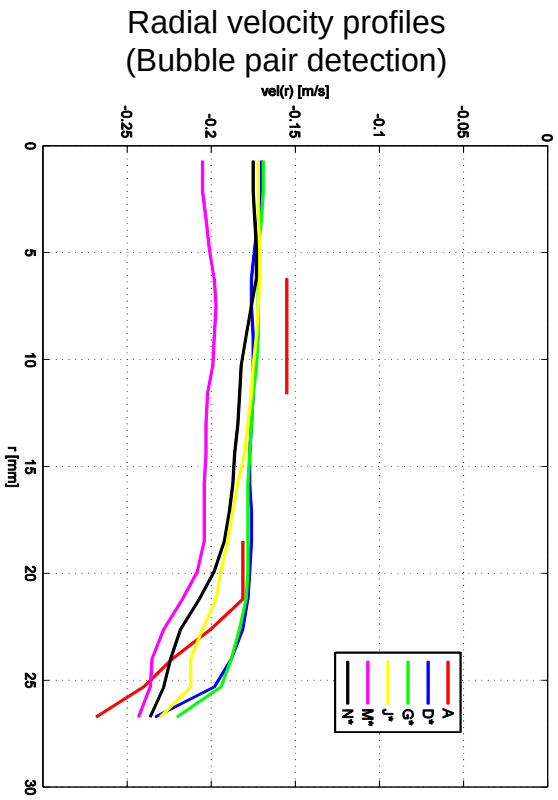
Radial velocity profiles
(Bubble pair detection)
vel(r) [m/s]
r [mm]
N*
M*
J*
G*
D*
A

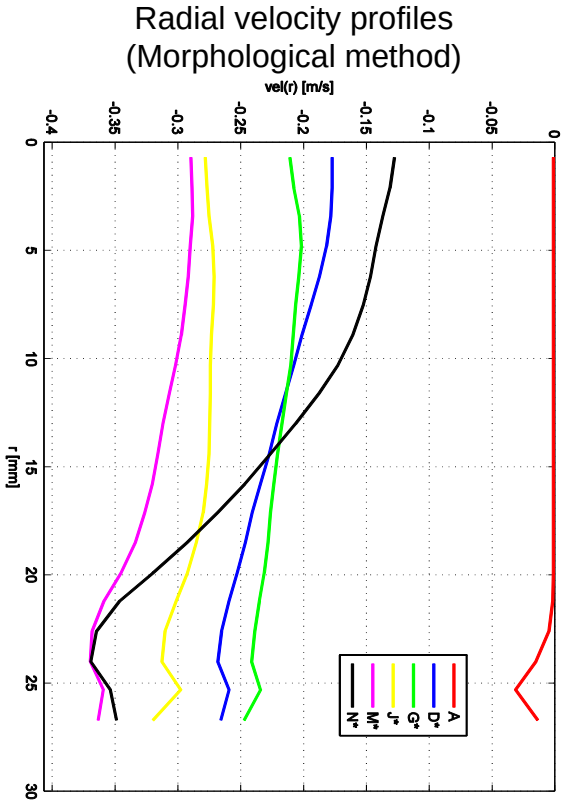
Radial velocity profiles
(Morphological method)
vel(r) [m/s]
r [mm]
N*
M*
J*
G*
D*
A

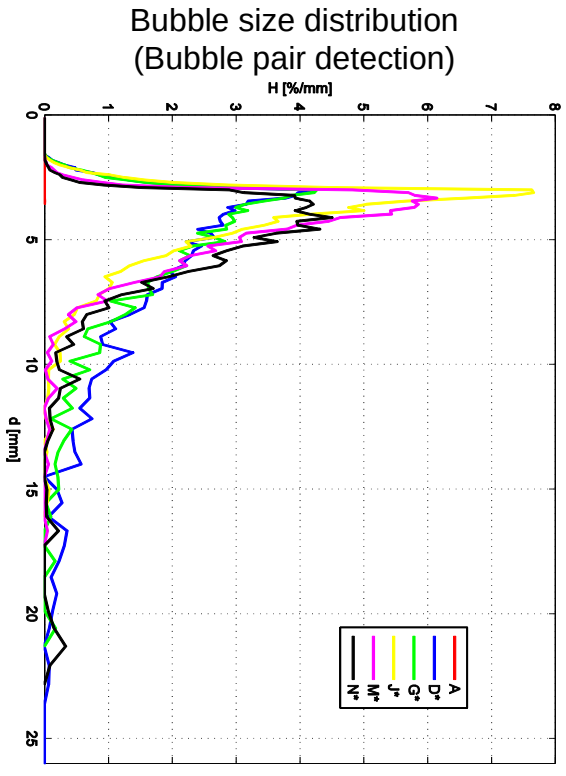
Bubble size distribution
(Bubble pair detection)
H [%/mm]
d [mm]
N*
M*
J*
G*
D*
A

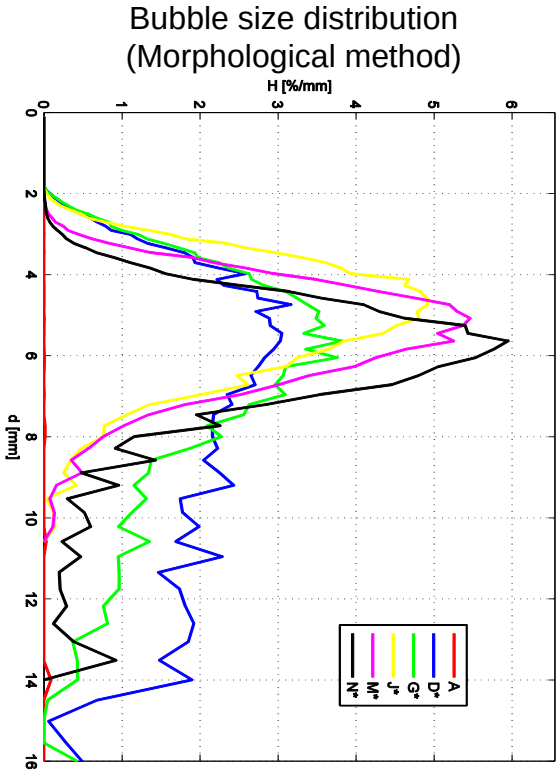
Bubble size distribution
(Morphological method)
H [%/mm]
d [mm]
N*
M*
J*
G*
D*
A

L20 – 084 (jl = -0.641 m/s; jg = -0.0574 m/s), 2x1000Hz
Void development
eps [%]
L/D [-]
Theory (u_d = 0.235 m/s)
Measurement
Radial gas fraction profiles
eps(r) [%]
r [mm]
A
D
G
J*
M*
N*
Radial velocity profiles
(Cross-correlation)
vel(r) [m/s]
r [mm]
Bubble size distribution
(Cross-correlation)
H [%/mm]
d [mm]

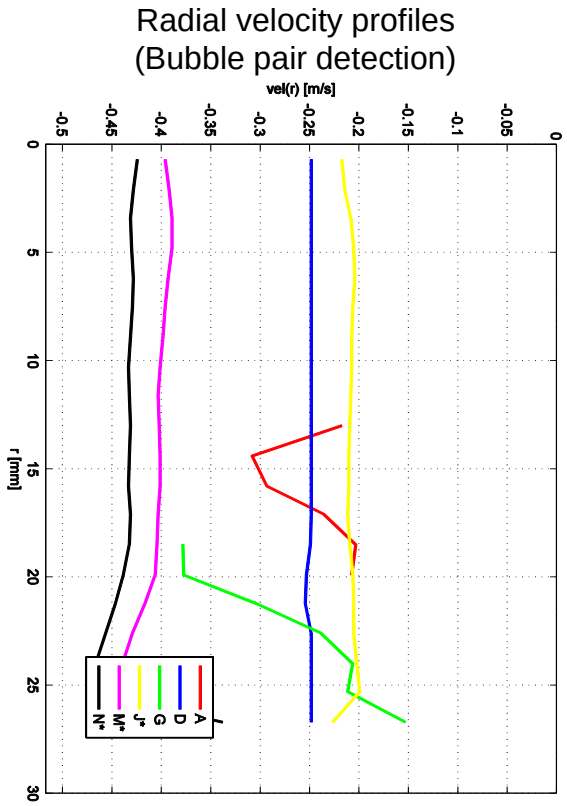
Radial velocity profiles
(Bubble pair detection)
vel(r) [m/s]
r [mm]
A
D
G
J*
M*
N*

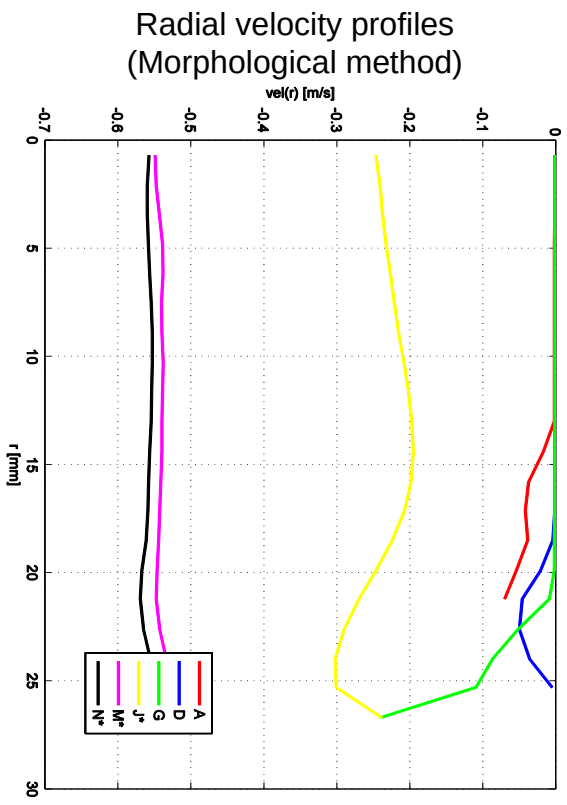
Radial velocity profiles
(Morphological method)
vel(r) [m/s]
r [mm]
A
D
G
J*
M*
N*

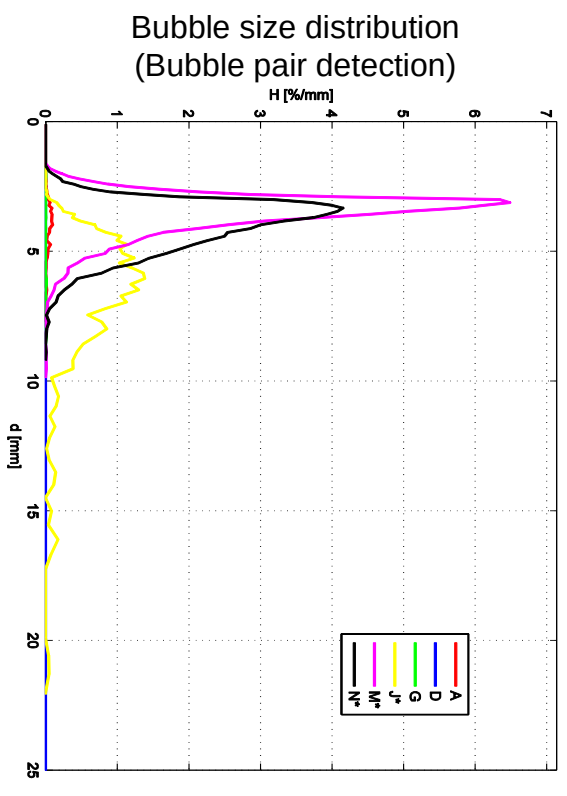
Bubble size distribution
(Bubble pair detection)
H [%/mm]
d [mm]
A
D
G
J*
M*
N*

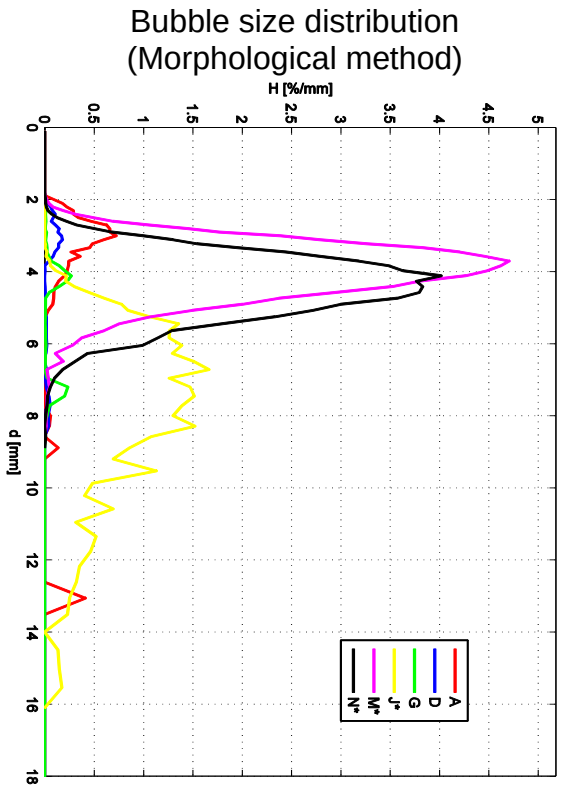
Bubble size distribution
(Morphological method)
H [%/mm]
d [mm]
A
D
G
J*
M*
N*

L20 – 085 (jl = -1.017 m/s; jg = -0.0574 m/s), 2x1000Hz

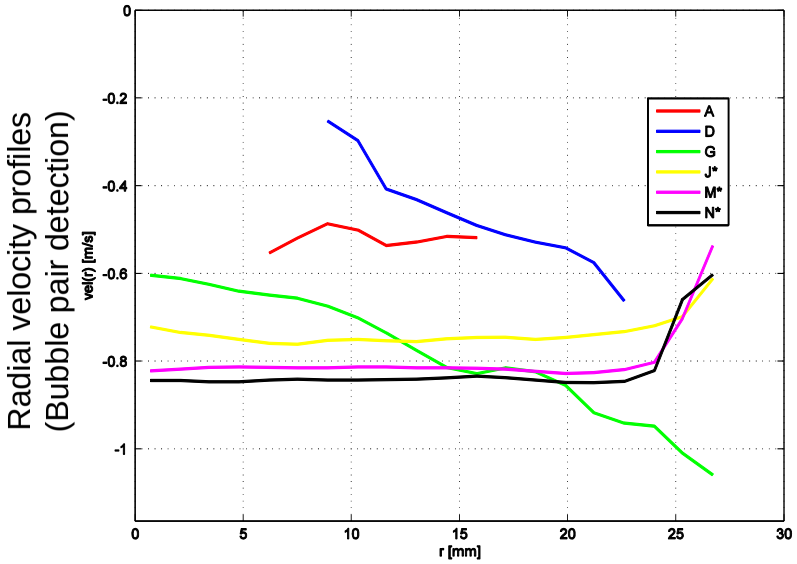
Radial velocity profiles
(Bubble pair detection)
vel(r) [m/s]
r [mm]
A
D
G
J*
M*
N*

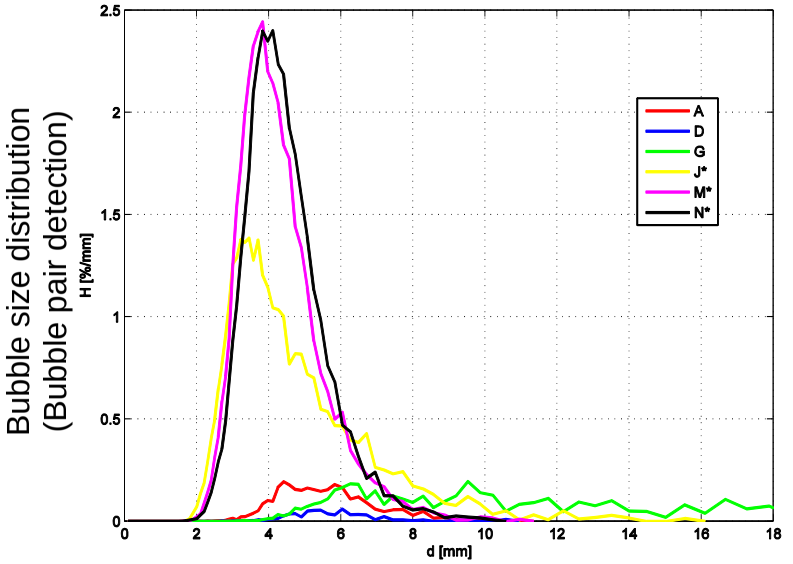
Bubble size distribution
(Bubble pair detection)
H [%/mm]
d [mm]
A
D
G
J*
M*
N*

L20 – 086 (jl = -1.611 m/s; jg = -0.0574 m/s), 2x2000Hz
Void development
eps [%]
L/D [-]
Theory (u_d = 0.235 m/s)
Measurement
Radial gas fraction profiles
eps(r) [%]
r [mm]
A
D
G*
J*
M*
N*
Radial velocity profiles
(Cross-correlation)
vel(r) [m/s]
r [mm]
Bubble size distribution
(Cross-correlation)
H [%/mm]
d [mm]

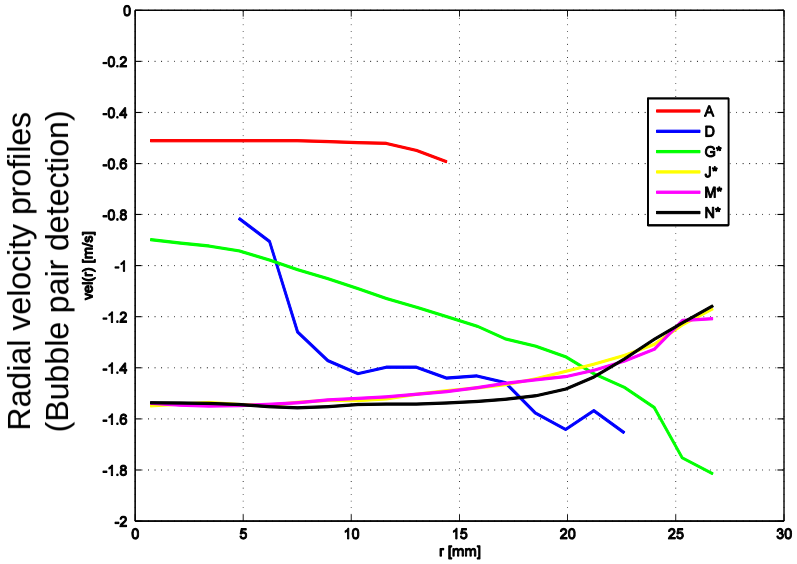
Radial velocity profiles
(Bubble pair detection)
vel(r) [m/s]
r [mm]
A
D
G*
J*
M*
N*

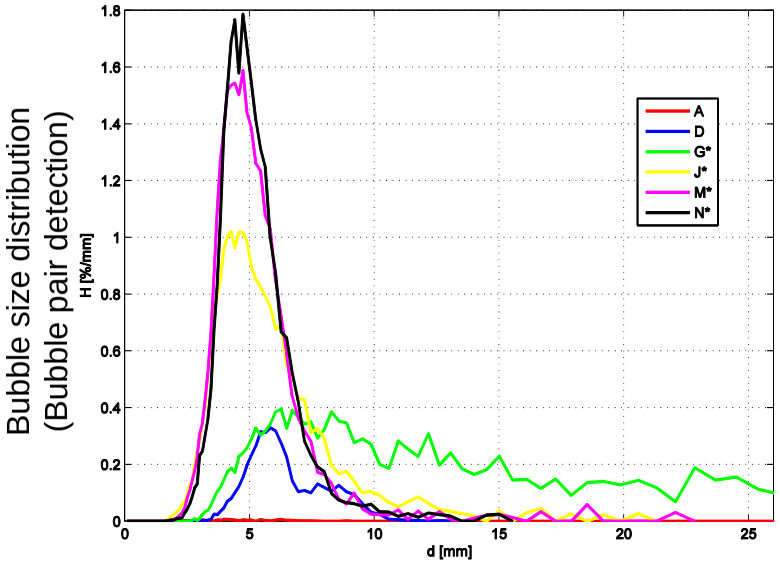
Bubble size distribution
(Bubble pair detection)
H [%/mm]
d [mm]
A
D
G*
J*
M*
N*

L21 – 116 (jl = -0.405 $^{m}/_{s}$; jg = -0.219 $^{m}/_{s}$), 2x1000Hz

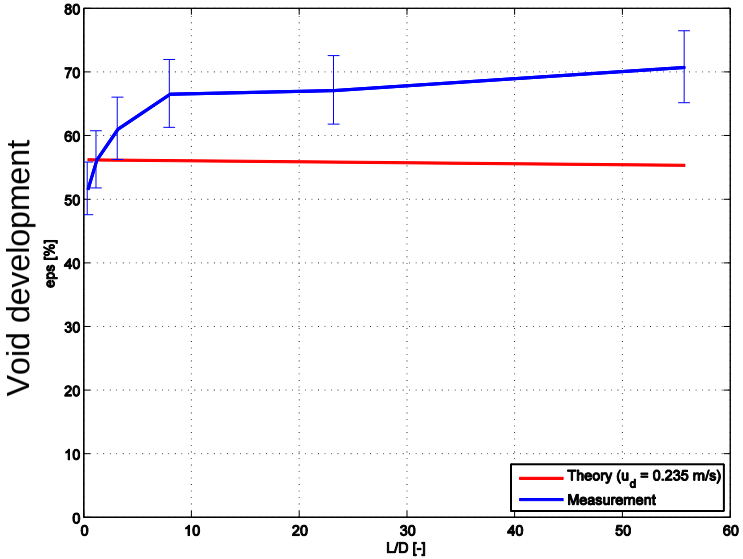

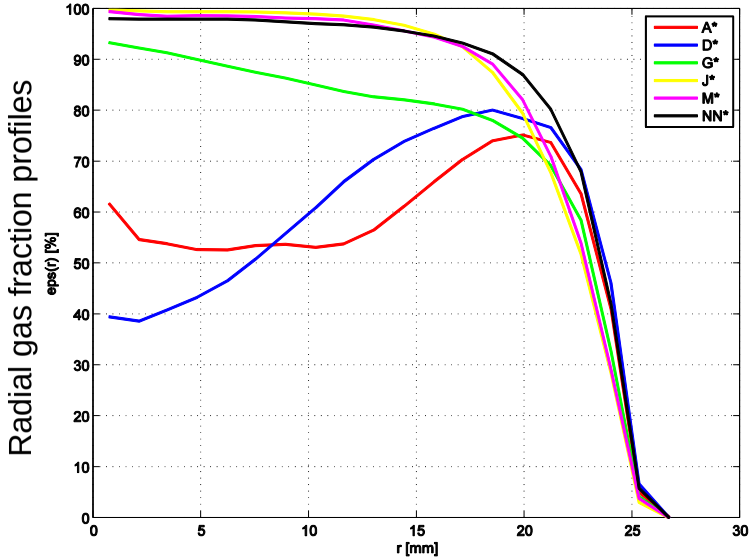

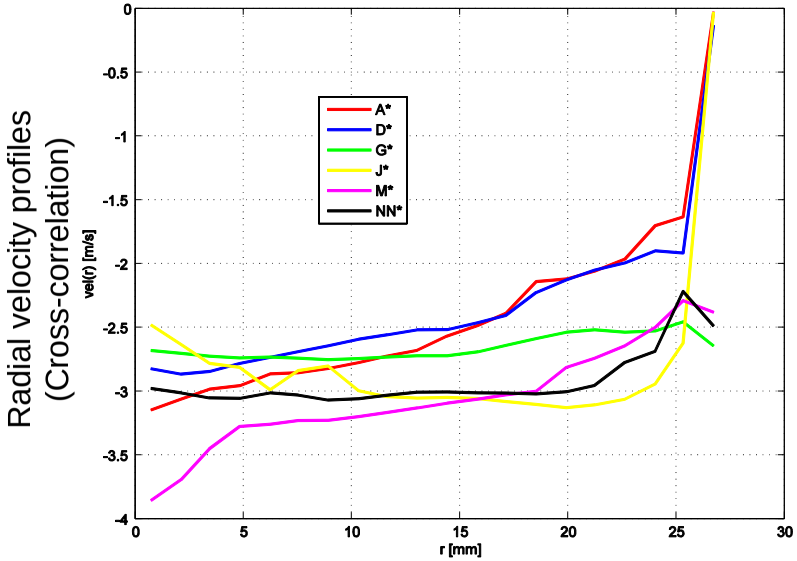

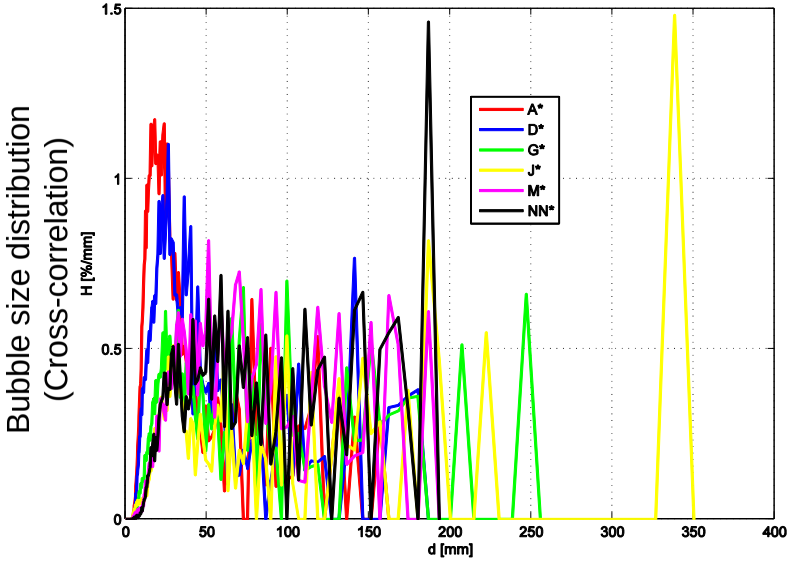

L21 – 117 (jl = -0.641 $^{m}/_{s}$; jg = -0.219 $^{m}/_{s}$), 2x1000Hz

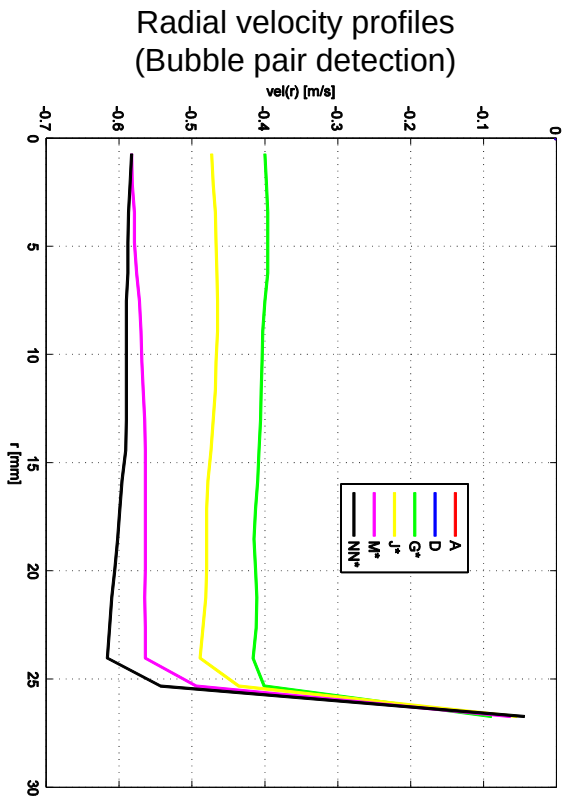
Radial velocity profiles
(Bubble pair detection)
vel(r) [m/s]
r [mm]
A
D
G*
J*
M*
NN*

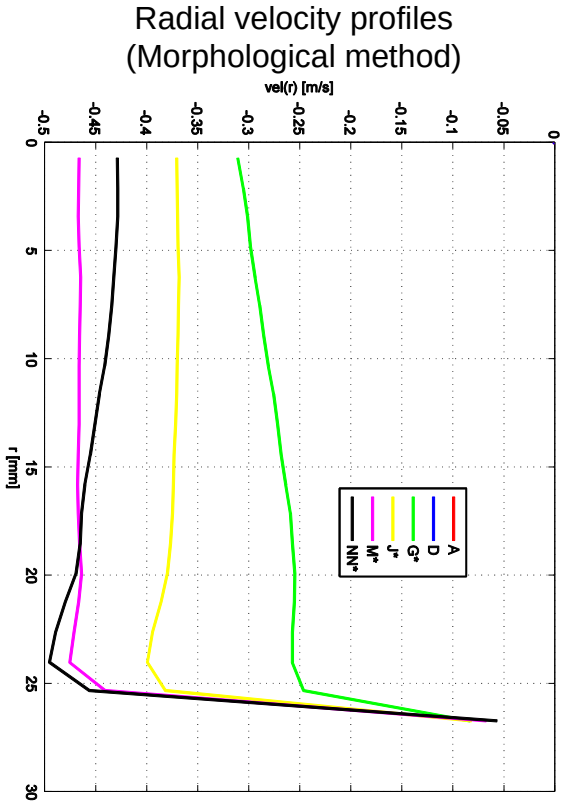
Radial velocity profiles
(Morphological method)
vel(r) [m/s]
r [mm]
A
D
G*
J*
M*
NN*

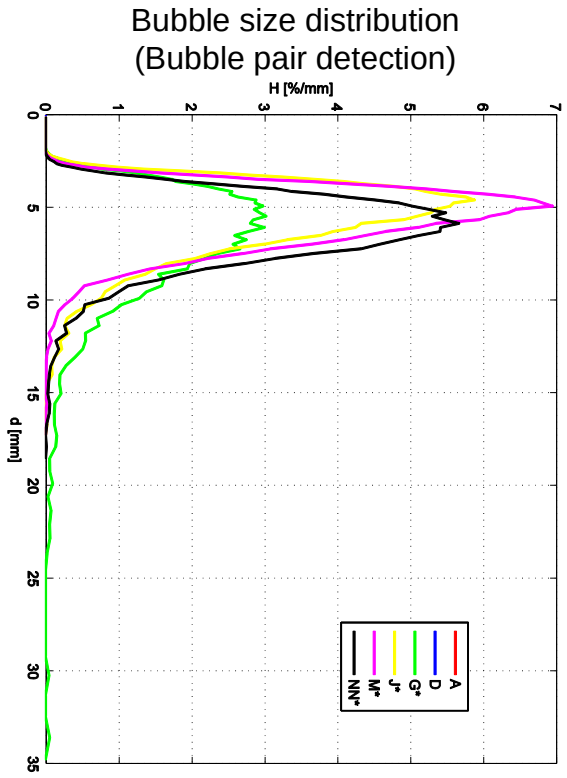
Bubble size distribution
(Bubble pair detection)
H [%/mm]
d [mm]
A
D
G*
J*
M*
NN*

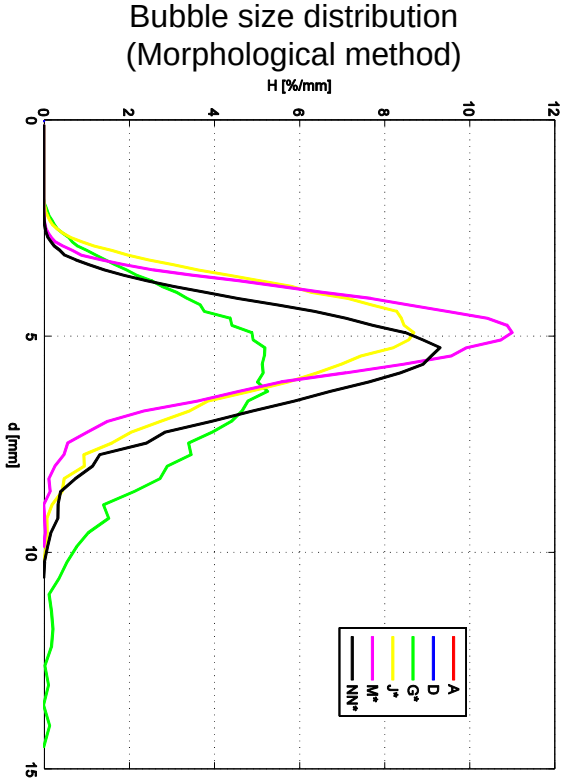
Bubble size distribution
(Morphological method)
H [%/mm]
d [mm]
A
D
G*
J*
M*
NN*

L21 – 118 (jl = -1.017 $^{m}/_{s}$; jg = -0.219 $^{m}/_{s}$), 2x1000Hz

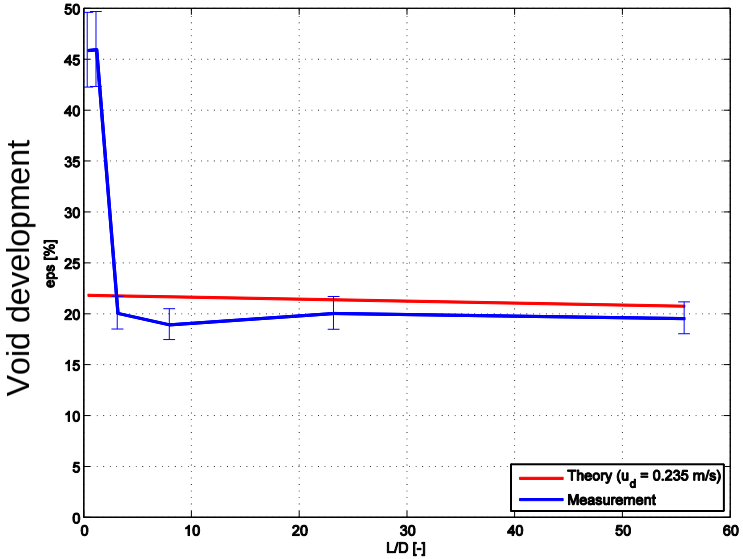

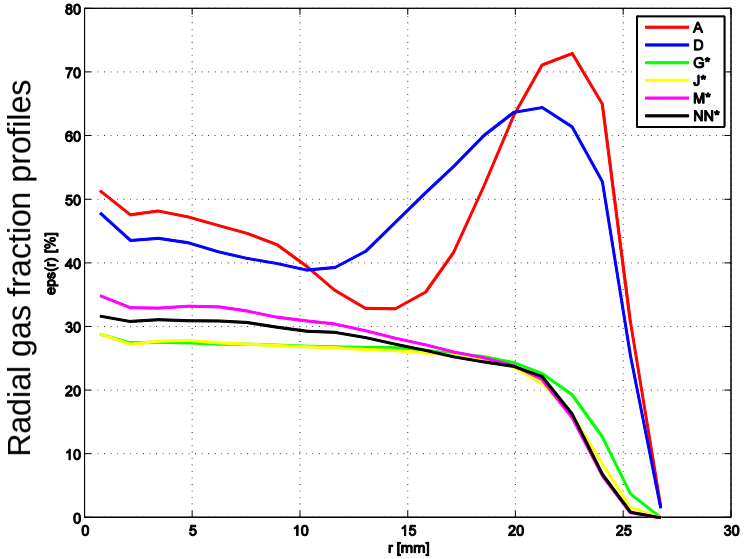

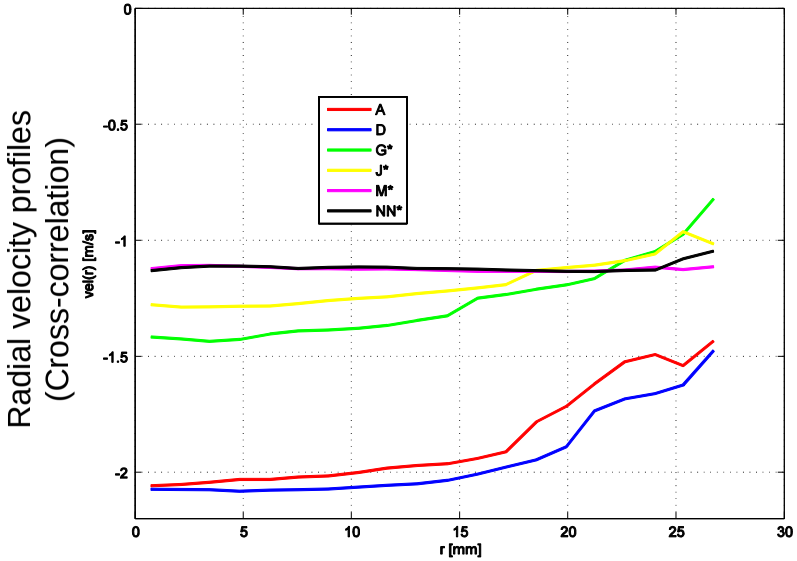

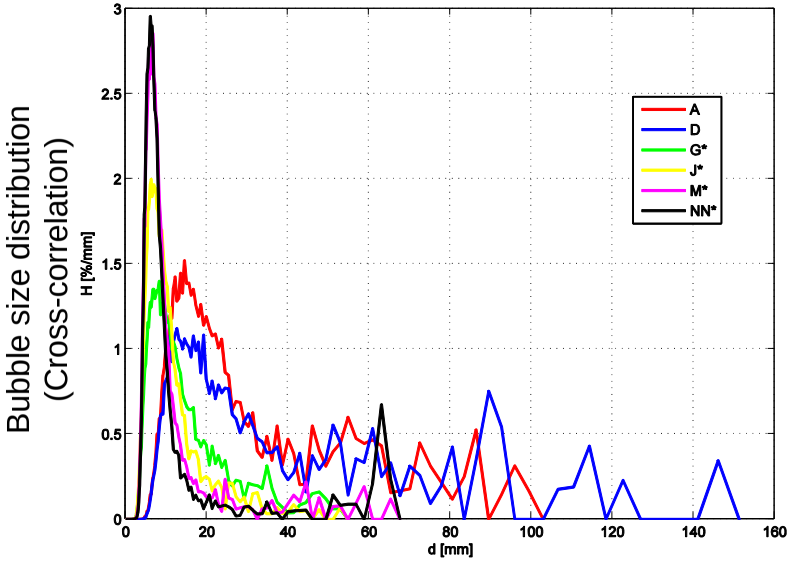

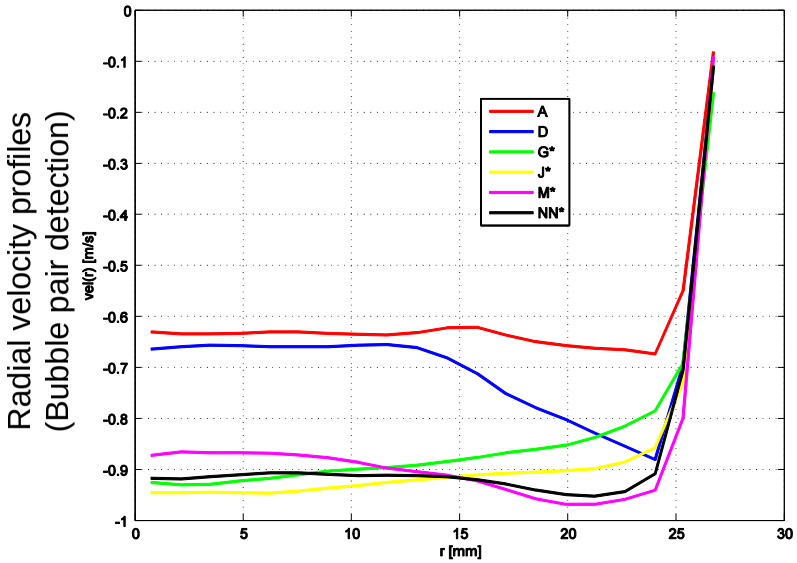
Radial velocity profiles
(Bubble pair detection)
vel(r) [m/s]
r [mm]
A
D
G*
J*
M*
NN*

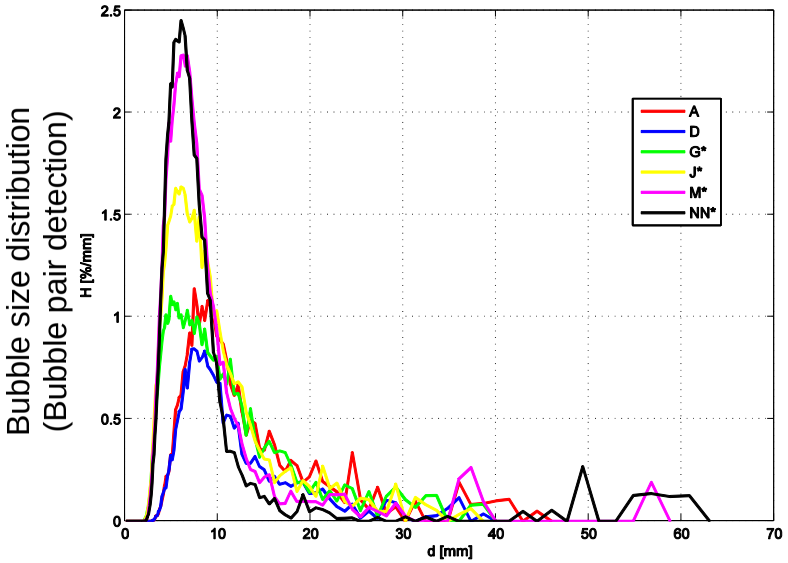
Bubble size distribution
(Bubble pair detection)
H [%/mm]
d [mm]
A
D
G*
J*
M*
NN*

L21 – 119 (jl = -1.611 m/s; jg = -0.219 m/s), 2x2500Hz
Void development
eps [%]
L/D [-]
Theory (u_d = 0.235 m/s)
Measurement
Radial gas fraction profiles
eps(r) [%]
r [mm]
A*
D*
G*
J*
M*
NN*
Radial velocity profiles
(Cross-correlation)
vel(r) [m/s]
r [mm]
Bubble size distribution
(Cross-correlation)
H [%/mm]
d [mm]

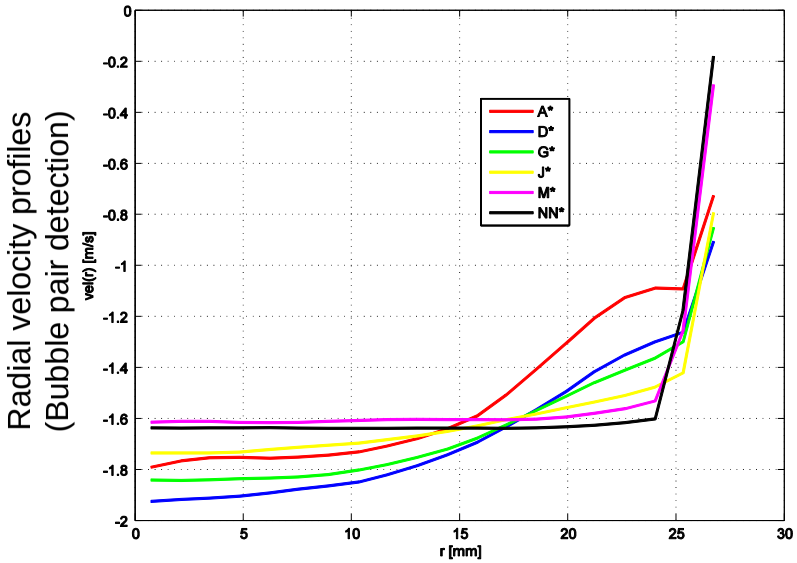
Radial velocity profiles
(Bubble pair detection)
vel(r) [m/s]
r [mm]
A*
D*
G*
J*
M*
NN*

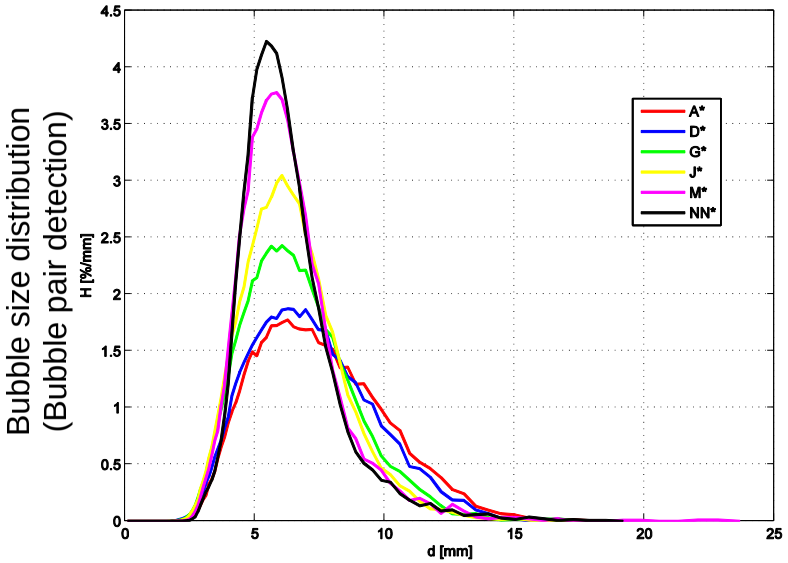
Bubble size distribution
(Bubble pair detection)
H [%/mm]
d [mm]
A*
D*
G*
J*
M*
NN*

L21 – 138 (jl = -0.405 $^{m}/_{s}$; jg = -0.534 $^{m}/_{s}$), 2x1000Hz

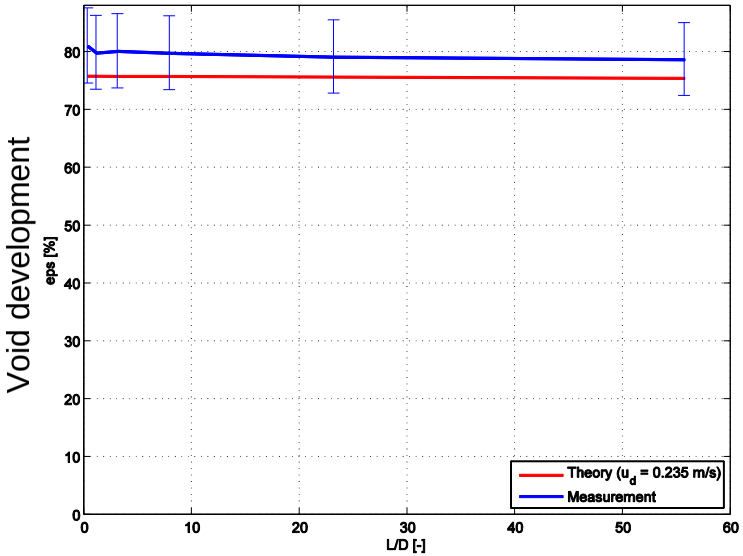

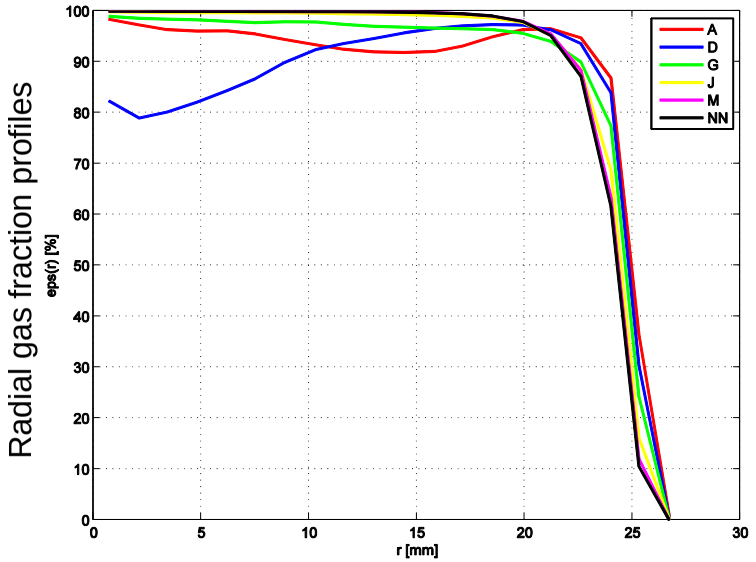

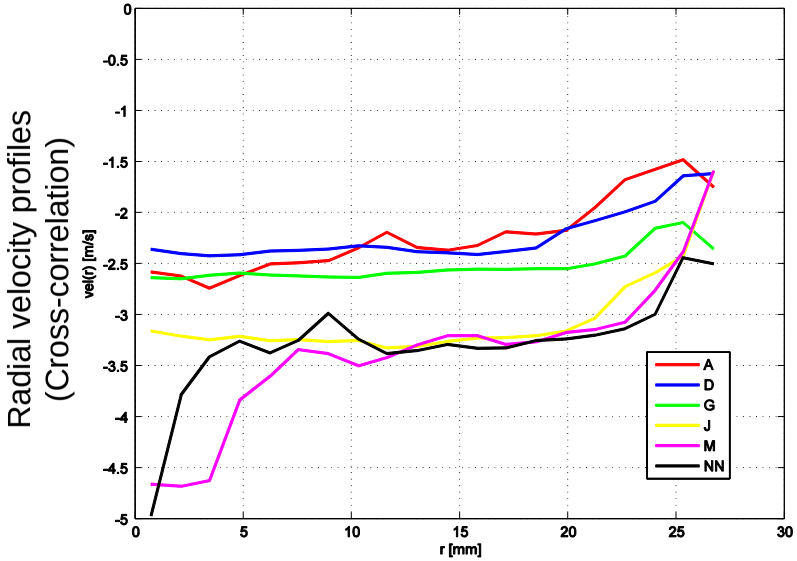

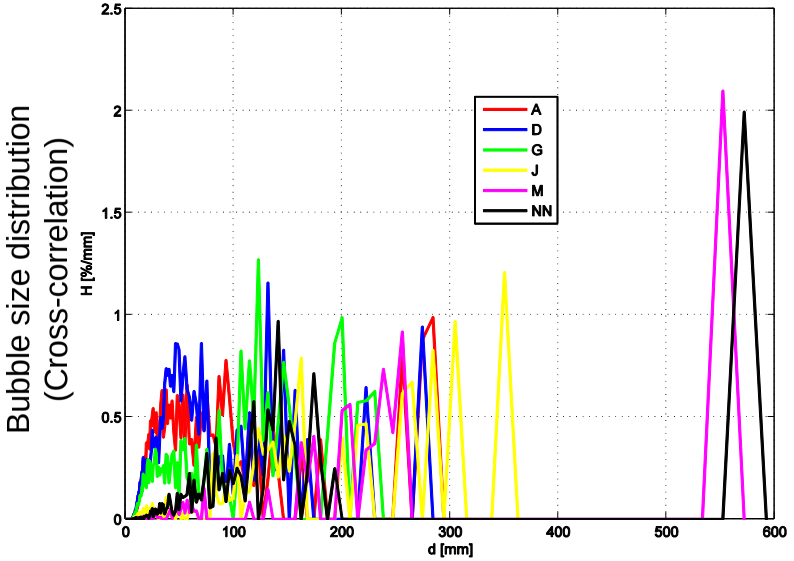

L21 – 139 (jl = -0.641 $^{m}/_{s}$; jg = -0.534 $^{m}/_{s}$), 2x2000Hz

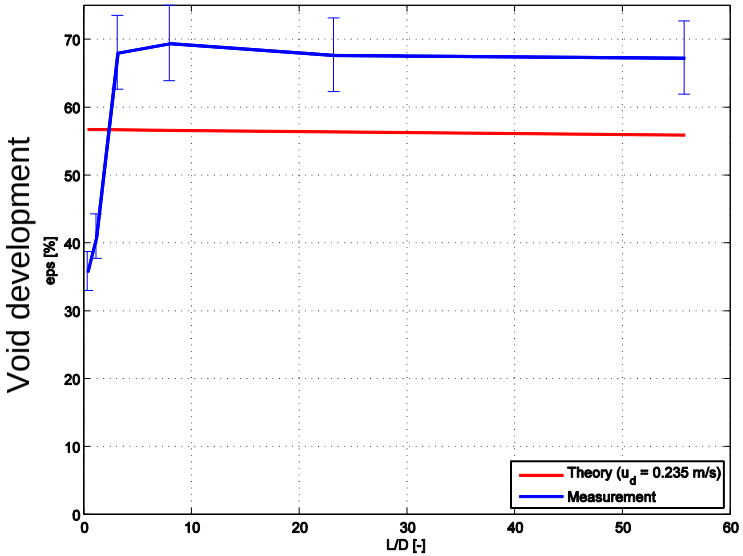

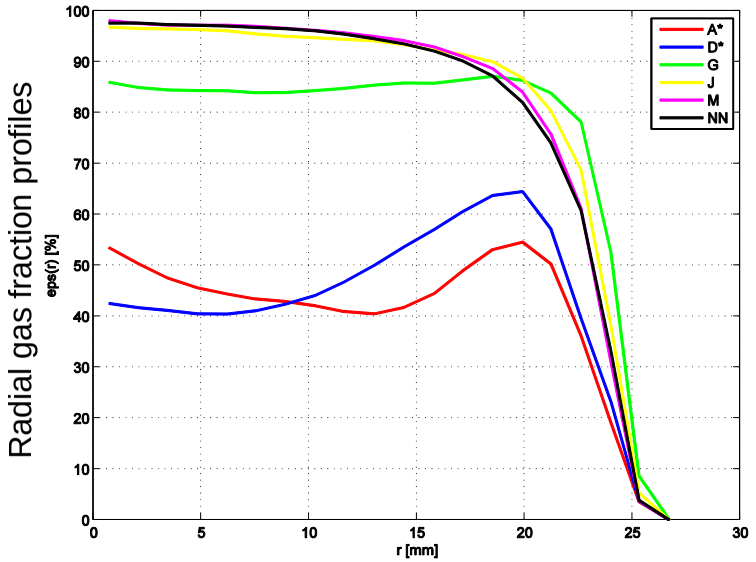

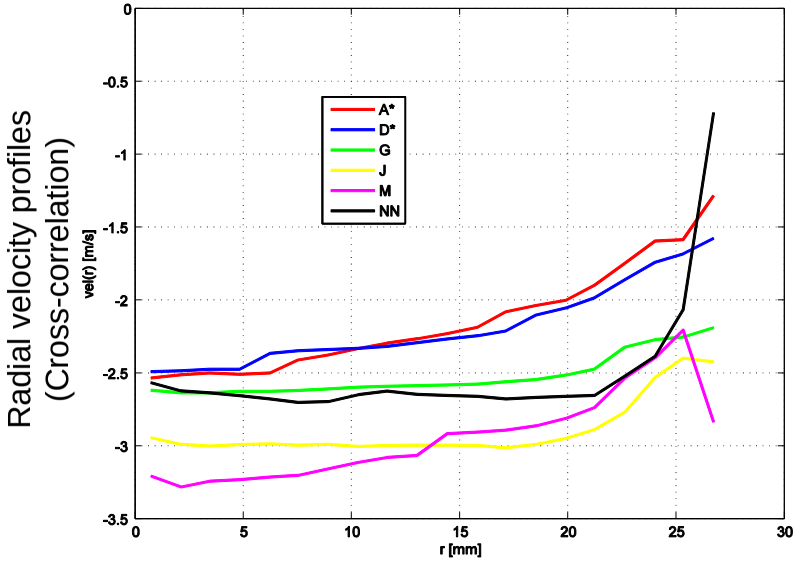

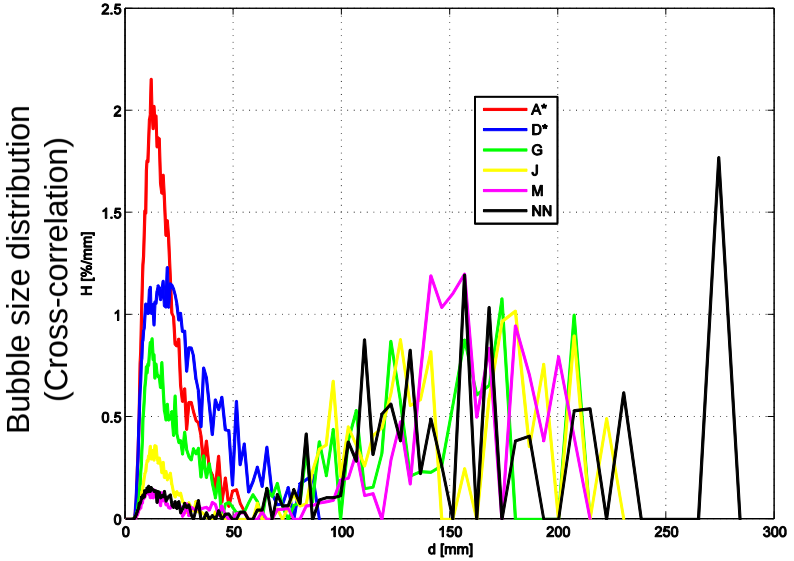

L21 – 150 (jl = -0.641 $^{m}/_{s}$; jg = -0.835 $^{m}/_{s}$), 2x2000Hz

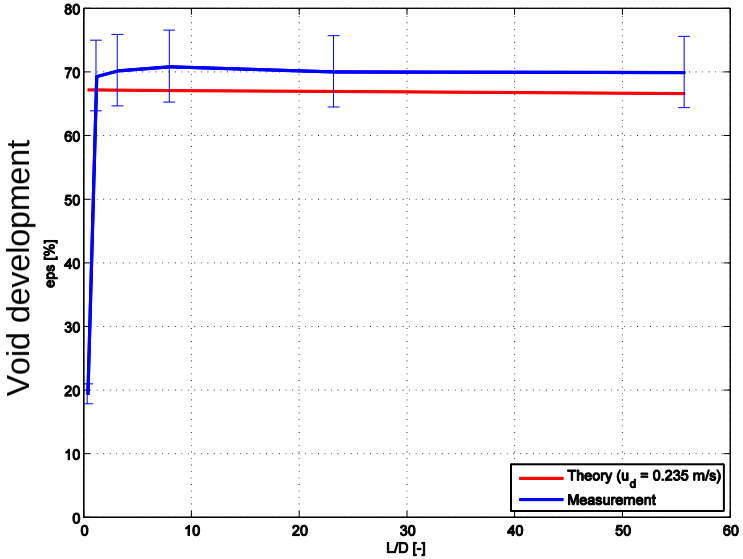

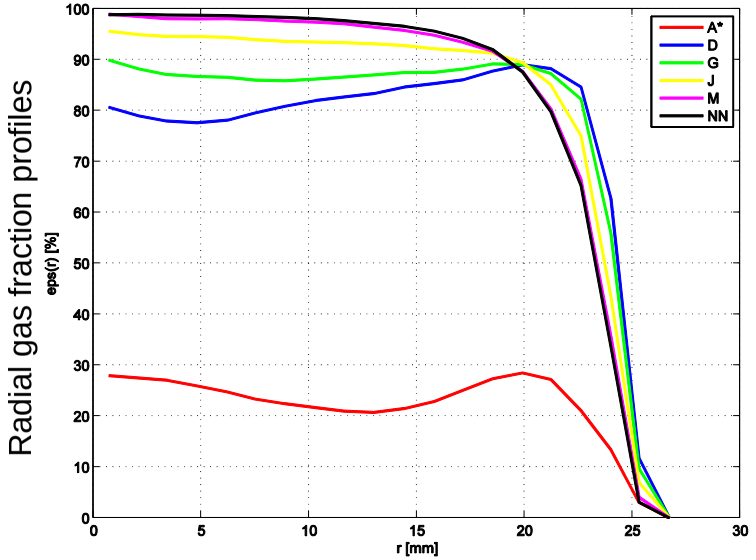

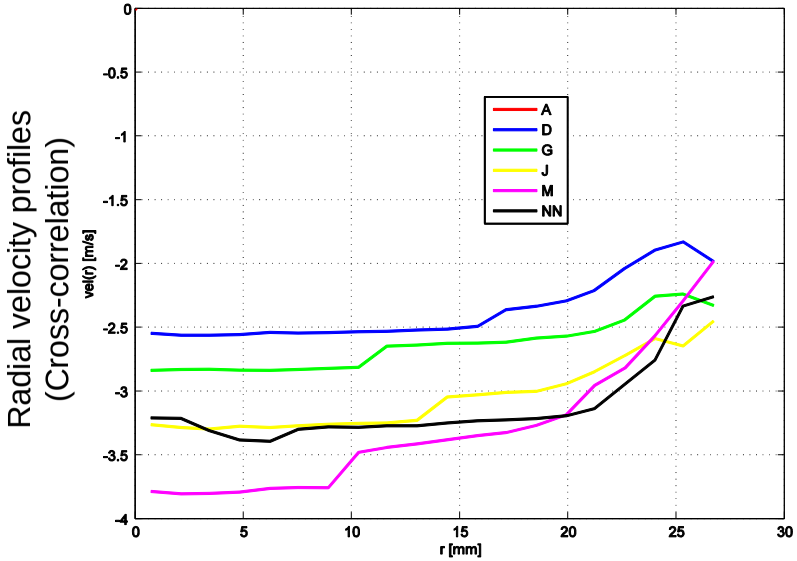

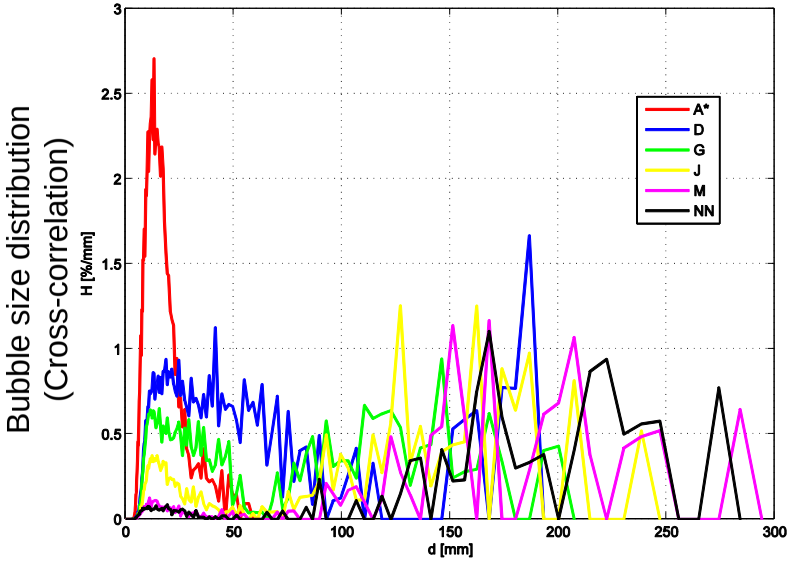

L21 – 151 (jl = -1.017 $^{m}/_{s}$; jg = -0.835 $^{m}/_{s}$), 2x2500Hz

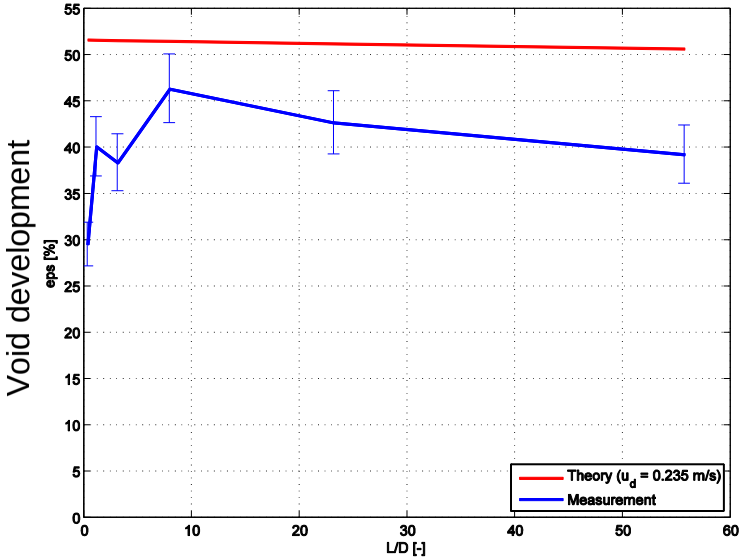

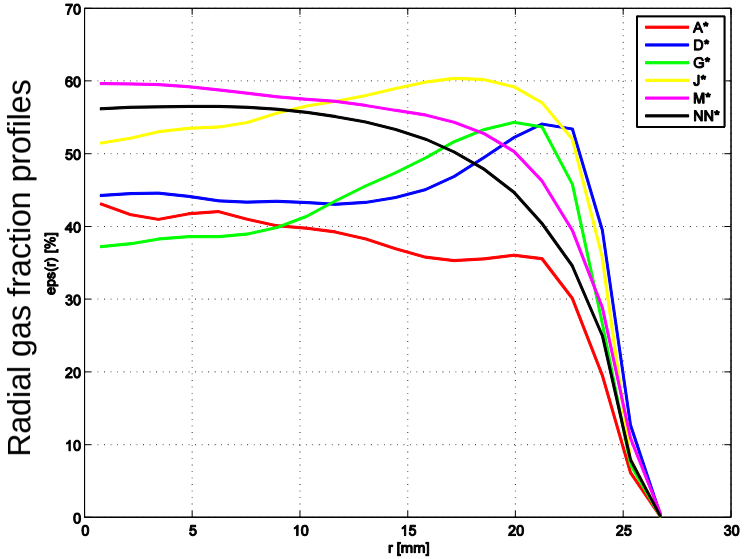

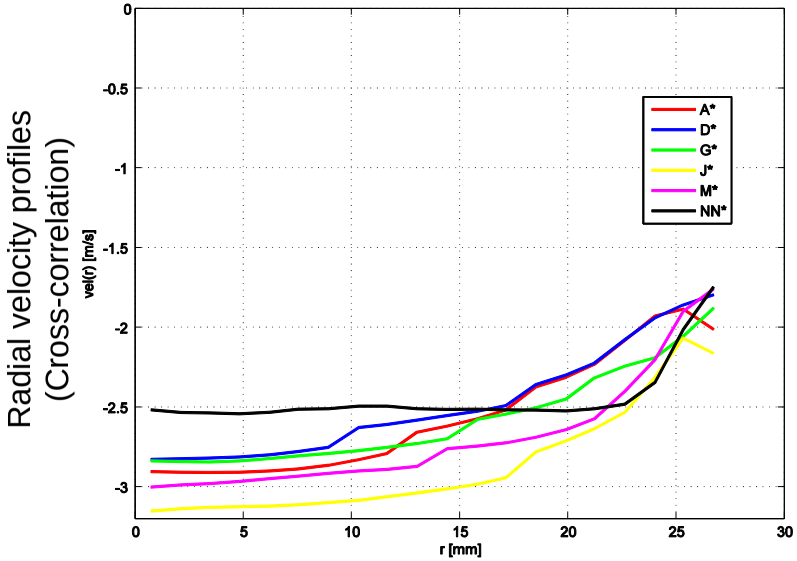

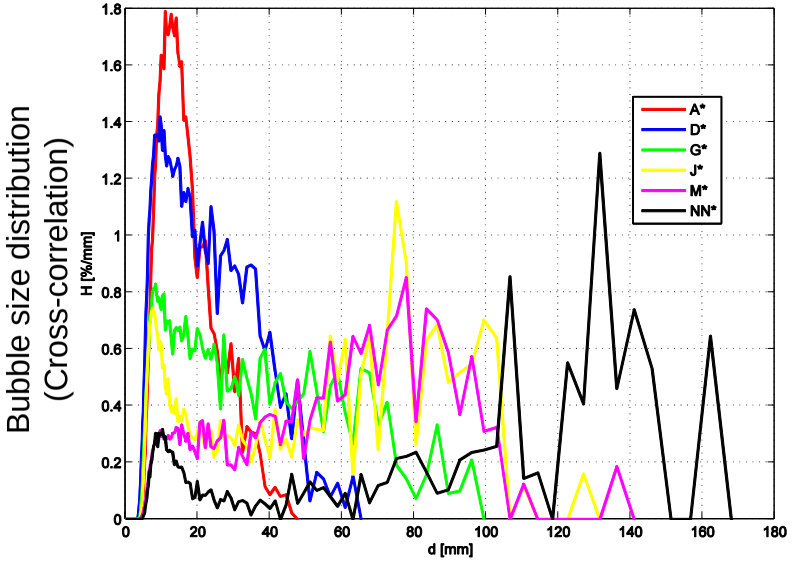

L21 – 152 (jl = -1.611 $^{m}/_{s}$; jg = -0.835 $^{m}/_{s}$), 2x2500Hz

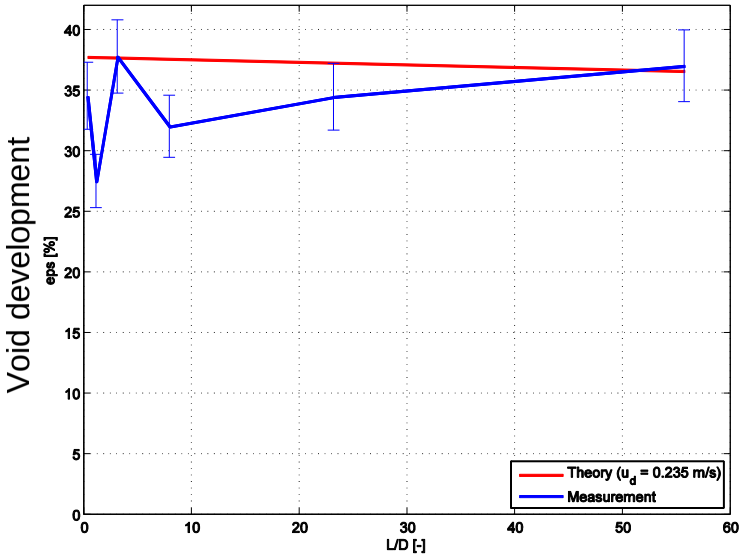

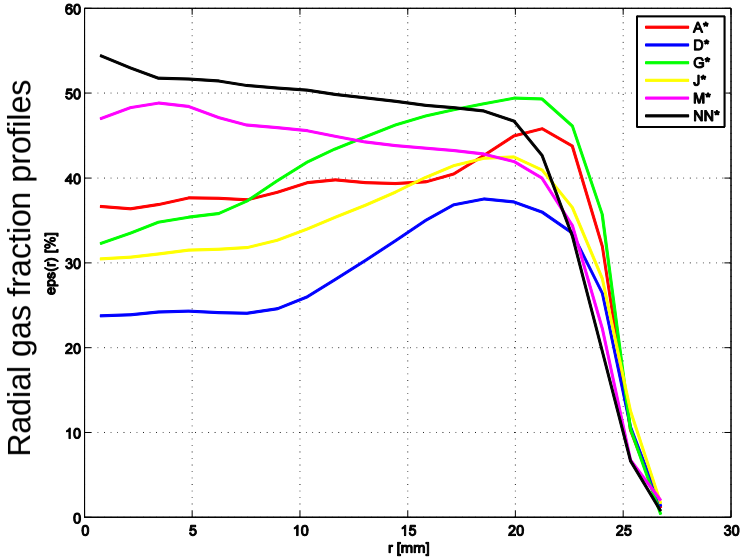

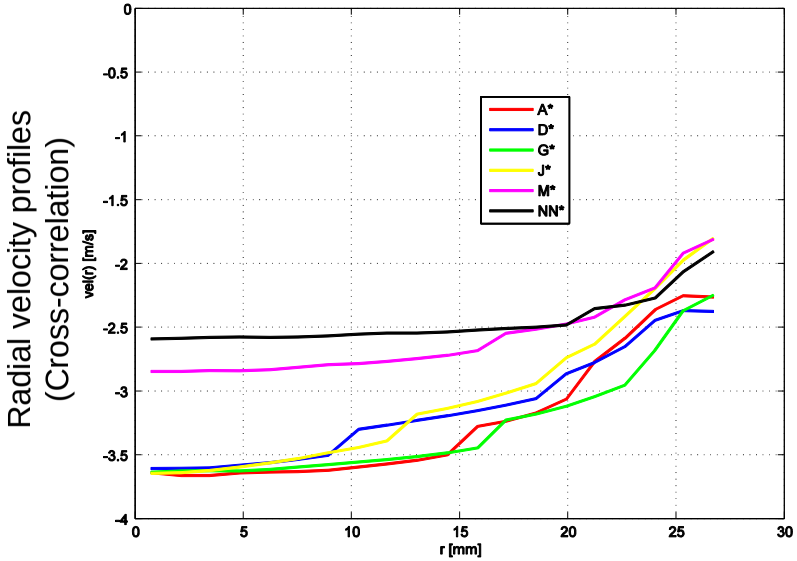

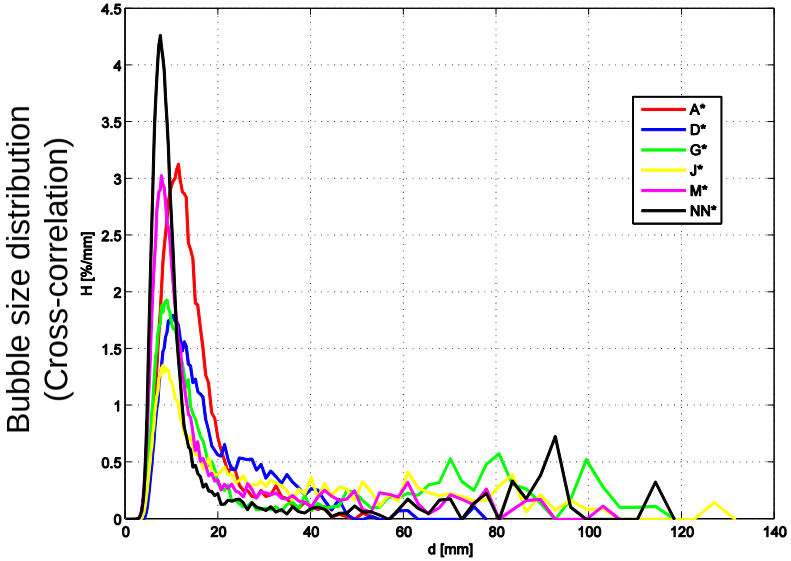

L21 – 162 (jl = -1.017 m/s; jg = -1.305 m/s), 2x2500Hz
Void development
eps [%]
L/D [-]
Theory (u_d = 0.235 m/s)
Measurement
Radial gas fraction profiles
eps(r) [%]
r [mm]
A*
D*
G*
J*
M*
NN*
Bubble size distribution
(Cross-correlation)
H [%/mm]
d [mm]
Radial velocity profiles
(Cross-correlation)
vel(r) [m/s]
r [mm]

L21 – 163 (jl = -1.611 $^{m}/_{s}$; jg = -1.305 $^{m}/_{s}$), 2x2500Hz

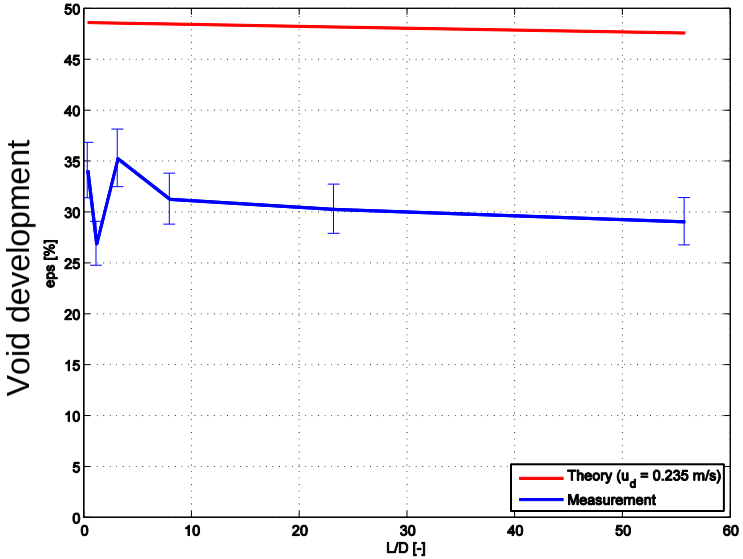

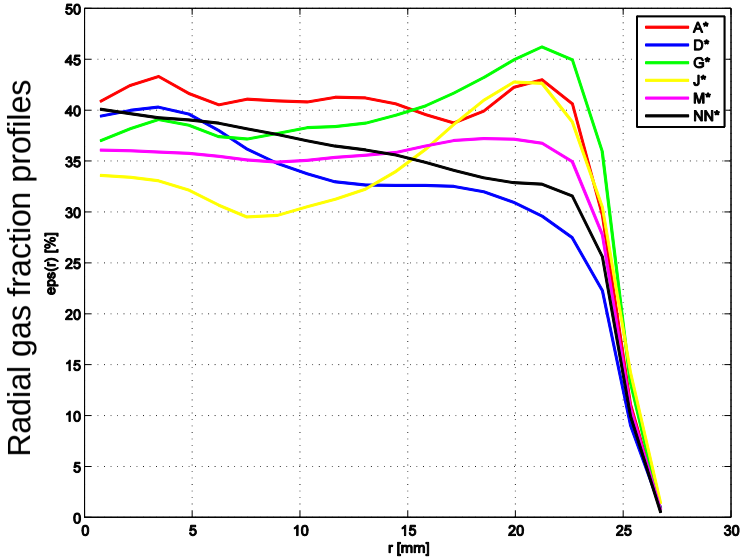

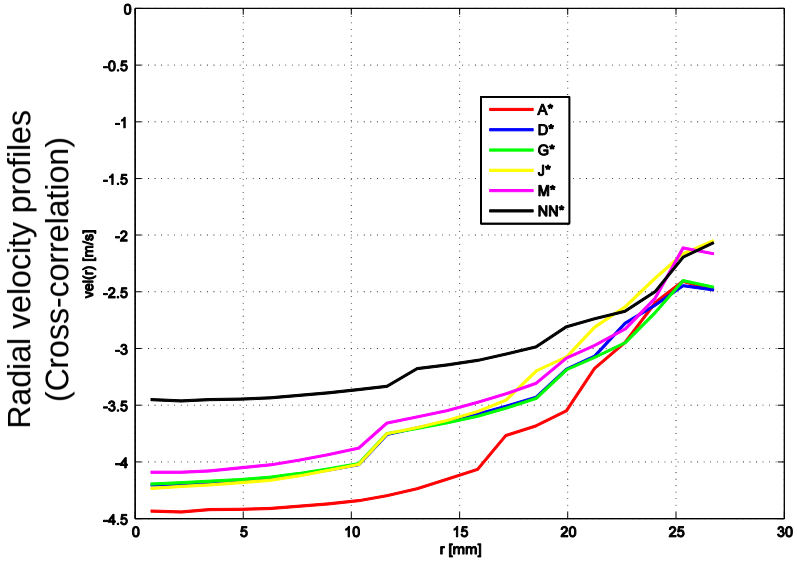

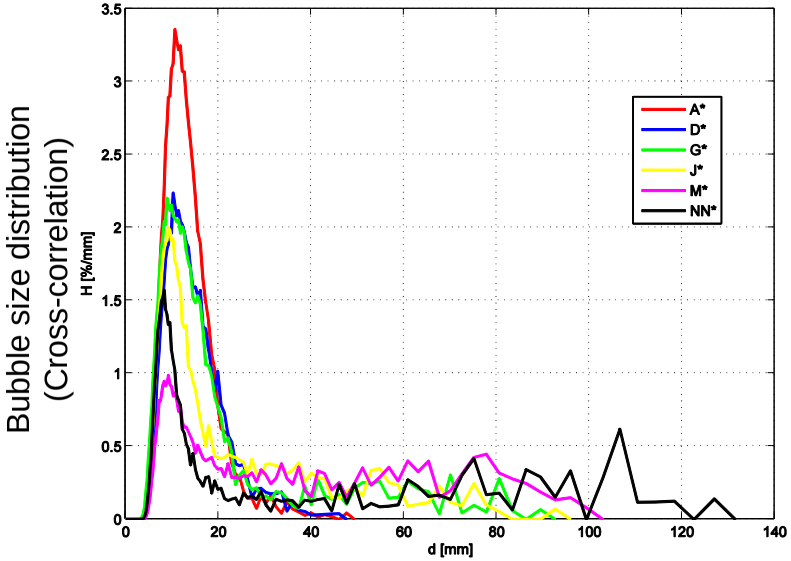

D19 – 151 (jl = 1.017 $^{m}/_{s}$; jg = 0.835 $^{m}/_{s}$), 4.0 MPa, 2x2500Hz

Void development

Radial gas fraction profiles

Radial velocity profiles
(Cross-correlation)

Bubble size distribution
(Cross-correlation)

D19 – 160 (jl = 0.405 $^{m}/_{s}$; jg = 1.305 $^{m}/_{s}$), 4.0 MPa, 2x2500Hz

D19 – 163 (jl = 1.611 $^{m}/_{s}$; jg = 1.305 $^{m}/_{s}$), 4.0 MPa, 1x5000Hz

Void development

Radial gas fraction profiles

Bubble size distribution
(Cross-correlation)

Radial velocity profiles used from
D19 – 163, 2x2500Hz used
(Cross-correlation)

D19 – 163 (jl = 1.611 $^{m}/_{s}$; jg = 1.305 $^{m}/_{s}$), 4.0 MPa, 2x2500Hz

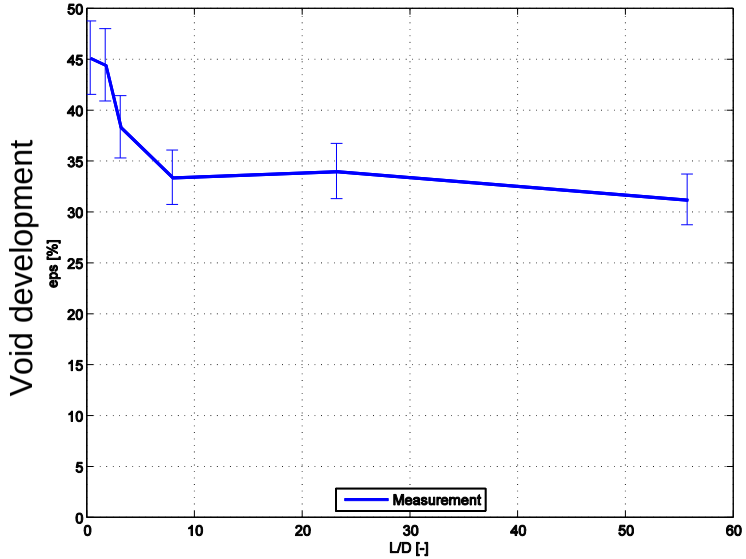

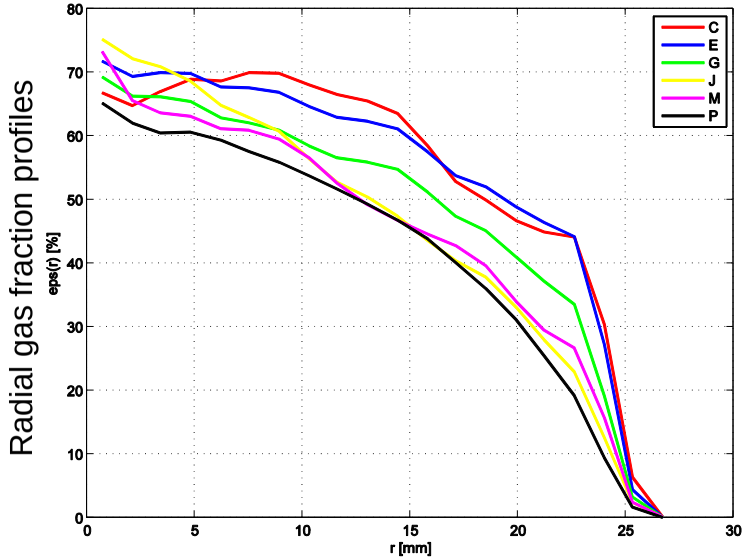

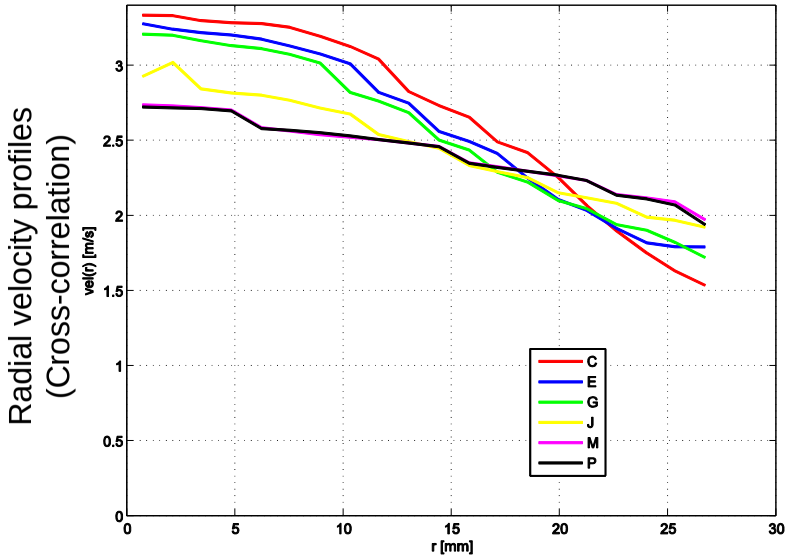

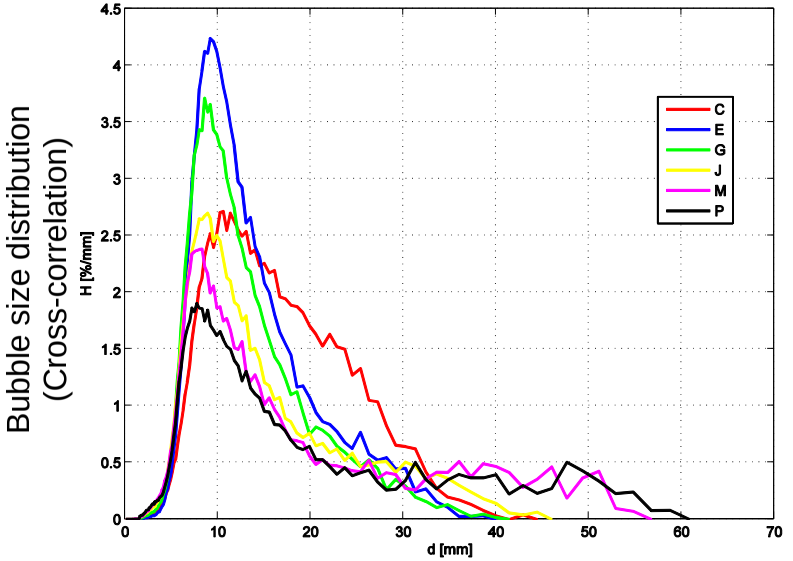

D19 – 173 (jl = 1.017 $^{m}/_{s}$; jg = 2.038 $^{m}/_{s}$), 4.0 MPa, 1x5000Hz

Void development

Radial gas fraction profiles

Bubble size distribution
(Cross-correlation)

Radial velocity profiles used from
D19 – 173, 2x2500Hz used
(Cross-correlation)

D19 – 173 (jl = 1.017 $^{m}/_{s}$; jg = 2.038 $^{m}/_{s}$), 4.0 MPa, 2x2500Hz

Void development

Radial gas fraction profiles

Radial velocity profiles
(Cross-correlation)

Bubble size distribution
(Cross-correlation)

D19 – 151 (jl = 1.017 $^{m}/_{s}$; jg = 0.835 $^{m}/_{s}$), 6.5 MPa, 2x2500Hz

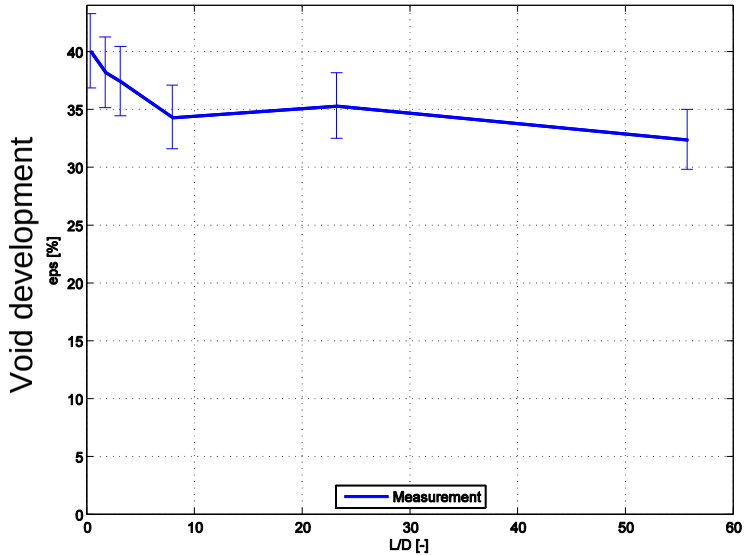

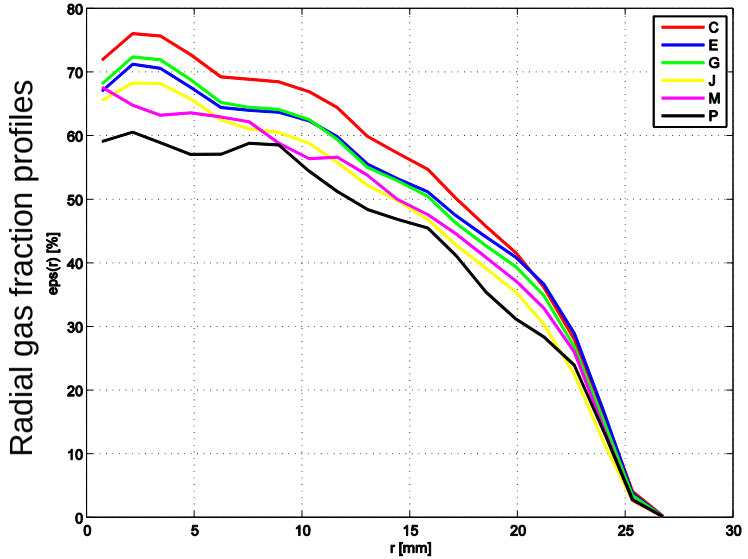

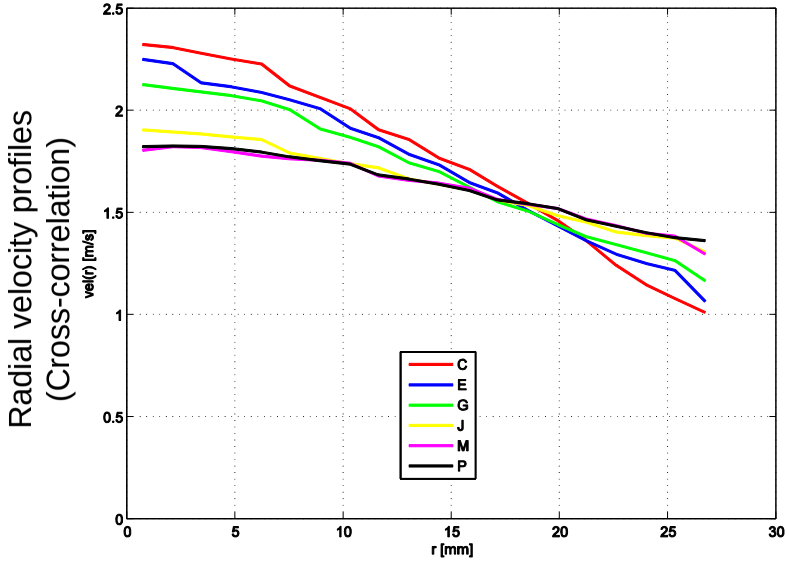

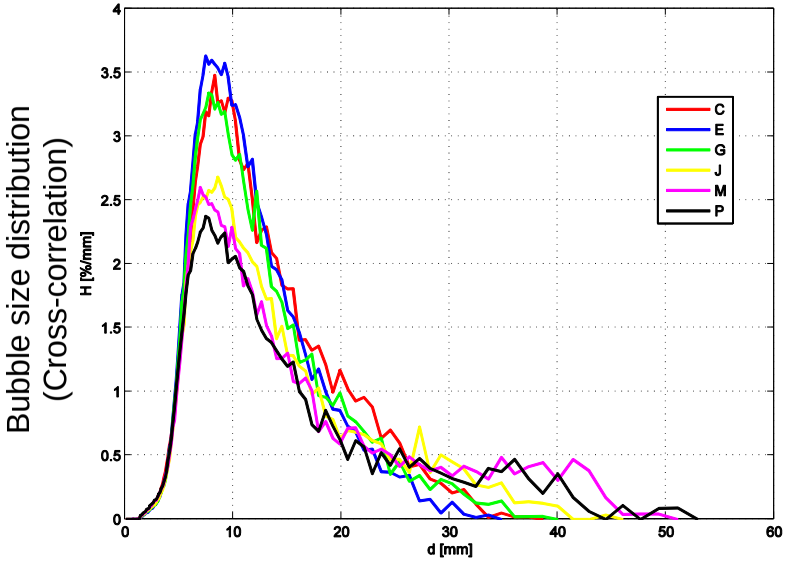

D19 – 160 (jl = 0.405 $^{m}/_{s}$; jg = 1.305 $^{m}/_{s}$), 6.5 MPa, 2x2500Hz

Void development

Radial gas fraction profiles

Radial velocity profiles
(Cross-correlation)

Bubble size distribution
(Cross-correlation)

D19 – 163 (j_l = 1.611 $^m/_s$; j_g = 1.305 $^m/_s$), 6.5 MPa, 1x5000Hz

Void development

Radial gas fraction profiles

Bubble size distribution
(Cross-correlation)

Radial velocity profiles used from
D19 – 163, 2x2500Hz used
(Cross-correlation)

D19 – 163 (j_l = 1.611 $^m/_s$; j_g = 1.305 $^m/_s$), 6.5 MPa, 2x2500Hz

Void development

Radial gas fraction profiles

Radial velocity profiles
(Cross-correlation)

Bubble size distribution
(Cross-correlation)

Radial velocity profiles used from D19 – 173, 2x2500Hz used (Cross-correlation)

Void development

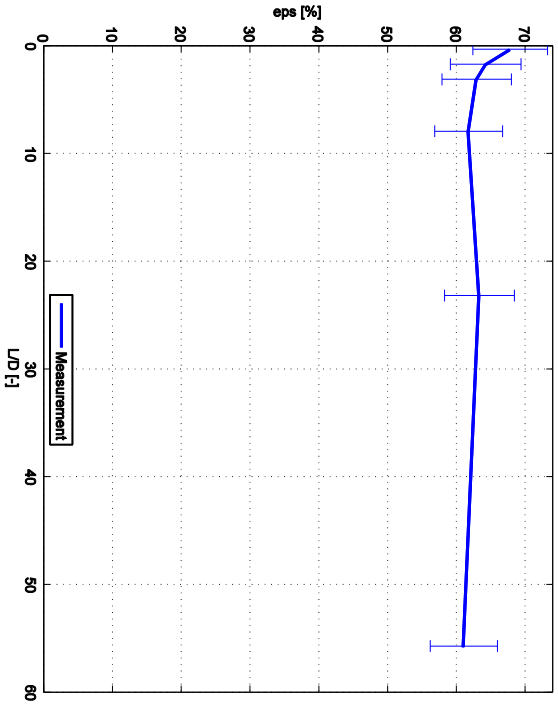

D19 – 173 (jl = 1.017 $^{m}/_{s}$; jg = 2.038 $^{m}/_{s}$), 6.5 MPa, 1x5000Hz

Radial gas fraction profiles

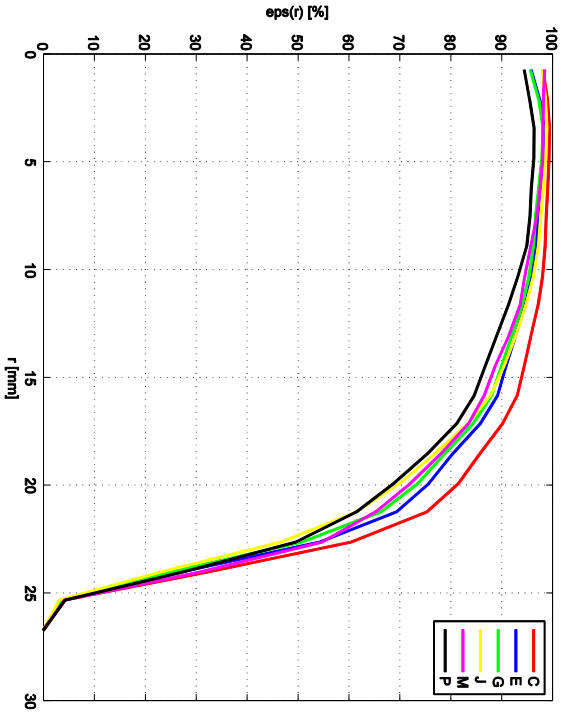

Bubble size distribution (Cross-correlation)

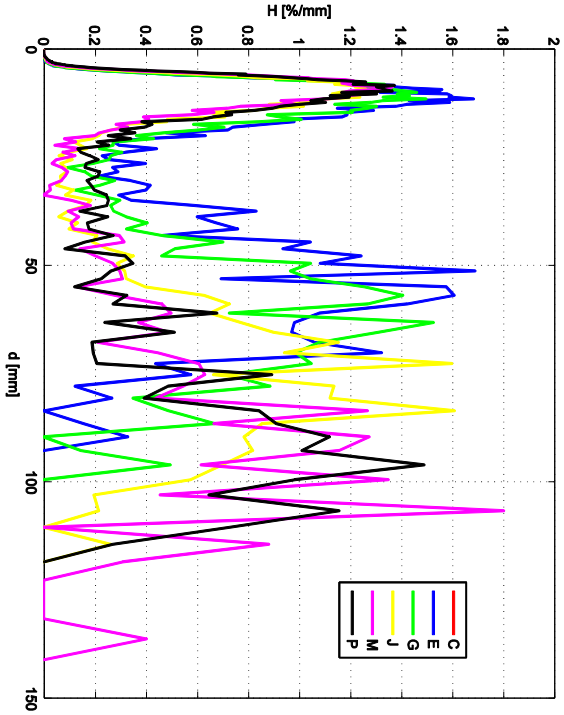

D19 – 173 (jl = 1.017 $^{m}/_{s}$; jg = 2.038 $^{m}/_{s}$), 6.5 MPa, 2x2500Hz

Void development

Radial gas fraction profiles

Radial velocity profiles
(Cross-correlation)

Bubble size distribution
(Cross-correlation)

D20 – 150 (jl = -0.641 $^{m}/_{s}$; jg = -0.835 $^{m}/_{s}$), 4.0 MPa, 2x2000Hz

D20 – 151 (jl = -1.017 $^{m}/_{s}$; jg = -0.835 $^{m}/_{s}$), 4.0 MPa, 2x2500Hz

D20 – 152 (jl = -1.611 $^{m}/_{s}$; jg = -0.835 $^{m}/_{s}$), 4.0 MPa, 2x2500Hz

D20 – 162 (jl = -1.017 $^{m}/_{s}$; jg = -1.305 $^{m}/_{s}$), 4.0 MPa, 2x2500Hz

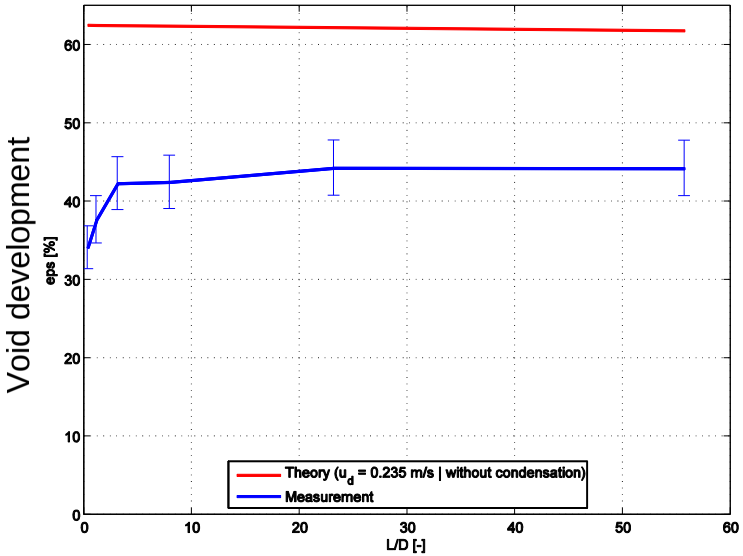

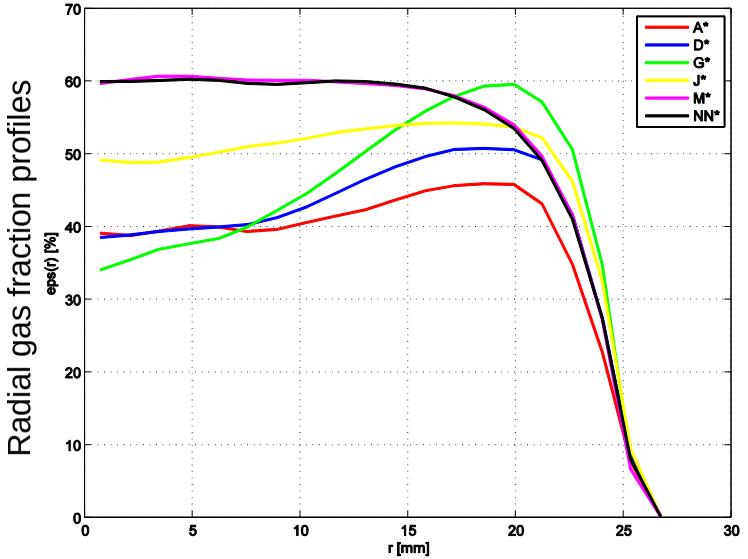

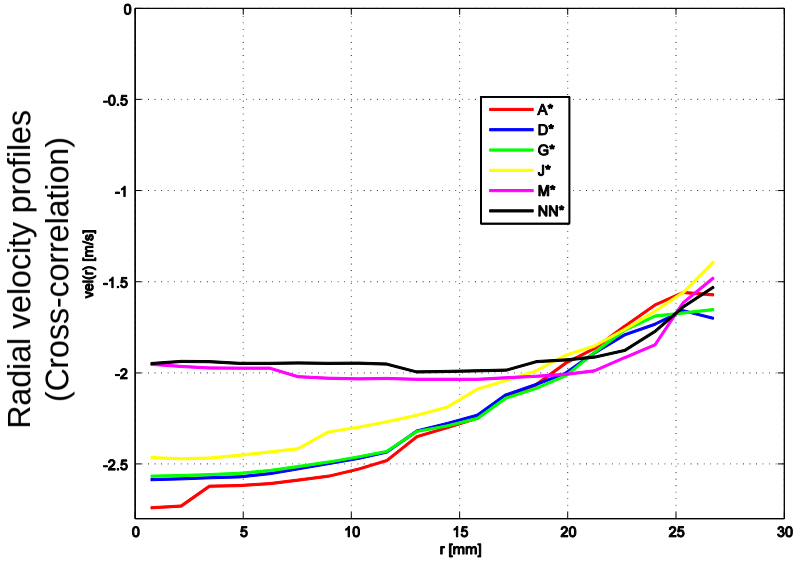

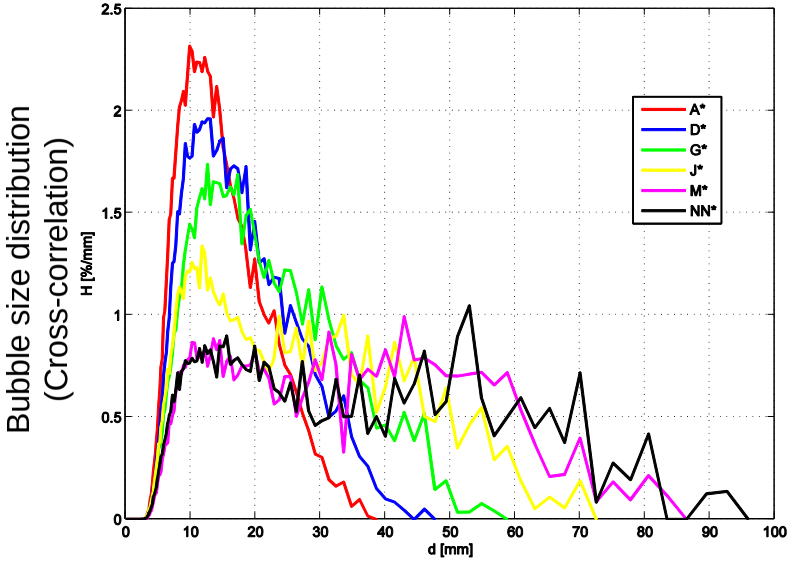

D20 – 163 (jl = -1.611 $^{m}/_{s}$; jg = -1.305 $^{m}/_{s}$), 4.0 MPa, 2x2500Hz

D20 – 150 (jl = -0.641 $^{m}/_{s}$; jg = -0.835 $^{m}/_{s}$), 6.5 MPa, 2x2000Hz

D20 – 151 (jl = -1.017 $^{m}/_{s}$; jg = -0.835 $^{m}/_{s}$), 6.5 MPa, 2x2500Hz

D20 – 152 (jl = -1.611 $^{m}/_{s}$; jg = -0.835 $^{m}/_{s}$), 6.5 MPa, 2x2500Hz

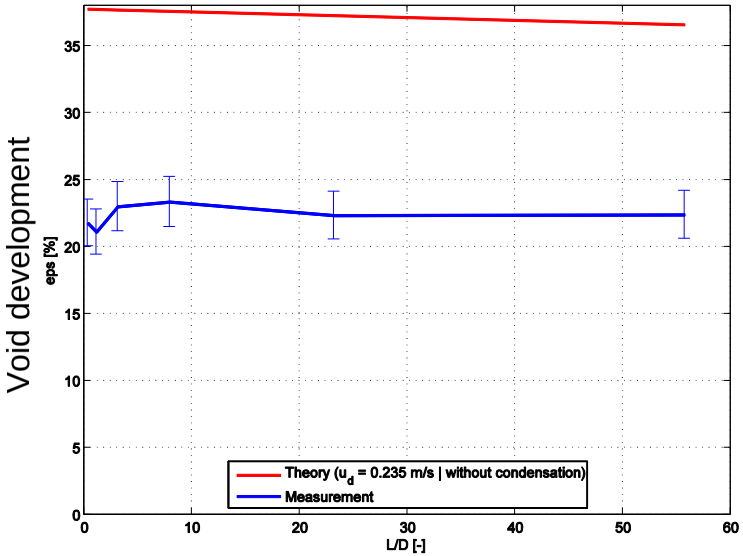

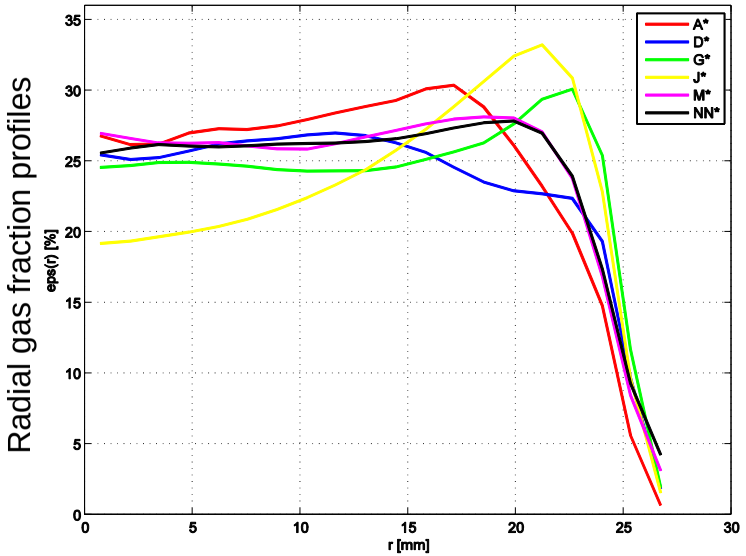

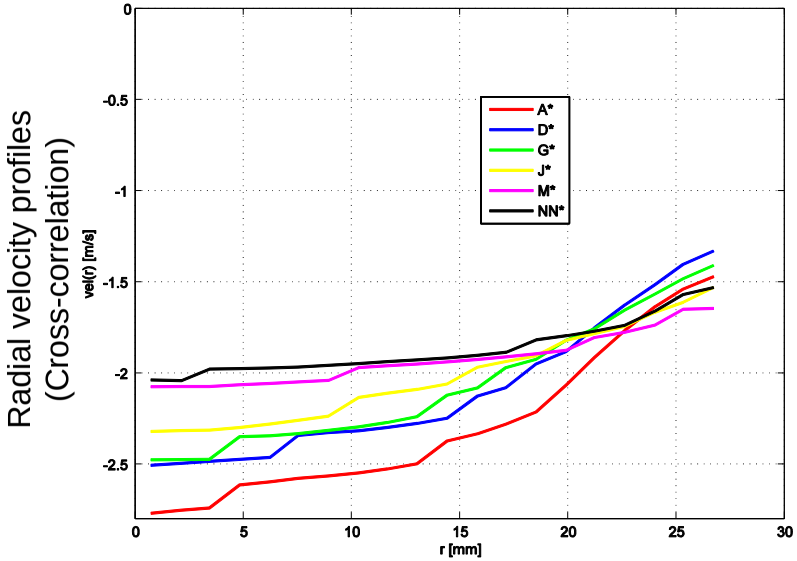

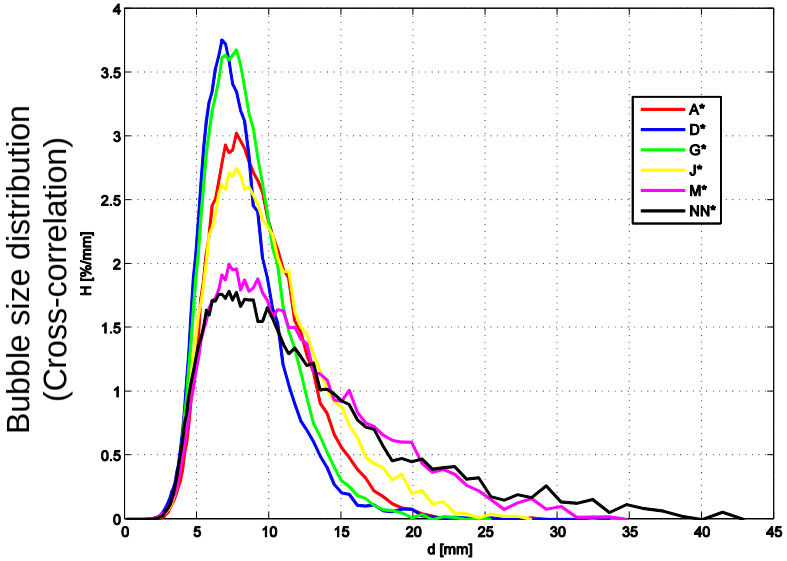

D20 – 162 (jl = -1.017 m/s; jg = -1.305 m/s), 6.5 MPa, 2x2500Hz
Void development
eps [%]
L/D [-]
Theory (u_d = 0.235 m/s | without condensation)
Measurement
Radial gas fraction profiles
eps(r) [%]
r [mm]
A*
D*
G*
J*
M*
NN*
Radial velocity profiles
(Cross-correlation)
vel(r) [m/s]
r [mm]
Bubble size distribution
(Cross-correlation)
H [%/mm]
d [mm]

D20 – 163 (jl = -1.611 $^{m}/_{s}$; jg = -1.305 $^{m}/_{s}$), 6.5 MPa, 2x2500Hz

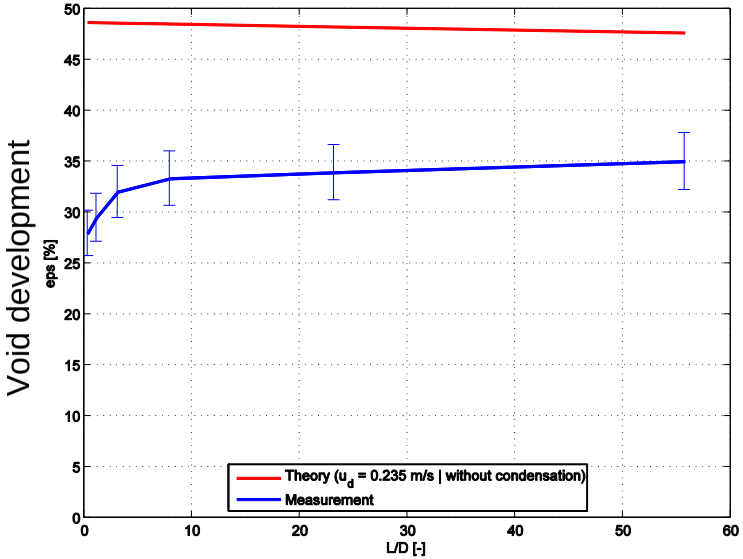

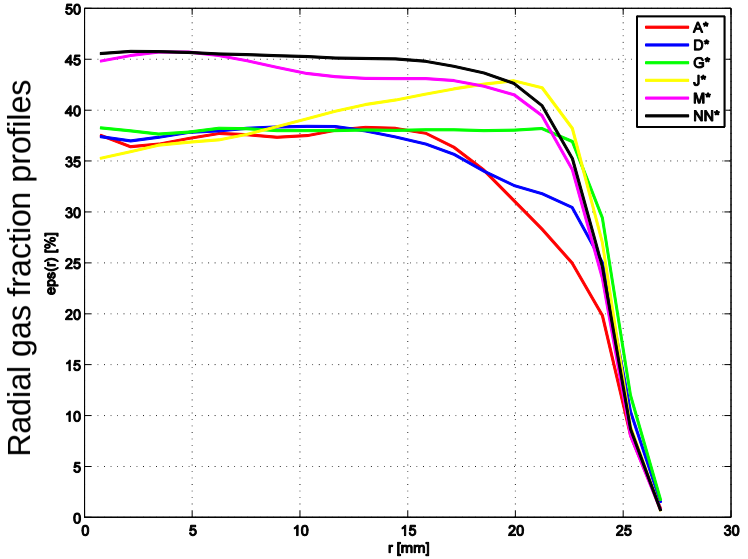

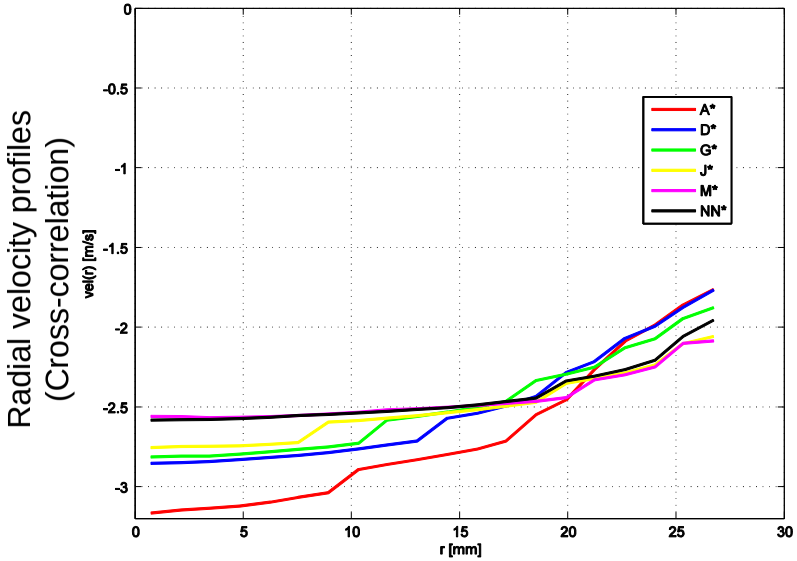

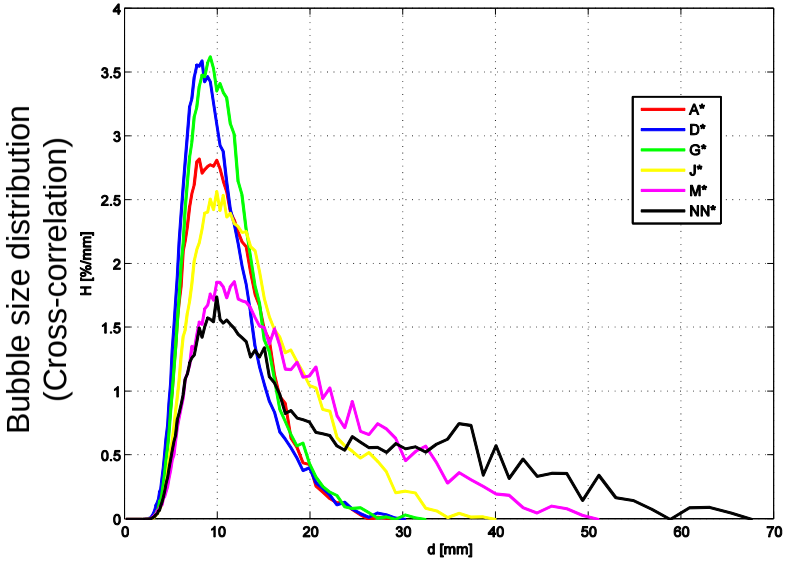

9.2. Calculated superficial gas velocities from air-water measurements

In the following table, the calculated superficial gas velocities taken from the air-water measurements are presented. The superfcial gas velocities are calculated as shown in equation (6.1) and are pressure corrected with the boyle's law.

L16:

Matrix point	Meas. Level	j_g [m/s] injected	j_g [m/s] cross-correlation		j_g [m/s] bubble pairs	j_g [m/s] morphology	
			O	U		O	U
001 2x1000Hz	A	0.0025	0.0070	0.0016	0.0001	0.0015	0.0005
	D		0.0021	0.0022	0.0016	0.0025	0.0025
	G		0.0022	0.0022	0.0017	0.0025	0.0025
	J		0.0022	0.0022	0.0017	0.0026	0.0026
	M		0.0021	0.0021	0.0018	0.0024	0.0024
	P		0.0020	0.0020	0.0017	0.0023	0.0023
004 2x1000Hz	A	0.0025	0.0053	0.0018	0.0002	0.0014	0.0007
	D		0.0022	0.0022	0.0019	0.0023	0.0024
	G		0.0023	0.0023	0.0020	0.0024	0.0024
	J		0.0023	0.0023	0.0021	0.0024	0.0024
	M		0.0022	0.0022	0.0020	0.0024	0.0024
	P		0.0020	0.0021	0.0020	0.0023	0.0022
006 2x1000Hz	A	0.0025	0.0013	0.0002	0.0001	0.0015	0.0004
	D		0.0025	0.0026	0.0025	0.0024	0.0025
	G		0.0026	0.0025	0.0025	0.0022	0.0022
	J		0.0026	0.0026	0.0025	0.0021	0.0021
	M		0.0028	0.0028	0.0027	0.0023	0.0023
	P		0.0027	0.0027	0.0026	0.0023	0.0023
006 2x2500Hz	A	0.0025	0.0017	0.0001	0.0001		
	D		0.0019	0.0020	0.0019		
	G		0.0019	0.0019	0.0019		
	J		0.0021	0.0021	0.0020		
	M		0.0021	0.0020	0.0020		
	P		0.0020	0.0020	0.0020		
008 2x2500Hz	A	0.0025	0.0018	0.0004	0.0020		
	D		0.0018	0.0019	0.0019		
	G		0.0021	0.0021	0.0021		
	J		0.0020	0.0022	0.0020		
	M		0.0025	0.0024	0.0023		
	P		0.0021	0.0020	0.0020		
028 2x1000Hz	A	0.0062	0.0021	0.0004	0.0000	0.0016	0.0008
	D		0.0060	0.0060	0.0057	0.0050	0.0048
	G		0.0067	0.0067	0.0064	0.0054	0.0055
	J		0.0067	0.0067	0.0065	0.0053	0.0053
	M		0.0067	0.0067	0.0064	0.0055	0.0054
	P		0.0062	0.0063	0.0060	0.0051	0.0052

028 2x2500Hz	A	0.0062	0.0236	0.0055	0.0002		
	D		0.0051	0.0053	0.0049		
	G		0.0052	0.0052	0.0051		
	J		0.0052	0.0053	0.0050		
	M		0.0053	0.0053	0.0052		
	P		0.0053	0.0054	0.0051		
030 2x2500Hz	A	0.0062	0.0166	0.0041	0.0002		
	D		0.0051	0.0051	0.0051		
	G		0.0056	0.0055	0.0054		
	J		0.0055	0.0056	0.0055		
	M		0.0056	0.0057	0.0055		
	P		0.0052	0.0052	0.0050		
034 2x1000Hz	A	0.0096	0.0544	0.0178	0.0004	0.0047	0.0017
	D		0.0092	0.0089	0.0057	0.0093	0.0091
	G		0.0094	0.0093	0.0066	0.0104	0.0103
	J		0.0090	0.0090	0.0062	0.0099	0.0100
	M		0.0096	0.0098	0.0065	0.0102	0.0104
	P		0.0089	0.0092	0.0064	0.0098	0.0101
037 2x1000Hz	A	0.0096	0.0371	0.0118	0.0004	0.0051	0.0014
	D		0.0094	0.0094	0.0077	0.0096	0.0092
	G		0.0099	0.0098	0.0083	0.0101	0.0101
	J		0.0096	0.0093	0.0081	0.0101	0.0100
	M		0.0096	0.0095	0.0084	0.0101	0.0101
	P		0.0090	0.0091	0.0078	0.0095	0.0096
039 2x1000Hz	A	0.0096	0.0059	0.0010	0.0003	0.0050	0.0007
	D		0.0113	0.0114	0.0106	0.0093	0.0093
	G		0.0115	0.0116	0.0109	0.0096	0.0096
	J		0.0117	0.0118	0.0112	0.0096	0.0097
	M		0.0115	0.0117	0.0112	0.0100	0.0100
	P		0.0113	0.0113	0.0109	0.0098	0.9397
039 2x2500Hz	A	0.0096	0.0065	0.0010	0.0005		
	D		0.0085	0.0084	0.0081		
	G		0.0031	0.0037	0.0050		
	J		0.0087	0.0087	0.0083		
	M		0.0087	0.0088	0.0084		
	P		0.0085	0.0086	0.0082		
041 2x2500Hz	A	0.0096	0.0000	0.0000	0.0000		
	D		0.0108	0.0106	0.0101		
	G		0.0119	0.0120	0.0115		
	J		0.0117	0.0120	0.0114		
	M		0.0105	0.0109	0.0105		
	P		0.0105	0.0106	0.0102		
042 2x2500Hz	A	0.0096	0.0000	0.0000	0.0000		
	D		0.0148	0.0145	0.0136		
	G		0.0171	0.0165	0.0157		
	J		0.0186	0.0182	0.0172		
	M		0.0171	0.0174	0.0162		
	P		0.0136	0.0140	0.0126		

050 2x1000Hz	A	0.0151	0.0277	0.0102	0.0001	0.0055	0.0012
	D		0.0167	0.0167	0.0153	0.0128	0.0123
	G		0.0173	0.0174	0.0165	0.0144	0.0143
	J		0.0172	0.0170	0.0165	0.0142	0.0142
	M		0.0166	0.0171	0.0162	0.0140	0.0143
	P		0.0165	0.0164	0.0158	0.0138	0.0138
050 2x2500Hz	A	0.0151	0.0181	0.0073	0.0006		
	D		0.0134	0.0133	0.0122		
	G		0.0132	0.0133	0.0128		
	J		0.0137	0.0140	0.0134		
	M		0.0133	0.0133	0.0128		
	P		0.0131	0.0133	0.0126		
052 2x2500Hz	A	0.0151	0.0088	0.0039	0.0009		
	D		0.0143	0.0141	0.0134		
	G		0.0149	0.0154	0.0144		
	J		0.0155	0.0159	0.0150		
	M		0.0149	0.0155	0.0150		
	P		0.0138	0.0144	0.0139		
067 2x1000Hz	A	0.0368	0.0182	0.0043	0.0011	0.0079	0.0032
	D		0.0396	0.0382	0.0136	0.0208	0.0196
	G		0.0362	0.0363	0.0170	0.0240	0.0239
	J		0.0337	0.0324	0.0173	0.0253	0.0240
	M		0.0320	0.0318	0.0185	0.0269	0.0262
	P		0.0312	0.0305	0.0185	0.0280	0.0270
074 2x2500Hz	A	0.0368	0.0072	0.0022	0.0004		
	D		0.0316	0.0312	0.0296		
	G		0.0342	0.0344	0.0330		
	J		0.0349	0.0349	0.0339		
	M		0.0348	0.0353	0.0340		
	P		0.0339	0.0345	0.0334		
077 2x2500Hz	A	0.0368	0.0022	0.0000	0.0000		
	D		0.0684	0.0615	0.0322		
	G		0.0832	0.0810	0.0382		
	J		0.0971	0.0907	0.0389		
	M		0.0952	0.1018	0.0393		
	P		0.0928	0.1226	0.0295		
089 2x1000Hz	A	0.0898	0.0278	0.0057	0.0011	0.0104	0.0034
	D		0.1273	0.1142	0.0311	0.0418	0.0379
	G		0.1033	0.1005	0.0415	0.0435	0.0423
	J		0.1052	0.0999	0.0413	0.0451	0.0406
	M		0.1005	0.1005	0.0455	0.0529	0.0524
	P		0.0735	0.0741	0.0466	0.0507	0.0483
096 2x2500Hz	A	0.0898	0.0000	0.0000	0.0000		
	D		0.0634	0.0601	0.0537		
	G		0.0751	0.0747	0.0691		
	J		0.0858	0.0844	0.0744		
	M		0.0856	0.0876	0.0782		
	P		0.0847	0.0857	0.0786		

099 2x2500Hz	A	0.0898	0.0063	0.0003	0.0000		
	D		0.0926	0.0923	0.0603		
	G		0.1271	0.1315	0.0834		
	J		0.1415	0.1345	0.0870		
	M		0.1376	0.1402	0.0835		
	P		0.1265	0.1452	0.0627		

L17

Matrix point	Meas. Level	j_g [m/s] injected	j_g [m/s] cross-correlation		j_g [m/s] bubble pairs	j_g [m/s] morphology	
			O	U		O	U
001 2x1000Hz	A	0.0025	0.0113	0.0012		0.0014	0.0001
	D		0.0022	0.0022		0.0024	0.0025
	G		0.0023	0.0023		0.0026	0.0027
	J		0.0022	0.0022		0.0026	0.0026
	M		0.0020	0.0021		0.0025	0.0026
	P		0.0022	0.0023		0.0028	0.0028
002 2x1000Hz	A	0.0025	0.0016	0.0006		0.0022	0.0008
	D		0.0006	0.0005		0.0026	0.0025
	G		0.0022	0.0021		0.0025	0.0025
	J		0.0021	0.0021		0.0025	0.0025
	M		0.0008	0.0008		0.0024	0.0025
	P		0.0018	0.0018		0.0021	0.0022
003 2x1000Hz	A	0.0025	0.0104	0.0067		0.0018	0.0007
	D		0.0021	0.0020		0.0023	0.0024
	G		0.0020	0.0020		0.0024	0.0024
	J		0.0021	0.0020		0.0025	0.0025
	M		0.0020	0.0022		0.0024	0.0028
	P		0.0021	0.0021		0.0026	0.0025
034 2x1000Hz	A	0.0096	0.0148	0.0088		0.0055	0.0029
	D		0.0085	0.0086		0.0100	0.0099
	G		0.0094	0.0095		0.0102	0.0106
	J		0.0088	0.0088		0.0102	0.0102
	M		0.0094	0.0094		0.0100	0.0099
	P		0.0090	0.0094		0.0098	0.0105
035 2x1000Hz	A	0.0096	0.0401	0.0199		0.0055	0.0029
	D		0.0091	0.0094		0.0108	0.0110
	G		0.0084	0.0085		0.0102	0.0102
	J		0.0085	0.0082		0.0103	0.0097
	M		0.0093	0.0091		0.0110	0.0108
	P		0.0097	0.0096		0.0105	0.0106
036 2x1000Hz	A	0.0096	0.0184	0.0149		0.0085	0.0084
	D		0.0085	0.0086		0.0122	0.0120
	G		0.0082	0.0083		0.0116	0.0117
	J		0.0076	0.0078		0.0103	0.0105
	M		0.0086	0.0083		0.0103	0.0105
	P		0.0085	0.0084		0.0101	0.0100

L18:

Matrix point	Meas. Level	j_g [m/s] injected	j_g [m/s] cross-correlation		j_g [m/s] bubble pairs	j_g [m/s] morphology	
			O	U		O	U
111 2x1000Hz	A	0.219	0.3044	0.3483	0.1152		
	D		0.3557	0.4030	0.1018		
	G		0.3270	0.3540	0.0958		
	J		0.3578	0.3584	0.0964		
	M		0.2602	0.2723	0.1067		
	P		0.1970	0.2075	0.1394		
114 2x1000Hz	A	0.219	0.1590	0.2259	0.1207		
	D		0.2615	0.2634	0.1594		
	G		0.2744	0.2661	0.1326		
	J		0.2726	0.2707	0.1271		
	M		0.2449	0.2476	0.1476		
	P		0.1851	0.1940	0.1359		
116 2x1000Hz	A	0.219	0.1816	0.1591	0.1103		
	D		0.1973	0.2225	0.1597		
	G		0.2048	0.2160	0.1639		
	J		0.2136	0.2085	0.1516		
	M		0.2086	0.2202	0.1353		
	P		0.1988	0.2060	0.1565		
118 2x2500Hz	A	0.219	0.2194	0.2243	0.1519		
	D		0.1846	0.2058	0.1470		
	G		0.1943	0.2280	0.1596		
	J		0.2199	0.2150	0.1848		
	M		0.2135	0.2289	0.1873		
	P		0.1994	0.2137	0.1761		
119 2x2500Hz	A	0.219	0.1737	0.1945	0.1166		
	D		0.1640	0.1807	0.1359		
	G		0.1854	0.1834	0.1517		
	J		0.1944	0.1942	0.1627		
	M		0.2214	0.2224	0.1880		
	P		0.2159	0.2188	0.1880		
120 2x2500Hz	A	0.219	0.1384	0.1716	0.0667		
	D		0.1350	0.1494	0.0839		
	G		0.1350	0.1506	0.0884		
	J		0.1595	0.1731	0.1071		
	M		0.2728	0.2765	0.1664		
	P		0.2570	0.2572	0.1707		
121 2x2500Hz	A	0.219	0.1333	0.1642	0.0155		
	D		0.1024	0.1222	0.0095		
	G		0.0974	0.0866	0.0097		
	J		0.1043	0.1328	0.0219		
	M		0.1545	0.1492	0.0413		
	P		0.1659	0.1998	0.0582		

133 2x1000Hz	A	0.534	0.6572	0.6743	0.0883		
	D		0.8620	0.8956	0.1050		
	G		0.6116	0.6343	0.0887		
	J		0.6879	0.7421	0.1081		
	M		0.5898	0.6448	0.0688		
	P		0.4512	0.4658	0.0778		
140 2x2500Hz	A	0.534	0.4574	0.4561	0.3026		
	D		0.4386	0.4620	0.3068		
	G		0.4592	0.4501	0.3172		
	J		0.4785	0.4754	0.3723		
	M		0.4993	0.5038	0.4156		
	P		0.4974	0.5074	0.4012		
143 2x2500Hz	A	0.534	0.1525	0.1511	0.0300		
	D		0.1175	0.1351	0.0199		
	G		0.1519	0.1812	0.0362		
	J		0.1904	0.1769	0.0599		
	M		0.2298	0.2960	0.0845		
	P		0.3658	0.3788	0.1303		
155 2x2500Hz	A	1.305	0.5953	0.6048	0.0270		
	D		0.8800	0.9372	0.0312		
	G		0.7652	0.7810	0.0330		
	J		0.9017	0.8964	0.0532		
	M		1.0137	1.0844	0.0650		
	P		1.0608	1.0761	0.1147		
162 2x2500Hz	A	1.305	0.9390	0.9552	0.2370		
	D		0.9285	0.9078	0.2221		
	G		0.9880	0.9859	0.2927		
	J		0.9381	0.9513	0.3430		
	M		0.9764	1.0182	0.4579		
	P		1.0560	1.0778	0.4833		
165 2x2500Hz	A	1.305	1.7014	0.5340	0.0168		
	D		1.6185	0.7224	0.0668		
	G		1.5311	1.5071	0.1801		
	J		1.6242	1.4802	0.2332		
	M		1.6945	1.6361	0.2613		
	P		1.5183	1.4279	0.2420		

L20:

Matrix point	Meas. Level	j_g [m/s] injected	j_g [m/s] cross-correlation		j_g [m/s] bubble pairs	j_g [m/s] morphology	
			O	U		O	U
006 2x1000Hz	A	-0.0025	-0.0029	-0.0046	-0.0018	-0.0027	-0.0029
	D		-0.0024	-0.0022	-0.0017	-0.0026	-0.0025
	G		-0.0020	-0.0019	-0.0017	-0.0026	-0.0025
	J		-0.0018	-0.0018	-0.0018	-0.0026	-0.0026
	M		-0.0016	-0.0018	-0.0016	-0.0025	-0.0026
	N		-0.0016	-0.0016	-0.0016	-0.0024	-0.0024

007 2x1000Hz	A	-0.0025	-0.0658	-0.0179	0.0000	-0.0007	-0.0002
	D		-0.0121	-0.0202	-0.0046	-0.0057	-0.0069
	G		-0.0021	-0.0024	-0.0014	-0.0015	-0.0017
	J		-0.0020	-0.0021	-0.0019	-0.0021	-0.0023
	M		-0.0019	-0.0016	-0.0016	-0.0023	-0.0020
	N		-0.0019	-0.0019	-0.0018	-0.0023	-0.0024
008 2x1000Hz	A	-0.0025	-0.1014	-0.0725	0.0000		
	D		-0.0026	-0.0026	-0.0018		
	G		-0.0027	-0.0026	-0.0020		
	J		-0.0030	-0.0027	-0.0024		
	M		-0.0026	-0.0027	-0.0024		
	N		-0.0032	-0.0032	-0.0025		
009 2x2000Hz	A	-0.0025	-0.0817	-0.0861	0.0000		
	D		-0.0025	-0.0025	-0.0018		
	G		-0.0023	-0.0024	-0.0016		
	J		-0.0031	-0.0024	-0.0018		
	M		-0.0025	-0.0030	-0.0019		
	N		-0.0038	-0.0034	-0.0029		
028 2x1000Hz	A	-0.0062	-0.0158	-0.0146	-0.0039	-0.0103	-0.0062
	D		-0.0068	-0.0068	-0.0044	-0.0062	-0.0062
	G		-0.0052	-0.0049	-0.0044	-0.0064	-0.0061
	J		-0.0047	-0.0047	-0.0045	-0.0066	-0.0066
	M		-0.0049	-0.0049	-0.0044	-0.0067	-0.0065
	N		-0.0051	-0.0048	-0.0044	-0.0066	-0.0062
029 2x1000Hz	A	-0.0062	-0.0851	-0.0382	0.0000	-0.0006	-0.0002
	D		-0.2691	-0.2765	0.0000	-0.0004	-0.0004
	G		-0.0080	-0.0083	-0.0038	-0.0045	-0.0043
	J		-0.0055	-0.0058	-0.0049	-0.0056	-0.0057
	M		-0.0045	-0.0046	-0.0044	-0.0055	-0.0059
	N		-0.0046	-0.0047	-0.0045	-0.0056	-0.0058
029Wh 2x1000Hz	A	-0.0062	-0.0975	-0.0466	0.0000	-0.0007	-0.0002
	D		-0.0402	-0.0490	-0.0095	-0.0149	-0.0111
	G		-0.0068	-0.0068	-0.0039	-0.0045	-0.0045
	J		-0.0049	-0.0049	-0.0045	-0.0053	-0.0054
	M		-0.0044	-0.0045	-0.0043	-0.0053	-0.0056
	N		-0.0047	-0.0047	-0.0045	-0.0057	-0.0056
030 2x1000Hz	A	-0.0062	-0.0180	-0.0055	-0.0002		
	D		-0.0139	-0.0395	-0.0080		
	G		-0.0064	-0.0062	-0.0046		
	J		-0.0064	-0.0083	-0.0058		
	M		-0.0075	-0.0068	-0.0063		
	N		-0.0069	-0.0069	-0.0063		
031 2x2000Hz	A	-0.0062	-0.1338	-0.1011	-0.1184		
	D		-0.0094	-0.0262	-0.0044		
	G		-0.0087	-0.0088	-0.0067		
	J		-0.0131	-0.0088	-0.0079		
	M		-0.0085	-0.0102	-0.0080		
	N		-0.0110	-0.0114	-0.0097		

050 2x1000Hz	A	-0.0151	-0.0942	-0.0926	-0.0145	-0.0278	-0.0216
	D		-0.0482	-0.0470	-0.0106	-0.0181	-0.0174
	G		-0.0302	-0.0301	-0.0092	-0.0136	-0.0134
	J		-0.0134	-0.0128	-0.0105	-0.0166	-0.0156
	M		-0.0138	-0.0134	-0.0107	-0.0167	-0.0160
	N		-0.0142	-0.0135	-0.0106	-0.0161	-0.0154
051 2x1000Hz	A	-0.0151	-0.0687	-0.0269	-0.0001	-0.0004	-0.0004
	D		-0.2992	-0.2927	-0.0008	-0.0019	-0.0030
	G		-0.0869	-0.1153	-0.0163	-0.0227	-0.0280
	J		-0.0136	-0.0128	-0.0093	-0.0115	-0.0107
	M		-0.0115	-0.0118	-0.0107	-0.0137	-0.0139
	N		-0.0106	-0.0110	-0.0100	-0.0128	-0.0130
052 2x1000Hz	A	-0.0151	-0.0115	-0.0045	-0.0012		
	D		-0.0136	-0.0134	-0.0109		
	G		-0.0145	-0.0147	-0.0133		
	J		-0.0146	-0.0140	-0.0133		
	M		-0.0141	-0.0145	-0.0137		
	N		-0.0140	-0.0145	-0.0137		
053 2x2000Hz	A	-0.0151	-0.0095	-0.0034	-0.0020		
	D		-0.0194	-0.0189	-0.0166		
	G		-0.0203	-0.0200	-0.0191		
	J		-0.0217	-0.0216	-0.0208		
	M		-0.0220	-0.0217	-0.0211		
	N		-0.0225	-0.0226	-0.0217		
083 2x1000Hz	A	-0.0574	-1.2843	-1.3360	0.0000	-0.0008	-0.0006
	D		-0.3336	-0.3219	-0.0342	-0.0611	-0.0569
	G		-0.1845	-0.1811	-0.0293	-0.0476	-0.0452
	J		-0.0843	-0.0788	-0.0290	-0.0517	-0.0476
	M		-0.0544	-0.0532	-0.0341	-0.0580	-0.0560
	N		-0.0720	-0.0687	-0.0340	-0.0559	-0.0531
084 2x1000Hz	A	-0.0574	-0.1533	-0.0707	-0.0003	-0.0028	-0.0003
	D		-0.2937	-0.2987	-0.1311	-0.0011	-0.0004
	G		-0.4714	-0.5202	0.0000	-0.0008	-0.0010
	J		-0.2185	-0.1272	-0.0126	-0.0352	-0.0177
	M		-0.0480	-0.0466	-0.0356	-0.0501	-0.0480
	N		-0.0482	-0.0468	-0.0388	-0.0522	-0.0504
085 2x1000Hz	A	-0.0574	-0.1607	-0.1068	-0.0027		
	D		-0.3658	-0.3831	-0.0006		
	G		-0.5062	-0.5789	-0.0118		
	J		-0.0508	-0.0519	-0.0314		
	M		-0.0538	-0.0535	-0.0454		
	N		-0.0580	-0.0556	-0.0493		
086 2x2000Hz	A	-0.0574	-0.1666	-0.1065	-0.0500		
	D		-0.3997	-0.3255	-0.0113		
	G		-0.1490	-0.1792	-0.0499		
	J		-0.0733	-0.0735	-0.0575		
	M		-0.0812	-0.0811	-0.0711		
	N		-0.0855	-0.0851	-0.0763		

L21:

Matrix point	Meas. Level	j_g [m/s] injected	j_g [m/s] cross-correlation		j_g [m/s] bubble pairs	j_g [m/s] morphology	
			O	U		O	U
116 2x1000Hz	A	-0.219	-1.2802	-1.2525			
	D		-1.2964	-1.2777			
	G		-1.6358	-1.5890			
	J		-2.0234	-1.9844			
	M		-2.0218	-2.0708			
	NN		-2.1553	-2.1322			
117 2x1000Hz	A	-0.219	-1.1091	-1.1409	-0.0000	-0.0000	-0.0000
	D		-0.4854	-0.5457	-0.0000	-0.0000	-0.0000
	G		-0.2499	-0.2658	-0.0786	-0.0619	-0.0647
	J		-0.2011	-0.2078	-0.1129	-0.0952	-0.0992
	M		-0.1884	-0.1932	-0.1425	-0.1215	-0.1238
	NN		-0.1941	-0.1966	-0.1530	-0.1244	-0.1252
118 2x1000Hz	A	-0.219	-0.7540	-0.8353	-0.0725		
	D		-0.7657	-0.9396	-0.0541		
	G		-0.2471	-0.2533	-0.1085		
	J		-0.2231	-0.2254	-0.1356		
	M		-0.2285	-0.2379	-0.1500		
	NN		-0.2294	-0.2359	-0.1442		
119 2x2500Hz	A	-0.219	-0.2945	-0.3308	-0.1651		
	D		-0.2421	-0.2462	-0.1824		
	G		-0.2378	-0.2402	-0.1965		
	J		-0.2524	-0.2523	-0.2119		
	M		-0.2668	-0.2712	-0.2346		
	NN		-0.2731	-0.2750	-0.2482		
138 2x1000Hz	A	-0.534	-1.7447	-1.7409			
	D		-1.7593	-1.7843			
	G		-2.0337	-2.0293			
	J		-2.5000	-2.4520			
	M		-2.6393	-2.6705			
	NN		-2.5906	-2.5734			
139 2x2000Hz	A	-0.534	-1.8977	-1.9104			
	D		-1.7735	-1.8110			
	G		-2.1515	-2.1361			
	J		-2.1950	-2.2003			
	M		-1.8770	-1.9797			
	NN		-2.3354	-2.3185			
150 2x2000Hz	A	-0.835	0.0000	0.0000			
	D		-1.6677	-1.5630			
	G		-1.8846	-1.7612			
	J		-2.2135	-2.0552			
	M		-2.3729	-2.3105			
	NN		-2.3175	-2.2487			

151 2x2500Hz	A	-0.835	-0.6787	-0.7786			
	D		-0.9457	-0.9497			
	G		-0.9821	-0.9179			
	J		-1.2953	-1.3042			
	M		-1.1664	-1.1730			
	NN		-1.0089	-1.0280			
152 2x2500Hz	A	-0.835	-1.0656	-1.0401			
	D		-0.8129	-0.7542			
	G		-1.1727	-1.1686			
	J		-0.9285	-0.9344			
	M		-0.9022	-0.9035			
	NN		-0.9725	-0.9492			
162 2x2500Hz	A	-1.305	-1.0887	-1.0972			
	D		-0.8336	-0.5315			
	G		-1.0887	-1.0820			
	J		-1.1631	-1.1447			
	M		-1.6692	-1.7132			
	NN		-1.4603	-1.4721			
163 2x2500Hz	A	-1.305	-1.2835	-1.1992			
	D		-0.9325	-0.8766			
	G		-1.1665	-1.1861			
	J		-0.9799	-1.0441			
	M		-0.9948	-1.0372			
	NN		-0.7715	-1.0678			

9.3. Operating data

In the following table, the operating data for the measurements of this test series are listed. The columns contain the following information:

Identifierer	Dimension	Description
inj. Module		number of the module / number of working injection needles
j Gas inj.	m/s	sup. Velocity gas injection (nominal value)
j water inj.	m/s	sup. Velocity water injection (nominal value)
V gas inj	nm³/h	gas volume flow above inj. module (nominal value)
m water inj.	kg/s	mass flow water above inj. Module (nominal value)
FIC4-1x	nm³/h	gas volume flow above inj. module (measurement)
FIC4-0x	kg/s	mass flow water above inj. Module (measurement)
FIC4-4/5	kg/s	mass flow steam above inj. module (measurement)
j w inj. meas.	m/s	sup. Velocity water injection (measurement)
PI4-06	bar	absolute pressure in the steam pipe
PI4-07	bar	absolute pressure at the outlet of VGE
PI4-200	bar	absolute pressure at wire-mesh sensor position (small meas. range)
PI4-201	bar	absolute pressure at wire-mesh sensor position
ts	°C	saturation temperature of PI4-201 (check sub-cooling water injection)
PI4-202	bar	absolute pressure at the outlet of Ti tube bottom (small meas. range) PI4-200(+PDI4-200)
PI4-203	bar	absolute pressure at the outlet of Ti tube bottom PI4-201(+PDI4-200)
ts	°C	saturation temperature of PI4-203 (check saturation condition)
PDI4-200	kPa	pressure differenz between TS in- and outlet
TI4-03	°C	water temperature after test section pump
TI4-05	°C	steam temperature in the steam pipe
TI4-07	°C	steam temperature in the steam pipe before TS Ti-tube
TI4-200	°C	water temperature before gas injection module
TI4-201	°C	water temperature after test section Ti-tube
dt	K	sub-cooling of water inlet
TI4-10	°C	water temperature between test section Ti-tube and steam drum
TI4-202	°C	gas temperature before gas injection module
TI4-203	°C	temperature at the outer surface of the thermal insulation
TI4-204	°C	temperature at the outer surface of the thermal insulation
TI4-205	°C	gas temperature before gas injection module top
PIC4-04	bar	absolute pressure in the steam drum B02
ts	°C	saturation temperature of PIC4-04 (check non-condensable gases)
TI4-35	°C	gas temperature in the steam drum
TI4-36	°C	gas temperature in the steam drum
freq	Hz	measurement frequency
j w inj. meas. corr.	m/s	sup. velocity water injection (measurement) with jg correction

L16 – 001

level code	L	data	DIAdem	inj. Module	j Gas inj.	j water inj	Vgas inj.	mWater inj.	FIC4-1x	FIC4-0x	PI4-200	PI4-201	PDI4-200	TI4-03	TI4-200	TI4-201	TI4-10	TI4-202	freq
[-]	[mm]	[-]	[-]	[-]	[m/s]	[m/s]	[nm³/h]	[kg/s]	[nm³/h]	[kg/s]	bar	bar	kPa	°C	°C	°C	°C	°C	Hz
A (tomo)	1	27.07.2012	63	M3 / 1	0,0025	0,041	0,076	0,095	**0,076**	**0,095**	**4,000**	4,041	0,38	29,9	**29,7**	**29,9**	29,5	**25,7**	2/1000
D (tomo)	62	27.07.2012	61	M3 / 1	0,0025	0,041	0,076	0,095	**0,076**	**0,095**	**3,999**	4,041	0,38	29,9	**29,8**	**30,0**	29,5	**25,7**	2/1000
G (tomo)	171	27.07.2012	55	M3 / 1	0,0025	0,041	0,076	0,095	**0,076**	**0,095**	**4,001**	4,038	0,39	30,0	**29,8**	**30,0**	29,4	**25,8**	2/1000
J (tomo)	435	27.07.2012	52	M3 / 1	0,0025	0,041	0,076	0,095	**0,076**	**0,095**	**4,001**	4,049	0,38	30,0	**29,7**	**29,9**	29,3	**25,8**	2/1000
M (tomo)	1271	27.07.2012	50	M3 / 1	0,0025	0,041	0,076	0,095	**0,076**	**0,095**	**4,001**	4,036	0,38	30,0	**29,7**	**29,9**	29,2	**25,8**	2/1000
P (tomo)	3270	27.07.2012	48	M3 / 1	0,0025	0,041	0,076	0,095	**0,076**	**0,095**	**3,999**	4,037	0,38	30,1	**29,6**	**29,8**	29,4	**25,9**	2/1000
S (wms)	4685	27.07.2012	48	M3 / 1	0,0025	0,041	0,076	0,095	**0,076**	**0,095**	**3,999**	4,037	0,38	30,1	**29,6**	**29,8**	29,4	**25,9**	2/5000

L16 – 004

level code	L	data	DIAdem	inj. Module	j Gas inj.	j water inj	Vgas inj.	mWater inj.	FIC4-1x	FIC4-0x	j w inj. meas.	PI4-200	PI4-201	PDI4-200	TI4-03	TI4-200	TI4-201	TI4-10	TI4-202	freq
[-]	[mm]	[-]	[-]	[-]	[m/s]	[m/s]	[nm³/h]	[kg/s]	[nm³/h]	[kg/s]	m/s	bar	bar	kPa	°C	°C	°C	°C	°C	Hz
A (tomo)	1	24.07.2012	35	M3 / 1	0,0025	0,161	0,076	0,378	**0,076**	**0,372**	**0,159**	**3,999**	4,039	0,22	30,6	**30,4**	**30,6**	29,8	**24,9**	2/1000
D (tomo)	62	24.07.2012	39	M3 / 1	0,0025	0,161	0,076	0,378	**0,076**	**0,372**	**0,159**	**3,999**	4,052	0,22	30,6	**30,6**	**30,7**	30,3	**24,7**	2/1000
G (tomo)	171	24.07.2012	43	M3 / 1	0,0025	0,161	0,076	0,378	**0,076**	**0,373**	**0,159**	**3,999**	4,046	0,23	30,7	**30,6**	**30,9**	30,5	**24,6**	2/1000
J (tomo)	435	24.07.2012	52	M3 / 1	0,0025	0,161	0,076	0,378	**0,076**	**0,372**	**0,159**	**3,999**	4,051	0,23	30,8	**30,6**	**30,9**	30,6	**24,6**	2/1000
M (tomo)	1271	24.07.2012	54	M3 / 1	0,0025	0,161	0,076	0,378	**0,076**	**0,373**	**0,159**	**3,999**	4,037	0,23	30,8	**30,6**	**30,9**	30,7	**24,5**	2/1000
P (tomo)	3270	24.07.2012	56	M3 / 1	0,0025	0,161	0,076	0,378	**0,076**	**0,373**	**0,159**	**4,000**	4,043	0,23	30,9	**30,7**	**31,0**	30,7	**24,5**	2/1000
S (wms)	4685	24.07.2012	56	M3 / 1	0,0025	0,161	0,076	0,378	**0,076**	**0,373**	**0,159**	**4,000**	4,043	0,23	30,9	**30,7**	**31,0**	30,7	**24,5**	2/5000

rho * Aq **2,34864**
FIC4-03 zero point correction

L16 – 006

level code	L	data	DIAdem	inj. Module	j Gas inj.	j water inj	Vgas inj.	mWater inj.	FIC4-1x	FIC4-0x	PI4-200	PI4-201	PDI4-200	TI4-03	TI4-200	TI4-201	TI4-10	TI4-202	freq
[-]	[mm]	[-]	[-]	[-]	[m/s]	[m/s]	[nm³/h]	[kg/s]	[nm³/h]	[kg/s]	bar	bar	kPa	°C	°C	°C	°C	°C	Hz
A (tomo)	1	18.07.2012	77	M3 / 1	0,0025	0,405	0,076	0,951	**0,076**	**0,951**	**4,001**	4,051	-0,24	29,8	**29,8**	**30,0**	30,0	**23,8**	2/2500
A (tomo)	1	18.07.2012	83	M3 / 1	0,0025	0,405	0,076	0,951	**0,076**	**0,951**	**4,000**	4,058	-0,24	29,8	**29,9**	**30,0**	29,9	**23,8**	2/1000
D (tomo)	62	18.07.2012	74	M3 / 1	0,0025	0,405	0,076	0,951	**0,076**	**0,951**	**4,001**	4,054	-0,24	29,8	**29,9**	**30,0**	29,9	**23,8**	2/2500
D (tomo)	62	18.07.2012	67	M3 / 1	0,0025	0,405	0,076	0,951	**0,076**	**0,951**	**4,001**	4,051	-0,24	29,8	**29,9**	**30,0**	29,9	**23,8**	2/1000
G (tomo)	171	18.07.2012	61	M3 / 1	0,0025	0,405	0,076	0,951	**0,076**	**0,951**	**4,000**	4,050	-0,24	29,9	**29,9**	**30,1**	30,0	**23,8**	2/2500
G (tomo)	171	18.07.2012	64	M3 / 1	0,0025	0,405	0,076	0,951	**0,076**	**0,951**	**4,002**	4,058	-0,24	29,8	**29,9**	**30,1**	30,0	**23,8**	2/1000
J (tomo)	435	18.07.2012	57	M3 / 1	0,0025	0,405	0,076	0,951	**0,076**	**0,952**	**4,000**	4,051	-0,23	29,9	**29,9**	**30,1**	30,1	**23,7**	2/2500
J (tomo)	435	18.07.2012	54	M3 / 1	0,0025	0,405	0,076	0,951	**0,076**	**0,951**	**4,003**	4,051	-0,24	30,0	**30,0**	**30,2**	30,1	**23,8**	2/1000
M (tomo)	1271	18.07.2012	50	M3 / 1	0,0025	0,405	0,076	0,951	**0,076**	**0,951**	**3,999**	4,053	-0,23	30,1	**30,2**	**30,4**	30,3	**23,8**	2/2500
M (tomo)	1271	18.07.2012	52	M3 / 1	0,0025	0,405	0,076	0,951	**0,076**	**0,951**	**3,996**	4,051	-0,24	30,0	**30,1**	**30,3**	30,2	**23,8**	2/1000
P (tomo)	3270	18.07.2012	47	M3 / 1	0,0025	0,405	0,076	0,951	**0,076**	**0,952**	**3,994**	4,040	-0,23	30,2	**30,3**	**30,4**	30,4	**23,8**	2/2500
P (tomo)	3270	18.07.2012	46	M3 / 1	0,0025	0,405	0,076	0,951	**0,076**	**0,952**	**4,002**	4,052	-0,22	30,3	**30,3**	**30,5**	30,4	**23,8**	2/1000
S (wms)	4685	18.07.2012	47	M3 / 1	0,0025	0,405	0,076	0,951	**0,076**	**0,952**	**3,994**	4,040	-0,23	30,2	**30,3**	**30,4**	30,4	**23,8**	2/5000

L16 – 008

level code	L	data	DIAdem	inj. Module	j Gas inj.	j water inj	Vgas inj.	mWater inj.	FIC4-1x	FIC4-0x	PI4-200	PI4-201	PDI4-200	TI4-03	TI4-200	TI4-201	TI4-10	TI4-202	freq
[-]	[mm]	[-]	[-]	[-]	[m/s]	[m/s]	[nm³/h]	[kg/s]	[nm³/h]	[kg/s]	bar	bar	kPa	°C	°C	°C	°C	°C	Hz
A (tomo)	1	24.07.2012	2	M3 / 1	0,0025	1,017	0,076	2,389	**0,076**	**2,388**	**4,003**	4,058	-2,41	29,9	**29,9**	**30,1**	30,0	**23,7**	2/2500
A (tomo)	1	24.07.2012	31	M3 / 1	0,0025	1,017	0,076	2,389	**0,076**	**2,392**	**4,000**	4,049	-2,42	30,4	**30,4**	**30,6**	30,5	**23,7**	1/1000
D (tomo)	62	24.07.2012	5	M3 / 1	0,0025	1,017	0,076	2,389	**0,076**	**2,388**	**4,002**	4,055	-2,44	29,9	**30,0**	**30,2**	30,0	**23,7**	2/2500
D (tomo)	62	24.07.2012	29	M3 / 1	0,0025	1,017	0,076	2,389	**0,076**	**2,387**	**4,001**	4,045	-2,37	30,4	**30,5**	**30,6**	30,5	**23,7**	1/1000
G (tomo)	171	24.07.2012	8	M3 / 1	0,0025	1,017	0,076	2,389	**0,076**	**2,381**	**4,001**	4,052	-2,43	30,0	**30,0**	**30,2**	30,1	**23,7**	2/2500
G (tomo)	171	24.07.2012	26	M3 / 1	0,0025	1,017	0,076	2,389	**0,076**	**2,393**	**3,999**	4,048	-2,41	30,3	**30,4**	**30,6**	30,4	**23,7**	1/1000
J (tomo)	435	24.07.2012	12	M3 / 1	0,0025	1,017	0,076	2,389	**0,076**	**2,391**	**4,001**	4,043	-2,44	30,0	**30,1**	**30,3**	30,1	**23,7**	2/2500
J (tomo)	435	24.07.2012	24	M3 / 1	0,0025	1,017	0,076	2,389	**0,076**	**2,394**	**3,999**	4,045	-2,43	30,3	**30,3**	**30,5**	30,4	**23,7**	1/1000
M (tomo)	1271	24.07.2012	14	M3 / 1	0,0025	1,017	0,076	2,389	**0,076**	**2,394**	**4,000**	4,054	-2,40	30,0	**30,1**	**30,3**	30,2	**23,7**	2/2500
M (tomo)	1271	24.07.2012	21	M3 / 1	0,0025	1,017	0,076	2,389	**0,076**	**2,392**	**4,000**	4,047	-2,51	30,2	**30,3**	**30,5**	30,3	**23,7**	1/1000
P (tomo)	3270	24.07.2012	16	M3 / 1	0,0025	1,017	0,076	2,389	**0,076**	**2,376**	**3,998**	4,051	-2,33	30,1	**30,2**	**30,4**	30,2	**23,7**	2/2500
P (tomo)	3270	24.07.2012	19	M3 / 1	0,0025	1,017	0,076	2,389	**0,076**	**2,392**	**3,998**	4,052	-2,48	30,1	**30,2**	**30,4**	30,3	**23,7**	1/1000
S (wms)	4685	24.07.2012	16	M3 / 1	0,0025	1,017	0,076	2,389	**0,076**	**2,376**	**3,998**	4,051	-2,33	30,1	**30,2**	**30,4**	30,2	**23,7**	2/5000

L16 – 028

level code	L	data	DIAdem	inj. Module	j Gas inj.	j water inj	Vgas inj.	mWater inj.	FIC4-1x	FIC4-0x	PI4-200	PI4-201	PDI4-200	TI4-03	TI4-200	TI4-201	TI4-10	TI4-202	freq
[-]	[mm]	[-]	[-]	[-]	[m/s]	[m/s]	[nm³/h]	[kg/s]	[nm³/h]	[kg/s]	bar	bar	kPa	°C	°C	°C	°C	°C	Hz
A (tomo)	1	18.07.2012	7	M3 / 1	0,0062	0,405	0,187	0,951	**0,187**	**0,951**	**3,998**	4,053	-0,01	29,8	**29,9**	**30,1**	29,9	**23,7**	2/2500
A (tomo)	1	18.07.2012	3	M3 / 1	0,0062	0,405	0,187	0,951	**0,187**	**0,952**	**4,001**	4,052	-0,01	29,6	**29,7**	**29,9**	29,7	**23,7**	2/1000
D (tomo)	62	18.07.2012	10	M3 / 1	0,0062	0,405	0,187	0,951	**0,187**	**0,951**	**4,000**	4,052	-0,01	29,9	**29,9**	**30,1**	29,9	**23,7**	2/2500
D (tomo)	62	18.07.2012	14	M3 / 1	0,0062	0,405	0,187	0,951	**0,187**	**0,951**	**4,004**	4,062	-0,01	30,0	**30,1**	**30,2**	30,1	**23,7**	2/1000
G (tomo)	171	18.07.2012	19	M3 / 1	0,0062	0,405	0,187	0,951	**0,187**	**0,955**	**3,999**	4,056	-0,01	30,1	**30,3**	**30,4**	30,2	**23,7**	2/2500
G (tomo)	171	18.07.2012	16	M3 / 1	0,0062	0,405	0,187	0,951	**0,187**	**0,951**	**3,998**	4,051	0,00	30,0	**30,2**	**30,3**	30,1	**23,7**	2/1000
J (tomo)	435	18.07.2012	24	M3 / 1	0,0062	0,405	0,187	0,951	**0,187**	**0,951**	**4,003**	4,058	0,00	30,2	**30,4**	**30,5**	30,3	**23,7**	2/2500
J (tomo)	435	18.07.2012	27	M3 / 1	0,0062	0,405	0,187	0,951	**0,187**	**0,949**	**4,006**	4,056	0,00	30,3	**30,4**	**30,6**	30,4	**23,7**	2/1000
M (tomo)	1271	18.07.2012	34	M3 / 1	0,0062	0,405	0,187	0,951	**0,187**	**0,954**	**4,002**	4,057	0,00	30,5	**30,6**	**30,8**	30,6	**23,7**	2/2500
M (tomo)	1271	18.07.2012	30	M3 / 1	0,0062	0,405	0,187	0,951	**0,187**	**0,952**	**3,998**	4,059	0,00	30,4	**30,5**	**30,7**	30,5	**23,7**	2/1000
P (tomo)	3270	18.07.2012	38	M3 / 1	0,0062	0,405	0,187	0,951	**0,187**	**0,951**	**4,005**	4,051	0,00	30,7	**30,6**	**30,9**	30,7	**23,7**	2/2500
P (tomo)	3270	18.07.2012	43	M3 / 1	0,0062	0,405	0,187	0,951	**0,187**	**0,950**	**3,999**	4,057	0,00	30,5	**30,6**	**30,7**	30,6	**23,8**	2/1000
S (wms)	4685	18.07.2012	38	M3 / 1	0,0062	0,405	0,187	0,951	**0,187**	**0,951**	**4,005**	4,051	0,00	30,7	**30,6**	**30,9**	30,7	**23,7**	2/5000

L16 – 030

level code	L	data	DIAdem	inj. Module	j Gas inj.	j water inj	Vgas inj.	mWater inj.	FIC4-1x	FIC4-0x	PI4-200	PI4-201	PDI4-200	TI4-03	TI4-200	TI4-201	TI4-10	TI4-202	freq
[-]	[mm]	[-]	[-]	[-]	[m/s]	[m/s]	[nm³/h]	[kg/s]	[nm³/h]	[kg/s]	bar	bar	kPa	°C	°C	°C	°C	°C	Hz
A (tomo)	1	27.07.2012	21	M3 / 1	0,0062	1,017	0,187	2,389	**0,187**	**2,391**	**3,999**	4,037	-2,36	29,5	**29,5**	**29,9**	29,6	**26,9**	2/2500
A (tomo)	1	27.07.2012	25	M3 / 1	0,0062	1,017	0,187	2,389	**0,187**	**2,398**	**4,004**	4,049	-2,38	29,5	**29,6**	**29,9**	29,6	**26,8**	1/1000
D (tomo)	62	27.07.2012	17	M3 / 1	0,0062	1,017	0,187	2,389	**0,187**	**2,397**	**4,001**	4,042	-2,34	29,4	**29,5**	**29,8**	29,5	**27,1**	2/2500
D (tomo)	62	27.07.2012	28	M3 / 1	0,0062	1,017	0,187	2,389	**0,187**	**2,391**	**4,000**	4,048	-2,38	29,6	**29,6**	**29,9**	29,6	**26,7**	1/1000
G (tomo)	171	27.07.2012	13	M3 / 1	0,0062	1,017	0,187	2,389	**0,187**	**2,391**	**4,003**	4,045	-2,47	29,4	**29,4**	**29,8**	29,5	**27,2**	2/2500
G (tomo)	171	27.07.2012	32	M3 / 1	0,0062	1,017	0,187	2,389	**0,187**	**2,393**	**4,001**	4,038	-2,37	29,7	**29,6**	**29,9**	29,7	**26,6**	1/1000
J (tomo)	435	27.07.2012	11	M3 / 1	0,0062	1,017	0,187	2,389	**0,187**	**2,396**	**4,003**	4,055	-2,39	29,4	**29,3**	**29,7**	29,4	**27,3**	2/2500
J (tomo)	435	27.07.2012	34	M3 / 1	0,0062	1,017	0,187	2,389	**0,187**	**2,385**	**4,004**	4,051	-2,32	29,7	**29,7**	**29,9**	29,8	**26,5**	1/1000
M (tomo)	1271	27.07.2012	7	M3 / 1	0,0062	1,017	0,187	2,389	**0,187**	**2,389**	**4,000**	4,051	-2,39	29,3	**29,3**	**29,6**	29,4	**27,4**	2/2500
M (tomo)	1271	27.07.2012	36	M3 / 1	0,0062	1,017	0,187	2,389	**0,187**	**2,380**	**4,002**	4,039	-2,29	29,7	**29,7**	**30,0**	29,8	**26,5**	1/1000
P (tomo)	3270	27.07.2012	5	M3 / 1	0,0062	1,017	0,187	2,389	**0,187**	**2,392**	**3,999**	4,044	-2,32	29,3	**29,3**	**29,6**	29,4	**27,6**	2/2500
P (tomo)	3270	27.07.2012	38	M3 / 1	0,0062	1,017	0,187	2,389	**0,187**	**2,389**	**4,002**	4,038	-2,36	29,8	**29,8**	**30,0**	29,8	**26,4**	1/1000
S (wms)	4685	27.07.2012	5	M3 / 1	0,0062	1,017	0,187	2,389	**0,187**	**2,392**	**3,999**	4,044	-2,32	29,3	**29,3**	**29,6**	29,4	**27,6**	2/5000

L16 – 034

level code	L	data	DIAdem	inj. Module	j Gas inj.	j water inj	Vgas inj.	mWater inj.	FIC4-1x	FIC4-0x	PI4-200	PI4-201	PDI4-200	TI4-03	TI4-200	TI4-201	TI4-10	TI4-202	freq
[-]	[mm]	[-]	[-]	[-]	[m/s]	[m/s]	[nm³/h]	[kg/s]	[nm³/h]	[kg/s]	bar	bar	kPa	°C	°C	°C	°C	°C	Hz
A (tomo)	1	25.07.2012	25	M3 / 3	0,0096	0,041	0,290	0,095	**0,290**	**0,095**	**4,004**	4,052	1,48	29,8	**29,1**	**29,4**	29,5	**24,4**	2/1000
D (tomo)	62	25.07.2012	28	M3 / 3	0,0096	0,041	0,290	0,095	**0,290**	**0,095**	**4,004**	4,053	1,51	29,9	**29,4**	**29,6**	29,5	**24,4**	2/1000
G (tomo)	171	25.07.2012	33	M3 / 3	0,0096	0,041	0,290	0,095	**0,290**	**0,095**	**3,999**	4,038	1,59	30,0	**29,7**	**29,9**	29,8	**24,4**	2/1000
J (tomo)	435	25.07.2012	36	M3 / 3	0,0096	0,041	0,290	0,095	**0,290**	**0,095**	**4,000**	4,038	1,55	30,0	**29,8**	**30,0**	29,7	**24,5**	2/1000
M (tomo)	1271	25.07.2012	39	M3 / 3	0,0096	0,041	0,290	0,095	**0,290**	**0,095**	**4,000**	4,045	1,60	30,0	**29,8**	**30,0**	29,7	**24,4**	2/1000
P (tomo)	3270	25.07.2012	43	M3 / 3	0,0096	0,041	0,290	0,095	**0,290**	**0,095**	**3,999**	4,050	1,60	29,9	**29,8**	**30,0**	29,7	**24,5**	2/1000
S (wms)	4685	25.07.2012	43	M3 / 3	0,0096	0,041	0,290	0,095	**0,290**	**0,095**	**3,999**	4,050	1,60	29,9	**29,8**	**30,0**	29,7	**24,5**	2/5000

L16 – 037

level code	L	data	DIAdem	inj. Module	j Gas inj.	j water inj	Vgas inj.	mWater inj.	FIC4-1x	FIC4-0x	PI4-200	PI4-201	PDI4-200	TI4-03	TI4-200	TI4-201	TI4-10	TI4-202	freq
[-]	[mm]	[-]	[-]	[-]	[m/s]	[m/s]	[nm³/h]	[kg/s]	[nm³/h]	[kg/s]	bar	bar	kPa	°C	°C	°C	°C	°C	Hz
A (tomo)	1	25.07.2012	20	M3 / 3	0,0096	0,161	0,290	0,378	**0,290**	**0,378**	**4,000**	4,050	1,01	30,3	**30,2**	**30,5**	30,3	**24,3**	2/1000
D (tomo)	62	25.07.2012	18	M3 / 3	0,0096	0,161	0,290	0,378	**0,290**	**0,378**	**4,000**	4,049	1,02	30,3	**30,3**	**30,5**	30,4	**24,4**	2/1000
G (tomo)	171	25.07.2012	12	M3 / 3	0,0096	0,161	0,290	0,378	**0,290**	**0,378**	**4,000**	4,053	1,03	30,4	**30,4**	**30,6**	30,5	**24,4**	2/1000
J (tomo)	435	25.07.2012	10	M3 / 3	0,0096	0,161	0,290	0,378	**0,290**	**0,378**	**4,000**	4,047	1,01	30,4	**30,4**	**30,6**	30,5	**24,4**	2/1000
M (tomo)	1271	25.07.2012	4	M3 / 3	0,0096	0,161	0,290	0,378	**0,290**	**0,378**	**4,002**	4,057	1,05	30,5	**30,6**	**30,8**	30,5	**24,5**	2/1000
P (tomo)	3270	25.07.2012	1	M3 / 3	0,0096	0,161	0,290	0,378	**0,290**	**0,378**	**3,998**	4,049	1,00	30,6	**30,5**	**30,7**	30,3	**24,6**	2/1000
S (wms)	4685	25.07.2012	1	M3 / 3	0,0096	0,161	0,290	0,378	**0,290**	**0,378**	**3,998**	4,049	1,00	30,6	**30,5**	**30,7**	30,3	**24,6**	2/5000

L16 – 039

level code	L	data	DIAdem	inj. Module	j Gas inj.	j water inj	Vgas inj.	mWater inj.	FIC4-1x	FIC4-0x	PI4-200	PI4-201	PDI4-200	TI4-03	TI4-200	TI4-201	TI4-10	TI4-202	freq
[-]	[mm]	[-]	[-]	[-]	[m/s]	[m/s]	[nm³/h]	[kg/s]	[nm³/h]	[kg/s]	bar	bar	kPa	°C	°C	°C	°C	°C	Hz
A (tomo)	1	19.07.2012	8	M3 / 3	0,0096	0,405	0,290	0,951	**0,290**	**0,955**	**4,002**	4,051	0,22	29,8	**29,8**	**30,1**	29,8	**23,8**	2/2500
A (tomo)	1	19.07.2012	5	M3 / 3	0,0096	0,405	0,290	0,951	**0,290**	**0,959**	**3,996**	4,051	0,21	29,7	**29,8**	**30,0**	29,8	**23,8**	2/1000
D (tomo)	62	19.07.2012	11	M3 / 3	0,0096	0,405	0,290	0,951	**0,290**	**0,951**	**3,996**	4,053	0,23	29,9	**29,9**	**30,1**	30,0	**23,8**	2/2500
D (tomo)	62	19.07.2012	13	M3 / 3	0,0096	0,405	0,290	0,951	**0,290**	**0,948**	**4,004**	4,055	0,24	30,0	**30,0**	**30,2**	30,0	**23,7**	2/1000
G (tomo)	171	19.07.2012	17	M3 / 3	0,0096	0,405	0,290	0,951	**0,290**	**0,949**	**3,997**	4,050	0,24	30,1	**30,2**	**30,4**	30,1	**23,8**	2/2500
G (tomo)	171	19.07.2012	15	M3 / 3	0,0096	0,405	0,290	0,951	**0,290**	**0,948**	**4,001**	4,051	0,23	30,0	**30,1**	**30,3**	30,1	**23,7**	2/1000
J (tomo)	435	19.07.2012	20	M3 / 3	0,0096	0,405	0,290	0,951	**0,290**	**0,949**	**4,000**	4,051	0,23	30,1	**30,3**	**30,4**	30,2	**23,8**	2/2500
J (tomo)	435	19.07.2012	22	M3 / 3	0,0096	0,405	0,290	0,951	**0,290**	**0,957**	**4,003**	4,051	0,22	30,2	**30,3**	**30,5**	30,3	**23,7**	2/1000
M (tomo)	1271	19.07.2012	27	M3 / 3	0,0096	0,405	0,290	0,951	**0,290**	**0,952**	**3,996**	4,051	0,24	30,4	**30,4**	**30,6**	30,4	**23,7**	2/2500
M (tomo)	1271	19.07.2012	25	M3 / 3	0,0096	0,405	0,290	0,951	**0,290**	**0,951**	**3,999**	4,056	0,24	30,3	**30,4**	**30,6**	30,3	**23,7**	2/1000
P (tomo)	3270	19.07.2012	29	M3 / 3	0,0096	0,405	0,290	0,951	**0,290**	**0,951**	**4,001**	4,057	0,23	30,4	**30,5**	**30,6**	30,5	**23,8**	2/2500
P (tomo)	3270	19.07.2012	32	M3 / 3	0,0096	0,405	0,290	0,951	**0,290**	**0,949**	**3,999**	4,057	0,24	30,5	**30,6**	**30,7**	30,5	**23,8**	2/1000
S (wms)	4685	19.07.2012	29	M3 / 3	0,0096	0,405	0,290	0,951	**0,290**	**0,951**	**4,001**	4,057	0,23	30,4	**30,5**	**30,6**	30,5	**23,8**	2/5000

L16 – 041

level code	L	data	DIAdem	inj. Module	j Gas inj.	j water inj	Vgas inj.	mWater inj.	FIC4-1x	FIC4-0x	PI4-200	PI4-201	PDI4-200	TI4-03	TI4-200	TI4-201	TI4-10	TI4-202	freq
[-]	[mm]	[-]	[-]	[-]	[m/s]	[m/s]	[nm³/h]	[kg/s]	[nm³/h]	[kg/s]	bar	bar	kPa	°C	°C	°C	°C	°C	Hz
A (tomo)	1	26.07.2012	28	M3 / 3	0,0096	1,017	0,290	2,389	**0,290**	**2,384**	**4,001**	4,058	-2,17	29,8	**29,8**	**30,1**	29,9	**24,2**	2/2500
A (tomo)	1	26.07.2012	32	M3 / 3	0,0096	1,017	0,290	2,389	**0,290**	**2,399**	**3,999**	4,058	-2,24	29,7	**29,9**	**30,1**	29,9	**24,6**	1/1000
D (tomo)	62	26.07.2012	24	M3 / 3	0,0096	1,017	0,290	2,389	**0,290**	**2,392**	**4,001**	4,053	-2,20	29,7	**29,8**	**30,0**	29,8	**24,3**	2/2500
D (tomo)	62	26.07.2012	35	M3 / 3	0,0096	1,017	0,290	2,389	**0,290**	**2,385**	**3,997**	4,055	-2,29	29,7	**29,8**	**30,0**	29,8	**24,3**	1/1000
G (tomo)	171	26.07.2012	14	M3 / 3	0,0096	1,017	0,290	2,389	**0,290**	**2,394**	**3,998**	4,052	-2,19	29,6	**29,7**	**30,0**	29,8	**24,4**	2/2500
G (tomo)	171	26.07.2012	39	M3 / 3	0,0096	1,017	0,290	2,389	**0,290**	**2,393**	**4,001**	4,058	-2,24	29,6	**29,8**	**29,9**	29,8	**24,2**	1/1000
J (tomo)	435	26.07.2012	12	M3 / 3	0,0096	1,017	0,290	2,389	**0,290**	**2,387**	**4,004**	4,055	-2,16	29,6	**29,6**	**29,9**	29,7	**24,5**	2/2500
J (tomo)	435	26.07.2012	41	M3 / 3	0,0096	1,017	0,290	2,389	**0,290**	**2,385**	**4,001**	4,054	-2,14	29,6	**29,7**	**30,0**	29,8	**24,0**	1/1000
M (tomo)	1271	26.07.2012	9	M3 / 3	0,0096	1,017	0,290	2,389	**0,290**	**2,391**	**4,003**	4,057	-2,24	29,6	**29,6**	**29,9**	29,7	**24,6**	2/2500
M (tomo)	1271	26.07.2012	43	M3 / 3	0,0096	1,017	0,290	2,389	**0,290**	**2,383**	**4,001**	4,060	-2,25	29,6	**29,8**	**29,9**	29,8	**23,9**	1/1000
P (tomo)	3270	26.07.2012	7	M3 / 3	0,0096	1,017	0,290	2,389	**0,290**	**2,394**	**3,998**	4,044	-2,22	29,3	**29,4**	**29,7**	29,4	**25,0**	2/2500
P (tomo)	3270	26.07.2012	45	M3 / 3	0,0096	1,017	0,290	2,389	**0,290**	**2,387**	**4,001**	4,052	-2,19	29,6	**29,7**	**29,9**	29,8	**23,8**	1/1000
S (wms)	4685	26.07.2012	7	M3 / 3	0,0096	1,017	0,290	2,389	**0,290**	**2,394**	**3,998**	4,044	-2,22	29,3	**29,4**	**29,7**	29,4	**25,0**	2/5000

L16 – 042

level code	L	data	DIAdem	inj. Module	j Gas inj.	j water inj	Vgas inj.	mWater inj.	FIC4-1x	FIC4-0x	PI4-200	PI4-201	PDI4-200	TI4-03	TI4-200	TI4-201	TI4-10	TI4-202	freq
[-]	[mm]	[-]	[-]	[-]	[m/s]	[m/s]	[nm³/h]	[kg/s]	[nm³/h]	[kg/s]	bar	bar	kPa	°C	°C	°C	°C	°C	Hz
A (tomo)	1	26.07.2012	68	M3 / 3	0,0096	1,611	0,290	3,784	**0,290**	**3,780**	**4,002**	4,052	-5,61	29,7	**29,8**	**30,0**	29,9	**23,6**	2/2500
A (tomo)	1	26.07.2012	58	M3 / 3	0,0096	1,611	0,290	3,784	**0,290**	**3,785**	**4,002**	4,051	-5,63	29,6	**29,8**	**29,9**	29,8	**23,7**	1/1000
D (tomo)	62	26.07.2012	70	M3 / 3	0,0096	1,611	0,290	3,784	**0,290**	**3,784**	**4,002**	4,051	-5,63	29,8	**29,9**	**30,1**	30,0	**23,6**	2/2500
D (tomo)	62	26.07.2012	55	M3 / 3	0,0096	1,611	0,290	3,784	**0,290**	**3,784**	**4,001**	4,051	-5,62	29,6	**29,7**	**29,9**	29,8	**23,7**	1/1000
G (tomo)	171	26.07.2012	73	M3 / 3	0,0096	1,611	0,290	3,784	**0,290**	**3,784**	**4,000**	4,051	-5,61	29,8	**29,9**	**30,1**	30,0	**23,6**	2/2500
G (tomo)	171	26.07.2012	53	M3 / 3	0,0096	1,611	0,290	3,784	**0,290**	**3,781**	**3,999**	4,058	-5,62	29,6	**29,7**	**29,9**	29,8	**23,7**	1/1000
J (tomo)	435	26.07.2012	77	M3 / 3	0,0096	1,611	0,290	3,784	**0,290**	**3,785**	**3,999**	4,064	-5,62	29,9	**29,9**	**30,2**	30,0	**23,6**	2/2500
J (tomo)	435	26.07.2012	52	M3 / 3	0,0096	1,611	0,290	3,784	**0,290**	**3,784**	**4,000**	4,052	-5,65	29,6	**29,7**	**29,9**	29,7	**23,7**	1/1000
M (tomo)	1271	26.07.2012	80	M3 / 3	0,0096	1,611	0,290	3,784	**0,290**	**3,783**	**3,998**	4,051	-5,62	29,9	**30,0**	**30,2**	30,1	**23,6**	2/2500
M (tomo)	1271	26.07.2012	50	M3 / 3	0,0096	1,611	0,290	3,784	**0,290**	**3,785**	**4,001**	4,059	-5,64	29,6	**29,7**	**29,9**	29,8	**23,8**	1/1000
P (tomo)	3270	26.07.2012	82	M3 / 3	0,0096	1,611	0,290	3,784	**0,290**	**3,785**	**4,001**	4,050	-5,64	30,0	**30,1**	**30,2**	30,1	**23,6**	2/2500
P (tomo)	3270	26.07.2012	47	M3 / 3	0,0096	1,611	0,290	3,784	**0,290**	**3,785**	**4,002**	4,059	-5,63	29,6	**29,7**	**29,9**	29,7	**23,8**	1/1000
S (wms)	4685	26.07.2012	82	M3 / 3	0,0096	1,611	0,290	3,784	**0,290**	**3,785**	**4,001**	4,050	-5,64	30,0	**30,1**	**30,2**	30,1	**23,6**	2/5000

L16 – 050

level code	L	data	DIAdem	inj. Module	j Gas inj.	j water inj	Vgas inj.	mWater inj.	FIC4-1x	FIC4-0x	PI4-200	PI4-201	PDI4-200	TI4-03	TI4-200	TI4-201	TI4-10	TI4-202	freq
[-]	[mm]	[-]	[-]	[-]	[m/s]	[m/s]	[nm³/h]	[kg/s]	[nm³/h]	[kg/s]	bar	bar	kPa	°C	°C	°C	°C	°C	Hz
A (tomo)	1	19.07.2012	68	M3 / 3	0,0151	0,405	0,456	0,951	**0,456**	**0,951**	**3,999**	4,048	0,58	30,1	**30,2**	**30,3**	30,2	**24,0**	2/2500
A (tomo)	1	19.07.2012	71	M3 / 3	0,0151	0,405	0,456	0,951	**0,456**	**0,951**	**4,002**	4,058	0,57	30,1	**30,2**	**30,3**	30,2	**24,0**	2/1000
D (tomo)	62	19.07.2012	64	M3 / 3	0,0151	0,405	0,456	0,951	**0,456**	**0,951**	**4,000**	4,050	0,57	30,1	**30,2**	**30,4**	30,3	**24,0**	2/2500
D (tomo)	62	19.07.2012	62	M3 / 3	0,0151	0,405	0,456	0,951	**0,456**	**0,951**	**4,003**	4,052	0,60	30,1	**30,2**	**30,4**	30,2	**23,9**	2/1000
G (tomo)	171	19.07.2012	55	M3 / 3	0,0151	0,405	0,456	0,951	**0,456**	**0,951**	**3,999**	4,051	0,59	30,1	**30,2**	**30,4**	30,3	**23,9**	2/2500
G (tomo)	171	19.07.2012	58	M3 / 3	0,0151	0,405	0,456	0,951	**0,456**	**0,951**	**4,000**	4,058	0,58	30,1	**30,2**	**30,4**	30,3	**23,9**	2/1000
J (tomo)	435	19.07.2012	52	M3 / 3	0,0151	0,405	0,456	0,951	**0,456**	**0,951**	**4,001**	4,056	0,59	30,1	**30,2**	**30,4**	30,3	**23,9**	2/2500
J (tomo)	435	19.07.2012	50	M3 / 3	0,0151	0,405	0,456	0,951	**0,456**	**0,951**	**4,003**	4,057	0,57	30,2	**30,2**	**30,4**	30,3	**23,9**	2/1000
M (tomo)	1271	19.07.2012	43	M3 / 3	0,0151	0,405	0,456	0,951	**0,456**	**0,950**	**4,002**	4,054	0,58	30,3	**30,4**	**30,6**	30,5	**23,8**	2/2500
M (tomo)	1271	19.07.2012	46	M3 / 3	0,0151	0,405	0,456	0,951	**0,456**	**0,951**	**4,001**	4,058	0,58	30,2	**30,3**	**30,5**	30,4	**23,8**	2/1000
P (tomo)	3270	19.07.2012	41	M3 / 3	0,0151	0,405	0,456	0,951	**0,456**	**0,951**	**4,002**	4,058	0,58	30,4	**30,5**	**30,6**	30,5	**23,8**	2/2500
P (tomo)	3270	19.07.2012	37	M3 / 3	0,0151	0,405	0,456	0,951	**0,456**	**0,951**	**3,999**	4,052	0,57	30,5	**30,5**	**30,7**	30,4	**23,8**	2/1000
S (wms)	4685	19.07.2012	41	M3 / 3	0,0151	0,405	0,456	0,951	**0,456**	**0,951**	**4,002**	4,058	0,58	30,4	**30,5**	**30,6**	30,5	**23,8**	2/5000

L16 – 052

level code	L	data	DIAdem	inj. Module	j Gas inj.	j water inj	Vgas inj.	mWater inj.	FIC4-1x	FIC4-0x	PI4-200	PI4-201	PDI4-200	TI4-03	TI4-200	TI4-201	TI4-10	TI4-202	freq
[-]	[mm]	[-]	[-]	[-]	[m/s]	[m/s]	[nm³/h]	[kg/s]	[nm³/h]	[kg/s]	bar	bar	kPa	°C	°C	°C	°C	°C	Hz
A (tomo)	1	01.08.2012	2	M3 / 3	0,0151	1,017	0,456	2,389	**0,456**	**2,389**	**4,004**	4,057	-2,05	29,4	**29,5**	**29,8**	29,6	**23,7**	2/2500
A (tomo)	1	01.08.2012	28	M3 / 3	0,0151	1,017	0,456	2,389	**0,456**	**2,390**	**3,999**	4,052	-2,05	30,3	**30,4**	**30,5**	30,4	**23,9**	1/1000
D (tomo)	62	01.08.2012	4	M3 / 3	0,0151	1,017	0,456	2,389	**0,456**	**2,389**	**3,998**	4,050	-2,05	29,5	**29,6**	**29,9**	29,6	**23,7**	2/2500
D (tomo)	62	01.08.2012	25	M3 / 3	0,0151	1,017	0,456	2,389	**0,456**	**2,389**	**4,001**	4,056	-2,04	30,2	**30,3**	**30,5**	30,4	**23,9**	1/1000
G (tomo)	171	01.08.2012	7	M3 / 3	0,0151	1,017	0,456	2,389	**0,456**	**2,389**	**3,998**	4,050	-2,04	29,6	**29,7**	**29,9**	29,7	**23,7**	2/2500
G (tomo)	171	01.08.2012	23	M3 / 3	0,0151	1,017	0,456	2,389	**0,456**	**2,389**	**3,997**	4,051	-2,04	30,1	**30,2**	**30,4**	30,3	**23,8**	1/1000
J (tomo)	435	01.08.2012	9	M3 / 3	0,0151	1,017	0,456	2,389	**0,456**	**2,389**	**4,000**	4,055	-2,05	29,7	**29,7**	**29,9**	29,8	**23,7**	2/2500
J (tomo)	435	01.08.2012	21	M3 / 3	0,0151	1,017	0,456	2,389	**0,456**	**2,390**	**4,002**	4,058	-2,04	30,1	**30,1**	**30,3**	30,2	**23,8**	1/1000
M (tomo)	1271	01.08.2012	11	M3 / 3	0,0151	1,017	0,456	2,389	**0,456**	**2,390**	**4,001**	4,050	-2,04	29,7	**29,8**	**30,0**	29,8	**23,7**	2/2500
M (tomo)	1271	01.08.2012	19	M3 / 3	0,0151	1,017	0,456	2,389	**0,456**	**2,390**	**3,999**	4,052	-2,04	30,0	**30,1**	**30,3**	30,1	**23,8**	1/1000
P (tomo)	3270	01.08.2012	14	M3 / 3	0,0151	1,017	0,456	2,389	**0,456**	**2,389**	**4,002**	4,050	-2,04	29,9	**30,0**	**30,2**	30,0	**23,8**	2/2500
P (tomo)	3270	01.08.2012	17	M3 / 3	0,0151	1,017	0,456	2,389	**0,456**	**2,389**	**4,000**	4,051	-2,04	29,9	**30,0**	**30,2**	30,0	**23,8**	1/1000
S (wms)	4685	01.08.2012	14	M3 / 3	0,0151	1,017	0,456	2,389	**0,456**	**2,389**	**4,002**	4,050	-2,04	29,9	**30,0**	**30,2**	30,0	**23,8**	2/5000

L16 – 067

level code	L	data	DIAdem	inj. Module	j Gas inj.	j water inj	Vgas inj.	mWater inj.	FIC4-1x	FIC4-0x	PI4-200	PI4-201	PDI4-200	TI4-03	TI4-200	TI4-201	TI4-10	TI4-202	freq
[-]	[mm]	[-]	[-]	[-]	[m/s]	[m/s]	[nm³/h]	[kg/s]	[nm³/h]	[kg/s]	bar	bar	kPa	°C	°C	°C	°C	°C	Hz
A (tomo)	5	22.05.2013	5	M3 / 4	0,0368	0,0405	1,112	0,095	**1,112**	**0,095**	**4,004**	4,072	7,12	30,7	**30,5**	**30,6**	29,9	**21,8**	2/1000
D (tomo)	62	22.05.2013	8	M3 / 4	0,0368	0,0405	1,112	0,095	**1,112**	**0,095**	**4,007**	4,073	7,02	30,8	**30,7**	**30,7**	29,9	**21,9**	2/1000
G (tomo)	171	22.05.2013	11	M3 / 4	0,0368	0,0405	1,112	0,095	**1,112**	**0,095**	**4,003**	4,072	7,14	30,8	**30,7**	**30,8**	30,0	**21,9**	2/1000
J (tomo)	435	22.05.2013	17	M3 / 4	0,0368	0,0405	1,112	0,095	**1,112**	**0,095**	**4,002**	4,072	7,06	30,8	**30,9**	**30,9**	30,1	**21,9**	2/1000
M (tomo)	1271	22.05.2013	21	M3 / 4	0,0368	0,0405	1,112	0,095	**1,112**	**0,095**	**3,993**	4,059	7,10	30,5	**30,7**	**30,8**	30,2	**21,8**	2/1000
P (tomo)	3270	22.05.2013	28	M3 / 4	0,0368	0,0405	1,112	0,095	**1,112**	**0,095**	**4,006**	4,072	7,09	30,3	**30,4**	**30,5**	30,2	**21,8**	2/1000
S (wms)	4685	22.05.2013	28	M3 / 4	0,0368	0,0405	1,112	0,095	**1,112**	**0,095**	**4,006**	4,072	7,09	30,3	**30,4**	**30,5**	30,2	**21,8**	2/5000

L16 – 074

level code	L	data	DIAdem	inj. Module	j Gas inj.	j water inj	Vgas inj.	mWater inj.	FIC4-1x	FIC4-0x	PI4-200	PI4-201	PDI4-200	TI4-03	TI4-200	TI4-201	TI4-10	TI4-202	freq
[-]	[mm]	[-]	[-]	[-]	[m/s]	[m/s]	[nm³/h]	[kg/s]	[nm³/h]	[kg/s]	bar	bar	kPa	°C	°C	°C	°C	°C	Hz
A (tomo)	5	23.05.2013	2	M3 / 4	0,0368	1,017	1,112	2,389	**1,112**	**2,390**	**4,006**	4,073	-1,20	29,5	**29,9**	**29,9**	29,7	**21,2**	2/2500
D (tomo)	62	23.05.2013	4	M3 / 4	0,0368	1,017	1,112	2,389	**1,112**	**2,388**	**4,003**	4,072	-1,18	29,5	**29,9**	**30,0**	29,8	**21,1**	2/2500
G (tomo)	171	23.05.2013	6	M3 / 4	0,0368	1,017	1,112	2,389	**1,112**	**2,388**	**4,002**	4,072	-1,20	29,5	**30,0**	**30,0**	29,9	**21,1**	2/2500
J (tomo)	435	23.05.2013	10	M3 / 4	0,0368	1,017	1,112	2,389	**1,112**	**2,391**	**4,005**	4,070	-1,19	29,6	**30,1**	**30,1**	29,9	**21,1**	2/2500
M (tomo)	1271	23.05.2013	14	M3 / 4	0,0368	1,017	1,112	2,389	**1,112**	**2,388**	**4,002**	4,072	-1,19	29,7	**30,1**	**30,1**	30,0	**21,1**	2/2500
P (tomo)	3270	23.05.2013	20	M3 / 4	0,0368	1,017	1,112	2,389	**1,112**	**2,390**	**4,007**	4,072	-1,19	29,8	**30,1**	**30,2**	30,1	**21,1**	2/2500
S (wms)	4685	23.05.2013	20	M3 / 4	0,0368	1,017	1,112	2,389	**1,112**	**2,390**	**4,007**	4,072	-1,19	29,8	**30,1**	**30,2**	30,1	**21,1**	2/2500

L16 – 077

level code	L	data	DIAdem	inj. Module	j Gas inj.	j water inj	Vgas inj.	mWater inj.	FIC4-1x	FIC4-0x	PI4-200	PI4-201	PDI4-200	TI4-03	TI4-200	TI4-201	TI4-10	TI4-202	freq
[-]	[mm]	[-]	[-]	[-]	[m/s]	[m/s]	[nm³/h]	[kg/s]	[nm³/h]	[kg/s]	bar	bar	kPa	°C	°C	°C	°C	°C	Hz
A (tomo)	5	24.05.2013	22	M3 / 3	0,0368	4,047	1,112	9,505	**1,112**	**9,510**	**3,997**	4,065	-29,05	29,9	**30,3**	**30,3**	30,2	**23,3**	2/2500
A (tomo)	5	24.05.2013	26	M3 / 3	0,0368	4,047	1,112	9,505	**1,112**	**9,507**	**4,007**	4,073	-28,97	30,0	**30,4**	**30,5**	30,4	**23,1**	1/5000
D (tomo)	62	24.05.2013	20	M3 / 3	0,0368	4,047	1,112	9,505	**1,112**	**9,513**	**3,995**	4,069	-29,07	29,8	**30,2**	**30,3**	30,1	**23,4**	2/2500
D (tomo)	62	24.05.2013	30	M3 / 3	0,0368	4,047	1,112	9,505	**1,112**	**9,506**	**4,000**	4,072	-28,97	30,3	**30,6**	**30,7**	30,6	**23,1**	1/5000
G (tomo)	171	24.05.2013	17	M3 / 3	0,0368	4,047	1,112	9,505	**1,112**	**9,507**	**4,006**	4,072	-29,27	29,6	**30,1**	**30,1**	30,0	**23,5**	2/2500
G (tomo)	171	24.05.2013	35	M3 / 3	0,0368	4,047	1,112	9,505	**1,112**	**9,500**	**4,002**	4,069	-28,98	30,4	**30,7**	**30,8**	30,7	**23,0**	1/5000
J (tomo)	435	24.05.2013	12	M3 / 3	0,0368	4,047	1,112	9,505	**1,112**	**9,504**	**3,996**	4,066	-29,15	29,5	**29,9**	**30,0**	29,9	**23,7**	2/2500
J (tomo)	435	24.05.2013	40	M3 / 3	0,0368	4,047	1,112	9,505	**1,112**	**9,504**	**3,996**	4,066	-29,09	30,4	**30,8**	**31,0**	30,8	**23,0**	1/5000
M (tomo)	1271	24.05.2013	8	M3 / 3	0,0368	4,047	1,112	9,505	**1,112**	**9,519**	**3,999**	4,066	-29,34	29,3	**29,8**	**29,8**	29,7	**23,9**	2/2500
M (tomo)	1271	24.05.2013	43	M3 / 3	0,0368	4,047	1,112	9,505	**1,112**	**9,505**	**4,002**	4,073	-29,20	30,5	**30,8**	**31,0**	30,9	**22,9**	1/5000
P (tomo)	3270	24.05.2013	4	M3 / 3	0,0368	4,047	1,112	9,505	**1,112**	**9,510**	**3,990**	4,063	-29,33	29,2	**29,6**	**29,7**	29,5	**24,2**	2/2500
P (tomo)	3270	24.05.2013	46	M3 / 3	0,0368	4,047	1,112	9,505	**1,112**	**9,516**	**4,006**	4,072	-29,23	30,4	**30,7**	**30,8**	30,8	**22,8**	1/5000
S (wms)	4685	24.05.2013	-	M3 / 3	0,0368	4,047	1,112	9,505											

L16 – 089

level code	L	data	DIAdem	inj. Module	j Gas inj.	j water inj	Vgas inj.	mWater inj.	FIC4-1x	FIC4-0x	PI4-200	PI4-201	PDI4-200	TI4-03	TI4-200	TI4-201	TI4-10	TI4-202	freq
[-]	[mm]	[-]	[-]	[-]	[m/s]	[m/s]	[nm³/h]	[kg/s]	[nm³/h]	[kg/s]	bar	bar	kPa	°C	°C	°C	°C	°C	Hz
A (tomo)	5	22.05.2013	51	M3 / 4	0,0898	0,0405	2,713	0,095	**2,713**	**0,095**	**4,003**	4,072	14,22	30,7	**30,7**	**30,7**	30,1	**20,7**	2/1000
D (tomo)	62	22.05.2013	48	M3 / 4	0,0898	0,0405	2,713	0,095	**2,713**	**0,095**	**4,010**	4,072	14,23	30,7	**30,7**	**30,7**	30,1	**20,8**	2/1000
G (tomo)	171	22.05.2013	43	M3 / 4	0,0898	0,0405	2,713	0,095	**2,713**	**0,095**	**3,992**	4,064	13,96	30,6	**30,6**	**30,6**	30,1	**20,9**	2/1000
J (tomo)	435	22.05.2013	40	M3 / 4	0,0898	0,0405	2,713	0,095	**2,713**	**0,095**	**4,001**	4,072	13,63	30,5	**30,5**	**30,5**	30,1	**21,0**	2/1000
M (tomo)	1271	22.05.2013	36	M3 / 4	0,0898	0,0405	2,713	0,095	**2,713**	**0,095**	**3,997**	4,066	14,08	30,5	**30,5**	**30,5**	30,1	**21,2**	2/1000
P (tomo)	3270	22.05.2013	32	M3 / 4	0,0898	0,0405	2,713	0,095	**2,713**	**0,095**	**3,988**	4,060	13,64	30,4	**30,4**	**30,4**	30,2	**21,4**	2/1000
S (wms)	4685	22.05.2013	32	M3 / 4	0,0898	0,0405	2,713	0,095	**2,713**	**0,095**	**3,988**	4,060	13,64	30,4	**30,4**	**30,4**	30,2	**21,4**	2/5000

L16 – 096

level code	L	data	DIAdem	inj. Module	j Gas inj.	j water inj	Vgas inj.	mWater inj.	FIC4-1x	FIC4-0x	PI4-200	PI4-201	PDI4-200	TI4-03	TI4-200	TI4-201	TI4-10	TI4-202	freq
[-]	[mm]	[-]	[-]	[-]	[m/s]	[m/s]	[nm³/h]	[kg/s]	[nm³/h]	[kg/s]	bar	bar	kPa	°C	°C	°C	°C	°C	Hz
A (tomo)	5	23.05.2013	42	M3 / 4	0,0898	1,017	2,713	2,389	**2,714**	**2,388**	**4,002**	4,065	0,41	30,0	**30,4**	**30,4**	30,3	**20,2**	2/2500
D (tomo)	62	23.05.2013	38	M3 / 4	0,0898	1,017	2,713	2,389	**2,714**	**2,388**	**3,997**	4,063	0,37	29,9	**30,3**	**30,4**	30,2	**20,2**	2/2500
G (tomo)	171	23.05.2013	34	M3 / 4	0,0898	1,017	2,713	2,389	**2,714**	**2,392**	**4,007**	4,072	0,37	29,9	**30,4**	**30,3**	30,2	**20,3**	2/2500
J (tomo)	435	23.05.2013	29	M3 / 4	0,0898	1,017	2,713	2,389	**2,714**	**2,391**	**4,008**	4,072	0,38	29,9	**30,3**	**30,3**	30,2	**20,5**	2/2500
M (tomo)	1271	23.05.2013	25	M3 / 4	0,0898	1,017	2,713	2,389	**2,714**	**2,387**	**4,004**	4,073	0,37	29,8	**30,2**	**30,2**	30,1	**20,7**	2/2500
P (tomo)	3270	23.05.2013	23	M3 / 4	0,0898	1,017	2,713	2,389	**2,714**	**2,389**	**4,000**	4,072	0,37	29,8	**30,1**	**30,2**	30,0	**20,9**	2/2500
S (wms)	4685	23.05.2013	23	M3 / 4	0,0898	1,017	2,713	2,389	**2,714**	**2,389**	**4,000**	4,072	0,37	29,8	**30,1**	**30,2**	30,0	**20,9**	2/2500

L16 – 099

level code	L	data	DIAdem	inj. Module	j Gas inj.	j water inj	Vgas inj.	mWater inj.	FIC4-1x	FIC4-0x	PI4-200	PI4-201	PDI4-200	TI4-03	TI4-200	TI4-201	TI4-10	TI4-202	freq
[-]	[mm]	[-]	[-]	[-]	[m/s]	[m/s]	[nm³/h]	[kg/s]	[nm³/h]	[kg/s]	bar	bar	kPa	°C	°C	°C	°C	°C	Hz
A (tomo)	5	24.05.2013	73	M3 / 3	0,0898	4,047	2,713	9,505	**2,713**	**9,502**	**4,010**	4,081	-29,23	29,4	**29,9**	**29,9**	29,8	**22,4**	2/2500
A (tomo)	5	24.05.2013	69	M3 / 3	0,0898	4,047	2,713	9,505	**2,713**	**9,513**	**3,998**	4,070	-29,40	29,5	**29,9**	**30,0**	29,9	**22,4**	1/5000
D (tomo)	62	24.05.2013	4	M3 / 3	0,0898	4,047	2,713	9,505	**2,713**	**9,497**	**4,010**	4,084	-29,27	29,3	**29,8**	**29,8**	29,7	**21,0**	2/2500
D (tomo)	62	24.05.2013	66	M3 / 3	0,0898	4,047	2,713	9,505	**2,713**	**9,507**	**3,998**	4,065	-29,25	29,6	**30,1**	**30,1**	30,0	**22,5**	1/5000
G (tomo)	171	24.05.2013	6	M3 / 3	0,0898	4,047	2,713	9,505	**2,713**	**9,503**	**3,992**	4,064	-29,19	29,4	**29,9**	**29,9**	29,8	**21,0**	2/2500
G (tomo)	171	24.05.2013	60	M3 / 3	0,0898	4,047	2,713	9,505	**2,713**	**9,507**	**4,004**	4,073	-29,17	29,7	**30,1**	**30,2**	30,1	**22,5**	1/5000
J (tomo)	435	24.05.2013	10	M3 / 3	0,0898	4,047	2,713	9,505	**2,713**	**9,506**	**3,995**	4,066	-29,21	29,5	**30,0**	**30,0**	29,9	**21,1**	2/2500
J (tomo)	435	24.05.2013	58	M3 / 3	0,0898	4,047	2,713	9,505	**2,713**	**9,498**	**4,000**	4,063	-29,15	29,8	**30,2**	**30,2**	30,1	**22,6**	1/5000
M (tomo)	1271	24.05.2013	14	M3 / 3	0,0898	4,047	2,713	9,505	**2,713**	**9,487**	**4,004**	4,072	-29,06	29,7	**30,2**	**30,2**	30,1	**21,1**	2/2500
M (tomo)	1271	24.05.2013	55	M3 / 3	0,0898	4,047	2,713	9,505	**2,713**	**9,499**	**4,011**	4,077	-29,22	29,9	**30,3**	**30,3**	30,2	**22,7**	1/5000
P (tomo)	3270	24.05.2013	17	M3 / 3	0,0898	4,047	2,713	9,505	**2,713**	**9,503**	**3,992**	4,062	-29,14	29,9	**30,3**	**30,3**	30,3	**21,2**	2/2500
P (tomo)	3270	24.05.2013	49	M3 / 3	0,0898	4,047	2,713	9,505	**2,713**	**9,510**	**3,999**	4,069	-29,21	30,1	**30,4**	**30,5**	30,5	**23,0**	1/5000
S (wms)	4685	24.05.2013	-	M3 / 3	0,0898	4,047	2,713	9,505											

L17 – 001

level code	L	data	DIAdem	inj. Module	j Gas inj.	j water inj	Vgas inj.	mWater inj.	FIC4-1x	FIC4-0x	j w inj. meas.	PI4-200	PI4-201	PDI4-200	TI4-03	TI4-200	TI4-201	TI4-10	TI4-202	j w inj. meas. corr
[-]	[mm]	[-]	[-]	[-]	[m/s]	[m/s]	[nm³/h]	[kg/s]	[nm³/h]	[kg/s]	m/s	bar	bar	kPa	°C	°C	°C	°C	°C	m/s
A (tomo)	1	20.07.2012	3	M3 / 1	0,0025	0,0405	0,076	0,095	**0,076**	**0,077**	**0,0327**	**4,003**	4,051	0,60	30,0	**29,3**	**29,6**	29,3	**24,8**	**0,0352**
D (tomo)	62	20.07.2012	5	M3 / 1	0,0025	0,0405	0,076	0,095	**0,076**	**0,077**	**0,0327**	**4,003**	4,057	0,59	30,1	**29,2**	**29,5**	29,2	**24,6**	**0,0352**
G (tomo)	171	20.07.2012	7	M3 / 1	0,0025	0,0405	0,076	0,095	**0,076**	**0,077**	**0,0327**	**4,003**	4,058	0,59	30,3	**29,2**	**29,5**	29,2	**24,5**	**0,0352**
J (tomo)	435	20.07.2012	11	M3 / 1	0,0025	0,0405	0,076	0,095	**0,076**	**0,077**	**0,0327**	**4,003**	4,051	0,59	30,4	**29,1**	**29,4**	29,2	**24,5**	**0,0352**
M (tomo)	1271	20.07.2012	14	M3 / 1	0,0025	0,0405	0,076	0,095	**0,076**	**0,077**	**0,0327**	**4,002**	4,051	0,60	30,6	**29,1**	**29,5**	29,1	**24,3**	**0,0352**
P (tomo)	3270	20.07.2012	22	M3 / 1	0,0025	0,0405	0,076	0,095	**0,076**	**0,077**	**0,0327**	**3,999**	4,057	0,70	30,8	**29,2**	**29,5**	29,1	**24,3**	**0,0352**
S (wms)	4685	20.07.2012	22	M3 / 1	0,0025	0,0405	0,076	0,095	**0,076**	**0,077**	**0,0327**	**3,999**	4,057	0,70	30,8	**29,2**	**29,5**	29,1	**24,3**	**0,0352**

rho * Aq	**2,34864**
FIC4-03 zero point correction	

L17 – 002

level code	L	data	DIAdem	inj. Module	j Gas inj.	j water inj	Vgas inj.	mWater inj.	FIC4-1x	FIC4-0x	j w inj. meas.	PI4-200	PI4-201	PDI4-200	TI4-03	TI4-200	TI4-201	TI4-10	TI4-202	j w inj. meas. corr
[-]	[mm]	[-]	[-]	[-]	[m/s]	[m/s]	[nm³/h]	[kg/s]	[nm³/h]	[kg/s]	m/s	bar	bar	kPa	°C	°C	°C	°C	°C	m/s
A (tomo)	1	20.07.2012	38	M3 / 1	0,0025	0,0641	0,076	0,151	**0,076**	**0,135**	**0,0576**	**3,999**	4,051	0,66	30,8	**30,2**	**30,5**	30,1	**24,3**	**0,0601**
D (tomo)	62	20.07.2012	35	M3 / 1	0,0025	0,0641	0,076	0,151	**0,076**	**0,135**	**0,0577**	**4,001**	4,058	0,66	30,9	**30,1**	**30,4**	29,9	**24,3**	**0,0602**
G (tomo)	171	20.07.2012	33	M3 / 1	0,0025	0,0641	0,076	0,151	**0,076**	**0,135**	**0,0576**	**4,002**	4,051	0,66	30,9	**29,9**	**30,2**	29,7	**24,3**	**0,0601**
J (tomo)	435	20.07.2012	31	M3 / 1	0,0025	0,0641	0,076	0,151	**0,076**	**0,135**	**0,0576**	**4,000**	4,057	0,66	30,9	**29,8**	**30,0**	29,5	**24,4**	**0,0601**
M (tomo)	1271	20.07.2012	28	M3 / 1	0,0025	0,0641	0,076	0,151	**0,076**	**0,135**	**0,0576**	**4,000**	4,054	0,66	31,0	**29,6**	**29,9**	29,4	**24,4**	**0,0601**
P (tomo)	3270	20.07.2012	26	M3 / 1	0,0025	0,0641	0,076	0,151	**0,076**	**0,135**	**0,0577**	**4,002**	4,059	0,66	31,0	**29,4**	**29,8**	29,2	**24,5**	**0,0602**
S (wms)	4685	20.07.2012	26	M3 / 1	0,0025	0,0641	0,076	0,151	**0,076**	**0,135**	**0,0577**	**4,002**	4,059	0,66	31,0	**29,4**	**29,8**	29,2	**24,5**	**0,0602**

rho * Aq **2,34864**
FIC4-03 zero point correction

L17 – 003

level code	L	data	DIAdem	inj. Module	j Gas inj.	j water inj	Vgas inj.	mWater inj.	FIC4-1x	FIC4-0x	j w inj. meas.	PI4-200	PI4-201	PDI4-200	TI4-03	TI4-200	TI4-201	TI4-10	TI4-202	j w inj. meas. corr
[-]	[mm]	[-]	[-]	[-]	[m/s]	[m/s]	[nm³/h]	[kg/s]	[nm³/h]	[kg/s]	m/s	bar	bar	kPa	°C	°C	°C	°C	°C	m/s
A (tomo)	1	20.07.2012	41	M3 / 1	0,0025	0,102	0,076	0,240	**0,076**	**0,228**	**0,0972**	**4,003**	4,058	0,86	30,8	**30,2**	**30,5**	30,1	**24,3**	**0,0997**
D (tomo)	62	20.07.2012	44	M3 / 1	0,0025	0,102	0,076	0,240	**0,076**	**0,228**	**0,0971**	**4,001**	4,051	0,84	30,8	**30,4**	**30,6**	30,3	**24,2**	**0,0996**
G (tomo)	171	20.07.2012	47	M3 / 1	0,0025	0,102	0,076	0,240	**0,076**	**0,229**	**0,0973**	**4,002**	4,052	0,85	30,8	**30,5**	**30,8**	30,5	**24,2**	**0,0998**
J (tomo)	435	20.07.2012	51	M3 / 1	0,0025	0,102	0,076	0,240	**0,076**	**0,228**	**0,0971**	**4,000**	4,051	0,85	30,8	**30,6**	**30,8**	30,5	**24,2**	**0,0996**
M (tomo)	1271	20.07.2012	53	M3 / 1	0,0025	0,102	0,076	0,240	**0,076**	**0,228**	**0,0973**	**4,002**	4,059	0,84	30,9	**30,6**	**30,8**	30,6	**24,2**	**0,0998**
P (tomo)	3270	20.07.2012	57	M3 / 1	0,0025	0,102	0,076	0,240	**0,076**	**0,228**	**0,0971**	**4,003**	4,057	0,84	30,9	**30,6**	**30,9**	30,7	**24,2**	**0,0996**
S (wms)	4685	20.07.2012	58	M3 / 1	0,0025	0,102	0,076	0,240	**0,076**	**0,229**	**0,0976**	**4,002**	4,057	0,83	30,9	**30,6**	**30,9**	30,7	**24,2**	**0,1001**

rho * Aq **2,34864**
FIC4-03 zero point correction

L17 – 034

level code	L	data	DIAdem	inj. Module	j Gas inj.	j water inj	Vgas inj.	mWater inj.	FIC4-1x	FIC4-0x	j w inj. meas.	PI4-200	PI4-201	PDI4-200	TI4-03	TI4-200	TI4-201	TI4-10	TI4-202	j w inj. meas. corr
[-]	[mm]	[-]	[-]	[-]	[m/s]	[m/s]	[nm³/h]	[kg/s]	[nm³/h]	[kg/s]	m/s	bar	bar	kPa	°C	°C	°C	°C	°C	m/s
A (tomo)	1	23.07.2012	23	M3 / 3	0,0096	0,0405	0,290	0,095	**0,290**	**0,077**	**0,0326**	**3,996**	4,045	2,48	29,5	**29,4**	**29,7**	29,5	**23,5**	**0,0422**
D (tomo)	62	23.07.2012	16	M3 / 3	0,0096	0,0405	0,290	0,095	**0,290**	**0,077**	**0,0327**	**4,001**	4,051	2,52	29,6	**29,1**	**29,4**	29,1	**23,4**	**0,0423**
G (tomo)	171	23.07.2012	14	M3 / 3	0,0096	0,0405	0,290	0,095	**0,290**	**0,077**	**0,0326**	**4,003**	4,051	2,60	29,6	**29,1**	**29,4**	29,1	**23,4**	**0,0422**
J (tomo)	435	23.07.2012	12	M3 / 3	0,0096	0,0405	0,290	0,095	**0,290**	**0,076**	**0,0324**	**4,002**	4,056	2,46	29,5	**29,1**	**29,4**	29,1	**23,4**	**0,0420**
M (tomo)	1271	23.07.2012	6	M3 / 3	0,0096	0,0405	0,290	0,095	**0,290**	**0,077**	**0,0327**	**4,001**	4,055	2,52	29,4	**29,1**	**29,4**	29,0	**23,4**	**0,0423**
P (tomo)	3270	23.07.2012	3	M3 / 3	0,0096	0,0405	0,290	0,095	**0,290**	**0,077**	**0,0327**	**4,001**	4,056	2,49	29,2	**29,1**	**29,5**	29,0	**23,3**	**0,0423**
S (wms)	4685	23.07.2012	3	M3 / 3	0,0096	0,0405	0,290	0,095	**0,290**	**0,077**	**0,0327**	**4,001**	4,056	2,49	29,2	**29,1**	**29,5**	29,0	**23,3**	**0,0423**

rho * Aq **2,34864**
FIC4-03 zero point correction

L17 – 035

level code	L	data	DIAdem	inj. Module	j Gas inj.	j water inj	Vgas inj.	mWater inj.	FIC4-1x	FIC4-0x	j w inj. meas.	PI4-200	PI4-201	PDI4-200	TI4-03	TI4-200	TI4-201	TI4-10	TI4-202	j w inj. meas. corr
[-]	[mm]	[-]	[-]	[-]	[m/s]	[m/s]	[nm³/h]	[kg/s]	[nm³/h]	[kg/s]	m/s	bar	bar	kPa	°C	°C	°C	°C	°C	m/s
A (tomo)	1	23.07.2012	26	M3 / 3	0,0096	0,0641	0,290	0,151	**0,290**	**0,136**	**0,0577**	**3,998**	4,051	3,49	29,4	**29,3**	**29,5**	29,0	**23,7**	**0,0673**
D (tomo)	62	23.07.2012	29	M3 / 3	0,0096	0,0641	0,290	0,151	**0,290**	**0,135**	**0,0577**	**4,000**	4,039	3,09	29,7	**29,2**	**29,6**	29,3	**23,7**	**0,0673**
G (tomo)	171	23.07.2012	32	M3 / 3	0,0096	0,0641	0,290	0,151	**0,290**	**0,135**	**0,0576**	**3,990**	4,043	3,14	29,9	**29,2**	**29,5**	29,2	**23,7**	**0,0672**
J (tomo)	435	23.07.2012	36	M3 / 3	0,0096	0,0641	0,290	0,151	**0,290**	**0,135**	**0,0576**	**3,996**	4,041	3,01	30,0	**29,2**	**29,5**	29,2	**23,7**	**0,0672**
M (tomo)	1271	23.07.2012	38	M3 / 3	0,0096	0,0641	0,290	0,151	**0,290**	**0,136**	**0,0577**	**4,001**	4,052	3,06	30,0	**29,1**	**29,5**	29,2	**23,7**	**0,0673**
P (tomo)	3270	23.07.2012	40	M3 / 3	0,0096	0,0641	0,290	0,151	**0,290**	**0,134**	**0,0571**	**3,999**	4,049	2,95	30,1	**29,3**	**29,6**	29,2	**23,7**	**0,0667**
S (wms)	4685	23.07.2012	40	M3 / 3	0,0096	0,0641	0,290	0,151	**0,290**	**0,134**	**0,0571**	**3,999**	4,049	2,95	30,1	**29,3**	**29,6**	29,2	**23,7**	**0,0667**

rho * Aq **2,34864**
FIC4-03 zero point correction

L17 – 036

level code	L	data	DIAdem	inj. Module	j Gas inj.	j water inj	Vgas inj.	mWater inj.	FIC4-1x	FIC4-0x	j w inj. meas.	PI4-200	PI4-201	PDI4-200	TI4-03	TI4-200	TI4-201	TI4-10	TI4-202	j w inj. meas. corr
[-]	[mm]	[-]	[-]	[-]	[m/s]	[m/s]	[nm³/h]	[kg/s]	[nm³/h]	[kg/s]	m/s	bar	bar	kPa	°C	°C	°C	°C	°C	m/s
A (tomo)	1	23.07.2012	61	M3 / 3	0,0096	0,1020	0,290	0,240	**0,290**	**0,228**	**0,0971**	**4,001**	4,051	4,84	30,4	**30,0**	**30,2**	30,0	**23,8**	**0,1067**
D (tomo)	62	23.07.2012	58	M3 / 3	0,0096	0,1020	0,290	0,240	**0,290**	**0,228**	**0,0972**	**4,001**	4,051	4,80	30,4	**30,0**	**30,2**	29,9	**23,8**	**0,1068**
G (tomo)	171	23.07.2012	49	M3 / 3	0,0096	0,1020	0,290	0,240	**0,290**	**0,228**	**0,0972**	**4,003**	4,052	4,98	30,3	**29,8**	**30,0**	29,6	**23,8**	**0,1068**
J (tomo)	435	23.07.2012	47	M3 / 3	0,0096	0,1020	0,290	0,240	**0,290**	**0,227**	**0,0968**	**3,998**	4,052	4,40	30,3	**29,7**	**30,0**	29,6	**23,7**	**0,1064**
M (tomo)	1271	23.07.2012	45	M3 / 3	0,0096	0,1020	0,290	0,240	**0,290**	**0,228**	**0,0971**	**4,001**	4,052	5,01	30,2	**29,6**	**29,9**	29,5	**23,7**	**0,1067**
P (tomo)	3270	23.07.2012	43	M3 / 3	0,0096	0,1020	0,290	0,240	**0,290**	**0,229**	**0,0973**	**3,995**	4,038	4,37	30,2	**29,4**	**29,8**	29,3	**23,7**	**0,1069**
S (wms)	4685	23.07.2012	43	M3 / 3	0,0096	0,1020	0,290	0,240	**0,290**	**0,229**	**0,0973**	**3,995**	4,038	4,37	30,2	**29,4**	**29,8**	29,3	**23,7**	**0,1069**

rho * Aq **2,34864**
FIC4-03 zero point correction

L18 – 111

level code	L	data	DIAdem	inj. Module	j Gas inj.	j water inj	Vgas inj.	mWater inj.	FIC4-1x	FIC4-0x	PI4-200	PI4-201	PDI4-200	TI4-03	TI4-200	TI4-201	TI4-10	TI4-202	freq
[-]	[mm]	[-]	[-]	[-]	[m/s]	[m/s]	[nm³/h]	[kg/s]	[nm³/h]	[kg/s]	bar	bar	kPa	°C	°C	°C	°C	°C	Hz
A (tomo)	18	28.05.2013	9	M4 / 6	0,2190	0,0405	6,616	0,095	**6,616**	**0,095**	**3,987**	4,064	23,42	29,6	**29,6**	**29,4**	28,7	**20,8**	2/1000
D (tomo)	62	28.05.2013	12	M4 / 6	0,2190	0,0405	6,616	0,095	**6,618**	**0,095**	**4,006**	4,081	23,38	29,6	**29,6**	**29,4**	28,8	**20,8**	2/1000
G (tomo)	171	28.05.2013	16	M4 / 6	0,2190	0,0405	6,616	0,095	**6,616**	**0,095**	**3,997**	4,070	23,62	29,7	**29,8**	**29,5**	28,8	**20,8**	2/1000
J (tomo)	435	28.05.2013	23	M4 / 6	0,2190	0,0405	6,616	0,095	**6,613**	**0,095**	**4,005**	4,079	23,56	29,8	**29,8**	**29,6**	28,8	**20,8**	2/1000
M (tomo)	1271	28.05.2013	27	M4 / 6	0,2190	0,0405	6,616	0,095	**6,615**	**0,095**	**3,991**	4,065	23,83	29,8	**29,9**	**29,6**	28,9	**20,8**	2/1000
P (tomo)	3205	28.05.2013	32	M4 / 6	0,2190	0,0405	6,616	0,095	**6,617**	**0,095**	**3,999**	4,070	23,15	29,9	**30,0**	**29,7**	29,0	**20,8**	2/1000
S (wms)	4685	28.05.2013	32	M4 / 6	0,2190	0,0405	6,616	0,095	**6,617**	**0,095**	**3,999**	4,070	23,15	29,9	**30,0**	**29,7**	29,0	**20,8**	2/5000

L18 – 114

level code	L	data	DIAdem	inj. Module	j Gas inj.	j water inj	Vgas inj.	mWater inj.	FIC4-1x	FIC4-0x	PI4-200	PI4-201	PDI4-200	TI4-03	TI4-200	TI4-201	TI4-10	TI4-202	freq
[-]	[mm]	[-]	[-]	[-]	[m/s]	[m/s]	[nm³/h]	[kg/s]	[nm³/h]	[kg/s]	bar	bar	kPa	°C	°C	°C	°C	°C	Hz
A (tomo)	18	28.05.2013	53	M4 / 6	0,2190	0,161	6,616	0,378	**6,617**	**0,378**	**4,005**	4,076	18,57	30,2	**30,5**	**30,5**	30,2	**20,6**	2/1000
D (tomo)	62	28.05.2013	47	M4 / 6	0,2190	0,161	6,616	0,378	**6,614**	**0,378**	**3,998**	4,071	18,48	30,0	**30,4**	**30,4**	30,1	**20,7**	2/1000
G (tomo)	171	28.05.2013	45	M4 / 6	0,2190	0,161	6,616	0,378	**6,452**	**0,377**	**3,995**	4,068	18,40	30,0	**30,4**	**30,3**	30,1	**20,7**	2/1000
G_2 (tomo)	171	29.05.2013	6	M4 / 6	0,2190	0,161	6,616	0,378	**6,606**	**0,378**	**3,997**	4,068	19,00	30,1	**30,4**	**30,4**	30,0	**20,8**	2/1000
J (tomo)	435	28.05.2013	40	M4 / 6	0,2190	0,161	6,616	0,378	**6,615**	**0,377**	**4,007**	4,082	18,54	30,0	**30,4**	**30,4**	30,1	**20,7**	2/1000
M (tomo)	1271	28.05.2013	38	M4 / 6	0,2190	0,161	6,616	0,378	**6,616**	**0,378**	**4,002**	4,074	18,51	30,1	**30,4**	**30,4**	29,8	**20,7**	2/1000
P (tomo)	3205	28.05.2013	36	M4 / 6	0,2190	0,161	6,616	0,378	**6,617**	**0,377**	**4,005**	4,077	18,48	30,0	**30,3**	**30,2**	29,1	**20,8**	2/1000
S (wms)	4685	28.05.2013	36	M4 / 6	0,2190	0,161	6,616	0,378	**6,617**	**0,377**	**4,005**	4,077	18,48	30,0	**30,3**	**30,2**	29,1	**20,8**	2/5000

L18 – 116

level code	L	data	DIAdem	inj. Module	j Gas inj.	j water inj	Vgas inj.	mWater inj.	FIC4-1x	FIC4-0x	PI4-200	PI4-201	PDI4-200	TI4-03	TI4-200	TI4-201	TI4-10	TI4-202	freq
[-]	[mm]	[-]	[-]	[-]	[m/s]	[m/s]	[nm³/h]	[kg/s]	[nm³/h]	[kg/s]	bar	bar	kPa	°C	°C	°C	°C	°C	Hz
A (tomo)	18	28.05.2013	57	M4 / 6	0,2190	0,405	6,616	0,951	**6,615**	**0,951**	**3,998**	4,073	11,51	30,0	**30,5**	**30,5**	30,5	**20,5**	2/1000
D (tomo)	62	28.05.2013	61	M4 / 6	0,2190	0,405	6,616	0,951	**6,616**	**0,953**	**4,002**	4,071	11,36	29,8	**30,3**	**30,3**	30,3	**20,6**	2/1000
G (tomo)	171	28.05.2013	63	M4 / 6	0,2190	0,405	6,616	0,951	**6,615**	**0,950**	**4,001**	4,068	11,49	29,6	**30,0**	**30,0**	30,0	**20,5**	2/1000
J (tomo)	435	28.05.2013	66	M4 / 6	0,2190	0,405	6,616	0,951	**6,617**	**0,947**	**4,003**	4,072	11,60	29,7	**30,2**	**30,1**	30,0	**20,5**	2/1000
M (tomo)	1271	28.05.2013	68	M4 / 6	0,2190	0,405	6,616	0,951	**6,613**	**0,938**	**4,005**	4,073	11,75	29,8	**30,2**	**30,2**	30,1	**20,4**	2/1000
P (tomo)	3205	28.05.2013	74	M4 / 6	0,2190	0,405	6,616	0,951	**6,615**	**0,948**	**3,998**	4,072	11,42	30,0	**30,4**	**30,3**	30,2	**20,4**	2/1000
S (wms)	4685	28.05.2013	74	M4 / 6	0,2190	0,405	6,616	0,951	**6,615**	**0,948**	**3,998**	4,072	11,42	30,0	**30,4**	**30,3**	30,2	**20,4**	2/5000

L18 – 118

level code	L	data	DIAdem	inj. Module	j Gas inj.	j water inj	Vgas inj.	mWater inj.	FIC4-1x	FIC4-0x	PI4-200	PI4-201	PDI4-200	TI4-03	TI4-200	TI4-201	TI4-10	TI4-202	freq
[-]	[mm]	[-]	[-]	[-]	[m/s]	[m/s]	[nm³/h]	[kg/s]	[nm³/h]	[kg/s]	bar	bar	kPa	°C	°C	°C	°C	°C	Hz
A (tomo)	18	31.05.2013	4	M4 / 6	0,2190	1,017	6,616	2,389	**6,618**	**2,387**	**3,998**	4,072	3,26	28,9	**29,3**	**29,3**	29,2	**20,6**	2/2500
D (tomo)	62	31.05.2013	8	M4 / 6	0,2190	1,017	6,616	2,389	**6,617**	**2,390**	**4,000**	4,064	3,28	28,9	**29,4**	**29,4**	29,2	**20,5**	2/2500
G (tomo)	171	31.05.2013	10	M4 / 6	0,2190	1,017	6,616	2,389	**6,619**	**2,387**	**3,999**	4,069	3,25	29,0	**29,5**	**29,5**	29,3	**20,2**	2/2500
J (tomo)	435	31.05.2013	13	M4 / 6	0,2190	1,017	6,616	2,389	**6,618**	**2,388**	**4,000**	4,069	3,28	29,1	**29,5**	**29,5**	29,4	**20,2**	2/2500
M (tomo)	1271	31.05.2013	15	M4 / 6	0,2190	1,017	6,616	2,389	**6,618**	**2,389**	**3,999**	4,067	3,20	29,1	**29,6**	**29,6**	29,5	**20,1**	2/2500
P (tomo)	3205	31.05.2013	18	M4 / 6	0,2190	1,017	6,616	2,389	**6,621**	**2,390**	**4,002**	4,066	3,27	29,2	**29,7**	**29,7**	29,5	**20,0**	2/2500
S (wms)	4685	31.05.2013	18	M4 / 6	0,2190	1,017	6,616	2,389	**6,621**	**2,390**	**4,002**	4,066	3,27	29,2	**29,7**	**29,7**	29,5	**20,0**	2/5000

L18 – 119

level code	L	data	DIAdem	inj. Module	j Gas inj.	j water inj	Vgas inj.	mWater inj.	FIC4-1x	FIC4-0x	PI4-200	PI4-201	PDI4-200	TI4-03	TI4-200	TI4-201	TI4-10	TI4-202	freq
[-]	[mm]	[-]	[-]	[-]	[m/s]	[m/s]	[nm³/h]	[kg/s]	[nm³/h]	[kg/s]	bar	bar	kPa	°C	°C	°C	°C	°C	Hz
A (tomo)	18	31.05.2013	57	M4 / 6	0,2190	1,611	6,616	3,784	**6,619**	**3,781**	**3,999**	4,071	-3,65	29,8	**30,3**	**30,3**	30,2	**19,7**	2/2500
D (tomo)	62	31.05.2013	54	M4 / 6	0,2190	1,611	6,616	3,784	**6,617**	**3,781**	**4,003**	4,076	-3,67	29,8	**30,2**	**30,2**	30,1	**19,7**	2/2500
G (tomo)	171	31.05.2013	45	M4 / 6	0,2190	1,611	6,616	3,784	**6,618**	**3,784**	**3,999**	4,065	-3,68	29,6	**30,1**	**30,1**	29,9	**19,7**	2/2500
J (tomo)	435	31.05.2013	39	M4 / 6	0,2190	1,611	6,616	3,784	**6,617**	**3,781**	**4,005**	4,081	-3,71	29,5	**30,0**	**30,0**	29,8	**19,8**	2/2500
M (tomo)	1271	31.05.2013	23	M4 / 6	0,2190	1,611	6,616	3,784	**6,617**	**3,785**	**4,005**	4,072	-3,69	29,3	**29,8**	**29,8**	29,7	**19,9**	2/2500
P (tomo)	3205	31.05.2013	21	M4 / 6	0,2190	1,611	6,616	3,784	**6,617**	**3,788**	**3,998**	4,071	-3,75	29,3	**29,8**	**29,8**	29,6	**19,9**	2/2500
S (wms)	4685	31.05.2013	21	M4 / 6	0,2190	1,611	6,616	3,784	**6,617**	**3,788**	**3,998**	4,071	-3,75	29,3	**29,8**	**29,8**	29,6	**19,9**	2/5000

L18 – 120

level code	L	data	DIAdem	inj. Module	j Gas inj.	j water inj	Vgas inj.	mWater inj.	FIC4-1x	FIC4-0x	PI4-200	PI4-201	PDI4-200	TI4-03	TI4-200	TI4-201	TI4-10	TI4-202	freq
[-]	[mm]	[-]	[-]	[-]	[m/s]	[m/s]	[nm³/h]	[kg/s]	[nm³/h]	[kg/s]	bar	bar	kPa	°C	°C	°C	°C	°C	Hz
A (tomo)	5	03.06.2013	3	M4 / 6	0,2190	2,554	6,616	5,998	**6,615**	**5,992**	**4,002**	4,081	-16,27	28,5	**29,0**	**29,0**	28,9	**19,8**	2/2500
A (tomo)	5	03.06.2013	33	M4 / 6	0,2190	2,554	6,616	5,998	**6,615**	**5,998**	**3,997**	4,065	-16,34	28,9	**29,4**	**29,5**	29,3	**19,1**	1/5000
D (tomo)	62	03.06.2013	5	M4 / 6	0,2190	2,554	6,616	5,998	**6,617**	**6,006**	**4,008**	4,081	-16,41	28,5	**29,0**	**29,1**	28,9	**19,7**	2/2500
D (tomo)	62	03.06.2013	31	M4 / 6	0,2190	2,554	6,616	5,998	**6,616**	**6,005**	**4,000**	4,069	-16,32	28,9	**29,3**	**29,4**	29,3	**19,2**	1/5000
G (tomo)	171	03.06.2013	9	M4 / 6	0,2190	2,554	6,616	5,998	**6,615**	**5,999**	**4,004**	4,076	-16,43	28,6	**29,0**	**29,1**	29,0	**19,7**	2/2500
G (tomo)	171	03.06.2013	29	M4 / 6	0,2190	2,554	6,616	5,998	**6,614**	**5,999**	**3,996**	4,064	-16,34	28,8	**29,3**	**29,4**	29,2	**19,1**	1/5000
J (tomo)	435	03.06.2013	13	M4 / 6	0,2190	2,554	6,616	5,998	**6,616**	**5,998**	**4,002**	4,077	-16,38	28,6	**29,1**	**29,2**	29,0	**19,6**	2/2500
J (tomo)	435	03.06.2013	27	M4 / 6	0,2190	2,554	6,616	5,998	**6,616**	**5,997**	**3,997**	4,067	-16,29	28,8	**29,3**	**29,4**	29,2	**19,2**	1/5000
M (tomo)	1271	03.06.2013	15	M4 / 6	0,2190	2,554	6,616	5,998	**6,616**	**5,994**	**4,001**	4,070	-16,35	28,7	**29,2**	**29,2**	29,1	**19,6**	2/2500
M (tomo)	1271	03.06.2013	25	M4 / 6	0,2190	2,554	6,616	5,998	**6,615**	**6,004**	**4,005**	4,077	-16,31	28,8	**29,3**	**29,4**	29,2	**19,2**	1/5000
P (tomo)	3270	03.06.2013	18	M4 / 6	0,2190	2,554	6,616	5,998	**6,621**	**5,994**	**4,000**	4,071	-16,36	28,7	**29,2**	**29,2**	29,1	**19,4**	2/2500
P (tomo)	3270	03.06.2013	22	M4 / 6	0,2190	2,554	6,616	5,998	**6,615**	**5,994**	**4,003**	4,075	-16,34	28,7	**29,2**	**29,2**	29,1	**19,2**	1/5000
S (wms)	4685	03.06.2013	18	M4 / 6	0,2190	2,554	6,616	5,998	**6,621**	**5,994**	**4,000**	4,071	-16,36	28,7	**29,2**	**29,2**	29,1	**19,4**	2/5000

L18 – 121

level code	L	data	DIAdem	inj. Module	j Gas inj.	j water inj	Vgas inj.	mWater inj.	FIC4-1x	FIC4-0x	PI4-200	PI4-201	PDI4-200	TI4-03	TI4-200	TI4-201	TI4-10	TI4-202	freq
[-]	[mm]	[-]	[-]	[-]	[m/s]	[m/s]	[nm³/h]	[kg/s]	[nm³/h]	[kg/s]	bar	bar	kPa	°C	°C	°C	°C	°C	Hz
A (tomo)	5	05.06.2013	5	M4 / 6	0,2190	4,047	6,616	9,505	**6,619**	**9,490**	**4,000**	4,067	-41,69	28,8	**29,3**	**29,4**	29,2	**20,2**	2/2500
A (tomo)	5	05.06.2013	48	M4 / 6	0,2190	4,047	6,616	9,505	**6,616**	**9,492**	**4,000**	4,062	-41,81	28,9	**29,4**	**29,5**	29,3	**19,4**	1/5000
D (tomo)	62	05.06.2013	7	M4 / 6	0,2190	4,047	6,616	9,505	**6,622**	**9,506**	**3,994**	4,068	-41,84	29,0	**29,5**	**29,5**	29,4	**20,0**	2/2500
D (tomo)	62	05.06.2013	46	M4 / 6	0,2190	4,047	6,616	9,505	**6,582**	**9,500**	**3,996**	4,068	-41,71	29,0	**29,5**	**29,5**	29,4	**19,4**	1/5000
G (tomo)	171	05.06.2013	12	M4 / 6	0,2190	4,047	6,616	9,505	**6,617**	**9,507**	**4,001**	4,072	-41,90	29,1	**29,6**	**29,7**	29,5	**19,9**	2/2500
G (tomo)	171	05.06.2013	44	M4 / 6	0,2190	4,047	6,616	9,505	**6,615**	**9,521**	**3,997**	4,067	-41,74	29,1	**29,5**	**29,5**	29,5	**19,4**	1/5000
J (tomo)	435	05.06.2013	15	M4 / 6	0,2190	4,047	6,616	9,505	**6,614**	**9,504**	**4,001**	4,071	-41,81	29,3	**29,7**	**29,8**	29,7	**19,8**	2/2500
J (tomo)	435	05.06.2013	42	M4 / 6	0,2190	4,047	6,616	9,505	**6,615**	**9,474**	**4,000**	4,071	-41,54	29,2	**29,6**	**29,7**	29,6	**19,4**	1/5000
M (tomo)	1271	05.06.2013	21	M4 / 6	0,2190	4,047	6,616	9,505	**6,615**	**9,495**	**4,001**	4,066	-41,65	29,5	**29,9**	**30,0**	29,8	**19,7**	2/2500
M (tomo)	1271	05.06.2013	40	M4 / 6	0,2190	4,047	6,616	9,505	**6,616**	**9,482**	**3,999**	4,072	-41,70	29,3	**29,7**	**29,7**	29,6	**19,5**	1/5000
P (tomo)	3270	05.06.2013	26	M4 / 6	0,2190	4,047	6,616	9,505	**6,614**	**9,500**	**4,000**	4,066	-41,65	29,7	**30,1**	**30,2**	30,0	**19,6**	2/2500
P (tomo)	3270	05.06.2013	38	M4 / 6	0,2190	4,047	6,616	9,505	**6,618**	**9,514**	**3,995**	4,060	-41,49	29,4	**29,9**	**29,9**	29,8	**19,6**	1/5000
S (wms)	4685		-	M4 / 6	0,2190	4,047	6,616	9,505											

L18 – 133

level code	L	data	DIAdem	inj. Module	j Gas inj.	j water inj	Vgas inj.	mWater inj.	FIC4-1x	FIC4-0x	PI4-200	PI4-201	PDI4-200	TI4-03	TI4-200	TI4-201	TI4-10	TI4-202	freq
[-]	[mm]	[-]	[-]	[-]	[m/s]	[m/s]	[nm³/h]	[kg/s]	[nm³/h]	[kg/s]	bar	bar	kPa	°C	°C	°C	°C	°C	Hz
A (tomo)	18	28.05.2013	97	M4 / 48	0,5340	0,0405	16,132	0,095	**16,116**	**0,095**	**4,003**	4,067	35,60	30,4	**30,4**	**30,1**	29,7	**18,9**	2/1000
D (tomo)	62	28.05.2013	94	M4 / 48	0,5340	0,0405	16,132	0,095	**16,124**	**0,095**	**3,990**	4,062	35,21	30,3	**30,4**	**30,0**	29,7	**19,0**	2/1000
G (tomo)	171	28.05.2013	92	M4 / 48	0,5340	0,0405	16,132	0,095	**16,128**	**0,095**	**3,993**	4,066	34,87	30,3	**30,4**	**30,0**	29,8	**19,2**	2/1000
J (tomo)	435	28.05.2013	84	M4 / 48	0,5340	0,0405	16,132	0,095	**16,121**	**0,095**	**3,986**	4,059	34,52	30,2	**30,3**	**29,9**	29,9	**19,4**	2/1000
M (tomo)	1271	28.05.2013	82	M4 / 48	0,5340	0,0405	16,132	0,095	**16,125**	**0,095**	**4,010**	4,083	34,88	30,1	**30,3**	**29,9**	29,9	**19,5**	2/1000
P (tomo)	3205	28.05.2013	79	M4 / 48	0,5340	0,0405	16,132	0,095	**16,119**	**0,095**	**4,001**	4,066	34,65	30,1	**30,2**	**29,8**	30,2	**19,8**	2/1000
S (wms)	4685	28.05.2013	79	M4 / 48	0,5340	0,0405	16,132	0,095	**16,119**	**0,095**	**4,001**	4,066	34,65	30,1	**30,2**	**29,8**	30,2	**19,8**	2/5000

L18 – 140

level code	L	data	DIAdem	inj. Module	j Gas inj.	j water inj	Vgas inj.	mWater inj.	FIC4-1x	FIC4-0x	PI4-200	PI4-201	PDI4-200	TI4-03	TI4-200	TI4-201	TI4-10	TI4-202	freq
[-]	[mm]	[-]	[-]	[-]	[m/s]	[m/s]	[nm³/h]	[kg/s]	[nm³/h]	[kg/s]	bar	bar	kPa	°C	°C	°C	°C	°C	Hz
A (tomo)	18	04.06.2013	2	M4 / 48	0,5340	1,017	16,132	2,389	**16,135**	**2,390**	**3,991**	4,071	9,37	29,1	**29,5**	**29,5**	29,4	**18,6**	2/1000
D (tomo)	62	04.06.2013	5	M4 / 48	0,5340	1,017	16,132	2,389	**16,136**	**2,388**	**3,994**	4,066	9,45	29,2	**29,7**	**29,7**	29,5	**18,3**	2/1000
G (tomo)	171	04.06.2013	11	M4 / 48	0,5340	1,017	16,132	2,389	**16,135**	**2,389**	**3,994**	4,064	9,37	29,3	**29,7**	**29,8**	29,6	**18,2**	2/1000
J (tomo)	435	04.06.2013	13	M4 / 48	0,5340	1,017	16,132	2,389	**16,137**	**2,389**	**3,990**	4,061	9,46	29,4	**29,9**	**29,9**	29,8	**18,0**	2/1000
M (tomo)	1271	04.06.2013	16	M4 / 48	0,5340	1,017	16,132	2,389	**16,132**	**2,388**	**3,991**	4,064	9,52	29,4	**29,9**	**30,0**	29,8	**18,0**	2/1000
P (tomo)	3205	04.06.2013	18	M4 / 48	0,5340	1,017	16,132	2,389	**16,137**	**2,390**	**4,003**	4,072	9,47	29,4	**29,9**	**30,0**	29,8	**18,0**	2/1000
S (wms)	4685	04.06.2013	18	M4 / 48	0,5340	1,017	16,132	2,389	**16,137**	**2,390**	**4,003**	4,072	9,47	29,4	**29,9**	**30,0**	29,8	**18,0**	2/5000

L18 – 143

level code	L	data	DIAdem	inj. Module	j Gas inj.	j water inj	Vgas inj.	mWater inj.	FIC4-1x	FIC4-0x	PI4-200	PI4-201	PDI4-200	TI4-03	TI4-200	TI4-201	TI4-10	TI4-202	freq
[-]	[mm]	[-]	[-]	[-]	[m/s]	[m/s]	[nm³/h]	[kg/s]	[nm³/h]	[kg/s]	bar	bar	kPa	°C	°C	°C	°C	°C	Hz
A (tomo)	5	06.06.2013	27	M4 / 48	0,5340	4,047	16,132	9,505	**16,138**	**9,506**	**4,000**	4,071	-42,46	29,3	**29,7**	**29,8**	29,6	**18,3**	2/2500
A (tomo)	5	*05.06.2013*	57	M4 / 48	0,5340	4,047	16,132	9,505	**16,136**	**9,498**	**4,004**	4,076	-42,41	29,1	**29,5**	**29,6**	29,5	**19,0**	1/5000
D (tomo)	62	06.06.2013	22	M4 / 48	0,5340	4,047	16,132	9,505	**16,138**	**9,497**	**4,006**	4,071	-42,36	29,3	**29,7**	**29,8**	29,7	**18,3**	2/2500
D (tomo)	62	*05.06.2013*	59	M4 / 48	0,5340	4,047	16,132	9,505	**16,134**	**9,505**	**3,998**	4,061	-42,63	29,2	**29,7**	**29,7**	29,5	**19,0**	1/5000
G (tomo)	171	06.06.2013	14	M4 / 48	0,5340	4,047	16,132	9,505	**16,134**	**9,500**	**3,995**	4,069	-42,63	29,4	**29,9**	**29,9**	29,7	**18,4**	2/2500
G (tomo)	171	*05.06.2013*	63	M4 / 48	0,5340	4,047	16,132	9,505	**16,126**	**9,517**	**3,994**	4,061	-42,51	29,3	**29,7**	**29,7**	29,6	**18,9**	1/5000
J (tomo)	435	06.06.2013	11	M4 / 48	0,5340	4,047	16,132	9,505	**16,137**	**9,514**	**3,995**	4,070	-42,56	29,4	**29,9**	**30,0**	29,8	**18,5**	2/2500
J (tomo)	435	*05.06.2013*	65	M4 / 48	0,5340	4,047	16,132	9,505	**16,135**	**9,527**	**4,002**	4,065	-42,37	29,3	**29,8**	**29,9**	29,7	**18,9**	1/5000
M (tomo)	1271	06.06.2013	8	M4 / 48	0,5340	4,047	16,132	9,505	**16,134**	**9,486**	**3,997**	4,071	-42,38	29,5	**30,0**	**30,1**	29,9	**18,7**	2/2500
M (tomo)	1271	*05.06.2013*	71	M4 / 48	0,5340	4,047	16,132	9,505	**16,129**	**9,528**	**4,003**	4,072	-42,35	29,5	**29,9**	**29,9**	29,9	**18,9**	1/5000
P (tomo)	3270	06.06.2013	6	M4 / 48	0,5340	4,047	16,132	9,505	**16,132**	**9,497**	**3,992**	4,056	-42,33	29,6	**30,1**	**30,1**	29,9	**19,0**	2/2500
P (tomo)	3270	*05.06.2013*	73	M4 / 48	0,5340	4,047	16,132	9,505	**16,134**	**9,505**	**4,000**	4,062	-42,30	29,6	**30,1**	**30,2**	30,0	**18,9**	1/5000
S (wms)	4685		-	M4 / 48	0,5340	4,047	16,132	9,505											

L18 – 155

level code	L	data	DIAdem	inj. Module	j Gas inj.	j water inj	Vgas inj.	mWater inj.	FIC4-1x	FIC4-0x	PI4-200	PI4-201	PDI4-200	TI4-03	TI4-200	TI4-201	TI4-10	TI4-202	freq
[-]	[mm]	[-]	[-]	[-]	[m/s]	[m/s]	[nm³/h]	[kg/s]	[nm³/h]	[kg/s]	bar	bar	kPa	°C	°C	°C	°C	°C	Hz
A (tomo)	18	28.05.2013	11	M4 / 54	1,3050	0,0405	39,424	0,095	**39,408**	**0,095**	**3,992**	4,063	37,17	30,1	**30,4**	**29,7**	30,0	**19,7**	2/2500
D (tomo)	62	28.05.2013	14	M4 / 54	1,3050	0,0405	39,424	0,095	**39,417**	**0,095**	**3,991**	4,057	37,27	30,3	**30,3**	**29,6**	29,7	**18,0**	2/2500
G (tomo)	171	28.05.2013	21	M4 / 54	1,3050	0,0405	39,424	0,095	**39,409**	**0,095**	**4,001**	4,073	37,24	30,3	**30,4**	**29,6**	29,5	**17,5**	2/2500
J (tomo)	435	28.05.2013	29	M4 / 54	1,3050	0,0405	39,424	0,095	**39,412**	**0,095**	**4,007**	4,076	37,56	30,4	**30,4**	**29,6**	29,4	**17,1**	2/2500
M (tomo)	1271	28.05.2013	33	M4 / 54	1,3050	0,0405	39,424	0,095	**39,409**	**0,095**	**4,001**	4,069	37,66	30,4	**30,4**	**29,6**	29,4	**16,9**	2/2500
P (tomo)	3205	28.05.2013	36	M4 / 54	1,3050	0,0405	39,424	0,095	**39,413**	**0,095**	**3,992**	4,062	37,53	30,5	**30,5**	**29,7**	29,3	**16,8**	2/2500
S (wms)	4685	28.05.2013	36	M4 / 54	1,3050	0,0405	39,424	0,095	**39,413**	**0,095**	**3,992**	4,062	37,53	30,5	**30,5**	**29,7**	29,3	**16,8**	2/5000

L18 – 162

level code	L	data	DIAdem	inj. Module	j Gas inj.	j water inj	Vgas inj.	mWater inj.	FIC4-1x	FIC4-0x	PI4-200	PI4-201	PDI4-200	TI4-03	TI4-200	TI4-201	TI4-10	TI4-202	freq
[-]	[mm]	[-]	[-]	[-]	[m/s]	[m/s]	[nm³/h]	[kg/s]	[nm³/h]	[kg/s]	bar	bar	kPa	°C	°C	°C	°C	°C	Hz
A (tomo)	5	03.06.2013	88	M4 / 54	1,3050	1,017	39,424	2,389	**39,417**	**2,390**	**4,004**	4,074	16,82	29,8	**30,2**	**30,2**	30,1	**16,2**	2/2500
A (tomo)	5	03.06.2013	37	M4 / 54	1,3050	1,017	39,424	2,389	**39,416**	**2,387**	**3,999**	4,067	17,06	29,1	**29,6**	**29,6**	29,5	**17,7**	1/5000
D (tomo)	62	03.06.2013	84	M4 / 54	1,3050	1,017	39,424	2,389	**39,412**	**2,389**	**4,006**	4,084	17,01	29,7	**30,1**	**30,1**	30,0	**16,3**	2/2500
D (tomo)	62	03.06.2013	39	M4 / 54	1,3050	1,017	39,424	2,389	**39,419**	**2,390**	**4,004**	4,071	16,76	29,2	**29,6**	**29,6**	29,5	**17,5**	1/5000
G (tomo)	171	03.06.2013	80	M4 / 54	1,3050	1,017	39,424	2,389	**39,416**	**2,391**	**3,998**	4,071	16,86	29,6	**30,1**	**30,1**	29,9	**16,4**	2/2500
G (tomo)	171	03.06.2013	44	M4 / 54	1,3050	1,017	39,424	2,389	**39,412**	**2,388**	**4,002**	4,069	17,03	29,2	**29,7**	**29,7**	29,6	**17,2**	1/5000
J (tomo)	435	03.06.2013	69	M4 / 54	1,3050	1,017	39,424	2,389	**39,416**	**2,388**	**3,997**	4,069	16,95	29,5	**30,0**	**30,0**	29,8	**16,4**	2/2500
J (tomo)	435	03.06.2013	47	M4 / 54	1,3050	1,017	39,424	2,389	**39,415**	**2,390**	**4,000**	4,071	16,71	29,2	**29,8**	**29,7**	29,6	**17,0**	1/5000
M (tomo)	1271	03.06.2013	65	M4 / 54	1,3050	1,017	39,424	2,389	**39,407**	**2,390**	**4,002**	4,076	16,91	29,5	**29,9**	**30,0**	29,8	**16,5**	2/2500
M (tomo)	1271	03.06.2013	51	M4 / 54	1,3050	1,017	39,424	2,389	**39,413**	**2,387**	**3,995**	4,063	16,90	29,3	**29,8**	**29,8**	29,6	**16,8**	1/5000
P (tomo)	3270	03.06.2013	62	M4 / 54	1,3050	1,017	39,424	2,389	**39,417**	**2,390**	**4,001**	4,073	16,63	29,4	**29,9**	**29,9**	29,7	**16,5**	2/2500
P (tomo)	3270	03.06.2013	55	M4 / 54	1,3050	1,017	39,424	2,389	**39,414**	**2,388**	**4,001**	4,075	16,81	29,3	**29,8**	**29,9**	29,7	**16,7**	1/5000
S (wms)	4685	03.06.2013	55	M4 / 54	1,3050	1,017	39,424	2,389	**39,414**	**2,388**	**4,001**	4,075	16,81	29,3	**29,8**	**29,9**	29,7	**16,7**	2/5000

L18 – 165

level code	L	data	DIAdem	inj. Module	j Gas inj.	j water inj	Vgas inj.	mWater inj.	FIC4-1x	FIC4-0x	PI4-200	PI4-201	PDI4-200	TI4-03	TI4-200	TI4-201	TI4-10	TI4-202	freq
[-]	[mm]	[-]	[-]	[-]	[m/s]	[m/s]	[nm³/h]	[kg/s]	[nm³/h]	[kg/s]	bar	bar	kPa	°C	°C	°C	°C	°C	Hz
A (tomo)	5	06.06.2013	30	M4 / 54	1,3050	4,047	39,424	9,505	**39,408**	**9,487**	**4,002**	4,066	-46,17	29,3	**29,7**	**29,8**	29,7	**17,2**	2/2500
A (tomo)	5	06.06.2013	74	M4 / 54	1,3050	4,047	39,424	9,505	**39,416**	**9,495**	**4,004**	4,069	-46,45	29,1	**29,6**	**29,7**	29,5	**19,1**	1/5000
D (tomo)	62	06.06.2013	32	M4 / 54	1,3050	4,047	39,424	9,505	**39,417**	**9,495**	**3,992**	4,054	-46,31	29,5	**30,0**	**30,1**	29,9	**17,0**	2/2500
D (tomo)	62	06.06.2013	71	M4 / 54	1,3050	4,047	39,424	9,505	**39,422**	**9,501**	**4,002**	4,065	-46,51	29,1	**29,5**	**29,6**	29,5	**18,9**	1/5000
G (tomo)	171	06.06.2013	36	M4 / 54	1,3050	4,047	39,424	9,505	**39,412**	**9,510**	**3,991**	4,050	-46,34	29,6	**30,1**	**30,1**	30,0	**17,6**	2/2500
G (tomo)	171	06.06.2013	68	M4 / 54	1,3050	4,047	39,424	9,505	**39,417**	**9,506**	**4,002**	4,066	-46,51	29,1	**29,6**	**29,6**	29,5	**18,8**	1/5000
J (tomo)	435	06.06.2013	39	M4 / 54	1,3050	4,047	39,424	9,505	**39,421**	**9,506**	**3,992**	4,061	-46,44	29,5	**29,9**	**30,0**	29,9	**17,6**	2/2500
J (tomo)	435	06.06.2013	65	M4 / 54	1,3050	4,047	39,424	9,505	**39,405**	**9,505**	**4,001**	4,070	-46,39	29,2	**29,6**	**29,7**	29,5	**18,5**	1/5000
M (tomo)	1271	06.06.2013	42	M4 / 54	1,3050	4,047	39,424	9,505	**39,417**	**9,483**	**3,996**	4,065	-46,31	29,4	**29,8**	**29,9**	29,8	**17,7**	2/2500
M (tomo)	1271	06.06.2013	58	M4 / 54	1,3050	4,047	39,424	9,505	**39,424**	**9,501**	**4,002**	4,072	-46,35	29,2	**29,5**	**29,6**	29,5	**18,3**	1/5000
P (tomo)	3270	06.06.2013	50	M4 / 54	1,3050	4,047	39,424	9,505	**39,409**	**9,507**	**3,996**	4,061	-46,39	29,3	**29,7**	**29,7**	29,6	**18,0**	2/2500
P (tomo)	3270	06.06.2013	56	M4 / 54	1,3050	4,047	39,424	9,505	**39,410**	**9,507**	**4,003**	4,066	-46,33	29,2	**29,6**	**29,6**	29,5	**18,2**	1/5000
S (wms)	4685		-	M4 / 54	1,3050	4,047	39,424	9,505											

L20 – 006

level code	L	data	DIAdem	inj. Module	j Gas inj.	j water inj	Vgas inj.	mWater inj.	FIC4-1x	FIC4-0x	PI4-202	PI4-203	PDI4-200	TI4-03	TI4-200	TI4-201	TI4-10	TI4-205	freq
[-]	[mm]	[-]	[-]	[-]	[m/s]	[m/s]	[nm³/h]	[kg/s]	[nm³/h]	[kg/s]	bar	bar	kPa	°C	°C	°C	°C	°C	Hz
A (tomo)	5	14.02.2014	26	M3 / 1	0,0025	0,4050	0,0755	0,951	**0,0754**	**0,951**	**4,006**	3,950	2,05	28,9	**29,3**	**29,3**	29,2	**20,1**	2 x 1000
D (tomo)	62	14.02.2014	24	M3 / 1	0,0025	0,4050	0,0755	0,951	**0,0754**	**0,951**	**3,995**	3,927	2,10	28,9	**29,3**	**29,3**	29,2	**20,1**	2 x 1000
G (tomo)	171	14.02.2014	22	M3 / 1	0,0025	0,4050	0,0755	0,951	**0,0754**	**0,951**	**4,000**	3,938	2,09	28,8	**29,3**	**29,3**	29,2	**20,1**	2 x 1000
J (tomo)	435	14.02.2014	16	M3 / 1	0,0025	0,4050	0,0755	0,951	**0,0754**	**0,950**	**4,001**	3,938	2,08	28,8	**29,3**	**29,3**	29,1	**20,0**	2 x 1000
M (tomo)	1271	14.02.2014	14	M3 / 1	0,0025	0,4050	0,0755	0,951	**0,0754**	**0,951**	**4,000**	3,937	2,21	28,8	**29,2**	**29,2**	29,1	**19,9**	2 x 1000
N (tomo)	3113	14.02.2014	12	M3 / 1	0,0025	0,4050	0,0755	0,951	**0,0754**	**0,952**	**4,003**	3,945	2,21	28,8	**29,2**	**29,2**	29,1	**19,9**	2 x 1000

L20 – 007

level code	L	data	DIAdem	inj. Module	j Gas inj.	j water inj	Vgas inj.	mWater inj.	FIC4-1x	FIC4-0x	PI4-202	PI4-203	PDI4-200	TI4-03	TI4-200	TI4-201	TI4-10	TI4-205	freq
[-]	[mm]	[-]	[-]	[-]	[m/s]	[m/s]	[nm³/h]	[kg/s]	[nm³/h]	[kg/s]	bar	bar	kPa	°C	°C	°C	°C	°C	Hz
A (tomo)	5	13.02.2014	4	M3 / 1	0,0025	0,6410	0,0755	1,505	**0,0754**	**1,512**	**4,000**	3,942	2,28	28,9	**29,4**	**29,4**	29,3	**20,0**	2 x 1000
D (tomo)	62	13.02.2014	7	M3 / 1	0,0025	0,6410	0,0755	1,505	**0,0754**	**1,505**	**4,001**	3,944	2,24	28,9	**29,4**	**29,4**	29,3	**20,1**	2 x 1000
G (tomo)	171	13.02.2014	11	M3 / 1	0,0025	0,6410	0,0755	1,505	**0,0754**	**1,507**	**4,001**	3,946	2,27	28,9	**29,4**	**29,4**	29,3	**20,1**	2 x 1000
J (tomo)	435	13.02.2014	16	M3 / 1	0,0025	0,6410	0,0755	1,505	**0,0754**	**1,566**	**4,000**	3,946	2,34	28,9	**29,5**	**29,5**	29,3	**20,1**	2 x 1000
M (tomo)	1271	13.02.2014	20	M3 / 1	0,0025	0,6410	0,0755	1,505	**0,0754**	**1,508**	**4,001**	3,938	2,30	28,9	**29,4**	**29,4**	29,3	**20,1**	2 x 1000
N (tomo)	3113	13.02.2014	23	M3 / 1	0,0025	0,6410	0,0755	1,505	**0,0754**	**1,505**	**3,999**	3,938	2,29	28,9	**29,4**	**29,4**	29,3	**20,1**	2 x 1000

L20 – 008

level code	L	data	DIAdem	inj. Module	j Gas inj.	j water inj	Vgas inj.	mWater inj.	FIC4-1x	FIC4-0x	PI4-202	PI4-203	PDI4-200	TI4-03	TI4-200	TI4-201	TI4-10	TI4-205	freq
[-]	[mm]	[-]	[-]	[-]	[m/s]	[m/s]	[nm³/h]	[kg/s]	[nm³/h]	[kg/s]	bar	bar	kPa	°C	°C	°C	°C	°C	Hz
A (tomo)	5	12.02.2014	33	M3 / 1	0,0025	1,0170	0,0755	2,389	**0,0754**	**2,391**	**3,999**	3,940	3,35	29,2	**29,6**	**29,6**	29,6	**19,8**	2 x 1000
D (tomo)	62	12.02.2014	31	M3 / 1	0,0025	1,0170	0,0755	2,389	**0,0754**	**2,379**	**4,004**	3,949	3,33	29,1	**29,6**	**29,6**	29,5	**19,9**	2 x 1000
G (tomo)	171	12.02.2014	28	M3 / 1	0,0025	1,0170	0,0755	2,389	**0,0754**	**2,386**	**3,999**	3,942	3,34	29,1	**29,5**	**29,5**	29,5	**19,9**	2 x 1000
J (tomo)	435	12.02.2014	25	M3 / 1	0,0025	1,0170	0,0755	2,389	**0,0754**	**2,383**	**4,002**	3,945	3,35	29,1	**29,5**	**29,5**	29,4	**19,8**	2 x 1000
M (tomo)	1271	12.02.2014	14	M3 / 1	0,0025	1,0170	0,0755	2,389	**0,0754**	**2,401**	**3,999**	3,935	3,35	29,0	**29,5**	**29,5**	29,4	**19,8**	2 x 1000
N (tomo)	3113	12.02.2014	9	M3 / 1	0,0025	1,0170	0,0755	2,389	**0,0754**	**2,389**	**4,000**	3,946	3,33	29,0	**29,5**	**29,5**	29,4	**19,8**	2 x 1000

L20 – 009

level code	L	data	DIAdem	inj. Module	j Gas inj.	j water inj	Vgas inj.	mWater inj.	FIC4-1x	FIC4-0x	PI4-202	PI4-203	PDI4-200	TI4-03	TI4-200	TI4-201	TI4-10	TI4-205	freq
[-]	[mm]	[-]	[-]	[-]	[m/s]	[m/s]	[nm³/h]	[kg/s]	[nm³/h]	[kg/s]	bar	bar	kPa	°C	°C	°C	°C	°C	Hz
A (tomo)	5	11.02.2014	7	M3 / 1	0,0025	1,6110	0,0755	3,784	**0,0754**	**3,783**	**4,003**	3,935	6,64	29,4	**29,9**	**29,9**	29,8	**20,1**	2 x 2000
D (tomo)	62	11.02.2014	9	M3 / 1	0,0025	1,6110	0,0755	3,784	**0,0754**	**3,783**	**4,006**	3,942	6,63	29,5	**30,0**	**30,0**	30,0	**20,1**	2 x 2000
G (tomo)	171	11.02.2014	15	M3 / 1	0,0025	1,6110	0,0755	3,784	**0,0754**	**3,785**	**4,001**	3,932	6,63	29,8	**30,2**	**30,2**	30,1	**20,2**	2 x 2000
J (tomo)	435	11.02.2014	18	M3 / 1	0,0025	1,6110	0,0755	3,784	**0,0754**	**3,786**	**4,002**	3,937	6,64	29,9	**30,4**	**30,4**	30,4	**20,2**	2 x 2000
M (tomo)	1271	11.02.2014	21	M3 / 1	0,0025	1,6110	0,0755	3,784	**0,0754**	**3,784**	**4,003**	3,936	6,63	30,2	**30,6**	**30,6**	30,6	**20,2**	2 x 2000
N (tomo)	3113	11.02.2014	25	M3 / 1	0,0025	1,6110	0,0755	3,784	**0,0754**	**3,784**	**4,002**	3,940	6,63	30,4	**30,7**	**30,8**	30,8	**20,2**	2 x 2000

L20 – 028

level code	L	data	DIAdem	inj. Module	j Gas inj.	j water inj	Vgas inj.	mWater inj.	FIC4-1x	FIC4-0x	PI4-202	PI4-203	PDI4-200	TI4-03	TI4-200	TI4-201	TI4-10	TI4-205	freq
[-]	[mm]	[-]	[-]	[-]	[m/s]	[m/s]	[nm³/h]	[kg/s]	[nm³/h]	[kg/s]	bar	bar	kPa	°C	°C	°C	°C	°C	Hz
A (tomo)	5	14.02.2014	29	M3 / 1	0,0062	0,4050	0,1873	0,951	**0,1873**	**0,952**	**3,996**	3,933	3,33	29,0	**29,5**	**29,5**	29,4	**20,3**	2 x 1000
D (tomo)	62	14.02.2014	34	M3 / 1	0,0062	0,4050	0,1873	0,951	**0,1873**	**0,952**	**4,007**	3,947	3,33	29,1	**29,5**	**29,5**	29,4	**20,3**	2 x 1000
G (tomo)	171	14.02.2014	36	M3 / 1	0,0062	0,4050	0,1873	0,951	**0,1873**	**0,951**	**4,002**	3,946	3,29	29,1	**29,5**	**29,5**	29,4	**20,3**	2 x 1000
J (tomo)	435	14.02.2014	41	M3 / 1	0,0062	0,4050	0,1873	0,951	**0,1873**	**0,951**	**4,001**	3,946	3,37	29,1	**29,5**	**29,6**	29,4	**20,4**	2 x 1000
M (tomo)	1271	14.02.2014	44	M3 / 1	0,0062	0,4050	0,1873	0,951	**0,1873**	**0,952**	**3,997**	3,933	3,35	29,1	**29,5**	**29,6**	29,5	**20,3**	2 x 1000
N (tomo)	3113	14.02.2014	48	M3 / 1	0,0062	0,4050	0,1873	0,951	**0,1873**	**0,950**	**4,002**	3,946	3,35	29,1	**29,5**	**29,6**	29,5	**20,3**	2 x 1000

L20 – 029

level code	L	data	DIAdem	inj. Module	j Gas inj.	j water inj	Vgas inj.	mWater inj.	FIC4-1x	FIC4-0x	PI4-202	PI4-203	PDI4-200	TI4-03	TI4-200	TI4-201	TI4-10	TI4-205	freq
[-]	[mm]	[-]	[-]	[-]	[m/s]	[m/s]	[nm³/h]	[kg/s]	[nm³/h]	[kg/s]	bar	bar	kPa	°C	°C	°C	°C	°C	Hz
A (tomo)	5	17.02.2014	23	M3 / 1	0,0062	0,6410	0,1873	1,505	**0,1873**	**1,505**	**3,999**	3,931	2,93	28,9	**29,4**	**29,4**	29,4	**20,4**	2 x 1000
D (tomo)	62	17.02.2014	21	M3 / 1	0,0062	0,6410	0,1873	1,505	**0,1873**	**1,505**	**4,006**	3,949	2,94	28,9	**29,4**	**29,4**	29,3	**20,4**	2 x 1000
D (tomo)	62	17.02.2014	19	M3 / 1	0,0062	0,6410	0,1873	1,505	**0,1873**	**1,504**	**3,995**	3,931	2,90	28,8	**29,3**	**29,3**	29,2	**20,4**	2 x 1000
G (tomo)	171	17.02.2014	15	M3 / 1	0,0062	0,6410	0,1873	1,505	**0,1873**	**1,506**	**4,003**	3,938	2,90	28,8	**29,3**	**29,3**	29,2	**20,3**	2 x 1000
J (tomo)	435	17.02.2014	8	M3 / 1	0,0062	0,6410	0,1873	1,505	**0,1873**	**1,505**	**4,000**	3,938	2,92	28,8	**29,3**	**29,3**	29,2	**20,4**	2 x 1000
M (tomo)	1271	17.02.2014	5	M3 / 1	0,0062	0,6410	0,1873	1,505	**0,1873**	**1,505**	**4,003**	3,948	2,89	28,8	**29,3**	**29,3**	29,2	**20,3**	2 x 1000
N (tomo)	3113	17.02.2014	2	M3 / 1	0,0062	0,6410	0,1873	1,505	**0,1873**	**1,505**	**3,999**	3,937	2,95	28,8	**29,3**	**29,2**	29,2	**20,3**	2 x 1000

WH

level code	L	data	DIAdem	inj. Module	j Gas inj.	j water inj	Vgas inj.	mWater inj.	FIC4-1x	FIC4-0x	PI4-202	PI4-203	PDI4-200	TI4-03	TI4-200	TI4-201	TI4-10	TI4-205	freq
[-]	[mm]	[-]	[-]	[-]	[m/s]	[m/s]	[nm³/h]	[kg/s]	[nm³/h]	[kg/s]	bar	bar	kPa	°C	°C	°C	°C	°C	Hz
A (tomo)	5	18.02.2014	21	M3 / 3	0,0062	0,6410	0,1873	1,505	**0,1873**	**1,505**	**3,999**	3,932	2,73	28,6	**29,1**	**29,1**	29,0	**19,8**	2 x 1000
D (tomo)	62	18.02.2014	15	M3 / 3	0,0062	0,6410	0,1873	1,505	**0,1873**	**1,505**	**3,994**	3,932	2,73	28,7	**29,1**	**29,1**	29,0	**19,8**	2 x 1000
G (tomo)	171	18.02.2014	13	M3 / 3	0,0062	0,6410	0,1873	1,505	**0,1873**	**1,505**	**4,003**	3,939	2,75	28,7	**29,1**	**29,1**	29,0	**19,8**	2 x 1000
J (tomo)	435	18.02.2014	9	M3 / 3	0,0062	0,6410	0,1873	1,505	**0,1873**	**1,503**	**4,006**	3,940	2,73	28,7	**29,1**	**29,1**	29,0	**19,8**	2 x 1000
M (tomo)	1271	18.02.2014	7	M3 / 3	0,0062	0,6410	0,1873	1,505	**0,1873**	**1,506**	**4,001**	3,944	2,70	28,7	**29,1**	**29,1**	29,0	**19,8**	2 x 1000
N (tomo)	3113	18.02.2014	5	M3 / 3	0,0062	0,6410	0,1873	1,505	**0,1873**	**1,505**	**4,002**	3,940	2,73	28,6	**29,1**	**29,1**	29,0	**19,8**	2 x 1000

L20 – 030

level code	L	data	DIAdem	inj. Module	j Gas inj.	j water inj	Vgas inj.	mWater inj.	FIC4-1x	FIC4-0x	PI4-202	PI4-203	PDI4-200	TI4-03	TI4-200	TI4-201	TI4-10	TI4-205	freq
[-]	[mm]	[-]	[-]	[-]	[m/s]	[m/s]	[nm³/h]	[kg/s]	[nm³/h]	[kg/s]	bar	bar	kPa	°C	°C	°C	°C	°C	Hz
A (tomo)	5	19.02.2014	2	M3 / 1	0,0062	1,0170	0,1873	2,389	**0,1873**	**2,388**	**4,001**	3,942	4,49	28,6	**29,2**	**29,2**	29,4	**19,1**	2 x 1000
A (tomo)	5	19.02.2014	4	M3 / 1	0,0062	1,0170	0,1873	2,389	**0,1873**	**2,389**	**3,997**	3,933	3,60	28,7	**29,1**	**29,1**	29,1	**19,3**	2 x 1000
D (tomo)	62	19.02.2014	7	M3 / 1	0,0062	1,0170	0,1873	2,389	**0,1873**	**2,389**	**3,998**	3,933	3,60	28,7	**29,2**	**29,2**	29,1	**19,3**	2 x 1000
G (tomo)	171	19.02.2014	10	M3 / 1	0,0062	1,0170	0,1873	2,389	**0,1873**	**2,388**	**4,000**	3,939	3,59	28,7	**29,2**	**29,2**	29,1	**19,3**	2 x 1000
J (tomo)	435	19.02.2014	13	M3 / 1	0,0062	1,0170	0,1873	2,389	**0,1873**	**2,389**	**4,002**	3,945	3,60	28,7	**29,2**	**29,2**	29,2	**19,4**	2 x 1000
M (tomo)	1271	19.02.2014	16	M3 / 1	0,0062	1,0170	0,1873	2,389	**0,1873**	**2,389**	**4,003**	3,943	3,61	28,8	**29,2**	**29,2**	29,2	**19,4**	2 x 1000
N (tomo)	3113	19.02.2014	19	M3 / 1	0,0062	1,0170	0,1873	2,389	**0,1873**	**2,390**	**4,003**	3,946	3,61	28,8	**29,3**	**29,3**	29,2	**19,4**	2 x 1000

L20 – 031

level code	L	data	DIAdem	inj. Module	j Gas inj.	j water inj	Vgas inj.	mWater inj.	FIC4-1x	FIC4-0x	PI4-202	PI4-203	PDI4-200	TI4-03	TI4-200	TI4-201	TI4-10	TI4-205	freq
[-]	[mm]	[-]	[-]	[-]	[m/s]	[m/s]	[nm³/h]	[kg/s]	[nm³/h]	[kg/s]	bar	bar	kPa	°C	°C	°C	°C	°C	Hz
A (tomo)	5	17.02.2014	26	M3 / 1	0,0062	1,6110	0,1873	3,784	**0,1873**	**3,783**	**3,994**	3,930	6,78	29,1	**29,5**	**29,5**	29,5	**20,4**	2 x 2000
D (tomo)	62	17.02.2014	29	M3 / 1	0,0062	1,6110	0,1873	3,784	**0,1873**	**3,783**	**4,006**	3,946	6,74	29,1	**29,6**	**29,6**	29,5	**20,4**	2 x 2000
G (tomo)	171	17.02.2014	36	M3 / 1	0,0062	1,6110	0,1873	3,784	**0,1873**	**3,784**	**4,000**	3,938	6,72	29,2	**29,7**	**29,7**	29,6	**20,5**	2 x 2000
J (tomo)	435	17.02.2014	41	M3 / 1	0,0062	1,6110	0,1873	3,784	**0,1873**	**3,785**	**4,001**	3,938	6,73	29,3	**29,7**	**29,7**	29,7	**20,5**	2 x 2000
M (tomo)	1271	17.02.2014	47	M3 / 1	0,0062	1,6110	0,1873	3,784	**0,1873**	**3,785**	**4,001**	3,938	6,72	29,3	**29,7**	**29,8**	29,7	**20,5**	2 x 2000
N (tomo)	3113	17.02.2014	49	M3 / 1	0,0062	1,6110	0,1873	3,784	**0,1873**	**3,784**	**3,999**	3,938	6,76	29,4	**29,8**	**29,8**	29,8	**20,5**	2 x 2000

L20 – 050

level code	L	data	DIAdem	inj. Module	j Gas inj.	j water inj	Vgas inj.	mWater inj.	FIC4-1x	FIC4-0x	PI4-202	PI4-203	PDI4-200	TI4-03	TI4-200	TI4-201	TI4-10	TI4-205	freq
[-]	[mm]	[-]	[-]	[-]	[m/s]	[m/s]	[nm³/h]	[kg/s]	[nm³/h]	[kg/s]	bar	bar	kPa	°C	°C	°C	°C	°C	Hz
A (tomo)	5	20.02.2014	30	M3 / 3	0,0151	0,4050	0,4562	0,951	**0,4563**	**0,952**	**4,003**	3,943	5,60	28,8	**29,2**	**29,2**	29,2	**20,0**	2 x 1000
D (tomo)	62	20.02.2014	32	M3 / 3	0,0151	0,4050	0,4562	0,951	**0,4563**	**0,951**	**4,002**	3,943	5,55	28,8	**29,2**	**29,2**	29,2	**20,0**	2 x 1000
G (tomo)	171	20.02.2014	36	M3 / 3	0,0151	0,4050	0,4562	0,951	**0,4562**	**0,951**	**3,999**	3,941	5,76	28,8	**29,2**	**29,2**	29,2	**20,0**	2 x 1000
J (tomo)	435	20.02.2014	39	M3 / 3	0,0151	0,4050	0,4562	0,951	**0,4562**	**0,952**	**4,002**	3,944	5,42	28,8	**29,2**	**29,2**	29,2	**20,1**	2 x 1000
M (tomo)	1271	20.02.2014	43	M3 / 3	0,0151	0,4050	0,4562	0,951	**0,4563**	**0,950**	**4,000**	3,929	5,38	28,8	**29,2**	**29,2**	29,1	**20,1**	2 x 1000
N (tomo)	3113	20.02.2014	45	M3 / 3	0,0151	0,4050	0,4562	0,951	**0,4562**	**0,951**	**4,004**	3,934	5,38	28,8	**29,2**	**29,2**	29,1	**20,1**	2 x 1000

L20 – 051

level code	L	data	DIAdem	inj. Module	j Gas inj.	j water inj	Vgas inj.	mWater inj.	FIC4-1x	FIC4-0x	PI4-202	PI4-203	PDI4-200	TI4-03	TI4-200	TI4-201	TI4-10	TI4-205	freq
[-]	[mm]	[-]	[-]	[-]	[m/s]	[m/s]	[nm³/h]	[kg/s]	[nm³/h]	[kg/s]	bar	bar	kPa	°C	°C	°C	°C	°C	Hz
A (tomo)	5	20.02.2014	23	M3 / 3	0,0151	0,6410	0,4562	1,505	**0,4562**	**1,505**	**4,003**	3,940	4,25	28,7	**29,1**	**29,1**	29,0	**19,8**	2 x 1000
D (tomo)	62	20.02.2014	16	M3 / 3	0,0151	0,6410	0,4562	1,505	**0,4562**	**1,504**	**4,005**	3,948	4,26	28,7	**29,1**	**29,1**	29,0	**19,7**	2 x 1000
G (tomo)	171	20.02.2014	13	M3 / 3	0,0151	0,6410	0,4562	1,505	**0,4563**	**1,505**	**4,002**	3,938	4,21	28,7	**29,1**	**29,1**	29,0	**19,7**	2 x 1000
J (tomo)	435	20.02.2014	9	M3 / 3	0,0151	0,6410	0,4562	1,505	**0,4563**	**1,504**	**4,005**	3,950	4,23	28,7	**29,1**	**29,1**	29,0	**19,7**	2 x 1000
M (tomo)	1271	20.02.2014	7	M3 / 3	0,0151	0,6410	0,4562	1,505	**0,4563**	**1,505**	**4,001**	3,940	4,21	28,7	**29,1**	**29,1**	29,0	**19,7**	2 x 1000
N (tomo)	3113	20.02.2014	4	M3 / 3	0,0151	0,6410	0,4562	1,505	**0,4563**	**1,505**	**3,996**	3,927	4,04	28,7	**29,2**	**29,1**	29,1	**19,7**	2 x 1000

L20 – 052

level code	L	data	DIAdem	inj. Module	j Gas inj.	j water inj	Vgas inj.	mWater inj.	FIC4-1x	FIC4-0x	PI4-202	PI4-203	PDI4-200	TI4-03	TI4-200	TI4-201	TI4-10	TI4-205	freq
[-]	[mm]	[-]	[-]	[-]	[m/s]	[m/s]	[nm³/h]	[kg/s]	[nm³/h]	[kg/s]	bar	bar	kPa	°C	°C	°C	°C	°C	Hz
A (tomo)	5	19.02.2014	41	M3 / 3	0,0151	1,0170	0,4562	2,389	**0,4562**	**2,389**	**3,999**	3,938	4,11	29,2	**29,6**	**29,6**	29,6	**19,7**	2 x 1000
D (tomo)	62	19.02.2014	39	M3 / 3	0,0151	1,0170	0,4562	2,389	**0,4562**	**2,389**	**4,000**	3,936	4,11	29,2	**29,6**	**29,6**	29,5	**19,6**	2 x 1000
G (tomo)	171	19.02.2014	34	M3 / 3	0,0151	1,0170	0,4562	2,389	**0,4562**	**2,390**	**4,000**	3,940	4,11	29,1	**29,5**	**29,5**	29,5	**19,6**	2 x 1000
J (tomo)	435	19.02.2014	30	M3 / 3	0,0151	1,0170	0,4562	2,389	**0,4562**	**2,388**	**4,003**	3,949	4,10	29,1	**29,5**	**29,5**	29,5	**19,6**	2 x 1000
M (tomo)	1271	19.02.2014	26	M3 / 3	0,0151	1,0170	0,4562	2,389	**0,4562**	**2,390**	**4,000**	3,940	4,12	29,0	**29,5**	**29,5**	29,5	**19,5**	2 x 1000
N (tomo)	3113	19.02.2014	23	M3 / 3	0,0151	1,0170	0,4562	2,389	**0,4562**	**2,389**	**4,004**	3,945	4,11	29,0	**29,4**	**29,4**	29,5	**19,5**	2 x 1000

L20 – 053

level code	L	data	DIAdem	inj. Module	j Gas inj.	j water inj	Vgas inj.	mWater inj.	FIC4-1x	FIC4-0x	PI4-202	PI4-203	PDI4-200	TI4-03	TI4-200	TI4-201	TI4-10	TI4-205	freq
[-]	[mm]	[-]	[-]	[-]	[m/s]	[m/s]	[nm³/h]	[kg/s]	[nm³/h]	[kg/s]	bar	bar	kPa	°C	°C	°C	°C	°C	Hz
A (tomo)	5	19.02.2014	48	M3 / 3	0,0151	1,6110	0,4562	3,784	**0,4562**	**3,782**	**4,001**	3,940	7,01	29,2	**29,7**	**29,7**	29,6	**19,7**	2 x 2000
D (tomo)	62	19.02.2014	51	M3 / 3	0,0151	1,6110	0,4562	3,784	**0,4562**	**3,783**	**4,005**	3,942	7,04	29,3	**29,7**	**29,7**	29,6	**19,7**	2 x 2000
G (tomo)	171	19.02.2014	60	M3 / 3	0,0151	1,6110	0,4562	3,784	**0,4562**	**3,785**	**4,002**	3,943	7,01	29,3	**29,8**	**29,7**	29,7	**19,8**	2 x 2000
J (tomo)	435	19.02.2014	64	M3 / 3	0,0151	1,6110	0,4562	3,784	**0,4562**	**3,783**	**4,004**	3,944	7,02	29,4	**29,8**	**29,8**	29,8	**19,8**	2 x 2000
M (tomo)	1271	19.02.2014	68	M3 / 3	0,0151	1,6110	0,4562	3,784	**0,4562**	**3,785**	**4,004**	3,941	7,02	29,4	**29,8**	**29,8**	29,8	**19,8**	2 x 2000
N (tomo)	3113	19.02.2014	73	M3 / 3	0,0151	1,6110	0,4562	3,784	**0,4562**	**3,784**	**4,000**	3,938	7,02	29,4	**29,8**	**29,8**	29,8	**19,8**	2 x 2000

L20 – 083

level code	L	data	DIAdem	inj. Module	j Gas inj.	j water inj	Vgas inj.	mWater inj.	FIC4-1x	FIC4-0x	PI4-202	PI4-203	PDI4-200	TI4-03	TI4-200	TI4-201	TI4-10	TI4-205	freq
[-]	[mm]	[-]	[-]	[-]	[m/s]	[m/s]	[nm³/h]	[kg/s]	[nm³/h]	[kg/s]	bar	bar	kPa	°C	°C	°C	°C	°C	Hz
A (tomo)	5	20.02.2014	68	M3 / 4	0,0574	0,4050	1,7340	0,951	**1,7344**	**0,951**	**3,996**	3,937	14,88	28,9	**29,3**	**29,3**	29,2	**20,2**	2 x 1000
D (tomo)	62	20.02.2014	61	M3 / 4	0,0574	0,4050	1,7340	0,951	**1,7344**	**0,952**	**4,002**	3,939	13,95	28,9	**29,3**	**29,3**	29,2	**20,2**	2 x 1000
G (tomo)	171	20.02.2014	58	M3 / 4	0,0574	0,4050	1,7340	0,951	**1,7342**	**0,952**	**4,000**	3,934	13,93	28,9	**29,4**	**29,3**	29,2	**20,2**	2 x 1000
J (tomo)	435	20.02.2014	55	M3 / 4	0,0574	0,4050	1,7340	0,951	**1,7342**	**0,951**	**4,008**	3,949	13,96	28,9	**29,3**	**29,3**	29,2	**20,1**	2 x 1000
M (tomo)	1271	20.02.2014	52	M3 / 4	0,0574	0,4050	1,7340	0,951	**1,7344**	**0,949**	**4,013**	3,952	13,94	28,9	**29,3**	**29,3**	29,2	**20,1**	2 x 1000
N (tomo)	3113	20.02.2014	49	M3 / 4	0,0574	0,4050	1,7340	0,951	**1,7342**	**0,948**	**4,006**	3,951	13,97	28,9	**29,4**	**29,4**	29,4	**20,1**	2 x 1000

L20 – 084

level code	L	data	DIAdem	inj. Module	j Gas inj.	j water inj	Vgas inj.	mWater inj.	FIC4-1x	FIC4-0x	PI4-202	PI4-203	PDI4-200	TI4-03	TI4-200	TI4-201	TI4-10	TI4-205	freq
[-]	[mm]	[-]	[-]	[-]	[m/s]	[m/s]	[nm³/h]	[kg/s]	[nm³/h]	[kg/s]	bar	bar	kPa	°C	°C	°C	°C	°C	Hz
A (tomo)	5	21.02.2014	51	M3 / 4	0,0574	0,6410	1,7340	1,505	**1,7346**	**1,505**	**3,993**	3,938	10,12	29,1	**29,5**	**29,5**	29,4	**19,9**	2 x 1000
D (tomo)	62	21.02.2014	54	M3 / 4	0,0574	0,6410	1,7340	1,505	**1,7346**	**1,504**	**4,003**	3,951	10,17	29,0	**29,5**	**29,5**	29,4	**19,9**	2 x 1000
G (tomo)	171	21.02.2014	56	M3 / 4	0,0574	0,6410	1,7340	1,505	**1,7348**	**1,504**	**4,001**	3,934	10,18	29,0	**29,5**	**29,5**	29,4	**19,9**	2 x 1000
J (tomo)	435	21.02.2014	59	M3 / 4	0,0574	0,6410	1,7340	1,505	**1,7347**	**1,506**	**4,000**	3,940	10,13	29,0	**29,4**	**29,5**	29,4	**20,0**	2 x 1000
M (tomo)	1271	21.02.2014	62	M3 / 4	0,0574	0,6410	1,7340	1,505	**1,7347**	**1,505**	**4,001**	3,942	10,14	29,0	**29,4**	**29,4**	29,4	**20,0**	2 x 1000
N (tomo)	3113	21.02.2014	64	M3 / 4	0,0574	0,6410	1,7340	1,505	**1,7347**	**1,507**	**4,001**	3,941	10,08	29,0	**29,4**	**29,4**	29,3	**20,0**	2 x 1000

L20 – 085

level code	L	data	DIAdem	inj. Module	j Gas inj.	j water inj	Vgas inj.	mWater inj.	FIC4-1x	FIC4-0x	PI4-202	PI4-203	PDI4-200	TI4-03	TI4-200	TI4-201	TI4-10	TI4-205	freq
[-]	[mm]	[-]	[-]	[-]	[m/s]	[m/s]	[nm³/h]	[kg/s]	[nm³/h]	[kg/s]	bar	bar	kPa	°C	°C	°C	°C	°C	Hz
A (tomo)	5	21.02.2014	46	M3 / 4	0,0574	1,0170	1,7340	2,389	**1,7346**	**2,389**	**4,004**	3,944	7,74	29,1	**29,6**	**29,6**	29,5	**19,8**	2 x 1000
D (tomo)	62	21.02.2014	43	M3 / 4	0,0574	1,0170	1,7340	2,389	**1,7346**	**2,388**	**4,004**	3,938	7,74	29,1	**29,6**	**29,5**	29,5	**19,8**	2 x 1000
G (tomo)	171	21.02.2014	41	M3 / 4	0,0574	1,0170	1,7340	2,389	**1,7346**	**2,389**	**4,003**	3,944	7,71	29,1	**29,6**	**29,6**	29,5	**19,8**	2 x 1000
J (tomo)	435	21.02.2014	36	M3 / 4	0,0574	1,0170	1,7340	2,389	**1,7347**	**2,389**	**4,001**	3,936	7,78	29,1	**29,6**	**29,5**	29,5	**19,8**	2 x 1000
M (tomo)	1271	21.02.2014	34	M3 / 4	0,0574	1,0170	1,7340	2,389	**1,7346**	**2,388**	**4,000**	3,936	7,71	29,1	**29,6**	**29,6**	29,5	**19,8**	2 x 1000
N (tomo)	3113	21.02.2014	31	M3 / 4	0,0574	1,0170	1,7340	2,389	**1,7346**	**2,388**	**4,000**	3,937	7,70	29,1	**29,5**	**29,6**	29,5	**19,8**	2 x 1000

L20 – 086

level code	L	data	DIAdem	inj. Module	j Gas inj.	j water inj	Vgas inj.	mWater inj.	FIC4-1x	FIC4-0x	PI4-202	PI4-203	PDI4-200	TI4-03	TI4-200	TI4-201	TI4-10	TI4-205	freq
[-]	[mm]	[-]	[-]	[-]	[m/s]	[m/s]	[nm³/h]	[kg/s]	[nm³/h]	[kg/s]	bar	bar	kPa	°C	°C	°C	°C	°C	Hz
A (tomo)	5	21.02.2014	6	M3 / 4	0,0574	1,6110	1,7340	3,784	**1,7346**	**3,784**	**4,004**	3,953	9,07	29,0	**29,4**	**29,4**	29,4	**19,6**	2 x 2000
D (tomo)	62	21.02.2014	9	M3 / 4	0,0574	1,6110	1,7340	3,784	**1,7348**	**3,784**	**4,004**	3,949	9,00	29,0	**29,5**	**29,5**	29,4	**19,7**	2 x 2000
G (tomo)	171	21.02.2014	14	M3 / 4	0,0574	1,6110	1,7340	3,784	**1,7347**	**3,788**	**3,998**	3,938	9,01	29,1	**29,5**	**29,5**	29,5	**19,7**	2 x 2000
J (tomo)	435	21.02.2014	20	M3 / 4	0,0574	1,6110	1,7340	3,784	**1,7347**	**3,785**	**3,998**	3,932	8,99	29,1	**29,6**	**29,6**	29,5	**19,7**	2 x 2000
M (tomo)	1271	21.02.2014	24	M3 / 4	0,0574	1,6110	1,7340	3,784	**1,7347**	**3,784**	**4,006**	3,946	8,98	29,2	**29,6**	**29,6**	29,6	**19,7**	2 x 2000
N (tomo)	3113	21.02.2014	28	M3 / 4	0,0574	1,6110	1,7340	3,784	**1,7347**	**3,783**	**3,999**	3,938	9,05	29,2	**29,6**	**29,7**	29,6	**19,7**	2 x 2000

L21 – 116

level code	L	data	DIAdem	inj. Module	j Gas inj.	j water inj	Vgas inj.	mWater inj.	FIC4-1x	FIC4-0x	PI4-202	PI4-203	PDI4-200	TI4-03	TI4-200	TI4-201	TI4-10	TI4-205	freq
[-]	[mm]	[-]	[-]	[-]	[m/s]	[m/s]	[nm³/h]	[kg/s]	[nm³/h]	[kg/s]	bar	bar	kPa	°C	°C	°C	°C	°C	Hz
A (tomo)	5	28.02.2014	48	M4 / 6	0,2190	0,4050	6,6159	0,951	**6,6135**	**0,949**	**4,005**	3,940	50,00	29,1	**29,5**	**29,5**	29,4	**19,4**	2 x 1000
D (tomo)	62	28.02.2014	46	M4 / 6	0,2190	0,4050	6,6159	0,951	**6,6132**	**0,955**	**3,991**	3,925	49,91	29,1	**29,5**	**29,5**	29,4	**19,4**	2 x 1000
G (tomo)	171	28.02.2014	41	M4 / 6	0,2190	0,4050	6,6159	0,951	**6,6129**	**0,957**	**4,000**	3,939	49,83	29,1	**29,6**	**29,5**	29,4	**19,4**	2 x 1000
J (tomo)	435	28.02.2014	37	M4 / 6	0,2190	0,4050	6,6159	0,951	**6,6118**	**0,950**	**3,999**	3,931	50,02	29,1	**29,6**	**29,5**	29,5	**19,4**	2 x 1000
M (tomo)	1271	28.02.2014	34	M4 / 6	0,2190	0,4050	6,6159	0,951	**6,6143**	**0,946**	**3,996**	3,941	49,96	29,1	**29,8**	**29,8**	29,8	**19,4**	2 x 1000
NN (tomo)	3054	28.02.2014	29	M4 / 6	0,2190	0,4050	6,6159	0,951	**6,6150**	**0,946**	**4,010**	3,949	50,65	29,1	**29,5**	**29,5**	29,4	**19,4**	2 x 1000

L21 – 117

level code	L	data	DIAdem	inj. Module	j Gas inj.	j water inj	Vgas inj.	mWater inj.	FIC4-1x	FIC4-0x	PI4-202	PI4-203	PDI4-200	TI4-03	TI4-200	TI4-201	TI4-10	TI4-205	freq
[-]	[mm]	[-]	[-]	[-]	[m/s]	[m/s]	[nm³/h]	[kg/s]	[nm³/h]	[kg/s]	bar	bar	kPa	°C	°C	°C	°C	°C	Hz
A (tomo)	5	28.02.2014	7	M4 / 6	0,2190	0,6410	6,6159	1,505	**6,6124**	**1,507**	**3,994**	3,938	20,27	28,9	**29,3**	**29,2**	29,2	**19,4**	2 x 1000
D (tomo)	62	28.02.2014	9	M4 / 6	0,2190	0,6410	6,6159	1,505	**6,6117**	**1,503**	**4,002**	3,941	20,28	28,8	**29,3**	**29,3**	29,2	**19,4**	2 x 1000
G (tomo)	171	28.02.2014	14	M4 / 6	0,2190	0,6410	6,6159	1,505	**6,6126**	**1,506**	**3,996**	3,934	20,23	28,8	**29,3**	**29,3**	29,2	**19,5**	2 x 1000
J (tomo)	435	28.02.2014	18	M4 / 6	0,2190	0,6410	6,6159	1,505	**6,6108**	**1,506**	**4,001**	3,940	20,21	28,8	**29,2**	**29,2**	29,2	**19,4**	2 x 1000
M (tomo)	1271	28.02.2014	22	M4 / 6	0,2190	0,6410	6,6159	1,505	**6,6141**	**1,504**	**4,003**	3,940	20,14	28,8	**29,2**	**29,2**	29,2	**19,4**	2 x 1000
NN (tomo)	3054	28.02.2014	24	M4 / 6	0,2190	0,6410	6,6159	1,505	**6,6120**	**1,504**	**4,007**	3,942	20,24	28,8	**29,2**	**29,2**	29,2	**19,4**	2 x 1000

L21 – 118

level code	L	data	DIAdem	inj. Module	j Gas inj.	j water inj	Vgas inj.	mWater inj.	FIC4-1x	FIC4-0x	PI4-202	PI4-203	PDI4-200	TI4-03	TI4-200	TI4-201	TI4-10	TI4-205	freq
[-]	[mm]	[-]	[-]	[-]	[m/s]	[m/s]	[nm³/h]	[kg/s]	[nm³/h]	[kg/s]	bar	bar	kPa	°C	°C	°C	°C	°C	Hz
A (tomo)	5	27.02.2014	41	M4 / 6	0,2190	1,0170	6,6159	2,389	**6,6085**	**2,388**	**4,000**	3,937	16,88	29,1	**29,6**	**29,5**	29,4	**19,3**	2 x 1000
D (tomo)	62	27.02.2014	39	M4 / 6	0,2190	1,0170	6,6159	2,389	**6,6111**	**2,390**	**4,002**	3,940	17,26	29,1	**29,6**	**29,5**	29,5	**19,3**	2 x 1000
G (tomo)	171	27.02.2014	37	M4 / 6	0,2190	1,0170	6,6159	2,389	**6,6128**	**2,381**	**4,000**	3,942	17,18	29,1	**29,6**	**29,5**	29,5	**19,3**	2 x 1000
J (tomo)	435	27.02.2014	35	M4 / 6	0,2190	1,0170	6,6159	2,389	**6,6078**	**2,393**	**3,995**	3,935	16,73	29,1	**29,6**	**29,5**	29,5	**19,3**	2 x 1000
M (tomo)	1271	27.02.2014	33	M4 / 6	0,2190	1,0170	6,6159	2,389	**6,6119**	**2,400**	**3,991**	3,931	16,75	29,1	**29,6**	**29,6**	29,5	**19,3**	2 x 1000
NN (tomo)	3054	27.02.2014	31	M4 / 6	0,2190	1,0170	6,6159	2,389	**6,6086**	**2,395**	**4,006**	3,940	16,69	29,1	**29,6**	**29,6**	29,5	**19,3**	2 x 1000

L21 – 119

level code	L	data	DIAdem	inj. Module	j Gas inj.	j water inj	Vgas inj.	mWater inj.	FIC4-1x	FIC4-0x	PI4-202	PI4-203	PDI4-200	TI4-03	TI4-200	TI4-201	TI4-10	TI4-205	freq
[-]	[mm]	[-]	[-]	[-]	[m/s]	[m/s]	[nm³/h]	[kg/s]	[nm³/h]	[kg/s]	bar	bar	kPa	°C	°C	°C	°C	°C	Hz
A (tomo)	5	27.02.2014	10	M4 / 6	0,2190	1,6110	6,6159	3,784	**6,6119**	**3,786**	**4,007**	3,947	16,50	29,1	**29,6**	**29,5**	29,5	**19,3**	2 x 2500
D (tomo)	62	27.02.2014	13	M4 / 6	0,2190	1,6110	6,6159	3,784	**6,6082**	**3,782**	**3,997**	3,934	16,56	29,1	**29,6**	**29,5**	29,5	**19,3**	2 x 2500
G (tomo)	171	27.02.2014	17	M4 / 6	0,2190	1,6110	6,6159	3,784	**6,6068**	**3,783**	**3,999**	3,943	16,50	29,1	**29,6**	**29,6**	29,5	**19,3**	2 x 2500
J (tomo)	435	27.02.2014	20	M4 / 6	0,2190	1,6110	6,6159	3,784	**6,6109**	**3,783**	**3,997**	3,932	16,51	29,1	**29,6**	**29,6**	29,5	**19,2**	2 x 2500
M (tomo)	1271	27.02.2014	24	M4 / 6	0,2190	1,6110	6,6159	3,784	**6,6112**	**3,784**	**4,006**	3,947	16,50	29,2	**29,6**	**29,6**	29,5	**19,3**	2 x 2500
NN (tomo)	3054	27.02.2014	27	M4 / 6	0,2190	1,6110	6,6159	3,784	**6,6083**	**3,783**	**3,991**	3,926	16,55	29,2	**29,6**	**29,6**	29,6	**19,3**	2 x 2500

L21 – 138

level code	L	data	DIAdem	inj. Module	j Gas inj.	j water inj	Vgas inj.	mWater inj.	FIC4-1x	FIC4-0x	PI4-202	PI4-203	PDI4-200	TI4-03	TI4-200	TI4-201	TI4-10	TI4-205	freq
[-]	[mm]	[-]	[-]	[-]	[m/s]	[m/s]	[nm³/h]	[kg/s]	[nm³/h]	[kg/s]	bar	bar	kPa	°C	°C	°C	°C	°C	Hz
A (tomo)	5	28.02.2014	54	M4 / 6	0,5340	0,4050	16,132	0,951	**16,129**	**0,951**	**3,991**	3,926	50,68	29,0	**29,5**	**29,4**	29,4	**19,2**	2 x 1000
D (tomo)	62	28.02.2014	58	M4 / 6	0,5340	0,4050	16,132	0,951	**16,132**	**0,950**	**3,993**	3,929	50,78	29,0	**29,4**	**29,4**	29,3	**19,1**	2 x 1000
G (tomo)	171	28.02.2014	60	M4 / 6	0,5340	0,4050	16,132	0,951	**16,130**	**0,947**	**4,010**	3,942	50,76	29,0	**29,4**	**29,4**	29,3	**19,0**	2 x 1000
J (tomo)	435	28.02.2014	62	M4 / 6	0,5340	0,4050	16,132	0,951	**16,129**	**0,955**	**3,997**	3,939	50,69	28,9	**29,4**	**29,4**	29,3	**18,9**	2 x 1000
M (tomo)	1271	28.02.2014	66	M4 / 6	0,5340	0,4050	16,132	0,951	**16,122**	**0,953**	**4,002**	3,942	50,73	29,0	**29,4**	**29,4**	29,3	**18,8**	2 x 1000
NN (tomo)	3054	28.02.2014	69	M4 / 6	0,5340	0,4050	16,132	0,951	**16,129**	**0,951**	**3,996**	3,939	50,69	28,9	**29,4**	**29,4**	29,3	**18,7**	2 x 1000

L21 – 139

level code	L	data	DIAdem	inj. Module	j Gas inj.	j water inj	Vgas inj.	mWater inj.	FIC4-1x	FIC4-0x	PI4-202	PI4-203	PDI4-200	TI4-03	TI4-200	TI4-201	TI4-10	TI4-205	freq
[-]	[mm]	[-]	[-]	[-]	[m/s]	[m/s]	[nm³/h]	[kg/s]	[nm³/h]	[kg/s]	bar	bar	kPa	°C	°C	°C	°C	°C	Hz
A (tomo)	5	04.03.2014	70	M4 / 48	0,5340	0,6410	16,1320	1,505	**16,1256**	**1,507**	**4,005**	3,944	45,30	29,0	**29,5**	**29,4**	29,3	**16,8**	2 x 2000
D (tomo)	62	04.03.2014	73	M4 / 48	0,5340	0,6410	16,1320	1,505	**16,1347**	**1,500**	**4,004**	3,947	46,02	29,0	**29,5**	**29,5**	29,4	**17,0**	2 x 2000
G (tomo)	171	04.03.2014	76	M4 / 48	0,5340	0,6410	16,1320	1,505	**16,1308**	**1,507**	**4,005**	3,946	45,48	29,0	**29,4**	**29,4**	29,4	**17,0**	2 x 2000
J (tomo)	435	04.03.2014	78	M4 / 48	0,5340	0,6410	16,1320	1,505	**16,1292**	**1,508**	**4,002**	3,944	45,48	29,0	**29,5**	**29,5**	29,4	**17,1**	2 x 2000
M (tomo)	1271	04.03.2014	84	M4 / 48	0,5340	0,6410	16,1320	1,505	**16,1269**	**1,509**	**4,001**	3,945	45,16	29,1	**29,5**	**29,5**	29,4	**17,1**	2 x 2000
NN (tomo)	3054	04.03.2014	87	M4 / 48	0,5340	0,6410	16,1320	1,505	**16,1338**	**1,502**	**4,004**	3,945	45,64	29,1	**29,5**	**29,5**	29,4	**17,2**	2 x 2000

L21 – 150

level code	L	data	DIAdem	inj. Module	j Gas inj.	j water inj	Vgas inj.	mWater inj.	FIC4-1x	FIC4-0x	PI4-202	PI4-203	PDI4-200	TI4-03	TI4-200	TI4-201	TI4-10	TI4-205	freq
[-]	[mm]	[-]	[-]	[-]	[m/s]	[m/s]	[nm³/h]	[kg/s]	[nm³/h]	[kg/s]	bar	bar	kPa	°C	°C	°C	°C	°C	Hz
A (tomo)	5	04.03.2014	65	M4 / 48	0,8350	0,6410	25,2252	1,505	**25,2294**	**1,505**	**4,000**	3,944	48,40	29,0	**29,5**	**29,4**	29,4	**16,8**	2 x 2000
D (tomo)	62	04.03.2014	60	M4 / 48	0,8350	0,6410	25,2252	1,505	**25,2293**	**1,505**	**4,002**	3,942	48,48	29,0	**29,4**	**29,4**	29,4	**16,8**	2 x 2000
G (tomo)	171	04.03.2014	57	M4 / 48	0,8350	0,6410	25,2252	1,505	**25,2254**	**1,505**	**4,000**	3,944	48,37	29,0	**29,4**	**29,4**	29,4	**16,8**	2 x 2000
J (tomo)	435	04.03.2014	55	M4 / 48	0,8350	0,6410	25,2252	1,505	**25,2279**	**1,504**	**3,999**	3,945	48,52	29,0	**29,5**	**29,5**	29,3	**16,8**	2 x 2000
M (tomo)	1271	04.03.2014	53	M4 / 48	0,8350	0,6410	25,2252	1,505	**25,2311**	**1,503**	**4,004**	3,946	48,57	29,0	**29,4**	**29,4**	29,4	**16,8**	2 x 2000
NN (tomo)	3054	04.03.2014	50	M4 / 48	0,8350	0,6410	25,2252	1,505	**25,2249**	**1,508**	**3,998**	3,937	48,55	29,0	**29,4**	**29,4**	29,3	**16,8**	2 x 2000

L21 – 151

level code	L	data	DIAdem	inj. Module	j Gas inj.	j water inj	Vgas inj.	mWater inj.	FIC4-1x	FIC4-0x	PI4-202	PI4-203	PDI4-200	TI4-03	TI4-200	TI4-201	TI4-10	TI4-205	freq
[-]	[mm]	[-]	[-]	[-]	[m/s]	[m/s]	[nm³/h]	[kg/s]	[nm³/h]	[kg/s]	bar	bar	kPa	°C	°C	°C	°C	°C	Hz
A (tomo)	5	04.03.2014	24	M4 / 48	0,8350	1,0170	25,2252	2,389	**25,2260**	**2,392**	**3,991**	3,927	39,75	29,0	**29,4**	**29,4**	29,4	**17,1**	2 x 2500
D (tomo)	62	04.03.2014	27	M4 / 48	0,8350	1,0170	25,2252	2,389	**25,2250**	**2,392**	**3,991**	3,931	40,15	29,0	**29,4**	**29,4**	29,3	**17,1**	2 x 2500
G (tomo)	171	04.03.2014	34	M4 / 48	0,8350	1,0170	25,2252	2,389	**25,2236**	**2,393**	**4,002**	3,941	39,78	29,0	**29,4**	**29,4**	29,4	**17,0**	2 x 2500
J (tomo)	435	04.03.2014	37	M4 / 48	0,8350	1,0170	25,2252	2,389	**25,2261**	**2,390**	**4,004**	3,943	40,14	29,0	**29,4**	**29,4**	29,4	**16,9**	2 x 2500
M (tomo)	1271	04.03.2014	40	M4 / 48	0,8350	1,0170	25,2252	2,389	**25,2215**	**2,392**	**4,011**	3,945	39,76	29,0	**29,4**	**29,4**	29,4	**16,9**	2 x 2500
NN (tomo)	3054	04.03.2014	43	M4 / 48	0,8350	1,0170	25,2252	2,389	**25,2251**	**2,391**	**4,006**	3,947	39,62	29,0	**29,4**	**29,4**	29,4	**16,9**	2 x 2500

L21 – 152

level code	L	data	DIAdem	inj. Module	j Gas inj.	j water inj	Vgas inj.	mWater inj.	FIC4-1x	FIC4-0x	PI4-202	PI4-203	PDI4-200	TI4-03	TI4-200	TI4-201	TI4-10	TI4-205	freq
[-]	[mm]	[-]	[-]	[-]	[m/s]	[m/s]	[nm³/h]	[kg/s]	[nm³/h]	[kg/s]	bar	bar	kPa	°C	°C	°C	°C	°C	Hz
A (tomo)	5	04.03.2014	20	M4 / 48	0,8350	1,6110	25,2252	3,784	**25,2248**	**3,784**	**3,999**	3,942	34,59	29,0	**29,4**	**29,4**	29,4	**17,3**	2 x 2500
D (tomo)	62	04.03.2014	17	M4 / 48	0,8350	1,6110	25,2252	3,784	**25,2279**	**3,787**	**3,998**	3,944	34,37	28,9	**29,4**	**29,4**	29,4	**17,4**	2 x 2500
G (tomo)	171	04.03.2014	12	M4 / 48	0,8350	1,6110	25,2252	3,784	**25,2237**	**3,786**	**4,001**	3,946	34,29	28,9	**29,4**	**29,3**	29,3	**17,5**	2 x 2500
J (tomo)	435	04.03.2014	7	M4 / 48	0,8350	1,6110	25,2252	3,784	**25,2293**	**3,784**	**4,005**	3,949	34,29	28,8	**29,3**	**29,2**	29,2	**17,7**	2 x 2500
M (tomo)	1271	04.03.2014	5	M4 / 48	0,8350	1,6110	25,2252	3,784	**25,2250**	**3,785**	**4,002**	3,945	34,30	28,8	**29,3**	**29,2**	29,2	**17,9**	2 x 2500
NN (tomo)	3054	04.03.2014	3	M4 / 48	0,8350	1,6110	25,2252	3,784	**25,2285**	**3,783**	**3,998**	3,940	34,50	28,7	**29,2**	**29,2**	29,1	**18,0**	2 x 2500

L21 – 162

level code	L	data	DIAdem	inj. Module	j Gas inj.	j water inj	Vgas inj.	mWater inj.	FIC4-1x	FIC4-0x	PI4-202	PI4-203	PDI4-200	TI4-03	TI4-200	TI4-201	TI4-10	TI4-205	freq
[-]	[mm]	[-]	[-]	[-]	[m/s]	[m/s]	[nm³/h]	[kg/s]	[nm³/h]	[kg/s]	bar	bar	kPa	°C	°C	°C	°C	°C	Hz
A (tomo)	5	03.03.2014	23	M4 / 54	1,3050	1,0170	39,4238	2,389	**39,4250**	**2,392**	**4,005**	3,945	46,47	29,1	**29,6**	**29,5**	29,5	**16,2**	2 x 2500
D (tomo)	62	03.03.2014	30	M4 / 54	1,3050	1,0170	39,4238	2,389	**39,4282**	**2,388**	**4,002**	3,940	46,42	29,1	**29,6**	**29,5**	29,5	**16,1**	2 x 2500
G (tomo)	171	03.03.2014	32	M4 / 54	1,3050	1,0170	39,4238	2,389	**39,4301**	**2,387**	**4,004**	3,946	46,41	29,1	**29,5**	**29,5**	29,4	**16,1**	2 x 2500
J (tomo)	435	03.03.2014	35	M4 / 54	1,3050	1,0170	39,4238	2,389	**39,4258**	**2,391**	**3,995**	3,935	46,30	29,1	**29,6**	**29,6**	29,5	**16,0**	2 x 2500
M (tomo)	1271	03.03.2014	37	M4 / 54	1,3050	1,0170	39,4238	2,389	**39,4245**	**2,390**	**3,997**	3,937	46,38	29,1	**29,6**	**29,6**	29,5	**16,0**	2 x 2500
NN (tomo)	3054	03.03.2014	40	M4 / 54	1,3050	1,0170	39,4238	2,389	**39,4254**	**2,387**	**4,001**	3,943	46,27	29,1	**29,6**	**29,5**	29,5	**15,9**	2 x 2500

L21 – 163

level code	L	data	DIAdem	inj. Module	j Gas inj.	j water inj	Vgas inj.	mWater inj.	FIC4-1x	FIC4-0x	PI4-202	PI4-203	PDI4-200	TI4-03	TI4-200	TI4-201	TI4-10	TI4-205	freq
[-]	[mm]	[-]	[-]	[-]	[m/s]	[m/s]	[nm³/h]	[kg/s]	[nm³/h]	[kg/s]	bar	bar	kPa	°C	°C	°C	°C	°C	Hz
A (tomo)	5	03.03.2014	19	M4 / 54	1,3050	1,6110	39,4238	3,784	**39,4247**	**3,784**	**3,996**	3,937	42,13	29,1	**29,6**	**29,5**	29,5	**16,5**	2 x 2500
D (tomo)	62	03.03.2014	15	M4 / 54	1,3050	1,6110	39,4238	3,784	**39,4262**	**3,783**	**4,000**	3,939	42,12	29,0	**29,5**	**29,5**	29,4	**16,7**	2 x 2500
G (tomo)	171	03.03.2014	11	M4 / 54	1,3050	1,6110	39,4238	3,784	**39,4279**	**3,781**	**3,999**	3,942	42,31	29,0	**29,5**	**29,5**	29,4	**17,0**	2 x 2500
J (tomo)	435	03.03.2014	8	M4 / 54	1,3050	1,6110	39,4238	3,784	**39,4242**	**3,784**	**4,004**	3,944	42,14	29,0	**29,4**	**29,4**	29,4	**17,3**	2 x 2500
M (tomo)	1271	03.03.2014	6	M4 / 54	1,3050	1,6110	39,4238	3,784	**39,4217**	**3,783**	**4,003**	3,943	42,31	29,0	**29,4**	**29,4**	29,4	**17,6**	2 x 2500
NN (tomo)	3054	03.03.2014	3	M4 / 54	1,3050	1,6110	39,4238	3,784	**39,4254**	**3,785**	**4,003**	3,944	42,16	28,9	**29,4**	**29,4**	29,4	**18,0**	2 x 2500

L22

MP	level code	L	data	DIAdem	inj. Module	j Gas inj.	j water inj	Vgas inj.	mWater inj.	FIC4-1x	FIC4-0x	PI4-200	PI4-201	PDI4-200	TI4-03	TI4-200	TI4-201	TI4-10	TI4-202	freq Tomo
	[-]	[mm]	[-]	[-]	[-]	[m/s]	[m/s]	[nm³/h]	[kg/s]	[nm³/h]	[kg/s]	bar	bar	kPa	°C	°C	°C	°C	°C	Hz
001	N (tomo)	2740	11.08.2014	27	M3 / 1	0,0025	0,0405	0,0542	0,091	**0,0543**	**0,091**	**3,005**	3,033	0,69	30,5	**29,7**	**29,5**	29,9	**23,4**	2 x 1000
	(wms)	2755																		
004	N (tomo)	2740	11.08.2014	29	M3 / 1	0,0025	0,161	0,0542	0,362	**0,0543**	**0,362**	**3,006**	3,033	0,53	30,8	**30,6**	**30,6**	29,7	**24,1**	2 x 1000
	(wms)	2755																		
006	N (tomo)	2740	11.08.2014	33	M3 / 1	0,0025	0,405	0,0542	0,910	**0,0542**	**0,909**	**3,002**	3,034	0,13	29,8	**30,0**	**30,0**	30,1	**23,8**	2 x 1000
	(wms)	2755																		
008	N (tomo)	2740	11.08.2014	10	M3 / 1	0,0025	1,017	0,0542	2,285	**0,0542**	**2,283**	**3,003**	3,033	-1,83	29,5	**29,8**	**29,7**	29,8	**23,5**	2 x 2500
	(wms)	2755																		
034	N (tomo)	2740	11.08.2014	26	M3 / 3	0,0096	0,0405	0,2081	0,091	**0,2081**	**0,091**	**3,004**	3,037	1,70	30,2	**29,5**	**29,4**	30,0	**23,3**	2 x 1000
	(wms)	2755																		
037	N (tomo)	2740	11.08.2014	30	M3 / 3	0,0096	0,161	0,2081	0,362	**0,2081**	**0,361**	**3,002**	3,033	1,30	30,3	**30,7**	**30,7**	30,1	**24,1**	2 x 1000
	(wms)	2755																		
039	N (tomo)	2740	11.08.2014	35	M3 / 3	0,0096	0,405	0,2081	0,910	**0,2081**	**0,910**	**3,005**	3,037	0,54	29,9	**30,0**	**30,0**	30,1	**23,8**	2 x 1000
	(wms)	2755																		
041	N (tomo)	2740	11.08.2014	7	M3 / 3	0,0096	1,017	0,2081	2,285	**0,2081**	**2,285**	**3,002**	3,033	-1,63	29,5	**29,8**	**29,7**	29,8	**23,5**	2 x 2500
	(wms)	2755																		
067	N (tomo)	2740	11.08.2014	25	M3 / 3	0,0368	0,0405	0,7977	0,091	**0,7974**	**0,091**	**3,002**	3,025	7,20	29,8	**29,5**	**29,3**	30,0	**23,2**	2 x 1000
	(wms)	2755																		
074	N (tomo)	2740	11.08.2014	5	M3 / 3	0,0368	1,017	0,7977	2,285	**0,7977**	**2,284**	**3,002**	3,019	-0,82	29,4	**29,6**	**29,6**	29,7	**23,2**	2 x 2500
	(wms)	2755																		
077	N (tomo)	2740	11.08.2014	12	M3 / 3	0,0368	4,047	0,7977	9,093	**0,7972**	**9,089**	**3,007**	3,033	-28,34	29,4	**29,6**	**29,6**	29,8	**23,3**	2 x 2500
	(wms)	2755																		
			11.08.2014	20	M3 / 3	0,0368	4,047	0,7977	9,093	**0,7976**	**9,097**	**3,000**	3,025	-28,47	29,7	**29,9**	**29,9**	30,1	**23,2**	1 x 5000
089	N (tomo)	2740	11.08.2014	24	M3 / 4	0,0898	0,0405	1,9465	0,091	**1,9458**	**0,091**	**3,001**	3,023	12,51	29,7	**29,5**	**29,5**	30,0	**23,2**	2 x 1000
	(wms)	2755																		
096	N (tomo)	2740	11.08.2014	1	M3 / 4	0,0898	1,017	1,9465	2,285	**1,9457**	**2,286**	**3,001**	3,032	0,71	29,4	**29,6**	**29,5**	29,7	**23,1**	2 x 2500
	(wms)	2755																		
099	N (tomo)	2740	11.08.2014	15	M3 / 4	0,0898	4,047	1,9465	9,093	**1,9458**	**9,078**	**2,995**	3,021	-28,32	29,5	**29,7**	**29,7**	29,9	**23,2**	2 x 2500
	(wms)	2755																		
			11.08.2014	18	M3 / 4	0,0898	4,047	1,9465	9,093	**1,9455**	**9,065**	**3,003**	3,028	-28,15	29,7	**29,8**	**29,8**	30,0	**23,2**	1 x 5000

L23

MP	level code	L	data	DIAdem	inj. Module	j Gas inj.	j water inj	Vgas inj.	mWater inj.	FIC4-1x	FIC4-0x	PI4-200	PI4-201	PDI4-200	TI4-03	TI4-200	TI4-201	TI4-10	TI4-202	freq Tomo
	[-]	[mm]	[-]	[-]	[-]	[m/s]	[m/s]	[nm³/h]	[kg/s]	[nm³/h]	[kg/s]	bar	bar	kPa	°C	°C	°C	°C	°C	Hz
111	N (tomo)	2740	06.08.2014	10	M4 / 6	0,2190	0,0405	4,747	0,091	**4,748**	**0,091**	**2,995**	3,028	23,57	30,1	**29,7**	**29,4**	29,7	**22,4**	2 x 1000
	(wms)	2755																		
114	N (tomo)	2740	06.08.2014	14	M4 / 6	0,2190	0,161	4,747	0,362	**4,748**	**0,362**	**3,005**	3,035	18,36	30,4	**30,6**	**30,5**	29,8	**22,4**	2 x 1000
	(wms)	2755																		
116	N (tomo)	2740	06.08.2014	16	M4 / 6	0,2190	0,405	4,747	0,910	**4,748**	**0,910**	**3,002**	3,035	12,41	29,7	**30,1**	**30,0**	30,3	**22,3**	2 x 1000
	(wms)	2755																		
			06.08.2014	46	M4 / 6	0,2190	0,405	4,747	0,910	**4,748**	**0,908**	**3,007**	3,037	12,20	30,0	**30,2**	**30,1**	30,2	**18,9**	2 x 2500
118	N (tomo)	2740	06.08.2014	49	M4 / 6	0,2190	1,017	4,747	2,285	**4,748**	**2,284**	**3,006**	3,032	3,97	29,9	**30,1**	**30,0**	30,2	**19,3**	2 x 2500
	(wms)	2755																		
121	N (tomo)	2740	06.08.2014	51	M4 / 6	0,2190	4,047	4,747	9,093	**4,748**	**9,118**	**3,006**	3,036	-37,24	30,0	**30,2**	**30,1**	30,3	**19,7**	2 x 2500
	(wms)	2755																		
			07.08.2014	2	M4 / 6	0,2190	4,047	4,747	9,093	**4,748**	**9,089**	**2,999**	3,027	-37,10	29,8	**30,2**	**30,1**	30,3	**22,4**	1 x 5000
133	N (tomo)	2740	06.08.2014	19	M4 / 48	0,534	0,0405	11,575	0,091	**11,572**	**0,091**	**2,994**	3,024	33,85	29,7	**30,0**	**29,6**	29,8	**22,0**	2 x 1000
	(wms)	2755																		
			06.08.2014	24	M4 / 48	0,534	0,0405	11,575	0,091	**11,579**	**0,091**	**2,998**	3,020	33,65	29,5	**29,7**	**29,3**	30,0	**20,7**	2 x 2500
140	N (tomo)	2740	06.08.2014	26	M4 / 48	0,534	1,017	11,575	2,285	**11,580**	**2,285**	**3,010**	3,035	10,23	29,7	**30,0**	**29,9**	30,0	**20,3**	2 x 2500
	(wms)	2755																		
143	N (tomo)	2740	06.08.2014	28	M4 / 48	0,534	4,047	11,575	9,093	**11,582**	**9,072**	**2,997**	3,022	-37,76	29,7	**30,0**	**30,0**	30,0	**20,6**	2 x 2500
	(wms)	2755																		
			07.08.2014	4	M4 / 48	0,534	4,047	11,575	9,093	**11,584**	**9,085**	**2,999**	3,030	-37,78	29,7	**30,0**	**30,0**	30,1	**21,3**	1 x 5000
155	N (tomo)	2740	06.08.2014	53	M4 / 54	1,305	0,0405	28,287	0,091	**28,227**	**0,091**	**3,000**	3,026	37,67	30,0	**30,1**	**29,5**	30,3	**19,2**	2 x 2500
	(wms)	2755																		
162	N (tomo)	2740	06.08.2014	38	M4 / 54	1,305	1,017	28,287	2,285	**28,284**	**2,275**	**2,998**	3,021	17,91	29,9	**30,2**	**30,1**	30,2	**19,0**	2 x 2500
	(wms)	2755																		
			07.08.2014	12	M4 / 54	1,305	1,017	28,287	2,285	**28,288**	**2,286**	**2,993**	3,017	17,85	29,4	**29,6**	**29,5**	29,7	**18,3**	1 x 5000
165	N (tomo)	2740	06.08.2014	30	M4 / 54	1,305	4,047	28,287	9,093	**28,285**	**9,073**	**2,999**	3,031	-41,19	29,9	**30,2**	**30,1**	30,2	**19,6**	2 x 2500
	(wms)	2755																		
			07.08.2014	8	M4 / 54	1,305	4,047	28,287	9,093	**28,291**	**9,091**	**2,999**	3,033	-41,27	29,5	**29,8**	**29,8**	29,9	**20,1**	1 x 5000
177	N (tomo)	2740	06.08.2014	57	M4 / 54	3,185	0,0405	69,038	0,091	**69,093**	**0,091**	**2,992**	3,019	44,92	30,1	**30,1**	**28,4**	30,3	**17,2**	2 x 2500
	(wms)	2755																		
			07.08.2014	18	M4 / 54	3,185	0,0405	69,038	0,091	**69,065**	**0,091**	**3,001**	3,026	44,53	29,3	**29,2**	**27,8**	29,6	**17,5**	1 x 5000
184	N (tomo)	2740	06.08.2014	55	M4 / 54	3,185	1,017	69,038	2,285	**69,085**	**2,284**	**2,989**	3,020	23,76	30,1	**30,3**	**30,1**	30,3	**17,8**	2 x 2500
	(wms)	2755																		
			07.08.2014	14	M4 / 54	3,185	1,017	69,038	2,285	**69,079**	**2,282**	**3,000**	3,031	23,26	29,3	**29,5**	**29,4**	29,6	**18,0**	1 x 5000

D19 – p=4.0 MPa – 151

level code	L	data	DIAdem	inj. Module	j Gas inj.	j water inj.	m gas inj.	m water inj.	FIC4-4/5	FIC4-0x	PI4-06	PI4-201	PI4-07	PDI4-200	TI4-05	TI4-07	TI4-202	TI4-03	TI4-200	TI4-201	TI4-203	TI4-204	TI4-10	Frequency
[-]	[mm]	[-]	[-]	[-]	[m/s]	[m/s]	[kg/s]	[kg/s]	[kg/s]	[kg/s]	bar	bar	bar	kPa	°C	°C	°C	°C	°C	°C	°C	°C	°C	Hz
C (tomo)	18	10.07.2013	2	M4 / 54	2,0380	1,017	0,162	1,796	**0,161**	**1,796**	67,520	**64,992**	64,794	32,75	283,7	281,8	**282,9**	277,0	**278,0**	**280,7**	80,6	76,3	280,8	2 x 2500
C (tomo)	18	10.07.2013	42	M4 / 54	2,0380	1,017	0,162	1,796	**0,163**	**1,795**	67,644	**64,997**	64,797	33,46	283,8	282,0	**282,9**	277,8	**278,7**	**280,7**	81,1	78,1	280,8	1 x 5000
E (tomo)	94	10.07.2013	4	M4 / 54	2,0380	1,017	0,162	1,796	**0,162**	**1,796**	67,564	**65,002**	64,798	32,89	283,7	281,8	**283,0**	277,2	**278,2**	**280,7**	80,5	75,9	280,8	2 x 2500
E (tomo)	94	10.07.2013	37	M4 / 54	2,0380	1,017	0,162	1,796	**0,162**	**1,795**	67,629	**65,004**	64,799	33,30	283,7	281,9	**282,9**	277,7	**278,6**	**280,8**	80,6	78,2	280,8	1 x 5000
G (tomo)	171	10.07.2013	9	M4 / 54	2,0380	1,017	0,162	1,796	**0,162**	**1,796**	67,563	**64,989**	64,800	32,99	283,7	281,8	**283,0**	277,2	**278,2**	**280,6**	80,4	75,8	280,8	2 x 2500
G (tomo)	171	10.07.2013	34	M4 / 54	2,0380	1,017	0,162	1,796	**0,162**	**1,796**	67,616	**64,991**	64,788	33,34	283,8	281,9	**282,9**	277,4	**278,5**	**280,8**	80,8	78,6	280,8	1 x 5000
J (tomo)	435	10.07.2013	14	M4 / 54	2,0380	1,017	0,162	1,796	**0,162**	**1,796**	67,607	**64,998**	64,799	33,10	283,8	281,9	**283,0**	277,3	**278,3**	**280,8**	80,7	76,7	280,8	2 x 2500
J (tomo)	435	10.07.2013	32	M4 / 54	2,0380	1,017	0,162	1,796	**0,162**	**1,797**	67,614	**64,999**	64,797	33,28	283,7	281,9	**282,9**	277,5	**278,4**	**280,8**	80,4	78,2	280,8	1 x 5000
M (tomo)	1271	10.07.2013	17	M4 / 54	2,0380	1,017	0,162	1,796	**0,161**	**1,792**	67,579	**65,001**	64,797	32,53	283,7	281,8	**282,9**	276,3	**276,6**	**280,7**	80,2	75,7	280,8	2 x 2500
M (tomo)	1271	10.07.2013	28	M4 / 54	2,0380	1,017	0,162	1,796	**0,161**	**1,795**	67,603	**65,000**	64,804	33,26	283,7	281,9	**282,9**	277,4	**278,5**	**280,8**	81,2	76,9	280,8	1 x 5000
P (tomo)	3270	10.07.2013	21	M4 / 54	2,0380	1,017	0,162	1,796	**0,161**	**1,795**	67,572	**64,997**	64,789	33,08	283,7	281,8	**282,9**	277,3	**278,3**	**280,7**	79,9	78,6	280,8	2 x 2500
P (tomo)	3270	10.07.2013	25	M4 / 54	2,0380	1,017	0,162	1,796	**0,163**	**1,796**	67,651	**64,997**	64,790	33,33	283,8	282,0	**282,9**	277,4	**278,4**	**280,7**	79,8	79,9	280,8	1 x 5000
S (wms)	4685	10.07.2013	21	M4 / 54	2,0380	1,017	0,162	1,796	**0,161**	**1,795**	67,572	**64,997**	64,789	33,08	283,7	281,8	**282,9**	277,3	**278,3**	**280,7**	79,9	78,6	280,8	2 x 5000

D19 – p=4.0 MPa – 160

level code	L	data	DIAdem	inj. Module	j Gas inj.	j water inj.	m gas inj.	m water inj.	FIC4-4/5	FIC4-0x	PI4-06	PI4-201	PI4-07	PDI4-200	TI4-05	TI4-07	TI4-202	TI4-03	TI4-200	TI4-201	TI4-203	TI4-204	TI4-10	Frequency
[-]	[mm]	[-]	[-]	[-]	[m/s]	[m/s]	[kg/s]	[kg/s]	[kg/s]	[kg/s]	bar	bar	bar	kPa	°C	°C	°C	°C	°C	°C	°C	°C	°C	Hz
C (tomo)	18	04.07.2013	79	M4 / 54	1,3050	0,405	0,062	0,763	**0,062**	**0,762**	40,796	**40,001**	39,861	31,42	251,8	250,2	**251,0**	247,0	**246,2**	**250,2**	74,7	68,9	250,4	2 x 2500
E (tomo)	94	04.07.2013	82	M4 / 54	1,3050	0,405	0,062	0,763	**0,061**	**0,762**	40,792	**39,999**	39,861	31,42	251,7	250,2	**250,9**	247,1	**246,3**	**250,2**	73,7	69,1	250,4	2 x 2500
G (tomo)	171	04.07.2013	84	M4 / 54	1,3050	0,405	0,062	0,763	**0,062**	**0,762**	40,812	**40,004**	39,860	31,45	251,7	250,2	**251,0**	247,1	**246,4**	**250,2**	74,1	69,3	250,4	2 x 2500
J (tomo)	435	04.07.2013	89	M4 / 54	1,3050	0,405	0,062	0,763	**0,062**	**0,764**	40,803	**40,004**	39,860	31,65	251,7	250,2	**251,1**	247,1	**246,4**	**250,2**	74,4	69,2	250,4	2 x 2500
M (tomo)	1271	04.07.2013	91	M4 / 54	1,3050	0,405	0,062	0,763	**0,062**	**0,763**	40,812	**40,006**	39,868	31,51	251,7	250,2	**251,1**	247,1	**246,5**	**250,2**	74,6	69,7	250,4	2 x 2500
P (tomo)	3270	04.07.2013	97	M4 / 54	1,3050	0,405	0,062	0,763	**0,062**	**0,763**	40,808	**40,002**	39,866	31,74	251,7	250,2	**251,0**	247,1	**246,5**	**250,2**	74,2	66,4	250,4	2 x 2500
S (wms)	4685	04.07.2013	97	M4 / 54	1,3050	0,405	0,062	0,763	**0,062**	**0,763**	40,808	**40,002**	39,866	31,74	251,7	250,2	**251,0**	247,1	**246,5**	**250,2**	74,2	66,4	250,4	2 x 5000

D19 – p=4.0 MPa – 163

level code	L	data	DIAdem	inj. Module	j Gas inj.	j water inj.	m gas inj.	m water inj.	FIC4-4/5	FIC4-0x	PI4-06	PI4-201	PI4-07	PDI4-200	TI4-05	TI4-07	TI4-202	TI4-03	TI4-200	TI4-201	TI4-203	TI4-204	TI4-10	Frequency
[-]	[mm]	[-]	[-]	[-]	[m/s]	[m/s]	[kg/s]	[kg/s]	[kg/s]	[kg/s]	bar	bar	bar	kPa	°C	°C	°C	°C	°C	°C	°C	°C	°C	Hz
C (tomo)	18	04.07.2013	15	M4 / 54	1,3050	1,611	0,062	3,034	**0,062**	**3,033**	40,946	**39,987**	39,712	14,91	252,0	250,4	**251,2**	247,3	**248,0**	**250,2**	74,2	67,7	250,1	2 x 2500
C (tomo)	18	04.07.2013	62	M4 / 54	1,3050	1,611	0,062	3,034	**0,063**	**3,036**	40,962	**40,004**	39,732	15,69	252,0	250,4	**251,3**	247,5	**248,4**	**250,1**	75,2	69,8	250,3	1 x 5000
E (tomo)	94	04.07.2013	17	M4 / 54	1,3050	1,611	0,062	3,034	**0,063**	**3,035**	40,932	**39,982**	39,707	15,29	251,9	250,3	**251,2**	247,4	**248,1**	**250,2**	74,2	68,2	250,1	2 x 2500
E (tomo)	94	04.07.2013	57	M4 / 54	1,3050	1,611	0,062	3,034	**0,062**	**3,034**	40,943	**40,001**	39,724	15,46	252,0	250,4	**251,4**	247,5	**248,4**	**250,2**	74,6	69,2	250,3	1 x 5000
G (tomo)	171	04.07.2013	19	M4 / 54	1,3050	1,611	0,062	3,034	**0,061**	**3,036**	40,922	**40,001**	39,724	15,04	251,9	250,3	**251,2**	247,4	**248,1**	**250,2**	74,1	68,1	250,2	2 x 2500
G (tomo)	171	04.07.2013	53	M4 / 54	1,3050	1,611	0,062	3,034	**0,062**	**3,034**	40,911	**39,996**	39,715	15,72	251,9	250,3	**251,3**	247,5	**248,4**	**250,2**	74,1	69,2	250,3	1 x 5000
J (tomo)	435	04.07.2013	25	M4 / 54	1,3050	1,611	0,062	3,034	**0,062**	**3,033**	40,962	**40,003**	39,725	15,07	252,0	250,4	**251,2**	247,5	**248,2**	**250,2**	74,1	67,3	250,2	2 x 2500
J (tomo)	435	04.07.2013	48	M4 / 54	1,3050	1,611	0,062	3,034	**0,061**	**3,035**	40,921	**40,006**	39,732	15,26	251,9	250,4	**251,3**	247,5	**248,4**	**250,2**	74,8	69,8	250,3	1 x 5000
M (tomo)	1271	04.07.2013	29	M4 / 54	1,3050	1,611	0,062	3,034	**0,063**	**3,035**	40,928	**40,001**	39,723	15,55	251,9	250,4	**251,2**	247,5	**248,3**	**250,2**	74,4	68,2	250,2	2 x 2500
M (tomo)	1271	04.07.2013	45	M4 / 54	1,3050	1,611	0,062	3,034	**0,062**	**3,034**	40,921	**40,004**	39,732	15,45	251,9	250,4	**251,3**	247,5	**248,4**	**250,1**	74,2	69,0	250,2	1 x 5000
P (tomo)	3270	04.07.2013	34	M4 / 54	1,3050	1,611	0,062	3,034	**0,062**	**3,033**	40,926	**39,994**	39,724	15,43	251,9	250,4	**251,4**	247,5	**248,3**	**250,2**	74,0	64,7	250,2	2 x 2500
P (tomo)	3270	04.07.2013	42	M4 / 54	1,3050	1,611	0,062	3,034	**0,061**	**3,033**	40,911	**40,004**	39,734	15,28	251,9	250,3	**251,3**	247,5	**248,4**	**250,2**	74,8	66,9	250,3	1 x 5000
S (wms)	4685	04.07.2013	34	M4 / 54	1,3050	1,611	0,062	3,034	**0,062**	**3,033**	40,926	**39,994**	39,724	15,43	251,9	250,4	**251,4**	247,5	**248,3**	**250,2**	74,0	64,7	250,2	2 x 5000

D19 – p=4.0 MPa – 173

level code	L	data	DIAdem	inj. Module	j Gas inj.	j water inj.	m gas inj.	m water inj.	FIC4-4/5	FIC4-0x	PI4-06	PI4-201	PI4-07	PDI4-200	TI4-05	TI4-07	TI4-202	TI4-03	TI4-200	TI4-201	TI4-203	TI4-204	TI4-10	Frequency
[-]	[mm]	[-]	[-]	[-]	[m/s]	[m/s]	[kg/s]	[kg/s]	[kg/s]	[kg/s]	bar	bar	bar	kPa	°C	°C	°C	°C	°C	°C	°C	°C	°C	Hz
C (tomo)	18	08.07.2013	8	M4 / 54	2,0380	1,017	0,097	1,915	**0,096**	**1,913**	41,518	**39,997**	39,785	28,00	252,8	251,2	**252,0**	246,5	**246,8**	**250,1**	75,7	71,2	250,4	2 x 2500
C (tomo)	18	08.07.2013	65	M4 / 54	2,0380	1,017	0,097	1,915	**0,096**	**1,916**	41,527	**40,003**	39,785	28,65	252,8	251,2	**252,0**	247,2	**247,8**	**250,2**	74,4	67,0	250,3	1 x 5000
E (tomo)	94	08.07.2013	11	M4 / 54	2,0380	1,017	0,097	1,915	**0,096**	**1,913**	41,542	**40,004**	39,785	28,33	252,9	251,2	**252,1**	246,8	**247,2**	**250,1**	76,2	70,6	250,4	2 x 2500
E (tomo)	94	08.07.2013	61	M4 / 54	2,0380	1,017	0,097	1,915	**0,098**	**1,915**	41,534	**39,987**	39,768	28,93	252,8	251,2	**252,0**	247,2	**247,7**	**250,1**	75,8	69,3	250,3	1 x 5000
G (tomo)	171	08.07.2013	14	M4 / 54	2,0380	1,017	0,097	1,915	**0,097**	**1,914**	41,551	**40,009**	39,782	28,50	252,9	251,2	**252,1**	247,0	**247,3**	**250,2**	75,1	68,1	250,4	2 x 2500
G (tomo)	171	08.07.2013	58	M4 / 54	2,0380	1,017	0,097	1,915	**0,098**	**1,915**	41,565	**39,991**	39,770	28,79	252,8	251,2	**252,0**	247,2	**247,7**	**250,1**	75,5	68,0	250,3	1 x 5000
J (tomo)	435	08.07.2013	18	M4 / 54	2,0380	1,017	0,097	1,915	**0,096**	**1,914**	41,522	**40,005**	39,782	28,36	252,8	251,1	**252,0**	247,1	**247,4**	**250,2**	74,8	68,1	250,3	2 x 2500
J (tomo)	435	08.07.2013	53	M4 / 54	2,0380	1,017	0,097	1,915	**0,097**	**1,915**	41,541	**39,995**	39,777	28,77	252,7	251,1	**252,0**	247,2	**247,7**	**250,1**	76,1	68,2	250,3	1 x 5000
M (tomo)	1271	08.07.2013	22	M4 / 54	2,0380	1,017	0,097	1,915	**0,097**	**1,915**	41,541	**40,009**	39,789	28,55	252,9	251,3	**252,0**	247,1	**247,5**	**250,1**	74,8	66,6	250,3	2 x 2500
M (tomo)	1271	08.07.2013	48	M4 / 54	2,0380	1,017	0,097	1,915	**0,097**	**1,915**	41,546	**39,992**	39,769	28,85	252,8	251,2	**251,9**	247,2	**247,7**	**250,1**	76,3	69,2	250,3	1 x 5000
P (tomo)	3270	08.07.2013	40	M4 / 54	2,0380	1,017	0,097	1,915	**0,098**	**1,914**	41,562	**39,988**	39,771	28,80	252,8	251,2	**252,0**	247,2	**247,7**	**250,1**	75,5	67,2	250,4	2 x 2500
P (tomo)	3270	08.07.2013	46	M4 / 54	2,0380	1,017	0,097	1,915	**0,097**	**1,914**	41,543	**39,996**	39,781	28,72	252,8	251,2	**252,0**	247,2	**247,6**	**250,1**	76,0	67,4	250,3	1 x 5000
S (wms)	4685	08.07.2013	40	M4 / 54	2,0380	1,017	0,097	1,915	**0,098**	**1,914**	41,562	**39,988**	39,771	28,80	252,8	251,2	**252,0**	247,2	**247,7**	**250,1**	75,5	67,2	250,4	2 x 5000

D19 – p=6.5 MPa – 151

level code	L	data	DIAdem	inj. Module	j Gas inj.	j water inj.	m gas inj.	m water inj.	FIC4-4/5	FIC4-0x	PI4-06	PI4-201	PI4-07	PDI4-200	TI4-05	TI4-07	TI4-202	TI4-03	TI4-200	TI4-201	TI4-203	TI4-204	TI4-10	Frequency
[-]	[mm]	[-]	[-]	[-]	[m/s]	[m/s]	[kg/s]	[kg/s]	[kg/s]	[kg/s]	bar	bar	bar	kPa	°C	°C	°C	°C	°C	°C	°C	°C	°C	Hz
C (tomo)	18	10.07.2013	51	M4 / 54	0,8350	1,017	0,066	1,796	**0,066**	**1,795**	65,920	**65,006**	64,827	22,27	282,1	280,2	**281,3**	277,9	**278,6**	**280,7**	81,2	78,9	280,8	2 x 2500
E (tomo)	94	10.07.2013	54	M4 / 54	0,8350	1,017	0,066	1,796	**0,066**	**1,797**	65,893	**64,997**	64,828	22,21	282,1	280,2	**281,3**	277,9	**278,7**	**280,8**	80,8	78,5	280,8	2 x 2500
G (tomo)	171	10.07.2013	56	M4 / 54	0,8350	1,017	0,066	1,796	**0,066**	**1,796**	65,892	**64,997**	64,816	22,26	282,0	280,2	**281,3**	277,9	**278,7**	**280,7**	81,3	78,4	280,8	2 x 2500
J (tomo)	435	10.07.2013	60	M4 / 54	0,8350	1,017	0,066	1,796	**0,066**	**1,796**	65,914	**64,988**	64,814	22,19	282,1	280,2	**281,2**	277,9	**278,6**	**280,7**	80,9	79,3	280,8	2 x 2500
M (tomo)	1271	10.07.2013	62	M4 / 54	0,8350	1,017	0,066	1,796	**0,066**	**1,797**	65,901	**64,990**	64,816	22,37	282,0	280,2	**281,2**	277,9	**278,7**	**280,7**	81,0	77,9	280,8	2 x 2500
P (tomo)	3270	10.07.2013	68	M4 / 54	0,8350	1,017	0,066	1,796	**0,066**	**1,796**	65,937	**65,009**	64,823	22,23	282,1	280,3	**281,3**	277,9	**278,8**	**280,7**	80,8	79,3	280,8	2 x 2500
S (wms)	4685	10.07.2013	68	M4 / 54	0,8350	1,017	0,066	1,796	**0,066**	**1,796**	65,937	**65,009**	64,823	22,23	282,1	280,3	**281,3**	277,9	**278,8**	**280,7**	80,8	79,3	280,8	2 x 5000

D19 – p=6.5 MPa – 160

level code	L	data	DIAdem	inj. Module	j Gas inj.	j water inj.	m gas inj.	m water inj.	FIC4-4/5	FIC4-0x	PI4-06	PI4-201	PI4-07	PDI4-200	TI4-05	TI4-07	TI4-202	TI4-03	TI4-200	TI4-201	TI4-203	TI4-204	TI4-10	Frequency
[-]	[mm]	[-]	[-]	[-]	[m/s]	[m/s]	[kg/s]	[kg/s]	[kg/s]	[kg/s]	bar	bar	bar	kPa	°C	°C	°C	°C	°C	°C	°C	°C	°C	Hz
C (tomo)	18	09.07.2013	77	M4 / 54	1,3050	0,405	0,104	0,715	**0,104**	**0,715**	66,275	**65,010**	64,886	35,21	282,3	280,4	**281,4**	275,9	**275,3**	**280,7**	80,9	78,4	280,8	2 x 2500
E (tomo)	94	09.07.2013	72	M4 / 54	1,3050	0,405	0,104	0,715	**0,105**	**0,716**	66,274	**65,001**	64,883	35,39	282,2	280,5	**281,5**	275,9	**275,3**	**280,6**	81,3	78,9	280,9	2 x 2500
G (tomo)	171	09.07.2013	68	M4 / 54	1,3050	0,405	0,104	0,715	**0,104**	**0,715**	66,267	**65,003**	64,896	35,06	282,2	280,5	**281,5**	275,9	**275,3**	**280,7**	81,4	77,8	280,8	2 x 2500
J (tomo)	435	09.07.2013	64	M4 / 54	1,3050	0,405	0,104	0,715	**0,103**	**0,715**	66,272	**65,002**	64,891	35,08	282,3	280,5	**281,4**	275,8	**275,3**	**280,8**	81,5	77,8	280,8	2 x 2500
M (tomo)	1271	09.07.2013	60	M4 / 54	1,3050	0,405	0,104	0,715	**0,102**	**0,714**	66,256	**65,004**	64,889	35,01	282,2	280,4	**281,4**	275,8	**275,2**	**280,6**	81,6	76,9	280,8	2 x 2500
P (tomo)	3270	09.07.2013	58	M4 / 54	1,3050	0,405	0,104	0,715	**0,105**	**0,714**	66,266	**64,998**	64,883	35,32	282,3	280,4	**281,4**	275,7	**275,2**	**280,6**	80,2	78,0	280,8	2 x 2500
S (wms)	4685	09.07.2013	58	M4 / 54	1,3050	0,405	0,104	0,715	**0,105**	**0,714**	66,266	**64,998**	64,883	35,32	282,3	280,4	**281,4**	275,7	**275,2**	**280,6**	80,2	78,0	280,8	2 x 5000

D19 – p=6.5 MPa – 163

level code	L	data	DIAdem	inj. Module	j Gas inj.	j water inj.	m gas inj.	m water inj.	FIC4-4/5	FIC4-0x	PI4-06	PI4-201	PI4-07	PDI4-200	TI4-05	TI4-07	TI4-202	TI4-03	TI4-200	TI4-201	TI4-203	TI4-204	TI4-10	Frequency
[-]	[mm]	[-]	[-]	[-]	[m/s]	[m/s]	[kg/s]	[kg/s]	[kg/s]	[kg/s]	bar	bar	bar	kPa	°C	°C	°C	°C	°C	°C	°C	°C	°C	Hz
C (tomo)	18	09.07.2013	29	M4 / 54	1,3050	1,611	0,104	2,845	**0,104**	**2,847**	66,397	**65,005**	64,749	19,82	282,4	280,6	**281,7**	277,8	**278,8**	**280,8**	81,7	78,8	280,7	2 x 2500
C (tomo)	18	09.07.2013	34	M4 / 54	1,3050	1,611	0,104	2,845	**0,103**	**2,844**	66,383	**65,003**	64,752	19,62	282,4	280,6	**281,6**	277,8	**278,8**	**280,8**	81,6	78,9	280,6	1 x 5000
E (tomo)	94	09.07.2013	25	M4 / 54	1,3050	1,611	0,104	2,845	**0,104**	**2,846**	66,417	**65,018**	64,771	19,81	282,4	280,7	**281,7**	277,8	**278,8**	**280,8**	82,0	79,4	280,7	2 x 2500
E (tomo)	94	09.07.2013	36	M4 / 54	1,3050	1,611	0,104	2,845	**0,104**	**2,845**	66,374	**64,995**	64,741	19,72	282,4	280,6	**281,6**	277,8	**278,8**	**280,7**	81,8	78,9	280,7	1 x 5000
G (tomo)	171	09.07.2013	20	M4 / 54	1,3050	1,611	0,104	2,845	**0,104**	**2,843**	66,401	**65,005**	64,748	19,83	282,4	280,7	**281,7**	277,8	**278,8**	**280,8**	81,6	77,6	280,7	2 x 2500
G (tomo)	171	09.07.2013	38	M4 / 54	1,3050	1,611	0,104	2,845	**0,105**	**2,843**	66,405	**64,995**	64,737	20,01	282,4	280,6	**281,6**	277,8	**278,8**	**280,8**	81,8	79,1	280,7	1 x 5000
J (tomo)	435	09.07.2013	15	M4 / 54	1,3050	1,611	0,104	2,845	**0,105**	**2,845**	66,389	**64,990**	64,731	19,82	282,4	280,7	**281,7**	277,7	**278,7**	**280,8**	81,1	78,6	280,7	2 x 2500
J (tomo)	435	09.07.2013	45	M4 / 54	1,3050	1,611	0,104	2,845	**0,104**	**2,842**	66,389	**64,999**	64,740	19,72	282,3	280,6	**281,6**	277,8	**278,8**	**280,8**	82,0	78,8	280,7	1 x 5000
M (tomo)	1271	09.07.2013	8	M4 / 54	1,3050	1,611	0,104	2,845	**0,104**	**2,847**	66,397	**65,001**	64,752	19,64	282,4	280,7	**281,7**	277,7	**278,7**	**280,8**	81,8	76,6	280,7	2 x 2500
M (tomo)	1271	09.07.2013	49	M4 / 54	1,3050	1,611	0,104	2,845	**0,104**	**2,845**	66,406	**64,979**	64,729	19,76	282,4	280,6	**281,7**	277,8	**278,8**	**280,7**	81,9	77,9	280,7	1 x 5000
P (tomo)	3270	09.07.2013	6	M4 / 54	1,3050	1,611	0,104	2,845	**0,104**	**2,843**	66,371	**64,988**	64,739	19,67	282,4	280,6	**281,7**	277,6	**278,7**	**280,7**	81,0	74,7	280,7	2 x 2500
P (tomo)	3270	09.07.2013	53	M4 / 54	1,3050	1,611	0,104	2,845	**0,105**	**2,848**	66,410	**64,993**	64,736	19,92	282,4	280,6	**281,7**	277,8	**278,8**	**280,6**	80,3	79,1	280,7	1 x 5000
S (wms)	4685	09.07.2013	6	M4 / 54	1,3050	1,611	0,104	2,845	**0,104**	**2,843**	66,371	**64,988**	64,739	19,67	282,4	280,6	**281,7**	277,6	**278,7**	**280,7**	81,0	74,7	280,7	2 x 5000

D19 – p=6.5 MPa – 173

level code	L	data	DIAdem	inj. Module	j Gas inj.	j water inj.	m gas inj.	m water inj.	FIC4-4/5	FIC4-0x	PI4-06	PI4-201	PI4-07	PDI4-200	TI4-05	TI4-07	TI4-202	TI4-03	TI4-200	TI4-201	TI4-203	TI4-204	TI4-10	Frequency
[-]	[mm]	[-]	[-]	[-]	[m/s]	[m/s]	[kg/s]	[kg/s]	[kg/s]	[kg/s]	bar	bar	bar	kPa	°C	°C	°C	°C	°C	°C	°C	°C	°C	Hz
C (tomo)	18	10.07.2013	2	M4 / 54	2,0380	1,017	0,162	1,796	**0,161**	**1,796**	67,520	**64,992**	64,794	32,75	283,7	281,8	**282,9**	277,0	**278,0**	**280,7**	80,6	76,3	280,8	2 x 2500
C (tomo)	18	10.07.2013	42	M4 / 54	2,0380	1,017	0,162	1,796	**0,163**	**1,795**	67,644	**64,997**	64,797	33,46	283,8	282,0	**282,9**	277,8	**278,7**	**280,7**	81,1	78,1	280,8	1 x 5000
E (tomo)	94	10.07.2013	4	M4 / 54	2,0380	1,017	0,162	1,796	**0,162**	**1,796**	67,564	**65,002**	64,798	32,89	283,7	281,8	**283,0**	277,2	**278,2**	**280,7**	80,5	75,9	280,8	2 x 2500
E (tomo)	94	10.07.2013	37	M4 / 54	2,0380	1,017	0,162	1,796	**0,162**	**1,795**	67,629	**65,004**	64,799	33,30	283,7	281,9	**282,9**	277,7	**278,6**	**280,8**	80,6	78,2	280,8	1 x 5000
G (tomo)	171	10.07.2013	9	M4 / 54	2,0380	1,017	0,162	1,796	**0,162**	**1,796**	67,563	**64,989**	64,800	32,99	283,7	281,8	**283,0**	277,2	**278,2**	**280,6**	80,4	75,8	280,8	2 x 2500
G (tomo)	171	10.07.2013	34	M4 / 54	2,0380	1,017	0,162	1,796	**0,162**	**1,796**	67,616	**64,991**	64,788	33,34	283,8	281,9	**282,9**	277,4	**278,5**	**280,8**	80,8	78,6	280,8	1 x 5000
J (tomo)	435	10.07.2013	14	M4 / 54	2,0380	1,017	0,162	1,796	**0,162**	**1,796**	67,607	**64,998**	64,799	33,10	283,8	281,9	**283,0**	277,3	**278,3**	**280,8**	80,7	76,7	280,8	2 x 2500
J (tomo)	435	10.07.2013	32	M4 / 54	2,0380	1,017	0,162	1,796	**0,162**	**1,797**	67,614	**64,999**	64,797	33,28	283,7	281,9	**282,9**	277,5	**278,4**	**280,8**	80,4	78,2	280,8	1 x 5000
M (tomo)	1271	10.07.2013	17	M4 / 54	2,0380	1,017	0,162	1,796	**0,161**	**1,792**	67,579	**65,001**	64,797	32,53	283,7	281,8	**282,9**	276,3	**276,6**	**280,7**	80,2	75,7	280,8	2 x 2500
M (tomo)	1271	10.07.2013	28	M4 / 54	2,0380	1,017	0,162	1,796	**0,161**	**1,795**	67,603	**65,000**	64,804	33,26	283,7	281,9	**282,9**	277,4	**278,5**	**280,8**	81,2	76,9	280,8	1 x 5000
P (tomo)	3270	10.07.2013	21	M4 / 54	2,0380	1,017	0,162	1,796	**0,161**	**1,795**	67,572	**64,997**	64,789	33,08	283,7	281,8	**282,9**	277,3	**278,3**	**280,7**	79,9	78,6	280,8	2 x 2500
P (tomo)	3270	10.07.2013	25	M4 / 54	2,0380	1,017	0,162	1,796	**0,163**	**1,796**	67,651	**64,997**	64,790	33,33	283,8	282,0	**282,9**	277,4	**278,4**	**280,7**	79,8	79,9	280,8	1 x 5000
S (wms)	4685	10.07.2013	21	M4 / 54	2,0380	1,017	0,162	1,796	**0,161**	**1,795**	67,572	**64,997**	64,789	33,08	283,7	281,8	**282,9**	277,3	**278,3**	**280,7**	79,9	78,6	280,8	2 x 5000

D20 – p=4.0 MPa – 150

level code	L	data	DIAdem	inj. Module	j Gas inj.	j water inj.	m gas inj.	m water inj.	FIC4-4/5	FIC4-0x	PI4-06	PI4-07	PI4-201	ts	PI4-203	ts	PDI4-200	TI4-03	TI4-14	TI4-08	TI4-201	dt	TI4-200	TI4-10	TI4-07	TI4-205	TI4-203	TI4-204	PIC4-04	ts	TI4-35	TI4-36	Frequency
[-]	[mm]	[-]	[-]	[-]	[m/s]	[m/s]	[kg/s]	[kg/s]	[kg/s]	[kg/s]	bar	bar	bar	°C	bar	°C	kPa	°C	°C	°C	°C	K	°C	°C	°C	°C	°C	°C	bar	°C	°C	°C	Hz
A	18	31.03.2014	44	M4 / 54	0,8350	0,641	0,040	1,207	**0,040**	**1,206**	40,422	39,624	39,791	250,0	**39,992**	250,3	35,86	246,0	246,7	247,0	**245,7**	**4,4**	**250,6**	249,9	249,7	**250,3**	85,9	55,2	39,387	249,4	249,2	249,3	2 x 2000
D	62	31.03.2014	42	M4 / 54	0,8350	0,641	0,040	1,207	**0,040**	**1,208**	40,420	39,622	39,789	250,0	**39,993**	250,3	35,64	246,0	246,6	247,0	**245,6**	**4,4**	**250,6**	249,8	249,7	**250,3**	85,9	57,1	39,391	249,4	249,2	249,3	2 x 2000
G	171	31.03.2014	36	M4 / 54	0,8350	0,641	0,040	1,207	**0,040**	**1,207**	40,407	39,621	39,801	250,1	**40,003**	250,4	35,62	245,9	246,6	247,0	**245,6**	**4,5**	**250,6**	249,9	249,7	**250,4**	80,6	66,3	39,394	249,5	249,3	249,4	2 x 2000
J	435	31.03.2014	31	M4 / 54	0,8350	0,641	0,040	1,207	**0,040**	**1,208**	40,412	39,616	39,794	250,1	**40,000**	250,4	35,60	245,9	246,6	247,0	**245,5**	**4,5**	**250,6**	249,9	249,7	**250,2**	72,9	68,8	39,385	249,4	249,2	249,3	2 x 2000
M	1271	31.03.2014	25	M4 / 54	0,8350	0,641	0,040	1,207	**0,040**	**1,209**	40,406	39,623	39,792	250,0	**39,997**	250,4	35,72	245,9	246,6	247,0	**245,5**	**4,5**	**250,5**	249,9	249,7	**250,3**	71,2	72,1	39,389	249,4	249,2	249,3	2 x 2000
NN	3054	31.03.2014	15	M4 / 54	0,8350	0,641	0,040	1,207	**0,040**	**1,208**	40,411	39,608	39,781	250,0	**39,995**	250,3	34,57	245,7	246,4	246,7	**245,2**	**4,8**	**250,6**	249,9	249,7	**250,3**	70,6	71,0	39,382	249,4	249,3	249,4	2 x 2000

D20 – p=4.0 MPa – 151

level code	L	data	DIAdem	inj. Module	j Gas inj.	j water inj.	m gas inj.	m water inj.	FIC4-4/5	FIC4-0x	PI4-06	PI4-07	PI4-201	ts	PI4-203	ts	PDI4-200	TI4-03	TI4-14	TI4-08	TI4-201	dt	TI4-200	TI4-10	TI4-07	TI4-205	TI4-203	TI4-204	PIC4_04	ts	TI4-35	TI4-36	Frequency
[-]	[mm]	[-]	[-]	[-]	[m/s]	[m/s]	[kg/s]	[kg/s]	[kg/s]	[kg/s]	bar	bar	bar	°C	bar	°C	kPa	°C	°C	°C	°C	K	°C	°C	°C	°C	°C	°C	bar	°C	°C	°C	Hz
A	18	31.03.2014	48	M4 / 54	0,8350	1,017	0,040	1,915	**0,040**	**1,915**	40,310	39,553	39,702	249,9	**39,993**	250,3	27,19	246,4	247,4	248,0	**246,8**	**3,1**	**250,5**	249,8	249,6	**250,2**	85,5	53,6	39,319	249,3	249,1	249,2	2 x 2500
D	62	31.03.2014	51	M4 / 54	0,8350	1,017	0,040	1,915	**0,040**	**1,915**	40,321	39,546	39,698	249,9	**39,984**	250,3	27,25	246,5	247,3	248,0	**246,8**	**3,1**	**250,6**	249,7	249,6	**250,2**	85,5	55,4	39,323	249,3	249,1	249,2	2 x 2500
G	171	31.03.2014	55	M4 / 54	0,8350	1,017	0,040	1,915	**0,040**	**1,915**	40,331	39,569	39,719	249,9	**40,008**	250,4	27,49	246,4	247,3	248,1	**246,8**	**3,1**	**250,6**	249,8	249,5	**250,1**	81,9	63,0	39,335	249,4	249,1	249,3	2 x 2500
J	435	31.03.2014	59	M4 / 54	0,8350	1,017	0,040	1,915	**0,040**	**1,916**	40,321	39,548	39,698	249,9	**39,986**	250,3	27,19	246,5	247,4	248,1	**246,8**	**3,1**	**250,5**	249,7	249,6	**250,2**	74,6	65,1	39,318	249,3	249,1	249,2	2 x 2500
M	1271	31.03.2014	62	M4 / 54	0,8350	1,017	0,040	1,915	**0,040**	**1,914**	40,342	39,565	39,713	249,9	**40,003**	250,4	27,12	246,4	247,4	248,0	**246,8**	**3,1**	**250,6**	249,8	249,6	**250,3**	72,9	68,2	39,330	249,4	249,1	249,3	2 x 2500
NN	3054	31.03.2014	66	M4 / 54	0,8350	1,017	0,040	1,915	**0,040**	**1,915**	40,342	39,561	39,712	249,9	**40,000**	250,4	27,47	246,5	247,3	248,0	**246,8**	**3,1**	**250,6**	249,7	249,6	**250,2**	74,4	70,8	39,329	249,4	249,1	249,2	2 x 2500

D20 – p=4.0 MPa – 152

level code	L	data	DIAdem	inj. Module	j Gas inj.	j water inj.	m gas inj.	m water inj.	FIC4-4/5	FIC4-0x	PI4-06	PI4-07	PI4-201	ts	PI4-203	ts	PDI4-200	TI4-03	TI4-14	TI4-08	TI4-201	dt	TI4-200	TI4-10	TI4-07	TI4-205	TI4-203	TI4-204	PIC4_04	ts	TI4-35	TI4-36	Frequency
[-]	[mm]	[-]	[-]	[-]	[m/s]	[m/s]	[kg/s]	[kg/s]	[kg/s]	[kg/s]	bar	bar	bar	°C	bar	°C	kPa	°C	°C	°C	°C	K	°C	°C	°C	°C	°C	°C	bar	°C	°C	°C	Hz
A	18	01.04.2014	22	M4 / 54	0,8350	1,611	0,040	3,034	**0,040**	**3,034**	40,289	39,588	39,695	249,9	**40,011**	250,4	24,56	246,9	247,5	248,5	**247,3**	**2,6**	**250,0**	249,5	249,4	**249,7**	87,8	56,0	39,239	249,2	249,0	249,0	2 x 2500
D	62	01.04.2014	20	M4 / 54	0,8350	1,611	0,040	3,034	**0,040**	**3,033**	40,337	39,592	39,691	249,9	**40,004**	250,4	24,79	246,9	247,5	248,5	**247,3**	**2,6**	**250,0**	249,5	249,4	**249,7**	87,9	57,8	39,244	249,2	249,0	249,0	2 x 2500
G	171	01.04.2014	15	M4 / 54	0,8350	1,611	0,040	3,034	**0,040**	**3,035**	40,290	39,580	39,681	249,9	**39,997**	250,4	24,59	246,9	247,5	248,5	**247,3**	**2,6**	**250,0**	249,5	249,3	**249,7**	80,9	71,2	39,228	249,2	249,0	248,9	2 x 2500
J	435	01.04.2014	12	M4 / 54	0,8350	1,611	0,040	3,034	**0,040**	**3,033**	40,307	39,589	39,682	249,9	**39,998**	250,4	24,61	246,9	247,5	248,5	**247,3**	**2,6**	**250,0**	249,5	249,4	**249,7**	75,1	72,1	39,239	249,2	249,0	249,0	2 x 2500
M	1271	01.04.2014	7	M4 / 54	0,8350	1,611	0,040	3,034	**0,040**	**3,033**	40,308	39,601	39,699	249,9	**40,016**	250,4	24,47	246,9	247,5	248,5	**247,3**	**2,6**	**250,0**	249,5	249,4	**249,7**	76,0	75,2	39,243	249,2	249,0	249,0	2 x 2500
NN	3054	01.04.2014	3	M4 / 54	0,8350	1,611	0,040	3,034	**0,040**	**3,033**	40,284	39,581	39,681	249,9	**39,997**	250,4	24,37	246,9	247,5	248,5	**247,3**	**2,6**	**250,0**	249,5	249,3	**249,7**	75,8	73,2	39,228	249,2	249,0	249,1	2 x 2500

D20 – p=4.0 MPa – 162

level code	L	data	DIAdem	inj. Module	j Gas inj.	j water inj.	m gas inj.	m water inj.	FIC4-4/5	FIC4-0x	PI4-06	PI4-07	PI4-201	ts	PI4-203	ts	PDI4-200	TI4-03	TI4-14	TI4-08	TI4-201	dt	TI4-200	TI4-10	TI4-07	TI4-205	TI4-203	TI4-204	PIC4_04	ts	TI4-35	TI4-36	Frequency
[-]	[mm]	[-]	[-]	[-]	[m/s]	[m/s]	[kg/s]	[kg/s]	[kg/s]	[kg/s]	bar	bar	bar	°C	bar	°C	kPa	°C	°C	°C	°C	K	°C	°C	°C	°C	°C	°C	bar	°C	°C	°C	Hz
A	18	02.04.2014	24	M4 / 54	1,3050	1,017	0,062	1,915	**0,062**	**1,914**	40,590	39,637	39,791	250,0	**39,988**	250,3	36,35	246,2	246,9	247,7	**246,4**	**3,7**	**250,4**	249,9	249,7	**250,4**	88,1	90,4	39,398	249,5	249,3	249,3	2 x 2500
D	62	02.04.2014	21	M4 / 54	1,3050	1,017	0,062	1,915	**0,062**	**1,915**	40,595	39,644	39,795	250,1	**39,995**	250,4	36,30	246,2	246,9	247,7	**246,3**	**3,7**	**250,4**	249,9	249,7	**250,4**	85,8	90,2	39,403	249,5	249,3	249,3	2 x 2500
G	171	02.04.2014	17	M4 / 54	1,3050	1,017	0,062	1,915	**0,062**	**1,913**	40,596	39,645	39,797	250,1	**39,997**	250,4	36,28	246,2	246,9	247,6	**246,3**	**3,7**	**250,4**	249,9	249,7	**250,4**	75,7	84,0	39,396	249,5	249,4	249,4	2 x 2500
J	435	02.04.2014	13	M4 / 54	1,3050	1,017	0,062	1,915	**0,062**	**1,914**	40,594	39,642	39,791	250,0	**39,991**	250,3	36,24	246,1	246,9	247,6	**246,3**	**3,8**	**250,4**	249,9	249,8	**250,5**	71,5	70,8	39,393	249,5	249,3	249,3	2 x 2500
M	1271	02.04.2014	9	M4 / 54	1,3050	1,017	0,062	1,915	**0,062**	**1,915**	40,584	39,638	39,788	250,0	**39,989**	250,3	36,18	246,1	246,9	247,6	**246,3**	**3,7**	**250,4**	249,9	249,7	**250,5**	71,2	69,0	39,394	249,5	249,3	249,2	2 x 2500
NN	3054	02.04.2014	4	M4 / 54	1,3050	1,017	0,062	1,915	**0,062**	**1,916**	40,605	39,638	39,801	250,1	**40,000**	250,4	36,04	246,1	246,9	247,6	**246,3**	**3,8**	**250,4**	249,9	249,7	**250,5**	71,6	70,9	39,396	249,5	249,4	249,4	2 x 2500

D20 – p=4.0 MPa – 163

level code	L	data	DIAdem	inj. Module	j Gas inj.	j water inj.	m gas inj.	m water inj.	FIC4-4/5	FIC4-0x	PI4-06	PI4-07	PI4-201	ts	PI4-203	ts	PDI4-200	TI4-03	TI4-14	TI4-08	TI4-201	dt	TI4-200	TI4-10	TI4-07	TI4-205	TI4-203	TI4-204	PIC4_04	ts	TI4-35	TI4-36	Frequency
[-]	[mm]	[-]	[-]	[-]	[m/s]	[m/s]	[kg/s]	[kg/s]	[kg/s]	[kg/s]	bar	bar	bar	°C	bar	°C	kPa	°C	°C	°C	°C	K	°C	°C	°C	°C	°C	°C	bar	°C	°C	°C	Hz
A	18	01.04.2014	25	M4 / 54	1,3050	1,611	0,062	3,034	**0,062**	**3,032**	40,630	39,657	39,762	250,0	**39,997**	250,4	32,76	247,0	247,6	248,6	**247,3**	**2,7**	**250,1**	249,5	249,8	**250,4**	87,6	54,7	39,282	249,3	249,0	249,0	2 x 2500
D	62	01.04.2014	27	M4 / 54	1,3050	1,611	0,062	3,034	**0,062**	**3,032**	40,609	39,657	39,760	250,0	**39,991**	250,3	32,88	247,0	247,5	248,6	**247,4**	**2,6**	**250,1**	249,5	249,8	**250,3**	87,7	56,5	39,278	249,3	249,0	249,1	2 x 2500
G	171	01.04.2014	30	M4 / 54	1,3050	1,611	0,062	3,034	**0,062**	**3,035**	40,598	39,661	39,758	250,0	**39,991**	250,3	32,84	247,0	247,5	248,5	**247,4**	**2,6**	**250,1**	249,5	249,7	**250,3**	85,1	65,0	39,283	249,3	249,0	249,0	2 x 2500
J	435	01.04.2014	33	M4 / 54	1,3050	1,611	0,062	3,034	**0,062**	**3,034**	40,582	39,658	39,758	250,0	**39,990**	250,3	32,86	247,0	247,5	248,5	**247,3**	**2,7**	**250,1**	249,5	249,7	**250,3**	79,9	71,2	39,276	249,3	249,0	249,0	2 x 2500
M	1271	01.04.2014	36	M4 / 54	1,3050	1,611	0,062	3,034	**0,062**	**3,034**	40,579	39,655	39,759	250,0	**39,992**	250,3	32,77	247,0	247,5	248,5	**247,3**	**2,7**	**250,1**	249,5	249,7	**250,3**	77,0	73,7	39,278	249,3	249,1	249,0	2 x 2500
NN	3054	01.04.2014	40	M4 / 54	1,3050	1,611	0,062	3,034	**0,062**	**3,035**	40,580	39,662	39,780	250,0	**40,014**	250,4	32,79	247,0	247,5	248,5	**247,4**	**2,6**	**250,1**	249,5	249,7	**250,3**	76,3	75,5	39,283	249,3	249,1	249,0	2 x 2500

D20 – p=6.5 MPa – 150

level code	L	data	DIAdem	inj. Module	j Gas inj.	j water inj.	m gas inj.	m water inj.	FIC4-4/5	FIC4-0x	PI4-06	PI4-07	PI4-201	ts	PI4-203	ts	PDI4-200	TI4-03	TI4-14	TI4-08	TI4-201	dt	TI4-200	TI4-10	TI4-07	TI4-205	TI4-203	TI4-204	PIC4-04	ts	TI4-35	TI4-36	Frequency
[-]	[mm]	[-]	[-]	[-]	[m/s]	[m/s]	[kg/s]	[kg/s]	[kg/s]	[kg/s]	bar	bar	bar	°C	bar	°C	kPa	°C	°C	°C	°C	K	°C	°C	°C	°C	°C	°C	bar	°C	°C	°C	Hz
A	18	07.04.2014	23	M4 / 54	0,8350	0,641	0,066	1,132	**0,066**	**1,132**	65,866	64,625	64,785	280,6	**64,998**	280,9	34,89	275,4	275,6	276,1	**274,2**	**6,4**	**280,7**	280,5	280,0	**280,9**	99,9	99,9	64,447	280,3	280,1	280,0	2 x 2000
D	62	07.04.2014	20	M4 / 54	0,8350	0,641	0,066	1,132	**0,066**	**1,133**	65,886	64,626	64,780	280,6	**64,998**	280,9	34,63	275,4	275,6	276,1	**274,2**	**6,5**	**280,8**	280,5	280,0	**280,9**	98,1	99,6	64,433	280,3	280,1	280,0	2 x 2000
G	171	07.04.2014	15	M4 / 54	0,8350	0,641	0,066	1,132	**0,066**	**1,134**	65,923	64,633	64,768	280,6	**64,990**	280,8	33,94	275,3	275,4	275,9	**274,1**	**6,5**	**280,8**	280,5	280,0	**281,0**	86,5	79,9	64,435	280,3	280,1	280,0	2 x 2000
J	435	07.04.2014	11	M4 / 54	0,8350	0,641	0,066	1,132	**0,066**	**1,131**	65,936	64,637	64,787	280,6	**65,004**	280,9	34,34	275,2	275,4	275,8	**274,0**	**6,6**	**280,8**	280,5	280,1	**281,0**	74,9	77,1	64,451	280,3	280,1	280,0	2 x 2000
M	1271	07.04.2014	9	M4 / 54	0,8350	0,641	0,066	1,132	**0,066**	**1,130**	65,848	64,623	64,768	280,6	**64,990**	280,8	33,96	275,2	275,3	275,6	**273,8**	**6,8**	**280,8**	280,5	280,0	**280,9**	74,7	80,6	64,432	280,3	280,1	280,0	2 x 2000
NN	3054	07.04.2014	5	M4 / 54	0,8350	0,641	0,066	1,132	**0,066**	**1,133**	65,850	64,622	64,769	280,6	**64,997**	280,9	33,45	274,9	275,0	275,3	**273,4**	**7,2**	**280,8**	280,5	280,0	**280,9**	73,5	78,6	64,430	280,3	280,1	279,9	2 x 2000

D20 – p=6.5 MPa – 151

level code	L	data	DIAdem	inj. Module	j Gas inj.	j water inj.	m gas inj.	m water inj.	FIC4-4/5	FIC4-0x	PI4-06	PI4-07	PI4-201	ts	PI4-203	ts	PDI4-200	TI4-03	TI4-14	TI4-08	TI4-201	dt	TI4-200	TI4-10	TI4-07	TI4-205	TI4-203	TI4-204	PIC4_04	ts	TI4-35	TI4-36	Frequency
[-]	[mm]	[-]	[-]	[-]	[m/s]	[m/s]	[kg/s]	[kg/s]	[kg/s]	[kg/s]	bar	bar	bar	°C	bar	°C	kPa	°C	°C	°C	°C	K	°C	°C	°C	°C	°C	°C	bar	°C	°C	°C	Hz
A	18	07.04.2014	28	M4 / 54	0,8350	1,017	0,066	1,796	**0,066**	**1,794**	65,815	64,587	64,711	280,6	**64,982**	280,8	29,08	276,4	277,1	277,9	**276,3**	**4,3**	**280,8**	280,5	280,0	**280,9**	99,2	99,0	64,387	280,2	280,1	280,0	2 x 2500
D	62	07.04.2014	31	M4 / 54	0,8350	1,017	0,066	1,796	**0,066**	**1,795**	65,862	64,602	64,731	280,6	**65,000**	280,9	29,29	276,4	277,1	278,0	**276,3**	**4,2**	**280,8**	280,5	280,0	**280,9**	97,5	99,4	64,394	280,2	280,1	280,0	2 x 2500
G	171	07.04.2014	33	M4 / 54	0,8350	1,017	0,066	1,796	**0,066**	**1,796**	65,892	64,620	64,750	280,6	**65,021**	280,9	29,01	276,4	277,2	278,0	**276,4**	**4,2**	**280,8**	280,5	280,0	**280,9**	89,9	84,3	64,413	280,3	280,1	280,0	2 x 2500
J	435	07.04.2014	36	M4 / 54	0,8350	1,017	0,066	1,796	**0,066**	**1,795**	65,828	64,604	64,737	280,6	**65,003**	280,9	29,40	276,5	277,2	278,1	**276,4**	**4,2**	**280,8**	280,5	280,0	**280,9**	79,9	79,2	64,399	280,2	280,1	280,0	2 x 2500
M	1271	07.04.2014	38	M4 / 54	0,8350	1,017	0,066	1,796	**0,066**	**1,796**	65,840	64,600	64,731	280,6	**64,998**	280,9	29,53	276,4	277,2	278,1	**276,5**	**4,1**	**280,9**	280,6	280,0	**280,9**	73,2	78,2	64,395	280,2	280,1	280,0	2 x 2500
NN	3054	07.04.2014	41	M4 / 54	0,8350	1,017	0,066	1,796	**0,066**	**1,797**	65,821	64,585	64,713	280,6	**64,981**	280,8	29,64	276,5	277,2	278,1	**276,4**	**4,1**	**280,8**	280,5	279,9	**280,9**	72,8	78,9	64,383	280,2	280,1	280,0	2 x 2500

D20 – p=6.5 MPa – 152

level code	L	data	DIAdem	inj. Module	j Gas inj.	j water inj.	m gas inj.	m water inj.	FIC4-4/5	FIC4-0x	PI4-06	PI4-07	PI4-201	ts	PI4-203	ts	PDI4-200	TI4-03	TI4-14	TI4-08	TI4-201	dt	TI4-200	TI4-10	TI4-07	TI4-205	TI4-203	TI4-204	PIC4_04	ts	TI4-35	TI4-36	Frequency
[-]	[mm]	[-]	[-]	[-]	[m/s]	[m/s]	[kg/s]	[kg/s]	[kg/s]	[kg/s]	bar	bar	bar	°C	bar	°C	kPa	°C	°C	°C	°C	K	°C	°C	°C	°C	°C	°C	bar	°C	°C	°C	Hz
A	18	08.04.2014	28	M4 / 54	0,8350	1,611	0,066	2,845	**0,066**	**2,845**	65,693	64,621	64,703	280,6	**64,991**	280,8	27,52	277,2	278,0	279,0	**277,7**	**2,9**	**280,7**	280,3	279,8	**280,8**	99,7	99,7	64,302	280,1	280,0	279,8	2 x 2500
D	62	08.04.2014	25	M4 / 54	0,8350	1,611	0,066	2,845	**0,066**	**2,845**	65,777	64,627	64,711	280,6	**65,002**	280,9	27,20	277,2	277,9	279,0	**277,7**	**2,9**	**280,7**	280,3	279,9	**280,9**	95,4	96,3	64,313	280,2	280,0	279,8	2 x 2500
G	171	08.04.2014	23	M4 / 54	0,8350	1,611	0,066	2,845	**0,066**	**2,844**	65,732	64,625	64,720	280,6	**65,007**	280,9	27,52	277,2	277,8	279,0	**277,7**	**2,9**	**280,7**	280,2	279,8	**280,8**	88,9	83,5	64,302	280,1	279,9	279,8	2 x 2500
J	435	08.04.2014	16	M4 / 54	0,8350	1,611	0,066	2,845	**0,066**	**2,846**	65,705	64,598	64,676	280,5	**64,963**	280,8	27,38	277,1	277,8	278,9	**277,7**	**2,8**	**280,7**	280,2	279,8	**280,8**	76,7	78,4	64,262	280,1	279,8	279,8	2 x 2500
M	1271	08.04.2014	11	M4 / 54	0,8350	1,611	0,066	2,845	**0,066**	**2,845**	65,680	64,621	64,701	280,6	**64,990**	280,8	27,32	277,2	277,8	278,9	**277,6**	**2,9**	**280,7**	280,2	279,8	**280,7**	76,2	81,1	64,289	280,1	279,9	279,8	2 x 2500
NN	3054	08.04.2014	6	M4 / 54	0,8350	1,611	0,066	2,845	**0,066**	**2,845**	65,741	64,630	64,721	280,6	**65,007**	280,9	27,51	277,2	277,9	278,9	**277,6**	**3,0**	**280,7**	280,2	279,9	**280,8**	82,1	80,2	64,283	280,1	279,9	279,8	2 x 2500

D20 – p=6.5 MPa – 162

level code	L	data	DIAdem	inj. Module	j Gas inj.	j water inj.	m gas inj.	m water inj.	FIC4-4/5	FIC4-0x	PI4-06	PI4-07	PI4-201	ts	PI4-203	ts	PDI4-200	TI4-03	TI4-14	TI4-08	TI4-201	dt	TI4-200	TI4-10	TI4-07	TI4-205	TI4-203	TI4-204	PIC4_04	ts	TI4-35	TI4-36	Frequency
[-]	[mm]	[-]	[-]	[-]	[m/s]	[m/s]	[kg/s]	[kg/s]	[kg/s]	[kg/s]	bar	bar	bar	°C	bar	°C	kPa	°C	°C	°C	°C	K	°C	°C	°C	°C	°C	°C	bar	°C	°C	°C	Hz
A	18	08.04.2014	58	M4 / 54	1,3050	1,017	0,104	1,796	**0,104**	**1,796**	66,632	64,662	64,801	280,7	**64,995**	280,9	36,68	276,6	277,4	278,3	**276,7**	**3,9**	**280,9**	280,6	280,8	**281,9**	98,5	98,9	64,454	280,3	280,2	280,1	2 x 2500
D	62	08.04.2014	55	M4 / 54	1,3050	1,017	0,104	1,796	**0,104**	**1,797**	66,657	64,669	64,805	280,7	**65,000**	280,9	36,71	276,6	277,3	278,2	**276,7**	**3,9**	**280,9**	280,6	280,8	**281,9**	93,7	94,1	64,459	280,3	280,2	280,1	2 x 2500
G	171	08.04.2014	53	M4 / 54	1,3050	1,017	0,104	1,796	**0,104**	**1,797**	66,700	64,692	64,822	280,7	**65,020**	280,9	36,54	276,6	277,4	278,2	**276,7**	**4,0**	**281,0**	280,6	280,9	**281,9**	87,2	77,8	64,475	280,3	280,2	280,1	2 x 2500
J	435	08.04.2014	50	M4 / 54	1,3050	1,017	0,104	1,796	**0,104**	**1,795**	66,670	64,663	64,802	280,7	**64,997**	280,9	36,63	276,6	277,3	278,3	**276,7**	**4,0**	**280,9**	280,6	280,8	**281,9**	75,9	73,9	64,461	280,3	280,2	280,1	2 x 2500
M	1271	08.04.2014	48	M4 / 54	1,3050	1,017	0,104	1,796	**0,104**	**1,796**	66,643	64,674	64,813	280,7	**65,006**	280,9	36,71	276,6	277,3	278,2	**276,8**	**3,9**	**280,9**	280,6	280,8	**281,9**	73,4	77,7	64,466	280,3	280,2	280,1	2 x 2500
NN	3054	08.04.2014	46	M4 / 54	1,3050	1,017	0,104	1,796	**0,104**	**1,796**	66,680	64,679	64,804	280,7	**65,000**	280,9	36,57	276,6	277,3	278,3	**276,7**	**3,9**	**280,9**	280,6	280,9	**281,9**	75,5	77,9	64,465	280,3	280,2	280,0	2 x 2500

D20 – p=6.5 MPa – 163

level code	L	data	DIAdem	inj. Module	j Gas inj.	j water inj.	m gas inj.	m water inj.	FIC4-4/5	FIC4-0x	PI4-06	PI4-07	PI4-201	ts	PI4-203	ts	PDI4-200	TI4-03	TI4-14	TI4-08	TI4-201	dt	TI4-200	TI4-10	TI4-07	TI4-205	TI4-203	TI4-204	PIC4_04	ts	TI4-35	TI4-36	Frequency
[-]	[mm]	[-]	[-]	[-]	[m/s]	[m/s]	[kg/s]	[kg/s]	[kg/s]	[kg/s]	bar	bar	bar	°C	bar	°C	kPa	°C	°C	°C	°C	K	°C	°C	°C	°C	°C	°C	bar	°C	°C	°C	Hz
A	18	08.04.2014	31	M4 / 54	1,3050	1,611	0,104	2,845	**0,104**	**2,847**	66,585	64,677	64,771	280,6	**64,999**	280,9	33,47	277,2	277,9	279,1	**277,6**	**3,0**	**280,7**	280,4	280,7	**281,7**	99,3	99,3	64,335	280,2	280,0	279,9	2 x 2500
D	62	08.04.2014	33	M4 / 54	1,3050	1,611	0,104	2,845	**0,104**	**2,846**	66,620	64,686	64,769	280,6	**64,997**	280,9	33,24	277,2	278,0	279,1	**277,7**	**2,9**	**280,8**	280,4	280,8	**281,8**	98,1	99,6	64,339	280,2	280,0	279,8	2 x 2500
G	171	08.04.2014	35	M4 / 54	1,3050	1,611	0,104	2,845	**0,104**	**2,845**	66,630	64,699	64,789	280,6	**65,017**	280,9	33,34	277,2	278,0	279,2	**277,7**	**2,9**	**280,8**	280,4	280,8	**281,9**	88,2	82,2	64,347	280,2	280,0	279,9	2 x 2500
J	435	08.04.2014	37	M4 / 54	1,3050	1,611	0,104	2,845	**0,104**	**2,845**	66,607	64,677	64,764	280,6	**64,991**	280,9	33,33	277,2	278,0	279,2	**277,7**	**2,9**	**280,8**	280,4	280,8	**281,7**	79,0	78,2	64,329	280,2	280,0	279,9	2 x 2500
M	1271	08.04.2014	39	M4 / 54	1,3050	1,611	0,104	2,845	**0,104**	**2,844**	66,588	64,669	64,754	280,6	**64,982**	280,8	33,34	277,2	278,0	279,2	**277,7**	**2,9**	**280,8**	280,4	280,7	**281,8**	74,9	77,1	64,317	280,2	280,0	279,9	2 x 2500
NN	3054	08.04.2014	42	M4 / 54	1,3050	1,611	0,104	2,845	**0,104**	**2,845**	66,594	64,679	64,767	280,6	**64,994**	280,9	33,40	277,2	278,0	279,2	**277,8**	**2,9**	**280,8**	280,4	280,7	**281,8**	75,4	77,7	64,331	280,2	280,1	279,9	2 x 2500

9.4. Available data files and data structure

In this appendix, tomography data files and their structure are described only. The data file structure of corresponding wire-mesh sensor data is explained detailed in the experimental report Beyer et al. (2008). Nevertheless, the file types for quantitative data have the same extension and structure for both measurement systems.

9.4.1 Name convention for the data files

The measurement data and the results of the evaluation are stored in files with the following structure:

NNN_BB_pktY_WxFFFFHz_P_108x108.typ;

The letter combinations have the following meaning:

NNN	Identification number of the test series
BB	Nominal pressure value [bar] in case of steam-water experiments, at air-water experiments not used
pkt	Matrix number of current measurement, three digits, leading zeros
Y	Letter of measurement position, in case of L20 and D19 measurements two letters possible, respectively. Compare with Table 2.2 and section 2.2.3
WxFFFFHz	Measurement frequency [Hz], first number W signifies single or dual plane tomography measurements
P	Letter of tomography plane, O for upper one, U for lower one
typ -	Filetyp, cf. Table 9.1

9.4.2 Description of the data files

Table 9.1. File types available for the test series

File typ	Description	Format
*.a	Geometric characteristics of all identified bubbles (section 3.6)	ASCII
*.a_pair	Characteristics of all detected bubbles pairs (section 3.7.2)	ASCII
*.a_morph	Characteristics of all identified bubbles regarding morphological velocity estimation (section 3.7.3)	ASCII
*.b	Matrix with the bubble identification numbers (chapter: 1.5.4)	binary
*.epsr_stat	Time and azimuthally averaged gas fraction and their standard deviation interval	ASCII
*.epsrad_20	Time and azimuthally (inside of 20 radius domains) averaged gas fraction (section 3.5)	ASCII
*.epsrad_20_pair	Time and azimuthally (inside of 20 radius domains) averaged gas fraction (section 3.5), results of bubble pair detection	ASCII
*.epst	Cross-sectional averaged gas fraction per every frame	ASCII

*.epsxy	Time averaged gas fraction for all pixels in cross-section area (section 3.5)	ASCII
*.epsxy_pair	Time averaged gas fraction for all pixels in cross-section area (section 3.5), results of bubble pair detection	ASCII
*.his_lin	Bubble size distribution referring to linear bubble classes (section 3.8)	ASCII
*.his_lin_r	Bubble size distribution referring to linear bubble classes partitioned in 20 radius domains (section 3.8)	ASCII
*.his_log	Bubble size distribution referring to logarithmic bubble classes (section 3.8)	ASCII
*.his_log_morph	Bubble size distribution referring to logarithmic bubble classes, results of morphological velocity estimation	ASCII
*.his_log_pair	Bubble size distribution referring to logarithmic bubble classes, results of bubble pair detection	ASCII
*.jgs_morph	Calculated superficial gas velocity from measured gas fraction and velocity, without pressure correction, results of morphological velocity estimation	ASCII
*.jgs_pair	Calculated superficial gas velocity from measured gas fraction and velocity, without pressure correction, results of bubble pair detection	ASCII
*.log	File with all information about the evaluation programmes and the parameters used	ASCII
*.sigvelxy_pair	Time averaged standard deviation of axial velocity for each pixel in cross-sectional area as results from bubble pair detection	ASCII
*.sigvelxy_axial_pair	Time averaged standard deviation of axial velocity for each pixel in cross-sectional area as results from bubble pair detection, for each measured integer bubble size values	ASCII
*.sigvelxy_radial _pair	Time averaged standard deviation of radial velocity for each pixel in cross-sectional area as results from bubble pair detection, for each measured integer bubble size values	ASCII
*.sigvelxy_morph	Time averaged standard deviation of axial velocity for each pixel in cross-sectional area as results from morphological method	ASCII
*.sigvelxy_azimuthal _morph	Time averaged standard deviation of azimuthal velocity for each pixel in cross-sectional area as results from morphological method	ASCII
*.sigvelxy_radial_morph	Time averaged standard deviation of radial velocity for each pixel in cross-sectional area as results from morphological method	ASCII
*.v	Binarized values for all cross-sectional pixels for all measurement frames, values 0 or 100 % (section 3.3)	binär

*.vel	Local azimuthally (20 radius domains) averaged gas velocities obtained by cross-correlation (section 3.7.1)	ASCII
*.velxy_morph	Time averaged axial velocity for each pixel in cross-sectional area obtained by cross-correlation	ASCII
*.vel_pair	Local azimuthally (20 radius domains) averaged axial gas velocities obtained by bubble pair finding (section 3.7.2) including radial standard deviation	ASCII
*.vel_axial_pair	Local azimuthally (20 radius domains) averaged axial gas velocities obtained by bubble pair finding (section 3.7.2) including radial standard deviation for each measured integer bubble size values	ASCII
*.vel_azimuthal _pair	Local azimuthally (20 radius domains) averaged azimuthal gas velocities obtained by bubble pair finding (section 3.7.2)	ASCII
*.vel_radial_pair	Local azimuthally (20 radius domains) averaged radial gas velocities obtained by bubble pair finding (section 3.7.2)	ASCII
*.velxy_pair	Time averaged axial velocity for each pixel in cross-sectional area as results from bubble pair detection	ASCII
*.velxy_axial_pair	Time averaged axial velocity for each pixel in cross-sectional area as results from bubble pair detection, for each measured integer bubble size values	ASCII
*.velxy_azimuthal _pair	Time averaged azimuthal velocity for each pixel in cross-sectional area as results from bubble pair detection	ASCII
*.velxy_radial_pair	Time averaged radial velocity for each pixel in cross-sectional area as results from bubble pair detection, for each measured integer bubble size values	ASCII
*.vel_morph	Local azimuthally (20 radius domains) averaged axial gas velocities obtained by morphological method (section 3.7.3) including radial standard deviation	ASCII
*.vel_azimuthal _morph	Local azimuthally (20 radius domains) averaged azimuthal gas velocities obtained by morphological method (section 3.7.3) including radial standard deviation	ASCII
*.vel_radial_morph	Local azimuthally (20 radius domains) averaged radial gas velocities obtained by morphological method (section 3.7.3) including radial standard deviation	ASCII
*.velxy_morph	Time averaged axial velocity for each pixel in cross-sectional area as results from morphological method	ASCII
*.velxy_azimuthal _morph	Time averaged azimuthal velocity for each pixel in cross-sectional area as results from morphological method	ASCII
*.velxy_radial_morph	Time averaged radial velocity for each pixel in cross-sectional area as results from morphological method	ASCII

9.4.3 Bubble characteristics

****.a-File:***

Table 9.2. Part of a *.a file (bubble characteristics)

bb	im	jm	km	ifront	jfront	kfront	iback	jback	kback	rmi	rmj	rmk	rmxy	max	v	rv	n	deps	rxymax
-	ms	mm	mm	ms	mm	mm	ms	mm	mm	ms	mm	mm	mm	%	ms*mm²	f(ms*mm²)	-	%	mm
1	3256,3	24,5	29,2	3254,4	23	26,5	3259,2	23,5	32,5	2,4	4,8	4,5	6,6	100	174	3,46	1740	0,0007552	4,287
4	977,1	31	18,7	974,8	31,5	18,5	979,2	32,5	22	2,4	3,3	4	5,2	100	117,5	3,04	1175	0,00051	3,362
5	1940,2	22	24,7	1938,8	20,5	23,5	1942	21	26	1,8	4	3,1	5	100	83,1	2,71	831	0,0003607	3,302
6	5963,5	28,9	25	5962	28	24,5	5965,2	31,5	24	1,7	6	4,8	7,7	100	193,7	3,59	1937	0,0008407	5,202

The *.a – files contain a table (Tab VI.2), which summarises for all identify bubbles:

bb - Bubble identification number,

im, jm, km - Coordinates of the centre of the bubble in i – flow direction and j, k – measurement cross-section,

ifront, jfront

kfront - Coordinates of the bubble front,

iback, jback

kback - Coordinates of the bubble back,

rmi, rmj, rmk - Moments of the bubble in i – flow direction and j, k – measurement cross-section,

rmxy - Radial moment of the bubble in measurement cross-section plane,

max - Maximum of the gas fraction of the bubble,

v - Bubble volume,

rv - Radius of a volume equivalent sphere,

n - Number volume elements occupied by the bubble,

deps - Part of the gas fraction per bubble referring to the total flow volume,

rxymax - Maximal circle equivalent radius of the bubble in the measurement cross-section.

In the second line of Table 9.2, the units for the bubble characteristics are given. It is indicated once again that with the bubble characteristics contrary to the gas fraction calculation, the index i refers to the serial number of the frames (time axis or z-direction), and the indices j and k apply to the measurement cross-section, respectively. All characteristics in direction of the time axis are given in time unities (ms).

****.a_pair-file:***

Table 9.3. Part of a *.a_pair file (bubble pair characteristics)

bb_O	bb_O_n	bb_O_d_eq	bb_O_radpos	code_O	bb_U	bb_U_n	bb_O_d_eq	bb_U_radpos	code_U	Total	VelAxial	VelRadial	VelAzimuthal	VelExp_OU	VelExp_UO	phiradpos	phivelOU	phivelUO	phivolOU	phivolUO
197	548	5,2768	8,2037	5	131	551	5,2768	8,2037	5	0,9997	1,3973	0,0000	0,0000	1,4035	1,4035	1,0000	1,0000	1,0000	0,9999	0,9999
663	316	3,6534	25,0635	5	674	315	3,6534	25,0416	5	0,9989	0,8095	-0,0017	0,0111	1,0671	1,0683	0,9990	1,0000	1,0000	1,0000	1,0000
308	601	5,5098	7,4095	5	305	603	5,5098	7,5027	5	0,9982	1,4571	0,0133	-0,0052	1,4112	1,4103	0,9983	1,0000	1,0000	0,9999	1,0000
632	249	3,4197	24,0169	5	652	248	3,4197	24,2043	5	0,9977	0,8430	0,0155	0,0058	1,1172	1,1092	0,9977	1,0000	1,0000	1,0000	1,0000
544	461	4,2415	24,6008	5	591	468	4,2797	24,7002	5	0,9973	0,8718	0,0085	0,0086	1,0911	1,0862	0,9988	1,0000	1,0000	0,9993	0,9993

bb_O Bubble identification number, upper plane

bb_O_n Number volume elements occupied by the bubble

bb_O_d_eq Sphere equivalent bubble diameter [mm]

bb_O_radpos Radial bubble position [mm]

code_O Flow region of bubble (compare section 3.7.2)

bb_U	Bubble identification number, lower plane
bb_U_n, bb_U_d_eq, bb_U_radpos, code_U described above, for lower plane	
Total	Total probability of bubble pair bb_O and bb_U
VelAxial	Axial velocity of bubble pair bb_O and bb_U VelRadial Radial velocity of bubble pair bb_O and bb_U [m/s]
VelAzimuthal	Azimuthal velocity of bubble pair bb_O and bb_U [m/s]
VelRadial	Radial velocity of bubble pair bb_O and bb_U [m/s]
VelExp_OU	Expected axial velocity for bubble bb_O [m/s]
VelExp_UO	Expected axial velocity for bubble bb_U [m/s]
phiradpos	Radial position probability value of bubble pair bb_O and bb_U
phivelOU	Axial pair velocity probability value for bubble bb_O
phivelUO	Axial pair velocity probability value for bubble bb_U
phivolOU	Volume probability value for bubble bb_O
phivolUO	Volume probability value for bubble bb_U

.a_morph-file:

Table 9.4. Part of a *.a_morph file (morphological bubble characteristics)

bb	vel_axial	vel_rad	vel_azi	Eötvös	Aspect	Vol	d	BSclass	RadPos	n	dt
[-]	[m/s]	[m/s]	[m/s]	[-]	[-]	[mm³]	[mm]	[-]	[mm]	[-]	[ms]
1	0,232	-0,1401	-0,1035	9,1087	0,5353	153,7594	6,6468	53	3,8328	2651	19
2	0,2531	0,1116	-0,1928	7,8255	0,5638	118,3287	6,0911	50	13,0863	1870	17
3	0,2751	-0,1307	-0,2773	15,6066	0,4339	244,6888	7,7602	57	6,926	3558	17
5	0,2033	0,2894	0,0417	7,4847	0,5721	122,6062	6,1636	51	12,6921	2412	21
6	0,3187	-0,1517	0,0909	6,3704	0,6016	96,8797	5,6983	48	10,1119	1216	13

bb	Bubble identification number
vel_axial	Axial bubble velocity
vel_rad	Radial bubble velocity
vel_azi	Azimuthal bubble velocity
Eötvös	Eötvös number of bubble
Aspect	Aspect ratio of bubble
Vol	Bubble volume
d	Sphere equivalent bubble diameter
BSclass	Bubble size class
RadPos	Radial bubble position
n	Number volume elements occupied by the bubble
dt	Bubble time detection length

9.4.4 Gas fraction files

Radial gas fraction distributions:

The ASCII files *.epsr* contains the time and azimuthally averaged gas fractions presented by two columns: The left column contains the radial distance of each ring domain from axis of the pipe in mm while in the right column contains the gas fraction in percent. The bubble pair results *.epsrad_20_pair file represents only the gas volume fraction of defined bubble pairs. At *.epsr_stat a third and fourth column represent the gas fraction distribution sigma limits ‘eps+sig’ and ‘eps-sig’.

Table 9.5. Part of gas fraction files *.epsrad_20 and *.epsr_stat

r [mm]	eps(r) [%]
0,7	2,326
2,1	2,345
3,4	2,308
4,8	2,247
6,2	2,018
7,5	1,801
8,9	1,572
10,3	1,455
11,6	1,369
13	1,233
14,4	1,091
15,8	0,961
17,1	0,865
18,5	0,763
19,9	0,634
21,2	0,484
22,6	0,33
24	0,189
25,3	0,076
26,7	0,02
*.epsrad_20-file or *.epsrad_20_pair-file	

r [mm]	eps(r) [%]	eps+sig [%]	eps-sig [%]
0,68	2,326	2,455	2,163
2,05	2,345	2,731	2,069
3,42	2,308	2,726	1,943
4,79	2,247	2,59	1,807
6,17	2,018	2,387	1,616
7,53	1,801	2,275	1,414
8,9	1,572	2,09	1,219
10,27	1,455	1,836	1,103
11,64	1,369	1,622	1,035
13,01	1,233	1,515	0,923
14,38	1,091	1,398	0,813
15,75	0,961	1,254	0,717
17,13	0,865	1,142	0,619
18,49	0,763	1,104	0,519
19,86	0,634	0,962	0,39
21,23	0,484	0,756	0,269
22,61	0,33	0,524	0,162
23,97	0,189	0,363	0,062
25,34	0,076	0,207	0,011
26,71	0,02	0,092	0
*.epsr_stat file			

Temporal gas fraction distributions:

For each scanned frame the cross-sectional averaged gas fraction is given as in Table 9.6 presented.

Table 9.6. Part of gas fraction file *.epst

t	eps(t)
s	%
0,001	0
0,002	0,09
0,003	0,23
0,004	0,9
0,005	1,48
0,006	1,92
0,007	2,13
0,008	2,26
0,009	2,2
0,01	2,51
0,011	2,75

Time averaged gas fraction distribution:

The *.epsxy-files contain the time averaged volumetric gas fractions in percent [%] as matrix for all the measurement cross-section (108x108 values). Table 9.7 shows a detailed view of this matrix. In this presentation, the points outside of the pipe cross-section also have the value 0%. The bubble pair results *.epsxy_pair file represents only the gas volume fraction of defined bubble pairs.

Table 9.7 Visualisation time averaged gas fractions over a quarter of the measurement cross-section from a *.epsxy file

9.4.5 Bubble size distribution

Bubble size distributions with linear bubble class width:

These files (* his_lin) contain a table as shown at tab. VI.5.

Table 9.8. Bubble size distribution for linear bubble class width from the file *.his_lin

d	hdxy	hdrelxy	hdnxy	hdv	hdrelv	hdnv
[mm]	[%/mm]	[1/mm]	[1/mm/s]	[%/mm]	[1/mm]	[1/mm/s]
0,25	0	0	0	0	0	0
0,5	0	0	0	0	0	0
0,75	0	0	0	0	0,0042	0,4
1	0	0,0048	0,4	0,0015	0,1842	14,8
1,25	0,0002	0,0227	2	0,0073	0,8903	54,8
1,5	0,0056	0,6765	41,2	0,0092	1,1159	40,8
1,75	0,0057	0,6957	35,2	0,0061	0,739	16
2	0,0073	0,8894	31,2	0,0034	0,4158	5,6
2,25	0,0042	0,5066	12,8	0,0034	0,4133	4
2,5	0,0052	0,6267	10	0,004	0,4891	3,2
2,75	0,0035	0,4221	3,6	0,0022	0,2725	1,6
3	0,0046	0,5613	3,6	0,0026	0,3142	1,2

The single columns include the following information (see also section 3.8):

d	Bubble diameter [mm]
hd	Gas fraction of the bubbles of this class referring to bubble class width (0,25 mm) [%/mm]
hdrel	hd related to the total gas fraction [1/mm]
hdn	Number of bubbles in respective class referring to the class width and the sum of measurement time [1/(mm*s)]

These three distributions are available related to the area equivalent bubble diameter for the largest cross-section area of the bubble in the measurement plane (xy) and basing on the volume equivalent bubble diameter (v), respectively. For the calculation of the volume equivalent parameters, the local gas velocities obtained by cross-correlation are used, in order to convert the time coordinate from the *.a- files into a geometrical length.

Bubble size distribution for linear bubble class widths distributed in ring domains:
These files (*.his_lin_r) contain for each of the 20 rings a table. The minimum and maximum radius of the ring is given above each table. At the end, a table with the integral bubble size distributions is added, which correspond to the distributions in the file *.his_lin. The local gas velocities obtained by cross-correlation are used.

Bubble size distribution for logarithmic bubble class widths:
The *.his_log files contain the same bubble size distributions as the *.his_lin files, but in this case the bubble class width increases logarithmically starting from a diameter d of 3 mm:

$$Bubble\ size\ class = \frac{\ln \frac{d}{3mm}}{0.035} + \frac{3}{0.1}$$

For smaller bubbles, a linear class width of 0.1 mm is used. Appendix 9.1 includes the graphical presentation of the bubble size distributions basing on the *.his_log files. The local gas velocities obtained by cross-correlation are used.

The bubble size distributions estimated by using morphological method and bubble pair finding (*.his_log_morph and *.his_log_pair) contain only two columns: The sphere equivalent bubble diameter representing the bubble size class and the Gas fraction of the bubbles of this class referring to bubble class width basing on the volume equivalent bubble diameter (hdv).

9.4.6 Gas velocities

Similar to the gas fraction files, the velocity files exist in two formats: A radial profile one (time and azimuthal averaged) and a cross-sectional one (only time averaged). These files are created for axial velocity (*.vel or *.velxy) obtained by all three velocity estimation methods (additional for morphological method and bubble pair finding the suffixes “_morph” or “_pair”). For radial and azimuthal velocities values obtained by the morphological method as well as bubble pair finding are existing only (extension suffix “_azimuthal” or “_radial” plus method suffix).
For both single bubble velocity methods, files containing the velocity standard deviation exist additionally (*.sigvel*).

HZDR
HELMHOLTZ
ZENTRUM DRESDEN
ROSSENDORF

Bautzner Landstraße 400
01328 Dresden, Germany
Tel. +49 351 260-2047
Fax +49 351 260-12047
d.lucas@hzdr.de
http://www.hzdr.de